2017 European School of High-Energy Physics

Evora, Portugal
6 – 19 September 2017

Editors: M. Mulders
G. Zanderighi

This volume is indexed in: CERN Document Server (CDS), INSPIRE, Scopus.

This volume should be cited as:
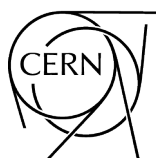
Proceedings of the 2017 European School of High-Energy Physics, Evora, Portugal, 6 – 19 September 2017,
edited by M. Mulders and G. Zanderighi, CERN Yellow Reports: School Proceedings, Vol. 3/2018,
CERN-2018-006-SP (CERN, Geneva, 2018), https://doi.org/10.23730/CYRSP-2018-003

A contribution in this volume should be cited as:

[Author name(s)], in Proceedings of the 2017 European School of High-Energy Physics, Evora, Portugal, 6 –
19 September 2017, edited by M. Mulders and G. Zanderighi, CERN Yellow Reports: School Proceedings,
Vol. 3/2018, CERN-2018-006-SP (CERN, Geneva, 2018), pp. [first page]–[last page],
https://doi.org/10.23730/CYRSP-2018-003.[first page]

Abstract

The European School of High-Energy Physics is intended to give young physicists an introduction to the theoretical aspects of recent advances in elementary particle physics. These proceedings contain lecture notes on the Electroweak standard model, the theory of quantum chromodynamics, physics beyond the standard model, Electroweak symmetry breaking after the Higgs discovery, neutrino physics, and practical statistics for High Energy Physics.

Preface

The twenty-fifth event in the series of the European School of High-Energy Physics took place in Evora, Portugal, from 6 to 19 September 2017. It was organized jointly by CERN, Geneva, Switzerland, and JINR, Dubna, Russia, with support from LIP, FCT, the University of Evora, the Agência de Promoção Turística do Alentejo and the Instituto de Turismo de Portugal. The local organization team was chaired by Patricia Conde Muíño (LIP). The other members of the local committee were: Natália Antunes, Gaspar Barreira, Mourad Bezzeghoud, Ruben Conceição, Michele Gallinaro, Ricardo Gonçalo, Isabel Lopes, José Maneira, António Onofre, Jorge Romão and João Varela.

A total of 100 students of 33 different nationalities attended the school, mainly from institutes in member states of CERN and/or JINR, but also some from other regions. The participants were generally students in experimental High-Energy Physics in the final years of work towards their PhDs.

The School was hosted at the Evora Hotel, just outside of the historic city centre. According to the tradition of the school, the students shared twin rooms mixing participants of different nationalities.

A total of 31 lectures were complemented by daily discussion sessions led by six discussion leaders. The students displayed their own research work in the form of posters in an evening session in the first week, and the posters stayed on display until the end of the School. The full scientific programme was arranged in the on-site conference facilities.

The School also included an element of outreach training, complementing the main scientific programme. This consisted of a two-part course from the Inside Edge media training company. Additionally, students had the opportunity to act out radio interviews under realistic conditions based on a hypothetical scenario.

The students from each discussion group subsequently carried out a collaborative project, preparing a talk on a physics-related topic at a level appropriate for a general audience. The talks were given by student representatives of each group in an evening session in the second week of the School. A jury, chaired by Catarina Espirito Santo (LIP), judged the presentations; other members of the jury were Pedro Abreu (LIP), and José Vítor Malheiros (Ciência Viva). We are very grateful to all of these people for their help.

Our thanks go to the local-organization team and, in particular, to Patricia Conde Muíño, for all of their work and assistance in preparing the School, on both scientific and practical matters, and for their presence throughout the event. Our thanks also go to the efficient and friendly hotel management and staff who assisted the School organizers and the participants in many ways. We are also extremely grateful for all of the support and assistance provided by the University of Evora.

Very great thanks are due to the lecturers and discussion leaders for their active participation in the School and for making the scientific programme so stimulating. The students, who in turn manifested their good spirits during two intense weeks, appreciated listening to and discussing with the teaching staff of world renown.

We would like to express our strong appreciation to Fabiola Gianotti, Director General of CERN, and Victor Matveev, Director of JINR, for their lectures on the scientific programmes of the two organizations and for discussing with the School participants.

In parallel with the School, a public outreach event was organised in collaboration with the University of Evora and LIP. This was introduced by Ana Costa Freitas, Rector of the University of Evora, Nick Ellis, Director of the CERN Schools of Physics, Manuel Heitor, Minister for Science and Higher Education, and Gaspar Barreira, Director of LIP. Fabiola Gianotti then gave a lecture entitled "The Higgs Particle and Our Life" in front of an audience of about 300 people with others watching a webcast. This was followed by questions from the audience that were answered by a panel composed of Gaspar Barreira, Fabiola Gianotti and Victor Matveev, chaired by Pedro Abreu.

In addition to the rich academic programme, the participants enjoyed numerous sports, leisure and cultural activities in and around Evora. There was a half-day excursion to the fascinating local sites of megalithic monuments, followed by a visit to the Convent Bom Jesus that included a wine tasting, buffet dinner and fado concert. During the full-day excursion to Monsaraz, participants were able visit the castle and the old town, and then spend the afternoon at the nautical club on the Alqueva reservoir with activities that included canoeing and archery, followed by a traditional dinner at a restaurant before returning to the hotel. On the final Saturday afternoon there was the option of a guided tour of the historic sites of Evora, followed by a buffet dinner hosted by the university. The excursions provided an excellent environment for informal interactions between staff and students.

We are very grateful to the School Administrators, Kate Ross (CERN) and Tatyana Donskova (JINR), for their untiring efforts in the lengthy preparations for and the day-to-day operation of the School. Their continuous care of the participants and their needs during the School was highly appreciated.

The success of the School was to a large extent due to the students themselves. Their poster session was very well prepared and highly appreciated, their group projects were a big success, and throughout the School they participated actively during the lectures, in the discussion sessions and in the different activities and excursions.

Nick Ellis
(On behalf of the Organizing Committee)

People in the photograph

1	Ana	Peixoto
2	Evgeniya	Cheremushkina
3	Tiago	Vale
4	Elisa	Minucci
5	Kirill	Melnikov
6	Susanna	Gaginyan
7	Sacha	Davidson
8	Petr	Mandrik
9	Pablo	De Castro Manzano
10	Martin	Beneke
11	Rostislav	Sotensky
12	Maria	Lavrova
13	Ellis	Kay
14	Alexander	Olshevskiy
15	Guillermo	Hamity
16	Yu-Heng	Chen
17	Alexander	Held
18	Karim	El Morabit
19	Adam	Parker
20	Tatiana	Lyubushkina
21	Tatyana	Donskova
22	Chiara	Amendola
23	Diallo	Boye
24	Johnny	Raine
25	Sebastien	Rettie
26	Evan	Ranken
27	Victor	Matveev
28	Despoina	Sampsonidou
29	Douglas	Burns
30	Matteo	Bedognetti
31	Joan	Arnau Romeu
32	Andrea	Rodriguez Perez
33	Mar	Barrio
34	Marco	Nardecchia
35	Charles	Delporte
36	Elias	Ruttinger
37	Claire	Antel
38	Tasneem	Rashid
39	Emanuele	Re
40	Emma	Winkels
41	Andrea	Scarpelli
42	Yu-Ting	Shen
43	Malgorzata	Pikies
44	Millie	McDonald
45	Michal	Sefcik
46	Michal	Zamkovsky
47	Johannes	Lange
48	Johannes	Junggeburth
49	Andrea	Selce
50	Andre	Cortez
51	Navid	Rad
52	Stephan	Duell
53	Olga	Bakina
54	Davide	Fazzini
55	Nick	Ellis
56	Alexey	Gladyshev
57	Emanuel	Gouveia
58	Zukhaimira	Zolkapli
59	Andrea	Beschi
60	Bruno	Galinhas
61	Maarten	van Veghel
62	Mazuza	Ghneimat
63	Stefanie	Todt
64	Klaudia	Burka
65	Fabrizio	Miano
66	Fabio	Tresoldi
67	Patricia	Conde Muino
68	Alexander	Bednyakov
69	Mick	Mulder
70	Lisa	Benato
71	Alexander	Mudrokh
72	Igor	Ivanov
73	Vincenzo	Ciriolo
74	Evangelos	Kourlitis
75	Harry	Moss
76	Fernando	Abudinen
77	Claudia	Merlassino
78	Elena	Dall'Occo
79	Rui	Santos
80	Philipp	Mogg
81	Magdalena	Kuich
82	Haifa	Rejeb Sfar
83	Irakli	Minashvili
84	Carl	Suster
85	Uli	Einhaus
86	Hualin	Mei
87	John	Myers
88	Cedric	Meaux
89	Krystian	Roslon
90	Jan Oliver	Rieger
91	Andres	Ramirez Morales
92	Kevin	De Vasconcelos Corga
93	Alessio	Piucci
94	Viesturs	Veckalns
95	Carlo Alberto	Gottardo
96	Marco	Valente
97	Grigore	Tarna
98	Po-Hsun	Chen
99	Robert	Wolff
100	Seth	Moortgat
101	Xuanhong	Lou
102	Oliver	Majersky
103	Guilherme	Milhano
104	Joao	Silva
105	Victor	Renaudin
106	Robert	Hankache
107	Nikolai	Hartmann
108	Antinea	Guerguichon
109	Jose	Maneira
110	Martijn	Mulders
111	Kate	Ross
112	Saskia	Falke
113	Marketa	Jansova
114	Jaana	Heikkilae

Photographs (montage)

The 2017 European School of High-Energy Physics
Evora, Portugal, 6 – 19 September 2017

Contents

Quantum Field Theory and the Electroweak Standard Model

A.B. Arbuzov
BLTP JINR, Dubna, Russia

Abstract

Lecture notes with a brief introduction to Quantum field theory and the Standard Model are presented. The lectures were given at the 2017 European School of High-Energy Physics. The main features, the present status, and problems of the Standard Model are discussed.

Keywords

Lectures; Standard Model; Quantum Field Theory; Gauge symmetry; Z boson; W boson; Higgs boson

1 Introduction

The lecture course consists of four main parts. In the Introduction, we will discuss what is the Standard Model (SM) [1–3], its particle content, and the main principles of its construction. The second Section contains brief notes on Quantum Field Theory (QFT), where we remind the main objects and rules required further for construction of the SM. Sect. 3 describes some steps of the SM development. The Lagrangian of the model is derived and discussed. Phenomenology and high-precision tests of the model are overviewed in Sect. 4. The present status, problems, and prospects of the SM are summarized in Conclusions. Some simple exercises and questions are given for students in each Section. These lectures give only an overview of the subject while for details one should look in textbooks, e.g., [4–7], and modern scientific papers.

1.1 What is the Standard Model?

Let us start with the definition of the main subject of the lecture course. It is the so-called *Standard Model*. This name is quite widely accepted and commonly used to define a certain theoretical model in high energy physics. This model is suited to describe properties and interactions of *elementary* particles. One can say that at the present moment, the Standard Model is the most successful physical model ever. In fact it describes with a high precision hundreds and hundreds independent observables. The model made also a lot of predictions which have been verified later experimentally. Among other physical models pretending to describe fundamental properties of Nature, the SM has the highest predictive power. Moreover, the model is minimal: it is constructed using only fields, interactions, and parameters which are necessary for consistency and/or observed experimentally. The minimality and in general the success of the model is provided to a great extent by application of symmetry principles.

In spite of the nice theoretical features and successful experimental verification of the SM, we hardly can believe that it is the true fundamental theory of Nature. First of all, it is only one of an infinite number of possible models within Quantum field theory. So it has well defined grounds but its uniqueness is questionable. Second, we will see that the SM and QFT itself do not seem to be the most adequate (mathematical) language to describe Nature. One can also remind that gravity is not (yet) joined uniformly with the SM interactions.

In any case, the SM is presently the main theoretical tool in high-energy physics. Most likely this status will be preserved even if some new more fundamental physical model would be accepted by the community. In this case the SM will be treated as an approximation (a low-energy limit) of that more general theory. But for practical applications (in a certain energy domain) we will still use the SM.
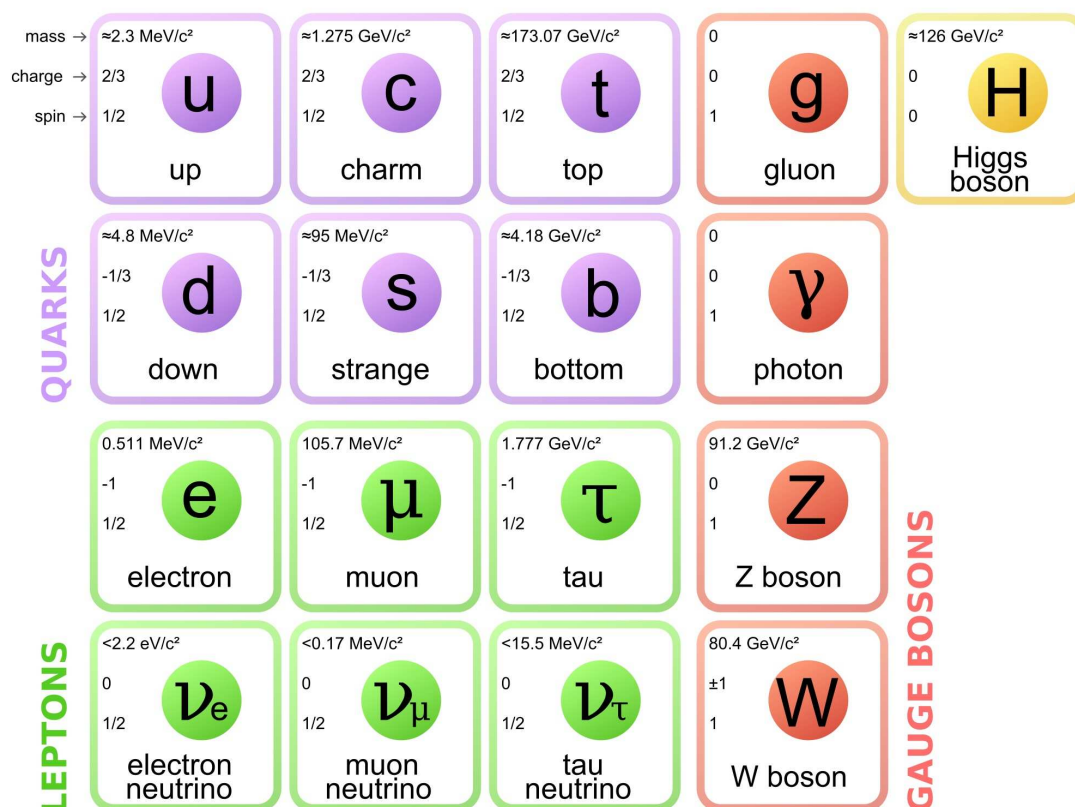
Fig. 1: Particle content of the Standard Model. Courtesy to Wikipedia: 'Standard Model of Elementary Particles' by MissMJ — Own work by uploader, PBS NOVA, Fermilab, Office of Science, United States Department of Energy, Particle Data Group.

1.2 Particle content of the Standard Model

Before construction of the SM, let us defined its content in the sense of fields and particles.

We would like to underline that the discovery of the Higgs boson at LHC in 2012 [8, 9] just finalized the list of SM particles from the experimental point of view. Meanwhile the Higgs boson is one of the key ingredients of the SM, so it was always in the list even so that its mass was unknown.

The particle content of the SM is given on Fig. 1. It consists of 12 fermions (spin = 1/2), 4 vector gauge bosons (spin = 1), and one scalar Higgs boson (spin = 0). For each particle the chart contains information about its mass, electric charge, and spin. One can see that the data on neutrino masses is represented in the form of upper limits, since they have not been yet measured. Strictly speaking the information about neutrino masses should be treated with care. According to the present knowledge, as discussed in the course of lectures on Neutrino Physics, a neutrino particle of a given lepton flavor e.g., ν_τ, is not a mass eigenstate but a superposition of (at least) three states with different masses.

Fermions are of two types: *leptons* and *quarks*. They are:
— 3 charged leptons (e, μ, τ);
— 3 neutrinos ν_e, ν_μ, ν_τ (or ν_1, ν_2, ν_3, see lectures on Neutrino physics);
— 6 quarks of different *flavors*, see lectures on Flavor Physics.

Each quark can have one of three *colours*, see lectures on QCD. Each fermion has 2 degrees of freedom e.g., can have spin up or down, or can be either *left* or *right*. Each fermion particle in the SM has an *anti-particle*, $f \neq \bar{f}$. The later statement is not yet verified for neutrinos, they might be Majorana particles.

Traditionally fermions are called *matter fields*, contrary the the so-called *force fields*, i.e., intermediate vector bosons which mediate gauge interactions. Please keep in mind that this notion doesn't correspond to the common sense directly. In fact most of fermions are unstable and do not form the 'ordinary matter' around us, while e.g., the mass of nuclear matter is provided to a large extent by gluons. Moreover, looking at various Feynman diagrams we can see that fermions can serve as intermediate particles in interaction processes.

In the SM we have the following boson fields:
— 8 vector (spin=1) *gluons*;
— 4 vector (spin=1) *electroweak bosons*: γ, Z, W^+, W^-;
— 1 scalar (spin=0) *Higgs boson*.

Gluons and photon are *massless* and have 2 degrees of freedom (polarizations), Z and W bosons are *massive* and have 3 degrees of freedom (polarizations). By saying massless or massive we mean the absence or presence of the corresponding terms in the Lagrangian of the SM. This is not always related to observables in a straightforward way: e.g., gluons are not observed as free asymptotic massless states, and masses of unstable W and Z bosons are defined indirectly from kinematics of their decay products.

Gluons and Electroweak (EW) bosons are *gauge bosons*, their interactions with fermions are fixed by certain symmetries of the SM Lagrangian. Note that electrically neutral bosons (H, γ, Z, and gluons) coincide with their anti-particles e.g., $\gamma \equiv \bar{\gamma}$. Each of 8 gluons carries one color and one anti-color.

Besides the particle content, we have to list the interactions which are described by the Standard Model. One of our final ultimate goals would be to answer the question *"How many fundamental interactions are there in Nature?"* But we should understand that it is only a dream, a primary motivation of our studies. Being scientists we should be always unsure about the true answer to this question. On the other hand, we can certainly say, how many different interactions is there in a given model, for example in the SM. To answer this question we have to look at the complete Lagrangian of the model, see e.g., book [10]. For the SM it looks very long and cumbersome. The SM Lagrangian contains kinetic terms for all listed above fields and dozens of terms that describe interactions between them. So, before trying to count the number of interactions we should understand the structure and symmetries of the Lagrangian.

1.3 Principles of the Standard Model

We are going to construct the SM Lagrangian. For this purpose, we have to define first the guiding principles. That is important for optimization of the procedure. The same principles might be used further in construction of other models.

First of all, we have to keep in mind that the SM is a model that is built within the local Quantum field theory. From the beginning this condition strongly limits the types of terms that can appear in the Lagrangian because of the Lorentz invariance, the Hermitian condition, the locality etc. One can make a long list of various conditions. Here I list only the main principles which will be exploited in our way of the SM construction:

- the *generalized correspondence* to various existing theories and models like Quantum Mechanics, QED, the Fermi model etc.;
- the *minimality*, i.e., only observed and/or unavoidable objects (fields and interactions) are involved;
- the *unitarity* which is a general condition for cross sections and various transformations of fields related to the fact that any probability limited from above by unity;
- the *renormalizability* is necessary for derivation of finite predictions for observable quantities at the quantum level;
- the *gauge* principle for introduction of interactions (were possible).

The main guiding principle is the *symmetry* one. The SM possesses several different symmetries:
— the Lorentz (and Poincaré) symmetry,

— the CPT symmetry,
— three gauge symmetries $SU(3)_C \otimes SU(2)_L \otimes U(1)_Y$,
— the global $SU(2)_L \times SU(2)_R$ symmetry in the Higgs sector (it is broken spontaneously);
— some other symmetries, like the one between three generation of fermions, the one that provides cancellation of axial anomalies etc.
In this context, one can mention also the conformal symmetry which is obviously broken in the SM, but the mechanism of its breaking and the consequences are very important for the model.

2 Brief notes on Quantum field theory

The Standard Model is a model constructed within the local relativistic Quantum field theory. It means that the SM obeys the general QFT rules. We should keep in mind that there are many other possible QFT models, and the SM is distinguished between them mostly because of its successful experimental verifications but also because of a number of its features like renormalizablity, unitarity, and cancellation of axial anomalies. I assume that all students of the ESHEP school had courses on Quantum field theory. Here we will just remind several features of QFT which are important for further construction of the SM Lagrangian.

As it was already mentioned, we are going to preserve the correspondence to Quantum Mechanics (QM). Historically, QFT was developed on the base of QM, in particular using the quantum oscillator ansatz. But by itself QFT can be considered as a more profound fundamental construction, so one should be able to define this theory without referring to QM. In fact, QFT can be formulated starting from the basic classification of fields as unitary irreducible representations of the Lorentz group.

Let us first of all fix the notation. We will work in the natural system of units where the speed of light $c = 1$ and the reduced Planck constant $\hbar = 1$. The Lorentz indexes will be denoted by Greek letters, like $\mu = 0, 1, 2, 3$; p_μ is a four-momentum of a particle, $\mathbf{p} = (p_1, p_2, p_3)$ is a three-momentum, $p_0 = E$ is the particle energy. The metric tensor of the Minkowsky space is chosen in the form

$$g_{\mu\nu} = \begin{pmatrix} 1 & 0 & 0 & 0 \\ 0 & -1 & 0 & 0 \\ 0 & 0 & -1 & 0 \\ 0 & 0 & 0 & -1 \end{pmatrix}, \quad g_{\mu\nu} p_\nu = p_\mu, \quad g_{\mu\mu} = 4. \tag{1}$$

We will always assume summation over a Lorentz index if it is repeated twice: $A_\mu B_\mu \equiv A_0 B_0 - A_1 B_1 - A_2 B_2 - A_3 B_3$, where the metric tensor is used. In particular, the scalar product of two four-vectors is defined as $pq = p_\mu q_\mu = p_0 q_0 - p_1 q_1 - p_2 q_2 - p_3 q_3$. It is a relativistic *invariant*.

We will assume that there exist so-called asymptotic free final states for particle-like excitation of quantum fields. These asymptotic states will be associated with initial or final state (elementary) particles which fly in a free space without interactions. For such states we apply the *on-mass-shell condition* $p^2 = pp = p_0^2 - \mathbf{p}^2 = E^2 - \mathbf{p}^2 = m^2$ where m is the mass of the particle.

Now we will postulate the properties of fields that are required for the construction of the SM. A neutral scalar field can be defined as

$$\varphi(x) = \frac{1}{(2\pi)^{3/2}} \int \frac{d\mathbf{p}}{\sqrt{2p_0}} \left(e^{-ipx} a^-(\mathbf{p}) + e^{+ipx} a^+(\mathbf{p}) \right), \tag{2}$$

where $a^\pm(\mathbf{p})$ are *creation* and *annihilation* operators. Their commutation relations read

$$[a^-(\mathbf{p}), a^+(\mathbf{p}')] \equiv a^-(\mathbf{p}) a^+(\mathbf{p}') - a^+(\mathbf{p}') a^-(\mathbf{p}) = \delta(\mathbf{p} - \mathbf{p}'),$$
$$[a^-(\mathbf{p}), a^-(\mathbf{p}')] = [a^+(\mathbf{p}), a^+(\mathbf{p}')] = 0. \tag{3}$$

The field is a function of four-coordinate x in the Minkowsky space. It behaves as a plane wave in the

whole space. The Lagrangian[1] for the neutral scalar field can be chosen in the form

$$\mathcal{L}(x) = \frac{1}{2}(\partial_\mu \varphi \partial_\mu \varphi - m^2 \varphi^2). \tag{4}$$

Note that it depends only on the field and its first derivative. Variation of the action $A \equiv \int \mathrm{d}^4 \mathcal{L}(x)$ with respect to variations of the field $\varphi \to \varphi + \delta\varphi$ according to the *least action principle* gives

$$\delta \int \mathrm{d}x \mathcal{L}(x) = \int \mathrm{d}x \left(\frac{\partial \mathcal{L}}{\partial \varphi} \delta\varphi + \frac{\partial \mathcal{L}}{\partial(\partial_\mu \varphi)} \delta(\partial_\mu \varphi) \right) = 0. \tag{5}$$

Here we apply quite natural for QFT problems zero boundary conditions for the field and its derivative at infinity and get the well-known Klein–Fock–Gordon equation of motion

$$(\partial_\mu^2 + m^2)\varphi(x) = 0. \tag{6}$$

EXERCISE: Check that the postulated above field $\varphi(x)$ satisfies the equation.

Creation and annihilation operators act in the Fock space which consists of *vacuum* ground state denoted as $|0\rangle$ and *excitations* over it. For the vacuum state we postulate

$$a^-(\mathbf{p})|0\rangle = 0, \quad \langle 0|a^+(\mathbf{p}) = 0, \quad \langle 0|0\rangle = 1. \tag{7}$$

Actually, $a^-(\mathbf{p})|0\rangle = 0 \cdot |0\rangle$ but the vacuum state can be dropped since finally all observable quantities are proportional to $\langle 0|0\rangle$. The field excitations are states of the form

$$|f\rangle = \int \mathrm{d}\mathbf{p}\, f(\mathbf{p})a^+(\mathbf{p})|0\rangle, \quad |g\rangle = \int \mathrm{d}\mathbf{p}\mathrm{d}\mathbf{q}\, g(\mathbf{p},\mathbf{q})a^+(\mathbf{p})a^+(\mathbf{q})|0\rangle, \quad \dots \tag{8}$$

The most simple excitation $a^+(\mathbf{p})|0\rangle \equiv |p\rangle$ is used to describe a single on-mass-shell particle with momentum $\mathbf{p}$. Then $a^+(\mathbf{p})a^+(\mathbf{q})|0\rangle$ is a two-particle state and so on. Because of the presence of modulating functions like $f(\mathbf{p})$ and $g(\mathbf{p},\mathbf{q})$, the Fock space is infinite-dimensional.

EXERCISES: 1) Find the norm $\langle p|p\rangle$; 2) check that operator $\hat{N} = \int \mathrm{d}\mathbf{p}\, a^+(\mathbf{p})a^-(\mathbf{p})$ acts as a particle number operator.

A charged scalar field is defined as

$$\varphi(x) = \frac{1}{(2\pi)^{3/2}} \int \frac{\mathrm{d}\mathbf{p}}{\sqrt{2p_0}} \left(e^{-ipx} a^-(\mathbf{p}) + e^{+ipx} b^+(\mathbf{p}) \right),$$

$$\varphi^*(x) = \frac{1}{(2\pi)^{3/2}} \int \frac{\mathrm{d}\mathbf{p}}{\sqrt{2p_0}} \left(e^{-ipx} b^-(\mathbf{p}) + e^{+ipx} a^+(\mathbf{p}) \right),$$

$$[a^-(\mathbf{p}), a^+(\mathbf{p}')] = [b^-(\mathbf{p}), b^+(\mathbf{p}')] = \delta(\mathbf{p} - \mathbf{p}'), \quad [a^\pm, b^\pm] = 0,$$

where operators $a^\pm(\mathbf{p})$ create and annihilate particles, while operators $b^\pm(\mathbf{p})$ are used for the same purpose for *anti-particles*. Note that the choice of what is particle and what is anti-particle is arbitrary here. The corresponding Lagrangian reads

$$\mathcal{L}(\phi, \phi^*) = \partial_\mu \varphi^* \partial_\mu \varphi - m^2 \varphi^* \varphi. \tag{9}$$

Note that φ and φ^* are related by a generalized complex conjugation which involves operator transformations: $(a^\pm)^* = a^\mp$ and $(b^\pm)^* = b^\mp$. It is worth to note also that φ and φ^* are not "a particle and an anti-particle".

---

[1]Actually it is a Lagrangian density.

A massive charged vector field (remind $W^\pm$ bosons) is defined as

$$U_\mu(x) = \frac{1}{(2\pi)^{3/2}} \int \frac{d\mathbf{p}}{\sqrt{2p_0}} \sum_{n=1,2,3} e_\mu^n(\mathbf{p}) \left(e^{-ipx} a_n^-(\mathbf{p}) + e^{+ipx} b_n^+(\mathbf{p})\right),$$

$$U_\mu^*(x) = \frac{1}{(2\pi)^{3/2}} \int \frac{d\mathbf{p}}{\sqrt{2p_0}} \sum_{n=1,2,3} e_\mu^n(\mathbf{p}) \left(e^{-ipx} b_n^-(\mathbf{p}) + e^{+ipx} a_n^+(\mathbf{p})\right),$$

$$[a_n^-(\mathbf{p}), a_l^+(\mathbf{p}')] = [b_n^-(\mathbf{p}), b_l^+(\mathbf{p}')] = \delta_{nl}\delta(\mathbf{p} - \mathbf{p}'), \quad [a^\pm, b^\pm] = 0.$$

For *polarization vectors* $e_\mu^n(\mathbf{p})$ the following conditions are applied:

$$e_\mu^n(\mathbf{p}) e_\mu^l(\mathbf{p}) = -\delta_{nl}, \qquad p_\mu e_\mu^n(\mathbf{p}) = 0. \tag{10}$$

EXERCISE: Using the above orthogonality conditions, show that

$$\sum_{n=1,2,3} e_\mu^n(\mathbf{p}) e_\nu^n(\mathbf{p}) = -\left(g_{\mu\nu} - \frac{p_\mu p_\nu}{m^2}\right). \tag{11}$$

The Lagrangian for a massive charged vector field takes the form

$$\mathcal{L} = -\frac{1}{2}\left(\partial_\mu U_\nu^* - \partial_\nu U_\mu^*\right)\left(\partial_\mu U_\nu - \partial_\nu U_\mu\right) + m^2 U_\mu^* U_\mu. \tag{12}$$

The corresponding Euler–Lagrange equation reads

$$\partial_\nu(\partial_\mu U_\nu - \partial_\nu U_\mu) + m^2 U_\mu = 0.$$

EXERCISE: Using the above equation, show that $\partial_\nu U_\nu(x) = 0$, i.e., derive the Lorentz condition. Note that the Lorentz condition removes from the field one of four independent degrees of freedom (components).

A massless neutral vector field (a photon) is defined as

$$A_\mu(x) = \frac{1}{(2\pi)^{3/2}} \int \frac{d\mathbf{p}}{\sqrt{2p_0}} e_\mu^\lambda(\mathbf{p}) \left(e^{-ipx} a_\lambda^-(\mathbf{p}) + e^{+ipx} a_\lambda^+(\mathbf{p})\right), \tag{13}$$

$$[a_\lambda^-(\mathbf{p}), a_\nu^+(\mathbf{p}')] = -g_{\lambda\nu}\delta(\mathbf{p} - \mathbf{p}') \qquad e_\mu^\lambda(\mathbf{p}) e_\nu^\lambda(\mathbf{p}) = g_{\mu\nu}, \qquad e_\mu^\lambda(\mathbf{p}) e_\mu^\nu(\mathbf{p}) = g_{\lambda\nu}.$$

Formally this field has four polarizations, but only two of them correspond to physical degrees of freedom. The corresponding Lagrangian reads

$$\mathcal{L} = -\frac{1}{4} F_{\mu\nu} F_{\mu\nu}, \qquad F_{\mu\nu} \equiv \partial_\mu A_\nu - \partial_\nu A_\mu. \tag{14}$$

A Dirac fermion field is defined as

$$\Psi(x) = \frac{1}{(2\pi)^{3/2}} \int \frac{d\mathbf{p}}{\sqrt{2p_0}} \sum_{r=1,2} \left(e^{-ipx} a_r^-(\mathbf{p}) u_r(\mathbf{p}) + e^{+ipx} b_r^+(\mathbf{p}) v_r(\mathbf{p})\right), \tag{15}$$

$$\overline{\Psi}(x) = \frac{1}{(2\pi)^{3/2}} \int \frac{d\mathbf{p}}{\sqrt{2p_0}} \sum_{r=1,2} \left(e^{-ipx} b_r^-(\mathbf{p}) \bar{v}_r(\mathbf{p}) + e^{+ipx} a_r^+(\mathbf{p}) \bar{u}_r(\mathbf{p})\right),$$

$$[a_r^-(\mathbf{p}), a_s^+(\mathbf{p}')]_+ = [b_r^-(\mathbf{p}), b_s^+(\mathbf{p}')]_+ = \delta_{rs}\delta(\mathbf{p} - \mathbf{p}'),$$

$$[a_r^+(\mathbf{p}), a_s^+(\mathbf{p}')]_+ = [a_r^-(\mathbf{p}), b_s^+(\mathbf{p}')]_+ = \ldots = 0.$$

EXERCISE: Show that $a_r^+(\mathbf{p}) a_r^+(\mathbf{p}) = 0$, i.e., verify the Pauli principle.

Here, u_r, u_r, $\bar{u}_r$, and $\bar{v}_r$ are four-component spinors, so $\Psi(x) \equiv \{\Psi_\alpha(x)\}$ is a four-vector column, $\alpha = 1, 2, 3, 4$, and $\overline{\Psi}(x)$ is a four-vector row,

$$\bar{u}u = \sum_{\alpha=1}^{4} \bar{u}_\alpha u_\alpha = \sum_{\alpha=1}^{4} u_\alpha \bar{u}_\alpha = \mathrm{Tr}(u\bar{u}).$$

Spinors are solutions of the (Dirac) equations:

$$(\hat{p} - m)u_r(\mathbf{p}) = 0, \qquad \bar{u}_r(\mathbf{p})(\hat{p} - m) = 0, \tag{16}$$
$$(\hat{p} + m)v_r(\mathbf{p}) = 0, \qquad \bar{v}_r(\mathbf{p})(\hat{p} + m) = 0,$$
$$\hat{p} \equiv p_\mu \gamma_\mu = p_0 \gamma_0 - p_1 \gamma_1 - p_2 \gamma_2 - p_3 \gamma_3, \qquad m \equiv m\mathbf{1},$$

where $\mathbf{1}$ is the unit four-by-four matrix. For the solutions of the above equations we impose the normalization conditions

$$\bar{u}_r(\mathbf{p})u_s(\mathbf{p}) = -\bar{v}_r(\mathbf{p})v_s(\mathbf{p}) = 2m\delta_{rs}.$$

The gamma matrixes (should) satisfy the commutation condition

$$[\gamma_\mu, \gamma_\nu]_+ = 2g_{\mu\nu}\mathbf{1} \quad \Rightarrow \quad \gamma_0^2 = \mathbf{1}, \quad \gamma_1^2 = \gamma_2^2 = \gamma_3^2 = -\mathbf{1}$$

and the condition of Hermitian conjugation

$$\gamma_\mu^\dagger = \gamma_0 \gamma_\mu \gamma_0.$$

The latter leads to the rule of the *Dirac conjugation*:

$$\overline{\Psi} = \Psi^\dagger \gamma_0, \quad \bar{u} = u^\dagger \gamma_0, \quad \bar{v} = v^\dagger \gamma_0. \tag{17}$$

EXERCISE: Show that the Dirac conjugation rule is consistent with the set of Dirac equations (16).

Note that explicit expressions for gamma matrixes are not unique, but they are not necessary for construction of observables, *QUESTION: Why is that so?* The most common representations of gamma matrixes are so-called Dirac's (standard) and Weyl's (spinor) ones.

Two values of index r in Eq. (15) correspond to two independent degrees of freedom for each spinor in other words to two independent solutions of the Dirac equations. In most cases these two degrees of freedom can be treated as two polarization states like 'spin up' and 'spin down'. But in the Standard Model, there is one special choice of the basis for spinors, namely we will distinguish *Left* (L) and *Right* (R) chiral states of spinors. By definition,

$$\Psi_L \equiv P_L\Psi, \quad \Psi_R \equiv P_R\Psi, \quad P_{L,R} \equiv \frac{\mathbf{1} -, + \gamma_5}{2}, \quad \Psi = \Psi_L + \Psi_R. \tag{18}$$

Here $\gamma_5 \equiv i\gamma_0\gamma_1\gamma_2\gamma_3$, this gamma-matrix has the properties

$$[\gamma_\mu, \gamma_5]_+ = 0, \qquad \gamma_5^2 = \mathbf{1}, \quad \gamma_5^\dagger = \gamma_5. \tag{19}$$

As can be seen from Eq. (18), $P_{L,R}$ form a complete set of orthogonal projection operators,

$$P_{L,R}^2 = P_{L,R} \qquad P_L P_R = P_R P_L = 0, \qquad P_L + P_R = 1. \tag{20}$$

The sign before γ_5 in the definition of the projection operators in Eq. (18) corresponds to the standard representation of gamma matrixes[2]. The Dirac conjugation (17) of left and right spinors gives

$$\overline{\Psi}_L \equiv \overline{\Psi}\frac{1 + \gamma_5}{2}, \qquad \overline{\Psi}_R \equiv \overline{\Psi}\frac{1 - \gamma_5}{2}.$$

---

[2]In the spinor representation the sign is opposite: $P_L \equiv (1 + \gamma_5)/2$ and $P_R \equiv (1 - \gamma_5)/2$.

Note that the definition of the left and right chiral states was done without referring to spin projections (helicity states). In fact, these are different ways to select a basis. Helicity and chirality states can be identified to each other only for massless fermions.

Remind some properties of gamma matrixes

$$\mathrm{Tr}\gamma_\mu = \mathrm{Tr}\gamma_5 = 0, \quad \mathrm{Tr}\gamma_\mu\gamma_\nu = 4g_{\mu\nu}, \quad \mathrm{Tr}\gamma_5\gamma_\mu\gamma_\nu = 0,$$
$$\mathrm{Tr}\gamma_\mu\gamma_\nu\gamma_\alpha\gamma_\beta = 4(g_{\mu\nu}g_{\alpha\beta} - g_{\mu\alpha}g_{\nu\beta} + g_{\mu\beta}g_{\nu\alpha}), \qquad \mathrm{Tr}\gamma_5\gamma_\mu\gamma_\nu\gamma_\alpha\gamma_\beta = -4i\varepsilon_{\mu\nu\alpha\beta}.$$

The equations for u and v are chosen so that we get the conventional *Dirac equations*

$$(i\gamma_\mu\partial_\mu - m)\Psi(x) = 0, \qquad i\partial_\mu\overline{\Psi}(x)\gamma_\mu + m\overline{\Psi}(x) = 0.$$

These equations follow also from the Lagrangian

$$\mathcal{L} = \frac{i}{2}\left[\overline{\Psi}\gamma_\mu(\partial_\mu\Psi) - (\partial_\mu\overline{\Psi})\gamma_\mu\Psi\right] - m\overline{\Psi}\Psi \equiv i\overline{\Psi}\gamma_\mu\partial_\mu\Psi - m\overline{\Psi}\Psi.$$

Note that the right-hand side is a short notation for the explicit Lagrangian which is given in the middle.

In QFT, Lagrangians (Hamiltonians) should be Hermitian: $\mathcal{L}^\dagger = \mathcal{L}$. *QUESTION: What kind of problems one can have with a non-Hermitian Hamiltonian?*

Up to now we considered only *free* non-interacting fields. Studies of transitions between free states is the main task of QFT[3].

Let us postulate the transition *amplitude* (matrix element) $\mathcal{M}$ of a physical process:

$$\mathcal{M} \equiv \langle out|S|in\rangle, \qquad S \equiv T\exp\left(i\int \mathrm{d}x\mathcal{L}_I(\varphi(x))\right). \tag{21}$$

Here S is the so-called S-matrix which is the general evolution operator of quantum states. Letter T means the *time ordering* operator, it will be discussed a bit later. The initial and final states are

$$|in\rangle = a^+(\mathbf{p}_1)\ldots a^+(\mathbf{p}_s)|0\rangle, \qquad |out\rangle = a^+(\mathbf{p}'_1)\ldots a^+(\mathbf{p}'_r)|0\rangle. \tag{22}$$

The differential probability to evolve from $|in\rangle$ to $|out\rangle$ is

$$\mathrm{d}w = (2\pi)^4\delta(\sum p'_i)\frac{n_1\ldots n_s}{2E_1\ldots E_s}|\mathcal{M}|^2\prod_{j=1}^r\frac{\mathrm{d}\mathbf{p}'_j}{(2\pi)^3 2E'_j}.$$

Here n_i is the particle number density of ith particle beam.

Nontrivial transitions happen due to interactions of fields. QFT prefers dealing with *local* interactions $\Rightarrow \quad \mathcal{L}_I = \mathcal{L}_I(\varphi(x))$. By 'local' we mean that all interaction terms in the Lagrangian are constructed as products of fields (or their first derivatives) taken at the same space-time coordinate.

Here are some examples of interaction Lagrangians:

$$g\varphi^3(x), \qquad h\varphi^4(x), \qquad y\varphi(x)\overline{\Psi}(x)\Psi(x),$$
$$e\overline{\Psi}(x)\gamma_\mu\Psi(x)A_\mu(x), \qquad G\overline{\Psi}_1(x)\gamma_\mu\Psi_1(x)\cdot\overline{\Psi}_2(x)\gamma_\mu\Psi_2(x).$$

IMPORTANT: Always keep in mind the dimension *of your objects!* The reference unit is the dimension of energy (mass):

$$[E] = [m] = 1 \quad \Rightarrow \quad [p] = 1, \qquad [x] = -1. \tag{23}$$

---

[3]Collective, nonperturbative effects, bound states etc. are also of interest, but that goes beyond the scope of these lectures.

An action should be dimensionless

$$\left[\int \mathrm{d}x \mathcal{L}(x) \right] = 0 \;\Rightarrow\; [\mathcal{L}] = 4. \tag{24}$$

EXERCISE: Show that $[\varphi] = [A_\mu] = 1$ *and* $[\Psi] = 3/2$. *Find the dimensions of the coupling constants g, h, y, e, and G in the examples above.*

By definition the time ordering operator acts as follows:

$$T\, A_1(x_1) \dots A_n(x_n) = (-1)^l A_{i_1}(x_{i_1}) \dots A_{i_n}(x_{i_n}) \;\text{ with }\; x_{i_1}^0 > \dots > x_{i_n}^0, \tag{25}$$

where l is the number of fermion field permutations.

The perturbative expansion of the S matrix exponent (21) leads to terms like

$$\frac{i^n g^n}{n!} \langle 0| a^-(\mathbf{p}'_1) \dots a^-(\mathbf{p}'_r) \int \mathrm{d}x_1 \dots \mathrm{d}x_n T \varphi^3(x_1) \dots \varphi^3(x_n) a^+(\mathbf{p}_1) \dots a^+(\mathbf{p}_s) |0\rangle.$$

Remind that fields φ also contain creation and annihilation operators. By permutation of operators $a^-(\mathbf{p}) a^+(\mathbf{p}') = a^+(\mathbf{p}') a^-(\mathbf{p}) + \delta(\mathbf{p} - \mathbf{p}')$ we move a^- to the right and a^+ to the left. At the end we get either zero because $a^-|0\rangle = 0$ and $\rangle 0|a^+ = 0$, or some finite terms proportional to $\langle 0|0\rangle = 1$.

EXERCISE: Show that $[a^-(\mathbf{p}), \varphi(x)] = \frac{e^{ipx}}{(2\pi)^{3/2}\sqrt{2p_0}}$ *and* $[a_r^-(\mathbf{p}), \overline{\Psi}(x)]_+ = \frac{e^{ipx}\bar{u}_r(\mathbf{p})}{(2\pi)^{3/2}\sqrt{2p_0}}$.

By definition the *causal Green function* is given by

$$\langle 0|T\varphi(x)\varphi(y)|0\rangle \equiv -iD^c(x-y). \tag{26}$$

It is a building block for construction of amplitudes. One can show (see textbooks) that

$$(\partial^2 + m^2)D^c(x) = \delta(x), \tag{27}$$

so that D^c is the Green function of the Klein–Fock–Gordon operator,

$$D^c(x) = \frac{-1}{(2\pi)^4} \int \frac{\mathrm{d}p\, e^{-ipx}}{p^2 - m^2 + i0}, \tag{28}$$

where $+i0$ is an infinitesimally small imaginary quantity which shifts the poles of the Green function from the real axis in the complex plane. The sign of this quantity is chosen to fulfil the requirement of the time ordering operation in Eq. (26).

For other fields we have

$$\langle 0|T\, \Psi(x)\overline{\Psi}(y)|0\rangle = \frac{i}{(2\pi)^4} \int \frac{\mathrm{d}p\, e^{-ip(x-y)}(\hat{p}+m)}{p^2 - m^2 + i0},$$

$$\langle 0|T\, U_\mu(x)U_\nu^*(y)|0\rangle = \frac{-i}{(2\pi)^4} \int \frac{\mathrm{d}p\, e^{-ip(x-y)}(g_{\mu\nu} - p_\mu p_\nu/m^2)}{p^2 - m^2 + i0}, \tag{29}$$

$$\langle 0|T\, A_\mu(x)A_\nu(y)|0\rangle = \frac{-i}{(2\pi)^4} \int \frac{\mathrm{d}p\, e^{-ip(x-y)} g_{\mu\nu}}{p^2 + i0}.$$

The Wick theorem states that for any combinations of fields

$$T\, A_1 \dots A_n \equiv \sum (-1)^l \langle 0|TA_{i_1}A_{i_2}|0\rangle \dots \langle 0|TA_{i_{k-1}}A_{i_k}|0\rangle \; : A_{i_{k+1}} \dots A_{i_n} : \tag{30}$$

The sum is taken over all possible ways to pair the fields.

The *normal ordering* operation acts as

$$: a_1^- a_2^+ a_3^- a_4^- a_5^+ a_6^- a_7^+ : = (-1)^l a_2^+ a_5^+ a_7^+ a_1^- a_3^- a_4^- a_6^- \tag{31}$$

so that all annihilation operators go to the right and all creation operators go to the left. The number of fermion operator permutations l provides the factor $(-1)^l$.

Using the Wick theorem we construct the *Feynman rules* for simple $g\phi^3$ and $h\varphi^4$ interactions. But for the case of gauge interactions we need something more as we will see below.

It appears that symmetries play a crucial role in the QFT. There are two major types of symmetries in the SM: *global* and *local* ones. By a global symmetry we mean invariance of a Lagrangian and observables with respect to certain transformations of coordinates and/or fields if the transformations are the same in each space-time point. If the transformations do depend on coordinates, the corresponding symmetry is called local.

The **1st Noether (Nöther) theorem**:
If an action is invariant with respect to transformations of a global Lie group G_r with r parameters, then there are r linearly independent combinations of Lagrange derivatives which become complete divergences; and vice versa.

If the field satisfies the Euler–Lagrange equations, then $\mathrm{div}J = \nabla J = 0$, i.e., the *Noether currents* are conserved. Integration of those divergences over a 3-dimensional volume (with certain boundary conditions) leads to r *conserved charges*. Remind that conservation of the electric charge in QED is related to the global $U(1)$ symmetry of this model, and that Poincaré symmetries lead to conservation of energy, momentum, and angular momentum.

Much more involved and actually important for us is the **2nd Noether theorem**:
If the action is invariant with respect to the infinite-dimensional r-parametric group $G_{\infty,r}$ with derivatives up to the kth order, then there are r independent relations between Lagrange derivatives and derivatives of them up to the kth order; and vice versa.

The importance of the second theorem is justified by the fact that gauge groups (and also the general coordinate transformation in Einstein's gravitational theory) are infinite-dimensional groups. The 2nd Noether theorem provides r conditions on the fields which are additional to the standard Euler–Lagrange equations. These conditions should be used to exclude *double counting* of physically *equivalent* field configurations.

2.1 Gauge symmetries

Let us start the discussion of local gauge symmetries with Quantum Electrodynamics (QED). The free Lagrangians for electrons and photons

$$\mathcal{L}_0(\Psi) = i\overline{\Psi}\gamma_\mu\partial_\mu\Psi - m\overline{\Psi}\Psi, \quad \mathcal{L}_0(A) = -\frac{1}{4}F_{\mu\nu}F_{\mu\nu} \tag{32}$$

are invariant with respect to the *global $U(1)$* transformations

$$\Psi(x) \to \exp(ie\theta)\Psi(x), \quad \overline{\Psi}(x) \to \exp(-ie\theta)\overline{\Psi}(x), \quad A_\mu(x) \to A_\mu(x). \tag{33}$$

One can note that $F_{\mu\nu}$ is invariant also with respect to *local* transformations $A_\mu(x) \to A_\mu(x) + \partial_\mu\omega(x)$, where $\omega(x)$ is an arbitrary (differentiable) function. For fermions the corresponding transformations are

$$\Psi(x) \to \exp(ie\omega(x))\Psi(x), \quad \overline{\Psi}(x) \to \exp(-ie\omega(x))\overline{\Psi}(x), \tag{34}$$

i.e., where the global constant angle θ in Eq. (33) is substituted by a local function $\omega(x)$ which varies from one space-time point to another.

The question is how to make the fermion Lagrangian being also invariant with respect to the local transformations? The answer is to introduce the so-called *covariant derivative*:

$$\partial_\mu \to D_\mu, \qquad D_\mu\Psi \equiv (\partial_\mu - ieA_\mu)\Psi, \quad D_\mu\overline{\Psi} \equiv (\partial_\mu + ieA_\mu)\overline{\Psi}. \tag{35}$$

Then we get the QED Lagrangian

$$
\begin{aligned}
\mathcal{L}_{\text{QED}} &= -\frac{1}{4}F_{\mu\nu}F_{\mu\nu} + i\overline{\Psi}\gamma_\mu D_\mu\Psi - m\overline{\Psi}\Psi \\
&= -\frac{1}{4}F_{\mu\nu}F_{\mu\nu} + i\overline{\Psi}\gamma_\mu\partial_\mu\Psi - m\overline{\Psi}\Psi + e\overline{\Psi}\gamma_\mu\Psi A_\mu,
\end{aligned}
$$

where the last term describes interaction of electrons and positrons with photons. The most important point here is that the structure of the interaction term is completely fixed by the gauge symmetry. Nevertheless, there is one specific feature of the abelian $U(1)$ case, namely the values of electric charges (coupling constants) can be different for different fermions e.g., for up and down quarks.

EXERCISES: 1) Check the covariance: $D_\mu\Psi \to e^{ie\omega(x)}(D_\mu\Psi)$; 2) construct the Lagrangian of scalar QED (use Eqs. (9) and (14)).

Let's look now again at the free photon Lagrangian

$$
\mathcal{L}_0(A) = -\frac{1}{4}(\partial_\mu A_\nu - \partial_\nu A_\mu)^2 = -\frac{1}{2}A_\nu K_{\mu\nu}A_\nu,
$$
$$
K_{\mu\nu} = g_{\mu\nu}\partial^2 - \partial_\mu\partial_\nu \quad \Rightarrow K_{\mu\nu}(p) = p_\mu p_\nu - g_{\mu\nu}p^2.
$$

Operator $K_{\mu\nu}(p)$ has zero modes (since $p_\mu K_{\mu\nu} = 0$), so it is not invertable. Definition of the photon propagator within the *functional integral formalism* becomes impossible. The reason is the unresolved symmetry. The solution is to introduce a *gauge fixing term* into the Lagrangian:

$$
\mathcal{L}_0(A) = -\frac{1}{4}F_{\mu\nu}F_{\mu\nu} - \frac{1}{2\alpha}(\partial_\mu A_\mu)^2 \quad \Rightarrow
$$
$$
\langle 0|T\, A_\mu(x)A_\nu(y)|0\rangle = \frac{-i}{(2\pi)^4}\int dp\, e^{-ip(x-y)}\frac{g_{\mu\nu} + (\alpha-1)p_\mu p_\nu/p^2}{p^2 + i0}.
$$

It is very important that physical quantities do not depend on the value of α.

Let us briefly discuss the features of non-abelian Gauge symmetries which will be also used in the construction of the SM. Transformations for a *non-abelian* case read

$$
\Psi_i \to \exp ig\omega^a t^a_{ij}\Psi_j, \qquad [t^a, t^b] = if^{abc}t^c,
$$
$$
B_\mu^a \to B_\mu^a + \partial_\mu\omega^a + gf^{abc}B_\mu^b\omega^c, \quad F_{\mu\nu}^a \equiv \partial_\mu B_\nu^a - \partial_\nu B_\mu^a + gf^{abc}B_\mu^b B_\nu^c,
$$

where t^a are the group generators, f^{abc} are the structure constants (see details in the lectures on QCD).

We introduce the covariant derivative

$$
\partial_\mu\Psi \to D_\mu\Psi \equiv (\partial_\mu - igB_\mu^a t^a)\Psi
$$

and get

$$
\begin{aligned}
\mathcal{L}(\Psi, B) &= i\overline{\Psi}\gamma_\mu D_\mu\Psi + \mathcal{L}(B), \\
\mathcal{L}(B) &= -\frac{1}{4}F_{\mu\nu}^a F_{\mu\nu}^a - \frac{1}{2\alpha}(\partial_\mu B_\mu^a)^2 = -\frac{1}{4}\left(\partial_\mu B_\nu^a - \partial_\nu B_\mu^a\right)^2 - \frac{1}{2\alpha}(\partial_\mu B_\mu^a)^2 \\
&\quad - \frac{g}{2}f^{abc}\left(\partial_\mu B_\nu^a - \partial_\nu B_\mu^a\right)B_\mu^b B_\nu^c - \frac{g^2}{4}f^{abc}f^{ade}B_\mu^b B_\nu^c B_\mu^d B_\nu^e.
\end{aligned}
$$

Note that $\mathcal{L}(B)$ contains self-interactions and can not be treated as a 'free Lagrangian'. There is no any mass term for the gauge field in the Lagrangian, $m_B \equiv 0$, because such a term would be not gauge-invariant. It is worth to note that the non-abelian charge g is *universal*, i.e., it is the same for all fields which are transformed by the given group.

Exclusion of double-counting due to the physical equivalence of the field configurations related to each other by non-abelian gauge transformations is nontrivial. Functional integration over those identical configurations (or application of the BRST method) leads to the appearance of the so-called *Faddeev–Popov ghosts*:

$$\mathcal{L}(\Psi, B) \to \mathcal{L}(\Psi, B) + \mathcal{L}_{gh},$$
$$\mathcal{L}_{gh} = -\partial_\mu \bar{c}^a \partial_\mu c^a + g f^{acb} \bar{c}^a B_\mu^c \partial_\mu c^a = -\partial_\mu \bar{c}^a \partial_\mu c^a - g f^{acb} \partial_\mu \bar{c}^a B_\mu^c c^a, \tag{36}$$

where c and $\bar{c}$ are ghost fields, they are fermion-like states with a boson-like kinetic term. Keep in mind that Faddeev–Popov ghosts are *fictitious* particles. In the Feynman rules they (should) appear only as virtual states in propagators but not in the initial and final asymptotic states. Formally, ghosts can be found also in QED, but they are non-interacting since $f^{abc} = 0$ there, and can be totally omitted.

2.2 Regularization and renormalization

Higher-order terms in the perturbative series contain loop integrals which can be ultraviolet (UV) divergent, e.g.,

$$I_2 \equiv \int \frac{\mathrm{d}^4 p}{(p^2 + i0)((k - p)^2 + i0)} \sim \int \frac{|p|^3 \, \mathrm{d}|p|}{|p|^4} \sim \ln \infty. \tag{37}$$

Introduction of an upper cut-off M on the integration variable leads to a finite, i.e., *regularized* value of the integral:

$$I_2^{\text{cut-off}} = i\pi^2 \left(\ln \frac{M^2}{k^2} + 1 \right) + \mathcal{O}\left(\frac{k^2}{M^2} \right) = i\pi^2 \left(\ln \frac{M^2}{\mu^2} - \ln \frac{k^2}{\mu^2} + 1 \right) + \mathcal{O}\left(\frac{k^2}{M^2} \right). \tag{38}$$

Another possibility is the *dimensional regularization* where $dim = 4 \to dim = 4 - 2\varepsilon$

$$I_2^{\text{dim.reg.}} = \mu^{2\varepsilon} \int \frac{\mathrm{d}^{4-2\varepsilon} p}{(p^2 + i0)((k - p)^2 + i0)} = i\pi^2 \left(\frac{1}{\varepsilon} - \ln \frac{k^2}{\mu^2} + 2 \right) + \mathcal{O}(\varepsilon). \tag{39}$$

Here the divergence is parameterized by the ε^{-1} term. The origin of UV divergences is the *locality* of interactions in QFT.

Let's consider a three-point (vertex) function in the $g\phi^3$ model, it looks like

$$G = \int \mathrm{d}x \, \mathrm{d}y \, \mathrm{d}z \; \varphi(x)\varphi(y)\varphi(z) F(x, y, z),$$
$$F^{\text{dim.reg.}} = \frac{A}{\varepsilon} \delta(y - x)\delta(z - x) + \dots$$

IMPORTANT: It means that UV-divergent terms are *local* (here because of the delta-functions).

*A QFT model is called **renormalizable** if all UV-divergent terms are of the type of the ones existing in the original (semi)classical Lagrangian. Otherwise the model is **non-renormalizable**.*

EXAMPLES:
a) renormalizable models: QED, QCD, the SM [proved by 't Hooft & Veltman], $h\varphi^4$, $g\varphi^3$;
b) non-renormalizable models: the Fermi model with $\mathcal{L} \sim G(\overline{\Psi}\gamma_\mu \Psi)^2$ and General Relativity.

It can be shown that models with dimensionful ($[G] < 0$) coupling constants are non-renormalizable.

In renormalizable models all UV divergences can be *subtracted* from amplitudes and shifted into *counter terms* in $\mathcal{L}$. In this way each term in $\mathcal{L}$ gets a *renormalization constant*. For the model describing a scalar field with the φ^4 self-interaction we get

$$\mathcal{L} = \frac{Z_2}{2}(\partial\varphi)^2 - \frac{Z_m m^2}{2}\varphi^2 + Z_4 h\varphi^4 = \frac{1}{2}(\partial\varphi_B)^2 - \frac{m_B^2}{2}\varphi^2 + h_B \varphi^4,$$
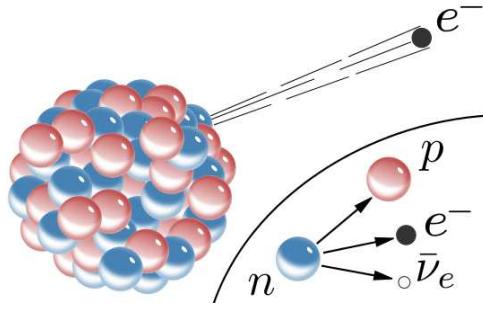
Fig. 2: Beta decay.

where $\varphi_B = \sqrt{Z_2}\varphi$, $m_B^2 = m^2 Z_M Z_2^{-1}$, $h_B = h Z_4 Z_2^{-2}$ are so-called *bare* field, mass, and charge,

$$Z_i(h, \varepsilon) = 1 + \frac{Ah}{\varepsilon} + \frac{Bh^2}{\varepsilon^2} + \frac{Ch^2}{\varepsilon} + \mathcal{O}(h^3).$$

Renormalization constants are chosen in such a way that divergences in amplitudes are *cancelled out* with divergences in Z_i. By construction, that happens order by order.

R. Feynman said once: *"I think that the renormalization theory is simply a way to sweep the difficulties of the divergences of electrodynamics under the rug."* Physicists are still not fully satisfied by the renormalization procedure, but the method has been verified in many models. Moreover, renormalizable models including the SM appear to be the most successful ones in the description of phenomenology. For these reasons we say now that renormalization is the general feature of physical theories.

Physical results should not depend on the auxiliary scale μ. This condition leads to the appearance of the renormalization group (RG). Schematically in calculation of an observable, we proceed in the following way

$$F(k, g, m) \xrightarrow{\infty} F_{\text{reg}}(k, M, g, m) \xrightarrow{M \to \infty} F_{\text{ren}}(k, \mu, g, m) \xrightarrow{RG} F_{\text{phys}}(k, \Lambda, m),$$

where Λ is a dimensionful scale. Charge (and mass) become *running*, i.e., energy-dependent:

$$g \to g\left(g, \frac{\mu'}{\mu}\right), \qquad \beta(g) \equiv \left.\frac{\mathrm{d}g}{\mathrm{d}\ln\mu}\right|_{g_B = Const}. \tag{40}$$

Note that the renormalization scale μ unavoidably appears in any scheme. Scheme and scale dependencies are reduced after including higher and higher orders of the perturbation theory.

At this point we stop the brief introduction to Quantum field theory, comprehensive details can be found in textbooks, e.g., Refs. [4, 6, 7].

3 Construction of the Standard Model

3.1 The Fermi model and Cabibbo–Kobayashi–Maskawa mixing matrix

To describe the β-decay $n \to p + e^- + \nu_e$ in 1933, see Fig. 2, Enrico Fermi suggested a simple model:

$$\mathcal{L}_{int} = G \underbrace{\overline{\Psi}_n \gamma_\rho \Psi_p}_{J_\rho^{(N)}} \cdot \underbrace{\overline{\Psi}_\nu \gamma_\rho \Psi_e}_{J_\rho^{(l)\dagger}} + h.c.$$

with interactions in the form of a product of two vector currents. This model was inspired by QED where similar vector currents appear.

In 1957 R. Marshak & G. Sudarshan; and R. Feynman & M. Gell-Mann modified the model:

$$\mathcal{L}_{\text{Fermi}} = \frac{G_{\text{Fermi}}}{\sqrt{2}} J_\mu J_\mu^\dagger,$$

$$J_\mu = \overline{\Psi}_e \gamma_\rho \frac{1 - \gamma_5}{2} \Psi_{\nu_e} + \overline{\Psi}_\mu \gamma_\rho \frac{1 - \gamma_5}{2} \Psi_{\nu_\mu} + (V - A)_{\text{nucleons}} + h.c. \tag{41}$$

Explicit *V-A* (Vector minus Axial–vector) form of weak interactions means the 100% violation of parity. In fact, it appears that only left fermions participate in weak interactions, while right fermions don't. Please remind that massive left fermions are not states with a definite spin. The modification of the model was required to describe differential distributions of *beta*-decays. Note that the CP symmetry in Lagrangian (41) is still preserved.

The modern form of the Fermi Lagrangian includes 3 fermion generations:

$$\mathcal{L}_{\text{Fermi}} = \frac{G_{\text{Fermi}}}{\sqrt{2}} (\overline{e}_L \ \overline{\mu}_L \ \overline{\tau}_L) \gamma_\rho \begin{pmatrix} \nu_{e,L} \\ \nu_{\mu,L} \\ \nu_{\tau,L} \end{pmatrix} \cdot (\overline{u}'_L \ \overline{c}'_L \ \overline{t}'_L) V_u^\dagger \gamma_\rho V_d \begin{pmatrix} d'_L \\ s'_L \\ b'_L \end{pmatrix} + \ldots$$

Quarks $\{q'\}$ are the *eigenstates* of the strong interactions, and $\{q\}$ are the eigenstates of the weak ones.

Matrixes V_d and V_u describe quark mixing (see details in lectures on Flavour Physics):

$$\begin{pmatrix} d \\ s \\ b \end{pmatrix} = V_d \times \begin{pmatrix} d' \\ s' \\ b' \end{pmatrix}, \qquad V_u^\dagger V_d \equiv V_{\text{CKM}} = \begin{pmatrix} V_{ud} & V_{us} & V_{ub} \\ V_{cd} & V_{cs} & V_{cb} \\ V_{td} & V_{ts} & V_{tb} \end{pmatrix}.$$

By construction, in this model (and further in the SM) the mixing matrixes are unitary: $V_i^\dagger V_i = \mathbf{1}$. In a sense, this property just keeps the number of quarks during the transformation to be conserved. V_{CKM} contains 4 independent parameters: 3 angles and 1 phase.

QUESTION: What is mixed by V_{CKM}? E.g., what is mixed by the V_{ud} element of V_{CKM}?

The Fermi model describes β-decays and the muon decay $\mu \to e + \bar{\nu}_e + \nu_\mu$ with a very high precision. Nevertheless, there are two critical problems:
1. The model is non-renormalizable, remind that the dimension of the Fermi coupling constant $[G_{\text{Fermi}}] = -2$.
2. Unitarity in this model is violated: consider, e.g., within the Fermi model the total cross section of electron-neutrino scattering

$$\sigma_{\text{total}}(e\nu_e \to e\nu_e) \sim \frac{G_{\text{Fermi}}^2}{\pi} s, \qquad s = (p_e + p_{\nu_e})^2. \tag{42}$$

This cross section obviously growth with energy. Meanwhile the unitarity condition for l^{th} partial wave in the scattering theory requires that $\sigma_l < \frac{4\pi(2l+1)}{s}$. For $l = 1$ we reach the *unitarity limit* at $s_0 = 2\pi\sqrt{3}/G_{\text{Fermi}} \approx 0.9 \cdot 10^6$ GeV^2. So at energies above $\sim 10^3$ GeV the Fermi model is completely senseless and somewhere below this scale another model should enter the game.

3.2 (Electro)Weak interactions in SM

The modern point of view is: *a renormalizable QFT model which preserves unitarity is a Yang–Mills (non-abelian) gauge model*. So we have to try to construct an interaction Lagrangian using the principle of gauge symmetry.

Let's try to do that for description of weak interactions. At the first step we introduce a massive vector W boson

$$\mathcal{L}_{\text{int}} = -g_w (J_\alpha W_\alpha + J_\alpha^\dagger W_\alpha^\dagger). \tag{43}$$
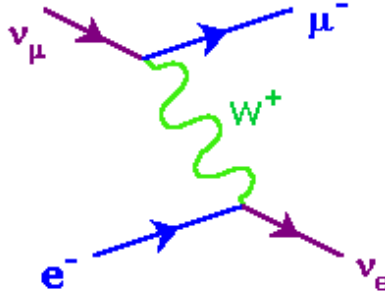
Fig. 3: Feynman diagram for electron-neutrino scattering with W boson exchange.

Then the scattering amplitude, see Fig. 3, takes the form

$$T = i(2\pi)^4 g_w^2 J_\alpha \, \frac{g_{\alpha\beta} - k_\alpha k_\beta / M_W^2}{k^2 - M_W^2} \, J_\beta^\dagger,$$ (44)

where k is the W boson momentum. If $|k| \ll M_W$ we reproduce the Fermi model with

$$\frac{G_{\text{Fermi}}}{\sqrt{2}} = \frac{g_w^2}{M_W^2}.$$

However such a way to introduce interactions again leads to a non-renormalizable model. The problem appears due to the specific momentum dependence in the propagator of a massive vector particle, see Eq. (29). Moreover, the mass term of the gauge boson is not gauge invariant.

The *minimal* way to introduce electromagnetic and weak interactions as gauge ones is to take the group $SU(2) \otimes U(1)$. The abelian group $U(1)$ is the same as the one that gives conservation of the electric charge in QED. Instead of the electric charge Q we introduce now the *hypercharge Y*. The $U(1)$ gauge symmetry provides interactions of fermions with a massless vector (photon-like) field B_μ. The non-abelian group $SU(2)$ is the same as the one used for description of spinors in Quantum mechanics. Instead of spin we use here the notion of *weak isospin I*. There are three massless vector Yang–Mills bosons in the adjoint representation of this group: W_μ^a, $a = 1, 2, 3$. Two of them can be electrically charged and the third one should be neutral. Introduction of the third (electro)weak boson is unavoidable, even so that we had not have experimental evidences of weak neutral currents at the times of the SM invention.

QUESTION: Why weak interactions in the charged current (like muon and beta decays) were discovered experimentally much earlier than the neutral current ones?

One can show that the model built above for gauge $SU(2) \otimes U(1)$ interactions of fermions and vector bosons is renormalizable and unitary. But this model doesn't describe the reality since all gauge bosons should be massless because of the gauge symmetry condition. To resolve this problem we need a mechanism that will provide masses for some vector bosons without an explicit breaking of the gauge symmetry.

3.3 The Brout–Englert–Higgs mechanism

Let's consider the simple abelian $U(1)$ symmetry for interaction of a charged scalar field φ with a vector field A_μ:

$$\mathcal{L} = \partial_\mu \varphi^* \partial_\mu \varphi - V(\varphi) - \frac{1}{4} F_{\mu\nu}^2 + ie(\varphi^* \partial_\mu \varphi - \partial_\mu \varphi^* \varphi) A_\mu + e^2 A_\mu A_\mu \varphi^* \varphi.$$
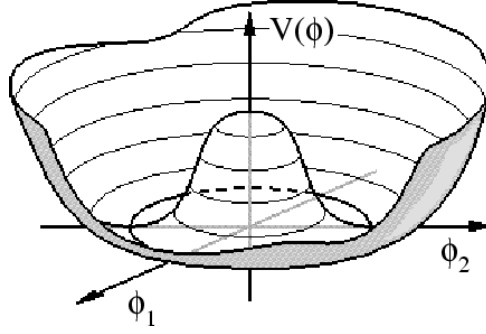
Fig. 4: The Higgs field potential. Picture courtesy: E.P.S. Shellard, DAMTP, Cambridge. From http://www.geocities.com/CapeCanaveral/ 2123/breaking.htm.

If $V(\varphi) \equiv V(\varphi^* \cdot \varphi)$, $\mathcal{L}$ is invariant with respect to local $U(1)$ gauge transformations

$$\varphi \to e^{ie\omega(x)}\varphi, \quad \varphi^* \to e^{-ie\omega(x)}\varphi^*, \quad A_\mu \to A_\mu + \partial_\mu\omega(x). \tag{45}$$

In polar coordinates $\varphi \equiv \sigma(x)e^{i\theta(x)}$ and $\varphi^* \equiv \sigma(x)e^{-i\theta(x)}$ and the Lagrangian takes the form

$$\mathcal{L} = \partial_\mu\sigma\partial_\mu\sigma + e^2\sigma^2 \underbrace{\left(A_\mu - \frac{1}{e}\partial_\mu\theta\right)}_{\equiv B_\mu} \underbrace{\left(A_\mu - \frac{1}{e}\partial_\mu\theta\right)}_{\equiv B_\mu} - V(\varphi^*\varphi) - \frac{1}{4}F_{\mu\nu}^2. \tag{46}$$

Note that after the change of variables $A_\mu + \frac{1}{e}\partial_\mu\theta \to B_\mu$, we have $F_{\mu\nu}(A) = F_{\mu\nu}(B)$ since $\theta(x)$ is a double differentiable function.

We see that $\theta(x)$ is completely swallowed by the field $B_\mu(x)$. So we made just a change of variables. But which set of variables is the true physical one? This question is related to the choice of variables in which the secondary quantization should be performed. And the answer can be given by measurements. In fact, according to Quantum mechanics only quantum eigenstates can be observed, so we have a reference point. Another argument can be given by a condition on the system stability.

R. Brout & F. Englert [11], and P. Higgs [12], see also a brief review in the Scientific Background on the Nobel Prize in Physics 2013 [13], suggested to take the scalar potential in the form

$$V(\varphi^*\varphi) = \lambda(\varphi^*\varphi)^2 + m^2\varphi^*\varphi. \tag{47}$$

For $\lambda > 0$ and $m^2 < 0$ we get the shape of a *Mexican hat*, see Fig. 4. We have chosen a potential for which $V(\varphi^*\varphi) = V(\sigma^2)$, while $\theta(x)$ corresponds to the rotational symmetry of the potential.

By looking at the derivative of the potential $\frac{dV(\sigma)}{d\sigma} = 0$, we find two critical points: $\sigma = 0$ is the local maximum, and $\sigma_0 = \sqrt{-\frac{m^2}{2\lambda}}$ is the global minimum. The stability condition suggest to shift from zero to the global minimum: $\sigma(x) \to h(x) + \sigma_0$. So we get

$$\mathcal{L} = \partial_\mu h \partial_\mu h + e^2 h^2 B_\mu B_\mu + 2e^2\sigma_0 h B_\mu B_\mu + e^2\sigma_0^2 B_\mu B_\mu - V(h) - \frac{1}{4}F_{\mu\nu}^2. \tag{48}$$

We see that field B_μ got the mass

$$m_B^2 = 2e^2\sigma_0^2 = -\frac{e^2 m^2}{\lambda} > 0. \tag{49}$$

So, we generated a mass term for the vector field without putting it into the Lagrangian by hand. That is the core of the Brout–Englert–Higgs mechanism.

The quantity $\sigma_0 \equiv v$ is the *vacuum expectation value* (vev) of $\sigma(x)$,

$$v \equiv \langle 0|\sigma|0\rangle, \qquad v = \frac{1}{V_0}\int_{V_0} \mathrm{d}^3x\ \sigma(x). \tag{50}$$

Look now at the potential (keep in mind $m^2 = -2\lambda v^2$)

$$\begin{aligned} V(h) &= \lambda(h+v)^4 + m^2(h+v)^2 \\ &= \lambda h^4 + 4\lambda v h^3 + h^2 \underbrace{\left(6\lambda v^2 + m^2\right)}_{2m_h^2 = 4\lambda v^2} + h\underbrace{\left(4\lambda v^3 + 2m^2 v\right)}_{=0} + \lambda v^4 + m^2 v^2. \end{aligned}$$

So, the scalar field h has a normal (not tachyon-like) mass term, $m_h^2 > 0$. One can see that the initial tachyons φ are not physically observable, since they are not pure states in the basis of the secondary quantized system of fields.

It is worth to note that even so that the field content of the Lagrangian is changed, but the number of degrees of freedom is conserved. In fact initially we had two components of the scalar field and two components of the massless vector field, and after the change of variables we have a single scalar field plus a massive vector field with 3 independent components: $2 + 2 = 1 + 3$.

The field $\theta(x)$ is a *Nambu–Goldstone boson* (a goldstone). It is massless, $m_\theta = 0$, and corresponds to effortless rotations around the vertical symmetry axis of the potential. In general, the Goldstone theorem claims that in a model with spontaneous breaking of a continuous global symmetry G_n (remind the first Noether theorem) there exist as many massless modes, as there are group generators which do not preserve the vacuum invariance.

The constant term $\lambda v^4 + m^2 v^2$ obviously doesn't affect equations of motion in QFT, but it contributes to the Universe energy density (too much, actually). That makes a problem for Cosmology. Formally, one can make a shift of the initial Lagrangian just by this term and avoid the problem at the present time of the Universe evolution.

One has to keep in mind that the term "spontaneous breaking of the gauge symmetry" is just a common notation, while in fact a (local) gauge symmetry can not be broken spontaneously as proved by S. Elitzur [14]. A detailed discussion can be found in [15], see also [16].

Now let us return to the case of the Standard Model. To generate masses for 3 vector bosons we need at least 3 goldstones. The minimal possibility is to introduce one complex scalar doublet field:

$$\Phi \equiv \begin{pmatrix} \Phi_1 \\ \Phi_2 \end{pmatrix}, \qquad \Phi^\dagger = (\Phi_1^*\ \Phi_2^*). \tag{51}$$

Then the following Lagrangian is $SU(2) \otimes U(1)$ invariant

$$\mathcal{L} = (D_\mu\Phi)^\dagger(D_\mu\Phi) - m^2\Phi^\dagger\Phi - \lambda(\Phi^\dagger\Phi)^2 - \frac{1}{4}W_{\mu\nu}^a W_{\mu\nu}^a - \frac{1}{4}B_{\mu\nu}B_{\mu\nu},$$

$$B_{\mu\nu} \equiv \partial_\mu B_\nu - \partial_\nu B_\mu, \qquad W_{\mu\nu}^a \equiv \partial_\mu W_\nu^a - \partial_\nu W_\mu^a + g\varepsilon^{abc}W_\mu^b W_\nu^c,$$

$$D_\mu\Phi \equiv \partial_\mu\Phi + igW_\mu^a\frac{\tau^a}{2}\Phi + \frac{i}{2}g'B_\mu\Phi. \tag{52}$$

Again for $m^2 < 0$ there is a non-trivial minimum of the Higgs potential and a non-zero vev of a component: $\langle 0|\Phi_2|0\rangle = \eta/\sqrt{2}$. In accord with the Goldstone theorem, three massless bosons appear. The global $SU(2) \times SU(2)$ symmetry of the Higgs sector is reduced to the *custodial $SU(2)$* symmetry.

3.4 Electroweak bosons

The gauge bosons of the $SU(2) \otimes U(1)$ group can be represented as

$$W_\mu^+ = \frac{W_\mu^1 + iW_\mu^2}{\sqrt{2}}, \qquad W_\mu^- = \frac{W_\mu^1 - iW_\mu^2}{\sqrt{2}}, \qquad W_\mu^0 = W_\mu^3, \qquad B_\mu. \tag{53}$$

W_μ^0 and B_μ are both neutral and have the same quantum numbers, so they can mix. In a quantum world, "can" means "do":

$$W_\mu^0 = \cos\theta_w \, Z_\mu + \sin\theta_w \, A_\mu,$$
$$B_\mu = -\sin\theta_w \, Z_\mu + \cos\theta_w \, A_\mu, \tag{54}$$

where θ_w is the *weak mixing angle*, introduced first by S. Glashow, θ_w is known also the Weinberg angle. Remind that we have to choose variables which correspond to observables. Vector bosons Z_μ and A_μ are linear combinations of the primary fields W_μ^0 and B_μ.

It is interesting to note that Sheldon Glashow, Abdus Salam, and Steven Weinberg have got the Nobel Prize in 1979, *before* the discovery of Z and W bosons in 1983, and even much longer before the discovery of the Higgs boson. So the Standard Model had been distinguished before experimental confirmation of its key components.

Look now at the scalar fields:

$$\Phi \equiv \frac{1}{\sqrt{2}} \left(\begin{array}{c} \Psi_2(x) + i\Psi_1(x) \\ \eta + \sigma(x) + i\xi(x) \end{array} \right), \qquad \Phi^\dagger = \ldots$$

Fields $\Psi_{1,2}$ and ξ become massless Goldstone bosons. We *hide* them into the vector fields:

$$W_\mu^i \to W_\mu^i + \frac{2}{g\eta}\partial_\mu\Psi_i \quad \Rightarrow \quad M_W = \frac{g\eta}{2},$$
$$Z_\mu = \frac{g}{\sqrt{g^2+g'^2}}W_\mu^0 - \frac{g'}{\sqrt{g^2+g'^2}}B_\mu - \frac{2}{\eta\sqrt{g^2+g'^2}}\partial_\mu\xi \quad \Rightarrow \quad M_Z = \frac{\eta\sqrt{g^2+g'^2}}{2}. \tag{55}$$

The photon field appears massless by construction. Looking at the mixing we get

$$\cos\theta_w = \frac{g}{\sqrt{g^2+g'^2}} = \frac{M_W}{M_Z}.$$

The non-abelian tensor

$$W_{\mu\nu}^a \equiv \partial_\mu W_\nu^a - \partial_\nu W_\mu^a + g\varepsilon^{abc}W_\mu^b W_\nu^c$$

leads to triple and quartic self-interactions of the *primary* W_μ^a bosons, since

$$\mathcal{L} = -\frac{1}{4}W_{\mu\nu}^a W_{\mu\nu}^a + \ldots \tag{56}$$

Fields B_μ and W_μ^a were not interacting between each other. But after the spontaneous breaking of the global symmetry in the Higgs sector, and the consequent change of the basis $\{W_\mu^0, B_\mu\} \to \{Z_\mu, A_\mu\}$, we get interactions of charged $W_\mu^\pm$ bosons with photons. And the charge of the physical W bosons is well known from the condition of charge conservation applied to *beta*-decays. That allows to fix the relation between the constants:

$$e = \frac{gg'}{\sqrt{g^2+g'^2}} = g\sin\theta_w. \tag{57}$$

We see that the very construction of the SM requires phenomenological input. So on the way of the SM building, not everything comes out automatically from symmetry principles etc.

3.5 EW interactions of fermions

We have chosen the $SU(2) \otimes U(1)$ symmetry group. To account for parity violation in weak decays, we assume different behavior of left and right fermions under $SU(2)_L$ transformations:

$$\text{left doublets} \quad \begin{pmatrix} \nu_e \\ e \end{pmatrix}_L, \quad \begin{pmatrix} u \\ d \end{pmatrix}_L \quad + 2 \text{ other generations,}$$

$$\text{right singlets} \quad e_R, \ u_R, \ d_R, \ (\nu_{e,R}) \quad + 2 \text{ other generations.}$$

To preserve the gauge invariance, the fermion Lagrangian is constructed with the help of covariant derivatives:

$$\mathcal{L}(\Psi) = \sum_{\Psi_i} \left[\frac{i}{2} \left(\overline{\Psi}_L \gamma_\alpha D_\alpha \Psi_L - D_\alpha \overline{\Psi}_L \gamma_\alpha \Psi_L \right) + \frac{i}{2} \left(\overline{\Psi}_R \gamma_\alpha D_\alpha \Psi_R - D_\alpha \overline{\Psi}_R \gamma_\alpha \Psi_R \right) \right],$$

$$D_\alpha \Psi_L \equiv \partial_\alpha \Psi_L + \frac{i g \tau^b}{2} W_\alpha^b \Psi_L - i g_1 B_\alpha \Psi_L, \qquad D_\alpha \Psi_R \equiv \partial_\alpha \Psi_L - i g_2 B_\alpha \Psi_L.$$

All interactions of the SM fermions with electroweak vector bosons are here. But coupling constants $g_{1,2}$ still have to be fixed and related to observables.

Fermions have weak isospins and hypercharges (I, Y):

$$\Psi_L : \quad \left(\frac{1}{2}, \ -\frac{2g_1}{g'} \right), \qquad \Psi_R : \quad \left(0, \ -\frac{2g_2}{g'} \right). \tag{58}$$

Looking at interactions of left and right electrons with A_μ in $\mathcal{L}(\Psi)$ we fix their hypercharges:

$$e_L : \quad \left(-\frac{1}{2}, \ -1 \right), \qquad e_R : \quad \left(0, \ -2 \right). \tag{59}$$

The *Gell-Mann–Nishijima formula* works for all fermions:

$$Q = I_3 + \frac{Y}{2}, \tag{60}$$

where Q is the electric charge of the given fermion, I_3 is its weak isospin projection, and Y is its hypercharge.

Interactions of leptons with $W^\pm$ and Z bosons come out in the form

$$\mathcal{L}_I = -\frac{g}{\sqrt{2}} \bar{e}_L \gamma_\mu \nu_{e,L} W_\mu^- + h.c. - \frac{g Z_\mu}{2 \cos \theta_w} \left[\bar{\nu}_{e,L} \gamma_\mu \nu_{e,L} \right.$$

$$\left. + \bar{e} \gamma_\mu \left(-(1 - 2 \sin^2 \theta_w) \frac{1 - \gamma_5}{2} + 2 \sin^2 \theta_w \frac{1 + \gamma_5}{2} \right) e \right]$$

$$\Rightarrow g_w = \frac{g}{2\sqrt{2}}, \quad M_W^2 = \frac{g^2 \sqrt{2}}{8 G_{\text{Fermi}}} = \frac{e^2 \sqrt{2}}{8 G_{\text{Fermi}} \sin^2 \theta_w} = \frac{\pi \alpha}{\sqrt{2} G_{\text{Fermi}} \sin^2 \theta_w}.$$

That gives $M_W = \frac{38.5}{\sin \theta_w}$ GeV, remind $M_Z = \frac{M_W}{\cos \theta_w}$.

We can see that the Higgs boson vev is directly related to the Fermi coupling constant:

$$v = (\sqrt{2} G_{\text{Fermi}})^{-1/2} \approx 246.22 \text{ GeV}. \tag{61}$$

So this quantity had been known with a high precision long before the discovery of the Higgs boson and the experimental measurement of its mass.

QUESTION: Why neutral weak currents in the SM do not change flavour (at the tree level)?
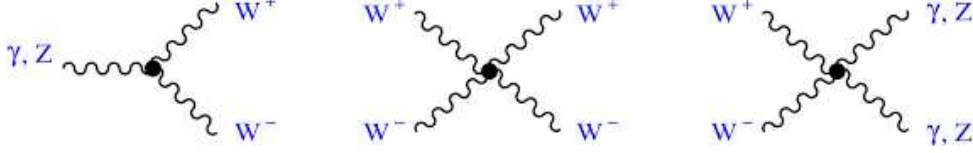
Fig. 5: Vertexes of EW boson self-interactions.

3.6 Self-interactions of EW bosons and Faddeev–Popov ghosts

Because of the non-abelian $SU(2)_L$ group structure and mixing of the neutral vector bosons, we have a rather reach structure of EW boson self-interactions, see Fig. 5. The corresponding contributions to the SM Lagrangian look as follows:

$$
\mathcal{L}_3 \sim ie\frac{\cos\theta_w}{\sin\theta_w}\bigg[(\partial_\mu W_\nu^- - \partial_\nu W_\mu^-)W_\mu^+ Z_\nu - (\partial_\mu W_\nu^+ - \partial_\nu W_\mu^+)W_\mu^- Z_\nu
$$

$$
+W_\mu^- W_\nu^+(\partial_\mu Z_\nu - \partial_\nu Z_\mu)\bigg]
$$

$$
\mathcal{L}_4 \sim -\frac{e^2}{2\sin^2\theta_w}\bigg[(W_\mu^+ W_\mu^-)^2 - W_\mu^+ W_\mu^+ W_\nu^- W_\nu^-\bigg],
$$

$$
-\frac{e^2\cos^2\theta_w}{\sin^2\theta_w}\bigg[W_\mu^+ W_\mu^- Z_\nu Z_\nu - W_\mu^+ Z_\mu W_\mu^- Z_\nu\bigg]
$$

$$
-\frac{e^2\cos^2\theta_w}{\sin^2\theta_w}\bigg[2W_\mu^+ W_\mu^- Z_\nu A_\nu - W_\mu^+ Z_\mu W_\mu^- A_\nu - W_\mu^+ A_\mu W_\mu^- Z_\nu\bigg]
$$

$$
-e^2\bigg[W_\mu^+ W_\mu^- A_\nu A_\nu - W_\mu^+ A_\mu W_\mu^- A_\nu\bigg].
$$

As we discussed earlier, an accurate treatment of non-abelian gauge symmetries leads to introduction of Faddeev–Popov ghosts. For the $SU(2)$ case we obtain 3 ghosts: $c_a(x)$, $a = 1, 2, 3$,

$$
c_1 = \frac{X^+ + X^-}{\sqrt{2}}, \quad c_2 = \frac{X^+ - X^-}{\sqrt{2}}, \quad c_3 = Y_Z\cos\theta_w - Y_A\sin\theta_w,
$$

$$
\mathcal{L}_{gh} = \underbrace{\partial_\mu\bar{c}_i(\partial_\mu c_i - g\varepsilon_{ijk}c_j W_\mu^k)}_{\text{kinetic + int. with } W^a} + \underbrace{\text{int. with }\Phi}_{M_{gh}, \text{ int. with } H}.
$$

Propagators of the ghost fields read

$$
D_{Y_\gamma}(k) = \frac{i}{k^2 + i0}, \qquad D_{Y_Z}(k) = \frac{i}{k^2 - \xi_Z M_Z^2 + i0}, \qquad D_X(k) = \frac{i}{k^2 - \xi_W M_W^2 + i0},
$$

where ξ_i are the gauge parameters. Note that masses of the ghosts Y_γ, Y_Z, and $X^\pm$ coincide with the ones of photon, Z, and $W^\pm$, respectively. That is important for *gauge invariance* of total amplitudes. The ghosts appear only in propagators, but not in the final or initial asymptotic states.

3.7 Generation of fermion masses

We observe massive fermions, but the $SU(2)_L$ gauge symmetry forbids fermion mass terms, since

$$
m\overline{\Psi}\Psi = m\left(\overline{\Psi}\frac{1+\gamma_5}{2} + \overline{\Psi}\frac{1-\gamma_5}{2}\right)\left(\frac{1+\gamma_5}{2}\Psi + \frac{1-\gamma_5}{2}\Psi\right) = m(\overline{\Psi}_L\Psi_R + \overline{\Psi}_R\Psi_L) \tag{62}
$$

while Ψ_L and Ψ_R are transformed in different ways under $SU(2)_L$. The SM solution is to introduce Yukawa interactions of fermions with the primary Higgs boson doublet field:

$$
\mathcal{L}_Y = -y_d(\bar{u}_L\bar{d}_L)\begin{pmatrix}\phi^+\\\phi^0\end{pmatrix}d_R - y_u(\bar{u}_L\bar{d}_L)\begin{pmatrix}\phi^{0*}\\-\phi^-\end{pmatrix}u_R
$$

$$- \quad y_l(\bar{\nu}_L\bar{l}_L) \begin{pmatrix} \phi^+ \\ \phi^0 \end{pmatrix} l_R - y_\nu(\bar{\nu}_L\bar{l}_L) \begin{pmatrix} \phi^{0*} \\ -\phi^- \end{pmatrix} \nu_R + h.c.$$

The form of this Lagrangian is fixed by the condition of the $SU(2)_L$ gauge invariance. It is worth to note that neutrino masses can be generated exactly in the same way as the up quark ones. Of course, that requires introduction of additional Yukawa constants y_ν. The Pontecorvo–Maki–Nakagawa–Sakata (PMNS) mixing matrix for (Dirac) neutrinos can be embedded in the SM.

QUESTION: Why do we need "h.c." in $\mathcal{L}_Y$?

Spontaneous breaking of the global symmetry in the Higgs sector provides mass terms for fermions and Yukawa interactions of fermions with the Higgs boson:

$$\mathcal{L}_Y = -\frac{v+H}{\sqrt{2}} \left[y_d\bar{d}d + y_u\bar{u}u + y_l\bar{l}l + y_\nu\bar{\nu}\nu \right] \quad \Rightarrow \quad m_f = \frac{y_f}{\sqrt{2}}v.$$

By construction, the coupling of the Higgs boson to a fermion is proportional to its mass m_f. It is interesting to note that the top quark Yukawa coupling is very close to 1. And there is a very strong hierarchy of fermion masses:

$$y_t \approx 0.99 \quad \gg \quad y_e \approx 3 \cdot 10^{-6} \quad \gg \quad y_\nu \approx?$$

The question mark in the last case is given not only because we do not know neutrino masses, but also since we are not sure the they are generated by the same mechanism.

Quarks can mix and Yukawa interactions are not necessarily diagonal neither in the basis of weak interaction eigenstates, nor in the basis of the strong ones. In the eigenstate basis of a given interaction for the case of three generations, the Yukawa coupling constants are 3×3 matrixes:

$$\begin{aligned} \mathcal{L}_Y \quad = \quad & -\sum_{j,k=1}^{3} \left\{ (\bar{u}_{jL}\bar{d}_{jL}) \left[\begin{pmatrix} \phi^+ \\ \phi^0 \end{pmatrix} y_{jk}^{(d)}d_{kR} + \begin{pmatrix} \phi^{0*} \\ -\phi^- \end{pmatrix} y_{jk}^{(u)}u_{kR} \right] \right. \\ & + \quad \left. (\bar{\nu}_{jL}\bar{l}_{jL}) \left[\begin{pmatrix} \phi^+ \\ \phi^0 \end{pmatrix} y_{jk}^{(l)}l_{kR} + \begin{pmatrix} \phi^{0*} \\ -\phi^- \end{pmatrix} y_{jk}^{(\nu)}\nu_{kR} \right] \right\} + h.c. \end{aligned}$$

where indexes j and k mark the generation number.

Charged lepton mixing is formally allowed in the SM, but not (yet) observed experimentally. Searches for lepton flavour violating processes, like the $\mu \to e\gamma$ decay, are being performed.

3.8 Short form of the SM Lagrangian

At CERN one can buy souvenirs with the Standard Model Lagrangian represented in a very short compressed form:

$$\begin{aligned} \mathcal{L}_{\text{SM}} \quad = \quad & -\frac{1}{4}F_{\mu\nu}F^{\mu\nu} \\ & + \quad i\bar{\Psi}\,\slashed{D}\,\Psi + h.c. \\ & + \quad \Psi_i y_{ij} \Psi_j \Phi + h.c. \\ & + \quad |D_\mu\Phi|^2 - V(\Phi). \end{aligned} \tag{63}$$

We can understand now the meaning of each term. First of all, we see that the Lagrangian is given in the initial form before the spontaneous symmetry breaking. Summation over $SU(3)_C$, $SU(2)_L$, and $U(1)_Y$ gauge groups is implicitly assumed in the first term. The second line represents the kinetic terms and gauge interactions of fermions provided by the covariant derivative(s). The third line is the Yukawa interaction of fermions with the primary scalar doublet field. And the fourth line represents the kinetic and potential terms of the scalar field.

EXERCISE: Find two 'misprints' in the Lagrangian (63) which break the commonly accepted QFT notation discussed in Sect. 2.
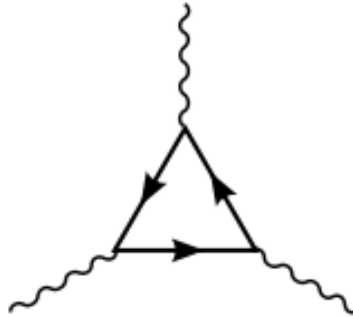
Fig. 6: Triangular anomaly diagram.

3.9 Axial anomaly

There are *axial-vector* currents in the SM:

$$J_\mu^A = \overline{\Psi}\gamma_\mu\gamma_5\Psi. \tag{64}$$

In the case of massless fermions, the unbroken global symmetry (via the Noether theorem) leads to conservation of these currents: $\partial_\mu J_\mu = 0$. For massive fermions $\partial_\mu J_\mu^A = 2im\overline{\Psi}\gamma_5\Psi$. But *one-loop corrections*, see Fig. 6, give

$$\partial_\mu J_\mu^A = 2im\overline{\Psi}\gamma_5\Psi + \frac{\alpha}{2\pi}F_{\mu\nu}\tilde{F}_{\mu\nu}, \qquad \tilde{F}_{\mu\nu} \equiv \frac{1}{2}\varepsilon_{\mu\nu\alpha\beta}F_{\alpha\beta}. \tag{65}$$

That fact is known as the *axial* or *chiral* or *triangular* Adler–Bell–Jackiw anomaly, see [6] for details. So at the quantum level the classical symmetry is lost. That is a real problem for the theory. In simple words, such a symmetry breaking makes the classical and quantum levels of the theory being inconsistent to each other. Moreover, the resulting quantum theory looses unitarity.

But in the SM the axial anomalies apparently cancel out. This can be seen for all possible combination of external gauge bosons:

1) $(W\,W\,W)$ and $(W\,B\,B)$ — automatically since left leptons and quarks are doublets;

2) $(B\,W\,W)$ — since $Q_e + 2Q_u + Q_d = 0$;

3) $(B\,B\,B)$ — since $Q_e = -1$, $Q_\nu = 0$, $Q_u = \frac{2}{3}$, $Q_d = -\frac{1}{3}$;

4) $(B\,g\,g)$ — automatically (g = gluon);

5) $(B\,gr\,gr)$ — the same as '3)' (gr = graviton).

Here B and W are the primary $U(1)$ and $SU(2)_L$ gauge bosons. Note that anomalies cancel out in each generation separately. It is interesting to note that condition '2)' means that the hydrogen atom is neutral.

It is very important that the axial anomalies cancel out in the *complete SM*: with the $SU(3)_C \otimes SU(2)_L \otimes U(1)_Y$ gauge symmetries. So there is a nontrivial connection between the QCD and EW sectors of the model.

QUESTION: Where is γ_5 in the $(B\,B\,B)$ case?

3.10 Parameters and interactions in the SM

The SM has quite a lot of parameters. We do not know (yet) where do they come from and have to define their values from observations. Let us fist count the number of independent free parameters in the SM. It is convenient to perform this exercise by looking at the initial form of the SM Lagrangian before the change of variables invoked by the spontaneous symmetry breaking. So, we have:

– 3 gauge charges (g_1, g_2, g_s);

    – 2 parameters in the Higgs potential;

    – 9 Yukawa couplings for charged fermions;

    – 4 parameters in the CKM matrix.

It makes in total 18 free parameters for the *canonical* Standard Model. Sometimes, we add also as a free parameter θ_{CP} which is responsible for CP symmetry violation in the QCD sector. But at the present time this parameter is determined experimentally to be consistent with zero, so we can drop it for the time being. Moreover, we can include neutrino masses and mixing, as described above. That would give in addition 4 (or 6 for the Majorana case) parameters in the PMNS matrix and 3 more Yukawa couplings.

    QUESTION: How many independent dimensionful parameters is there in the SM?

    Most likely that many of the listed parameters are not true independent ones. There should be some hidden symmetries and relations. Those certainly go beyond the SM. In spite of a large number of parameters the SM is distinguished between many other models by its minimality and predictive power. For example, the supersymmetric extension of the SM formally has more than one hundred free parameters, and for this reason it is not able to provide unambiguous predictions for concrete observables.

    Let us now count the interactions in the SM. Obviously, we should do that in accord with the QFT rules. The key point is to exploit symmetries, first of all the gauge ones. But looking at the Lagrangian it might be not clear what actually should be counted:

— number of *different vertexes* in Feynman rules?

— number of particle which *mediate* interactions?

— number of *coupling constants*?

    Our choice here is to count coupling constants. In fact that will automatically help us to avoid double coupling of the same interactions. This way how to count interactions is dictated by the QFT rules. So we have:

    – 3 gauge charges $(g_1,\ g_2,\ g_s)$;

    – 1 self-coupling λ in the Higgs potential;

    – 9 Yukawa couplings for charged fermions.

If required we can add 3 Yukawa couplings for neutrinos. We see that the SM contains 5 types of interactions: 3 gauge ones, the self-interaction of scalar bosons, and the Yukawa interactions of the scalar bosons with fermions. Note also that even we like some interactions e.g., the gauge ones, in the SM more than others, we can not say that any of them is more fundamental than others just since they all are in the same Lagrangian.

3.11   The naturalness problem in the SM

The most serious and actually the only one real theoretical problem of the SM is the *naturalness problem* known also as *fine-tuning* or *hierarchy* one. Note that all but one masses in the SM are generated due to the spontaneous symmetry breaking in the Higgs sector. While the scalar boson mass itself has been introduced *by hands* (of Peter Higgs *et al.*) from the beginning. The tachyon mass term breaks the scale invariance (the conformal symmetry) *explicitly*.

    So the running of all but one masses is suppressed by the classical symmetries. As the result, all other masses run with energy only logarithmically, but the Higgs mass gets quadratically divergent radiative corrections. In the one-loop approximation we get

$$M_H^2 = (M_H^0)^2 + \frac{3\Lambda^2}{8\pi^2 v^2}\left[M_H^2 + 2M_W^2 + M_Z^2 - 4m_t^2\right],$$

where Λ is a formal UV cut-off. At the same time Λ can be the energy scale of a new physics which is coupled to the EW one. In particular Λ can be even the Planck mass scale. On the other hand, it is

unnatural to have $\Lambda \gg M_H$. The most natural option would be $\Lambda \sim M_H$ e.g., everything is defined by the EW scale. But that is not the case of the SM... There are two general ways to solve the problem:

— either to exploit some (super)symmetry to cancel out the huge terms;

— or to introduce some new physics at a scale not very far from the electroweak one, i.e., making Λ being not large. One can find in the literature quite a lot of models for both options. But the experimental data coming from modern accelerators and rare decay studies disfavor most of scenarios of new physics with scales up to about 1 TeV and even higher. Moreover, it was shown that the measured value of the Higgs boson mass makes the SM being self-consistent up to very high energies even up to the Planck mass scale [17]. Direct and indirect experimental searches push up and up possible energy scale of new physical phenomena. So the naturalness problem becomes nowadays more and more prominent. And the question, why the top quark mass, the Higgs boson mass and and vacuum expectation value v are of the same order becomes more and more intriguing. In a sense, the problem is not about how to deal with divergent radiative corrections, but how to understand the very origin of the EW energy scale.

After the discovery of the Higgs boson and the measurement of its mass, we found some remarkable empirical relation between parameters of the SM. In particular the equality

$$v = \sqrt{M_H^2 + M_W^2 + M_Z^2 + m_t^2} \tag{66}$$

holds within the experimental errors: $246.22 = 246 \pm 1$ GeV. Obviously, there should be some tight clear relation between the top quark mass and the Higgs boson one (or the EW scale in general). The present version of the SM does not explain this puzzle.

EXERCISE: Divide both sides of Eq. (66) by v and find a relation between coupling constants.

Another interesting relation also involves the Higgs boson and the top quark:

$$2\frac{m_h^2}{m_t^2} = 1.05 \approx 1 \approx 2\frac{m_t^2}{v^2} \equiv y_t^2 = 0.99. \tag{67}$$

It might be that these relations are of a pure numerological nature, but they certainly indicate some hidden properties of the SM.

4 Phenomenology of the Standard Model

Let us discuss input parameters of the SM. It was convenient to count their number in the *primary* form of the Lagrangian. But for *practical* applications we use different sets, see e.g., Table 1. Various *EW schemes* with different sets of practical input parameters are possible (and actually used), since there are relations between them. One should keep in mind that the result of calculations does depend on the choice because we usually work in a limited order of the perturbation theory, while the true relations between the parameters (and between observed quantities) involve the complete series. So simple relations appear only at the lowest order, quantum effects (radiative corrections) make them complicated.

Table 1: Input parameters of the SM.

18(19)=	1	1	1	1	1	9	4	(1)
primary:	g'	g	g_s	m_Φ	λ	y_f	y_{jk}	θ_{CP}
practical:	α	M_W	α_s	G_{Fermi}	M_H	m_f	V_{CKM}	0

A comprehensive up-to-date set of the SM parameters can be found in the Review of Particle Physics published by the Particle Data Group Collaboration [18]. Let us look at some values of input parameters extracted from experiments:

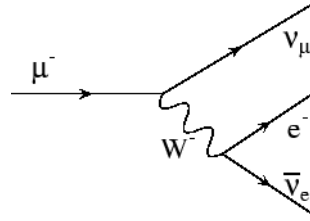– The *fine structure constant*: $\alpha^{-1}(0) = 137.035999074(44)$ from $(g-2)_e$;

Fig. 7: The Feynman diagram for muon decay in the SM.

– The SM predicts $M_W = M_Z \cos\theta_w \;\Rightarrow\; M_W < M_Z$, we have now
  $M_Z = 91.1876(21)$ GeV from LEP1/SLC, $M_W = 80.385(15)$ GeV from LEP2/Tevatron/LHC;
– The Fermi coupling constant: $G_{\mathrm{Fermi}} = 1.1663787(6) \cdot 10^{-5}$ GeV^{-2} from muon decay,
– The top quark mass: $m_t = 173.1(6)$ GeV from Tevatron/LHC;
– The Higgs boson mass: $M_H = 125.09(21)(11)$ GeV from ATLAS & CMS (March 2015).

One can see that the precision in definition of the parameters varies by several orders of magnitude. That is related to experimental uncertainties and to the limited accuracy of theoretical calculations which are required to extract the parameter values from the data.

QUESTION: What parameter of the canonical, i.e., without neutrino masses and mixing SM is known now with the least precision?

4.1 The muon decay

Let us consider a few examples of particle interaction processes and start with the muon decay $\mu^- \rightarrow e^- + \bar{\nu}_e + \nu_\mu$, see Fig. 7. It is the most clean weak-interaction process. One can say that this process is one of keystones of particle physics. The muon decay width reads

$$\Gamma_\mu = \frac{1}{\tau_\mu} = \frac{G_{\mathrm{Fermi}}^2 m_\mu^5}{192\pi^3}\left[f(m_e^2/m_\mu^2) + \mathcal{O}(m_\mu^2/M_W^2) + \mathcal{O}(\alpha)\right],$$
$$f(x) = 1 - 8x + 8x^3 - x^4 - 12x^2 \ln x,$$
$$\mathcal{O}(m_\mu^2/M_W^2) \sim 10^{-6}, \qquad \mathcal{O}(\alpha) \sim 10^{-3},$$

where $\mathcal{O}(\alpha)$ includes effects of radiative corrections due to loop (virtual) effects and real photon and/or e^+e^- pair emission.

As mentioned above, the value of the Fermi coupling constant is extracted from the data on the muon lifetime, $G_{\mathrm{Fermi}} = 1.1663787(6) \cdot 10^{-5}$ GeV^{-2}. The high precision is provided by a large experimental statistics, low systematical errors of the final state electron observation, and by accurate theoretical calculations of radiative corrections. But impressive precision ($\sim 1 \cdot 10^{-6}$) in the measurement of the muon life time doesn't give by itself any valuable test of the SM. *QUESTION: Why is that so?* On the other hand, studies of differential distributions in electron energy and angle do allow to test the $V - A$ structure of weak interactions and look for other possible types of interactions which can be parameterized in a model-independent way by the so-called *Michel parameters*.

4.2 Electron and muon anomalous magnetic moments

The Dirac equations predict gyromagnetic ratio $g_f = 2$ in the fermion magnetic moment $\vec{M} = g_f \frac{e}{2m_f}\vec{s}$. Julian Schwinger in 1948 found that one-loop QED corrections to the vertex function give the so-called *anomalous magnetic moment*:

$$a_f \equiv \frac{g_f - 2}{2} \approx \frac{\alpha}{2\pi} = 0.001\,161\,\ldots \tag{68}$$

For the electron case, the Harvard experiment [19] obtained

$$a_e^{\text{exp}} = 1\,159\,652\,18\mathbf{0.73}\,(28) \cdot 10^{-12} \quad [0.24\text{ppb}].$$

The SM predicts [20]

$$a_e^{\text{SM}} = 1\,159\,652\,18\mathbf{1.643}\,(25)_{8th}(23)_{10th}(16)_{EW+had.}(763)_{\delta\alpha} \cdot 10^{-12}.$$

The perfect agreement between the measurement and the theoretical prediction is a triumph of Quantum electrodynamics. In particular, we note that $a_f \neq 0$ is a pure quantum loop effect which is absent as in classical physics as well as in Quantum mechanics.

It is worth to note that the extremely high precision in the experimental measurement of the electron anomalous magnetic moment allows to use it as a reference point for definition of the fine structure constant: $a_e^{\text{exp}} \Rightarrow \alpha^{-1}(0) = 137.035999074(44)$.

For the anomalous magnetic moment of muon, the E821 experiment at BNL in 2006 published the following result of data analysis:

$$a_\mu^{\text{exp}} = 116\,592\,\mathbf{089}\,(54)(33) \cdot 10^{-11} \quad [0.5\text{ppm}].$$

The corresponding theoretical value and the difference are

$$a_\mu^{\text{SM}} = 116\,591\,\mathbf{840}\,(59) \cdot 10^{-11} \quad [0.5\text{ppm}] \tag{69}$$

$$\Delta a_\mu \equiv a_\mu^{\text{exp}} - a_\mu^{\text{SM}} = \mathbf{249}\,(87) \cdot 10^{-11} \quad [\sim 3\sigma].$$

First, one can see that both experimental and theoretical values are very accurate. Second, there is a discrepancy of the order of three standard deviations. That is a rather rare case for the SM tests. Moreover, this discrepancy remains for a long period of time in spite of intensive efforts of experimentalists and theoreticians.

The SM prediction consists of the QED, hadronic, and weak contributions:

$$a_\mu = a_\mu(\text{QED}) + a_\mu(\text{hadronic}) + a_\mu(\text{weak}), \tag{70}$$

$$a_\mu(\text{QED}) = 116\,584\,718\,845\,(9)(19)(7)(30) \cdot 10^{-14} \qquad [5\text{ loops}],$$

$$a_\mu(\text{hadronic}) = a_\mu(\text{had. vac.pol.}) + a_\mu(\text{had. l.b.l}), = 6949\,(37)(21) \cdot 10^{-11} + 116\,(40) \cdot 10^{-11},$$

$$a_\mu(\text{weak}) = 154\,(2) \cdot 10^{-11} \qquad [2\text{ loops}].$$

Note that the QED contribution to the muon anomalous magnetic moment is essentially the same as the one to the electron magnetic moment. The only difference is coming from the dependence on electron and muon masses. As concerning the hadronic and weak interaction contributions, they are enhanced by the factor m_μ^2/m_e^2 with respect to the electron case. The same factor typically appears for hypothetical contributions of new interactions beyond the SM. For this reason anomalous magnetic moments of muon and tau lepton are potentially more sensitive to new physics contributions.

One can see that the difference between the theoretical prediction and the experimental data is almost twice the contribution of weak interactions: $\Delta a_\mu \sim 2 \times a_\mu(\text{weak})$. Here by 'weak' we mean the complete electroweak calculation minus the pure QED contribution. The weak interactions have been directly tested with high precision experimentally. So it is not so simple to attribute the difference to an effect of new physics. Nevertheless, there is a bunch of theoretical models that try to resolve the problem by introduction of new interactions and/or new particles.

4.3 Vacuum polarization

By direct calculation in QED, one can see that virtual charged fermion anti-fermion pairs provide a screening effect for the electric force between probe charges. Resummation of bubbles, see Fig. 8, gives

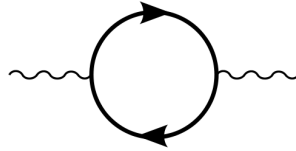$$\alpha(q^2) = \frac{\alpha(0)}{1 - \Pi(q^2)}, \qquad \text{e.g. } \alpha^{-1}(M_Z^2) \approx 128.944(19),$$

Fig. 8: The one-loop Feynman diagram for QED vacuum polarization.

$$\Pi(q^2) = \frac{\alpha(0)}{\pi}\left(\frac{1}{3}\ln\left(\frac{-q^2}{m_e^2}\right) - \frac{5}{9} + \delta(q^2)\right) + \mathcal{O}(\alpha^2),$$
$$\delta(q^2) = \delta_\mu(q^2) + \delta_\tau(q^2) + \delta_W(q^2) + \delta_{\text{hadr.}}(q^2). \tag{71}$$

The hadronic contribution to vacuum polarization $\delta_{\text{hadr.}}(q^2)$ for $|q^2|$ below a few GeV^2 is not calculable within the perturbation theory. Now we get it from experimental data on $e^+e^- \to$ hadrons and $\tau \to \nu_\tau +$ hadrons with the help of dispersion relations, see e.g., review [21]. Lattice results for this quantity are approaching.

Note that screening, i.e., an effective reduction of the observed charge with increasing of distance, is related to the minus sign attributed to a fermion loop in the Feynman rules.

QUESTION: Estimate the value of q_0^2 at which $\alpha(q_0^2) = \infty$.

This singularity is known as the *Landau pole*. Formally, such a behaviour of QED brakes unitarity at large energies. But that happens at energies much higher than any practical energy scale including the Planck mass and the mass of the visible part of the Universe. So we keep this problem in mind as a theoretical issue which stimulates our searches for a more fundamental description of Nature.

4.4 Experimental tests of the SM at LEP

After the analysis of LEP1 and LEP2 experimental data, the LEP Electroweak Working Group (LEP-EWWG) [22] illustrated the overall status of the Standard Model by the so-called *pulls*, see Fig. 9. The pulls are defined as differences between the measurement and the SM prediction calculated for the central values of the fitted SM input parameters [$\alpha(M_Z^2) = 1/128.878$, $\alpha_s(M_Z^2) = 0.1194$, $M_Z = 91.1865$ GeV, $m_t = 171.1$ GeV] divided by the experimental error. Although there are several points where deviations between the theory and experiment approach two standard deviations, the average situation should be ranked as extremely good. We note that the level of precision reached is of the order of $\sim 10^{-3}$, and that it is extremely non-trivial to control all experimental systematics at this level.

Through quantum effects the observed cross sections of electron-positron annihilation at LEP depend on all parameters of the Standard Model including the Higgs boson mass. The so-called yellow band plot Fig. 10 shows the fit of M_H performed by LEPEWWG [22] with the LEP data in March 2012. The left yellow area has been excluded by direct searches at LEP, and the right one was also excluded by LHC. The plot is derived from a combined fit of all the world experimental data to the SM exploiting the best knowledge of precision theoretical calculations which is realized in computer codes ZFITTER [23] and TOPAZ0 [24]. One can see that the data was not very sensitive to M_H, but the fit unambiguously prefers a relatively light Higgs boson. Now we can say that the measured value of this parameter agrees very well with the LEP fit. That indirectly confirms again the consistency and the power of the Standard Model.

It is interesting also to look at the behavior of the cross sections of electron-positron annihilation into hadrons as a function of energy Fig. 11. A clear peak at the Z boson mass is seen. The excellent agreement of the experimental data with the SM predictions is achieved only after inclusion of QCD and electroweak radiative corrections which reach dozens of percent in the vicinity of the peak.

A peculiar result was obtained at LEP for the number of (light) neutrinos, see Fig. 12. Even so that the final state neutrinos in the process $e^+ + e^- \to Z \to \nu + \bar\nu$ was not observed, the corresponding cross

Stanford 1999
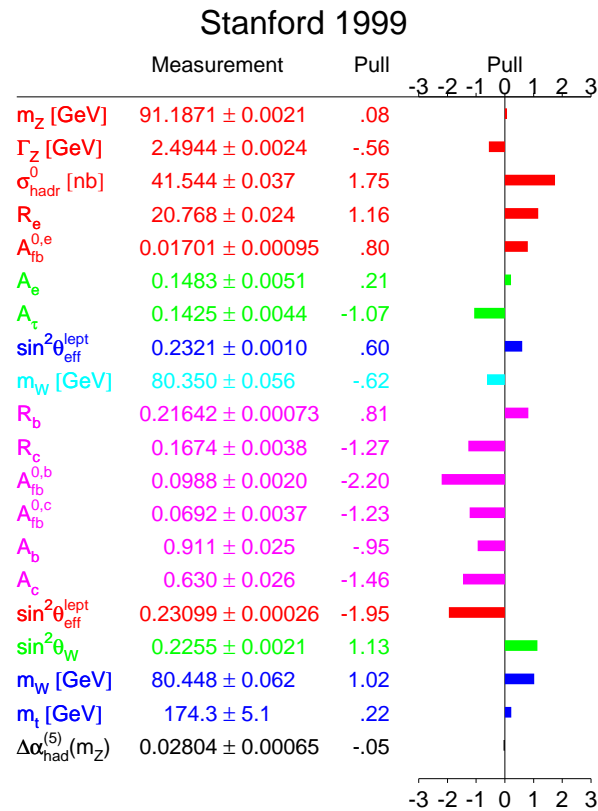
	Measurement	Pull	Pull
			-3 -2 -1 0 1 2 3
m_Z [GeV]	91.1871 ± 0.0021	.08	
Γ_Z [GeV]	2.4944 ± 0.0024	-.56	
σ^0_{hadr} [nb]	41.544 ± 0.037	1.75	
R_e	20.768 ± 0.024	1.16	
$A^{0,e}_{fb}$	0.01701 ± 0.00095	.80	
A_e	0.1483 ± 0.0051	.21	
A_τ	0.1425 ± 0.0044	-1.07	
$\sin^2\theta^{lept}_{eff}$	0.2321 ± 0.0010	.60	
m_W [GeV]	80.350 ± 0.056	-.62	
R_b	0.21642 ± 0.00073	.81	
R_c	0.1674 ± 0.0038	-1.27	
$A^{0,b}_{fb}$	0.0988 ± 0.0020	-2.20	
$A^{0,c}_{fb}$	0.0692 ± 0.0037	-1.23	
A_b	0.911 ± 0.025	-.95	
A_c	0.630 ± 0.026	-1.46	
$\sin^2\theta^{lept}_{eff}$	0.23099 ± 0.00026	-1.95	
$\sin^2\theta_W$	0.2255 ± 0.0021	1.13	
m_W [GeV]	80.448 ± 0.062	1.02	
m_t [GeV]	174.3 ± 5.1	.22	
$\Delta\alpha^{(5)}_{had}(m_Z)$	0.02804 ± 0.00065	-.05	
			-3 -2 -1 0 1 2 3

Fig. 9: Pulls of pseudo-observables at LEP [22].

section was restored with the help of the separately measured hadronic and leptonic cross sections [22], and the total Z boson width.

It appears that the dependence of LEP observables on quantum loop effects involving top quark is rather strong. So even without approaching the direct production of top quark, LEP experiments were able to extract information about its mass. The top quark mass 'history' (till 2006) is shown by Fig. 13.
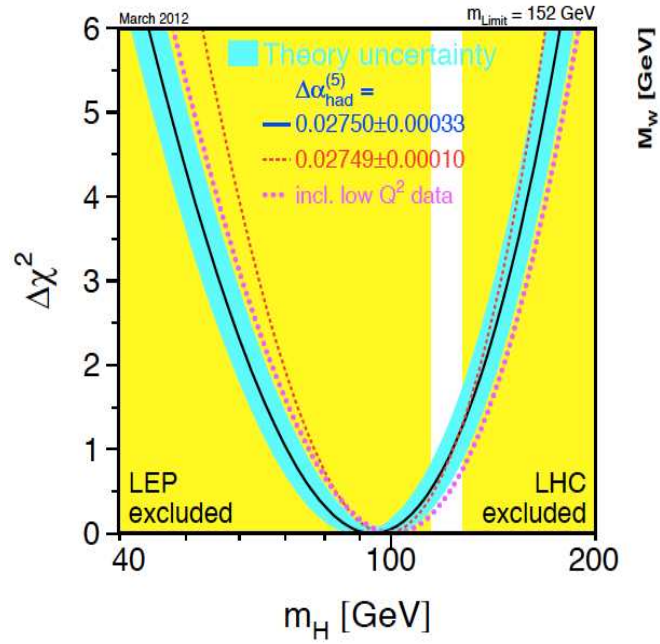
Fig. 10: The curve shows $\Delta\chi^2_{\min}(M_H^2) = \chi^2_{\min}(M_H^2) - \chi^2_{\min}$ as a function of M_H. The width of the shaded band around the curve shows the theoretical uncertainty. The vertical bands show the 95% CL exclusion limit on M_H from the direct searches at LEP (left) and at LHC (right). The dashed curve is the result obtained using the evaluation of $\Delta\alpha^{(5)}(M_Z^2)$. The dotted curve corresponds to a fit including also the low-Q^2 data.
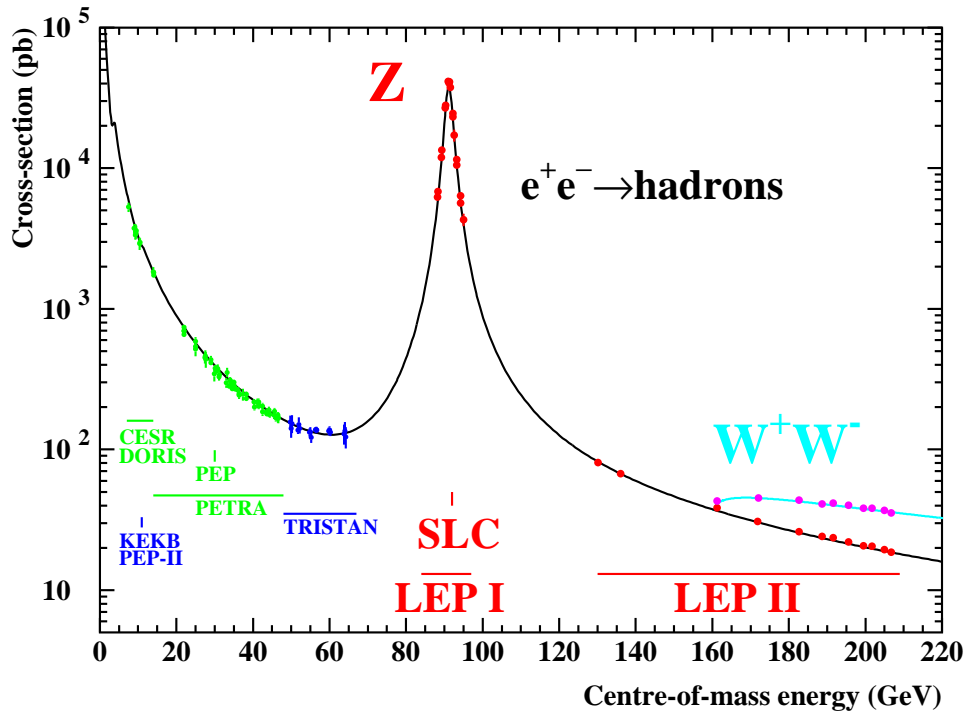

Fig. 11: Measurements of the $e^+e^- \to$ hadrons cross section.
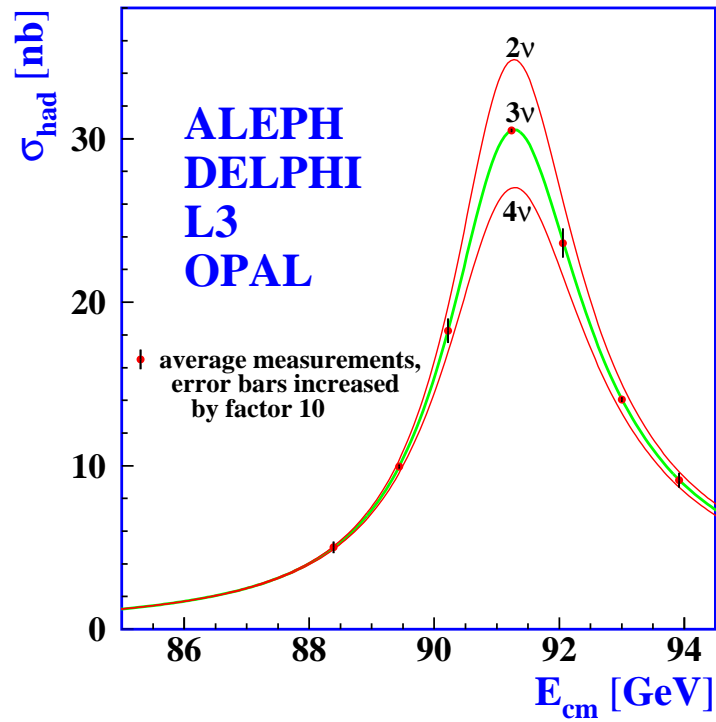
Fig. 12: Annihilation cross section $e^+e^- \to \text{hadrons}$ for different numbers of light neutrinos: measured distribution vs. the SM prediction.
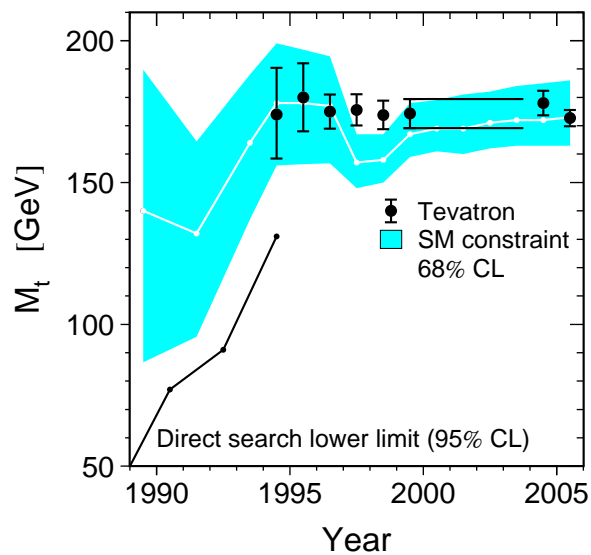

Fig. 13: Indirect (LEP) and direct (Tevatron) measurements of the top quark mass.
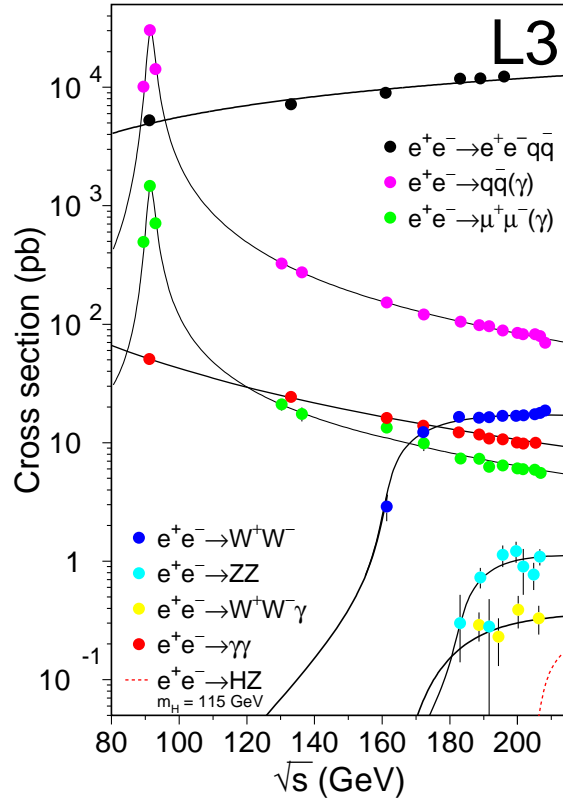
Fig. 14: Cross-sections of electroweak SM processes at LEP2.

In general, all LEP measurements of various cross-sections of electroweak SM processes were found in a very good agreement with theoretical predictions obtained within the SM, see plot Fig. 14 from the LEPEWWG [22] 2013 report. The dots show the measurements and curves are the SM predictions with radiative corrections taken into account.

4.5 Measurements of SM processes at LHC

The Large Hadron Collider at CERN is not only a discovery machine. In fact the large luminosity and advanced detectors allow to perform there high-precision tests of the Standard Model. High statistics on many SM processes is collected. Plots Fig. 15 and Fig. 16 show the public preliminary results of the ATLAS and CMS collaborations. One can see that we have again a good agreement for all channels. Certainly, the tests of the SM will be continued at LHC at higher energies and luminosity. That is one of the main tasks the LHC physical programme. The proton-antiproton collider Tevatron has proven that hadronic colliders can do high-precision studies of the SM. In particular, CDF and D0 experiments at Tevatron managed to exceed LEP in the precision of the W boson mass measurement.

At LHC the best precision in SM processes measurement is reached for the Drell–Yan-like processes. A schematic diagram for such a process is shown on Fig. 17. These processes are distinguished by production of final state leptons which can be accurately detected. We differ the neutral current (NC) Drell–Yan-like processes which involve intermediate Z bosons and photons, and the charged current (CC) ones which go through $W^{\pm}$ bosons. The main contribution to the (observed) total cross section of these processes comes from the domain where the invariant mass of the final state lepton pair is close to the masses of Z and W bosons. So these processes are also known as single Z and W production reactions. The CC and NC Drell–Yan-like processes at LHC are used for:

Fig. 15: SM cross sections measured by ATLAS (public results).

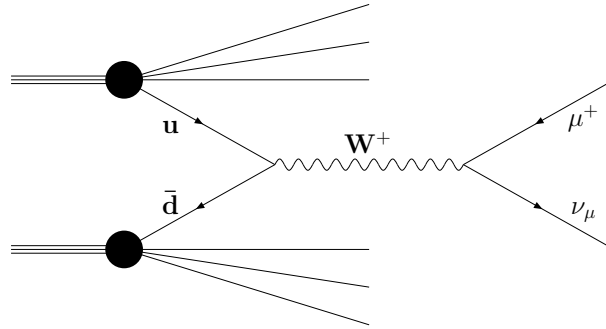**Fig. 16:** SM cross sections measured by CMS (public results).

Fig. 17: Schematic Feynman diagram for the charged current Drell–Yan-like process.

- luminosity monitoring;
- W mass and width measurements;
- extraction of parton density functions;
- detector calibration;
- background to many other processes;
- and new physics searches.

In particular, a new peak in the observed invariant-mass distribution of final leptons can indicate the presence of a new intermediate particle.

5   Conclusions

Let us summarize the status of the SM. We see that it is a rather elegant construction which allows making systematic predictions for an extremely wide range of observables in particle physics. The energy range of its applicability covers the whole domain which is explored experimentally while the true limits remain unknown. We do not understand all features of the model, the origin(s) of its symmetries and parameter values. But we see that the SM has the highest predictive power among all models in particle physics and it successfully passed verification at thousands of experiments.

There are several particularly nice features of the SM:

- it is renormalizable and unitary $\Rightarrow$ it gives finite predictions;
- its predictions do agree with experimental data;
- symmetry principles are extensively exploited;
- it is minimal;
- all its particles are discovered;
- the structure of interactions is fixed (but not yet tested everywhere);
- not so many free parameters, all are fixed;
- CP violation is allowed;
- tree-level flavor-changing neutral currents are not present;
- there is a room to incorporate neutrino masses and mixing.

In principle in the future, the SM can be embedded into a more general theory as an effective low-energy approximation. But in any case the SM will remain the working tool in the energy domain relevant for the absolute majority of our experiments.

For many reasons we do not believe that the SM is the final 'theory of everything'. Of course first of all, we have to mention that the SM is not joined with General Relativity. But frankly speaking,

that is mostly the problem of GR, since the SM itself is ready to be incorporated into a generalized joint QFT construction, while GR is not (yet) quantized. The naturalness problem discussed above in Sect. 3.11 indicates that either some new physics should be very close to the EW energy scale, or we do not understand features of the renormalization procedure in the SM. In general, we have a lot of open questions within the SM:

- the origin of symmetries;
- the origin of EW and QCD energy scales;
- the origin of 3 fermion generations;
- the origin of neutrino masses;
- the hierarchy of lepton masses;
- the absence of strong CP violation in the QCD sector;
- confinement in QCD, and so on. . .

There are also some phenomenological issues:

- the baryon asymmetry in the Universe;
- the dark matter;
- the dark energy;
- the proton charge radius, $(g-2)_\mu$, and not much else. . .

The first three items above are related to Cosmology, see the corresponding lecture course. We should note also that most of observations in Cosmology and Astrophysics are well described within the Standard Model (and General Relativity). But for the listed cases we need most likely something beyond the SM. The last item in the list claims that there are some tensions in the predictions of the SM and measurements at experiments in particle physics.

So we see that the SM is build using some nice fundamental principles but also with a substantial phenomenological input. The most *valuable task* for high-energy physicists now is to find the limits of the SM applicability energy domain. Yes, we hope to discover soon new physical phenomena. But any kind of new physics ought to preserve the correspondence to the SM. The SM contains good mechanisms to generate masses of vector bosons and fermions, but it doesn't show the *origin(s)* of the electroweak and QCD energy scales.

So, the SM can not be the full story in particle physics, we still have a lot to explore. Good luck!

References

[1] S. L. Glashow, Nucl. Phys. **22** (1961) 579.

[2] S. Weinberg, Phys. Rev. Lett. **19** (1967) 1264.

[3] A. Salam, Conf. Proc. C **680519** (1968) 367.

[4] N. N. Bogoliubov, D. V. Shirkov, *Introduction to the theory of quantized fields,* Interscience Publishers, 1959.

[5] L. H. Ryder, *Quantum Field Theory,* 2nd Edition, Cambridge University Press, 1996.

[6] S. Weinberg, *The Quantum Theory of Fields,* Cambridge University Press, Vol.1, 1995, Vol.2, 1996.

[7] M. E. Peskin, D. V. Schroeder, *An Introduction to Quantum Field Theory,* Westview Press, 1995.

[8] G. Aad *et al.* [ATLAS Collaboration], Phys. Lett. B **716** (2012) 1.

[9] S. Chatrchyan *et al.* [CMS Collaboration], Phys. Lett. B **716** (2012) 30.

[10] D. Y. Bardin and G. Passarino, *The standard model in the making: Precision study of the electroweak interactions,* Oxford University Press, International series of monographs on physics, 104 Oxford, 1999.

[11] F. Englert and R. Brout, Phys. Rev. Lett. **13** (1964) 321.

[12] P. W. Higgs, Phys. Rev. Lett. **13** (1964) 508.

[13] Scientific Background on the Nobel Prize in Physics 2013: The BEH-Mechanism, Interactions with Short Range Forces and Scalar Particles, `http://www.nobelprize.org/nobel_prizes/physics/laureates/2013/advanced-physicsprize2013.pdf`.

[14] S. Elitzur, Phys. Rev. D **12** (1975) 3978.

[15] M. N. Chernodub, L. Faddeev and A. J. Niemi, JHEP **0812** (2008) 014.

[16] F. Wilczek, Central Eur. J. Phys. **10** (2012) 1021.

[17] A. V. Bednyakov, B. A. Kniehl, A. F. Pikelner and O. L. Veretin, Phys. Rev. Lett. **115** (2015) 20, 201802.

[18] C. Patrignani *et al.* [Particle Data Group], Chin. Phys. C **40** (2016) 10, 100001.

[19] D. Hanneke, S. F. Hoogerheide and G. Gabrielse, Phys. Rev. A **83** (2011) 052122.

[20] T. Aoyama, M. Hayakawa, T. Kinoshita and M. Nio, Phys. Rev. Lett. **109** (2012) 111807.

[21] S. Actis *et al.* [Working Group on Radiative Corrections and Monte Carlo Generators for Low Energies Collaboration], Eur. Phys. J. C **66** (2010) 585.

[22] The LEP Electroweak Working Group, `http://lepewwg.web.cern.ch/LEPEWWG/`.

[23] A. B. Arbuzov, M. Awramik, M. Czakon, A. Freitas, M. W. Grunewald, K. Monig, S. Riemann and T. Riemann, Comput. Phys. Commun. **174** (2006) 728.

[24] G. Montagna, O. Nicrosini, F. Piccinini and G. Passarino, Comput. Phys. Commun. **117** (1999) 278.

Lectures on QCD for hadron colliders

K. Melnikov

Institute for Theoretical Particle Physics, Karlsurhe Institute of Technology, Karlsruhe, Germany

Abstract

I discuss how perturbative QCD can be used to describe outcomes of hard hadron collisions in a detailed and precise way. To an extent that four lectures permit, we touch upon fixed order computations, resummations, parton distribution functions and parton showers. Main ideas behind these concepts are explained and derivations of many important results are given. The importance of understanding the soft and collinear limits of scattering amplitudes for the perturbative QCD description of hadron collisions is repeatedly emphasized.

Keywords

Lectures; QCD; perturbative computations; collider physics

1 Introduction

Experiments at the LHC where proton beams collide with the center of mass energy of 13 TeV are rightfully described as experiments at the energy frontier. Being at the energy frontier is important since, by increasing the collision energy, we create a situation where events with larger momentum transfer or larger energy deposition become possible. Such events are interesting because, if enough energy is packed into a small volume, it becomes possible to knock out new heavy elementary particles from the vacuum and to study their properties. It is hoped that, in doing so, we will be able to determine the Lagrangian that governs physics beyond the Standard Model.

This approach is at the heart of many measurements performed by ATLAS and CMS collaborations at the LHC. While these experiments scored clear successes since the start of the LHC in 2010, for example by discovering the celebrated Higgs boson [1, 2], they keep struggling to break through the "Standard Model barrier", see Fig. 1. As many exclusion limits improve to the point, that masses of new heavy particles, that are still not excluded, become so large that their frequent production at the LHC is hardly possible, it becomes clear that further searches for physics beyond the Standard Model based on the idea of clear, resonance-like structures emerging on top of relatively flat backgrounds will have to be supplemented by entirely new search strategies. Indeed, if new particles are not seen directly at the LHC, they can hide in complex final states, if they are light, or, if they are heavy, they can be virtually produced for short periods of time and then disappear back into the vacuum. In the latter case, we may hope to detect these virtual particles since they affect properties of Standard Model particles that we observe experimentally.

Given this situation, we are forced to think if precision physics at the LHC is possible and whether or not it can become a tool to discover physics beyond the Standard Model. It is important to realize that systematic precision studies at hadron colliders – aimed at discovering New Physics through indirect effects – were never attempted before. This is not surprising given the fact that hadrons are composite particles kept together by a poorly understood strong force. If we can not understand or compute properties of a single proton, how can we confidently describe what happens if two protons collide?

It is generally believed that this can be done if the collision energy is high enough and if we select events where momentum transfer is very large. Such events occur at small distances and, since physics of strong interactions at short distances becomes more perturbative, the understanding of the strong force improves. Of course, it never becomes perfect. So the question is how far we can drive the idea of the precision LHC physics before poor control over the strong force catches up with us.
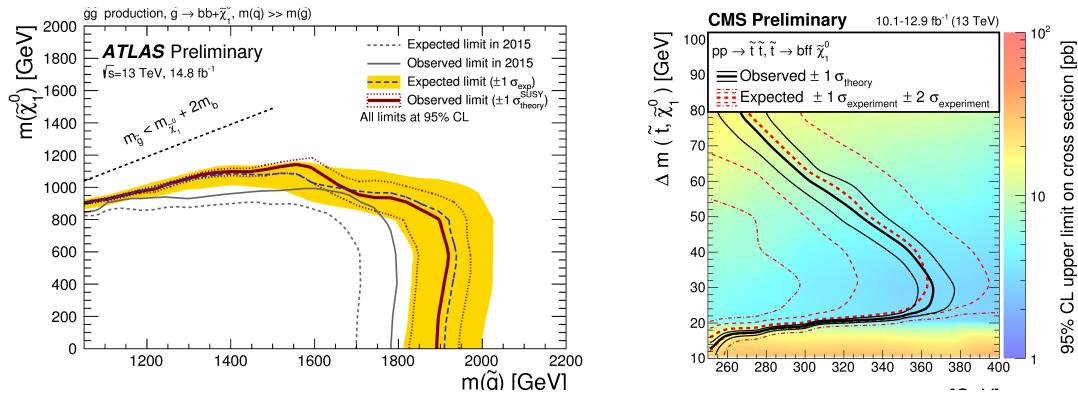
Fig. 1: Recent exclusion limits by ATLAS and CMS collaborations. The constraints on gluino and stop masses start challenging an established paradigm in high-energy physics.

This problem is non-trivial since, as we will see, we have very poor understanding of non-perturbative effects in hadron collisions. Unfortunately, non-perturbative effects need to be modeled anyhow, for instance to describe a transformation of partons to hadrons since it is the latter that interact with particle detectors. Since modeling non-perturbative effects necessarily involves some arbitrariness, it is important to find out which aspects of hadron collisions can be described and understood from first principles. This requirement is stronger than the ability of tools that we use to study hadron collisions (i.e. parton showers, fixed order computations, resummations etc.) to describe data since this can happen by accident or because one can tune these tools to do that.

As we will see in these lectures, all tools that we use to describe hadron collisions are based on approximations and all of them have limited range of applicability. For this reason, we need to understand, parametrically, the approximations that are made on the way from the Standard Model Lagrangian to a theory behind a particular measurement and we need to be convinced that a particular approximation is justified in each case. We need to be sure that the framework that we use is systematically improvable and, if not, we need to know its ultimate limit[1].

In short, we need to start asking questions about the foundations of what we do to describe hard hadron collisions and keep in mind that a significant fraction of the current lore, ideas and approaches dates back to times when even an order-of-magnitude understanding of hadron collider physics was considered a success. There is no question that currently we strive for more.

The key for describing hard scattering processes in hadron collisions is provided by the collinear factorization theorem in QCD [3]. Within this framework, colliding protons are viewed as beams of partons (massless quarks and gluons), each carrying a fraction of proton energy. Probabilities to find partons with definite energy fractions are called parton distribution functions (PDFs). These objects are universal, i.e. they do not depend on a process under investigation. Therefore, they can be determined in some processes and used to describe many other. Partons interact with each other and produce final states composed of Standard Model particles such a leptons, gauge bosons and QCD partons themselves. We interpret these QCD partons in final states as seeds of hadronic energy flows that are barely affected by non-perturbative QCD effects. We call these seeds jets.[2]

The production cross sections for processes with final states composed of QCD jets and Standard

---

[1]One of the possible questions is what is the order beyond which perturbative computations become *meaningless*?

[2] Unfortunately, due to time constraints, we could not discuss jets during the lectures. A comprehensive introduction into this very important subject can be found in Ref. [4].

Model particles in hard hadron collisions can thus be computed using the following formula

$$d\sigma = \sum_{i_1,i_2} \int dx_1 dx_2 f_{i_1}(x_1) f_{i_2}(x_2) d\sigma_{i_1 i_2}(x_1, x_2) F_J \left(1 + \mathcal{O}(\Lambda_{\text{QCD}}^n / Q^n)\right), \quad n \geq 1. \tag{1}$$

Here $x_{1,2}$ are fractions of incoming hadron's energies carried by partons i_1 and i_2 and $f_{i_{1,2}}$ are the parton distribution functions. Finally, F_J is a function that, if necessary, defines jets by combining in a smart way QCD partons that appear in the final state.

The last term in Eq. (1) represents genuine non-perturbative effects that take us beyond the simple picture of parton scattering and fragmentation into jets. These effects are expected to be suppressed by the ratio of Λ_{QCD}/Q where Q is the smallest of hard scales in the problem and $\Lambda_{\text{QCD}} \approx 300$ MeV is the non-perturbative parameter of QCD. Note that, according to Eq. (1) we *do not know how strongly* these effects are supposed to be suppressed. It is believed that, in many cases, the exponent n in Eq. (1) is $n = 2$ but there are arguments that suggest that $n = 1$ is possible especially if one studies complex kinematic distributions. Numerically, if $n = 1$ and $Q = 30$ GeV, the non-perturbative effects are estimated to be just a few percent. Note that non-perturbative of that magnitude are comparable to the accuracy to which partonic cross sections for certain hadron collider processes have been calculated. This implies that disentangling perturbative, non-perturbative and New Physics contributions to hadronic cross sections becomes problematic and may require careful investigation.

Note also that the non-perturbative contribution in Eq. (1) is highly non-trivial, in spite of its simple appearance since it contains different physical effects such as double-parton scattering, hadronization, contributions from the underlying events etc. Experimentalists know how important it is to simulate all these effects if one wants to extract real physics from hadron collisions but, according to the formula that we are going to use all the time, all these effects *are just power corrections* that can not be described from first principles. This fact alone should be worrisome enough since it shows a different take on what the LHC physics is all about by theorists and experimentalists. We will discuss how these two approaches can be reconciled when we will talk about the parton showers at the end of these lectures. Our next step is to discuss the basics of the quantum field theory of strong interactions, the QCD.

Before we dive into this discussion, let me state the obvious – it is impossible to explain the details of a complex quantum field theory, the QCD, and discuss its numerous applications to hadron collider physics in four lectures. Although I will do my best in communicating the main ideas of this theory, students should be well-advised to consult numerous textbooks on quantum field theory and the use of QCD to describe hadron collisions. An incomplete list of useful references can be found in the bibliography [5–9].

2 Basic facts about QCD for colliders

The upshot of the discussion in the previous Section and the collinear factorization formula Eq. (1) is that hard scattering processes at the LHC can be understood in terms of partons, i.e. quarks and gluons; only limited knowledge about protons is needed. Physics of quarks and gluons is governed by a field theory of strong interactions, the QCD. QCD is a non-abelian SU(3)-gauge theory so it is complicated and I can not describe all the details of this theory in these lectures. Instead, I will provide a few basic facts about QCD that we will use later. More information on QCD can be found in textbooks on particle physics and quantum field theory [5].

Similar to any other quantum field theory, QCD is described by a Lagrangian. It reads

$$\mathcal{L}_{\text{QCD}} = \sum \bar{q}_j \left(i\hat{D} - m_j\right) q_j - \frac{1}{4} G^a_{\mu\nu} G^{a,\mu\nu}, \tag{2}$$

where we sum over six quark flavors – up, down, strange, charm, bottom and top. The theory describes interactions of these quarks with carriers of the strong force, the gluons. Quarks (gluons) transform under

$$a,\mu \quad p \quad b,\nu \qquad = \frac{-i\delta^{ab}}{p^2}\left(-g_{\mu\nu}+\xi\frac{p_\mu p_\nu}{p^2}\right) \qquad j,\beta \xrightarrow{\quad p \quad} i,\alpha \qquad = \left(\frac{i}{\hat{p}}\right)_{\alpha\beta}\delta^{ij}$$

$$\begin{aligned} &= g_s f^{abc}(\quad g^{\mu\nu}(k-p)^\rho \\ &\qquad\qquad + g^{\nu\rho}(p-q)^\mu \\ &\qquad\qquad + g^{\rho\mu}(q-k)^\nu) \end{aligned}$$

$$= ig_s\gamma^\mu T^a_{ij}$$

$$= -ig_s^2\left[f^{abe}f^{cde}(g^{\mu\rho}g^{\nu\sigma}-g^{\mu\sigma}g^{\nu\rho}) \\ + f^{ace}f^{bed}(g^{\mu\nu}g^{\rho\sigma}-g^{\mu\sigma}g^{\nu\rho}) \\ + f^{ade}f^{bce}(g^{\mu\nu}g^{\rho\sigma}-g^{\mu\rho}g^{\nu\sigma})\right]$$

$$a \cdots\cdots\cdots b \qquad = \frac{i\delta^{ab}}{p^2}$$

$$= -g_s f^{abc}p^\mu$$

Fig. 2: QCD Feynman rules. Solid lines refer to quarks, wavy lines to gluons gluons and dashed lines to ghosts. Gluons in the three-gluon vertex are outgoing.

the fundamental (adjoined) representation of the gauge group SU(3), respectively. It is often said that there are also *unphysical* ghost particles in QCD; we will say a few words about them below. The various quantities that appear in the Lagrangian Eq. (2) are

$$D_\mu = \partial_\mu - ig_s T^a A^a_\mu, \quad G^a_{\mu\nu} = \partial_\mu A^a_\nu - \partial_\nu A^a_\mu + g_s f^{abc}A^b_\mu A^c_\nu, \tag{3}$$

where T^a and f^{abc} are generators and structure constants of the Lie algebra of the gauge group $SU(3)$.

It follows from the Lagrangian $\mathcal{L}_{\text{QCD}}$ that gluons interact with quarks and antiquarks and also with other gluons. We can associate these interactions with color charges of the corresponding particles; however, since there are eight Lie algebra generators and many structure constants, it becomes difficult to say what the color charges really are. Since we can not observe color, physical processes are sensitive to average color charges; those are provided by the corresponding Casimir invariants of a particular representation R $C_R = \sum T^a_R T^a_R$. These Casimir invariants evaluate to $C_F = 4/3$ and $C_A = 3$ for the fundamental and adjoined representations, respectively. The importance of these numbers is that they show that the color charge of a gluon is larger than the color charge of a quark. Physically, this means that gluons interact stronger and radiate more, leading to e.g. higher multiplicities in gluon-initiated jets as compared to quark-initiated.

Similar to any quantum field theory, QCD can be characterized by Feynman rules that describe elementary interactions between different particles in the theory. The Feynman rules are shown in Fig. 2. It is seen from Fig. (2) that, indeed quarks interact with gluons and gluons interact with quarks and gluons. Interaction between quarks and gluons is very much QED-like except for additional SU(3) matrices that describe the color chargers.

In addition to quarks and gluons there are additional particles – ghosts. Ghosts are described by scalar *anti-commuting* fields, directly violating the spin-statistics theorem. The reason ghosts are so strange is that they appear in the theory for technical reasons, i.e. as a tool to allow for the quantization

of QCD in covariant gauges where gluons are assigned *four* polarizations instead of two. When this is done in QED, two additional photon polarizations decouple from the theory automatically thanks to the so-called Ward identities. In QCD this does not happen and the primary role of a ghost is to ensure that contributions of unphysical gluon polarizations are removed from cross sections with on-shell gluons even if the latter are computed using unphysical density matrices.

If physical gluon polarizations are used to describe external states, ghosts do not appear as external particles. For a gluon that moves along the z direction with momentum k, the two physical polarizations are

$$k = (k_0, 0, 0, k_0), \quad \epsilon^+ = \frac{1}{\sqrt{2}} (0, 1, i, 0), \quad \epsilon^- = \frac{1}{\sqrt{2}} (0, 1, -i, 0). \tag{4}$$

Note that physical gluon polarizations satisfy the following transversality condition

$$k \cdot \epsilon^\pm = 0. \tag{5}$$

We will make use of this condition when discussing soft and collinear limits of real emission matrix elements.

The situation with internal gluons is somewhat more complex; one can, in principle, employ gluons with only physical polarizations (and the non-propagating color-electric field) to do loop computations, but this leads to additional complications. In practice, it is more convenient to use covariant gauges and ghosts for computing loop corrections to scattering amplitudes and Green's functions.

Fixed order computations in QCD employ an expansion in the strong coupling constant α_s. However, we do not know its numerical value since, thanks to confinement, we observe colorless states – hadrons – whereas α_s refers to interactions between color charges that we associate with quarks and gluons. To determine α_s, we measure it at high energies where description of final states in terms of jets produced by quarks and gluons becomes appropriate. For example, from studies of Z-boson decays, we know that $\alpha_s(M_z) \approx 0.12$. We also find that if we want to describe QCD processes at other energies, we can absorb significant part of quantum corrections into the "running", i.e. "energy"-dependent, coupling constant. In particular, we find that at higher energies or, more precisely, higher momentum transfers, quantum corrections can be described by using a *smaller* coupling constant. This phenomenon, known as asymptotic freedom, is described by the formula

$$\alpha_s(\mu) = \frac{1}{\beta_0 \ln \frac{\mu^2}{\Lambda_{\text{QCD}}^2}}, \quad \beta_0 = \frac{33 - 2n_f}{12\pi} \approx 0.5|_{n_f=5}, \tag{6}$$

where n_f is the number of "active" quark flavors.[3]

Asymptotic freedom is central to our ability to describe hard scattering processes at the LHC in QCD perturbative theory since the smallness of the coupling constant is a pre-requisite for the success of perturbative description. Note that for typical LHC processes the strong coupling constant is small but not tiny. This implies that quite often QCD corrections need to be computed to higher orders to claim high precision. The technology for computing next-to-leading QCD corrections to many processes of interest was developed in mid 1990s [10,11] and an important ingredient was added about ten years ago [12,13]. Since then, the development of theoretical methods for next-to-next-to-leading order (NNLO) computations became of great interest to the community of theorists interested in precision LHC phenomenology. Very recently, we have seen the emergence of several key technologies for NNLO computations [14] and dramatic increase in the number of their applications to LHC physics [15].

The use of QCD to describe hard scattering processes at the LHC is intimately connected with the detailed understanding of how scattering amplitudes behave in the so-called soft and collinear limits. The soft limit corresponds to a situation where energy of an emitted gluon becomes small. The collinear

---

[3]An "active" quark is a quark whose mass is smaller than the scale μ.
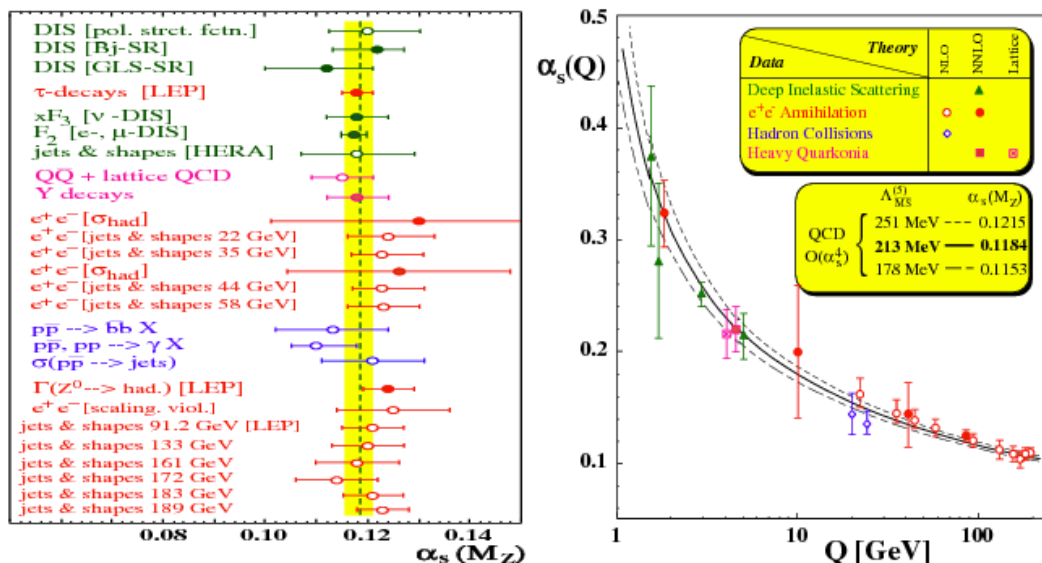
Fig. 3: The strong coupling constants as determined from different measurements and its evolution with momentum transfer.

limit corresponds to a situation where at least two external particles propagate in the same direction so that the relative angle between their momenta is small.

Scattering amplitudes become infinite if either soft or collinear limit is taken. Hence, soft and collinear limits describe kinematic situations where scattering amplitudes are large and which, therefore, provide dominant contributions to cross sections. This fact alone would have justified the need to understand soft and collinear limits of QCD amplitudes but there are more reasons to do that. They are listed below.

First, we can only apply perturbative QCD to describe observables that are *insensitive* to infrared and collinear dynamics. This is because infra-red and collinear dynamics is non-perturbative and, therefore, it can not be described as an expansion in α_s. Hence, it is important to understand soft and collinear limits of scattering amplitudes to enable construction of observables that *can* be described and understood in perturbative QCD.

Second, soft and collinear limits of amplitudes lead to non-integrable singularities in perturbative computations of cross sections. Obtaining finite fixed order predictions in high orders of perturbative QCD requires us to understand in detail how soft and collinear singularities cancel in the total cross section or in other infra-red safe observables.

Third, soft and collinear limits often determine enhanced contributions to scattering amplitudes and cross sections. These enhanced contributions may invalidate fixed order predictions and, for this reason, they are essential for resummations, PDF evolution and parton showers. Understanding universal factorization properties of matrix elements in these limits is crucial for the success of the resummation program.

Finally, soft and collinear emissions dominate high-multiplicity final states. Understanding high-multiplicity final state in QCD is important for describing the evolution from hard scattering processes that occur at short distances to large distances where non-perturbative transition from QCD partons to observable hadrons occurs.

In what follows, we will look at different ways to describe hard hadron collisions, emphasizing the role of soft and collinear limits for these descriptions. We will start with a relatively simple picture of fixed order computations. We will continue by making it more complex in order to improve the description of certain observables. Quite often, I will use toy models and examples from QED to explain the

relevant physics, instead of talking about QCD directly. The reason for this is that QED physics is similar to QCD but QCD, being a non-abelian theory, is technically more involved. Therefore, understanding physics of hard collisions in a simpler gauge theory – QED – is a crucial step towards mastering QCD.

The remainder of these lectures is organized as follows. In the next Section I will discuss the production of lepton pairs in hadron collisions at leading order in perturbative expansion in QCD. We will find that the results of the calculation provide a decent description of rapidity and invariant mass distributions of a lepton pair but completely fail to describe its transverse momentum distribution. We will attempt to improve on this result by considering NLO QCD corrections to dilepton pair production in hadron collisions in Section 4. We will find that, although we can describe the transverse momentum distribution of a lepton pair at high $p_\perp$, we fail to do that at low values of the transverse momentum. In Section 5 we explain that at low values of the transverse momenta, perturbative expansion is in expansion in $\alpha_s \ln^2(s/p_\perp^2)$, rather than α_s, which can be of order one, so that all such contributions need to be resummed. We explain how to resum such terms in QCD perturbative series in Section 5. Upon doing so, we will discover that it is necessary to choose the factorization scale of parton distribution proportional to $p_\perp$, in order to achieve the resummation of $p_\perp$-dependent logarithms at small values of the transverse momentum. To understand the reason for that, we will discuss the parton distribution functions and the meaning of the factorization scale in Section 6. Parton distribution functions provide a limited information about the composition of the final state. To improve on that, parton showers are used. In Section 7 we explain the basic ideas behind parton showers and show how parton showers can be used to generate unweighted events. We conclude in Section 8.

3 Lepton pair production at leading order

In this Section, we discuss production of lepton pairs (e^+e^-, $\mu^+\mu^-$, $\tau^+\tau^-$) in hadron collisions at leading order in perturbative QCD. We will only consider the photon-mediated process; the exchange of the Z-boson between quarks and leptons will be neglected.

According to the factorization theorem Eq. (1), production of a lepton pair in hadron collisions is described by the following formula at leading order in perturbative QCD

$$
\mathrm{d}\sigma_{H_1+H_2\to l^+l^-} = \sum_{i\in[q,\bar{q}]} \int \mathrm{d}x_1\mathrm{d}x_2 f_i(x_1) f_{\bar{i}}(x_2) \, \mathrm{d}\sigma_{i\bar{i}\to l^+l^-}(x_1P_1, x_2P_2). \tag{7}
$$

Here $P_{1,2}$ are the momenta of the colliding hadrons $H_{1,2}$, respectively. The momenta of incoming hadrons are taken to be light-like $P_1^2 = P_2^2 = 0$, i.e. all the mass effects are neglected. The four-momenta of the colliding massless quarks are then $p_1 = x_1P_1$ and $p_2 = x_2P_2$. Parton distribution functions $f_{q,\bar{q}}(x)$ are extracted from experimental measurements and are considered to be known for our purposes. Although there are gluon partons in a proton, they do not contribute to leading order cross section for lepton pair production.

To compute the hadronic cross section we need the cross section for the partonic process $q\bar{q} \to l^+l^-$. Computation of this cross section proceeds in a standard way. The matrix element reads

$$
i\mathcal{M} = \frac{ie^2 Q_q \delta_{km}}{Q^2} \left[\bar{u}(k_1, \lambda_1)\gamma_\mu v(k_2, \lambda_2)\right] \left[\bar{v}(p_2, \xi_2)\gamma^\mu u(p_1, \xi_1)\right], \tag{8}
$$

where Q_q is the electric charge of colliding quarks, k and m are their colors, $\lambda_{1,2}$ and $\xi_{1,2}$ are the polarization labels and $k_{1,2}$ are the four-momenta of a lepton and an anti-lepton, respectively. We will treat leptons as massless particles. We also introduced the four-momentum $Q = p_1 + p_2 = k_1 + k_2$ that flows through the propagator of a virtual photon.

To compute the cross section, we need to square the matrix element in Eq. (8) and sum it over polarizations of the initial and final state particles. This computation is simplified if we use the standard

trick that allows us to turn sums over polarizations into traces of products of Dirac matrices. The key formula reads

$$\sum_\lambda u(p,\lambda)_\alpha \bar{u}(p,\lambda)_\beta = \sum_\lambda v(p,\lambda)_\alpha \bar{v}(p,\lambda)_\beta = \hat{p}_{\alpha\beta}. \tag{9}$$

We use Eq. (9) and write

$$\sum_{\{\lambda,\xi\}} \sum_{\text{color}} |\mathcal{M}|^2 = N_c \frac{(e^2 Q_q)^2}{Q^4} \text{Tr}\left[\hat{k}_1 \gamma_\mu \hat{k}_2 \gamma_\nu\right] \ \text{Tr}\left[\hat{p}_2 \gamma^\mu \hat{p}_1 \gamma^\nu\right], \tag{10}$$

where $N_c = 3$ is the number of colors. We calculate the two traces using the standard formula

$$\text{Tr}\left[\hat{a}\gamma_\mu \hat{b}\gamma_\nu\right] = 4\left(a_\mu b_\nu + a_\nu b_\mu - g_{\mu\nu} a \cdot b\right), \tag{11}$$

and find

$$\sum_{\{\lambda,\xi\}} \sum_{\text{color}} |\mathcal{M}|^2 = \frac{32 N_c (e^2 Q_q)^2}{Q^4} \left[(k_1 p_2)(k_2 p_1) + (k_1 p_1)(k_1 p_2)\right]. \tag{12}$$

To compute the cross section, we write

$$\mathrm{d}\sigma_{q\bar{q}\to e^+ e^-} = \frac{1}{2s}\frac{1}{4}\frac{1}{N_c^2} \sum_{\{\lambda,\xi\}} \sum_{\text{color}} |\mathcal{M}|^2 \ \ [\mathrm{d}k_1][\mathrm{d}k_2](2\pi)^4 \delta^{(4)}(p_1 + p_2 - k_1 - k_2), \tag{13}$$

where the prefactors describe the flux factor $2s = 4p_1 p_2$ and the averaging over spins and colors of the incoming quarks. We also introduced a convenient notation for the Lorentz-invariant phase space of a single particle with momentum p

$$[\mathrm{d}p] = \frac{\mathrm{d}^3 p}{(2\pi)^3 2p_0}. \tag{14}$$

We will now rewrite the phase-space in a way that will allow us to separate two processes – the production of a virtual photon with the total momentum $Q = k_1 + k_2$ and the decay of this virtual photon to a lepton pair. For $q\bar{q} \to l^+ l^-$ process the procedure that we describe is perhaps an overkill, but it is useful to understand it since it can be very helpful in more complicated cases. To this end, we introduce an auxiliary vector Q and write

$$1 = \int \mathrm{d}^4 Q \, \delta^{(4)}(Q - p_1 - p_2). \tag{15}$$

We insert this integral into the phase space and simplify it by separating integration over $Q^2 = M^2$

$$
\begin{aligned}
&[\mathrm{d}k_1][\mathrm{d}k_2](2\pi)^4 \delta(p_1 + p_2 - k_1 - k_2) \\
&= [\mathrm{d}k_1][\mathrm{d}k_2](2\pi)^4 \delta(p_1 + p_2 - k_1 - k_2)\mathrm{d}^4 Q \delta^{(4)}(Q - p_1 - p_2) \\
&= \mathrm{d}M^2 \delta(M^2 - Q^2)\mathrm{d}^4 Q \delta^{(4)}(Q - p_1 - p_2)[\mathrm{d}k_1][\mathrm{d}k_2](2\pi)^4 \delta(Q - k_1 - k_2) \\
&= \mathrm{d}M^2 \delta(M^2 - s) \ [\mathrm{d}k_1][\mathrm{d}k_2](2\pi)^4 \delta(Q - k_1 - k_2)|_{Q=p_1+p_2, Q^2=M^2}.
\end{aligned}
\tag{16}
$$

This formula does what we wanted since it separates the production of a (virtual) particle with the mass $M^2 = s$ from its decay to a di-lepton final state.

To compute the cross section we need to integrate over lepton momenta. There are different ways to do that. Since, according to Eqs. (12,13,16)

$$\mathrm{d}\sigma_{q\bar{q}\to e^+ e^-} \sim \int [\mathrm{d}k_1][\mathrm{d}k_2]\delta(Q - k_1 - k_2) \, k_1^\mu k_2^\nu (p_{1,\mu} p_{2,\nu} + p_{1,\nu} p_{2,\mu}), \tag{17}$$

we need to understand how to compute the following tensor integral

$$\int [\mathrm{d}k_1][\mathrm{d}k_2](2\pi)^4 \delta(Q - k_1 - k_2)k_1^\mu k_2^\nu = I^{\mu\nu}. \tag{18}$$

This integral is a rank-two tensor; therefore, it can only depend on the metric tensor and a rank-two tensor constructed using the vector Q. Thus, we write

$$I^{\mu\nu} = I_1 Q^2 g^{\mu\nu} + I_2 Q^\mu Q^\nu. \tag{19}$$

To compute the form factors $I_{1,2}$, it is convenient to contract $I_{\mu\nu}$ with $g_{\mu\nu}$ and $Q_\mu Q_\nu$, compute the contracted integrals separately and solve the system of linear equations for the two form factors. To illustrate this procedure, consider $g_{\mu\nu}I^{\mu\nu}$. This integral reads

$$Q^2 (4I_1 + I_2) = \int [\mathrm{d}k_1][\mathrm{d}k_2](2\pi)^4 \delta(Q - k_1 - k_2)(k_1 k_2). \tag{20}$$

We use $k_1 k_2 = Q^2/2$ and find

$$8I_1 + 2I_2 = \int [\mathrm{d}k_1][\mathrm{d}k_2](2\pi)^4 \delta(Q - k_1 - k_2). \tag{21}$$

The integral on the right hand side is the two-particle phase space. To compute it, it is convenient to use the fact that it is Lorentz-invariant and choose a frame where $Q = (Q_0, \vec{0})$ with $Q_0 = \sqrt{Q^2}$. The integral becomes

$$I_{\mathrm{Lips}} = \int [\mathrm{d}k_1][\mathrm{d}k_2](2\pi)^4 \delta(Q - k_1 - k_2) = \int [\mathrm{d}k_1][\mathrm{d}k_2](2\pi)^4 \delta(Q_0 - \omega_1 - \omega_2)\delta^{(3)}(\vec{k}_1 + \vec{k}_2). \tag{22}$$

The integration over $\vec{k}_2$ is used to eliminate the three-momentum conserving δ-function; the integration over the absolute value of $|k_1|$ is used to eliminate the energy-conserving δ-function. The remaining integration over directions of the three-momentum k_1 are unconstrained. Therefore, we obtain

$$I_{\mathrm{Lips}} = \frac{1}{8\pi} \int \frac{\mathrm{d}\Omega_1}{4\pi} = \frac{1}{8\pi} \int_0^\pi \frac{\mathrm{d}\theta \sin\theta}{2} \int_0^{2\pi} \frac{\mathrm{d}\phi}{2\pi} = \frac{1}{8\pi}. \tag{23}$$

A very similar computation can be performed for $Q_\mu Q_\nu I^{\mu\nu} = Q^4(I_1 + I_2)$. In fact, since $Qk_1 = Qk_2 = Q^2/2$, the calculation is almost identical. Solving the two linear equations for I_1, I_2, we find

$$I^{\mu\nu} = \frac{1}{96\pi} \left(Q^2 g^{\mu\nu} + 2Q^\mu Q^\nu \right). \tag{24}$$

We employ Eq. (24) to compute the cross section for $q\bar{q} \to l^+ l^-$ and use $N_c = 3$, $p_1 p_2 = Q^2/2 = s/2$ and $Qp_1 = Q^2/2 = s/2$, to arrive at the final result

$$\frac{\mathrm{d}\sigma_{q\bar{q}\to e^+e^-}}{\mathrm{d}M^2} = \frac{4\pi\alpha^2 Q_q^2}{9s} \delta(s - M^2). \tag{25}$$

We will use Eq. (25) to compute the hadronic cross section for lepton pair production. To this end, we employ the collinear factorization formula Eq. (7) and the partonic cross section Eq. (25), integrated over M^2, to obtain

$$\sigma_{H_1+H_2\to p_1+p_2} = \sum_{i\in[q,\bar{q}]} \int \mathrm{d}x_1 \mathrm{d}x_2 f_i(x_1) f_{\bar{i}}(x_2) \frac{4\pi\alpha^2 Q_i^2}{9M^2}. \tag{26}$$

Here the invariant mass of the lepton pair M^2 is expressed through the center of mass energy squared of the two colliding hadrons S as $M^2 = Sx_1x_2$.

It is convenient to rewrite the integration over x_1 and x_2 through the invariant mass M^2 and the *rapidity* of the lepton pair. The rapidity is defined as

$$Y = \frac{1}{2} \ln \frac{Q_0 + Q_z}{Q_0 - Q_z}, \tag{27}$$

where Q_z is the component of the four-momentum of the lepton pair $Q = k_1 + k_2$ along the collision axis. Using the momentum conservation $Q = k_1 + k_2 = p_1 + p_2 = x_1 P_1 + x_2 P_2$ and the fact that hadrons collide in the center-of-mass frame along the z-axis, we find

$$Y = \frac{1}{2} \ln \frac{Q_0 + Q_z}{Q_0 - Q_z} = \frac{1}{2} \ln \frac{P_2 Q}{P_1 Q} = \frac{1}{2} \ln \frac{x_1}{x_2} \frac{p_2 Q}{p_1 Q} = \frac{1}{2} \ln \frac{x_1}{x_2}. \tag{28}$$

Since $M^2 = Sx_1x_2$ we can write

$$x_1 = \sqrt{\frac{M^2}{S}} e^Y, \quad x_2 = \sqrt{\frac{M^2}{S}} e^{-Y}. \tag{29}$$

Finally, we can trade the integration over x_1, x_2 for the integration over M^2 and Y. Computing the Jacobian of the transformation, we obtain

$$\mathrm{d}x_1 \mathrm{d}x_2 = \frac{\mathrm{d}M^2 \mathrm{d}Y}{S}. \tag{30}$$

Integration boundaries follow from the conditions on the momenta fractions $0 < x_{1,2} < 1$ and read

$$|Y| < \frac{1}{2} \ln \frac{S}{M^2}, \quad 0 < M^2 < S. \tag{31}$$

The final result for the hadronic cross-section reads

$$\frac{M^2 \, \mathrm{d}\sigma_{H_1+H_2 \to l^+l^-}}{\mathrm{d}M^2 \mathrm{d}Y} = \frac{4\pi\alpha^2}{9S} \sum_{i \in [q,\bar{q}]} Q_i^2 f_i(x_1^*) f_{\bar{i}}(x_2^*), \tag{32}$$

where $x_{1,2}^* = \sqrt{M^2/S} e^{\pm Y}$.

The above formula provides interesting information about kinematics of lepton pairs that are produced in hadron collisions. It predicts non-trivial distributions in the invariant mass and the rapidity of a lepton pair. However, the very same formula also predicts that momenta of lepton pairs are aligned with the collision axis and that no lepton pairs with non-vanishing momenta components transverse to the collision axis are produced in hadron collisions. Indeed, since $Q = x_1 P_1 + x_2 P_2$, the transverse momentum distribution predicted by our computation reads $\mathrm{d}\sigma/\mathrm{d}^2\vec{Q}_\perp \sim \delta(\vec{Q}_\perp)$.

It is instructive to compare these predictions with the results of actual measurements. The measured distributions of the invariant masses of lepton pairs and the rapidity are shown in Fig. 4. The experimental results include the Z exchange between quarks and leptons, c.f. the peak in the left pane at around $M_{ll} \sim 90$ Gev, so they can not be directly compared with our computation. However, if we were to include the Z-exchange into our theoretical prediction, we would describe data shown in Fig. 4 reasonably well.

However, the situation becomes very different for the transverse momentum distribution of a lepton pair, shown in Fig. 5. As we explained earlier, the leading order computation predicts that lepton
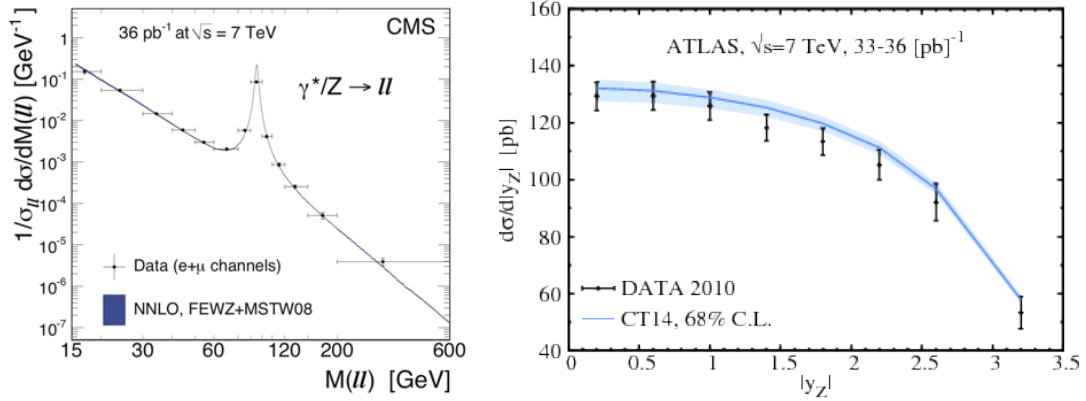
Fig. 4: Invariant mass (left) and rapidity (right) distributions of lepton pairs at the LHC. Z-exchanges are included and the results compared with theoretical predictions that include higher order QCD corrections. If we were to include the Z-exchange in our cross section computation and then plot the invariant mass and the rapidity distributions, we would describe experimental data reasonably well.
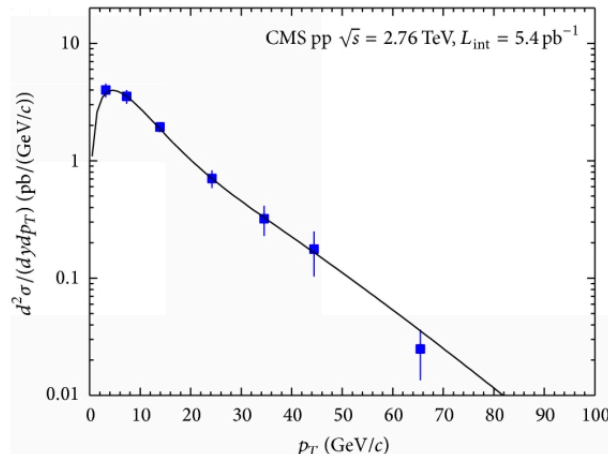

Fig. 5: The lepton pair transverse momentum distribution measured by the CMS collaboration. Clearly, it is very different from $\mathrm{d}\sigma/\mathrm{d}^2 p_\perp \sim \delta^{(2)}(\vec{p}_\perp)$ predicted by the leading order computation.

pairs produced in hadron collisions have vanishing transverse momenta. This prediction is in *direct contradiction* with the results of experimental measurements shown in Fig. 5. To summarize, we see that leading order QCD theory works reasonably well for the invariant mass and the rapidity distributions but that it fails for the transverse momentum distribution of a lepton pair. So, what is going on?

To understand how non-trivial transverse momentum distribution of a lepton pair can be produced, we recall that our computation of the lepton pair production cross section was performed at leading order in perturbative QCD. If we go to higher orders, two things can happen. First, the interaction strengths between quarks and photons changes because of the *virtual* QCD corrections. Second, a gluon can be emitted by an incoming quark or an incoming anti-quark; such contributions are called *real-emission* corrections. If this gluon happens to have a non-vanishing transverse momentum, the lepton pair will have to balance it because of momentum conservation; this may generate a continuous spectrum of lepton pairs with different transverse momenta in accord with experimental measurements. We will substantiate these considerations with mathematical formulas in the next Section.

4 Lepton pair production at next-to-leading order in perturbative QCD

To make this discussion more quantitative, we need to be able to compute next-to-leading order QCD corrections to lepton pair production cross section in hadron collisions. We will start with the discussion of the real emission process $q\bar{q} \to e^+e^- + g$. We will denote the gluon momentum as p_3. We write the real-emission cross section in a particular way

$$\mathrm{d}\sigma_R = \frac{1}{2s} \int [\mathrm{d}p_3] F_{\mathrm{LM}}(1, 2, 3), \tag{33}$$

where

$$F_{\mathrm{LM}}(1, 2, 3) = N_A \overline{|M(1, 2, 3)|}^2 (2\pi)^4 \delta(p_1 + p_2 - p_3 - k_1 - k_2) \, \mathrm{dLips}_{e^+e^-}, \tag{34}$$

N_A is the required symmetry factor that includes averaging over spins and colors of the colliding partons and $\overline{|(M(1, 2, 3)|}^2$ is the matrix element squared for $q\bar{q} \to e^+e^- + g$ process, summed over polarizations and colors of all particles. Also, $\mathrm{dLips}_{e^+e^-} = [\mathrm{d}k_1][\mathrm{d}k_2]$ is the phase-space of the lepton pair. Note also that observables are reconstructed from the momenta of particles that appear in the function F_{LM}; this remark will be important once we get to the discussion of the *subtraction procedure* later in this Section.

We would like to compute the contribution of the the real-emission process to the production rate of lepton pairs in hadron collisions. This requires integrating over gluon and dilepton phase spaces in Eq. (33). We will show now that this integral *can not be computed*.

To see this, let us understand the conditions on the matrix elements that ensure that the real emission contribution can be computed. We begin by considering the integration over gluon energy. The phase space element scales as

$$[\mathrm{d}p_3] \sim \frac{E_3^2 \mathrm{d}E_3}{E_3} \sim E_3 \mathrm{d}E_3. \tag{35}$$

The lower integration boundary is $E_3 = 0$, the upper integration boundary follows from the energy conservation. Therefore

$$\mathrm{d}\sigma_R \sim \int_0^{E_3^{\mathrm{max}}} \mathrm{d}E_3 E_3 |\mathcal{M}(1, 2, 3)|^2. \tag{36}$$

It follows that if $\lim_{E_3 \to 0} M(1, 2, 3) \sim E_3^{-1}$, the integral over E_3 does not converge at the lower integration boundary.

We can check how the matrix element behaves when the energy of the gluon becomes small. The matrix element reads

$$\mathcal{M}(1, 2, 3) = g_s T_{ji}^a \bar{v}(p_2) \left[\frac{\gamma^\mu(\hat{p}_1 - \hat{p}_3)\hat{\epsilon}}{(p_1 - p_3)^2} - \frac{\hat{\epsilon}(\hat{p}_2 - \hat{p}_3)\gamma^\mu}{(p_2 - p_3)^2} \right] u(p_1) \times \frac{[e^2 Q_q]}{Q^2} \bar{u}(k_1)\gamma_\mu v(k_2), \tag{37}$$

where, as before, Q is the four-momentum of the lepton pair, g_s is the strong coupling constant and ϵ^μ is the gluon polarization vector.

We are interested in the behavior of the amplitude Eq. (37) in the limit $E_3 \to 0$; this implies that p_3 vanishes, component by component. Since $(p_{1,2} - p_3)^2 = -2p_{1,2}p_3 \sim O(E_3)$ and since we are only interested in the contribution to $\mathcal{M}$ that scales as E_3^{-1}, we can neglect p_3 in the numerators of the two terms in square brackets in Eq. (37) and keep it in the denominators.

Further simplifications are possible in Eq. (37). Consider the first term in square brackets as an example. We find

$$\bar{v}(p_2) \left[\frac{\gamma^\mu(\hat{p}_1 - \hat{p}_3)\hat{\epsilon}}{(p_1 - p_3)^2} \right] u(p_1) \to \frac{\bar{v}(p_2)\gamma^\mu \hat{p}_1 \hat{\epsilon} u(p_1)}{(-2p_1 p_3)} \to -\frac{p_1 \cdot \epsilon}{p_1 \cdot p_3} \, \bar{v}(p_2)\gamma^\mu u(p_1), \tag{38}$$

where we used $\hat{p}_1\hat{\epsilon}u(p_1) = (2p_1 \cdot \epsilon - \hat{\epsilon}\hat{p}_1)u(p_1) = 2p_1 \cdot \epsilon u(p_1)$ as follows from the anticommutation relations of the Dirac matrices and the Dirac equation $\hat{p}_1 u(p_1) = 0$.

Repeating the calculation to simplify the second term in the square brackets in Eq. (37), we find the soft limit of the amplitude

$$\lim_{E_3 \to 0} \mathcal{M}(1,2,3) = -g_s T_{ij}^a \left(\frac{p_1 \epsilon}{p_1 p_3} - \frac{p_2 \epsilon}{p_2 p_3} \right) \mathcal{M}'(1,2). \tag{39}$$

Here $\mathcal{M}'(1,2)$ is the amplitude for the elastic process $q\bar{q} \to e^+ e^-$ with the color factor δ_{ij} removed. It is now straightforward to compute the amplitude squared summed over colors and polarizations. We obtain

$$\lim_{E_3 \to 0} |\mathcal{M}(1,2,3)|^2 = \mathrm{Eik}(1,2,3)|\mathcal{M}(1,2)|^2, \tag{40}$$

where the eikonal factor reads

$$\mathrm{Eik}(1,2,3) = g_s^2 C_F \frac{2p_1 p_2}{(p_1 p_3)(p_2 p_3)}. \tag{41}$$

There are two comments to make about this result. First, soft limits of scattering amplitudes are *universal*; they depend on the color charges of colliding energetic particles and their momenta. The hard scattering amplitude that appears in the soft limit describes a process without soft gluon radiation, i.e. $q\bar{q} \to e^+ e^-$ in our case. Second, it is clear from Eqs. (40,41) that the amplitude squared for the $q\bar{q} \to e^+ e^- + g$ process indeed scales as E_3^{-2} in the soft limit. As the result, its contribution to the real emission cross section diverges at $E_3 = 0$

$$\sigma_R \sim \int\limits_0^{E_{\max}} \frac{\mathrm{d}E_3}{E_3} = \infty, \tag{42}$$

and, therefore, can not be computed.

We will discuss how to solve this problem below. For now, we will study another kinematic region where integration over the gluon four-momentum becomes problematic. To appreciate that there might be another problem, consider again the gluon emission amplitude shown in Eq. (37) and look at the first term in square brackets that describes gluon emission off the incoming quark. The denominator of this term is $s_{13} = (p_1 - p_3)^2 = -2p_1 p_3 = -2E_1 E_3(1 - \cos\theta_{13})$. It vanishes if the energy of the emitted gluon vanishes – this is the situation that we just discussed. However, s_{13} also vanishes if $\theta_{13} \to 0$ that corresponds to a situation when the gluon is emitted along the direction of the incoming quark. Since the gluon emission phase space scales as $[\mathrm{d}p_3] \sim \theta_{13}\mathrm{d}\theta_{13}$, for small θ_{13} the amplitude squared should diverge weaker than $|\mathcal{M}(1,2,3)|^2 \sim \theta_{13}^{-2}$ for the rate to be calculable. Unfortunately, a naive computation of this *collinear* limit

$$|\mathcal{M}(1,2,3)|^2 \sim s_{13}^{-2} \sim \theta_{13}^{-4}, \tag{43}$$

indicates a very strong singularity which, however, is inconsistent with e.g. the soft limit of the amplitude squared, c.f. Eq. (41).

To understand what is going on, we need to study the collinear limit of the amplitude more carefully. To this end, it is convenient to employ the so-called Sudakov decomposition for the gluon momentum

$$p_3 = xp_1 + \beta p_2 + p_{3\perp}, \tag{44}$$

where the transverse momentum is defined by the conditions $p_1 p_{3\perp} = p_2 p_{3\perp} = 0$. Since the gluon p_3 is on the mass shell, $p_3^2 = 0$, we find

$$sx\beta = \vec{p}_{3,\perp}^2. \tag{45}$$

If the gluon is emitted along the direction of the incoming quark, $x \sim 1$, $p_{3,\perp} \sim \sqrt{s}\theta_{13}$ and $\beta \sim \theta_{13}^2$; the latter scaling follows from Eq. (45).

We use the Sudakov decomposition in the matrix element for $q\bar{q} \to e^+e^- + g$ assuming that the gluon is emitted collinearly to the momentum of the incoming quark. We will first show that the singularity that appears when $\theta_{13} \to 0$ is *significantly weaker* than the naive estimate Eq. (43). To see this, consider the most singular contribution to the amplitude in the $\theta_{13} \to 0$ limit that arises from the term that describes gluon emission off the quark line

$$\mathcal{M}_q(1,2,3) = g_s T^a_{ji} \bar{v}(p_2) \left[\frac{\gamma^\mu(\hat{p}_1 - \hat{p}_3)\hat{\epsilon}}{-2p_1p_3} \right] u(p_1) \times \frac{[e^2 Q_q]}{Q^2} \bar{u}(k_1)\gamma_\mu v(k_2). \qquad (46)$$

We use the Sudakov decomposition for the gluon momentum in this expression and look for the most singular term in the limit $\theta_{13} \to 0$. We replace p_3 using the Sudakov decomposition as in Eq. (44) and use scalings of β and $p_{3,\perp}$ with θ_{13} to discard subleading terms. The most singular term corresponds to the amplitude Eq. (46) with p_3 in the numerator replaced with xp_1. We find

$$\begin{aligned}
\lim_{\theta_{13}\to 0} \mathcal{M}_q(1,2,3) &= -\frac{g_s T^a_{ij}}{2p_1p_3}(1-x)\bar{v}(p_2)\gamma^\mu \hat{p}_1 \epsilon u(p_1) \times \frac{[e^2 Q_q]}{Q^2}\bar{u}(k_1)\gamma_\mu v(k_2) \\
&= -\frac{g_s T^a_{ij}}{2p_1p_3}(1-x)(2p_1\epsilon)\,\bar{v}(p_2)\gamma^\mu u(p_1) \times \frac{[e^2 Q_q]}{Q^2}\bar{u}(k_1)\gamma_\mu v(k_2),
\end{aligned} \qquad (47)$$

where again at the last step we used the anti-commutation relation of the Dirac matrices and the Dirac equation $\hat{p}_1 u(p_1) = 0$.

The expression Eq. (47) seems to confirm the naive estimate of the strength of the singularity of the amplitude in the $\theta_{13} \to 0$ limit since $p_1p_3 \sim \beta \sim \theta_{13}^2$ and the numerator in Eq. (47) contains no θ_{13}. However this conclusion is misleading. Indeed, since ϵ is the polarization vector of a physical gluon, it satisfies the transversality condition $p_3\epsilon = 0$. We use this equation to find the scaling of the scalar product $p_1\epsilon$ that appears in in Eq.(47) using the Sudakov decomposition for p_3. We obtain $x(p_1\epsilon) + \beta(p_2\epsilon) + (p_{3\perp}\epsilon) = 0$, so that

$$p_1\epsilon = -\frac{p_{3\perp}\epsilon}{x} - \frac{\beta p_2\epsilon}{x} \sim \mathcal{O}(\theta_{13}). \qquad (48)$$

Hence, thanks to the fact that we deal with the gauge theory, the matrix element in the collinear limit is less singular than the naive estimate shows. Using Eqs. (47,48), we find $\mathcal{M}(1,2,3) \sim \theta_{13}^{-1}$.

To compute the collinear limit of the amplitude, we need to account for all terms that scale as θ_{13}^{-1} but all other terms can be neglected. In particular, we do not need to consider contributions to the amplitude which describe the emission of gluons by an anti-quark since they scale as $\mathcal{O}(1)$. The calculation is straightforward but somewhat messy and we do not present it here. Instead, we just report the result

$$\lim_{\theta_{13}\to 0} \overline{|\mathcal{M}(1,2,3)|}^2 = \frac{2g_s^2}{(p_1-p_3)^2} P_{qq}\left(\frac{E_1}{E_1-E_3}\right) \overline{|\mathcal{M}(1-3,2)|}^2, \qquad (49)$$

where

$$P_{qq} = C_F \frac{1+z^2}{1-z} \qquad (50)$$

is the so-called $q \to qg$ splitting function and the notation $\mathcal{M}(1-3,2)$ means that the matrix element for the leading order process $q\bar{q} \to e^+e^-$ has to be computed for the four-momenta of the incoming quark given by $p_q^\mu = (E_1 - E_3)/E_1\, p_1^\mu$. Clearly, p_q can be thought of as the four-momentum of a quark *after* it emitted the collinear gluon with the energy E_3.

It should be clear from this discussion that a very similar situation occurs when the gluon is emitted by an incoming anti-quark. The limit for the amplitude squared in this case is obtained after simple modifications in Eq. (49)

$$\lim_{\theta_{23}\to 0} \overline{|\mathcal{M}(1,2,3)|}^2 = \frac{2g_s^2}{(p_2-p_3)^2} P_{qq}\left(\frac{E_2}{E_2-E_3}\right) \overline{|\mathcal{M}(1,2-3)|}^2, \tag{51}$$

where $\mathcal{M}(1,2-3)$ refers to leading order matrix element where the four-momentum of an anti-quark is taken to be $p_{\bar{q}}^\mu = (E_2-E_3)/E_2\, p_2^\mu$.

Clearly, since the matrix element squared scales as $|\mathcal{M}(1,2,3)|^2 \sim \theta^{-2}$ for small emission angles, it is not possible to compute the contribution of the real emission process to the production rate

$$\sigma_R \sim \int [\mathrm{d}p_3]|\mathcal{M}(1,2,3)|^2 \sim \int\limits_0^\pi \theta \mathrm{d}\theta\, \theta^{-2} = \infty. \tag{52}$$

To understand what to do with these infinities, we need to turn them into something tractable. To this end, we use an idea of the *regularization* that appears in theoretical physics over and again. It is based on the understanding that all infinities look *similar* and so it is difficult to trace where they come from. On the other hand, if we introduce a parameter that allows us to control how these infinities arise in the corresponding limits, we can start to distinguish between them thereby making the first step towards understanding what to do about them.

There are different ways to regularize these infinities. One option is to imagine that the scattering process occurs in a space-time whose dimensionality is *larger* than four. Scalings of amplitudes in the soft and collinear limits remain the same but the scaling of the gluon phase space changes. Indeed, if we consider, for the sake of example, the process $q\bar{q} \to e^+e^- + g$ in the five-dimensional space-time, we find

$$[\mathrm{d}p_3]_{5d} \sim E_3^2 \mathrm{d}E_3, \quad [\mathrm{d}p_3]_{5d} \sim \theta^2 \mathrm{d}\theta. \tag{53}$$

These scalings of the phase space imply that soft and collinear limits of the amplitude squared can be integrated in five-dimensional space-time without a problem. Of course at this point it is not clear how this observation can be used to perform computations in four-dimensional space-time since four- and five-dimensional space-times are clearly rather different.

An interesting idea [16] is to treat the dimensionality of space-time as a formal parameter *without* assuming it to be integer. It is conventional to denote the space-time dimensionality as d and to write $d = 4 - 2\epsilon$. If we are able to perform all the relevant computations without requiring d to be integer and if, at the end, we can take the $\epsilon \to 0$ limit, we will be able to write our results as an expansion around four-dimensional space-time and regularize infinities that we observed earlier.

It is easy to see that this strategy is quite sensible. Indeed, the phase-space element for a massless particle with four momentum $k = (k_0, \vec{k})$, $k^2 = 0$ in a d-dimensional space-time is defined as

$$[\mathrm{d}k] = \frac{k_0^{d-2}\mathrm{d}k_0 \mathrm{d}\Omega^{(d-1)}}{2(2\pi)^{d-1}}. \tag{54}$$

The solid angle in non-integer number of dimensions is defined recursively

$$\mathrm{d}\Omega^{(d-1)} = \mathrm{d}\cos\theta\,(1-\cos^2\theta)^{(d-4)/2}\,\mathrm{d}\Omega^{(d-2)}, \quad \Omega^{(d)} = \frac{2\pi^{d/2}}{\Gamma(d/2)}. \tag{55}$$

We will now show that this modification of the phase-space regularizes soft and collinear singularities. To this end, consider the integral of the eikonal factor over the single gluon phase space. It reads

$$I_E = \int [\mathrm{d}p_3]\frac{2p_1\cdot p_2}{p_3\cdot p_1 p_3\cdot p_2}\theta(E_{\max}-E_3). \tag{56}$$

The momenta $p_{1,2}$ are back-to-back and we choose the z-axis to be the collision axis. The resulting integral becomes

$$
\begin{aligned}
I_E &= \int\limits_0^{E\text{max}} \frac{4E_3^{d-2}\mathrm{d}E_3}{2(2\pi)^{d-1}E_3^3} \int\limits_{-1}^1 \frac{\mathrm{d}\cos\theta(1-\cos^2\theta)^{(d-4)/2}\,\mathrm{d}\Omega^{(d-2)}}{(1-\cos^2\theta)} \\
&= \frac{2\Omega^{(d-2)}}{(2\pi)^{d-1}} \int\limits_0^{E_\text{max}} \frac{\mathrm{d}E_3}{E_3^{1+2\epsilon}} \int\limits_{-1}^1 \frac{\mathrm{d}\cos\theta}{(1-\cos^2\theta)^{1+\epsilon}}.
\end{aligned}
\tag{57}
$$

The last two integrals are easy to compute assuming that $\epsilon < 0$, so that integrals converge at the otherwise problematic boundaries. The integral over gluon energy is straightforward

$$
\int\limits_0^{E\text{max}} \frac{\mathrm{d}E_3}{E_3^{1+2\epsilon}} = -\frac{E_\text{max}^{-2\epsilon}}{2\epsilon}.
\tag{58}
$$

To compute the integral over the polar angle in Eq. (57) we need to change the integration variable $\cos\theta = 1 - 2x$, $0 < x < 1$. Then

$$
\int\limits_{-1}^1 \frac{\mathrm{d}\cos\theta}{(1-\cos^2\theta)^{1+\epsilon}} = 2^{-1-2\epsilon} \int\limits_0^1 \mathrm{d}x(x(1-x))^{-1-\epsilon} = -2^{-2\epsilon} \frac{\Gamma^2(1-\epsilon)}{\epsilon\Gamma(1-2\epsilon)}.
\tag{59}
$$

Since $\Gamma(1+x\epsilon) \approx 1 + \mathcal{O}(\epsilon)$, we find

$$
I_E = \frac{1}{4\pi^2\epsilon^2} + \mathcal{O}(1/\epsilon).
\tag{60}
$$

It follows from the above equation that that integrations over energy and the polar angle produce terms that become infinite in the $d \to 4$ limit. However, the relevant integrals are indeed regularized and we can study how the $1/\epsilon$ singularities disappear when all the different contributions to cross sections are combined.

We will try to achieve this *without* integrating over any measureable degrees of freedom of the emitted gluon. Since, as we saw, the $1/\epsilon$ singularities appear only after integration over gluon energies and angles, we need to design a procedure that allows us to integrate over emitted gluons *without* affecting the observables. This is accomplished with the help of the so-called so-called *subtraction* procedure. The idea is to systematically subtract simplified versions of real emission contributions that, on one hand, make the (subtracted) real emission cross sections integrable in $d = 4$ and, on the other hand, are simple enough to be integrated over the unresolved phase-space in $d \neq 4$.

To see how this procedure works in detail, it is convenient to introduce particular notation to extract soft and collinear limits from the matrix elements and the corresponding phase space. We write

$$
S_3 F_\text{LM}(1,2,3) = \lim_{p_3\to 0} F_\text{LM}(1,2,3) = g_s^2 C_F \frac{2p_1 p_2}{(p_1 p_3)(p_2 p_3)} F_\text{LM}(1,2),
$$

$$
C_{31} F_\text{LM}(1,2,3) = \lim_{\theta_{13}\to 0} F_\text{LM}(1,2,3) = \frac{2g_s^2}{(p_1-p_3)^2} P_{qq}\left(\frac{E_1}{E_1-E_3}\right) F_\text{LM}(1-3,2),
\tag{61}
$$

$$
C_{32} F_\text{LM}(1,2,3) = \lim_{\theta_{23}\to 0} F_\text{LM}(1,2,3) = \frac{2g_s^2}{(p_2-p_3)^2} P_{qq}\left(\frac{E_2}{E_2-E_3}\right) F_\text{LM}(1,2-3),
$$

where the splitting function P_{qq} is given by

$$
P_{qq}(z) = C_F\left(\frac{1+z^2}{1-z} - \epsilon(1-z)\right).
\tag{62}
$$

Note that the $\mathcal{O}(\epsilon)$ term that appears in P_{qq} in Eq. (62) is the consequence of additional gluon polarizations that need to be accounted for in case of the $(4 - 2\epsilon)$-dimensional space-time.

We now use the operators introduced in Eq. (61) to subtract soft and collinear singularities. It is convenient to denote integration over the relevant phase spaces, continued to d dimensions, using angle brackets

$$d\sigma_R = \langle F_{\text{LM}}(1,2,3) \rangle. \tag{63}$$

As we already discussed, $d\sigma_R$ can not be computed in four-dimensional space-time since it exhibits soft and collinear singularities. To isolate them, we rewrite Eq. (63) in the following way

$$
\begin{aligned}
\langle F_{\text{LM}}(1,2,3) \rangle &= \langle (I - S_3) F_{\text{LM}}(1,2,3) \rangle + \langle S_3 F_{\text{LM}}(1,2,3) \rangle \\
&= \langle (I - C_{31} - C_{32})(I - S_3) F_{\text{LM}}(1,2,3) \rangle \\
&\quad + \langle (C_{31} + C_{32})(I - S_3) F_{\text{LM}}(1,2,3) \rangle + \langle S_3 F_{\text{LM}}(1,2,3) \rangle,
\end{aligned} \tag{64}
$$

where I is an identity operator. It is instructive to explore different terms on the right hand side of Eq. (64) keeping an eye on the simplifications in hard matrix elements that occur once soft and collinear operators act on $F_{\text{LM}}(1,2,3)$.

First, we note that the term

$$\langle \mathcal{O}_{\text{NLO}} F_{\text{LM}}(1,2,3) \rangle = \langle (I - C_{31} - C_{32})(I - S_3) F_{\text{LM}}(1,2,3) \rangle \tag{65}$$

does not have infra-red and collinear singularities and, therefore, can be computed in four dimensions. This is so because all the potentially singular limits are subtracted from the hard matrix element. Note that it is important to perform the subtraction in a "nested" way, i.e. the collinear subtraction is applied to the *soft-subtracted* matrix element squared.

The remaining two terms in Eq. (64) depend on the *simplified* matrix elements where gluon momentum does not appear at all (soft subtraction) or changes the energy of the incoming partons (collinear subtraction). Therefore, one can integrate these terms over some parts of the gluon phase-space without specifying the hard matrix element. Before we discuss this step in detail, we would like to simplify Eq. (64). To this end, we rewrite the last two terms in the following way

$$
\begin{aligned}
&\langle (C_{31} + C_{32})(I - S_3) F_{\text{LM}}(1,2,3) \rangle + \langle S_3 F_{\text{LM}}(1,2,3) \rangle \\
&= \langle (C_{31} + C_{32}) F_{\text{LM}}(1,2,3) \rangle + \langle (I - C_{31} - C_{32}) S_3 F_{\text{LM}}(1,2,3) \rangle,
\end{aligned} \tag{66}
$$

and focus on the last term. Taking $S_3 F_{\text{LM}}(1,2,3)$ from Eq. (61), we compute

$$
\begin{aligned}
C_{31} S_3 F_{\text{LM}}(1,2,3) &= g_s^2 C_F \frac{2E_1}{E_3 (p_1 p_3)} F_{\text{LM}}(1,2), \\
C_{32} S_3 F_{\text{LM}}(1,2,3) &= g_s^2 C_F \frac{2E_2}{E_3 (p_2 p_3)} F_{\text{LM}}(1,2),
\end{aligned} \tag{67}
$$

For the head-on collisions, we find

$$\frac{2E_1}{E_3(p_1 p_3)} + \frac{2E_2}{E_3(p_2 p_3)} = \frac{2E_1(p_2 p_3) + 2E_2(p_1 p_3)}{E_3(p_1 p_3)(p_2 p_3)} = \frac{2p_1 p_2}{(p_3 p_1)(p_2 p_1)}. \tag{68}$$

Therefore,

$$\langle (I - C_{31} - C_{32}) S_3 F_{\text{LM}}(1,2,3) \rangle = 0, \tag{69}$$

which implies a simplified subtraction formula

$$\langle F_{\text{LM}}(1,2,3) \rangle = \langle \mathcal{O}_{\text{NLO}} F_{\text{LM}}(1,2,3) \rangle + \langle (C_{31} + C_{32}) F_{\text{LM}}(1,2,3) \rangle. \tag{70}$$

As we already mentioned, the first term on the right hand side of Eq. (70) is finite and can be computed in a straightforward way. We will now study the collinear subtraction terms.

We take $\langle C_{31} F_{\mathrm{LM}}(1, 2, 3) \rangle$ as an example and write

$$
\langle C_{31} F_{\mathrm{LM}}(1, 2, 3) \rangle = \int [\mathrm{d}p_3] \frac{g_s^2}{(p_1 - p_3)^2} P_{qq}\left(\frac{E_1}{E_1 - E_3}\right) (2s)^{-1} F_{\mathrm{LM}}(1 - 3, 2)
$$

$$
= \int \frac{E_3^{d-3} \mathrm{d}E_3 \, \mathrm{d}\Omega^{(d-1)}}{2(2\pi)^{d-1}} \frac{g_s^2}{-2 E_1 E_3 (1 - \cos\theta_{13})} P_{qq}\left(\frac{E_1}{E_1 - E_3}\right) (2s)^{-1} F_{\mathrm{LM}}\left(\frac{E_1 - E_3}{E_3} 1, 2\right). \tag{71}
$$

Since $F_{\mathrm{LM}}(1-3, 2)$ is independent of the gluon emission angle, we can integrate over it. This is a typical simplification that occurs with the subtraction terms since hard matrix elements in the subtraction terms depend on a limited number of gluon kinematic variables, if at all. Integration over the gluon emission angle is straightforward and we obtain

$$
\int \frac{\mathrm{d}\Omega^{(d-1)}}{1 - \cos\theta_{13}} = -\Omega^{(d-2)} \frac{2^{-2\epsilon} \Gamma^2(1 - \epsilon)}{\epsilon \, \Gamma(1 - 2\epsilon)}. \tag{72}
$$

The $1/\epsilon$ factor that appears after the integration over angle is the collinear divergence that we discussed earlier.

The remaining integration over energy of the emitted gluon in Eq. (71) can not be performed without specifying the hard matrix element. However, it is possible to write the integrand in Eq. (71) in a more transparent way by changing the integration variable. We write $E_3 = E_1(1 - z)$ and use $P_{qq}(1/z) = -P_{qq}(z)/z$ which can be verified using explicit expression for the splitting function in Eq. (62). Putting everything together, we obtain

$$
\langle C_{31} F_{\mathrm{LM}}(1, 2, 3) \rangle = -\frac{[\alpha_s]}{\epsilon} \frac{\Gamma^2(1 - \epsilon)}{\Gamma(1 - 2\epsilon)} (2E_1)^{-2\epsilon} \int\limits_{z_{\min}}^{1} \frac{\mathrm{d}z}{(1 - z)^{2\epsilon}} P_{qq}(z) \left\langle \frac{F_{\mathrm{LM}}(z \cdot 1, 2)}{z} \right\rangle, \tag{73}
$$

where

$$
[\alpha_s] = \frac{\alpha_s \mu^{2\epsilon} e^{\epsilon \gamma_E}}{2\pi \Gamma(1 - \epsilon)}, \tag{74}
$$

is the strong coupling constant at the scale μ and $z_{\min} = 1 - E_{\max}/E_1$.

A glance at the splitting function in Eq. (62) reveals that the remaining integration in Eq. (73) leads to divergences. Indeed, in the $z \to 1$ limit, $P_{qq} \sim 2C_F/(1 - z)$, so that the integration over z can not be preformed in four dimensions. The first thing we need to do is to extract the $z \to 1$ singularity without specifying the hard matrix element. This is easy to accomplish – since this singularity is logarithmic it can be easily subtracted. More precisely, we split the P_{qq} function into singular and regular parts and write

$$
P_{qq} = \frac{2C_F}{1 - z} + P_{qq}^{\mathrm{reg}}, \quad P_{qq}^{\mathrm{reg}} = -C_F(1 + z + \epsilon(1 - z)). \tag{75}
$$

Then, we introduce a new notation $G(z) = \langle F_{\mathrm{LM}}(z \cdot 1, 2)/z \rangle$ and write the relevant integral as

$$
\int\limits_{z_{\min}}^{1} \frac{\mathrm{d}z}{(1 - z)^{2\epsilon}} P_{qq}(z) \, G(z) = \int\limits_{0}^{1} \mathrm{d}z \left[\frac{2C_F}{(1 - z)^{1 + 2\epsilon}} + (1 - z)^{-2\epsilon} P_{qq}^{\mathrm{reg}} \right] G(z). \tag{76}
$$

Note that we replaced $z_{\min}$ with zero, as the lower integration boundary; this is allowed because the minimal value of z is determined by the energy-momentum conservation condition for the process $q(z p_1) + \bar{q}(p_2) \to l^+ l^-$ which implies that a non-vanishing energy of the incoming quark is required to produce a pair of leptons.

The first term on the right hand side in Eq. (76) requires further analysis; the second term does not lead to singularities and, therefore, can be integrated numerically, expanding around $d = 4$. To deal with the first term, we write

$$
\int_0^1 dz \, \frac{2C_F}{(1-z)^{1+2\epsilon}} G(z) = \int_0^1 dz \, \frac{2C_F}{(1-z)^{1+2\epsilon}} \left(G(z) - G(1) \right) - \frac{C_F}{\epsilon} G(1)
$$
$$
= -\frac{C_F}{\epsilon} G(1) + 2C_F \sum_{n=0}^{\infty} \frac{(-1)^n (2\epsilon)^n}{n!} \int_0^1 \mathcal{D}_n(z) G(z).
$$
(77)

In the last step we introduced the so-called "plus"-distributions that are defined as follows

$$
\mathcal{D}_n(z) = \left[\frac{\ln^n(1-z)}{1-z} \right]_+ \Rightarrow \int_0^1 dz \, \mathcal{D}_n(z) \, G(z) = \int_0^1 dz \, \frac{\ln^n(1-z)}{(1-z)} \left[G(z) - G(1) \right].
$$
(78)

Clearly, these distributions provide a way to regulate an integral that otherwise diverges at $z = 1$.

Putting everything together and expanding the result in powers of ϵ up to $\mathcal{O}(\epsilon^0)$, we obtain the following expression for the collinear subtraction term

$$
\langle C_{31} F_{\text{LM}}(1,2,3) \rangle = -\frac{[\alpha_s]}{\epsilon} \frac{\Gamma^2(1-\epsilon)}{\Gamma(1-2\epsilon)} s^{-\epsilon} \left[\left(-\frac{C_F}{\epsilon} + \frac{3C_F}{2} \right) \langle F_{\text{LM}}(1,2) \rangle \right.
$$
$$
\left. + \int_0^1 dz P_{qq,R}(z) \langle \frac{F_{\text{LM}}(z \cdot 1,2)}{z} \rangle \right],
$$
(79)

where

$$
P_{qq,R}(z) = P_{qq}^{(0)} + \epsilon P_{qq,R}^{\epsilon}(z) + \mathcal{O}(\epsilon^2),
$$
(80)

and

$$
P_{qq}^{(0)} = C_F \left(2D_0(z) - (1+z) + \frac{3}{2}\delta(1-z) \right),
$$
$$
P_{qq,R}^{(\epsilon)}(z) = C_F \left(2(1+z) \log(1-z) - (1-z) - 4D_1(z) \right).
$$
(81)

A similar analysis can be performed for the emission off the incoming anti-quark. Combining the relevant formulas, we derive the result for the real emission cross section

$$
2s d\sigma^R = 2[\alpha_s] s^{-\epsilon} \left(\frac{C_F}{\epsilon^2} + \frac{3C_F}{2\epsilon} \right) \times \frac{\Gamma^2(1-2\epsilon)}{\Gamma(1-2\epsilon)} \langle F_{\text{LM}}(1,2) \rangle
$$
$$
- \frac{[\alpha_s] s^{-\epsilon}}{\epsilon} \frac{\Gamma(1-\epsilon)^2}{\Gamma(1-2\epsilon)} \int_0^1 dz \, P_{qq}^{(0)}(z) \langle \frac{F_{\text{LM}}(z1,2)}{z} + \frac{F_{\text{LM}}(1,z2)}{z} \rangle
$$
$$
- [\alpha_s] s^{-\epsilon} \frac{\Gamma(1-\epsilon)^2}{\Gamma(1-2\epsilon)} \int_0^1 dz \, P_{qq,R}^{(\epsilon)}(z) \langle \frac{F_{\text{LM}}(z1,2)}{z} + \frac{F_{\text{LM}}(1,z2)}{z} \rangle
$$
$$
+ \langle \mathcal{O}_{\text{NLO}} F_{\text{LM}}(1,2,4) \rangle.
$$
(82)

Terms on the right hand side in Eq. (82) are written as an expansion in $1/\epsilon$. We note that the strongest singularity $\mathcal{O}(1/\epsilon^2)$ appears in terms that depend on the cross section of the elastic (no-emission) process

$q\bar{q} \to e^+e^-$ in leading order kinematics. We also note that there is a large number of terms in Eq. (82) that exhibit $\mathcal{O}(1/\epsilon)$ singularities and depend on cross sections of the leading order process in the *boosted* kinematics, i.e. when a quark with reduced energy annihilates with an anti-quark, or vice versa.

As it is clearly seen from Eq. (82), the partonic process with additional gluon radiated into a final state leads to divergent contribution to the production cross section. If perturbative approach to hard hadron collisions is to make sense, there should be other contributions that cancel the singularities. What are these additional contributions? Clearly, for the cancellation of the divergent terms to happen, the relevant pieces must at the very least have a similar dependence on the hard scattering cross section as divergent terms in Eq. (82). Since the most singular term has tree-level kinematics, it is reasonable to imagine that *virtual corrections* to leading order process may produce a divergent result and, hopefully, cancel the singularities in the integrated real-emission cross section.

We can compute the virtual corrections to $q\bar{q} \to e^+e^-$ process explicitly and it may be, in fact, necessary to do so if we want to understand their contribution to dilepton pair production fully. However, if we are interested in understanding how divergences in real and virtual contributions cancel out, there is a better way. Indeed, it was pointed out by S. Catani [17] that infra-red divergences of one-loop amplitudes in QCD are known for a generic process. Such infra-red divergences depend on the color charges of external particles, certain kinematic invariants and leading order scattering amplitudes. In case of dilepton pair production, the scattering amplitude can be written as

$$\mathcal{M}_{\text{full}} = \mathcal{M}_0 + \frac{\alpha_s(\mu)}{2\pi}\mathcal{M}_{1-\text{loop}} + \mathcal{O}(\alpha_s^2), \quad \mathcal{M}_{1-\text{loop}} = I_1(\epsilon)\mathcal{M}_0 + \mathcal{M}_{1-\text{loop}}^{\text{fin}}, \tag{83}$$

where

$$I_1(\epsilon) = -\frac{e^{\epsilon\gamma_E}}{\Gamma(1-\epsilon)}\left[\frac{C_F}{\epsilon^2} + \frac{3C_F}{2\epsilon}\right]\left(\frac{\mu^2}{-s - i0}\right)^{-\epsilon}. \tag{84}$$

Squaring the amplitude and accounting for the interference between $\mathcal{M}_0$ and $\mathcal{M}_{1-\text{loop}}$, we obtain the following result for the virtual corrections to leading order cross section

$$2s\mathrm{d}\sigma_V = -2[\alpha_s]\cos(\epsilon\pi)\left(\frac{C_F}{\epsilon^2} + \frac{3C_F}{2\epsilon}\right)s^{-\epsilon}\langle F_{\text{LM}}(1,2)\rangle + \langle F_{LV}^{\text{fin}}(1,2)\rangle. \tag{85}$$

The last term on the right hand side represents the finite contribution that can be computed in four dimensions; all $1/\epsilon$ divergences that appear in virtual contributions to cross sections are shown explicitly.

To compute the rate, we combine real Eq. (82) and virtual Eq. (85) corrections. It is easy to see that divergent parts of virtual corrections and contributions to real emission corrections proportional to $\langle F_{\text{LM}}(1,2)\rangle$ cancel almost entirely. Expanding in ϵ, we find

$$\begin{aligned} 2s\mathrm{d}\sigma^{R+V} = &-\frac{[\alpha_s]s^{-\epsilon}}{\epsilon}\frac{\Gamma(1-\epsilon)^2}{\Gamma(1-2\epsilon)}\int_0^1 \mathrm{d}z\, P_{qq}^{(0)}(z)\langle\frac{F_{\text{LM}}(z1,2)}{z} + \frac{F_{\text{LM}}(1,z2)}{z}\rangle \\ &+ \frac{2\pi^2 C_F}{3}\frac{\alpha_s}{2\pi}\langle F_{\text{LM}}(1,2)\rangle - \frac{\alpha_s}{2\pi}\int_0^1 \mathrm{d}z\, P_{qq,R}^{(\epsilon)}(z)\langle\frac{F_{\text{LM}}(z1,2)}{z} + \frac{F_{\text{LM}}(1,z2)}{z}\rangle \\ &+ \langle\mathcal{O}_{\text{NLO}}F_{\text{LM}}(1,2,3)\rangle. \end{aligned} \tag{86}$$

As can be seen from Eq. (86), the remaining divergences are associated with tree-level cross sections for dilepton pair production that, however, describe a situation where a pair is boosted along the collision axis. A boost along the collision axis changes rapidity distribution and can, in principle, be absorbed into a re-definition of parton distribution functions. Indeed, we have seen in discussing the leading order cross section that parton distribution functions determine the rapidity distribution of dilepton pairs.

When we talked about the leading order cross section, we said that parton distribution functions are universal non-perturbative objects that are determined in experiment. What does it mean then, that they can be changed to absorb divergent contributions to partonic cross sections? Well, the point is that theoretical predictions for experimental quantities *include* divergent contributions – what is measured in the experiment is a combination of *bare* parton distribution functions and the divergent terms that appear in perturbative computations. It is the combination of the two that defines physical parton distribution functions.

Therefore, similar to all other parameters that appear in perturbative computations in Quantum Field Theory, we start with the so-called bare parton distribution functions and write them as physical parton distributions and the counter-terms whose role is to remove the divergences. Similar to ordinary ultraviolet renormalization in Quantum Field Theory, counter-terms for parton distribution functions lead to the renormalization group equation which in this case is known as Dokshitzer-Gribov-Altarelli-Parisi (DGLAP) evolution equation [18]. We will talk about this equation in Section 6. For now, we just quote the relation between bare and renormalized parton distribution functions that we use to remove remaining singularities in the NLO cross section Eq.(86). The renomalization of parton distribution functions amounts to the replacement

$$f_i^{\text{bare}} \to \left[\hat{\delta}_{ij} + \frac{\alpha_s(\mu)}{2\pi\epsilon} P_{ij}^{(0)} + \mathcal{O}(\alpha_s^2)\right] \otimes f_j(\mu), \tag{87}$$

where summation over repeated index is assumed and the convolution is defined as follows

$$[f_1 \otimes f_2](z) = \int\limits_0^1 \mathrm{d}x_1 \mathrm{d}x_2 f_1(x_1) f_2(x_2) \delta(z - x_1 x_2). \tag{88}$$

Since we consider $q\bar{q}$ collisions, the function $P_{ij}^{(0)}$ needs to be substituted with the Altarelli-Parisi kernels $P_{qq}^{(0)}$ Eq. (81). In fact, a glance at Eq. (86) shows that the remaining divergences in our computation are proportional to $P_{qq}^{(0)}$ and have exactly the right form to be canceled by the renormalization of parton distribution functions Eq. (87). We use Eq. (87) in leading order cross section, expand it through $\mathcal{O}(\alpha_s)$ and combine the additional terms with the NLO cross section Eq. (86). We observe that all $1/\epsilon$ terms cancel and we find

$$2s\mathrm{d}\sigma^{\text{NLO}} = \langle F_{\text{LV}}^{\text{fin}}(1,2) + \frac{\alpha_s}{2\pi}\frac{2\pi^2}{3} C_F F_{\text{LM}}(1,2)\rangle + \langle \mathcal{O}_{\text{NLO}} F_{\text{LM}}(1,2,4)\rangle$$
$$+ \frac{\alpha_s}{2\pi}\int\limits_0^1 \mathrm{d}z \left[P_{qq}^{(0)}(z)\ln\frac{s}{\mu^2} - P_{qq,R}^{(\epsilon)}(z)\right]\langle\frac{F_{\text{LM}}(z1,2)}{z} + \frac{F_{\text{LM}}(1,z2)}{z}\rangle. \tag{89}$$

Since the NLO contribution to the partonic cross section Eq.(89) contains no $1/\epsilon$ singularities, all quantities there can be computed in four-dimensional space-time. We note that Eq. (89) provides a fully-differential cross-section for the lepton pair production in partonic collisions since no integration over resolved phase-space has been performed there. The NLO contribution to the hadronic cross section is obtained by convoluting the differential partonic cross section Eq. (89) with parton distribution functions.

Computation of NLO QCD corrections to dilepton pair production described in this Section shows the importance of soft and collinear limits of the matrix elements for computing physical infra-red safe quantities. Although our discussion focused on a particular process, it's main ingredients are universal and can be used to construct a *general algorithm* for NLO computations [10, 11]. Extensions of these approaches to even higher orders are also possible; in fact, recently several methods were proposed that can be used to perform fully-differential NNLO QCD computations [14]. Making these methods computationally more efficient is very important for extending their applicability to more complex processes and significant effort currently goes into that.
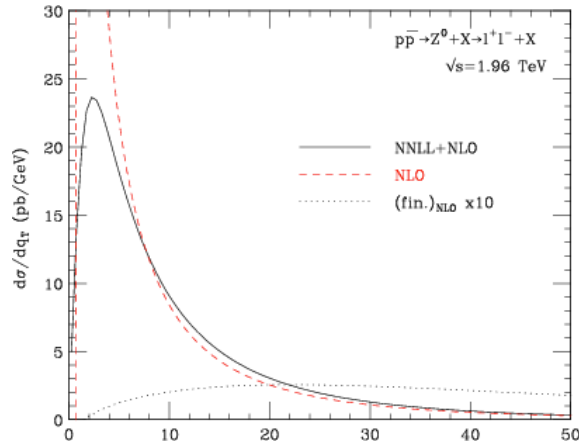
Fig. 6: Transverse momentum distribution of a lepton pair at the Tevatron. Fixed order and resummed results are compared [20].

Going back to our result Eq. (89), we can ask what will happen if we use it to compute kinematic distributions of a lepton pair. Recall that we started thinking about NLO QCD contribution to dilepton production cross section because the leading order result did not properly describe the transverse momentum distribution of a lepton pair. Using next-to-leading order predictions for the cross section, we find a refined description of the invariant mass and the rapidity distributions of a lepton pair. Although its qualitative features are similar to what we observed at leading order, they describe experimental data much better and their dependence on unphysical parameters such as the renormalization and the factorizations scales is significantly reduced. We also find a non-trivial transverse momentum distribution as shown in Fig. 6 which is a clear improvement over the leading order result. However, although the NLO QCD distribution provides a decent description of the experimental results (cf. Fig. 5) at high $p_\perp$, it keeps growing with the decrease of the transverse momentum in contrast to the experimental result that reaches maximum at finite $p_\perp$ and decrease after that. Therefore, in comparison to leading order computations, we have a partial success with understanding the $p_\perp$-spectrum of dilepton pairs since, apparently, its high-$p_\perp$ region is amenable to perturbative treatment, whereas something more complex occurs at low transverse momenta. We will try to understand what is happening there in the next Section.

5 Small-$p_\perp$ resummation

We will discuss the small-$p_\perp$ region in the context of QED, ignoring all complications related to the non-Abelian nature of QCD. However, the result that we will get will be valid in QCD as well provided that we trade electric charges for color ones. The QED analysis that we describe below follows the classic paper by Parisi and Petronzio [21]; their discussion of the problem was instrumental in setting up the stage for a modern understanding of small-$p_\perp$ resummation that is a very important topic for applications of perturbative QCD to hadron collider processes (see e.g. Ref. [22] for contemporary perspective).

We consider production of muon pairs in electron-positron collisions. We assume that muons are heavy and do not radiate photons. We are interested in understanding QED effects that are related to initial state radiation. This is very similar to gluon emissions in $q\bar{q}$ annihilation to lepton pairs studied in the previous Section.

We are interested in the transverse momentum distribution of a muon pair in the limit when the transverse momentum of a pair $p_\perp$ becomes very small. We will see that in each order of perturbation theory there are terms that contain *two* powers of $L = \log s/p_\perp^2 \gg 1$ per power of $\alpha \ll 1$. As the transverse momentum decreases, the logarithm increases whereas α stays fixed. Hence, we can reach

values of $p_\perp$ such that

$$\alpha L^2 \sim 1, \quad \alpha L \ll 1. \tag{90}$$

The appearance of αL^2 in each order of perturbative expansion does not allow us to truncate the series and forces us to resum contributions to perturbative cross sections that scale as $\sigma^{(k)} \sim \sigma_0 \ \alpha^k L^{2k} \sim \sigma_0, \quad k = 0, 1, 2, ...$ Clearly, all other contributions, for examples $\sigma^{(k)} \sim \sigma_0 \ \alpha^{k+1} L^{2k} \sim \alpha \ \sigma_0 \ll \sigma_0$, are small and can be neglected.

Two powers of $p_\perp$-dependent logarithms per power of α can only be generated by photon emissions that are *soft and collinear at the same time*. As we already know from the previous Section, a single *soft* photon emission can be described by the eikonal factor

$$\lim_{k \to 0} \overline{|\mathcal{M}(e^+, e^-; k)|}^2 \approx e^2 \frac{2p_1 p_2}{(p_1 k)(p_2 k)} \overline{|\mathcal{M}(e^+, e^-)|}^2. \tag{91}$$

Consider now the head-on collision where $p_1 = (E_1, 0, 0, E_1)$ and $p_2 = (E_2, 0, 0, -E_2)$. We parametrize the photon momentum as $k = \omega(1, \sin\theta\cos\phi, \sin\theta\sin\phi, \cos\theta)$. The eikonal factor becomes

$$\frac{2p_1 p_2}{(p_1 k)(p_2 k)} = \frac{4E_1 E_2}{E_1 E_2 \omega^2 (1 - \cos\theta)(1 + \cos\theta)} = \frac{4}{\vec{k}_\perp^2}, \tag{92}$$

where we used $|\vec{k}_\perp| = \omega \sin\theta$ for the absolute value of the photon transverse momentum. Hence, we find

$$|\mathcal{M}(e^+, e^-; k)|^2 \approx \frac{4e^2}{\vec{k}_\perp^2} \ |\mathcal{M}(e^+, e^-)|^2. \tag{93}$$

We need to understand what happens if we integrate the radiation amplitude squared Eq. (93) over the photon phase space. Since the photon is soft we can neglect the photon momentum k in the δ-function that enforces energy-momentum conservation. We then identify the $\mu^+\mu^-$ transverse momentum $p_\perp$ with the photon transverse momentum. The phase space element reads

$$\frac{\mathrm{d}^3 k}{(2\pi)^3 2\omega} = \frac{\mathrm{d}\cos\theta \mathrm{d}\phi \omega \mathrm{d}\omega}{16\pi^3} = \frac{1}{8\pi^2} \ \mathrm{d}\cos\theta \ \omega \mathrm{d}\omega. \tag{94}$$

Since $k_\perp = \omega \sin\theta$, we can express the emission angle θ in terms of the transverse momentum

$$\cos\theta = \pm\sqrt{1 - \frac{k_\perp^2}{\omega^2}}. \tag{95}$$

Changing variables $\cos\theta \to k_\perp$ in Eq. (94), we obtain

$$\frac{\mathrm{d}^3 k}{(2\pi)^3 2\omega} = \frac{1}{8\pi^2} \frac{2k_\perp \mathrm{d}k_\perp \mathrm{d}\omega}{\sqrt{\omega^2 - k_\perp^2}}. \tag{96}$$

We are interested in computing the real-emission cross section in the logarithmic approximation. Therefore, we write

$$\frac{\mathrm{d}\omega}{\sqrt{\omega^2 - k_\perp^2}} \approx \frac{\mathrm{d}\omega}{\omega}. \tag{97}$$

Integration over ω will have to be cut at $\omega \approx k_\perp$ from below and at $\omega \approx \sqrt{s}$ from above. The first condition follows from the approximation in Eq. (97); the second condition from the requirement that the emitted photon is soft.

Combining the matrix element with the phase space parametrization we obtain

$$\frac{d\sigma_\gamma}{dk_\perp^2} = \sigma_0 \frac{2\alpha}{\pi} \frac{1}{k_\perp^2} \int\limits_{k_\perp}^{\sqrt{s}} \frac{d\omega}{\omega} = \sigma_0 \frac{\alpha}{\pi} \frac{\ln \frac{s}{k_\perp^2}}{k_\perp^2}. \tag{98}$$

This formula shows once again that the transverse momentum distribution computed through first order in perturbation theory grows strongly in the limit $k_\perp \to 0$. In fact, the growth is so strong that is can overcome suppression provided by the fine structure constant α and make the radiation cross section larger than the Born one. Clearly, perturbative expansion in α becomes meaningless in this case.

It is important to understand the role of virtual corrections in shaping the transverse momentum distribution. The virtual corrections reside at $k_\perp = 0$. To understand how they can be included in our computation, we calculate the cross section to produce a $\mu^+ \mu^-$ pair with a transverse momentum between 0 and $p_\perp$. We define

$$\Sigma(p_\perp) = \frac{1}{\sigma_0} \int\limits_0^{p_\perp^2} \frac{d\sigma_{\text{tot}}}{dk_\perp^2} dk_\perp^2. \tag{99}$$

Expanding the total cross section in powers of α and introducing $d\sigma_{\gamma+V}$ to denote $\mathcal{O}(\alpha)$ contribution to the cross section that includes both real emission and virtual corrections, we write

$$\Sigma(p_\perp) - 1 = \frac{1}{\sigma_0} \int\limits_0^{p_\perp^2} \frac{d\sigma_{\gamma+V}}{dk_\perp^2} dk_\perp^2 = \frac{1}{\sigma_0} \int\limits_0^{s} \frac{d\sigma_{\gamma+V}}{dk_\perp^2} dk_\perp^2 - \frac{1}{\sigma_0} \int\limits_{p_\perp^2}^{s} \frac{d\sigma_\gamma}{dk_\perp^2} dk_\perp^2 \tag{100}$$

The first term – given by an integral from 0 to s represents the radiative correction to the total cross section for $\mu^+ \mu^-$ production in the logarithmic approximation, with both real and virtual corrections included. Such corrections contain no large logarithms and, since we only care about terms that scale as αL^2, can be set to zero. This identification, effectively, provides an infra-red regularization prescription that allows us to define the integrand at $k_\perp^2 = 0$ *without computing virtual corrections*. Thus, we require

$$\frac{1}{\sigma_0} \int\limits_0^{s} \frac{d\sigma_{\gamma+V}}{dk_\perp^2} dk_\perp^2 = \mathcal{O}(\alpha_s) \Rightarrow 0, \tag{101}$$

and use Eq. (100) to derive

$$\Sigma(p_\perp) = 1 - \frac{\alpha}{2\pi} \ln^2 \frac{s}{p_\perp^2}. \tag{102}$$

It is possible to re-write the integrand in Eq. (100) in such a way that Eq. (102) is obtained by the direct integration. The idea is to introduce the plus-distribution. We define

$$\frac{d\sigma}{\sigma_0 dk_\perp^2} = \delta(k_\perp^2) + \frac{\alpha}{\pi} \left[\frac{1}{k_\perp^2} \ln \frac{s}{k_\perp^2} \right]_+, \tag{103}$$

where the +-prescription is defined on an interval $k_\perp^2 \in [0, s]$. To illustrate how this works, we compute the total cross section using Eq. (103). We find

$$\Sigma(s^{1/2}) = \frac{1}{\sigma_0} \int\limits_0^{s} \frac{d\sigma}{dk_\perp^2} dk_\perp^2 = \int\limits_0^{s} dk_\perp^2 \left(\delta(k_\perp^2) + \frac{\alpha}{\pi} \left[\frac{1}{k_\perp^2} \ln \frac{s}{k_\perp^2} \right]_+ \right)$$
$$= 1 + \frac{\alpha}{\pi} \int\limits_0^{s} \frac{dk_\perp^2}{k_\perp^2} \ln \left(\frac{s}{k_\perp^2} \right) (1 - 1) = 1. \tag{104}$$

To extend this result to higher orders in α, we need to understand multiple photon emissions in the soft approximation. It is well-known [5] that soft photon emissions completely factorize so that a n-photon emission amplitude reads

$$\mathcal{M}_n = e^n \prod_{i=1}^{n} \left(\frac{p_1 \epsilon_i}{p_1 k_i} - \frac{p_2 \epsilon_i}{p_2 k_i} \right) \mathcal{M}_0. \tag{105}$$

Here ϵ_i and k_i are the polarization vector and the four-momentum of the i-th photon, respectively. Squaring $\mathcal{M}_n$ and summing over photon polarizations, we obtain

$$\sum_{\text{pol}} |\mathcal{M}_n|^2 = |\mathcal{M}_0|^2 \prod_{i=1}^{n} e^2 \frac{2p_1 p_2}{(p_1 k_i)(p_2 k_i)} \tag{106}$$

It follows from Eq. (106) that the emission probability of each of the n photons is determined by an eikonal factor studied at the beginning of this Section. We use the expression for the amplitude squared to compute the transverse momentum distribution of the muon pair. It reads

$$\frac{1}{\sigma_0} \frac{\mathrm{d}^2 \sigma_n}{\mathrm{d}^2 \vec{p}_\perp} = \frac{1}{n!} \int \prod_{i=1}^{n} \frac{\mathrm{d}^3 \vec{k}_i}{(2\pi)^3 2\omega_i} \left[\frac{e^2 2 p_1 p_2}{(p_1 \cdot k_i)(p_2 \cdot k_i)} \right] \delta^{(2)} \left(\vec{p}_\perp - \sum_i^n \vec{k}_{\perp,i} \right). \tag{107}$$

To proceed further, we need to find a way to factorize the δ-function that contains the sum of photon transverse momenta preventing us from integrating over any of them. To this end, we write the δ-function as an integral over auxiliary two-component vector that we will refer to as the "impact parameter"

$$\delta^{(2)} \left(\vec{p}_\perp - \sum \vec{k}_{i,\perp} \right) = \int \frac{\mathrm{d}^2 \vec{b}}{(2\pi)^2} e^{-i\vec{b} \left(\vec{p}_\perp - \sum_{i=1}^{n} \vec{k}_{i,\perp} \right)}. \tag{108}$$

Using this equation, we re-write the cross section for emitting n-photon, integrating along the way over their energies. We find

$$\frac{1}{\sigma_0} \frac{\mathrm{d}^2 \sigma_n}{\mathrm{d}^2 \vec{p}_\perp} = \frac{1}{n!} \int \frac{\mathrm{d}^2 \vec{b}}{(2\pi)^2} e^{-i\vec{b}\vec{p}_\perp} \left[\frac{\alpha}{\pi} \int \frac{\mathrm{d}^2 \vec{k}_\perp}{\pi \vec{k}_\perp^2} \ln \frac{s}{k_\perp^2} e^{-i\vec{b}\vec{k}_\perp} \right]^n, \tag{109}$$

where the integration over $k_\perp$ is cut at $k_\perp^2 = s$. The apparent singularity at $k_\perp = 0$ is regulated in the same way as in case of the single photon emission – we introduce a plus-prescription ensuring the cancellation of real and virtual corrections for fully inclusive quantities.

It is clear from Eq. (109) that the summation over n can be performed in a straightforward manner. We obtain

$$\frac{\mathrm{d}\sigma}{\sigma_0 \mathrm{d}^2 \vec{p}_\perp} = \sum_{n=0}^{\infty} \frac{\mathrm{d}^2 \sigma_n}{\sigma_0 \mathrm{d}^2 \vec{p}_\perp} = \int \frac{\mathrm{d}^2 \vec{b}}{(2\pi)^2} e^{-i\vec{b}\vec{p}_\perp} \hat{\sigma}(b), \tag{110}$$

where

$$\hat{\sigma}(b) = e^{\frac{\alpha}{\pi} \nu(b)}, \quad \nu(b) = \int\limits_{0}^{|k_\perp| < \sqrt{s}} \frac{\mathrm{d}^2 \vec{k}_\perp}{\pi} \left[\frac{1}{k_\perp^2} \ln \frac{s}{k_\perp^2} \right]_+ e^{i\vec{b}\vec{k}_\perp}. \tag{111}$$

The result given in Eq. (110) is the differential cross section for producing a muon pair with momentum $p_\perp$ in the double logarithmic approximation. This formula is implicit because of the integration over the impact parameter. In what follows, we will compute some of the integrals explicitly and arrive at the result for the cross section that is more transparent. In particular, we are interested in understanding if the differential cross section in Eq. (110) exhibits a turnover at low values of the transverse momentum, a feature that was clearly missing in the result of the next-to-leading order computation.

To proceed with sufficiently complicated integrations in Eq. (110), we note that the integrals in Eqs. (110,111) depend on $\vec{p}_\perp$, $\vec{b}$ and s. From Eq. (110) it follows that $b \sim 1/p_\perp$. Since $\sqrt{s} \gg p_\perp$, $sb^2 \gg 1$. We need to compute the various quantities in Eqs.(110,111) taking advantage of these hierarchical relations between the various parameters that appear there.

We begin with the computation of $\nu(b)$. We perform the angular integration and find

$$\nu(b) = \int_0^{|k_\perp|<\sqrt{s}} \frac{\mathrm{d}^2\vec{k}_\perp}{\pi} \left[\frac{1}{k_\perp^2} \ln \frac{s}{k_\perp^2}\right]_+ e^{i\vec{b}\vec{k}_\perp} = \int_0^{|k_\perp|<\sqrt{s}} \frac{\mathrm{d}k_\perp^2}{k_\perp^2} \ln \frac{s}{k_\perp^2} \int_0^{2\pi} \frac{\mathrm{d}\varphi}{2\pi} \left[e^{ibk_\perp \cos\varphi} - 1\right]$$

$$= \int_0^s \frac{\mathrm{d}k_\perp^2}{k_\perp^2} \ln \frac{s}{k_\perp^2} \left[J_0(b_\perp k_\perp) - 1\right], \tag{112}$$

where $J_0(x)$ is the Bessel function of the first kind.[4] To make the integral more tractable, we change variables $k_\perp \to \xi = b_\perp k_\perp$ and obtain

$$\nu(b) = 2 \int_0^{\sqrt{s}b} \frac{\mathrm{d}\xi}{\xi} \ln \left[\frac{sb^2}{\xi^2}\right] \left[J_0(\xi) - 1\right]. \tag{113}$$

We now integrate by parts, use $J_0(0) = 1$, $\mathrm{d}J_0(\xi)/\mathrm{d}\xi = -J_1(\xi)$, and find

$$\nu(b) = \frac{1}{2} \ln^2(sb^2) \left(J_0(\sqrt{s}b) - 1\right) + 2 \int_0^{\sqrt{s}b} \mathrm{d}\xi \left[\ln(sb^2) \ln\xi - \ln^2\xi\right] J_1(\xi). \tag{114}$$

Since $J_0(\sqrt{s}b) \sim (\sqrt{s}b)^{-1/2}$ and since the integral with $J_1(\xi)$ converges at infinity, we can neglect quite a number of terms in Eq. (114) if we focus on the double logarithmic contributions. We find

$$\nu(b) \approx -\frac{1}{2} \ln^2(sb^2) + \mathcal{O}(\ln(sb^2)). \tag{115}$$

The cross section becomes

$$\frac{1}{\sigma_0} \frac{\mathrm{d}^2\sigma}{\mathrm{d}^2\vec{p}_\perp} = \int \frac{\mathrm{d}^2\vec{b}}{(2\pi)^2} e^{-i\vec{b}\vec{p}_\perp} e^{-\frac{\alpha}{2\pi}\ln^2(sb^2)} = \frac{1}{2\pi} \int_0^\infty \mathrm{d}b\, b\, J_0(bp_\perp)\, e^{-\frac{\alpha}{2\pi}\ln^2(sb^2)}, \tag{116}$$

where in the last step we integrated over directions of the vector $\vec{b}$. To proceed further, we change integration variables $b \to y$ where $b = y/p_\perp$ and expand the integrand assuming that $\alpha \ln^2 s/p_\perp \sim 1$ but $\alpha \ln s/p_\perp \ll 1$. We obtain

$$\frac{1}{\sigma_0} \frac{\mathrm{d}^2\sigma}{\mathrm{d}^2\vec{p}_\perp} = \frac{1}{2\pi p_\perp^2} e^{-\frac{\alpha}{2\pi}\ln^2 \frac{s}{p_\perp^2}} \int_0^\infty \mathrm{d}y\, y\, J_0(y) \left(1 - \frac{2\alpha}{\pi} \ln \frac{s}{p_\perp^2} \ln y + ...\right), \tag{117}$$

where ellipses stand for $\mathcal{O}(\alpha^2)$ terms that can be neglected. Integration over y can be performed using the known results for definite integrals of the Bessel functions

$$\int_0^\infty \mathrm{d}y\, y\, J_0(y) = 0, \qquad \int_0^\infty \mathrm{d}y\, J_0(y) \ln y = -1. \tag{118}$$

---

[4]Vast amount of information about special functions in general and Bessel functions in particular can be found in a classic book by Abramowitz and Stegun [23].

Using these results in Eq. (117), we derive the resummed cross section

$$\frac{1}{\sigma_0} \frac{\mathrm{d}^2 \sigma}{\mathrm{d}^2 \vec{p}_\perp} = \frac{\alpha}{\pi^2 p_\perp^2} \ln \frac{s}{p_\perp^2} e^{-\frac{\alpha}{2\pi} \ln^2 \frac{s}{p_\perp^2}}. \tag{119}$$

It follows from Eq. (119) that the resummed $p_\perp$ distribution has a turnover, in contrast to the $p_\perp$ distribution that is predicted by a single photon emission. The distribution peaks at

$$p_\perp^{\max} \approx \sqrt{s} e^{-\frac{\pi}{2\alpha}}. \tag{120}$$

Note that $p_\perp^{\max}$ has a *non-analytic* dependence on the fine structure constant α and, for this reason, it can not be obtained in any finite order of perturbation theory.[5]

The transverse momentum distribution of a lepton pair in QED reflects all the subtleties of a resummed computation, but can be performed analytically until the very end thanks to the simplicity of this case. It is useful to take a look at the QCD formula that describes resummed transverse momentum distribution of a lepton pair in hadron collisions under the assumption that a pair is produced through a decay of an intermediate on-shell Z-boson; the Z-boson itself is produced in the $q\bar{q}$ annihilation. The resummed cross section reads [24]

$$\frac{\mathrm{d}\sigma_Z}{\mathrm{d}p_\perp^2} \approx \sum_q \frac{\sigma_0^{q\bar{q}}}{2} \int_0^\infty \mathrm{d}b\, b\, J_0(bp_\perp) e^{-S(b, M_Z)} \int_0^1 \mathrm{d}x_1 \mathrm{d}x_2 \delta\left(x_1 x_2 - \frac{M_Z^2}{S}\right) \tag{121}$$
$$\times \left[q(x_1, b_0/b)\bar{q}(x_2, b_0/b) + q \leftrightarrow \bar{q}\right],$$

where s is the hadronic center-of-mass energy squared, $\sigma_0^{q\bar{q}} = \pi\sqrt{2} G_F M_Z^2 (V_q^2 + A_q^2)/(3S)$, $b_0 = 2e^{-\gamma_E}$ and

$$S(b, Q) = \int_{(b_0/b)^2}^{Q^2} \frac{\mathrm{d}q^2}{q^2} \left[\ln \frac{Q^2}{q^2} A(\alpha_s(q)) + B(\alpha_s(q))\right], \tag{122}$$

where the two functions A and B can be computed in QCD perturbation theory

$$A(\alpha_s) = \sum_{n=1}^\infty \left(\frac{\alpha_s}{2\pi}\right)^n A_n, \quad B(\alpha_s) = \sum_{n=1}^\infty \left(\frac{\alpha_s}{2\pi}\right)^n B_n. \tag{123}$$

It is easy to see the similarities between the resummed cross sections in QCD and QED. However, an interesting feature of the QCD result is the appearance of the transverse momentum in parton distribution functions. Indeed, since $b \sim p_\perp$ and since the *factorization scale* for parton distribution functions in Eq. (121) is chosen to be $1/b$, it appears that one can only resum the $\ln \sqrt{s}/p_\perp$ contributions provided that the factorization scale is proportional to $p_\perp$. We already mentioned the dependence of parton distribution functions on the factorization scale when we talked about fixed order computations and the relation between bare and physical parton distribution functions. In the next Section we will discuss the origin of parton distribution functions and the physical meaning of the factorization scale.

6 Partons and their evolution

We have seen in the previous Section that the resummed formula for the transverse momentum distribution includes parton distribution functions evaluated at a particular scale $1/b \sim p_\perp$ which is correlated with the transverse momentum of the produced lepton pair. If we want to understand why it is so, we

---

[5]However, the vaue of $p_\perp$ for which the distribution reaches its maximum is *outside* the validity range of our computation since $\alpha/\pi \ln(\sqrt{s}/p_\perp^{\max}) \sim 1$.

need to understand the physics behind parton distribution functions. Similar to the discussion in the previous Section, it is much easier to discuss this problem in QED first and then explain how the QED results generalize to the QCD case.

Consider a process where an electron collides with a target that we will denote as X and produces a final state with a photon and another particle Y, $e + X \rightarrow \gamma + Y$. We will be interested in a situation where the final state photon is emitted in the forward direction, i.e. it follows the momentum of the incoming electron. To describe this kinematic situation, we employ the *collinear* approximation to the matrix element squared that we already used when discussing the NLO QCD corrections to the Drell-Yan process. We write

$$\sum_{\text{pol}} |\mathcal{M}_{e(p)+X\rightarrow\gamma+Y}|^2 \approx \frac{-2e^2}{(p-q)^2} \frac{1+z^2}{z(1-z)} \sum_{\text{pol}} |\mathcal{M}_{e(zp)+X\rightarrow Y}|^2, \tag{124}$$

where q is the four-momentum of the emitted photon that is parametrized as

$$q = (1-z)p + \beta\bar{p} + q_\perp. \tag{125}$$

Here $(1 - z)$ is the fraction of the original electron energy carried away by the photon. The photon emission angle θ_γ is assumed to be small. The transverse momentum and the component of the four-momentum q along the complementary light-cone direction $\bar{p}$, β, scale as $q_\perp/\sqrt{s} \sim \theta_\gamma \ll 1$ and $\beta \sim \theta_\gamma^2 \ll 1$.

We use the approximate formula for the matrix element squared Eq. (124) to compute the cross section

$$\mathrm{d}\sigma_{e+X\rightarrow\gamma+Y} = \int [\mathrm{d}q][\mathrm{d}p_Y](2\pi)^4\delta^{(4)}(p+p_X-q-p_Y)\frac{1}{4(p_X\cdot p)}\frac{1}{2}\sum_{\text{pol}} |\mathcal{M}_{e(p)+X\rightarrow\gamma+Y}|^2$$

$$\approx \int [\mathrm{d}q][\mathrm{d}p_Y](2\pi)^4\delta^{(4)}(zp+p_X-p_Y)\frac{-2e^2}{(p-q)^2}\frac{1+z^2}{1-z}\frac{1}{4(p_X\cdot zp)}\frac{1}{2}\sum_{\text{pol}} |\mathcal{M}_{e(zp)+X\rightarrow Y}|^2 \tag{126}$$

$$\approx \int [\mathrm{d}q]\frac{-2e^2}{(p-q)^2}\frac{1+z^2}{1-z}\ \mathrm{d}\sigma(e(zp)+X\rightarrow Y).$$

To arrive at the final formula, we used the collinear approximation for the photon momentum $q \rightarrow (1-z)p$ in the energy-momentum conserving δ-function and combined the reduced matrix element, the δ-function, $[\mathrm{d}p_Y]$ etc. into a differential cross section for the process $e + X \rightarrow Y$ where the four-momentum of the incoming electron is zp. To proceed further, we need to write the integration measure $[\mathrm{d}q]$ in Eq.(126) in a convenient way. It is easy to see that the following formula holds in the collinear $\theta_\gamma \rightarrow 0$ limit

$$\frac{\mathrm{d}^3q}{(2\pi)^3 2q_0}\frac{-2e^2}{(p-q)^2} = \frac{\alpha}{2\pi}\frac{\mathrm{d}q_\perp^2}{q_\perp^2}\ \mathrm{d}z. \tag{127}$$

Using this result in Eq. (126), we derive the forward photon emission contribution to the cross section of the process $e + X \rightarrow \gamma + Y$

$$\mathrm{d}\sigma_{e+X\rightarrow\gamma+Y} = \frac{\alpha}{2\pi}\int_0^1 \mathrm{d}z\,\frac{1+z^2}{1-z}\int\frac{\mathrm{d}q_\perp^2}{q_\perp^2}\,\mathrm{d}\sigma(e(zp)+X\rightarrow Y). \tag{128}$$

There are three problems with the cross section formula shown in Eq. (128). The first problem is that integration over z diverges at $z = 1$. The second problem is that integration over $q_\perp$ appears to be unrestricted from above. The third problem is that integration over $q_\perp$ diverges at $q_\perp = 0$.

It is easy to understand that the two last problems are, essentially, self-inflicted. Indeed, a divergence at large values of $q_\perp$ is related to the approximate treatment of the phase space that was justified because $q_\perp$ was considered small, $q_\perp \ll \sqrt{s}$. Therefore, with the logarithmic accuracy, integration over $q_\perp$ should be cut at some value $q_\perp = q_{\perp,\mathrm{max}} \sim \sqrt{s}$. The exact value of $q_{\perp,\mathrm{max}}$ is, at this point, impossible to determine but since the dependence on this parameter is logarithmic and, therefore, weak, we do not need to be careful about it. Since, parametrically, $q_{\perp,\mathrm{max}}$ is of the order of the center of mass energy of the collision, we will use $q_{\perp,\mathrm{max}} = \sqrt{s}$ in what follows. Physically, it corresponds to the largest transverse momentum of the photon that we believe can still be be treated in the collinear approximation. Similarly, the divergence at small $q_\perp$ is related to our treatment of an incoming electron as a massless particle. This approximation is only justified for $q_\perp \gg m_e$ and, therefore, we should cut the integration over $q_\perp$ from below at $q_\perp \sim m_e$. Again, the *exact* value of the lower integration boundary is not important if we are content with the logarithmic accuracy of the calculation.

The divergence at $z = 1$ is more subtle. Since $q \approx (1-z)p$, $z \to 1$ corresponds to a situation where a *soft* photon is emitted. As we know from the discussion of the NLO computations, the emission of soft photons is indeed divergent and the divergence is canceled by the virtual corrections. The virtual corrections corresponds to elastic scattering process and, therefore, reside at $z = 1$. We can regulate the real emission contribution and introduce virtual corrections by writing the *inclusive* production cross section for the particle Y in the following way

$$\mathrm{d}\sigma_{e+X \to Y}^{\mathrm{incl}} = \int\limits_0^1 \mathrm{d}z \ \mathrm{d}\sigma(e(zp) + X \to Y) \, f_{e/e}(z,s), \tag{129}$$

where

$$f_{e/e}(z,s) = \delta(1-z) + \frac{\alpha}{2\pi}\left(\left[\frac{1+z^2}{1-z}\right]_+ + V\delta(1-z)\right)\log\frac{s}{m_e^2}. \tag{130}$$

Note that the structure of Eq. (129) is analogous to what we do in hadron collider physics when we compute hadronic cross sections by convoluting parton distributions with partonic cross sections. We therefore interpret $f_{e/e}(z,s)$ as the distribution of an "electron parton" in an original physical electron generated by the (real and virtual) emissions of collinear photons. Note that similar to parton distribution functions, the function $f_{e/e}(z,s)$ has two arguments: the first argument describes the energy fraction of the incoming electron carried by a parton, the second argument refers to an upper boundary imposed on $q_\perp$ integration which, effectively, corresponds to a definition of the kinematic region where collinear description of the final state is considered to be sensible.

We expect that collinear photon emissions generate a non-trivial energy spectrum of the "electron partons", but the number of electrons remains unchanged. This implies

$$\int\limits_0^1 \mathrm{d}z \, f_{e/e}(z,s) = 1 \quad \Rightarrow \quad f_{e/e}(z,s) = \delta(1-z) + \frac{\alpha}{2\pi}\left[\frac{1+z^2}{1-z}\right]_+ \ln\frac{s}{m_e^2}. \tag{131}$$

Note that the "electron number conservation" condition allows us to fix virtual corrections without computing them. The plus-distribution that multiplies the logarithm $\ln s/m_e^2$ is the electron splitting function

$$P_{ee} = \left[\frac{1+z^2}{1-z}\right]_+ = 2D_0(z) - (1+z) + \frac{3}{2}\delta(1-z). \tag{132}$$

Note that, up to a color factor, it coincides with the quark splitting function $P_{qq}^{(0)}$ discussed in Section 3.

The electron distribution function Eq. (131) has a number of important properties. If the collision energy is small $s \sim m_e^2$, the electron PDF reads $f_{e/e}(z,m_e^2) = \delta(1-z)$. This implies that collinear

emissions at low energies do not happen often. If, on the other hand, $s \gg m_e^2$, $f_{e/e}(z, s)$ becomes very sensitive to additional radiation since corrections to the elastic piece are controlled by the parameter $\alpha/\pi \log(s/m_e^2)$ and not by the fine structure constant α. Although in QED this parameter becomes close to one at inconceivably large energies, in QCD this happens earlier, which implies that the resummation of these logarithmically enhanced terms needs to be carried out. We will return to this point shortly.

We have discussed the process $e + X \to \gamma + Y$ in the collinear approximation. However, it is also possible to consider a process $e + X \to e + Y$ which corresponds to $\gamma + X \to Y$ elastic process. Working in the collinear approximation for that process, one can define a distribution function of a *photon parton* in the physical electron. The corresponding function reads

$$f_{e/\gamma}(z, s) = \frac{\alpha}{2\pi} \frac{1 + (1 - z)^2}{z} \ln \frac{s}{m_e^2}. \tag{133}$$

Note that $f_{e/\gamma}(z, m_e^2) = 0$, i.e. there are no photons in an electron if the radiation is suppressed.

It is instructive to compute the average momentum carried by the photon and electron constituents in a physical electron. Since the two distribution functions originate from the same splitting $e \to e + \gamma$ with the only difference that in one case we tag an electron and in the other case a photon, we expect that the average momenta carried by a photon and by an electron sum up to the momentum of the incoming electron. Clearly, this is true in every individual splitting and, therefore, it should be true on average. Performing explicit computation of the energy fractions

$$\langle z \rangle_e = \int\limits_0^1 \mathrm{d}z \, f_{e/e}(z, s) \, z = 1 - \frac{2\alpha}{3\pi} \ln \frac{s}{m_e^2}, \quad \langle z \rangle_\gamma = \int\limits_0^1 \mathrm{d}z \, f_{\gamma/e}(z, s) \, z = \frac{2\alpha}{3\pi} \ln \frac{s}{m_e^2}, \tag{134}$$

we find

$$\langle z \rangle_e + \langle z \rangle_\gamma = 1, \tag{135}$$

in agreement with the expectations.

We would like to generalize these results to the case when multiple photons are emitted; we will start with the case of two photons. There are two diagrams that contribute in this case and a $1/2!$ factor in the phase space that is necessary to include because photons are identical particles. The two diagrams differ by order in which photons are emitted off the incoming electron line. We note that these diagrams change the production cross section by an amount proportional to $\mathcal{O}(\alpha^2)$. Since we are only interested in contributions where each power of α is accompanied by a large logarithm $\ln(s/m_e^2)$, we need to understand how these diagrams can generate two powers of $\ln(s/m_e^2)$.

To see this, it is sufficient to compare propagators of an electron after the first and the second emissions. Consider a diagram where electron emits a photon with momentum q_1 and then a photon with momentum q_2. Electron propagator after the first emission scales as $1/q_{1,\perp}^2$, so that integration over $q_{1,\perp}$ is already logarithmic. The integration over $q_{2,\perp}$ can only be logarithmic if $q_{1,\perp} \ll q_{2,\perp}$ so that $q_{1,\perp}$ can be neglected in the electron propagator after the second emission. Clearly, everything that has just been said applies also to the second diagram – where electron first emits a photon with momentum q_2 and then the photon with momentum q_1 – after the replacement $q_1 \leftrightarrow q_2$. Hence, to account for *both diagrams*, we can take the contribution of the first one and remove the $1/2!$ symmetry factor from the phase space.

The constraints on the transverse momenta of the emitted photons define integration regions over $q_\perp$ that lead to the double-logarithmic enhancement of these $\mathcal{O}(\alpha^2)$ contributions. Since the transverse momentum ordering described above implies sequential approach of the collinear limits, it is clear that the Sudakov decomposition of the second emission needs to be performed relative to the electron four-momentum *after* the emission of the first photon, i.e.

$$q_1 = (1 - z_1)p + ..., \qquad q_2 = (1 - z_2)z_1 p + ... \tag{136}$$

Generalizing this discussion to arbitrary number of photons and neglecting the possibility that an electron fluctuates into a virtual photon, we obtain the following result for the inclusive cross section

$$\sigma_{e+X\to Y+\text{anything}} = \int\limits_0^1 dz\, f_{e/e}(z,s)\, d\sigma(e(zp) + X \to Y).\tag{137}$$

where

$$f_{e/e}(z,s) = \delta(1-z) + \sum_{n=1}^\infty \left(\frac{\alpha}{2\pi}\right)^n \int\limits_0^1 dz_n P_{ee}(z_n) \int\limits_{m_e^2}^s \frac{dq_{n,\perp}^2}{q_{n,\perp}^2} \times$$

$$\int\limits_0^1 dz_{n-1} P_{ee}(z_{n-1}) \int\limits_{m_e^2}^{q_{n,\perp}^2} \frac{dq_{n-1,\perp}^2}{q_{n-1,\perp}^2} \times \cdots \times \int\limits_0^1 dz_1 P_{ee}(z_1) \int\limits_{m_e^2}^{q_{2,\perp}^2} \frac{dq_{1,\perp}^2}{q_{1,\perp}^2}\ \delta(z_1...z_n - z).\tag{138}$$

This expression appears to be relatively complicated. However, we can re-write it in a more compact form by computing logarithmic derivative of $f_{e/e}(s,z)$ with respect to s. Recall that $\sqrt{s}$ represents the largest value of the transverse momentum of an emitted photon that we agree to treat in the collinear approximation.

It is straightforward to compute the derivative since s appears only as an upper boundary of the left-most integral over $p_\perp$ in each term in Eq. (138). We obtain

$$s\frac{\partial f_{e/e}(z,s)}{\partial s} = \frac{\alpha}{2\pi}\int\limits_0^1 dz_1 P_{ee}(z_1)\left[\delta(z-z_1) + \frac{\alpha}{2\pi}\int\limits_0^1 dz_2 P_{ee}(z_2)\int\limits_{m_e^2}^s \frac{dq_{2,\perp}^2}{q_{2,\perp}^2}\delta(z-z_1z_2) + \cdots\right].\tag{139}$$

We can cast the right-hand side of this equation into a more recognizable expression by removing z_1 from all δ-functions that appear in square brackets in Eq. (139). We use the identity

$$\delta(z - z_1\cdots) = \frac{1}{z_1}\delta(z/z_1 - \cdots),\tag{140}$$

and realize that the expression in square brackets in Eq. (139) can be identified with $1/z_1 f_{e/e}(z/z_1, s)$. Hence, the differential equation Eq. (139) becomes

$$s\frac{\partial f_{e/e}(z,s)}{\partial s} = \frac{\alpha}{2\pi}\int\limits_0^1 \frac{dz_1}{z_1} P_{ee}(z_1) f_{e/e}(z/z_1, s) = \int\limits_0^1 dz_1 dz_2 P_{ee}(z_1) f_{e/e}(z_2, s)\delta(z - z_1z_2).\tag{141}$$

This is the QED version of the celebrated Dokshitzer-Gribov-Altarelli-Parisi (DGLAP) evolution equation [18]. We note that Eq. (141) is not complete since we neglected possible splittings of an electron to a photon or to a positron, but it gives us an idea of how the DGLAP equation looks like and how it appears.

The DGLAP equation can be solved provided that the distribution function is known for some value of s. In the QED case $s = m_e^2$ is special and $f_{e/e}(z, m_e^2) = \delta(1-z)$. We can find $f_{e/e}(z,s)$ for $s \neq m_e^2$ by solving the DGLAP equation Eq. (141).

We will now summarize what we have seen so far. Parton distribution functions naturally appear if we attempt to describe quasi-collinear emissions by colliding particles, including the *elementary ones*. These functions depend on two parameters – the fraction of energy of the incoming particle that a parton carries into a hard collision and the "factorization scale" which, roughly, corresponds to the

$$Q_0 = 3 \text{ GeV}$$

$$xu_V \sim x^{0.7}(1-x)^{3.5}, \quad xd_v \sim x^{0.7}(1-x)^{5.2}$$

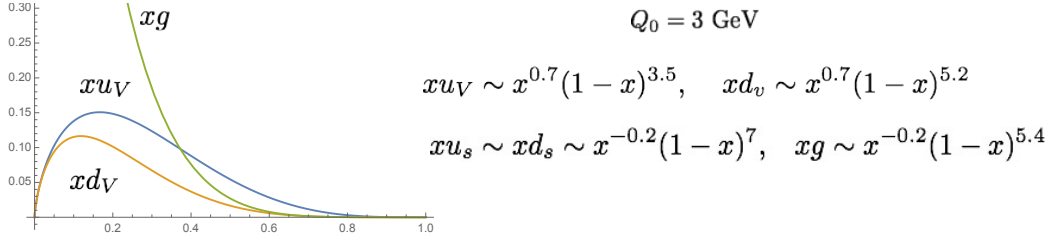$$xu_s \sim xd_s \sim x^{-0.2}(1-x)^7, \quad xg \sim x^{-0.2}(1-x)^{5.4}$$

Fig. 7: Typical proton parton distribution functions at the factorization scale 3 GeV.

maximal value of the transverse momentum that is considered acceptable to be treated in the collinear approximation and whose impact on final state kinematics is ignored. Although we have illustrated these points in the context of QED, they are valid in QCD as well. The most important difference between QED and QCD is that in QCD we do not know the initial condition for parton distribution functions at low factorization scale since QCD is non-perturbative and since we are mostly interested in parton distribution functions of non-elementary particles (protons, neutrons etc.). On the other hand, the QCD evolution equations are very similar to what we derived in QED, with obvious modifications to allow for transitions between different types of partons and the running of the coupling constant. The DGLAP equations in QCD read

$$s\frac{\partial q_i(z,s)}{\partial s} = \frac{\alpha_s(s)}{2\pi} \int\limits_0^1 \frac{\mathrm{d}\xi}{\xi} \Bigg[P_{q\to q}(\xi) q_i(\xi/z) + P_{\bar{q}\to q}(\xi)\bar{q}_i(z/\xi,s)$$

$$+ P_{q'\to q}(\xi) \sum_{j\neq i} \big(q_j(z/\xi,s) + \bar{q}_j(z/\xi,s)\big) + P_{g\to q}(\xi)\, g(z/\xi,s) \Bigg],$$

$$s\frac{\partial \bar{q}_i(z,s)}{\partial s} = \frac{\alpha_s(s)}{2\pi} \int\limits_0^1 \frac{\mathrm{d}\xi}{\xi} \Bigg[P_{q\to q}(\xi) \bar{q}_i(\xi/z) + P_{\bar{q}\to q}(\xi)q_i(z/\xi,s) \tag{142}$$

$$+ P_{q'\to q}(\xi) \sum_{j\neq i} \big(q_j(z/\xi,s) + \bar{q}_j(z/\xi,s)\big) + P_{g\to q}(\xi)\, g(z/\xi,s) \Bigg],$$

$$s\frac{\partial g(z,s)}{\partial s} = \frac{\alpha_s(s)}{2\pi} \int\limits_0^1 \frac{\mathrm{d}\xi}{\xi} \Big[P_{q\to g}(\xi) \sum \big(q_j(z/\xi,s) + \bar{q}_j(z/,\xi))\big) + P_{g\to g}(\xi)\, g(z/\xi,s) \Big].$$

The Altarelli-Parisi splitting functions in QCD are well-known. At leading order, all of them, except P_{gg}, can be obtained from the corresponding QED results. We present the leading order splitting functions here for completeness

$$P_{q\to q} = C_F \left[\frac{1+z^2}{1-z}\right]_+, \qquad P_{q\to g} = C_F \frac{1+(1-z)^2}{z}, \qquad P_{g\to q} = T_R(z^2 + (1-z)^2),$$

$$P_{g\to g} = 2C_A \left[\frac{1-z}{z} + \frac{z}{(1-z)_+} + z(1-z) + \left(\frac{11}{6}C_A - \frac{2n_f T_R}{3}\right)\delta(1-z)\right]. \tag{143}$$

The DGLAP equations imply that parton distribution functions at any scale can be determined if they are known at some scale. So, the strategy is to parametrize parton distributions at a relatively low scale and then use the DGLAP evolution and various data to determine them. Typical results are shown in Fig. 7 where quarks are split into *valence* (constituent) and *sea* (produced by the gluon splitting)
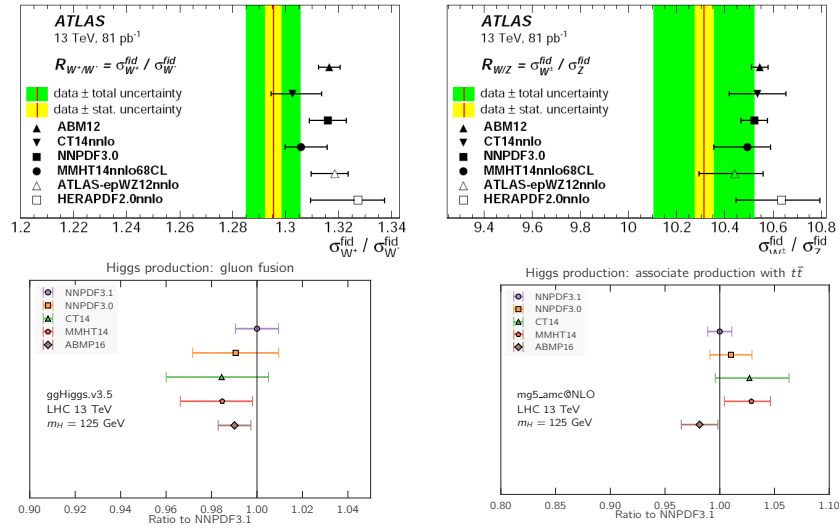
Fig. 8: Comparison of physical cross sections for a few selected processes computed with popular parton distribution functions.

contributions. Understanding uncertainties in the determination of parton distribution functions is an important question that is being constantly discussed and refined [25]. Another complication is that extraction of PDFs involves fixed order cross section computations. When fixed order results change (i.e. by accounting for higher order QCD corrections), the PDFs change as well (provided, of course, that data does not). It is therefore customary to extract PDFs employing fixed order cross sections of certain accuracy (LO, NLO, NNLO). These (LO, NLO, NNLO) PDFs sets should be used to predict physical observables using *matching orders* in computed partonic cross sections.

How well do we know parton distributions functions? A snapshot of the current situation is shown in Fig. 8 for a variety of Standard Model processes including $pp \to V$ with $V = W, Z$, $pp \to H$ and $pp \to t\bar{t}H$. We see that different PDF sets are in reasonable agreement and, at this point, there are no PDF sets that are in a clear disagreement with the other sets. This is quite encouraging and suggests that, with sufficient effort, parton distribution functions can be understood well-enough to allow for the precision physics program at the LHC.

7 Parton showers

Parton distribution functions provide limited information about final state particles. Indeed, to derive the DGLAP evolution equation, we integrate over momenta of the emitted particles loosing information about kinematics of the final state. This may not be ideal since, in certain cases, we may want to have a more detailed description of the final states. This can be done with the help of the so-called *parton shower programs*. The most famous examples of such programs are PYTHIA, HERWIG and SHERPA [26] whose relevance for experiments in high-energy physics is hard to overstate. The goal of this Section is to introduce basic ideas behind parton showers and explain how they can be used to simulate unweighted events.

7.1 The toy model

Following the spirit of the previous Sections, we will start the discussion of parton showers with a toy model inspired by soft emissions in QED. As we have already mentioned in these Lectures, soft emissions in QED completely factorize, c.f. Eq. (105). The cross section in the soft photon approximation is obtained by integrating over photon energies with an additional constraint that the total radiated en-

ergy and the energy that remains in the radiator E can not exceed the total energy available before the emissions. We write

$$\mathrm{d}\sigma_n = \frac{\alpha^n}{n!}\,\mathrm{d}\sigma_0\,\mathrm{d}E\,\prod_{i=1}^{n}\frac{\mathrm{d}\omega_i}{\omega_i}\,\delta(E_T - E - \sum_{i=1}^{n}\omega_i). \tag{144}$$

We integrate over the energy E of the radiator and find

$$\mathrm{d}\sigma_n = \frac{\alpha^n}{n!}\,\mathrm{d}\sigma_0\,\prod_{i=1}^{n}\frac{\mathrm{d}\omega_i}{\omega_i}\,\theta(E_T - \sum\omega_i). \tag{145}$$

Solving the θ-function constraint and introducing a lower integration boundary for integration over ω, we write

$$\mathrm{d}\sigma_n = \frac{\alpha^n}{n!}\mathrm{d}\sigma_0\int_{\lambda}^{E_T}\frac{\mathrm{d}\omega_1}{\omega_1}\int_{\lambda}^{E_T-\omega_1}\frac{\mathrm{d}\omega_2}{\omega_2}\int_{\lambda}^{E_T-\omega_1-\omega_2}\frac{\mathrm{d}\omega_3}{\omega_3}\cdots\int_{\lambda}^{E_T-\omega_1-\omega_2-\cdots-\omega_{n-1}}\frac{\mathrm{d}\omega_n}{\omega_n}. \tag{146}$$

The cross section σ_n is a function of E_T/λ; we would like to evaluate this function in the limit $\lambda \to 0$ which corresponds to $E_T/\lambda \to \infty$. We will now show that, in order to pick up the largest logarithmic contribution to the integral $\mathrm{d}\sigma_n$, we can neglect all dependencies on energies in integration boundaries in Eq. (146)

$$\int_{\lambda}^{E_T}\frac{\mathrm{d}\omega_1}{\omega_1}\int_{\lambda}^{E_T-\omega_1}\frac{\mathrm{d}\omega_2}{\omega_2}\int_{\lambda}^{E_T-\omega_1-\omega_2}\frac{\mathrm{d}\omega_3}{\omega_3}\cdots \to \int_{\lambda}^{E_T}\frac{\mathrm{d}\omega_1}{\omega_1}\int_{\lambda}^{E_T}\frac{\mathrm{d}\omega_2}{\omega_2}\int_{\lambda}^{E_T}\frac{\mathrm{d}\omega_3}{\omega_3}\cdots = \log^n\frac{E_T}{\lambda}. \tag{147}$$

To illustrate why this approximation gives the correct *highest* power of a large logarithm, we consider the case of the two emissions and compute

$$\begin{aligned}
I_2 &= \int_{\lambda}^{E_T}\frac{\mathrm{d}\omega_1}{\omega_1}\int_{\lambda}^{E_T-\omega_1}\frac{\mathrm{d}\omega_2}{\omega_2} = \int_{\lambda}^{E_T}\frac{\mathrm{d}\omega_1}{\omega_1}\log\frac{E_T-\omega_1}{\lambda} \\
&= \int_{\lambda}^{E_T}\frac{\mathrm{d}\omega_1}{\omega_1}\left[\ln\frac{E_T}{\lambda} + \ln\left(1 - \frac{\omega}{E_T}\right)\right] = \ln^2\frac{E_T}{\lambda} + \int_{\lambda}^{E_T}\frac{\mathrm{d}\omega_1}{\omega_1}\ln\left(1 - \frac{\omega_1}{E_T}\right)
\end{aligned} \tag{148}$$

Note that the last integral is convergent in the $\omega_1 \to 0$ limit, so that the dependence on λ can be neglected. Upon doing that and changing integration variables $\omega_1 = E_T\xi$, we arrive at

$$I_2 \approx \ln^2\frac{E_T}{\lambda} + \int_{0}^{1}\frac{\mathrm{d}\xi}{\xi}\ln(1-\xi) = \ln^2\frac{E_T}{\lambda} - \frac{\pi^2}{6} \approx \ln^2\frac{E_T}{\lambda}, \tag{149}$$

where in the last step we neglected the constant term. Clearly, the logarithmically-enhanced term can be obtained if we neglect the dependence of the integration boundaries on the photon energy

$$I_2 = \int_{\lambda}^{E_T}\frac{\mathrm{d}\omega_1}{\omega_1}\int_{\lambda}^{E_T-\omega_1}\frac{\mathrm{d}\omega_2}{\omega_2} \approx \int_{\lambda}^{E_T}\frac{\mathrm{d}\omega_1}{\omega_1}\int_{\lambda}^{E_T}\frac{\mathrm{d}\omega_2}{\omega_2} = \ln^2\frac{E_T}{\lambda}. \tag{150}$$

The generalization to the case of a larger number of photons is obvious. We conclude that, with the leading logarithmic accuracy, the cross section for producing n photons reads

$$\mathrm{d}\sigma_n \approx \frac{\alpha^n}{n!}\sigma_0\ln^n\frac{E_T}{\lambda}. \tag{151}$$

The cross section for emitting *any* number of photons is obtained by summing Eq. (151) over n. We obtain

$$d\sigma = \sum_{0}^{\infty} d\sigma_n = d\sigma_0 \, e^{\alpha \ln \frac{E_T}{\lambda}}. \tag{152}$$

The result shown in Eq. (152) is rather strange since it implies that soft emissions make the cross section very large. We know from previous discussions that this can only happen if *virtual* corrections are improperly neglected and, if real and virtual corrections are combined, no logarithmically enhanced corrections appear in the cross section integrated over all soft emissions. Since we work with the logarithmic accuracy, we have to find

$$d\sigma_{\text{full}} = d\sigma_0, \tag{153}$$

in variance with Eq. (152).

To account for virtual corrections we write, in accord with Eq. (153),

$$d\sigma_{\text{full}} = d\sigma_0 V e^{\alpha \ln E_T/\lambda}, \tag{154}$$

where $V = e^{-\alpha \ln E_T/\lambda}$ represents the effect of virtual corrections. We can now expand the real emission exponential back and find

$$1 = \sum_{n=0}^{\infty} P_n, \tag{155}$$

where

$$P_n = e^{-\alpha \ln E_T/\lambda} \, \alpha^n \int_{\lambda}^{E_T} \frac{d\omega_1}{\omega_1} \int_{\lambda}^{\omega_1} \frac{d\omega_2}{\omega_2} \int_{\lambda}^{\omega_2} \frac{d\omega_3}{\omega_3} \cdots \int_{\lambda}^{\omega_{n-1}} \frac{d\omega_n}{\omega_n}. \tag{156}$$

We interpret the different contributions in Eq. (155) as the relative probabilities to produce a final state with *certain number of photons*. Integrations over ω's in Eq. (156) represent sampling over different kinematic configurations that contribute to these final states. Our goal is to turn Eqs. (155,156) into a generator of *unweighted events* where, similar to experimental reality, each event is characterized by a collection of photons with definite energies.

To proceed further, we introduce a notation $\phi(x,y) = \alpha \ln x/y$, write

$$e^{-\alpha \ln E_T/\lambda} = e^{-\phi(E_T,\omega_1)} e^{-\phi(\omega_1,\omega_2)} ... e^{-\phi(\omega_{n-1},\omega_n)} e^{-\phi(\omega_n,\lambda)}, \tag{157}$$

and insert this representation into the integral in Eq. (156). We obtain

$$\mathcal{P}_n = \alpha^n \int_{\lambda}^{E_T} \frac{d\omega_1}{\omega_1} e^{-\phi(E_T,\omega_1)} \int_{\lambda}^{\omega_1} \frac{d\omega_2}{\omega_2} e^{-\phi(\omega_1,\omega_2)} .. \int_{\lambda}^{\omega_{n-1}} \frac{d\omega_n}{\omega_n} e^{-\phi(\omega_{n-1},\omega_n)} e^{-\phi(\omega_n,\lambda)} \tag{158}$$

We then change variables $\omega_i \to r_i = e^{-\phi(\omega_{i-1},\omega_i)}$, find the Jacobians of the variable transformations and the new integration boundaries

$$dr_i = \alpha \frac{d\omega_i}{\omega_i} e^{-\phi(\omega_{i-1},\omega_i)}, \qquad r_{\min}(\omega_{i-1}) < r_i < 1, \quad r_{\min}(\omega) = e^{-\alpha \ln \omega/\lambda}. \tag{159}$$

We then write $\mathcal{P}_n$ using new variables

$$\mathcal{P}_n = \int_{r^{\min}(\omega_0)}^{1} dr_1 \int_{r^{\min}(\omega_1)}^{1} dr_2 .. \int_{r^{\min}(\omega_{n-1})}^{1} dr_n \, e^{-\phi(\omega_n,\lambda)}, \tag{160}$$

71

where $\omega_0 = E_T$.

It is instructive to compute the probability to emit $n + X$ photons, where X is an arbitrary final state. This probability is given by

$$
\begin{aligned}
\mathcal{P}_{n+X} = &\int\limits_{r^{\min}(\omega_0)}^{1} \mathrm{d}r_1 \int\limits_{r^{\text{in}}(\omega_1)}^{1} \mathrm{d}r_2.. \int\limits_{r^{\min}(\omega_{n-1})}^{1} \mathrm{d}r_n \\
&\times \left[e^{-\phi(\omega_n,\lambda)} + \int\limits_{r^{\min}(\omega_n)}^{1} \mathrm{d}r_{n+1} e^{-\phi(\omega_{n+1},\lambda)} + \int\limits_{r^{\min}(\omega_n)}^{1} \mathrm{d}r_{n+1} \int\limits_{r^{\min}(\omega_{n+1})}^{1} \mathrm{d}r_{n+2} e^{-\phi(\omega_{n+2},\lambda)} + \cdots \right] \\
= &\int\limits_{r^{\min}(\omega_0)}^{1} \mathrm{d}r_1 \int\limits_{r^{\text{in}}(\omega_1)}^{1} \mathrm{d}r_2.. \int\limits_{r^{\min}(\omega_{n-1})}^{1} \mathrm{d}r_n,
\end{aligned}
$$

(161)

where in the last step we used the fact that the expression in square brackets is the total probability to produce *any* final state which isi equal to one.

The formula Eq. (161) suggests how events can be generated since the probability to emit a photon with particular energy is independent of whether or not subsequent emissions occur. The first step is to decide if at least one emission happened. The probability for at least one emission is given by

$$
\mathcal{P}_1 = \int\limits_{r^{\min}(E_T)}^{1} \mathrm{d}r_1.
$$

(162)

The probability that event contains no (resolved) emissions is given by $\mathcal{P}_0 = r^{\min}(E_T) = 1 - \mathcal{P}_1$.

To produce events with these probability distributions, we generate a random number with the flat probability distribution $0 < \xi_1 < 1$. If $\xi_1 < P_0$, no emission happened. We exit the generation process and register an event which contains *no photon emissions*. To generate *another* event, we return to the beginning of the generation process.

If, on the other hand, $\mathcal{P}_0 < \xi_1 < 1$, the photon emission did happen. We find the energy of the emitted photon by solving the equation $\xi_1 = e^{-\phi(\omega_0,\omega_1)}$ for ω_1. The result reads $\omega_1 = \omega_0 \xi_1^{1/\alpha}$. Next, we need to determine if the second photon is emitted. We repeat the first step with the only difference that we use ω_1 instead of E_T to compute the no-emission probability. For example, if the second emission does happen, the energy of the second photon reads $\omega_2 = \omega_1 \xi_2^{1/\alpha}$.

Clearly, we can keep doing that until a no-emission event is generated. Note that the probability to generate a no-emission event grows because energies of the radiated photons decrease as we generate more and more photons. Once the energy of the emitted photon becomes comparable to λ, the no-emission probability becomes close to one and the generation process has a high chance to terminate. At any rate, once the no-emission event is generated, we exit the event generation process. At this point, we have the list of photons with their energies; this list provides complete kinematic description of the generated event. If we need to generate another event, we start from the beginning. One can work with these unweighted events in the same way experimentalists work with real events recorded in experiments at the LHC and compute the relevant cross sections and distributions simply by combining them in an appropriate way.

The above procedure gives us a toy model of a parton shower. It shows that parton showers develop an approximate treatment of perturbative corrections to cross sections and distribution by picking up the

logarithmically enhanced terms, treating the radiation phase space in a simplified manner and preserving hard cross sections by requiring that integrated real emission and virtual corrections cancel each other exactly. This last feature allows us to define a "conserved quantity" that we then recast into a *probability* and use it to generate events with particular kinematic features of final state particles.

7.2 Parton shower description of collinear emissions

We would like to move beyond the toy model and develop a parton shower description of a gauge theory. We will again start with QED and make use of our discussion of parton distribution functions. To develop the probabilistic picture, inherent to parton showers, we need to understand what can play a role of a conserved quantity in case of collinear emissions. To this end, recall that an electron distribution in a physical electron satisfies the DGLAP evolution equation

$$s\frac{\partial}{\partial s}f_{e/e}(z,s) = \frac{\alpha}{2\pi}\int\limits_0^1 \mathrm{d}z_1\mathrm{d}z_2 P_{ee}(z_1)f_{e/e}(z_2,s)\delta(z - z_1 z_2). \tag{163}$$

We integrate both sides of this equation over z and find

$$s\frac{\partial}{\partial s}\int\limits_0^1 \mathrm{d}z\, f_{e/e}(z,s) = \int\limits_0^1 \mathrm{d}z_1 P_{ee}(z_1)\int\limits_0^1 \mathrm{d}z_2 f_{e/e}(z_2) = 0, \tag{164}$$

where the last step follows from the fact that $P_{ee}(z)$ is a plus-distribution, c.f. Eq. (132).

The above equation implies that the *integral* of $f_{e/e}(z,s)$ over z is independent of s and since $f_{e/e}(z,m_e^2) = \delta(1-z)$, we find

$$\int\limits_0^1 \mathrm{d}z f_{e/e}(z,s) = 1. \tag{165}$$

We would like to interpret Eq. (165) as a probability conservation condition that will allow us to compute the relative probabilities of collinear photon emissions. To this end, we re-write the DGLAP equation by separating real and virtual corrections in the splitting function

$$s\frac{\partial}{\partial s}f_{e/e}(z,s) = \frac{\alpha}{2\pi}\int\limits_0^1 \mathrm{d}\xi \tilde{P}_{ee}(\xi)\left[\frac{f_{e/e}(z/\xi,s)}{\xi} - f_{e/e}(z,s)\right], \tag{166}$$

where $\tilde{P}_{ee}(\xi) = (1+\xi^2)/(1-\xi)$. We would like to treat the two terms on the right hand side of Eq. (166) separately; to do that we need to introduce a cut-off on the integration over ξ, $\xi < 1 - \delta$. After moving $f_{e/e}(z,s)$ to the left hand side of Eq.(166), we obtain

$$s\frac{\partial}{\partial s}f_{e/e}(z,s) + \frac{\alpha}{2\pi}\left[\int\limits_0^{1-\delta} \mathrm{d}\xi\, \tilde{P}_{ee}(\xi)\right]f_{e/e}(z,s) = \int\limits_0^{1-\delta} \frac{\mathrm{d}\xi}{\xi}\tilde{P}_{ee}(\xi)f_{e/e}(\frac{z}{\xi},s). \tag{167}$$

We will solve Eq.(167) in the approximation $\delta \to 0$. Note that the singularity at $\xi = 0$ is irrelevant since it is protected by the fact that the splitting function vanishes for values of arguments that are bigger than one. To solve Eq. (167), we remove the homogeneous part of the equation by writing

$$f_{e/e}(z,s) = \Delta(s)g(z,s), \tag{168}$$

and choose $\Delta(s)$ to satisfy the differential equation

$$s\frac{\partial}{\partial s}\Delta(s) + \frac{\alpha}{2\pi}\left[\int\limits_0^{1-\delta} \mathrm{d}\xi\, \tilde{P}_{ee}(\xi)\right]\Delta(s) = 0. \tag{169}$$

The equation for $g(z,s)$ becomes

$$s\frac{\partial g(z,s)}{\partial s} = \frac{\alpha}{2\pi}\int\limits_0^{1-\delta}\frac{\mathrm{d}\xi}{\xi}\tilde{P}_{ee}(\xi)g(z/\xi,s). \tag{170}$$

To find the splitting function $f_{e/e}(z,s)$ we need to solve the differential equations Eqs. (169,170). We begin with Eq. (169). Its solution reads

$$\Delta(s,m_e^2) = \exp\left[-\frac{\alpha}{2\pi}\int\limits_{m_e^2}^{s}\frac{\mathrm{d}t}{t}\int\limits_0^{1-\delta}\mathrm{d}\xi\tilde{P}_{ee}(\xi)\right]. \tag{171}$$

We note that $\Delta(s,m_e^2)$ is known as the *Sudakov form factor*. As we will see later, it describes a probability of the elastic (no-emission) process.

We integrate Eq. (170) over s and find

$$g(z,s) = g(z,m_e^2) + \frac{\alpha}{2\pi}\int\limits_{m_e^2}^{s}\frac{\mathrm{d}t}{t}\int\limits_0^{1-\delta}\frac{\mathrm{d}\xi}{\xi}\tilde{P}_{ee}(\xi)g(z/\xi,t). \tag{172}$$

If we multiply both sides of this equation with $\Delta(s,m_e^2)$ and use the fact that $\Delta(m_e^2,m_e^2) = 1$, we obtain

$$f_{e/e}(z,s) = \Delta(s,m_e^2)f_{e/e}(z,m_e^2) + \frac{\alpha}{2\pi}\int\limits_{m_e^2}^{s}\frac{\mathrm{d}t}{t}\Delta(s,t)\int\limits_0^{1-\xi_{\min}}\frac{\mathrm{d}\xi}{\xi}\,\tilde{P}_{ee}(\xi)\,f_{e/e}(z/\xi,t). \tag{173}$$

We can expand the right hand side of Eq. (173) in power series in α, treating the Sudakov form factor as quantity of order one and using $f_{e/e}(z,m_e^2) = \delta(1-z)$. This is very similar to what we did when constructing the probability conservation equation in the toy model. We obtain

$$f_{e/e}(s,z) = \Delta(s,m_e^2)\delta(1-z) + \frac{\alpha}{2\pi}\int\limits_{m_e^2}^{s}\frac{\mathrm{d}t_1}{t_1}\Delta(s,t_1)\int\limits_0^{1-\delta}\mathrm{d}\xi_1\tilde{P}_{ee}(\xi_1)\Delta(t_1,m_e^2)\delta(z-\xi_1)$$

$$+\left(\frac{\alpha}{2\pi}\right)^2\int\limits_{m_e^2}^{s}\frac{\mathrm{d}t_1}{t_1}\Delta(s,t_1)\int\limits_0^{1-\delta}\mathrm{d}\xi_1\tilde{P}_{ee}(\xi_1)\int\limits_{m_e^2}^{t_1}\frac{\mathrm{d}t_2}{t_2}\Delta(t_1,t_2)\int\limits_0^{1-\delta}\mathrm{d}\xi_2\tilde{P}_{ee}(\xi_2)\Delta(t_2,m_e^2)\delta(z-\xi_1\xi_2) \tag{174}$$

$$+\cdots$$

We now integrate both sides of Eq. (174) over z, use the "probability conservation" condition Eq. (165)

and obtain an equation that we can use to generate events in exactly the same way as in the toy model

$$1 = \Delta(s, m_e^2) + \frac{\alpha}{2\pi} \int\limits_{m_e^2}^{s} \frac{dt_1}{t_1} \Delta(s, t_1) \int\limits_{0}^{1-\delta} d\xi_1 \tilde{P}_{ee}(\xi_1) \Delta(t_1, m_e^2)$$

$$+ \left(\frac{\alpha}{2\pi}\right)^2 \int\limits_{m_e^2}^{s} \frac{dt_1}{t_1} \Delta(s, t_1) \int\limits_{0}^{1-\delta} d\xi_1 \tilde{P}_{ee}(\xi_1) \int\limits_{m_e^2}^{t_1} \frac{dt_2}{t_2} \Delta(t_1, t_2) \int\limits_{0}^{1-\delta} d\xi_2 \tilde{P}_{ee}(\xi_2) \Delta(t_2, m_e^2) \tag{175}$$

$$+ \cdots$$

Each term in these series represents a probability of a process with a fixed number of resolved photons. The generation process works similarly to the toy model. Note that this similarity can be made exact if, similar to the toy model, we introduce a random variable

$$r_i = \Delta(t_{i-1}, t_i), \quad t_0 = s. \tag{176}$$

Indeed, since

$$dr_i = \frac{\alpha}{2\pi} \frac{dt_i}{t_i} \int\limits_{0}^{1-\delta} d\xi_1 \tilde{P}_{ee}(\xi_1) \, \Delta(t_{i-1}, t_i), \tag{177}$$

Eq. (175) can be cast into a form that is identical to e.g. Eq. (161) discussed in the context of the toy model. Therefore, we can generate events following our earlier discussion. The only difference is that we need more than one random variables to describe momentum of an emitted photon.

We now explain the procedure in detail. We begin with generating a random number $0 < r < 1$ and solving the equation

$$\Delta(s, t_1) = r \tag{178}$$

for t_1. If $t_1 < m_e^2$, then no emission happens, we exit the generation process and, if necessary, start anew. If, on the other hand, we find $t_1 > m_e^2$, then the emission happens. To determine the energy of the photon, we generate another random variable $0 < y_1 < 1$ and solve for ξ_1

$$y_1 = \frac{\int\limits_{0}^{\xi_1} d\bar{\xi} P_{ee}(\bar{\xi})}{\int\limits_{0}^{1-\delta} d\bar{\xi} P_{ee}(\bar{\xi})}. \tag{179}$$

The two variables, ξ_1 and t_1 allow us to compute the four-momentum of the radiated photon

$$q_1^\mu = (1 - \xi_1) p^\mu + \beta_1 \bar{p}^\mu + q_{\perp,1} n_{\perp,1}^\mu, \tag{180}$$

where $q_{\perp,1} = \sqrt{t_1}$, $n_{\perp,1}^\mu$ is a randomly generated unit vector, $n_{\perp,1}^2 = -1$, in a plane transverse to p and $\bar{p}$ and $\beta_1 = t_1/((1 - \xi_1)2p\bar{p})$.

Once the photon is generated, the next step is repeated with s replaced by t_1. This means that we again generate a random number $0 < r < 1$ and solve the equation

$$r = \Delta(t_1, t_2) \tag{181}$$

for t_2. If we find that $t_2 < m_e^2$, we declare that no further photon emission happened and we exit the generation process. If, on the other hand, $t_2 > m_e^2$, we generate abother random variable y_2, determine ξ_2 from an analog of Eq. (179) and compute the momentum of the second emitted photon as

$$q_2^\mu = (1 - \xi_2)\xi_1 p^\mu + \beta_2 \bar{p}^\mu + q_{\perp,2} n_{\perp,2}^\mu, \tag{182}$$

where $q_{\perp,2} = \sqrt{t_2}$ etc. This process continues unless at some stage the no-emission event is generated. If this happens, we exit the generation process. At this point we have a list of photon momenta that describes an event – with fully specified final state – for the process $e + X \rightarrow Y + \text{photons}$ in the collinear approximation for the emitted photons.

The generalization to QCD is, in principle, straightforward since the above discussion is built around the analysis of the DGLAP evolution equation for the structure functions. One can repeat all the steps almost verbatim and arrive at a similar conclusion. One aspect that, in principle, one should also consider in QED, is a possibility to split into different types of partons. Indeed, in QCD all different types of branchings $a \rightarrow b + c$ have to be taken into account. As the result, there are different Sudakov form factor for different partons and a sum over all types of possible branchings appears in the exponent. The other aspect that we have been systematically neglecting in our QED discussion is the running of the coupling constant that definitely has to be accounted for in QCD. The Sudakov form factor of a parton a reads

$$\Delta_a(s, s_0) = \exp\left[\int\limits_{s_0}^{s} \frac{\mathrm{d}t}{t} \frac{\alpha_s(t)}{2\pi} \int\limits_{0}^{1-\delta} \mathrm{d}\xi \sum_b P_{a \rightarrow b}(\xi) \right]. \tag{183}$$

We generate events in exactly the same way as discussed above except that at every step we need to decide which branching actually happens. This is done based on the relative probabilities for individual branchings

$$w_{a \rightarrow b} = \frac{\int\limits_{0}^{1-\delta} \mathrm{d}\xi P_{a \rightarrow b}(\xi)}{\int\limits_{0}^{1-\delta} \mathrm{d}\xi \sum_b P_{a \rightarrow b}(\xi)}. \tag{184}$$

7.3 Soft emissions and parton showers

We have discussed how to generate events that describe emissions of collinear partons from initial state particles. Note that since we generate collinear emissions and since collinear emissions from different particles do not interfere, it becomes straightforward to generalize our discussion to an arbitrary number of incoming and outgoing particles. However, we have also seen in the computation of NLO QCD corrections that infra-red divergences – and related logarithmically-enhanced contributions – can have either collinear or *soft* origin. The construction of a parton shower that we described addresses collinear singularities and large collinear logarithms. However, if soft contributions are to play an important role, how can they be accommodated into this framework?

The important difference between soft and collinear emissions is that soft gluons emitted by different color charges necessarily interfere so that emission of soft gluons does not occur locally in the phase space – it requires a snapshot of the whole system. This is very different from independent collinear emissions and it is unclear a priori if the parton shower framework can accommodate soft emissions.

It turns out that it is actually possible to describe soft emissions with parton showers. In fact, there are at least *two* ways to do that; I will explain below the classic one [7] based on the concept of the so-called *angular ordering*.[6] To understand what this is, consider a soft photon emission from an electron-positron pair that is produced in the splitting of a virtual photon $\gamma^* \rightarrow e^+ e^-$. We know that the full matrix element squared is given by the eikonal factor and the elastic matrix element squared, and that the differential cross section can be described by the following formula

$$\mathrm{d}\sigma = \mathrm{d}\sigma_0 \frac{\alpha}{2\pi} \frac{\mathrm{d}\omega}{\omega} \frac{\mathrm{d}\Omega}{(2\pi)} \frac{2p_1 p_2 \, \omega^2}{(p_1 k)(p_2 k)}. \tag{185}$$

---

[6] Another popular option is to employ a suitable color basis and the fact that certain color-order ampltudes do not interfere in the limit where number of colors is considered to be a large parameter, see Ref. [28].

It is convenient to denote the scalar products of four-vectors as $p_i p_j = E_i E_j (1 - \cos\theta_{ij}) = E_i E_j \xi_{ij}$, so that the eikonal factor that appears in the formula for the cross section reads

$$\frac{2 p_1 p_2 \, \omega^2}{(p_1 k)(p_2 k)} = \frac{2\xi_{12}}{\xi_{1k}\xi_{2k}} = 2W(1,2;k). \tag{186}$$

We now re-write the *radiator function* $W(1,2;k)$ in the following way

$$W(1,2;k) = \frac{\xi_{12}}{\xi_{1k}\xi_{2k}} = \frac{1}{2}\left(\frac{\xi_{12}}{\xi_{1k}\xi_{2k}} - \frac{1}{\xi_{2k}} + \frac{1}{\xi_{1k}}\right) + (1 \Leftrightarrow 2) = W_1(1,2;k) + W_2(1,2;k). \tag{187}$$

We would like to interpret the function $W_1(1,2;k)$ as the photon emission off the electron with momentum p_1 and the function $W_2(1,2;k)$ as the photon emission off the positron with momentum p_2. To understand why this interpretation is meaningful, it is useful to study the collinear limits of the two radiator functions. Consider $W_1(1,2;k)$ as an example. If the photon is emitted along the direction of the electron, $\xi_{1,k} \to 0$, $\xi_{2k} \to \xi_{1,2}$ and $W_1(1,2,k) \approx 1/\xi_{1,k} \gg W_2(1,2;k)$. On the contrary, if the photon is emitted along the direction of the positron, $\xi_{2,k} \to 0$, $\xi_{1k} \to \xi_{12}$ and $W_2(1,2;k) \approx 1/\xi_{2,k} \gg W_1(1,2;k)$.

The situation becomes particularly transparent if we integrate over the *azimuthal angle* of the emitted photon defined in the following way. For the function $W_1(1,2;k)$, we choose a reference frame where the electron momentum is the z-axis, i.e. $n_1 = (0,0,1)$, the momentum of the positron is in the $x - z$ plane, i.e. $n_2 = (\sin\theta_{12}, 0, \cos\theta_{12})$ and the photon momentum is arbitrary $\vec{n}_k = (\sin\theta\cos\phi, \sin\theta\sin\phi, \cos\theta)$. Suppose that we want to integrate the function $W_1(1,2;k)$ over the angle ϕ. The only ϕ-dependent scalar product in $W_1(1,2;k)$ is $\xi_{2,k} = 1 - \sin\theta_{12}\sin\theta\cos\phi - \cos\theta_{12}\cos\theta$. The relevant integral reads

$$\int\limits_0^{2\pi} \frac{\mathrm{d}\phi}{(2\pi)} \frac{1}{a + b\cos\phi} = \frac{1}{\sqrt{a^2 - b^2}} \quad \Rightarrow \quad \int\limits_0^{2\pi} \frac{\mathrm{d}\phi}{(2\pi)} \frac{1}{\xi_{2k}} = \frac{1}{|\xi_{1k} - \xi_{12}|}. \tag{188}$$

Using this result to integrate the radiator function W_1, we obtain

$$\int\limits_0^{2\pi} \frac{\mathrm{d}\phi}{(2\pi)} W_1(1,2;k) = \int\limits_0^{2\pi} \frac{\mathrm{d}\phi}{(2\pi)} \frac{1}{2\xi_{1k}}\left(\frac{\xi_{12} - \xi_{1k}}{\xi_{2k}} + 1\right) = \frac{1}{2\xi_{1k}}\left(\frac{\xi_{12} - \xi_{1k}}{|\xi_{12} - \xi_{1k}|} + 1\right) = \frac{\theta(\xi_{12} - \xi_{1k})}{\xi_{1k}}. \tag{189}$$

We repeat the same computation for the second radiator function $W_2(1,2;k)$. However, in this case we integrate over a *different azimuthal angle* since we align the z-axis with the positron direction vector n_2. If we do that, we find

$$\int\limits_0^{2\pi} \frac{\mathrm{d}\phi}{(2\pi)} W_2(1,2;k) = \frac{\theta(\xi_{12} - \xi_{2k})}{\xi_{2k}}. \tag{190}$$

Combining the results for $W_{1,2}$, we obtain a simple formula for the full radiator function

$$W(1,2;k) = W_1(1,2;k) + W_2(1,2;k) \Rightarrow \frac{\theta(\xi_{1k} - \xi_{12})}{\xi_{1k}} + \frac{\theta(\xi_{2k} - \xi_{12})}{\xi_{2k}}. \tag{191}$$

Note that this formula is obtained upon averaging the two contributing radiator functions over *different azimuthal angles*.

We can now use the radiator function Eq. (191) to compute the cross section. We find

$$\mathrm{d}\sigma = \mathrm{d}\sigma_0 \, \frac{\alpha}{2\pi} \, \frac{\mathrm{d}\omega}{\omega} \sum_{i=1}^{2} \frac{\mathrm{d}\xi_{1k}}{\xi_{1k}} \theta(\xi_{12} - \xi_{ik}). \tag{192}$$

This formula shows remarkable features that enable probabilistic interpretation of soft photon emissions. Indeed, since for small emission angles $\xi_{ij} \approx \theta_{ij}^2/2$, according to Eq. (192), electron and positron emit soft photons independently of each other provided that the emission angle is smaller than the opening angle of the pair, $\theta_{1k} < \theta_{12}$, $\theta_{2k} < \theta_{12}$. If emission at a larger angle happens, the *interference* of emissions by the electron and the positron effectively shuts off the radiation completely.

What makes this result interesting for the construction of a parton shower is that it appears to be possible to describe soft emissions by making *educated choices of evolution variables*. Indeed, we have so far discussed the parton shower evolution as being driven by the logarithmic integration over the transverse momentum of the emitted particle. However, since $k_\perp \sim \omega\theta$, one can trade logarithmic integration over the transverse momentum for the integration over emission angle

$$\frac{\mathrm{d}k_\perp}{k_\perp} = \frac{\mathrm{d}\theta}{\theta} = \frac{1}{2}\frac{\mathrm{d}\xi}{\xi} \tag{193}$$

The natural ordering of the emission angles, i.e. larger emission angles closer to a hard process followed by smaller emission angles at the end of the cascade, allows to resum both *soft* and *collinear* logarithms in an event.

Although the above discussion is sufficiently general to be used in QCD parton showers, there is one aspect of it that is too QED-specific and, for this reason, warrants a clarification. Indeed, in QED, the variety of charge-changing processes is very limited since in a splitting $a \to b + c$, one of the particles is always neutral. This is clearly not the case in QCD, where a color-charged gluon can split into a quark-anti-quark pair. Since working with QCD amplitudes and introducing convenient notations for color charges will take us astray, it is more useful to introduce a toy model that, on one hand, will be easy to work with and, on the other hand, will not suffer from the limitation of QED described above. To this end, we consider a soft photon emission amplitude off a final state with three charged particles

$$\mathcal{M} \sim \sum_{i=1}^{3} Q_i \frac{p_i\epsilon}{p_i k} \mathcal{M}_0. \tag{194}$$

Gauge-invariance dictates that $\sum_{i=1}^{3} Q_i = 0$, but does not impose constraints on individual charges. Upon squaring the amplitude and summing over photon polarizations, we find

$$|\mathcal{M}|^2 \sim -\sum_{ij} Q_i Q_j \frac{p_i p_j}{(p_i k)(p_j k)} |\mathcal{M}_0|^2. \tag{195}$$

Expressing this result in terms of the radiator function, we obtain

$$W = -Q_1 Q_2 W_{12} - Q_1 Q_3 W_{13} - Q_2 Q_3 W_{23}. \tag{196}$$

We then re-write charge products through charge squares, e.g. $-Q_1 Q_2 = (Q_1^2 + Q_2^2 - Q_3^2)/2$ using $Q_1 + Q_2 + Q_3 = 0$ and derive

$$W = \frac{1}{2}\left[Q_1^2 \left(W_{12} + W_{13} - W_{23}\right) + Q_2^2 \left(W_{12} + W_{23} - W_{13}\right) + Q_3^2 \left(W_{13} + W_{23} - W_{12}\right)\right]. \tag{197}$$

We would like to re-write this expression in a way that will make an interpretation in terms of successive independent emissions possible. To this end, we split each radiator function into a sum of relevant terms and average each such term over respective azimuthal angles. We also consider a kinematic configuration where the opening angle between p_1 and p_2 is much smaller than the opening angle between p_{12} and p_3, c.f. Fig. 9.
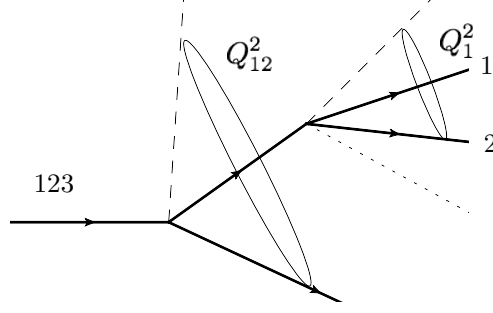
Fig. 9: Soft emissions after azimuthal ordering, see Eq. (202).

To see how the hierarchy of angles can be exploited, consider the term in Eq. (197) that is proportional to Q_1^2 and write

$$
\begin{aligned}
W_{12} + W_{13} - W_{23} &\to W_{12}^{[1]} + W_{12}^{[2]} + W_{13}^{[1]} + W_{13}^{[3]} - W_{23}^{[2]} - W_{23}^{[3]} \\
&= 2W_{12}^{[1]} + \left\{ (W_{13}^{[1]} - W_{12}^{[1]}) + (W_{12}^{[1]} - W_{23}^{[2]}) \right\} + \left\{ W_{13}^{[3]} - W_{23}^{[3]} \right\}.
\end{aligned}
\tag{198}
$$

We now study the different terms separately. We find

$$
\begin{aligned}
(W_{13}^{[1]} - W_{12}^{[1]}) + (W_{12}^{[1]} - W_{23}^{[2]}) &= \frac{(\theta(\xi_{13} - \xi_{1k}) - \theta(\xi_{12} - \xi_{1k}))}{\xi_{1k}} - \frac{(\theta(\xi_{23} - \xi_{2k}) - \theta(\xi_{12} - \xi_{2k}))}{\xi_{2k}} \\
&\Rightarrow \int d\Omega_k \left[(W_{13}^{[1]} - W_{12}^{[1]}) + (W_{12}^{[1]} - W_{23}^{[2]}) \right] = \ln \frac{\theta_{13}}{\theta_{23}} \sim 1,
\end{aligned}
\tag{199}
$$

for $\theta_{12} \ll \theta_{13}$. This result implies that the combination of radiator functions displayed in Eq. (199) *does not* lead to large logarithmic corrections and, for this reason, can be neglected. A similar analysis of the last term in Eq. (198) leads to a similar conclusion

$$
(W_{13}^{[3]} - W_{23}^{[3]}) = \frac{\theta(\xi_{13} - \xi_{3k})}{\xi_{3k}} - \frac{\theta(\xi_{23} - \xi_{3k})}{\xi_{3k}} \Rightarrow \int d\Omega_k (W_{13}^{[3]} - W_{23}^{[3]}) = \ln \frac{\theta_{13}}{\theta_{23}} \sim 1.
\tag{200}
$$

Hence, for the kinematic case that we are interested in, the following replacement is valid with the logarithmic accuracy

$$
W_{12} + W_{13} - W_{23} \to 2W_{12}.
\tag{201}
$$

Similar arguments allow us to simplify the radiator function in Eq. (197) and write it as

$$
W \approx Q_1^2 W_{12}^{[1]} + Q_2^2 W_{12}^{[2]} + (Q_1 + Q_2)^2 W_{12,3}^{[12]} + Q_3^2 W_{12,3}^{[3]}.
\tag{202}
$$

Here $W_{12,3}^{[12]}$ describes emission off the "parent parton" of the two partons 1 and 2. It reads $W_{12,3}^{[12]} = \theta(\xi_{12,3} - \xi_{12,k})\theta(\xi_{12,k} - \xi_{12})/\xi_{12,k}$.

The interpretation of Eq. (202) is straightforward. It shows that soft radiation can be described by independent emissions off *four* particles that appear in the amplitude – partons $1, 2$ and 3 and the "parent" of the two partons 1 and 2. The radiation off each of these particles is proportional to its charge squared. The radiation is restricted by the opening angles of the corresponding "dipoles". For example, the "parent" of 1 and 2 radiates to an opening angle between $\vec{n}_1 \sim \vec{n}_2$ an $\vec{n}_3$ but 1 and 2 radiate into an opening angle between themselves. It should be clear from previous discussions that this structure easily lends itself to a parton shower description provided that opening angles are chosen as independent evolution variables.

7.4   Parton showers connect perturbative and non-perturbative descriptions of hadron collisions

We have seen that parton showers can be used to generate unweighted events and, within certain approximations, produce final states with arbitrary number of quarks and gluons starting from a few energetic particles in the event. These initial hard particles provide seeds of energy flows that a hardly affected by non-perturbative effects. These energy flows provide foundations for hadron jets, a trademark of high-energy collisions. Collinear and soft radiation described by parton showers builds up these jets and fills them with large number of partons. When relative transverse momenta of gluons and quarks generated by parton showers become small, QCD turns into a non-perturbative theory and generation of further emissions of quarks and gluons becomes meaningless. At this point, one employs phenomenological models that describe a parton-to-hadron transition, i.e. they allow us to transform an ensemble of quarks and gluons into a *hadronic* final state. Although the description of such a transition is empirical (see e.g. Refs. [7, 26]), it is very important since hadrons, not partons, hit particle detectors. Therefore, properties of hard events that we strive to understand are deduced from particle composition, multiplicities and energy depositions of hadrons observed in particle detectors. Our ability to connect these measurements with properties of the hard scattering relies on parton shower Monte Carlo and the description of parton-to-hadron transition.

It is important to stress that the interplay between fixed orders and parton showers drives the development of both tools. In particular, spectacular progress in our ability to perform sophisticated fixed order computations lead to a possibility to describe better the kinematics of *hard* jets, as produced in short-distance collisions, leaving the parton shower with a task that it does best – filling these jets with the soft and collinear radiation. The ideas of *merging* and *matching* [27] emphasize the need to combine fixed orders with parton showers; they also put additional pressure on parton shower algorithms to become more refined theoretical tools with higher (and well-defined) parametric accuracy. The progress in this field will be crucial for extracting maximal physics information from the LHC and making precision physics at the LHC a viable opportunity.

8   Conclusions

The goal of these lectures was to describe how the theory of strong interactions – Quantum Chromodynamics – is applied to describe hard collisions at the LHC. QCD is crucial for the success of the LHC physics program since two strongly interacting particles – protons – are collided there. In spite of this fact, if we look at the right observables, LHC physics is mainly determined by interactions of quarks and gluons rather than hadrons and these interactions can be understood directly from the Standard Model Lagrangian. Recent theoretical developments that include advances in fixed order computations, resummations, parton shower algorithms and determination of parton distribution functions allowed us to describe hard scattering data at the LHC with very high precision. We hope that this high precision predictions for many LHC observabels will, one day, be used to find something unexpected and will, in this way, complectement direct searches for physics beyond the Standard Model at the LHC [29].

Acknowledgments

References

[1] ATLAS collaboration, *Observation of a new particle in the search for the Standard Model Higgs boson with the ATLAS detector at the LHC*, Phys. Lett. B **716** (2012) 1.

[2] CMS collaboration, *Observation of a new boson at a mass of 125 GeV with the CMS experiment at the LHC*, Phys. Lett. B **716** (2012) 30.

[3] J.C. Collins, D.E. Soper and G. Sterman, in *Perturbative Quantum Chromodynamics*, ed. A. H. Mueller (World Scientific, Singapore, 1989), p.1; J. C. Collins and D. E. Soper, *The Theorems of Perturbative QCD*, Ann. Rev. Nucl. Part. Sci. **37** (1987) 383.

[4] G. P. Salam, *Towards Jetography*, Eur. Phys. J. C **67** (2010) 637.

[5] M. E. Peskin and D. V. Schroeder, *An Introduction to quantum field theory*, Westview Press, 1995.

[6] M. D. Schwartz, *Quantum Field Theory and the Standard Model*, Cambridge University Press, 2014.

[7] R.K. Ellis, W.J. Stirling and B.R. Webber, *QCD and collider physics*, Cambridge Monographs on Particle Physics, Nuclear Physics and Cosmology, 1996.

[8] Yu.L. Dokshitzer, V.A. Khoze, A.H. Mueller and S.I. Troyan, *Basics of Perturbative QCD*, Editions Frontieres, 1991.

[9] G. Dissertori, I. Knowles, M. Schmelling, *Quantum Chromodynamics*, Oxford Science Publications, 2009.

[10] S. Catani and M. H. Seymour, *A General algorithm for calculating jet cross-sections in NLO QCD*, Nucl. Phys. B **485** (1997) 291; Erratum: [Nucl. Phys. B **510** (1998) 503].

[11] S. Frixione, Z. Kunszt and A. Signer, *Three jet cross-sections to next-to-leading order*, Nucl. Phys. B **467** (1996) 399.

[12] G. Ossola, C. G. Papadopoulos and R. Pittau, *'Reducing full one-loop amplitudes to scalar integrals at the integrand level*, Nucl. Phys. B **763** (2007) 147.

[13] C. F. Berger, Z. Bern, L. J. Dixon, F. Febres Cordero, D. Forde, H. Ita, D. A. Kosower and D. Maitre, *An Automated Implementation of On-Shell Methods for One-Loop Amplitudes*, Phys. Rev. D **78** (2008) 036003; R. K. Ellis, W. T. Giele and Z. Kunszt, *A Numerical Unitarity Formalism for Evaluating One-Loop Amplitudes* JHEP **0803** (2008) 003; W. T. Giele, Z. Kunszt and K. Melnikov, *Full one-loop amplitudes from tree amplitudes*, JHEP **0804** (2008) 049.

[14] S. Catani and M. Grazzini, *An NNLO subtraction formalism in hadron collisions and its application to Higgs boson production at the LHC*, Phys. Rev. Lett. **98** (2007) 222002; R. Boughezal, C. Focke, X. Liu and F. Petriello, *W-boson production in association with a jet at next-to-next-to-leading order in perturbative QCD*, Phys. Rev. Lett. **115** (2015) 062002; J. Gaunt, M. Stahlhofen, F. J. Tackmann and J. R. Walsh, *N-jettiness Subtractions for NNLO QCD Calculations*, JHEP **1509** (2015) 058; A. Gehrmann-De Ridder, T. Gehrmann and E. W. N. Glover, *Antenna subtraction at NNLO*, JHEP **0509** (2005) 056 E. W. Nigel Glover and J. Pires, *Antenna subtraction for gluon scattering at NNLO*, JHEP **1006**, 096 (2010) M. Czakon, *Double-real radiation in hadronic top quark pair production as a proof of a certain concept*, Nucl. Phys. B **849** (2011), 250; M. Czakon and D. Heymes, *Four-dimensional formulation of the sector-improved residue subtraction scheme*, Nucl. Phys. B **890** (2014) 152; F. Caola, K. Melnikov and R. Röntsch, *Nested soft-collinear subtractions in NNLO QCD computations*, Eur. Phys. J. C **77**, (2017) 248;

[15] See e.g. T. Gehrmann, M. Grazzini, S. Kallweit, P. Maierhöfer, A. von Manteuffel, S. Pozzorini, D. Rathlev and L. Tancredi, W^+W^- *Production at Hadron Colliders in Next to Next to Leading Order QCD*, Phys. Rev. Lett. **113**, no. 21, 212001 (2014); R. Boughezal, F. Caola, K. Melnikov, F. Petriello and M. Schulze, *Higgs boson production in association with a jet at next-to-next-to-leading order*, Phys. Rev. Lett. **115** (2015) 082003; M. Czakon, D. Heymes and A. Mitov, *High-precision differential predictions for top-quark pairs at the LHC* Phys. Rev. Lett. **116** (2016) 082003; J. Currie, A. Gehrmann-De Ridder, T. Gehrmann, E. W. N. Glover, A. Huss and J. Pires, *Precise predictions for dijet production at the LHC*, Phys. Rev. Lett. **119** (2017) 152001; A. Gehrmann-De Ridder, T. Gehrmann, E. W. N. Glover, A. Huss and T. A. Morgan, *Precise QCD predictions for the production of a Z boson in association with a hadronic jet*, Phys. Rev. Lett. **117**, no. 2, 022001 (2016); E. L. Berger, J. Gao, C.-P. Yuan and H. X. Zhu, *NNLO QCD Corrections to t-channel Single Top-Quark Production and Decay*, Phys. Rev. D **94** (2016) no.7, 071501.

[16] C. G. Bollini and J. J. Giambiagi, *Dimensional Renormalization: The Number of Dimensions as a Regularizing Parameter,* Nuovo Cim. B **12** (1972) 20.

[17] S. Catani, *The Singular behavior of QCD amplitudes at two loop order*, Phys. Lett. B **427** (1998) 161.

[18] V. N. Gribov and L. N. Lipatov, *Deep inelastic e p scattering in perturbation theory*, Sov. J. Nucl. Phys. **15** (1972) 438;

[19] Y. L. Dokshitzer, *Calculation of the Structure Functions for Deep Inelastic Scattering and e+ e- Annihilation by Perturbation Theory in Quantum Chromodynamics*, Sov. Phys. JETP **46** (1977) 641; G. Altarelli and G. Parisi, *Asymptotic Freedom in Parton Language*, Nucl. Phys. B **126** (1977) 298.

[20] G. Bozzi, S. Catani, G. Ferrera, D. de Florian and M. Grazzini, Phys. Lett. B **696** (2011) 207.

[21] G. Parisi and R. Petronzio, *Small Transverse Momentum Distributions in Hard Processes*, Nucl. Phys. B **154** (1979) 279.

[22] G. Luisoni and S. Marzani, *QCD resummation for hadronic final states,* J. Phys. G **42** (2015) 103101.

[23] M. Abramowitz and I. Stegun, *Handbook of Mathematical Functions*, NBS, 1964.

[24] J. C. Collins, D. E. Soper and G. F. Sterman, *Transverse Momentum Distribution in Drell-Yan Pair and W and Z Boson Production*, Nucl. Phys. B **250** (1985) 199.

[25] J. Butterworth *et al.*, *PDF4LHC recommendations for LHC Run II*, J. Phys. G **43** (2016) 023001; A. Accardi *et al.*, *A Critical Appraisal and Evaluation of Modern PDFs*, Eur. Phys. J. C **76** (2016) 471.

[26] A. Buckley *et al.*, *General-purpose event generators for LHC physics*, Phys. Rept. **504** (2011) 145.

[27] S. Catani, F. Krauss, R. Kuhn and B. R. Webber, *QCD matrix elements + parton showers*, JHEP **0111** (2001) 063; S. Frixione and B. R. Webber, *Matching NLO QCD computations and parton shower simulations*, JHEP **0206** (2002) 029; S. Frixione, P. Nason and C. Oleari, *Matching NLO QCD computations with Parton Shower simulations: the POWHEG method*, JHEP **0711** (2007) 070; S. Alioli, C. W. Bauer, C. J. Berggren, A. Hornig, F. J. Tackmann, C. K. Vermilion, J. R. Walsh and S. Zuberi, *Combining Higher-Order Resummation with Multiple NLO Calculations and Parton Showers in GENEVA*, JHEP **1309** (2013) 120.

[28] S. Plätzer, *Summing Large-N Towers in Colour Flow Evolution*, Eur. Phys. J. C **74** (2014) 2907.

[29] S. Alioli, M. Farina, D. Pappadopulo and J. T. Ruderman, *Catching a New Force by the Tail*, arXiv:1712.02347 [hep-ph]; C. Frye, M. Freytsis, J. Scholtz and M. J. Strassler, *Precision Diboson Observables for the LHC*, JHEP **1603** (2016) 171; A. Azatov, C. Grojean, A. Paul and E. Salvioni, *Resolving gluon fusion loops at current and future hadron colliders*, JHEP **1609** (2016) 123.

Beyond the Standard Model' 17

D. Kazakov

Bogoliubov Laboratory of Theoretical Physics, Joint Institute for Nuclear Research, Dubna, Russia

Abstract

We discuss the status of the Standard Model (SM): the principles; the Lagrangian; the problems; open questions and the ways beyond. Then we consider possible physics beyond the SM: New symmetries (Gauge, SUSY); New particles (gauge, axion, superpartners); New dimensions (extra, large, compact, etc) or a New Paradigm (strings, branes, gravity). In conclusion, we formulate the first priority tasks for the future HEP program.

Keywords

Lectures; physics beyond the Standard Model; supersymmetry; extra dimensions; grand unification; Axions, String theory

1 Introduction: The Standard Model

Physics of elementary particles today is perfectly described by the Standard Model of fundamental interactions which accumulates all achievements of the recent years. It is usually said that with the discovery of the Higgs boson the Standard Model is completed. Nevertheless, it still contains many puzzles and possibly requires some modification in future. The search for new physics beyond the Standard Model is inevitably based on comparison of experimental data with predictions of the Standard Model since the particles observed in the final states are the well-known stable ones and new physics as a rule manifests itself in the form of excess above the SM background.

It is instructive to remind the main principles in the foundation of the Standard Model and possible ways to go beyond it. They are:

– Three groups of gauged symmetries $SU(3) \times SU(2) \times U(1)$
– Three families of quarks and leptons in representations $(3 \times 2, 3 \times 1, 1 \times 2, 1 \times 1)$
– Brout-Englert-Higgs mechanism of spontaneous EW symmetry breaking accompanied by the Higgs boson
– Mixing of flavours with the help of the Cabibbo-Kobayashi-Maskawa (CKM) and the Pontecorvo-Maki-Nakagava-Sakato (PMNS) matrices
– CP violation via the phase factors in the flavour mixing matrices
– Confinement of quarks and gluons inside hadrons
– Baryon and lepton number conservation
– CPT invariance which leads to the existence of antimatter

The principles of the Standard Model allow its small modifications with respect to the minimal scheme. Thus, for instance, it is possible to add new families of matter particles, additional Higgs bosons, the presence or absence of right-handed neutrino, Dirac or Majorana nature of neutrino is fully acceptable.

The formalism of the Standard Model is based on local quantum field theory. The SM is described by Lagrangian which is built in accordance with the Lorentz invariance and invariance under three gauged groups of symmetry and also obeys the principle of renormalizability, which means that it contains only the operators of dimension 2, 3 and 4 [1].

$$\mathcal{L} = \mathcal{L}_{gauge} + \mathcal{L}_{Yukawa} + \mathcal{L}_{Higgs},$$ (1)

$$\mathcal{L}_{gauge} = -\frac{1}{4}G^a_{\mu\nu}G^a_{\mu\nu} - \frac{1}{4}A^i_{\mu\nu}A^i_{\mu\nu} - \frac{1}{4}B_{\mu\nu}B_{\mu\nu}$$
$$+i\overline{L}_\alpha\gamma^\mu D_\mu L_\alpha + i\overline{Q}_\alpha\gamma^\mu D_\mu Q_\alpha + i\overline{l}_\alpha\gamma^\mu D_\mu l_\alpha$$
$$+i\overline{U}_\alpha\gamma^\mu D_\mu U_\alpha + i\overline{D}_\alpha\gamma^\mu D_\mu D_\alpha + (D_\mu H)^\dagger(D_\mu H)$$
$$+i\bar{N}_\alpha\gamma^\mu\partial_\mu N_\alpha \quad \leftarrow \text{possible rigth-handed neutrino}$$

$$\mathcal{L}_{Yukawa} = y^l_{\alpha\beta}\overline{L}_\alpha l_\beta H + y^d_{\alpha\beta}\overline{Q}_\alpha D_\beta H + y^u_{\alpha\beta}\overline{Q}_\alpha U_\beta\tilde{H} + h.c.,$$
$$+y^N_{\alpha\beta}\bar{L}_\alpha N_\beta\tilde{H} \quad \leftarrow \text{possible rigth-handed neutrino}$$

where $\tilde{H} = i\tau_2 H^\dagger$.

$$\mathcal{L}_{Higgs} = -V = m^2 H^\dagger H - \frac{\lambda}{2}(H^\dagger H)^2.$$

Here y are the Yukawa and λ is the Higgs coupling constants, respectively, both dimensionless and m is the only dimensional mass parameter.

The symmetries of the SM allow one to fix all the interactions of quarks and leptons which are performed by the exchange of the force carriers, namely, by gluons, W and Z bosons, photons and the Higgs boson in the case of strong, weak, electromagnetic and Yukawa interactions, respectively. The only freedom is the choice of parameters: 3 gauge couplings g_i, 3 (or 4) Yukawa matrices $y^k_{\alpha\beta}$, the Higgs coupling λ, and the mass parameter m. All of them are not predicted by the SM but are measured experimentally. The existence of the right-handed neutrino leads to two additional terms in the Lagrangian, the kinetic one and the interaction with the Higgs boson. If the neutrino is a Majorana particle, then one should also add the Majorana mass term.

The Standard model has some drawbacks which, however, are manifested at very high energies where it can possibly be replaced by a new theory. Below, we list some of them.

1) The running couplings of the SM tend to infinity at finite energies (the Landau pole [2]). This is true for the $U(1)$ and the Higgs couplings (see Fig.1, left). Thus, the running of the $U(1)$ coupling in
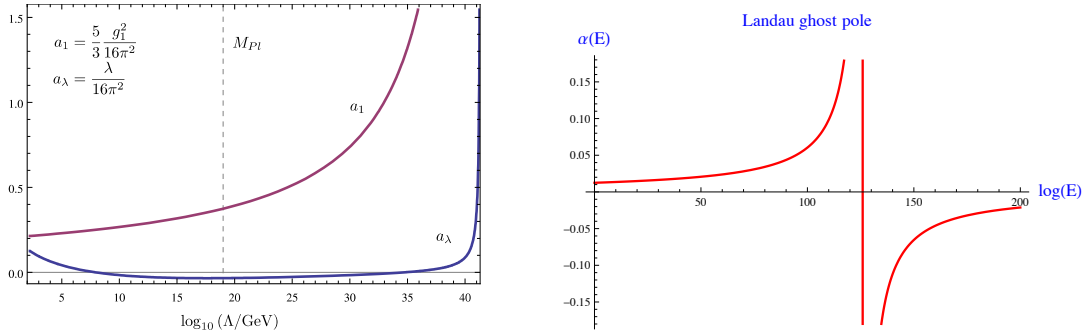
Fig. 1: The dependence of the abelian gauge and the Higgs couplings on momenta transfer (left). The behaviour of the coupling in the vicinity of the Landau pole (right).

the leading order is described by the formula

$$\alpha_1(Q^2) = \frac{\alpha_{10}}{1 - \frac{41}{10}\frac{\alpha_{10}}{4\pi}\log(Q^2/M_Z^2)} \tag{2}$$

and goes to infinity at $Q^* = M_Z exp(\frac{20\pi}{41\alpha_{10}}) \sim 10^{41}$ GeV (see Fig.1 right). The Landau pole has a wrong sign residue that indicates the presence of unphysical ghost fields - intrinsic problem and inconsistency of a theory, which leads to the violation of causality. And though it takes place at energies much higher

than the Planck mass where, as we assume, quantum gravity might change everything, formally a theory with the Landau pole is not self consistent.

2) Radiative corrections lead to the violation of stability of the electroweak vacuum. The whole construction of the SM may be in trouble being metastable or even unstable. This is also related to the behaviour of the Higgs coupling which crosses zero and then becomes negative at the energies close to 10^{11} GeV (see Fig 2. [3]) However, the situation strongly depends on the accuracy of the measurement
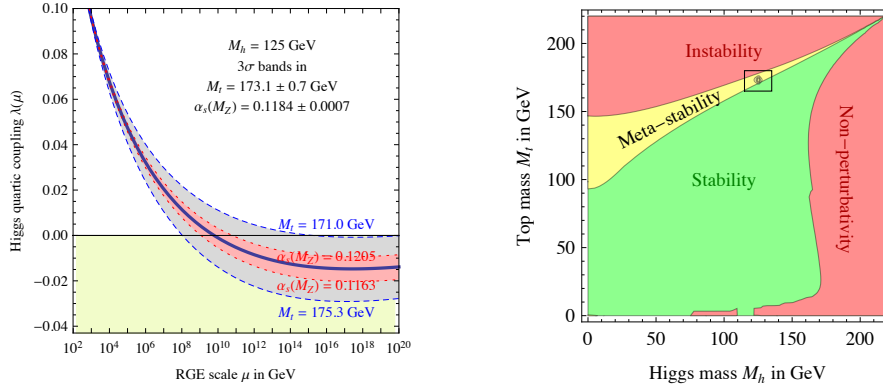
Fig. 2: Dependence of the Higgs coupling on energy scale for various values of the top quark mass in the region where it crosses zero and becomes negative (left) and the regions of stability of the Higgs potential as functions of the top quark and the Higgs boson masses (right).

of the top quark and the Higgs boson masses and on the order of perturbation theory. The tendency when accounting for higher orders is that with increasing accuracy the instability point moves toward higher energies and possibly might reach the Planck scale (see Fig. 3 [4]). The situation may change if there are
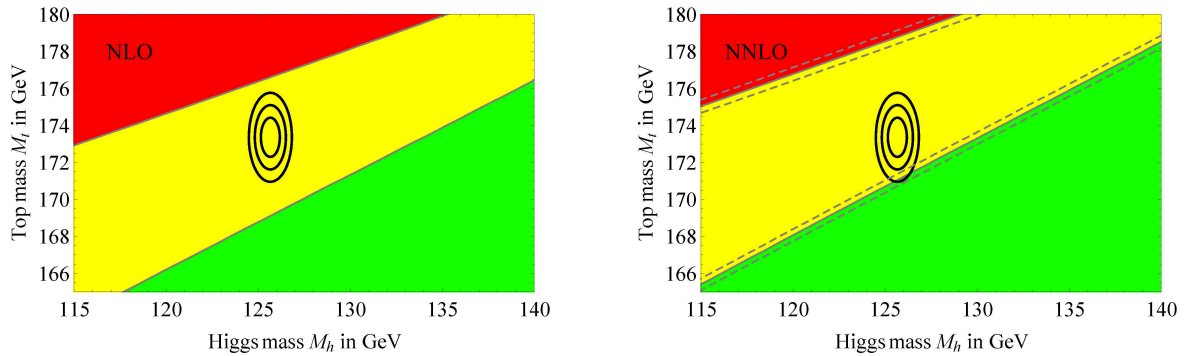
Fig. 3: The same as Fig.2 (right) but with bigger resolution. The left panel corresponds to the NLO corrections while the right panel to the NNLO ones. One can see that the allowed spot moves towards the stability border line

new heavy particles beyond the SM.

3) New physics at the high energy scale might destroy the electroweak scale of the Standard Model due to radiative corrections. This is because contrary to quarks, leptons and intermediate weak bosons the mass of the Higgs boson is not protected by any symmetry. For this reason the radiative correction to the mass of the Higgs boson due to the interaction with hypothetical heavy particles, which are proportional to their mass squared, destroy the electroweak scale. The example of such interaction in the Grand Unified theories is shown in Fig.4. The existing mass hierarchy $M_W/M_{GUT} \sim 10^{-14}$ might be broken.

This is called the hierarchy problem.
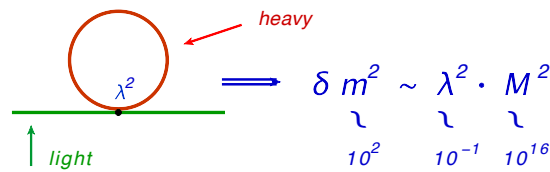
Fig. 4: The one loop diagram which gives the contribution to the renormalization of the Higgs boson mass due to the interaction with hypothetical heavy particles

Notice that this is not a problem of the SM itself (the quadratic divergences are absorbed into the redefinition of the bare mass which is unobservable), but leads to a quadratic dependence of low energy physics on unknown high energy one that is not acceptable. The way out of this situation might be a new physics at intermediate energies.

The Standard Model puts some questions, the answers to which might lie beyond it. They are:

– why is the symmetry group $SU(3) \times SU(2) \times U(1)$?
– why are there 3 generations of matter particles?
– why does the SM obey the quark-lepton symmetry?
– why does the weak interaction have a $V - A$ structure?
– why is the SM left-right asymmetric?
– why are the baryon and lepton numbers conserved?
– etc.

It is not clear also how some mechanisms inside the SM work. In particular, it is not clear

– how confinement actually works
– how the quark-hadron phase transition happens
– how neutrinos get a mass
– how CP violation occurs in the Universe
– how to protect the SM from would be heavy scale physics

There are other questions to the Standard Model:

– Is it self consistent quantum field theory?
– Does it describe <u>all</u> experimental data?
– Are there any indications for physics beyond the SM?
– Is there another scale except for the EW and the Planck ones?
– Is it compatible with Cosmology? (Where is Dark Matter?)

2 Possible Physics Beyond the Standard Model

Let us look at the high energy physics panorama from the point of view of the energy scale (see Fig.5). Besides the electroweak scale $\sim 10^2$ GeV and the Planck scale $\sim 10^{19}$ GeV there is a scale of quantum chromodynamics $\Lambda \sim 200$ MeV, the whole spectra of quark, lepton, intermediate vector boson and the Higgs boson masses, all related to the electroweak scale. Presumably, there is also a string scale $\sim 10^{18}$ GeV, the Grand unification scale $\sim 10^{16}$ GeV, the Majorana mass scale $\sim 10^{12}$ GeV, the vacuum stability
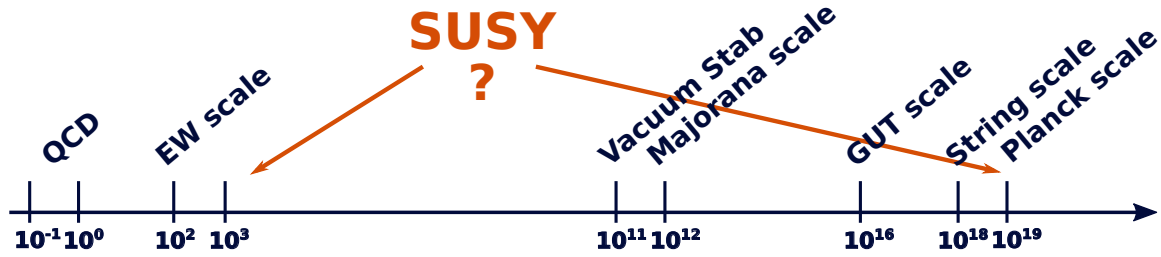
Fig. 5: The high energy physics panorama from the point of view of the energy scale

scale $\sim 10^{11}$ GeV and finally somewhere in the interval from 10^3 to 10^{19} GeV there is a supersymmetry scale.

So far there are no indications that all these scales and new physics related to them exist and high energy physics today stays in a kind of fog masking the horizon of knowledge. But sooner or later the fog will clear away and we will see the ways of future science. At the moment we live in the era of data when theory suggests various ways of development and only experiment can show the right road.

The way out beyond the Standard Model is performed along the following directions:

1. Extension of the symmetry group of the SM : supersymmetry, Grand Unified Theories, new U(1) factors, etc. This way one may solve the problem of the Landau pole, the problem of stability, the hierarchy problem, and also the Dark Matter problem.

2. Addition of new particles: extra generations of matter, extra gauge bosons, extra Higgs bosons, extra neutrinos, etc. This way one may solve the problem of stability and the Dark Matter problem.

3. Introduction of extra dimensions of space: compact or flat extra dimensions. This opportunity opens a whole new world of possibilities, one may solve the problem of stability and the hierarchy problem, get a new insight into gravity.

4. Transition to a new paradigm beyond the local QFT: string theory, brane world, etc. The main hope here is the unification of gravity with other interactions and the construction of quantum gravity.

Note the paradox in modern high energy physics. If usually a new theory emerges as a reply to experimental data which are not explained in an old theory, in our case we try to construct a new theory and persistently look for experimental data which go beyond the Standard Model but cannot find them so far. The existing small deviations from the SM at the level of a few sigma such as in the forward-backward asymmetries in electron-positron scattering or in the anomalous magnetic moment of muon are possibly due to uncertainty of the experiment or data processing. The neutrino oscillations indicating that neutrinos have a mass will probably require a slight modification of the SM: however, there might also be described inside it. Dark Matter, almost the only indication of incompleteness of the SM, yet might be related to heavy Majorana neutrinos and require nothing else.

Nevertheless, there is a vast field of theoretical models of physics beyond the Standard Model. The question is which of these models is correct and adequate to Nature. Note that the prevailing paradigm in most of the attempts to go beyond the SM is the idea of unification. It dates back to the unification of electricity and magnetism in Maxwell theory, unification of electromagnetic and weak forces in electroweak theory, merging of three forces in Grand unified theory, attempts to unify with gravity and creation of the theory of everything on the basis of a string theory. This scenario, though it did not find any experimental verification, still seems possible and has no reasonable alternative.

3   New Symmetries

Extension of the symmetry group of the SM can be performed along two directions: extension of the Lorentz group and extension of the internal symmetry group. In the first case, we are talking about supersymmetric extension.

3.1   Supersymmetry

Supersymmetry is a *boson-fermion* symmetry that is aimed to unify all forces in Nature including gravity within a singe framework [5–9]. Supersymmetry emerged from attempts to generalize the Poincaré algebra to mix representations with different spin [5]. It happened to be a problematic task due to "no-go" theorems preventing such generalizations [10]. The way out was found by introducing the so-called graded Lie algebras, i. e. adding anti-commutators to usual commutators of the Lorentz algebra. Such a generalization, described below, appeared to be the only possible one within the relativistic field theory.

If Q is a generator of the SUSY algebra, then acting on a boson state it produces a fermion one and vice versa

$$\bar{Q}\,|\text{boson}\rangle = |\text{fermion}\rangle, \quad Q\,|\text{fermion}\rangle = |\text{boson}\rangle.$$

Combined with the usual Poincaré and internal symmetry algebra the Super-Poincaré Lie algebra contains additional SUSY generators Q_α^i and $\bar{Q}_{\dot{\alpha}}^i$ [7]

$$
\begin{aligned}
&[P_\mu, P_\nu] = 0, \\
&[P_\mu, M_{\rho\sigma}] = i\,(g_{\mu\rho}P_\sigma - g_{\mu\sigma}P_\rho), \\
&[M_{\mu\nu}, M_{\rho\sigma}] = i\,(g_{\nu\rho}M_{\mu\sigma} - g_{\nu\sigma}M_{\mu\rho} - g_{\mu\rho}M_{\nu\sigma} + g_{\mu\sigma}M_{\nu\rho}), \\
&[B_r, B_s] = i\,C_{rs}^t B_t, \quad [B_r, P_\mu] = [B_r, M_{\mu\sigma}] = 0, \\
&[Q_\alpha^i, P_\mu] = [\bar{Q}_{\dot{\alpha}}^i, P_\mu] = 0, \\
&[Q_\alpha^i, M_{\mu\nu}] = \frac{1}{2}\,(\sigma_{\mu\nu})_\alpha^\beta Q_\beta^i, \quad [\bar{Q}_{\dot{\alpha}}^i, M_{\mu\nu}] = -\frac{1}{2}\,\bar{Q}_{\dot{\beta}}^i(\bar{\sigma}_{\mu\nu})_{\dot{\alpha}}^{\dot{\beta}}, \\
&\{Q_\alpha^i, \bar{Q}_{\dot{\beta}}^j\} = 2\,\delta^{ij}(\sigma^\mu)_{\alpha\dot{\beta}}P_\mu, \\
&[Q_\alpha^i, B_r] = (b_r)_j^i Q_\alpha^j, \quad \bar{Q}_{\dot{\alpha}}^i, B_r] = -\bar{Q}_{\dot{\alpha}}^j(b_r)_j^i, \\
&\{Q_\alpha^i, Q_\beta^j\} = 2\,\epsilon_{\alpha\beta}Z^{ij}, \quad Z_{ij} = a_{ij}^r b_r, \quad Z^{ij} = Z_{ij}^+,
\end{aligned}
\tag{3}
$$

$$
\begin{aligned}
&\{\bar{Q}_{\dot{\alpha}}^i, \bar{Q}_{\dot{\beta}}^j\} = -2\,\epsilon_{\dot{\alpha}\dot{\beta}}Z^{ij}, \quad [Z_{ij}, anything] = 0, \\
&\alpha, \dot{\alpha} = 1, 2 \quad i, j = 1, 2, \ldots, N.
\end{aligned}
\tag{4}
$$

Here P_μ and $M_{\mu\nu}$ are the four-momentum and angular momentum operators, respectively, B_r are the internal symmetry generators, Q^i and $\bar{Q}^i$ are the spinorial SUSY generators and Z_{ij} are the so-called central charges; $\alpha, \dot{\alpha}, \beta, \dot{\beta}$ are the spinorial indices. In the simplest case, one has one spinor generator Q_α (and the conjugated one $\bar{Q}_{\dot{\alpha}}$) that corresponds to the ordinary or $N = 1$ supersymmetry. When $N > 1$ one has the extended supersymmetry.

Motivation for supersymmetry in particle physics is based on the following remarkable features of SUSY theories:

Unification with gravity The representations of the Super-Poincaré algebra contain particles with different spin contrary to the Poincaré algebra where spin is a conserved quantity. This opens the way to unification of all other forces with gravity since the carriers of the gauge interactions have spin 1 and of gravity - spin2, and in the case of supersymmetry, they might be in the same multiplet. Starting with the graviton state of spin 2 and acting by the SUSY generators, we get the following chain of states:

$$\text{spin } 2 \;\to\; \text{spin } \frac{3}{2} \;\to\; \text{spin } 1 \;\to\; \text{spin } \frac{1}{2} \;\to\; \text{spin } 0.$$

Thus, the partial unification of matter (the fermions) with forces (the bosons) naturally arises from an attempt to unify gravity with other interactions.

Taking infinitesimal transformations $\delta_\epsilon = \epsilon^\alpha Q_\alpha$, $\bar{\delta}_{\bar{\epsilon}} = \bar{Q}_{\dot{\alpha}} \bar{\epsilon}^{\dot{\alpha}}$, and using Eqn. (4), one gets

$$\{\delta_\epsilon, \bar{\delta}_{\bar{\epsilon}}\} = 2\,(\epsilon \sigma^\mu \bar{\epsilon}) P_\mu, \tag{5}$$

where $\epsilon, \bar{\epsilon}$ are the transformation parameters. Choosing ϵ to be local, i. e. the function of the space-time point $\epsilon = \epsilon(x)$, one finds from Eqn. (5) that the anticommutator of two SUSY transformations is a local coordinate translation, and the theory, which is invariant under the local coordinate transformation is the General Relativity. Thus, making SUSY local, one naturally obtains the General Relativity, or the theory of gravity, or supergravity [6].

Unification of gauge couplings To see how the couplings change with energy, one has to consider the renormalization group equations. They are well known in the leading orders of perturbation theory in any given model. Besides, one has to know the initial conditions at low energy which are measured experimentally. After the precise measurement of the $SU(3) \times SU(2) \times U(1)$ coupling constants at LEP, it became possible to check the unification numerically. Using these numbers as input and running the RG equations one can check the unification hypothesis. Taking first just the SM, one can see that the couplings do not unify with an offset of 8 sigma. On the contrary, if one switches to supersymmetric generalization of the SM at some energy threshold, unification is perfectly possible with the SUSY scale around 1 TeV that gives additional indication at the low energy supersymmetry. The result is demonstrated in Fig. 6 [11] showing the evolution of the inverse of the couplings as a function of the logarithm of energy. In this presentation, the evolution becomes a straight line in the first order. The second order corrections are small and do not cause any visible deviation from the straight line.
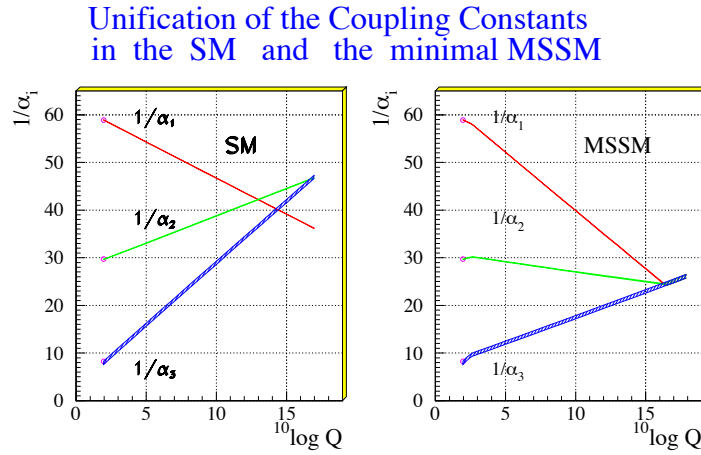
Fig. 6: The evolution of the inverse of the three coupling constants in the Standard Model (left) and in the supersymmetric extension of the SM (MSSM) (right).

Protection of the hierarchy Supersymmetry provides natural preservation of the hierarchy and protection of the low energy scale against radiative corrections. Moreover, SUSY automatically cancels the quadratic corrections in all orders of perturbation theory. This is due to the contributions of superpartners of ordinary particles. The contribution from boson loops cancels those from the fermion ones because of an additional factor (-1) coming from the Fermi statistics, as shown in Fig. 7.

One can see here two types of contribution. The first line is the contribution of the heavy Higgs boson and its superpartner (higgsino). The strength of the interaction is given by the Yukawa coupling constant λ. The second line represents the gauge interaction proportional to the gauge coupling constant g with the contribution from the heavy gauge boson and its heavy superpartner (gaugino).
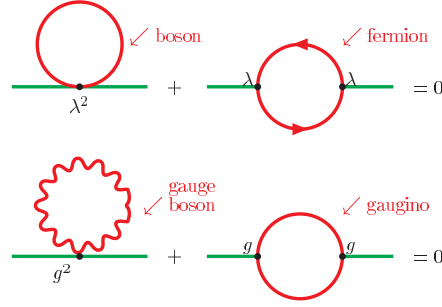
Fig. 7: Cancellation of the quadratic terms (divergencies).

Explanation of the EW symmetry breaking To break the Electroweak symmetry, we use the Brout-Englert-Higgs mechanism of spontaneous symmetry breaking. However, the form of the scalar field potential is taken ad hoc. On the contrary SUSY models provide such an explanation. One originally starts with unbroken potential shown in Fig.8 (left) and then arrives at the famous Mexican hat potential Fig.8 (right) as a result of radiative corrections [12]. Thus, supersymmetry provides the mechanism of radiative EW symmetry breaking in a natural way.
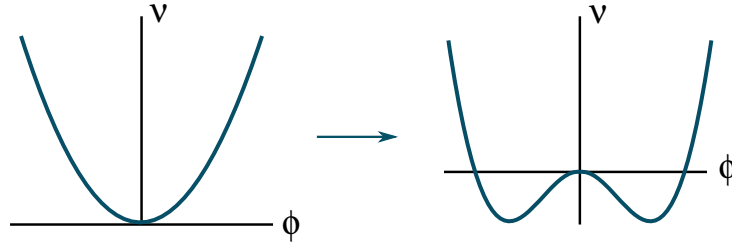
Fig. 8: EW symmetry breaking

Provides the DM particle Supersymmetry provides an excellent candidate for the cold dark matter, namely, the neutralino, the lightest superparticle which is the lightest combination of superparnters of the photon, Z-boson and two neutral Higgses.

$$|\tilde{\chi}_1^0\rangle = N_1|B_0\rangle + N_2|W_0^3\rangle + N_3|H_1\rangle + N_4|H_2\rangle.$$

It is neutral, heavy, stable and takes part in weak interactions, precisely what is needed for a WIMP. Besides, one can easily get the right amount of DM with the electroweak annihilation cross-section.

A natural question arises: what is the content of SUSY theory, what kind of states is possible? To answer this question, consider massless states. Let us start with the ground state labeled by the energy and the helicity, the projection of the spin on the direction of momenta, and let it be annihilated by Q_i [7]

$$\text{Vacuum} = |E, \lambda\rangle, \qquad Q_i|E, \lambda\rangle = 0.$$

Then one- and many-particle states can be constructed with the help of creation operators as

State	Expression	# of states
vacuum	$|E, \lambda\rangle$	1
1-particle	$\bar{Q}_i|E, \lambda\rangle = |E, \lambda + \frac{1}{2}\rangle_i$	N
2-particle	$\bar{Q}_i\bar{Q}_j|E, \lambda = |E, \lambda + 1\rangle_{ij}$	$\frac{N(N-1)}{2}$
...	...	...
N-particle	$\bar{Q}_1 \ldots \bar{Q}_N|E, \lambda\rangle = |E, \lambda + \frac{N}{2}\rangle$	1

The total # of states is: $\sum_{k=0}^{N} \begin{pmatrix} N \\ k \end{pmatrix} = 2^N = 2^{N-1}$ bosons + 2^{N-1} fermions. The energy E is not changed, since according to (4) the operators $\bar{Q}_i$ commute with the Hamiltonian.

Thus, one has a sequence of bosonic and fermionic states and the total number of the bosons equals that of the fermions. This is a generic property of any supersymmetric theory. However, in CPT invariant theories the number of states is doubled since CPT transformation changes the sign of helicity. Hence, in the CPT invariant theories, one has to add the states with the opposite helicity to the above mentioned ones.

Let us consider some examples. We take $N = 1$ and $\lambda = 0$. Then one has the following set of states:

$$
\begin{array}{llll}
N = 1 & \lambda = 0 & & \\
\text{helicity} & 0\ \tfrac{1}{2} & \text{helicity} & 0\ -\tfrac{1}{2} \\
& & \xRightarrow{CPT} & \\
\text{\# of states} & 1\ 1 & \text{\# of states} & 1\quad 1
\end{array}
$$

Hence, the complete $N = 1$ multiplet is

$$
\begin{array}{lccc}
N = 1 & \text{helicity} & -1/2 \quad 0 \quad 1/2 \\
& \text{\# of states} & 1 \quad\ 2 \quad\ 1
\end{array}
$$

which contains one complex scalar and one spinor with two helicity states.

This is an example of the so-called self-conjugated multiplet. There are also self-conjugated multiplets with $N > 1$ corresponding to the extended supersymmetry. Two particular examples are the $N = 4$ super Yang-Mills multiplet and the $N = 8$ supergravity multiplet

$$N = 4 \quad \text{SUSY YM} \quad \lambda = -1$$

helicity	-1	$-1/2$	0	$1/2$	1
# of states	1	4	6	4	1

$$N = 8 \quad \text{SUGRA} \quad \lambda = -2$$

-2	$-3/2$	-1	$-1/2$	0	$1/2$	1	$3/2$	2
1	8	28	56	70	56	28	8	1

One can see that the multiplets of extended supersymmetry are very rich and contain a vast number of particles.

In what follows, we shall consider simple supersymmetry, or the $N = 1$ supersymmetry, contrary to extended supersymmetries with $N > 1$. In this case, one has the following types of the supermultiplets with lower spins:

- chiral supermultiplet (ϕ, ψ) containing the scalar state ϕ and the chiral fermion ψ;

- vector supermultiplet (λ, A_μ) containing the Majorana spinor λ and the vector field A_μ;

- gravity supermultiplet $(\tilde{g}, g)$ containing graviton g of spin 2 and gravitino $\tilde{g}$ of spin 3/2.

Each of multiplets contains two physical states, one boson and one fermion. From these multiplets one constructs all supersymmetric models with N=1 supersymmetry.

To construct a supersymmetric generalization of the SM [13], one has to put all the particles into these multiplets. For instance, the quarks should go into the chiral multiplet and the photon into the vector multiplet. The members of the same multiplet have the same quantum numbers and differ only by spin. Since in the SM there are no particles of different spin having the same quantum numbers, one has to add the corresponding partner for all particles of the SM, thus doubling the number of particles (see fig. 9 [14]) The particle content of the MSSM then appears as shown in Table 3.1. Hereafter, the tilde
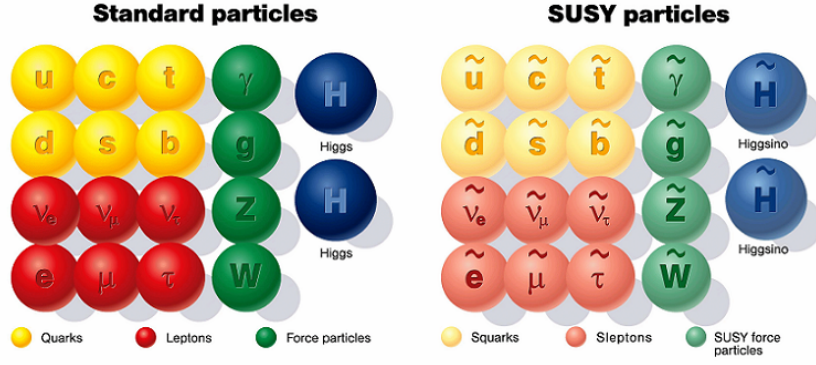
Fig. 9: The minimal supersymmetric generalization of the standard Model

Superfield	Bosons		Fermions		$SU(3)$	$SU(2)$	$U_Y(1)$
Gauge							
G^a	gluon	g^a	gluino	$\tilde{g}^a$	8	0	0
V^k	Weak	W^k $(W^\pm, Z)$	wino, zino	$\tilde{w}^k$ $(\tilde{w}^\pm, \tilde{z})$	1	3	0
V$'$	Hypercharge	B (γ)	bino	$\tilde{b}(\tilde{\gamma})$	1	1	0
Matter							
L$_i$	sleptons $\Big\{$	$\tilde{L}_i = (\tilde{\nu}, \tilde{e})_L$	leptons $\Big\{$	$L_i = (\nu, e)_L$	1	2	-1
E$_i$		$\tilde{E}_i = \tilde{e}_R$		$E_i = e_R^c$	1	1	2
Q$_i$		$\tilde{Q}_i = (\tilde{u}, \tilde{d})_L$		$Q_i = (u, d)_L$	3	2	1/3
U$_i$	squarks $\Big\{$	$\tilde{U}_i = \tilde{u}_R$	quarks $\Big\{$	$U_i = u_R^c$	3*	1	$-4/3$
D$_i$		$\tilde{D}_i = \tilde{d}_R$		$D_i = d_R^c$	3*	1	2/3
Higgs							
H$_1$	Higgses $\Big\{$	H_1	higgsinos $\Big\{$	$\tilde{H}_1$	1	2	-1
H$_2$		H_2		$\tilde{H}_2$	1	2	1
S	Singlet	s	singlino	s	1	1	0

Table 1: Particle content of the MSSM and the NMSSM (the last line)

denotes the superpartner of the ordinary particle. In the last line an extra singlet field is added which corresponds to the so-called Next-to-Minimal model (NMSSM) [15].

The presence of the extra Higgs doublet in the SUSY model is a novel feature of the theory. In the MSSM one has two doublets with the quantum numbers (1,2,-1) and (1,2,1). Thus, in the MSSM, as actually in any two Higgs doublet model, one has five physical Higgs bosons: two CP-even neutral Higgs, one CP-odd neutral Higgs and two charged ones.

The interactions of the superpartners are essentially the same as in the SM, but two of three particles involved into the interaction at any vertex are replaced by the superpartners. Typical vertices are shown in Fig. 10. The tilde above the letter denotes the corresponding superpartner. Note that the coupling in all the vertices involving the superpartners is the same as in the SM as dictated by supersymmtry.

The above-mentioned rule together with the Feynman rules for the SM enables one to draw diagrams describing creation of the superpartners. One of the most promising processes is the e^+e^- annihilation (see Fig. 11). The usual kinematic restriction is given by the c.m. energy $m_{sparticle}^{max} \leq \sqrt{s}/2$.
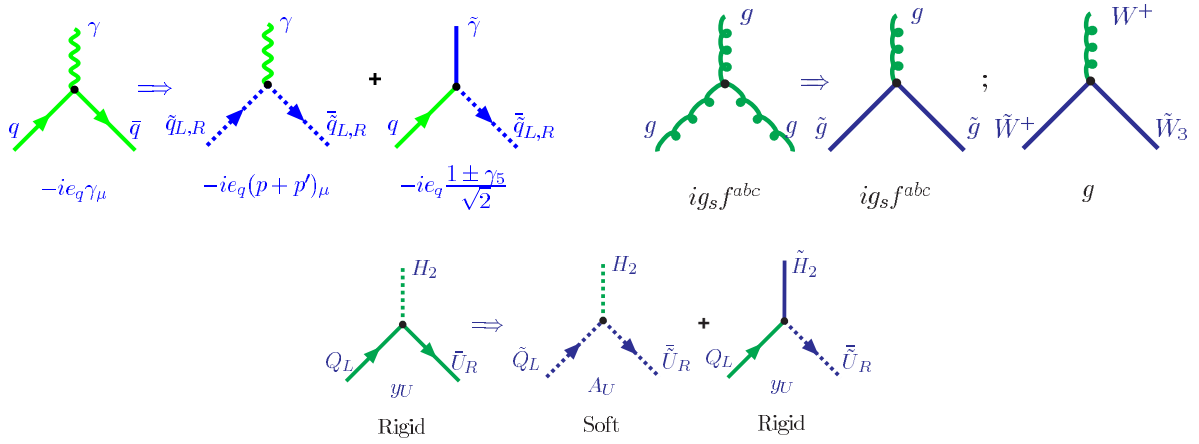
Fig. 10: The gauge-matter interaction, the gauge self-interaction and the Yukawa interaction.
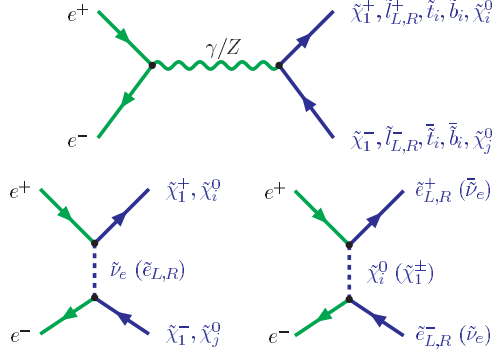

Fig. 11: Creation of the superpartners at electron-positron colliders.

At the hadron colliders the signatures are similar to those at the e^+e^- machines; however, here one has wider possibilities. Besides the usual annihilation channel, one has numerous processes of gluon fusion, quark-antiquark and quark-gluon scattering (see Fig. 12) [16]. The creation of superpartners can be accompanied by the creation of ordinary particles as well. They crucially depend on the SUSY breaking pattern and on the mass spectrum of the superpartners.

The decay properties of the superpartners also depend on their masses. For the quark and lepton superpartners the main processes are shown in Fig. 13. One can notice that the line of superpatners shown in blue is never broken. At the final state one always has a lighter superpartner. This is a consequence of additional new symmetry.
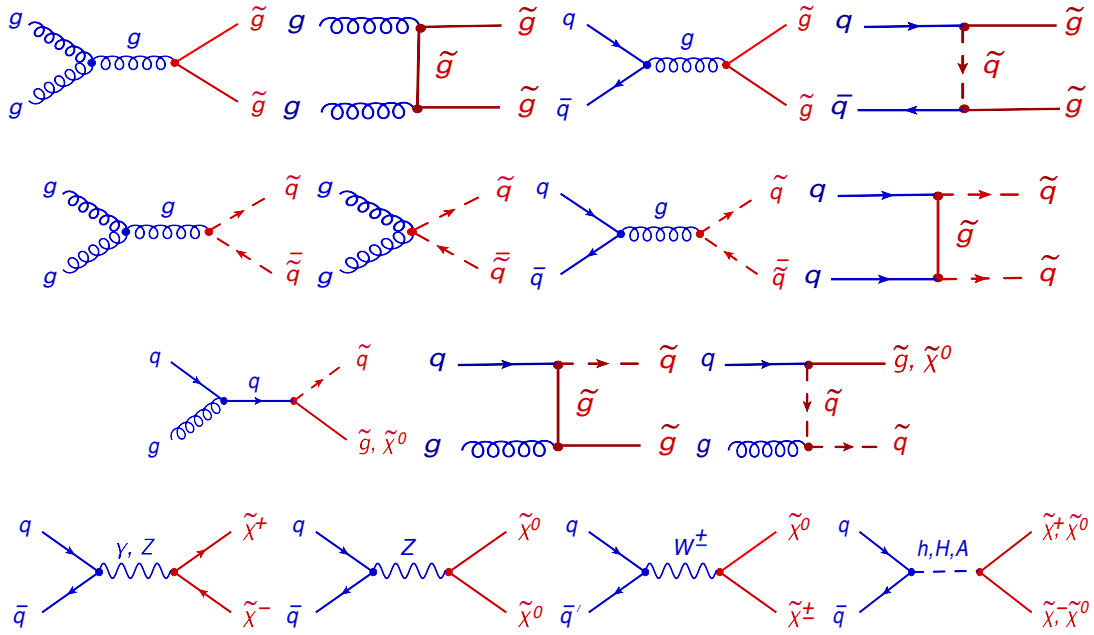
Fig. 12: Examples of diagrams for the SUSY particle production via the strong interactions (top rows for $\tilde{g}\tilde{g}$, $\tilde{q}\bar{\tilde{q}}$ and $\tilde{g}\tilde{q}$, respectively) and the electroweak interactions (the lowest row).

squarks	$\tilde{q}_{L,R} \to q + \tilde{\chi}_i^0$	
	$\tilde{q}_L \to q' + \tilde{\chi}_i^\pm$	
	$\tilde{q}_{L,R} \to q + \tilde{g}$	

sleptons	$\tilde{l} \to l + \tilde{\chi}_i^0$
	$\tilde{l}_L \to \nu_l + \tilde{\chi}_i^\pm$
chargino	$\tilde{\chi}_i^\pm \to e + \nu_e + \tilde{\chi}_i^0$
	$\chi_i^\pm \to q + \bar{q}' + \tilde{\chi}_i^0$

gluino	$\tilde{g} \to q = \bar{q} + \tilde{\gamma}$
	$\tilde{g} \to g + \tilde{\gamma}$

neutralino	$\tilde{\chi}_i^0 \to \tilde{\chi}_1^0 + l^+ + l^-$	final states	$l^+ l^- + \not{E}_T$
	$\tilde{\chi}_i^0 \to \tilde{\chi}_1^0 + q + \bar{q}'$		2jets $+ \not{E}_T$
	$\tilde{\chi}_i^0 \to \tilde{\chi}_1^\pm + l^\pm + \nu_l$		$\gamma + \not{E}_T$
	$\tilde{\chi}_i^0 \to \tilde{\chi}_1^0 + \nu_l + \bar{\nu}_l$		$\not{E}_T$
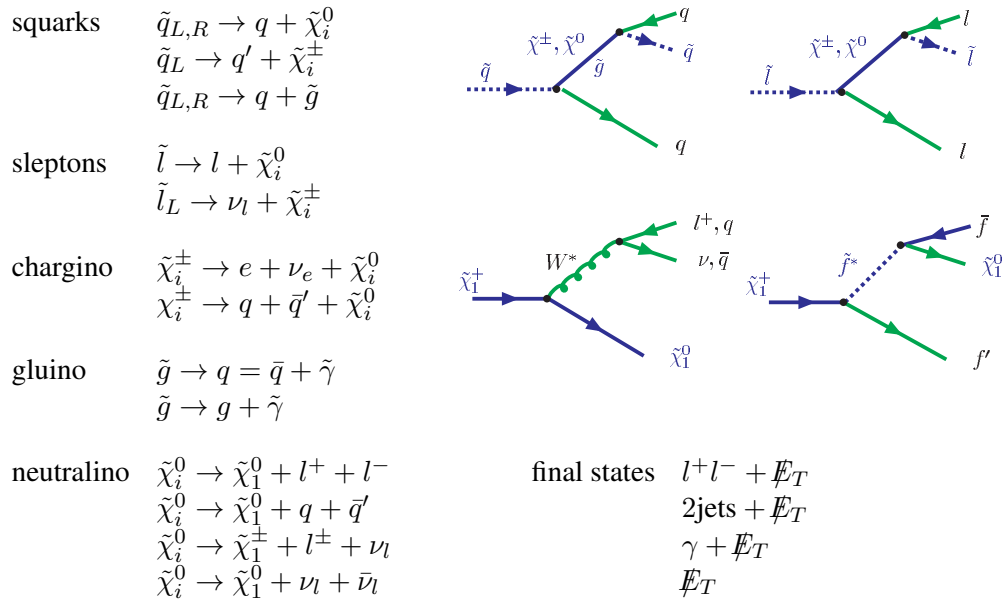
Fig. 13: Decay of superpartners

The interactions of superpartners in the MSSM obey new $U(1)$ symmetry called R-symmetry [17] which is reduced to the discrete group Z_2 and is called R-parity. The R-parity quantum number is

$$R = (-1)^{3(B-L)+2S} \qquad (6)$$

for the particles with the spin S. Thus, all the ordinary particles have the R-parity quantum number equal to $R = +1$, while all the superpartners have the R-parity quantum number equal to $R = -1$. Conservation of the R-parity has two important consequences: the superpartners are created in pairs and the lightest superparticle (LSP) is stable. Usually, it is the photino $\tilde{\gamma}$, the superpartner of the photon with some admixture of the neutral higgsino. This is the candidate for the DM particle which should be neutral and has survived since the Big Bang.

Breaking of SUSY in the MSSM Usually, it is assumed that supersymmetry is broken spontaneously via the v.e.v.s of some fields. However, in the case of supersymmetry, one can not use scalar fields like the Higgs field, but rather the auxiliary fields present in any SUSY multiplet. There are two basic mechanisms of spontaneous SUSY breaking: the Fayet-Iliopoulos (or D-type) mechanism [18] based on the D auxiliary field from the vector multiplet and the O'Raifeartaigh (or F-type) mechanism [19] based on the F auxiliary field from the chiral multiplet. Unfortunately, one can not explicitly use these mechanisms within the MSSM since none of the fields of the MSSM can develop the nonzero v.e.v. without spoiling the gauge invariance. Therefore, the spontaneous SUSY breaking should take place via some other fields.

The most common scenario for producing low-energy supersymmetry breaking is called the *hidden sector scenario* [20]. According to this scenario, there exist two sectors: the usual matter belongs to the "visible" one, while the second, "hidden" sector, contains the fields which lead to breaking of supersymmetry. These two sectors interact with each other by an exchange of some fields called *messengers*, which mediate SUSY breaking from the hidden to the visible sector. There might be various types of the messenger fields: gravity, gauge, etc. The hidden sector is the weakest part of the MSSM. It contains a lot of ambiguities and leads to uncertainties of the MSSM predictions.

All mechanisms of the soft SUSY breaking are different in details but are common in the results. To make certain predictions, one usually introduces the so-called soft supersymmetry breaking terms that violate supersymmetry by the operators of dimension lower than four. For the MSSM without the R-parity violation one has in general

$$-\mathcal{L}_{Breaking} = \qquad (7)$$
$$= \sum_i m_{0i}^2 |\varphi_i|^2 + \left(\frac{1}{2} \sum_\alpha M_\alpha \tilde{\lambda}_\alpha \tilde{\lambda}_\alpha + B H_1 H_2 + A_{ab}^U \tilde{Q}_a \tilde{U}_b^c H_2 + A_{ab}^D \tilde{Q}_a \tilde{D}_b^c H_1 + A_{ab}^L \tilde{L}_a \tilde{E}_b^c H_1 \right),$$

where we have suppressed the $SU(2)$ indices. Here φ_i are all the scalar fields, $\tilde{\lambda}_\alpha$ are the gaugino fields, $\tilde{Q}, \tilde{U}, \tilde{D}$ and $\tilde{L}, \tilde{E}$ are the squark and slepton fields, respectively, and $H_{1,2}$ are the SU(2) doublet Higgs fields.

Equation. (7) contains a vast number of free parameters which spoils the predictiive power of the model. To reduce their number, we adopt the so-called *universality hypothesis*, i. e., we assume the universality or equality of various soft parameters at the high energy scale, namely, we put all the spin-0 particle masses to be equal to the universal value m_0, all the spin-1/2 particle (gaugino) masses to be equal to $m_{1/2}$ and all the cubic and quadratic terms proportional to A and B, to repeat the structure of the Yukawa superpotential. This is an additional requirement motivated by the supergravity mechanism of SUSY breaking. The universality is not a necessary requirement and one may consider nonuniversal soft terms as well. In this case, Eqn. (7) takes the form

$$-\mathcal{L}_{Breaking} = \qquad (8)$$

$$= m_0^2 \sum_i |\varphi_i|^2 + \left(\frac{m_{1/2}}{2} \sum_\alpha \tilde{\lambda}_\alpha \tilde{\lambda}_\alpha + B\mu H_1 H_2 + A\left[y^U_{ab}\tilde{Q}_a\tilde{U}^c_b H_2 + y^D_{ab}\tilde{Q}_a\tilde{D}^c_b H_1 + y^L_{ab}\tilde{L}_a\tilde{E}^c_b H_1\right] \right).$$

<u>Manifestation of SUSY</u> Search for supersymmetry was and still is one of the main tasks in high energy physics. In particle physics this is direct production at colliders at high energies, indirect manifestation at low energies in high precision observables like rare decays or $g - 2$ of the muon and search for long-lived SUSY particles. In astrophysics this is a measurement of the dark matter abundance in the Universe, search for the DM annihilation signal in cosmic rays and direct interaction of DM with the nucleon target in underground experimrnts. So far there is no positive signal anywhere.

Under the assumption that supersymmetry exists at the TeV scale the superpartners of ordinary particles have to be produced at the LHC. Typical processes of creation of superpartners in strong and weak interaction are shown in Fig.14 [21]. A typical signature of supersymmetry is the presence of
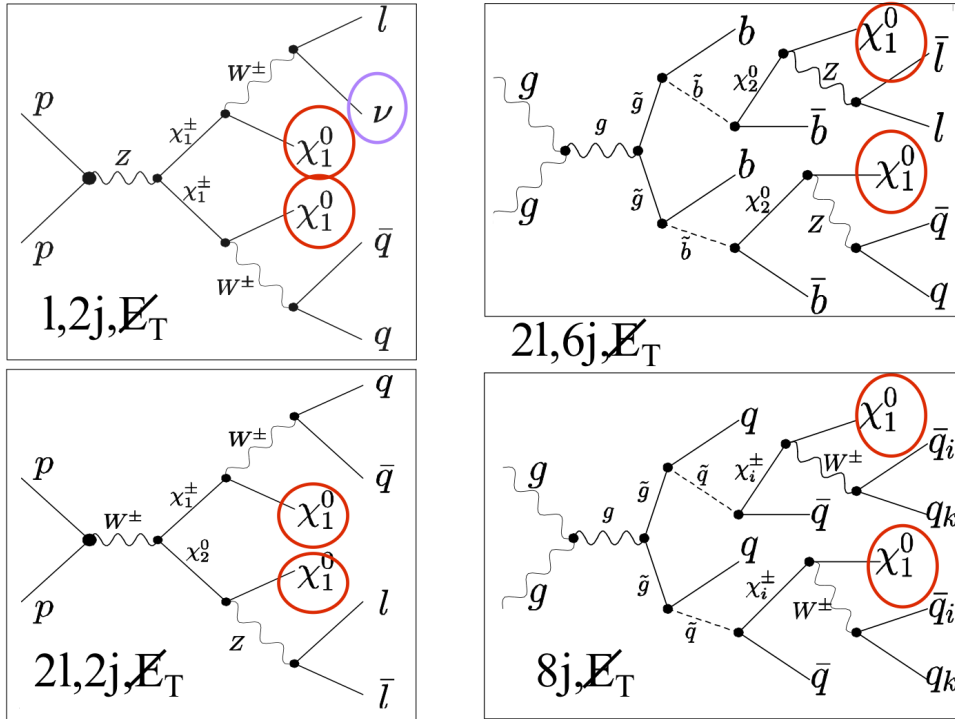
Fig. 14: Creation of superpartners in weak (left) and strong (right) interactions. The expected final states are also shown

missing energy and missing transverse momentum carried away by the lightest supersymmetric particle χ^0_1 which is neutral and stable.

So far the creation of superpartners at the LHC is not found, there are only limits on the masses of hypothetical new particles. To present and analyze the data, two different approaches are used: the high energy input and the low energy input. In the first case, one introduces universal high energy parameters like $m_0, m_{1/2}, A_0, \tan\beta$ of the MSSM [13] and performs the analysis in this universal parameter space. The advantage of this approach is that one has a small number of universal parameters for all particles. The disadvantage is that this set it model dependent (MSSM, NMSSM, etc). In the second case one uses the low energy parameters like masses of superpartners, $\tilde{m}_g, \tilde{m}_q, \tilde{m}_\chi$ or $m_A, \tan\beta$. The advantage is that it is model independent, the disadvantage is that one has many parameters and they are process dependent. Both the approaches are used in practice.

As one can see from Fig.15 [22], the progress achieved at the LHC run is rather remarkable. The

boundary of possible values of masses of the scalar quarks and gluino have reached approximately 1500 and 1000 GeV, respectively. For the stop quarks it is almost two times lower. This is because the created squark always decays into the corresponding quark and in the case of the top quark, due to its heaviness, the phase space decreases and so does the resulting branching ratio. For the lightest neutralino the mass boundary varies between 100 and 400 GeV depending on the values of other masses. The constraints on the masses of charged weakly interacting particles are almost two times higher than those for the neutral ones but depend on the decay mode. Let us stress once more that the obtained mass limits depend on the assumed decay modes which in their turn depend on the mass spectrum of superpartners, which is unknown. The presented constraints refer to the natural scenario.
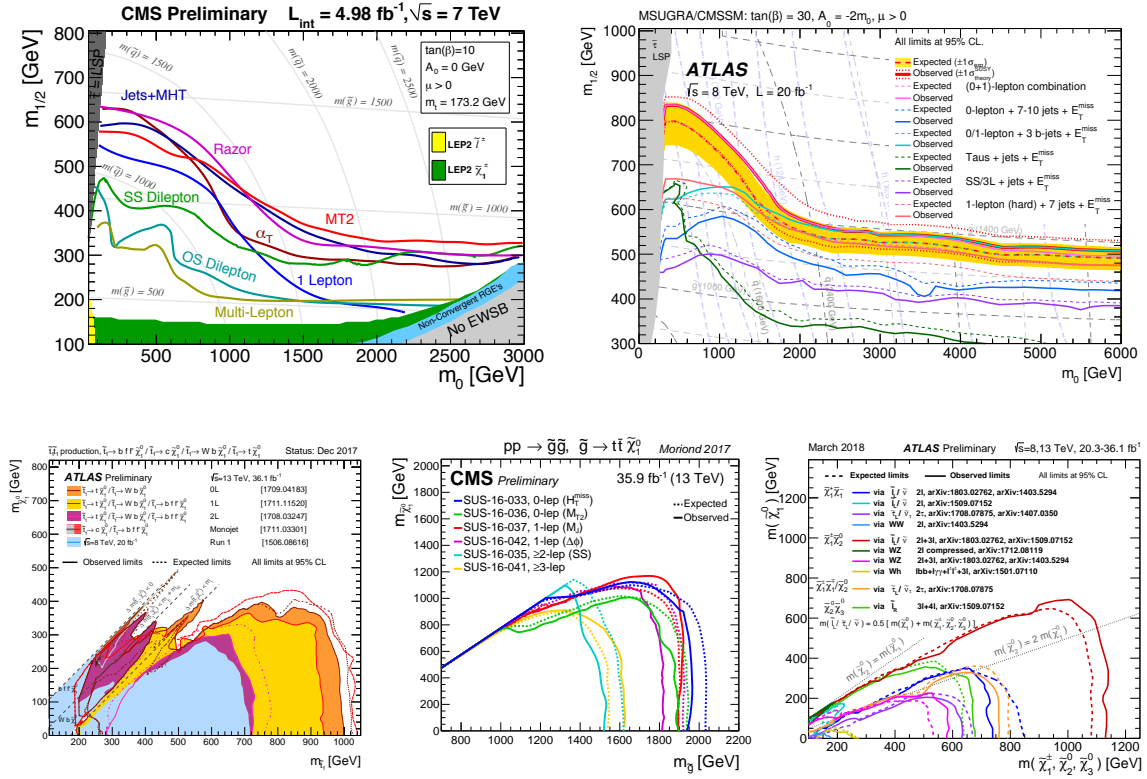
Fig. 15: Search for supersymmetry: the universal parameter plot (upper row) and the superpartner mass plot (lower row)

The enormous progress reached by the LHC is slightly disappointing. The natural question arises: Are we looking in the right direction? Or maybe we have not yet reached the needed mass interval? The answers to these questions can be obtained at the next runs of the accelerator. For the doubled energy the cross-sections of the particle production with the masses around 1 TeV rise almost by an order of magnitude, and one might expect much higher statistics. Taking the gauge coupling unification seriously, SUSY may have some chance to be seen at the LHC, and a good chance at the FCC. The mass range reach of the high luminosity LHC and the FCC collider are shown in Fig.16.

3.2 Grand Unification

Grand Unification is an extension of the Gauge symmetry of the SM. Grand Unified Theories (GUT) unify strong, weak and electromagnetic interactions in the framework of a single theory based on a simple symmetry group [24]. In this case the internal symmetry group of the SM, namely, $SU(3) \times SU(2) \times U(1)$ becomes a part of a wider group G_{GUT}. All known interactions are considered as different branches
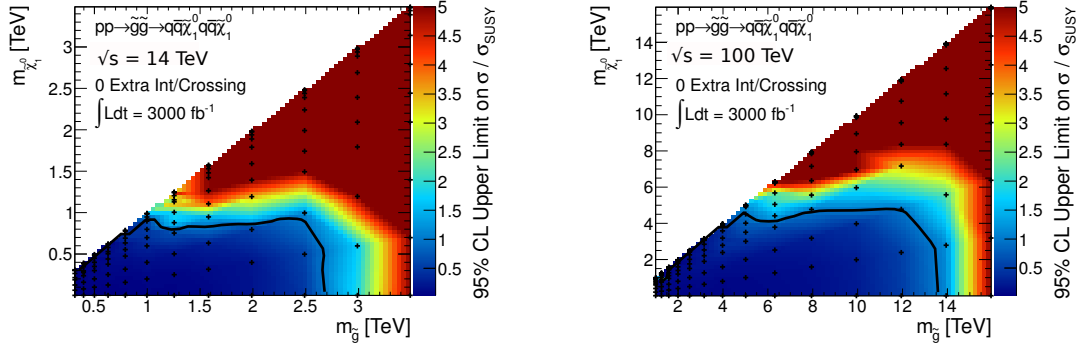
Fig. 16: Search for supersymmetry at the LHC and FCC [23]

of a unique interaction associated with a simple gauge group. The unification (or splitting) occurs at high energy

	Low energy		$\Rightarrow$	High energy
$SU_c(3)\otimes$	$SU_L(2)\otimes$	$U_Y(1)$	$\Rightarrow$	G_{GUT} $(or\ G^n + \text{discrete symmetry})$
gluons	W, Z	photon	$\Rightarrow$	gauge bosons
quarks	leptons		$\Rightarrow$	fermions
g_3	g_2	g_1	$\Rightarrow$	g_{GUT}

At first sight this is impossible due to a big difference in the values of the couplings of strong, weak and electromagnetic interactions. The crucial point here is the running coupling constants. According to the renormalization group equations, all the couplings depend on the energy scale. In the SM
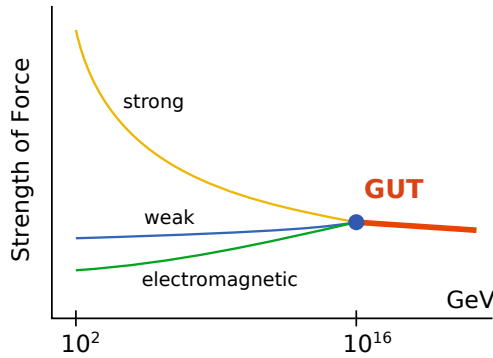
Fig. 17: The running coupling constants in the GUT scenario

the strong and weak couplings associated with non-abelian gauge groups decrease with energy, while the electromagnetic one associated with the abelian group on the contrary increases. Thus, it becomes possible that on some energy scale they become equal (see Fig.17).

According to the GUT idea, this equality is not occasional but is a manifestation of unique origin of these three interactions. As a result of spontaneous symmetry breaking, the unifying group is broken and unique interaction is splitted into three branches which we call strong, weak and electromagnetic interactions.

The symmetry group of a Grand Unified Theory should be sufficiently wide to include the group of the SM and should have appropriate complex representations to fit quarks and leptons inside them. This means that the rank of this group (the maximal number of linearly independent generators that commute with each other) should be equal or larger to that of the SM group, i.e. 4. Remind the

classical groups of rank l: $SU_{l+1}, SO_{2l+1}, SO_{2l}, Sp_{2l}$. Thus, the minimal group of rank 4 is $SU(5)$.

SU(5) GUT - Minimal GUT

$SU(5)$ is a minimal group (rank 4) into which $SU(3) \otimes SU(2) \otimes U(1)$ can be embedded and which has complex representations needed for chiral fermions. This group satisfies all the requirements mentioned above. Particle content of the $SU(5)$ GUT is the following:

Gauge sector. $W_\mu = W_\mu^A T^A$, $A = 1, 2, \ldots 24$, T^A are the generators of $SU(5)$. It is a $24 - plet$ which can be represented as a traceless 5×5 matrix

$$W_\mu = \begin{pmatrix} & & & \vdots & X_\mu^1 & Y_\mu^1 \\ & G_\mu^a \frac{\lambda^a}{2} & - \frac{1}{\sqrt{15}} B_\mu \mathbf{1}_3 & \vdots & X_\mu^2 & Y_\mu^2 \\ & & & \vdots & X_\mu^3 & Y_\mu^3 \\ \ldots & \ldots & \ldots & \vdots & \ldots & \ldots \\ X_\mu^{*1} & X_\mu^{*2} & X_\mu^{*3} & \vdots & \frac{1}{2} A_\mu^3 + \sqrt{\frac{3}{20}} B_\mu & W_\mu^+ \\ Y_\mu^{*1} & Y_\mu^{*2} & Y_\mu^{*3} & \vdots & W_\mu^- & -\frac{1}{2} A_\mu^3 + \sqrt{\frac{3}{20}} B_\mu \end{pmatrix}$$

Among 24 gauge bosons there are 8 gluons G_μ^a, 3 weak bosons $W_\mu^\pm$ and A_μ^3 and 1 $U(1)$ boson B_μ. There are also 12 *new* fields X_μ and Y_μ. They are usually called lepto-quarks because they mediate lepto-quark transition leading to baryon No violation. The gauge multiplet has the following $SU(3) \otimes SU(2)$ decomposition

$$\underline{24} = \underset{gluons}{(\underline{8}, \underline{1})} + \underset{W \ and \ Z}{(\underline{1}, \underline{3})} + \underset{leptoquarks}{(\underline{3}, \underline{2}) + (\underline{3}, \underline{2})}$$

All fermions are taken to be left-handed. Right-handed particles are replaced by the corresponding left-handed conjugated ones. The minimal fundamental representation of $SU(5)$ is $\underline{5}$. However, it is more convenient to use the conjugated one which has appropriate $SU(3) \otimes SU(2) \otimes U(1)$ quantum numbers

$$\underline{5}^* = (\underline{3}, \underline{1}, -2/3) + (\underline{1}, \underline{2}, 1)$$

It is naturally identified with d-quark and electron-neutrino doublet

$$\underline{5}^* = (d_1^c, d_2^c, d_3^c, e^-, \nu_e)_{Left}$$

To find place for the other members of the same family, we have to go beyond the fundamental representation. Surprisingly, the next (after $\underline{5}$) representation, $\underline{10} = (5 \times 5)_{asym}$ has precisely correct quantum numbers

$$\underline{10} = (\underline{3}, \underline{2}, 1/3) + (\underline{3}^*, \underline{1}, -4/3) + (\underline{1}, \underline{1}, -2)$$

It is a 5×5 antisymmetric matrix and its fermion assignment is

$$\underline{10} = \begin{pmatrix} 0 & u_3^c & -u_2^c & u_1 & d_1 \\ & 0 & u_1^c & u_2 & d_2 \\ & & 0 & u_3 & d_3 \\ & & & 0 & e^+ \\ & & & & 0 \end{pmatrix}_{Left} , \quad \begin{array}{c} u_L^c \to u_R \\ e_L^+ \to e_R \end{array} .$$

Thus, all known fermions exactly fit to $(\underline{5}^* + \underline{10})$ representations of $SU(5)$. Now new fermions appear. Note that there is no room for the right-handed neutrino ν_R. Hence either neutrino is massless in the $SU(5)$ model or it could be a singlet that does not take part in gauge interaction. In spite of the left- right asymmetry of the model there are no anomalies in the gauge currents. They are automatically cancelled between contributions of $\underline{5}^*$ and $\underline{10}$.

SO(10) - optimal GUT. The next popular GUT is based on the $SO(10)$ group of rank 5. The advantage of this model is that all the fermions of the same generation belong to a single irreducible representation $\underline{16}$

$$\underline{16} = (u_1 \ u_2 \ u_3 \ d_1 \ d_2 \ d_3 \ \nu_e \ e^- \ u_1^c \ u_2^c \ u_3^c \ d_1^c \ d_2^c \ d_3^c \ \nu_e^c \ e^+)_{Left}$$

Note that contrary to the $SU(5)$ model the right-handed neutrino (left-handed antineutrino) is present now. This means that the neutrino in the $SO(10)$ model is massive. The gauge field in the $SO(10)$ model has dimension 45. The $SO(10)$ multiplets find their natural decomposition in terms of that of $SU(5)$

$$\begin{aligned} \underline{16} &= \underline{5}^* + \underline{10} + \underline{1} \quad fermions, \\ \underline{45} &= \underline{24} + \underline{10} + \underline{10}^* + \underline{1} \quad gauge \ bosons. \end{aligned}$$

E(6) GUT The next example is the model based on the exceptional group $E(6)$ of rank 6. It is left-right symmetric

$$E(6) \ \supset \ SU_C(3) \otimes SU_L(3) \otimes SU_R(3).$$

Fermions belong to a single fundamental representation $\underline{27}$ which has the following decomposition under $SO(10)$

$$\underline{27} = \underline{16} + \underline{10} + \underline{1},$$

while the gauge bosons form an adjoint representation $\underline{78}$. This model contains a lot of new particles. Its attractiveness is mainly due to the appearance of $E(6)$ GUT in superstring inspired models.

The GUT symmetry is broken spontaneously via the same Brout-Englert-Higgs mechanism. In the case of $SU(5)$ it occurs in two stages: one introduces two Higgs multiplets: $\underline{24}$ which breaks $SU(5)$ down to $SU(3) \otimes SU(2) \otimes U(1)$ and $\underline{5}$ which breaks $SU(3) \otimes SU(2) \otimes U(1)$ down to $SU(3) \otimes U(1)$. The v.e.v are chosen to be

$$< \Phi_{24} > = \begin{pmatrix} V & & & & \\ & V & & & \\ & & V & & \\ & & & -3/2\,V & \\ & & & & -3/2\,V \end{pmatrix}, \quad < H_5 > = \begin{pmatrix} 0 \\ 0 \\ 0 \\ 0 \\ v/\sqrt{2} \end{pmatrix},$$

where $V \sim M_{GUT} \sim 10^{15}$ Gev and $v \sim 250$ Gev .

The symmetry breaking in the $SO(10)$ model can be achieved in two different ways and needs at least three different scales $M_1 \gg M_2 \gg \cdots M_W$

$$SO(10) \ \begin{array}{c} \nearrow \\ M_1 \\ \searrow \end{array} \ \begin{array}{l} SU(5) \ \overset{M_2}{\Rightarrow} \ SU(3) \otimes SU(2) \otimes U(1) \ \overset{M_W}{\Rightarrow} \ SU(3) \otimes U(1) \\ \\ SO(6) \otimes SO(4) \ \sim \ SU(4) \otimes SU_L(2) \otimes SU_R(2) \end{array}$$

The Grand Unified Theories solve many problems of the SM, for instance, the absence of the Landau pole, reduction of the number of parameters, all particles might sit in a single representation (16 of SO(10)), unification of quarks and leptons, open the way to baryon and lepton number violation, etc. However, they produce new problems. This is first of all the hierarchy problem. Indeed, the unification of the couplings takes place at the GUT scale $\sim 10^{15} - 10^{16}$ GeV where spontaneous symmetry breaking takes place. The new heavy particles acquire masses of the order of this scale. Interacting with the Higgs boson of the SM they create the radiative corrections to its mass of the order of their own, thus destroying the hierarchy (see Fig.4). The solution of this problem might be obtained in SUSY GUTs where these unwanted corrections are canceled with the contributions of superpartners in all orders of

PT. This way supersymmetry stabilizes GUTs eliminating the influence of unknown heavy physics on low energy observables preserving hierarchy.

Since in GUTs quarks and leptons belong to the same representation of the gauge group, the interactions with the new gauge bosons leads to the processes where quarks convert into leptons and vice versa, i.e. to the violation of the baryon and lepton numbers, contrary to the SM. The key prediction of GUTs is proton decay. It takes place according to the process shown in Fig.18 (left) with creation of π^0 meson and positron. The proton life time is proportional to the mass of the heavy X boson $\tau_P \sim M_X^4$
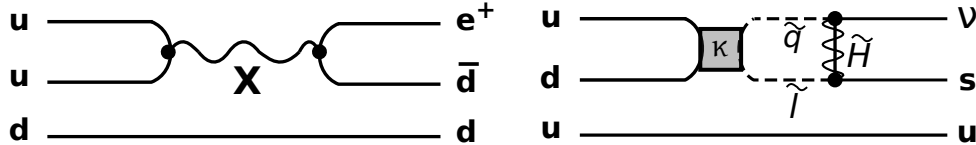
Fig. 18: The diagrams giving a contribution to proton decay in the usual GUT (left) and in the supersymmetric version (right)

that gives the value bigger than 10^{30} years. The modern experimental data give the lower bound $\sim 10^{34}$ years. At the same time, in the supersymmetric case there might be other modes of proton decay with creation of K^+ meson and antineutrino (see Fig.18 right). In this case, the decay rate is additionally suppressed due to the loop with superpartners inside. Experimental constraint here is weaker $\sim 10^{33}$ years. The search for the proton decay is continued. The observation of such a decay would be the confirmation of the GUT hypothesis.

3.3 Extra symmetry factors

A less radical change of the symmetry group of the SM is the presence of additional symmetry factors like $U(1)'$ or $SU(2)'$, etc. These additional factors are typical for the string theory models and might continue the symmetry pattern of the SM. The presence of such factors leads to the existence of additional gauge bosons A', Z', W', etc. At colliders they might appear as characteristic single or double jet events with high energy (see Fig.19 [25]).
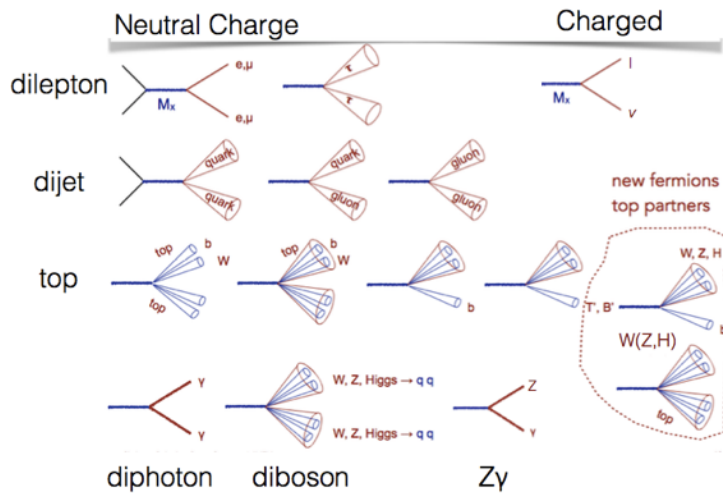
Fig. 19: Single jet and dijet events with high transverse energy

Experimentally studied are the processes with Z' boson production (dimuon events), W production (single muon/jets), resonant $t\bar{t}$ production, diboson events and monojet events with missing energy

(see Fig.20 [26]). So far there are no positive signatures and we have just the bounds on the masses of these hypothetical particles of an order of TeV.
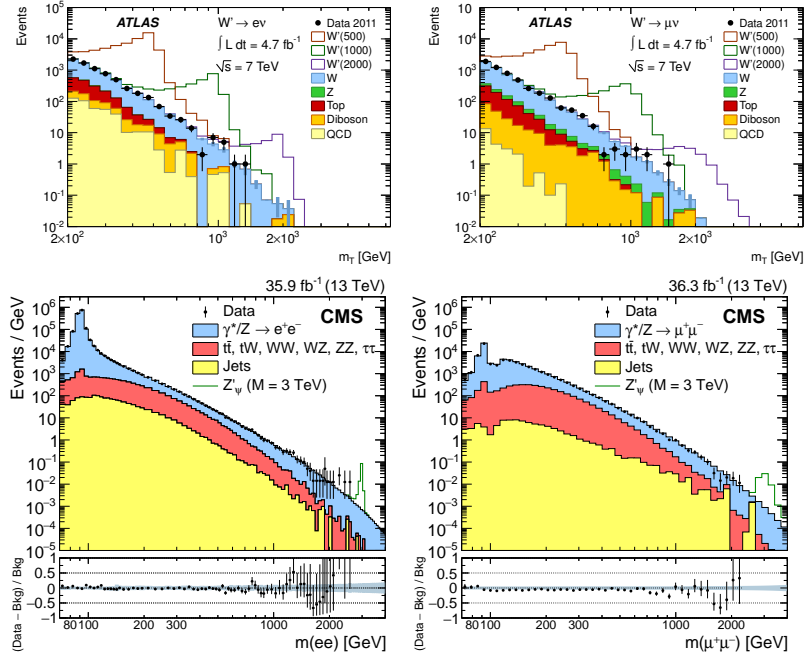
Fig. 20: Search for additional gauge bosons at the LHC

The other popular example of hypothetical new symmetries is the additional $U(1)'$ factor associated with the so-called dark photon. The mixture with the ordinary photon due to the non-diagonal term $\mathcal{L} \sim F_{\mu\nu} F'_{\mu\nu}$ leads to conversion of the ordinary photon into the dark one that might be observed experimentally. There are already some dedicated experiments. Presumably the dark photon might be the dark matter particle.

4 New Particles

The Standard model can be extended introducing new particles as we have seen by example of supersymmetry or additional symmetry factors. However, there are many other possibilities of addition of new particles which are not related to the extension of the symmetry group.

4.1 Extended Higgs sector

Possible extension of the Higgs sector of the SM is an actual question which might be answered in the near future. Is the discovered Higgs boson the only one or not? What are the alternatives to the one Higgs doublet model?

The nearest extension of the SM is the two Higgs doublet model [27]. It is also realized in the case of the Minimal Supersymmetric Standard Model (MSSM) [13]. Here the up and down quarks and leptons interact with different doublets each of which has a vacuum expectation value. In this case, one has 5 Higgs bosons: two CP-even, one CP-odd and two charged ones (see Fig.21 (left)).

The next popular step is the introduction of an additional Higgs field which is a singlet with respect to the gauge group of the SM. In the case of supersymmetry, this model is called the NMSSM, the next-to minimal [15]. Here one has already seven Higgs bosons. The sample spectrum of particles for various models is shown in Fig.21, right. Note that in the case of the NMSSM, one has two light CP-even Higgs bosons and the discovered particle might correspond to both H_1 and to H_2. The reason why we do not
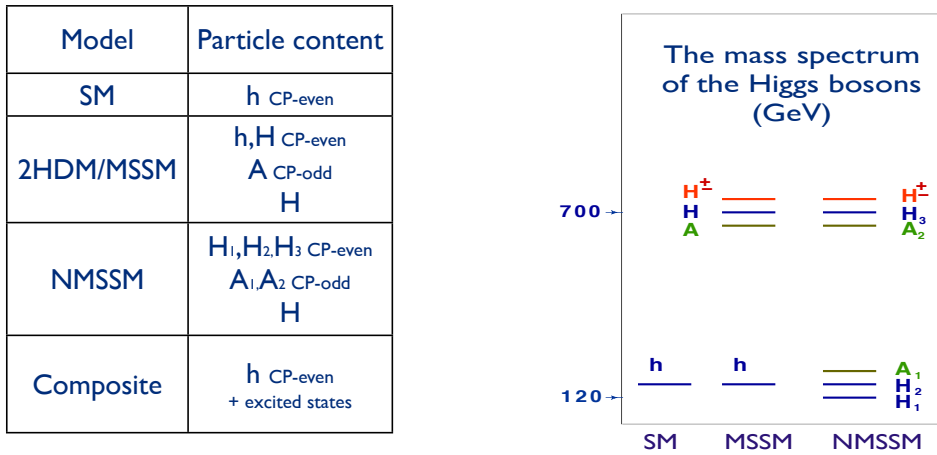
Fig. 21: The field content and the spectrum in various models of the Higgs sector

see the lightest Higgs boson H_1 in the second case is that it has a large admixture of the singlet state and hence very weakly interacts with the SM particles.

How to check these options experimentally? There are two methods: to measure the couplings of the 125-GeV Higgs boson with quarks, leptons and intermediate gauge bosons and check whether they deviate from the predictions of the SM. In the latter case they correspond to the straight line in the plot representing the couplings as functions of the masses of particles (see Fig.22 [28]). Here the name of the game is high precision which can be achieved increasing the luminosity.
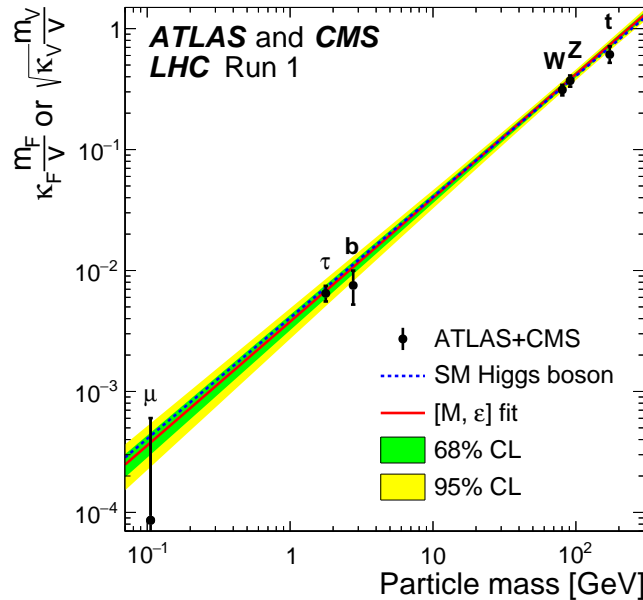
Fig. 22: Dependence of the Higgs couplings on the masses of quarks, leptons and intermediate gauge bosons

The task for the near future is the precision analysis of the discovered Higgs boson. It is necessary to measure its characteristics like the mass and the width and also all decay constants with the accuracy ten times higher than the reached one. Quite possible that this task requires a construction of the electron-positron collider, for instance, the linear collider ILC. Figure 23 shows the expected results for the Higgs
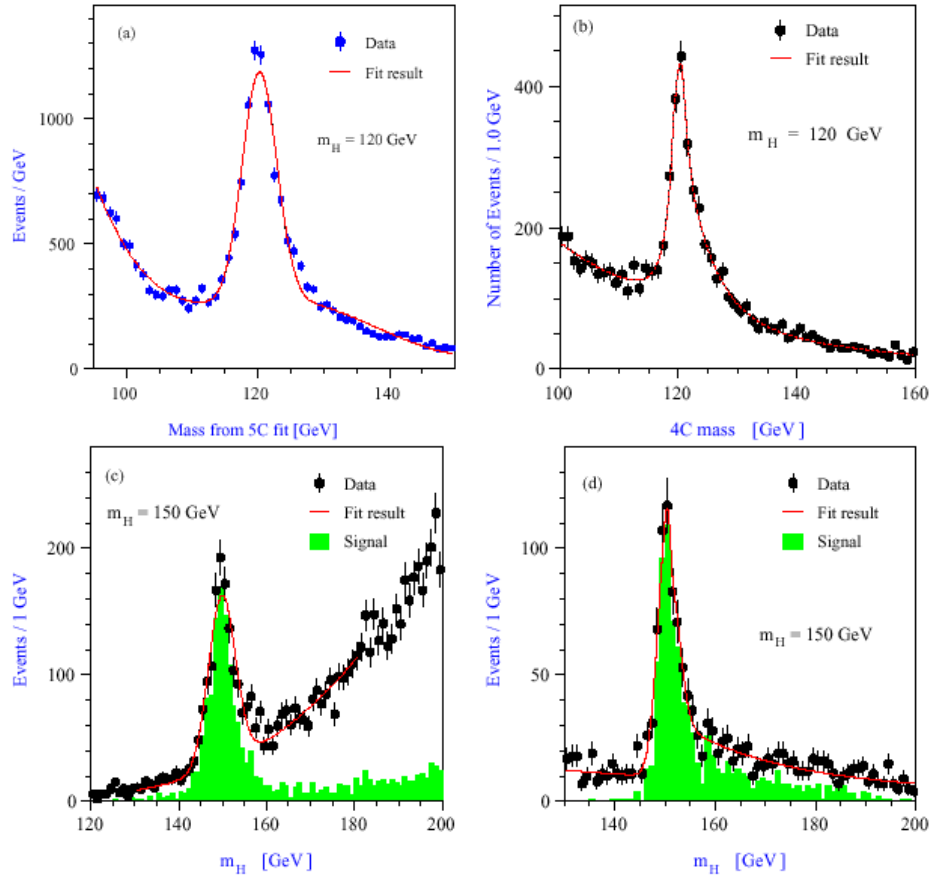
Fig. 23: The measurement of the mass and the width of the Higgs boson in various channels at the ILC: $e^+e^- \rightarrow HZ \rightarrow b\bar{b}q\bar{q}, q\bar{q}l^+l^-, W^+W^-q\bar{q}, W^+W^-l^+l^-$

boson mass measurement at the ILC in various channels [29].

It is planned that the accuracy of the Higgs mass measurement will achieve ~ 50 MeV that is 5-7 times higher than the achieved one. Another task is the accurate determination of the constants of all decays which will possibly allow one to distinguish the one-doublet model from the two-doublet one. Figure 24 shows the planned accuracies of the measurement of the couplings of the Higgs boson with the SM particles at the LHC for the integrated luminosity of 300 1/fb (left), which is ten times higher than today. For comparison we also show the same data for the ILC (middle). The accuracy of measurement of the couplings at the ILC will allow one not only to distinguish different models but also check the predictions of supersymmetric theories (right).
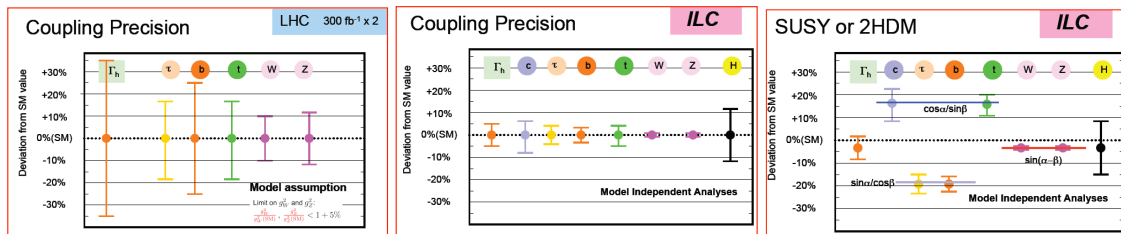
Fig. 24: The measurement of the Higgs boson couplings at the LHC and ILC [30]

The second way is the direct observation of additional Higgs bosons.
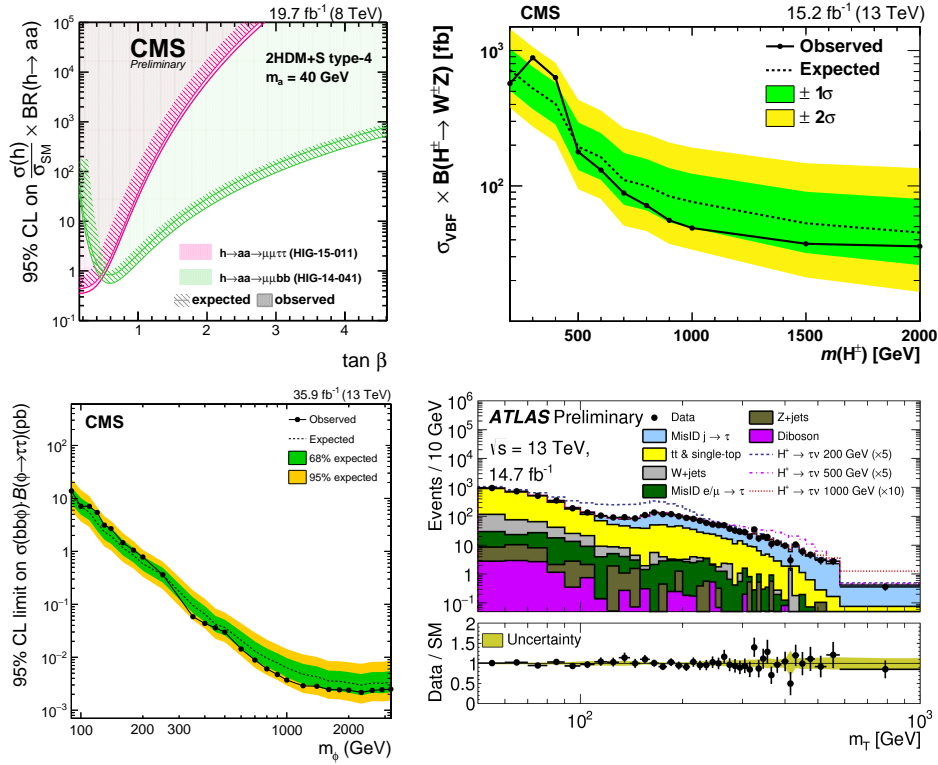
Fig. 25: The search for the heavy and charged Higgs bosons at the LHC

The search for additional Higgs bosons, both the neutral and the charged ones, are performed now at the LHC in various channels. Up to now no signature is seen and we have only the constraints on the masses and parameters of the interaction. Unfortunately, there are no clear predictions for these parameters as it was with the 125-GeV Higgs boson. The results of experimental analysis are shown in Fig.25 [31]. The search for additional Higgs bosons in the interval $200 < m_H < 1000$ GeV did not give positive results so far.

4.2 Axions and axion-like particles

A completely different type of particles is represented axions and axion-like particles. They are related to the problem of CP-violation in strong interactions. As is well known, in the SM CP-violation is due to the phase factors in the quark and lepton mixing matrices. In the quark sector this phase is very small $\delta_{13} = 1.2 \pm 0.1$ rad. However, strong interactions due to the axial anomaly produce a new effective interaction $\frac{\alpha_s}{8\pi} G\tilde{G}\theta_{QCD}$ which has a topological nature and changes the CP-violating phase $\theta = \theta_{QCD} + N_f\delta$.

$$\mathcal{L}_{SM} \in -\bar{q}_L \begin{pmatrix} m_u e^{i\delta/2} & 0 & ... \\ 0 & m_d e^{i\delta/2} & ... \\ 0 & 0 & ... \end{pmatrix} \begin{pmatrix} u \\ d \\ ... \end{pmatrix}_R - \frac{\alpha_s}{8\pi} G\tilde{G}\theta_{QCD}$$

The presence of this phase leads to the appearance of the neutron dipole moment $d_n = -4 \times 10^{-3} \times \theta$ [e fm]. At the same time, the experimental bound on the neutral dipole moment is very strict: $|d_n| < 3 \times 10^{-13}$ [e fm] that gives $\theta < 10^{-10}$. Such a small number requires some explanation. And it was found transforming the angle θ into the dynamic field $a(x) = \theta(x)f_a$ whose vacuum mean value

defines the CP-violating phase. This field interacts with gluons

$$\mathcal{L} = \frac{1}{2}(\partial_\mu a)(\partial^\mu a) - \frac{\alpha_s}{8\pi f_a^2} G_{\mu\nu}^a \tilde{G}_a^{\mu\nu} a \tag{9}$$

and develops a dynamical potential (see Fig.26). In the minimum of the potential it equals zero and
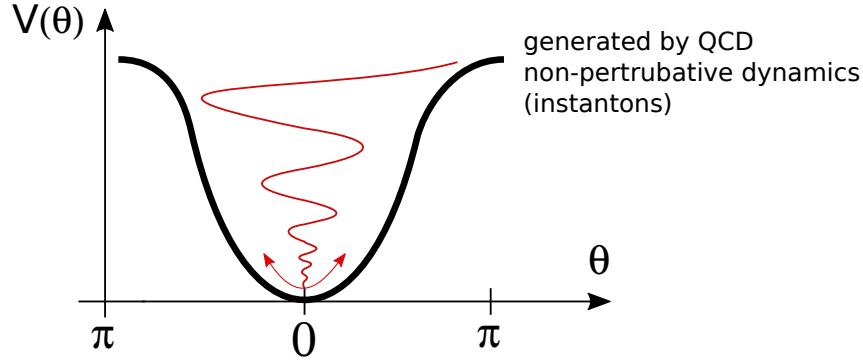
Fig. 26: The axion potential generated by QCD non-perturbative dynamics

then acquires a small value generated by non-perturbative dynamics. The axial symmetry related to this field is broken spontaneously, which leads to the appearance of a goldstone boson that later obtains a mass. This particle got the name of axion and the mechanism of dynamic suppression of θ was called the Peccei-Quinn mechanism [32].

The axion is characterized by two free parameters, its mass m_a and the interaction with gluons $1/f_a$. The search for axions has not given a result so far. The allowed regions in parameter space are shown in Fig.27 [33]. One can see that the allowed masses are extremely small and the scale of interaction f_a is very high.

Later it became clear that coherent oscillations of the axion field (remind that axion is a boson) may produce condensate that can be the form of Dark Matter. Despite the small mass of the axion, the axion Dark matter might be cold since it is not in the state of thermal equilibrium. Therefore, if the axion exists, some amount of Dark Matter of the axion type is inevitable.

4.3 Neutrinos

We know now 3 generations of matter particles. At the moment, there is no theoretical answer to the question of this fact. We have only the experimental data that can be interpreted as an indication of the existence of three generations. They assume the presence of the quark-lepton symmetry since refer to the number of light neutrinos and, due to this symmetry, to the number of generations.

The first fact is the measurement at the electron-positron collider LEP of the profile and width of the Z-boson. The Z-boson can decay into quarks, leptons and neutrinos with the total mass less than its own mass and measuring the width of the Z-boson, one can find out the number of light neutrinos. This is not true for neutrinos with the mass bigger than 45 GeV. The fit to the data corresponds to the number of neutrinos equal to $N_\nu = 2.984 \pm 0.008$, i.e. 3 (see Fig.28 left) [34].

The same conclusion follows from the fit of the spectrum of thermal fluctuations of the cosmic microwave background (CMB). The number of light neutrinos as well as the spectra of their masses are reliably defined from the CMB shape (see Fig.28 right). The obtained number is: $N_\nu =< 3.30 \pm 0.27$ [35], i.e. is also consistent with 3 but still leaves some space for an additional sterile neutrino.

The search for a sterile neutrino is on the way. Its existence may eliminate some tension in neutrino oscillation data coming from the LSND and MiniBoone experiments due to an admixture of the fourth
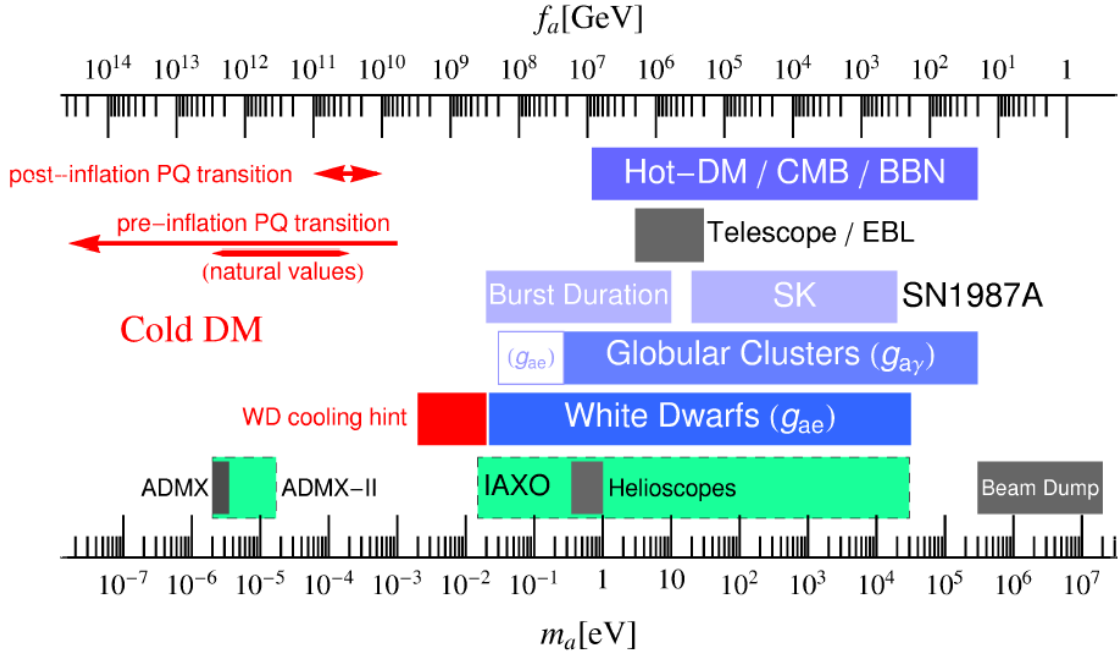
Fig. 27: The allowed regions for the mass and the coupling of the axion
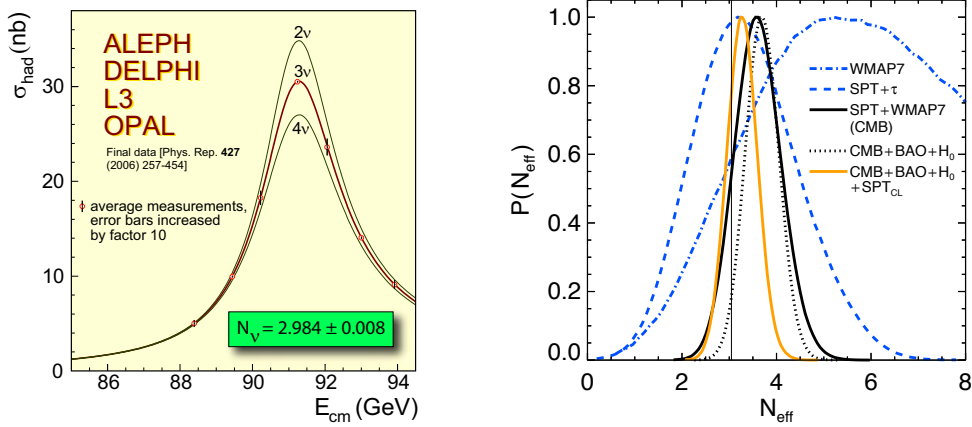
Fig. 28: Experimentally measured profile of the Z-boson, and the number of light neutrinos (left) and the fit of the number of light neutrinos from the temperature fluctuations of CMB (right)

component, which gives additional contribution to neutrino transformation probabilities

$$P_{\nu_e \to \nu_e} \approx 1 - 2|U_{e4}|^2(1 - |U_{e4}|^2)$$
$$P_{\nu_\mu \to \nu_\mu} \approx 1 - 2|U_{\mu4}|^2(1 - |U_{\mu4}|^2)$$
$$P_{\nu_\mu \to \nu_e} \approx 2|U_{e4}|^2|U_{e4}|^2$$

for $4\pi E/\Delta m_{41}^2 << L << 4\pi E/\Delta m_{31}^2$. Nevertheless, a recent direct search for a sterile neutrino gave negative results and imposed constraints on the mass and the mixing of the fourth neutrino (see Fig.29 [36]).

At last, there are complimentary data on precision measurements of the probabilities of rare decays
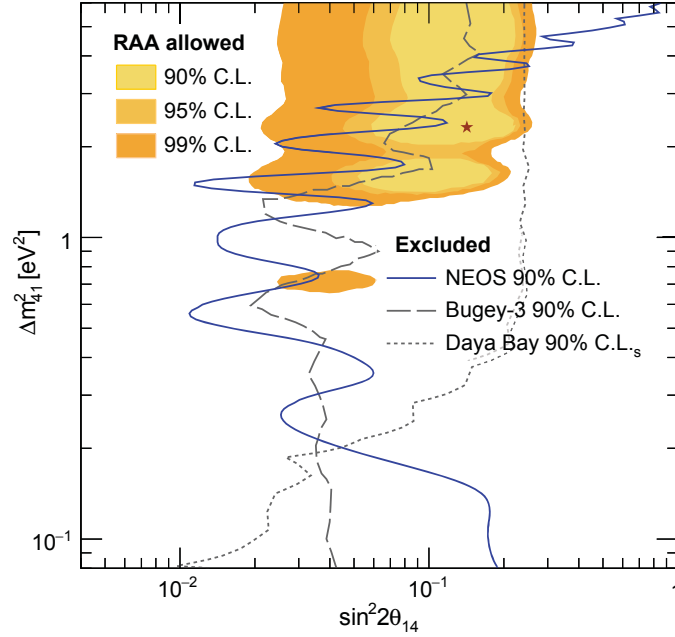
Fig. 29: Constraints on the mass and mixing parameters of a sterile neutrino

where hypothetical additional heavy quark generations might contribute. According to these data, the fourth generation is excluded at the 90% confidence level [37].

A natural question arises: Why does dNature need 3 copies of quarks and leptons? All what we see around us is made of protons, neutrons and electrons, i.e. of u and d quarks and electrons - particles of the first generation. The particles made of the quarks of the next two generations and heavy leptons, copies of the electron, quickly decay and are observed only in cosmic rays or accelerators. Why do we need them?

Possibly, the answer to this question is concealed not in the SM but in the properties of the Universe. The point is that for the existence of baryon asymmetry of the Universe, which is the necessary condition for the existence of a stable matter, one needs the CP-violation [38]. This requirement in its turn is achieved in the SM due to the nonzero phase in the mixing matrices of quarks and leptons.The nonzero phase appears only when the number of generations $N_g \geq 3$.

With the discovery of neutrino oscillations neutrino physics has entered the new phase: the mass differences of different neutrino types and the mixing angles were measured. At last, the answer to the question of neutrino mass was obtained. Now we know that neutrinos are massive. This way, the lepton sector of the SM took the form identical to the quark one and it was confirmed that the SM possesses the quark-lepton symmetry. Nevertheless, the reason for such symmetry remains unclear, it might well be that it is a consequence of the Grand unification of interactions. However, the answer to this question lies beyond the SM.

At the same time, the neutrino sector of the SM is still not fully understood. First of all, this concerns the mass spectrum. Neutrino oscillations allow one to determine only the squares of the mass difference for various neutrinos. The obtained picture is shown in Fig.30 [39]. The color pattern shows the fraction of various types of neutrino in mass eigenstates.

Besides the hierarchy problem (normal or inverted) there is also an unclear question of the absolute scale of neutrino masses. One may hope to get an answer to this question in two ways. The first one is a direct measurement of the electron neutrino mass in the β-decay experiment. According to the Troitsk-Mainz experiment, the upper bound on the neutrino mass today is $m_{\nu_e} < 2$ eV [40]. The upcoming
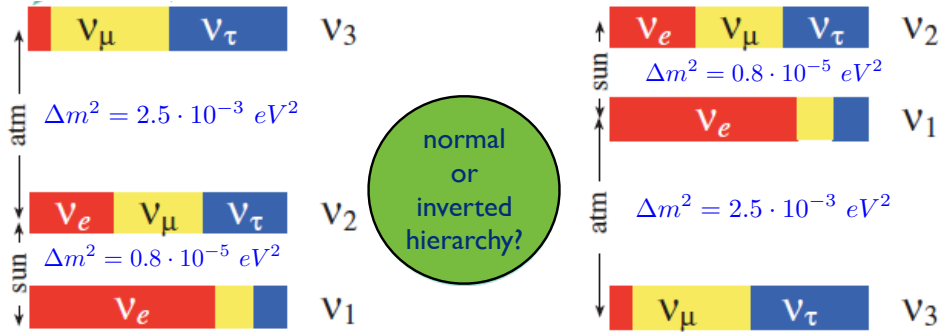
Fig. 30: Normal and inverse hierarchy of neutrino masses

experiment KATRIN [41] will be able to move this bound up to < 0.2 eV. However, this might not be enough if one believes in astrophysical data. The determination of the sum of neutrino masses from the spectrum of the cosmic microwave background is an indirect but rather an accurate way to find the absolute mass scale. At the early stage of the Universe during the fast cooling process particles fell out of the thermodynamic equilibrium at the temperature proportional to their masses and their abundance "froze down" influencing the spectrum. Hence, fitting the spectrum of the CMB fluctuations one can determine the number of neutrino species and the sum of their masses. The result of the latest space mission PLANK [42] looks like $\sum m_\nu < 0.23$ eV. This number is still much bigger than the neutrino mass difference shown in Fig.30. Thus, the absolute scale of neutrino masses is still an open question.

Another unsolved problem of the neutrino sector is the nature of neutrino: Is it a Majorana particle or a Dirac one, is it an antiparticle to itself or not? Remind that particles with spin 1/2 are described by the Dirac equation, the solutions being the bispinors. They can be divided into two parts corresponding to the left or right polarization

$$\nu_D = \begin{pmatrix} \nu_L \\ 0 \end{pmatrix} + \begin{pmatrix} 0 \\ \nu_R \end{pmatrix}, \quad \nu_L \neq \nu_R^*, \quad m_L = m_R. \tag{10}$$

Both parts have the same mass since this is just one particle with two polarization states. At the same time, in the case of a neutral particle the Dirac bispinor can be split into two real parts

$$\nu_D = \begin{pmatrix} \xi_1 \\ \xi_1^* \end{pmatrix} + \begin{pmatrix} \xi_2 \\ \xi_2^* \end{pmatrix}, \quad m_{\xi_1} \neq m_{\xi_2}. \tag{11}$$

each of these parts is a Majorana spinor obeying the condition $\nu_M = \nu_M^*$, i.e. if the neutrino is a Majorana spinor, then it is an antiparticle to itself. These two Majorana spinors can have different masses. Hence, if this possibility is realized in Nature, we have just discovered the light neutrino and the heavy ones can have much bigger masses.

An argument in favour of the Majorana neutrino is the smallness of their masses. If one gets them through the usual Brout-Englert-Higgs mechanism, the corresponding Yukawa couplings are extremely small of an order of 10^{-12}. In the case of the Majorana neutrino one can avoid it using the see-saw mechanism [43]: The small masses of light neutrinos appear due to the heaviness of the Majorana mass

$$M_\nu = \begin{array}{c} \\ L \\ R \end{array}\begin{array}{cc} L & R \\ \end{array}\begin{pmatrix} 0 & m_D \\ m_D & M \end{pmatrix}, \quad m_1 = \frac{m_D^2}{M}, \, m_2 = M. \tag{12}$$

Thus, the neutrino Yukawa coupling may have the usual lepton value and the Majorana mass M might be of the order of the Grand Unification scale. In this case, one also has the maximal mixing in the neutrino sector.

One can find out the nature of the neutrino studying the double β-decay. If the neutrinoless double β-decay is possible, then the neutrino is a Majorana since for the Dirac neutrino it is forbidden. The corresponding Feynman diagram is shown in Fig.31. It also shows the energy spectrum of electrons in the case of the usual and neutrinoless β-decay [46]. As one can see, two types of spectrum are easily
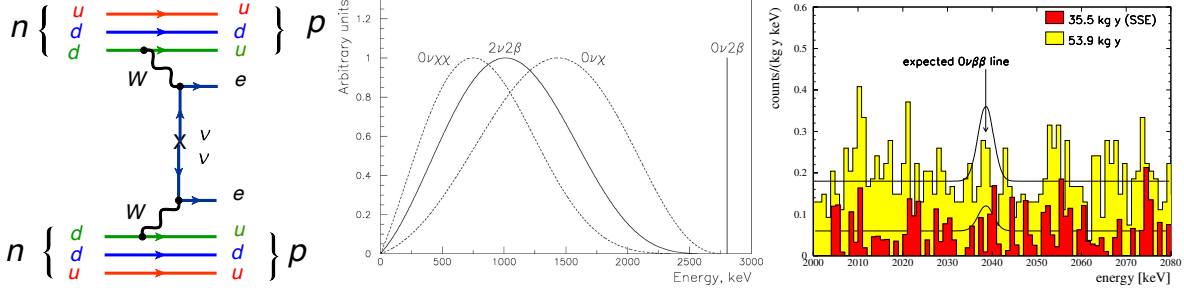
Fig. 31: Neutrinoless double β- decay (left) and the energy spectrum of electrons in the case of a usual and neutrinoless decay of the isotope ^{76}Ge (center). The experimentally measured spectrum of electrons is shown on the right [46]

distinguishable. However, practical observation is rather cumbersome. The histogram shown in Fig.31 (right) is the experimentally measured electron spectrum of the double β-decay. The solid line shows the expected position of the maximum in the spectrum of two electrons corresponding to the double neutrinoless β-decay.

As a result, today there are no clear indications of the existence of the double neutrinoless β-decay. The experiments are carried out on the isotopes $^{48}Ca, ^{76}Ge, ^{82}Se, ^{130}Te, ^{136}Xe, ^{150}Nd$. Modern estimates of the lifetime are [45]

$$T_{1/2}2\nu\beta\beta(^{136}Xe) \quad \times \quad 10^{21} \ yr = 2.23 \pm 0.017 \ stat \pm 0.22 \ sys,$$
$$T_{1/2}0\nu\beta\beta(^{136}Xe) \quad \times \quad 10^{25} \ yr > 1.6 \ (90\% \ CL).$$

It is an interesting question whether it will be possible to find the neutrinoless double beta decay increasing the accuracy of the observation in principle since the effective coupling might be very small. It so happens that the answer to this question depends on the hierarchy of neutrino masses: for the inverse hierarchy the situation is optimistic and there is a lower limit on effective mass while for the normal hierarchy the lower limit is absent and the effective mass can be unlimitedly small. The situation is illustrated in Fig.32 [47]. Thus, the nature of the neutrino remains an open problem of the SM.

4.4 Dark Matter

The existence of Dark Matter is known since the 30s of the last century. However, the situation has changed when the energy balance of the Universe was obtained and became clear that there is 6 times as much of Dark Matter than ordinary matter (see Fig.33, left) [48]. The existence of Dark Matter, which is known so far due to its gravitational influence, is supported by the rotational curves of the stars, galaxies and clusters of galaxies (see Fig.33 right), the gravitational lenses, and the large scale structure of the Universe [49]. Therefore, the question appears: What is the dark matter made of, can it be some non-shining macro objects like the extinct stars, molecular clouds, etc., or these are micro particles? In the last case Dark Matter becomes the object of particle physics.

According to the last astronomical data, at least in our galaxy, there is no evidence of the existence of macro objects, the so called MACHOs. At the same time, Dark Matter is required for a correct description of the star rotation. Therefore, the hypothesis of the microscopic nature of the Dark matter is the dominant one. In this case, in order to form the large scale structure of the Universe, Dark Matter has
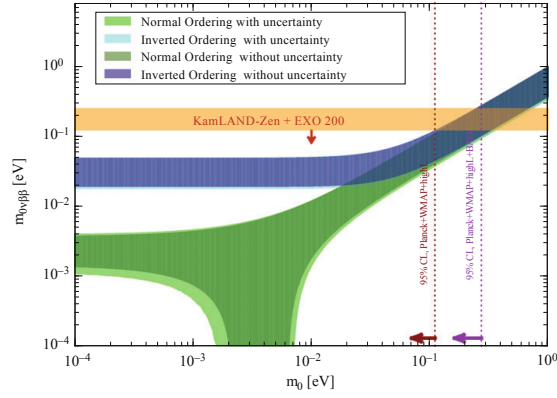
Fig. 32: Effective neutrino mass in neutrinoless double beta decay. Green and pink areas correspond to the inverse and normal hierarchy of neutrino masses, respectively
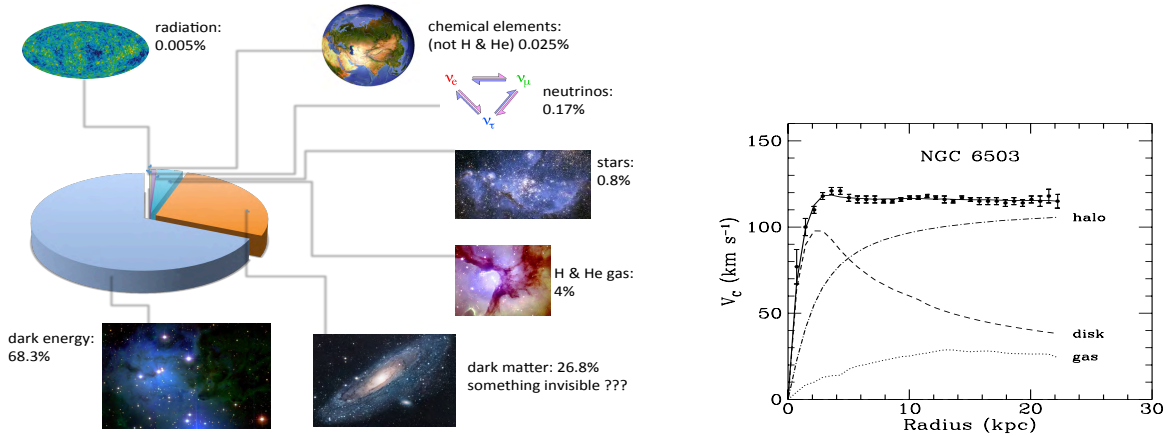
Fig. 33: The energy balance of the Universe (left) [50] and rotation curves of stars in the spiral galaxy (right) [51]

to be cold, i.e. nonrelativistic; hence, DM particles have to be heavy. According to the estimates, their mass has to be above a few dozens of keV [52]. Besides, DM particles have to be stable or long-lived to survive since the Big Bang. Thus, one needs a neutral, stable and relatively heavy particle.

If one looks at the SM, the only stable neutral particle is the neutrino. However, if the neutrino is the Dirac particle, its mass is too small to form Dark Matter. Therefore, within the SM the only possibility to describe Dark Matter is the existence of heavy Majorana neutrinos. Otherwise, one needs to assume some new physics beyond the SM. The possible candidates are: neutralino, sneutrino and gravitino in the case of supersymmetric extension of the SM [53], and also a new heavy neutrino [54], a heavy photon, a sterile Higgs boson, etc. [55]. An alternative way to form Dark Matter is the axion field, the hypothetical light strongly interacting particle [56]. In this case, Dark Matter differs by its properties.

The dominant hypothesis is that Dark Matter is made of weakly interacting massive particles - WIMPs. This hypothesis is supported by the following fact: the concentration of Dark Matter after the moment when a particle fell down from the thermal equilibrium is given by the Boltzmann equation [53]

$$\frac{dn_\chi}{dt} + 3Hn_\chi = - < \sigma v > (n_\chi^2 - n_{\chi,eq}^2),\tag{13}$$

where $H = \dot{R}/R$ is the Hubble constant, $n_{\chi,eq}$ is the concentration in the equilibrium, and σ is the Dark matter annihilation cross-section. The relic density is expressed through the concentration n_χ in the

following way:

$$\Omega_\chi h^2 = \frac{m_\chi n_\chi}{\rho_c} \approx \frac{2 \cdot 10^{27} \ cm^3 \ sec^{-1}}{<\sigma v>}. \tag{14}$$

Having in mind that $\Omega_\chi h^2 \approx 0.113 \pm 0.009$ and $v \sim 300$ km/sec, one gets for the cross-section

$$\sigma \approx 10^{-34} \ cm^2 = 100 \ pb, \tag{15}$$

that is a typical cross-section for a weakly interacting particle with the mass of the order of the Z-boson mass.

These particles presumably form an almost spherical galactic halo with the radius a few times bigger than the size of the shining matter. The DM particles cannot leave the halo being gravitationally bounded and cannot stop since they cannot drop down the energy emitting photons like the charged particles. In the Milky Way, in the region of the Sun the density of Dark Matter should be ~ 0.3 GeV/sm^3 in order to get the observed rotation velocity of the Sun around the center of the galaxy ~ 220 km/sec.

The search for Dark Matter particles is based on three reactions the cross-sections of which are related by the crossing symmetry (see Fig.34) [49].
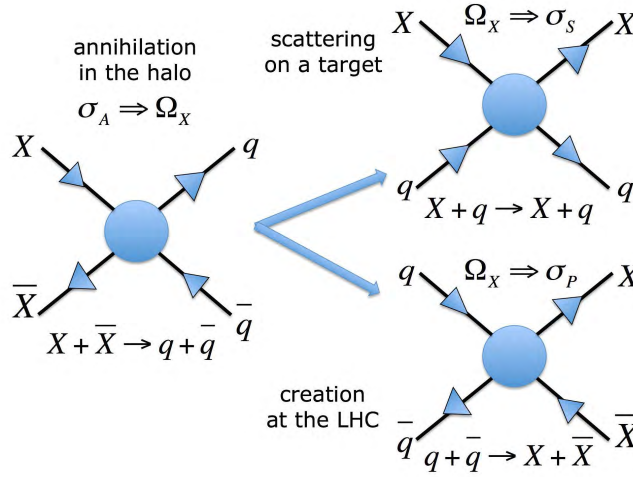
Fig. 34: The search for Dark Matter in three cross related channels

This is, first of all, the annihilation of Dark Matter in the galactic halo that leads to the creation of ordinary particles and should appear as the "knee" in the spectrum of the cosmic rays for diffused gamma rays, antiprotons and positrons. Secondly, this is the scattering of DM on the target which should lead to a recoil of the nucleus of the target when hit by a particle with the mass of the order of the Z-boson mass. And, third, this is a direct creation of DM particles at the LHC which, due to their neutrality, should manifest themselves in the form of missing energy and transverse momentum.

In all these directions there is an intensive search for a signal of the DM. The results of this search for all three cases are shown in Figs.35, 36. As one can see from the cosmic ray data (Fig.35), in the antiproton sector there is no any statistically significant excess above the background [57]. In the positron data there exists some confirmed increase; however, its origin is usually connected not with the DM annihilation but with the new astronomical source [58]. The spectrum of diffused gamma rays like antiprotons is consistent with the background within the uncertainties.

As for the direct detection of Dark Matter, there is no any positive signal so far. The results of the search are presented in the plane mass–cross-section. One can see from Fig.36 [61] that today the cross-sections up to 10^{-45} sm^2 are reached for the mass near 100 GeV. In the near future it is planned to advance two orders of magnitude.
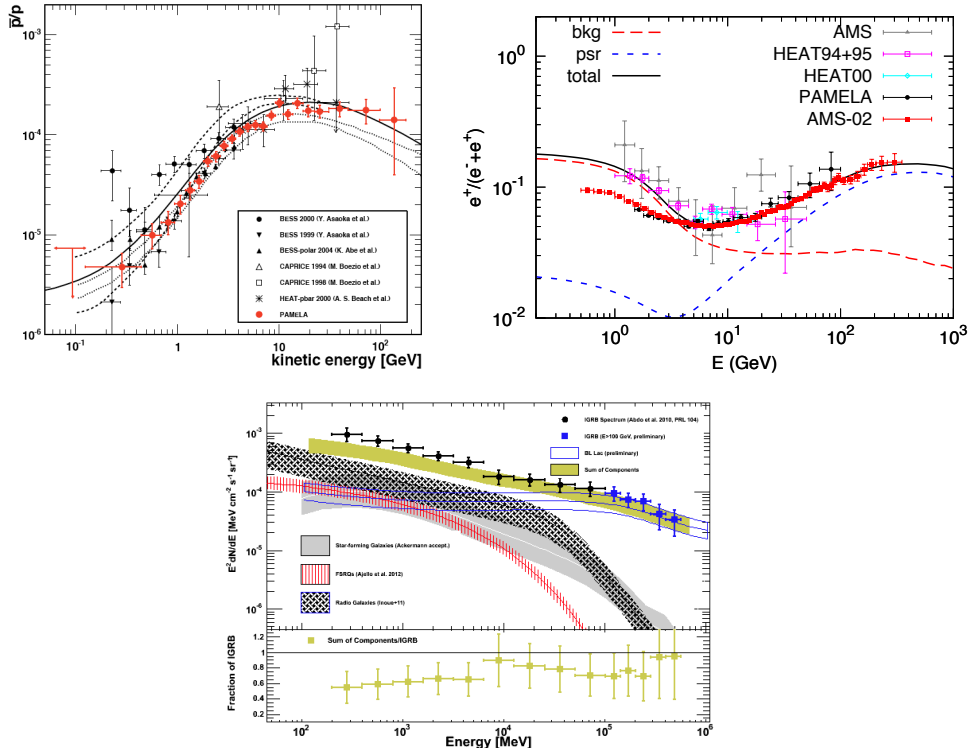
Fig. 35: Indirect search for Dark Matter: antiproton [57], positron [58], and diffuse γ ray [59] data

The results of the DM search at the LHC are also shown in the plane mass–cross-section [62]. Here the signal of the DM creation is also absent. As it follows from the plot, the achieved bound of possible cross-sections at the LHC is worse than in the underground experiments for all mass regions except for the small masses < 10 GeV where the accelerator is more efficient. Note, however, that the interpretation of the LHC data as the registration of DM particles is ambiguous and definite conclusions can be made only together with the data from the cosmic rays and direct detection of the scattering of DM.

All available experimental data combined (LHC,LUX,Planck) are still consistent with even the simplest versions of SUSY (cNMSSM, NUHM). The remaining parameter space is directly probed by direct WIMP searches with tonne scale detectors: DEAP-3600, XENON1T, LUX/LZ. Complimentarity with the LHC (cMSSM, NUHM are mostly out of reach of the 14 TeV run!)

The other possibility mentioned already is the dark photon. In the process of annihilation one may produce the dark photon together with the ordinary one. It will decay later producing the pair of charged particles which may be detected or invisible matter in the form of neutralino. The search for such decays is running and new dedicated experiments are in progress. The results are presented in the plane of the dark photon mass versus the mixing with ordinary photon (see Fig.37 [63]).

5 New Dimensions

The paradoxical idea of extra dimensions attracted considerable interest in recent years despite the absence of any experimental confirmation. This is mainly due to unusual possibilities and intriguing effects even in classical physics (For review see, e.g. Refs. [64]), and the requirement from the string theory which allows for consistent formulation in the critical dimension equal to 26 for the bosonic and 10 for the fermionic string [65]. This way the string theory stimulated the study of ED theories.

The natural question arises: why don't we see these extra space dimensions? There are two
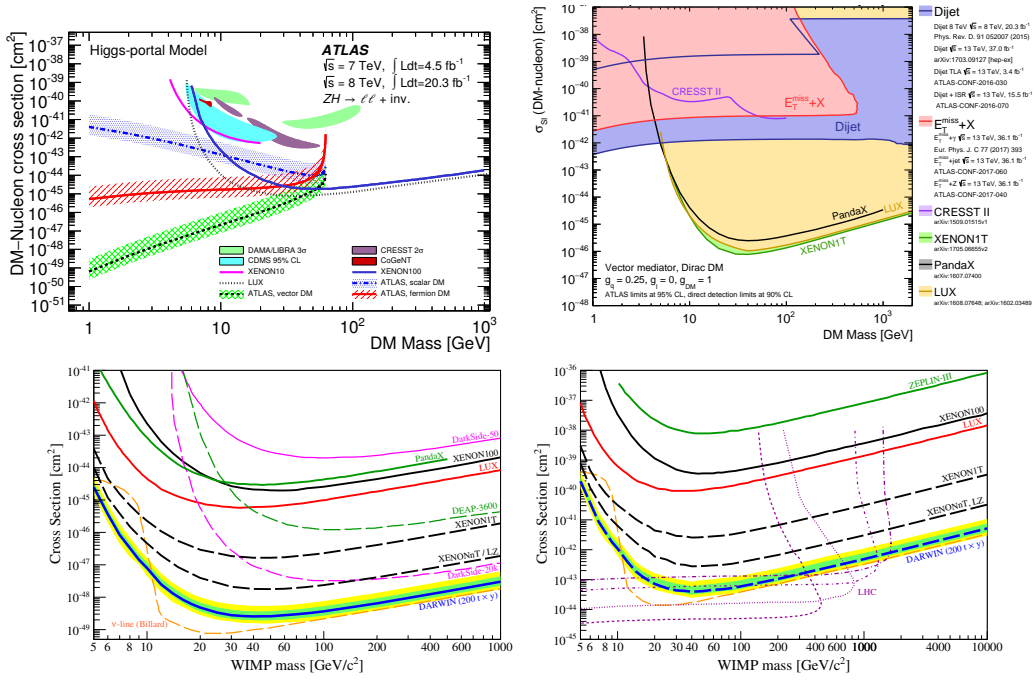
Fig. 36: Direct search for the Dark matter at accelerators [60] and underground experiments [61]
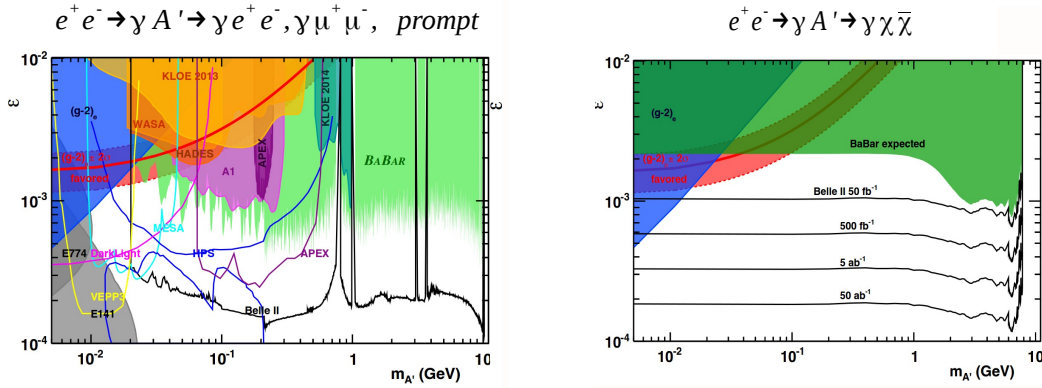
Fig. 37: The search for Dark photon

possibilities: compact ED of small radius and localization of observables on a 4-dimensional hyper surface (brane) (see Fig.38).

5.1 Compact Extra Dimensions

The idea of compact extra dimensions goes back to the so-called Kaluza-Klein theories [66]. We do not see ED because their radius is too small for the present energies, say, equal to the Planck length, 10^{-33} cm. The KK approach is based on the hypothesis that the space-time is a (4+d)-dimensional pseudo Euclidean space [67]

$$E_{4+d} = M_4 \times K_d,$$

where M_4 is the four-dimensional space-time and K_d is the d-dimensional compact space of characteristic size (scale) R. In accordance with the direct product structure of the space-time, the metric is usually chosen to be

$$ds^2 = \hat{G}_{MN}(\hat{x})d\hat{x}^M d\hat{x}^N = g_{\mu\nu}(x)dx^\mu dx^\nu + \gamma_{mn}(x,y)dy^m dy^n. \tag{16}$$
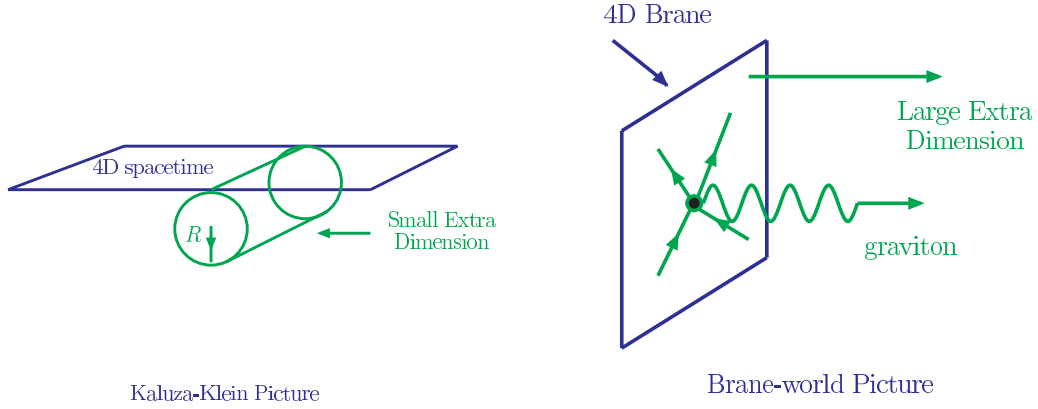
Fig. 38: Compact (left) and large (right) extra space dimensions

To interpret the theory as an effective four-dimensional one, the field $\hat{\phi}(x,y)$ depending on both coordinates is expanded in a Fourier series over the compact space

$$\hat{\phi}(x,y) = \sum_n \phi^{(n)}(x) Y_n(y), \tag{17}$$

where $Y_n(y)$ are orthogonal normalized eigenfunctions of the Laplace operator Δ_{K_d} on the internal space K_d,

$$\Delta_{K_d} Y_n(y) = \frac{\lambda_n}{R^2} Y_n(y). \tag{18}$$

The coefficients $\phi^{(n)}(x)$ of the Fourier expansion (17) are called the Kaluza-Klein modes and play the role of fields of the effective four-dimensional theory. Their masses are given by

$$m_n^2 = m^2 + \frac{\lambda_n}{R^2}, \tag{19}$$

where R is the radius of the compact dimension.

The coupling constant $g_{(4)}$ of the 4-dimensional theory is related to the coupling constant $g_{(4+d)}$ of the initial (4+d)-dimensional one by

$$g_{(4)} = \frac{g_{(4+d)}}{V_{(d)}}, \tag{20}$$

$V_{(d)} \propto R^d$ being the volume of the space of extra dimensions.

<u>Low scale gravity</u>

Consider now the Einstein $(4+d)$-dimensional gravity with the action

$$S_E = \int d^{4+d}\hat{x} \sqrt{-\hat{G}} \frac{1}{16\pi G_{N(4+d)}} \mathcal{R}^{(4+d)}[\hat{G}_{MN}],$$

where the scalar curvature $\mathcal{R}^{(4+d)}[\hat{G}_{MN}]$ is calculated using the metric $\hat{G}_{MN}$. Performing the mode expansion and integrating over K_d, one arrives at the four-dimensional action

$$S_E = \int d^4x \sqrt{-g} \left\{ \frac{1}{16\pi G_{N(4)}} \mathcal{R}^{(4)}[g_{MN}^{(0)}] + \text{non-zero KK modes} \right\},$$

Similar to eq.(20), the relation between the 4-dimensional and $(4+d)$-dimensional gravitational (Newton) constants is given by

$$G_{N(4)} = \frac{1}{V_{(d)}} G_{N(4+d)}. \tag{21}$$

One can rewrite this relation in terms of the 4-dimensional Planck mass $M_{Pl} = (G_{N(4)})^{-1/2} = 1.2 \cdot 10^{19}$ GeV and a fundamental mass scale of the $(4 + d)$-dimensional theory $M \equiv (G_{N(4+d)})^{-\frac{1}{d+2}}$. One gets

$$M_{Pl}^2 = V_{(d)} M^{d+2}. \tag{22}$$

This formula is often referred to as the reduction formula.

The presence of ED leads to the modification of classical gravity. The Newton potential between two test masses m_1 and m_2, separated by a distance r, is in this case equal to

$$V(r) = G_{N(4)} m_1 m_2 \sum_n \frac{1}{r} e^{-m_n r} = G_{N(4)} m_1 m_2 \left(\frac{1}{r} + \sum_{n \neq 0} \frac{1}{r} e^{-|n|r/R} \right).$$

The first term in the last bracket is the contribution of the usual massless graviton (zero mode) and the second term is the contribution of the massive gravitons. For the size R large enough (i.e. for the spacing between the modes small enough) this sum can be replaced by the integral and one gets [69]

$$V(r) = G_{N(4)} \frac{m_1 m_2}{r} \left[1 + S_{d-1} \int_1^\infty e^{-mr/R} m^{d-1} dm \right] = G_{N(4)} \frac{m_1 m_2}{r} \left[1 + S_{d-1} \left(\frac{R}{r} \right)^d \int_{r/R}^\infty e^{-z} z^{d-1} dz \right], \tag{23}$$

where S_{d-1} is the area of the $(d-1)$-dimensional sphere of the unit radius. This leads to the following behaviour of the potential at short and long distances

$$V \approx \begin{cases} G_{N(4)} \dfrac{m_1 m_2}{r} & r \gg R, \\ G_{N(4)} \dfrac{m_1 m_2}{r} S_{d-1} \left(\dfrac{R}{r} \right)^d \Gamma(d) = G_{N(4+d)} \dfrac{m_1 m_2}{r^{d+1}} S_{d-1} \Gamma(d) & r \ll R, \end{cases} \tag{24}$$

The attempts to observe the modification of the Newton law did not come out with a positive result but the accuracy was increased by two orders of magnitude. In Fig.39 [68] we show the allowed regions in parameter space for the modified potential of the form $V = -G \frac{m_1 m_2}{r} (1 + \alpha e^{-r/\lambda})$.
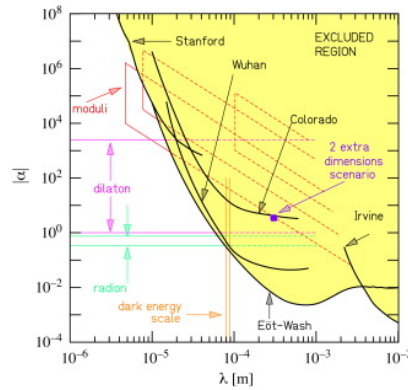
Fig. 39: The allowed region in parameter space for the modified Newton potential

The ADD model

The ADD model was proposed by N. Arkani-Hamed, S. Dimopoulos and G. Dvali in Ref. [69]. The model includes the SM localized on a 3-brane embedded into the $(4 + d)$-dimensional space-time with compact extra dimensions. The gravitational field is the only field which propagates in the bulk.

To analyze the field content of the effective (dimensionally reduced) four-dimensional model, consider the field $\hat{h}_{MN}(x, y)$ describing the linear deviation of the metric around the $(4+d)$-dimensional

Minkowski background η_{MN}

$$\hat{G}_{MN}(x, y) = \eta_{MN} + \frac{2}{M^{1+d/2}} \hat{h}_{MN}(x, y) \tag{25}$$

Let us assume, for simplicity, that the space of extra dimensions is the d-dimensional torus. Performing the KK mode expansion

$$\hat{h}_{MN}(x, y) = \sum_n h_{MN}^{(n)}(x) \frac{1}{\sqrt{V_{(d)}}} \exp(-i\frac{n_m y^m}{R}), \tag{26}$$

where $V_{(d)}$ is the volume of the space of extra dimensions, we obtain the KK tower of states $h_{MN}^{(n)}(x)$ with masses

$$m_n = \frac{1}{R}\sqrt{n_1^2 + n_2^2 + \ldots + n_d^2} \equiv \frac{|n|}{R}, \tag{27}$$

so that the mass splitting is $\Delta m \propto 1/R$.

The interaction of the KK modes $h_{MN}^{(n)}(x)$ with fields on the brane is determined by the universal minimal coupling of the $(4 + d)$-dimensional theory

$$S_{int} = \int d^{4+d}\hat{x} \sqrt{-\hat{G}} \hat{T}_{MN} \hat{h}^{MN}(x, y),$$

where the energy-momentum tensor of the matter localized on the brane at $y = 0$ has the form

$$\hat{T}_{MN}(x, y) = \delta_M^\mu \delta_N^\nu T_{\mu\nu}(x) \delta^{(d)}(y).$$

Using the reduction formula (22) and the KK expansion (26), one obtains that

$$S_{int} = \int d^4x T_{\mu\nu} \sum_n \frac{1}{M^{1+d/2}\sqrt{V_{(d)}}} h^{(n)\mu\nu}(x) = \sum_n \int d^4x \frac{1}{M_{Pl}} T^{\mu\nu}(x) h_{\mu\nu}^{(n)}(x), \tag{28}$$

which is the usual interaction of matter with gravity suppressed by M_{Pl}.

The degrees of freedom of the four-dimensional theory, which emerge from the multidimensional metric, include [70, 71]

1. the massless graviton and the massive KK gravitons $h_{\mu\nu}^{(n)}$ (spin-2 fields) with masses given by eq.(27);
2. $(d - 1)$ KK towers of spin-1 fields which do not couple to $T_{\mu\nu}$;
3. $(d^2 - d - 2)/2$ KK towers of real scalar fields (for $d \geq 2$), they do not couple to $T_{\mu\nu}$ either;
4. a KK tower of scalar fields coupled to the trace of the energy-momentum tensor T_μ^μ, its zero mode is called radion and describes fluctuations of the volume of extra dimensions.

Alternatively, one can consider the $(4 + d)$-dimensional theory with the $(4 + d)$-dimensional massless graviton $\hat{h}_{MN}(x, y)$ interacting with the SM fields with couplings $\sim 1/M^{1+d/2}$.

In the 4-dimensional picture the coupling of each individual graviton (both massless and massive) to the SM fields is small $\sim 1/M_{Pl}$. However, the smallness of the coupling constant is compensated by the high multiplicity of states with the same mass. Indeed, the number $d\mathcal{N}(|n|)$ of modes with the modulus $|n|$ of the quantum number being in the interval $(|n|, |n| + d|n|)$ is equal to

$$d\mathcal{N}(|n|) = S_{d-1}|n|^{d-1}d|n| = S_{d-1}R^d m^{d-1}dm \sim S_{d-1}\frac{M_{Pl}}{M^{d+2}}m^{d-1}dm, \tag{29}$$

where we used the mass formula $m = |n|/R$ and the reduction formula (22). The number of KK gravitons $h^{(n)}$ with masses $m_n \leq E < M$ is equal to

$$\mathcal{N}(E) \sim \int_0^{ER} d\mathcal{N}(|n|) \sim S_{d-1} \frac{M_{Pl}^2}{M^{d+2}} \int_0^E m^{d-1} dm = \frac{S_{d-1}}{d} \frac{M_{Pl}^2}{M^{d+2}} E^d \sim R^d E^d.$$

One can see that for $E \gg R^{-1}$ the multiplicity of states which can be produced is large. Hence, despite the fact that due to eq.(28) the amplitude of emission of the mode n is $\mathcal{A} \sim 1/M_{Pl}$, the total combined rate of emission of the KK gravitons with masses $m_n \leq E$ is

$$\sim \frac{1}{M_{Pl}^2} \mathcal{N}(E) \sim \frac{E^d}{M^{d+2}}. \tag{30}$$

We can see that there is a considerable enhancement of the effective coupling due to the large phase space of KK modes or due to the large volume of the space of extra dimensions. Because of this enhancement the cross-sections of processes involving the production of KK gravitons may turn out to be quite noticeable at future colliders.

HEP phenomenology

There are two types of processes at high energies in which the effect of the KK modes of the graviton can be observed in running or planned experiments. These are the graviton emission and virtual graviton exchange processes [70]- [74].

We start with the graviton emission, i.e., the reactions where the KK gravitons are created as final state particles. These particles escape from the detector so that a characteristic signature of such processes is missing energy. Though the rate of production of each individual mode is suppressed by the Planck mass, due to the high multiplicity of KK states the magnitude of the total rate of production is determined by the TeV scale (see eq.(30)). Taking eq.(29) into account, the relevant differential cross section [70] is

$$\frac{d^2\sigma}{dt\,dm} \sim S_{d-1} \frac{M_{Pl}^2}{M^{d+2}} m^{d-1} \frac{d\sigma_m}{dt} \sim \frac{1}{M^{d+2}}, \tag{31}$$

where $d\sigma_m/dt$ is the differential cross section of the production of a single KK mode with mass m.

At e^+e^- colliders the main contribution comes from the $e^+e^- \to \gamma h^{(n)}$ process. The main background comes from the process $e^+e^- \to \nu\bar{\nu}\gamma$ and can be effectively suppressed by using polarized beams. Figure 40 shows the total cross section of the graviton production in electron-positron collisions [74]. To the right is the same cross section as a function of M for $\sqrt{s} = 800$ GeV [75].

Effects due to gravitons can also be observed at hadron colliders. A characteristic process at the LHC would be $pp \to (\text{jet} + \text{missing } E)$. The subprocess that gives the largest contribution is the quark-gluon collision $qg \to qh^{(n)}$. Other subprocesses are $q\bar{q} \to gh^{(n)}$ and $gg \to gh^{(n)}$.

Processes of another type, in which the effects of extra dimensions can be observed, are exchanges of virtual KK modes, in particular, the virtual graviton exchanges. Contributions to the cross section from these additional channels lead to deviation from the behaviour expected in the 4-dimensional model. An example is $e^+e^- \to f\bar{f}$ with $h^{(n)}$ being the intermediate state (see Fig.41). Moreover, gravitons can mediate processes absent in the SM at the tree-level, for example, $e^+e^- \to HH$, $e^+e^- \to gg$. Detection of such events with large cross sections may serve as an indication of the existence of extra dimensions.

The s-channel amplitude of a graviton-mediated scattering process is given by

$$\mathcal{A} = \frac{1}{M_{Pl}^2} \sum_n \left\{ T_{\mu\nu} \frac{P^{\mu\nu} P^{\rho\sigma}}{s - m_n^2} T_{\rho\sigma} + \sqrt{\frac{3(d-1)}{d+2}} \frac{T_\mu^\mu T_\nu^\nu}{s - m_n^2} \right\}, \tag{32}$$

where $P_{\mu\nu}$ is the polarization factor coming from the propagator of the massive graviton and $T_{\mu\nu}$ is the energy-momentum tensor [70]. It contains a kinematic factor

$$\mathcal{S} = \frac{1}{M_{Pl}^2} \sum_n \frac{1}{s - m_n^2} \approx \frac{1}{M_{Pl}^2} S_{d-1} \frac{M_{Pl}^2}{M^{d+2}} \int^\Lambda \frac{m^{d-1} dm}{s - m^2}$$
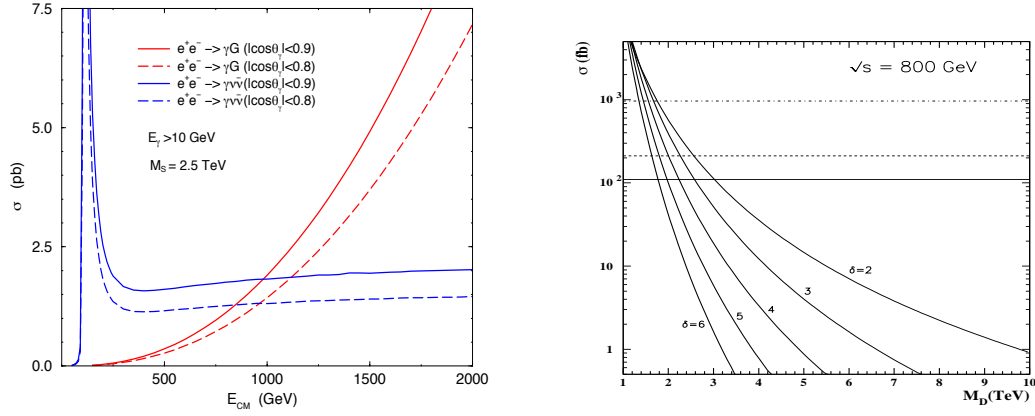
Fig. 40: The total cross sections for $e^+e^- \to \gamma\nu_i\bar{\nu}_i$ ($i = e, \mu, \tau$) and $e^+e^- \to \gamma h$ (faster growing curves) for $d = 2$ and $M = 2.5$ TeV [74] (left) and the cross section for $e^+e^- \to \gamma h^{(n)}$ at $\sqrt{s} = 800$ GeV as a function of the scale M for A different number δ of extra dimensions (right). Horizontal lines indicate the background. [75]
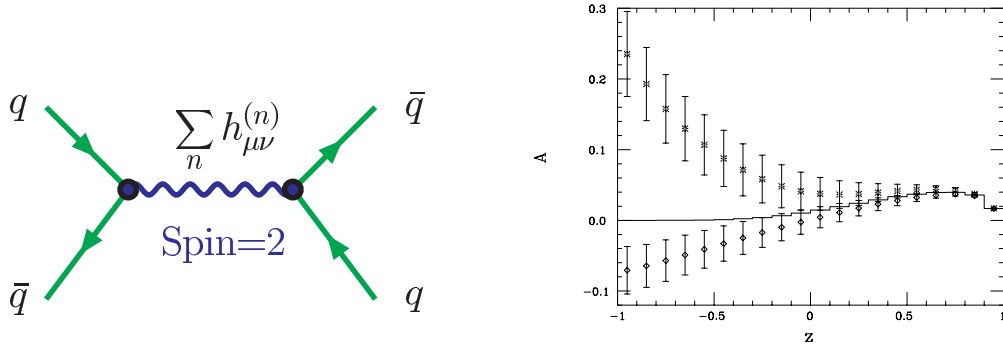

Fig. 41: The Feynman diagram for the virtual graviton exchange (left) and deviation from the expectations of the SM (histogram) for the Bhabha scattering at a 500 GeV e^+e^- collider for the Left-Right polarization asymmetry as a function of $z = \cos\theta$ for $M = 1.5$ TeV and the integrated luminosity $\mathcal{L} = 75$ fb^{-1} (right) [73].

$$= \frac{S_{d-1}}{2M^4}\left\{i\pi\left(\frac{s}{M^2}\right)^{d/2-1} + \sum_{k=1}^{[(d-1)/2]} c_k\left(\frac{s}{M^2}\right)^{k-1}\left(\frac{\Lambda}{M}\right)^{d-2k}\right\}. \tag{33}$$

Since the integrals are divergent for $d \geq 2$, the cutoff Λ was introduced. It sets the limit of applicability of the effective theory. Because of the cutoff, the amplitude cannot be calculated explicitly without the knowledge of a full fundamental theory. Usually, in the literature it is assumed that the amplitude is dominated by the lowest-dimensional local operator (see [70]).

The characteristic feature of expression (33) different from the 4-dimensional model is the increase of the cross section with energy. This is a consequence of the exchange of the infinite tower of the KK modes. Note, however, that this result is based on a tree-level amplitude, while the radiative corrections in this case are power-like and may well change this behaviour.

Typical processes, in which the virtual exchange via massive gravitons can be observed, are: (a) $e^+e^- \to \gamma\gamma$; (b) $e^+e^- \to f\bar{f}$, for example the Bhabha scattering $e^+e^- \to e^+e^-$ or Möller scattering $e^-e^- \to e^-e^-$; (c) graviton exchange contribution to the Drell-Yang production. A signal of the KK graviton mediated processes is the deviation in the number of events and in the left-right polarization asymmetry from those predicted by the SM (see Figs. 41) [73].

5.2 Large Extra Dimensions

The alternative to compact ED are the large ones which we do not see for the reason that observables are localized on a 4-dimensional hyper surface called *brane*. The particles can be pressed to the brane by some force, and to leave the brane, they have to gain high energy.

The Randal-Sundrum model [76] is a model of Einstein gravity in the five-dimensional Anti-de Sitter space-time with extra dimension being compactified to the orbifold S^1/Z_2. There are two 3-branes in the model located at the fixed points $y = 0$ and $y = \pi R$ of the orbifold, where R is the radius of the circle S^1. The brane at $y = 0$ is usually referred to as A Planck brane, whereas the brane at $y = \pi R$ is called A TeV brane (see Fig.42). The SM fields are constrained to the TeV brane, while gravity propagates in additional dimension.
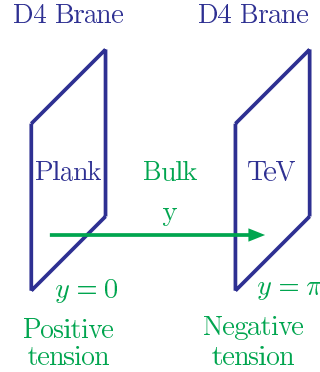
Fig. 42: The Randall-Sundrum construction of the extra-dimensional space

The action of the model is given by

$$
\begin{aligned}
S &= \int d^4x \int_{-\pi R}^{\pi R} dy \sqrt{-\hat{G}} \left\{ 2M^3 \mathcal{R}^{(5)} \left[\hat{G}_{MN} \right] + \Lambda \right\} \\
&+ \int_{B_1} d^4x \sqrt{-g^{(1)}} \left(L_1 - \tau_1 \right) + \int_{B_2} d^4x \sqrt{-g^{(2)}} \left(L_2 - \tau_2 \right),
\end{aligned}
\tag{34}
$$

where $\mathcal{R}^{(5)}$ is the five-dimensional scalar curvature, M is the mass scale (the five-dimensional "Planck mass") and Λ is the cosmological constant; L_j is a matter Lagrangian and τ_j is a constant vacuum energy on brane j $(j = 1, 2)$.

The RS solution describes the space-time with nonfactorizable geometry with the metric given by

$$
ds^2 = e^{-2\sigma(y)} \eta_{\mu\nu} dx^\mu dx^\nu + dy^2.
\tag{35}
$$

The additional coordinate changes inside the interval $-\pi R < y \leq \pi R$ and the function $\sigma(y)$ in the warp factor $\exp(-2\sigma)$ is equal to

$$
\sigma(y) = k|y|, \quad (k > 0).
\tag{36}
$$

For the solution to exist the parameters must be fine-tuned to satisfy the relations

$$
\tau_1 = -\tau_2 = 24M^3 k, \quad \Lambda = 24M^3 k^2.
$$

Here k is a dimensional parameter which was introduced for convenience. This fine-tuning is equivalent to the usual cosmological constant problem. If $k > 0$, then the tension on brane 1 is positive, whereas the tension τ_2 on brane 2 is negative.

For a certain choice of the gauge the most general perturbed metric is given by

$$ds^2 = e^{-2k|y|}\left(\eta_{\mu\nu} + \tilde{h}_{\mu\nu}(x,y)\right)dx^\mu dx^\nu + (1+\phi(x))dy^2.$$

and describes the graviton field $\tilde{h}_{\mu\nu}(x,y)$ and the radion field $\phi(x)$ [77].

As the next step, the field $h_{\mu\nu}(x,y)$ is decomposed over an appropriate system of orthogonal and normalized functions:

$$h_{\mu\nu}(x,y) = \sum_{n=0}^{\infty} h_{\mu\nu}^{(n)}(x)\frac{\chi_n(y)}{R}. \tag{37}$$

The particles localized on the branes are:

Brane 1 (Planck):

- massless graviton $h_{\mu\nu}^{(0)}(x)$,
- massive KK gravitons $h_{\mu\nu}^{(n)}(x)$ with masses $m_n = \beta_n k e^{-\pi k R}$, where $\beta_n = 3.83, 7.02, 10.17, 13.32, \ldots$ are the roots of the Bessel function,
- massless radion $\phi(x)$.

Brane 2 (TeV):

- massless graviton $h_{\mu\nu}^{(0)}(x)$,
- massive KK gravitons $h_{\mu\nu}^{(n)}(x)$ with masses $m_n = \beta_n k$,
- massless radion $\phi(x)$.

The brane 2 is most interesting from the point of view of high energy physics phenomenology. Because of the nontrivial warp factor $e^{-2\sigma(\pi R)}$, the Planck mass here is related to the fundamental 5-dimensional scale M by

$$M_{Pl}^2 = e^{2k\pi R}\int_{-\pi R}^{\pi R} dy\, e^{-2k|y|} = \frac{M^3}{k}\left(e^{2k\pi R} - 1\right). \tag{38}$$

This way one obtains the solution of the hierarchy problem. The large value of the 4-dimensional Planck mass is explained by an exponential wrap factor of geometrical origin, while the scale M stays small.

The general form of the interaction of the fields, emerging from the five-dimensional metric, with the matter localized on the branes is given by the expression:

$$\frac{1}{2M^{3/2}}\int_{B_1} d^4x\, h_{\mu\nu}(x,0)T_{\mu\nu}^{(1)} + \frac{1}{2M^{3/2}}\int_{B_2} d^4x\, h_{\mu\nu}(x,0)T_{\mu\nu}^{(2)}\sqrt{-\det\gamma_{\mu\nu}(\pi R)}$$

Decomposing the field $h_{\mu\nu}(x,y)$ according to (37) we can write the interaction Lagrangian as

$$\frac{1}{2}\int_{B_2} d^4z\left[\frac{1}{M_{Pl}}h_{\mu\nu}^{(0)}(z)T^{(2)\mu\nu} - \sum_{n=1}^{\infty}\frac{w_n}{\Lambda_\pi}h_{\mu\nu}^{(n)}T^{(2)\mu\nu} - \frac{1}{\Lambda_\pi\sqrt{3}}T_\mu^{(2)\mu}\right], \tag{39}$$

where $\Lambda_\pi = M_{Pl}e^{-k\pi R} \approx \sqrt{M^3/k}$ and M_{Pl} is given by eq.(38) .

The massless graviton, as in the standard gravity, interacts with matter with the coupling M_{Pl}^{-1}. The interaction of the massive gravitons and radion is considerably stronger: their couplings are $\propto \Lambda_\pi^{-1} \sim 1\,\text{TeV}^{-1}$. If the first few massive KK gravitons have masses $M_n \sim 1\text{TeV}$, then this leads to new effects which in principle can be seen at future colliders. To have this situation, the fundamental mass scale M and the parameter k are taken to be $M \sim k \sim 1\text{TeV}$.

HEP phenomenology

With the mass of the first KK mode $M_1 \sim 1$ TeV direct searches for the first KK graviton $h^{(1)}$ in the resonance production at future colliders become quite possible. Signals of the graviton detection can be [78]

- an excess in the Drell-Yan processes $\quad q\bar{q} \to h^{(1)} \to l^+l^-,$
$$gg \to h^{(1)} \to l^+l^-$$
- an excess in the dijet channel $\quad q\bar{q}, gg \to h^{(1)} \to q\bar{q}, gg.$

The plots of the exclusion regions for the LHC [78] are presented in Fig. 43.
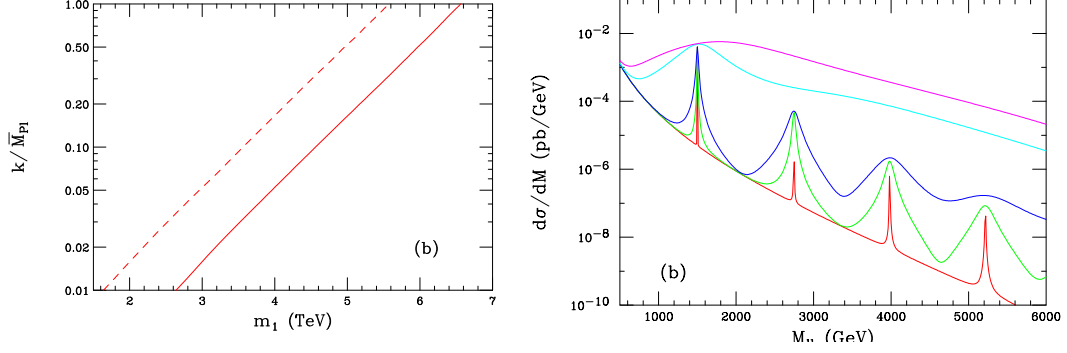

Fig. 43: Exclusion region for resonance production of the first KK graviton excitation in the Drell-Yan (corresponding to the diagonal lines) and dijet (represented by the bumpy curves) channels at the LHC. The dashed and solid curves correspond to 10, 100 fb^{-1} of integrated luminosity, respectively (left). Drell-Yan production of the KK graviton for the LHC (right) for $M_1 = 1500$GeV and its subsequent tower states (right)

They show the exclusion region for resonance production of the first KK graviton excitation in the Drell-Yan and dijet channels. The excluded region lies above and to the left of the curves.

The next plots present the behaviour of the cross-section of the Drell-Yan process as a function of the invariant mass of the final leptons. It is shown for two values of $M_1 = 1500$ GeV for the LHC in Fig. 43 [78]. One can see the characteristic peaks in the cross section for one or a series of massive graviton modes.

The possibility to detect the resonance production of the first massive graviton in the proton - proton collisions $pp \to h^{(1)} \to e^+e^-$ at the LHC depends on the cross section. The main background processes are $pp \to Z/\gamma^* \to e^+e^-$. The estimated cross section of the process $h^{(1)} \to e^+e^-$ as a function of M_1 in the RS model is shown in Fig. 44 [79]. One can see that the detection might be possible if $M_1 \leq 2080$ GeV .

To be able to conclude that the observed resonance is a graviton and not, for example, a spin-1 Z' resonance or a similar particle, it is necessary to check that it is produced by a spin-2 intermediate state. The spin of the intermediate state can be determined from the analysis of the angular distribution function $f(\theta)$ of the process, where θ is the angle between the initial and final beams. This function is

$$
\begin{aligned}
Spin\ 0 \quad &=> \quad f(\theta) = 1, \\
Spin\ 1 \quad &=> \quad f(\theta) = 1 + \cos^2\theta, \\
Spin\ 2 \quad &=> \quad \begin{cases} q\bar{q} \to h^{(1)} \to e^+e^- & f(\theta) = 1 - 3\cos^2\theta + 4\cos^4\theta, \\ gg \to h^{(1)} \to e^+e^- & f(\theta) = 1 - \cos^4\theta. \end{cases}
\end{aligned}
$$

The analysis, carried out in Ref. [79], shows that angular distributions allow one to determine the spin of the intermediate state with 90% C.L. for $M_1 \leq 1720$ GeV.

As the next step, it would be important to check the universality of the coupling of the first massive graviton $h^{(1)}$ by studying various processes, e.g. $pp \to h^{(1)} \to l^+l^-$, jets, $\gamma\gamma, W^+W^-, HH$, etc. If it
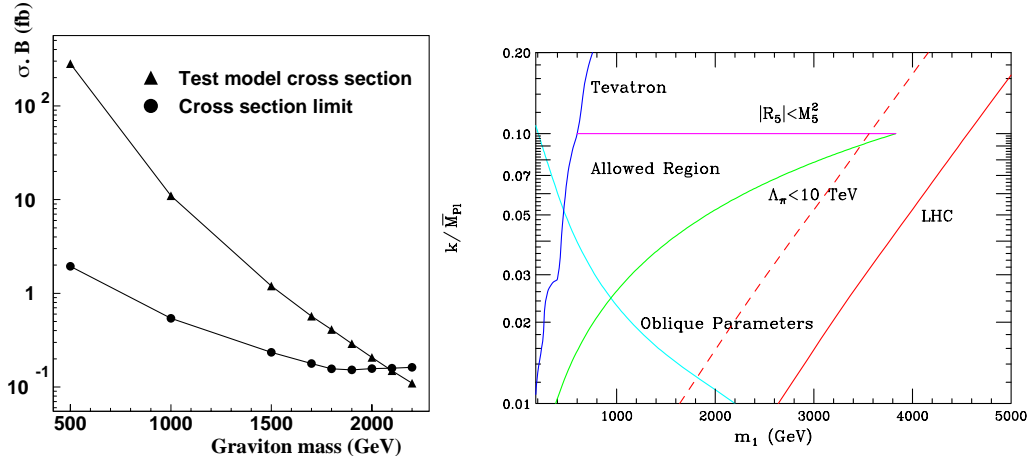
Fig. 44: The cross-section times branching ratio, $\sigma \cdot B$, for $h^{(1)} \to e^+ e^-$ in the RS model and the smallest detectable cross-section times the branching ratio, $(\sigma \cdot B)^{min}$ [79] (left) and the summary of experimental and theoretical constraints on the parameters M_1 and $\eta = (k/M_{Pl})e^{k\pi R}$ (right) [78]. The allowed region lies as indicated. The LHC sensitivity to graviton resonances in the Drell-Yan channel is represented by diagonal dashed and solid curves, corresponding to 10 and 100 fb^{-1} of integrated luminosity, respectively

is kinematically feasible to produce higher KK modes, measuring the spacings of the spectrum will be another strong indication in favour of the RS model.

The conclusion is [78] that with the integrated luminosity $\mathcal{L} = 100$ fb^{-1} the LHC will be able to cover the natural region of parameters $(M_1, \eta = (k/M_{Pl})e^{k\pi R})$ and, therefore, discover or exclude the RS model. This is illustrated in the r.h.s. of Fig. 44.

We finish with a short summary of the main features of the ADD and RS models.

ADD Model.

1. The ADD model removes the M_{EW}/M_{Pl} hierarchy, but replaces it by the hierarchy $\frac{R^{-1}}{M} \sim \left(\frac{M}{M_{Pl}}\right)^{2/d} \sim 10^{-\frac{30}{d}}$. For $d = 2$ this relation gives $R^{-1}/M \sim 10^{-15}$. This hierarchy is of a different type and might be easier to understand or explain, perhaps with no need for SUSY;

2. The model predicts the modification of the Newton law at short distances, which may be checked in precision experiments;

3. For M small enough high-energy physics effects, predicted by the model, can be discovered at future collider experiments.

RS model

1. The model solves the M_{EW}/M_{Pl} hierarchy problem without generating a new hierarchy.

2. A large part of the allowed range of parameters of the RS model will be studied in future collider experiments, which will either discover new phenomena or exclude the most "natural" region of its parameter space.

3. With a mechanism of radion stabilization added the model is quite viable. In this case, cosmological scenarios, based on the RS model, are consistent without additional fine-tuning of parameters (except the cosmological constant problem) [80].

6 New Paradigm

The most radical way out of the SM is the change of the paradigm of local quantum field theory and transition to non-local theories. And the first attempt of this kind is the string theory - the theory of one-dimensional extended objects [65]. The natural development of this idea is the consideration of the objects of an arbitrary dimension which are called branes (from membrane - two-dimensional surface). The theory of these objects is in progress but some qualitative features are widely discussed.

6.1 String Theory

The string theory describes one-dimensional extended objects which in their motion swap a two-dimensional world surface. The action for such objects is the straightforward generalization of the action for a point-
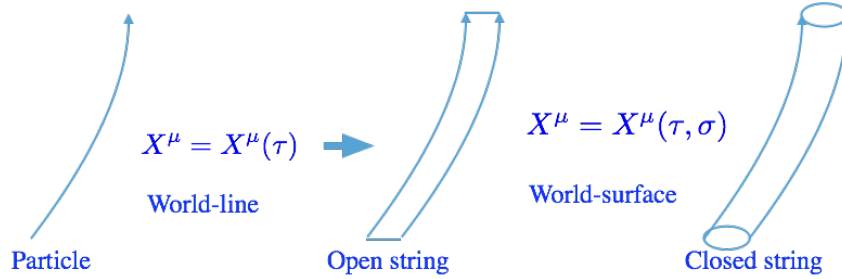
Fig. 45: From a point-like particle to a one-dimensional string

like particle

$$S = -m \int d\tau \sqrt{-\frac{dX^\mu}{d\tau}\frac{dX^\nu}{d\tau}\eta_{\mu\nu}} \Rightarrow S = -\frac{1}{2\pi l_S^2} \int d^2\sigma \sqrt{-det\left(\frac{dX^\mu}{d\sigma^\alpha}\frac{dX^\nu}{d\sigma^\beta}\eta_{\mu\nu}\right)}. \quad (40)$$

The strings may be open and closed. The spectrum of string excitations

$$l_S^2 M = \sum_n N_n(+\bar{N}_n) \in Z, \quad N_n = \alpha^\mu_{-n}\alpha^\mu_n, \quad (41)$$

contains zero modes associated with observed particles and heavy massive modes. The lowest string states are:

open string $\alpha^\mu_{-1}|0> \to A^\mu \to \int d^D x \sqrt{-g}\, tr(F_{\mu\nu}F^{\mu\nu})$ this state is associated with photon
closed string $\alpha^\mu_{-1}\bar{\alpha}^\nu_{-1}|0> \to g^{\mu\nu}, ... \to \int d^D x \sqrt{-g}\, R + ...$ this state is associated with graviton

The spectrum of open strings contains spin 0, 1/2 and 1 states associated with gauge and matter fields, the spectrum of closed strings contains spin 2 state associated with gravity. Besides the vibrational modes, strings contain also the modes connected with the winding of the world line on a string. All together these modes define the full spectrum of a string. Thus, for a string on a circle with radius R one has the momentum states with $M^2 = m^2/R^2$, the winding states with $M^2 = \omega^2 R^2/l_S^4$ and the full spectrum $M^2 = m^2/R^2 + \omega^2 R^2/l_S^4$. The string is characterized by a minimal size called the string length $l_S = \sqrt{\alpha'}$. It is assumed that this size is close to the Planck length.

Quantum theory of strings is formulated in critical dimension of space-time where it is free from conformal anomalies. For the bosonic string this critical dimension is equal to 26 and for the fermion string to 10. Besides, the string spectrum may contain taxions, particles with negative mass squared. To get rid of these states, one considers a supersymmetric fermion string which is free from taxions. Its

spectrum starts from zero modes which are usually associated with point-like particles of local quantum field theory.

To get from the string theory the effective 4-dimensional low energy theory containing massless modes, one needs to perform compactification of extra dimensions. The properties of the compact 6-dimensional manifold define the properties of the obtained low energy theory. Thus, the degeneracy of the compact manifold in size and shape manifested in the existence of the scalar fields called moduli, defines the values of the couplings, and different topologies define the symmetry group and the field content of the 4-dimensional theory. The gravity action defined in D dimensions and the matter field action defined on a p-brane

$$S_D = \frac{1}{l_S^{D-2}} \int d^D x \sqrt{-g}\, R + \cdots + \frac{1}{l_S^{p-3}} \int d^{p+1} x\, \sqrt{-\gamma}\, tr(F_{\alpha\beta} F^{\alpha\beta}) + \cdots \tag{42}$$

being compactified to 4-dimensions take the form

$$S_4 = \underbrace{\frac{V}{l_S^{D-2}}}_{\frac{1}{16\pi G_N}} \int d^4 x \sqrt{-g_4}\, R_4 + \cdots + \underbrace{\frac{v}{l_S^{p-3}}}_{\frac{1}{16\pi g_{YM}^2}} \int d^4 x\, \sqrt{-g_4}\, tr(F_{\mu\nu} F^{\mu\nu}) + \cdots \tag{43}$$

The existing multiple possibilities of multidimensional theories do not allow one at the moment to choose the preferable scheme and to make definite predictions.

Phenomenologically, the most acceptable is the so-called heterotic string. In this case, one has the unification of the gauge and the Higgs fields that allows in particular to predict the coupling constants and get the top-quark mass of the order of 170 GeV. In this theory one also gets the cancellation of anomalies which is possible for a fixed gauge group of associated GUT: $SO(32)$ or $E_8 \times E_8$. This theory possesses the right-handed neutrino and the Majorana mass term, permits the proton decay. The effective low energy theory gives the desired unification with gravity and contains the mechanism of spontaneous supersymmetry breaking via effects of supergravity in the hidden sector.

The string theory contains not only strings but other extended objects of various dimensions. The emerging picture of the world consists of branes, the open strings end up on the branes and the open strings propagate in the bulk.

6.2   M-theory and the Theory of Everything

There are five types of consistent string theories free from conformal and gauge anomalies and of taxions (type IIA, type IIB, type I, and two Heterotic) [81]. All five string theories are only consistent in 10 space-time dimensions, all five have world-sheet supersymmetry and lead to space-time-supersymmetry in 10 dimensions. They are believed to be different vacua of a single unified "theory" called $M - theory$. However, there is no adequate formulation of this theory. The other vacuum of M-theory is 11-dimensional supergravity (see Fig.46 [82]) It is assumed that the ultimate unified theory will be the "theory of everything", i.e. will describe on a fundamental level all laws of Nature. The form of this theory, however, is still unknown. It is not clear which degrees of freedom are fundamental. Moreover, is is quite possible that there are different, dual to each other, descriptions of the same reality. The example of such a duality is the so-called AdS/CFT correspondence when some characteristics of a theory can be described as in the framework of the 4-dimensional conformal field theory and also in the framework of classical gravity in the 5-dimensional de Sitter space [83]. Here we are still far from detailed predictions which allow experimental tests.

7   Conclusion. The priority tasks of high energy physics

The successes of the Standard Model and the enormous efforts for its tests and search for new physics at accelerators as well as in non-accelerator experiments define the future of high energy physics in the
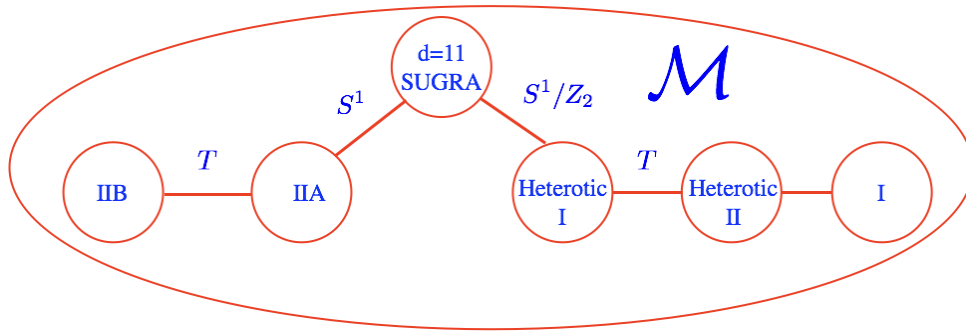
Fig. 46: The string landscape and $\mathcal{M}$ theory

coming years. The experiments at the Large Hadron Collider are at the edge of modern knowledge. The success of these experiments is the success of all high energy physics. However, the peculiarity of the modern situation is that there is no field where we may expect the guaranteed discovery. We make the first steps into the unknown land and try to unveil the mystery. We have to be persistent and patient. There are many theoretical models which suggest new physics at different scales. Which of these models happens to be correct and adequate to Nature we have to find experimentally. Today we may talk about priority tasks. They are:

– Investigation of the Higgs sector;
– Search for particles of Dark Matter;
– Study of the neutrino properties in non-accelerator experiments;
– Search for new physics (supersymmetry);
– The areas that were left behind come to the front: confinement, exotic hadrons, dense hadron matter

Further development of high energy physics crucially depends on the results of these searches.

Acknowledgements

References

[1] The Review of Particle Physics (2017), C. Patrignani et al. (Particle Data Group), Chin. Phys. **C 40** (2016) 100001 and 2017 update.

[2] L.D. Landau, On quantum field theory, in "Niels Bohr and the Development of Physics", London: Pergamon Press, 1955

[3] G. Degrassi, S.Di Vita, J.Elias-Miro, J.R. Espinosa, G.F. Giudice, G.Isidori, and A.Strumia, *Higgs mass and vacuum stability in the Standard Model at NNLO*, *JHEP* **1208** (2012) 098, arXiv:1205.6497

[4] J.R. Espinosa, *Vacuum stability and the Higgs boson*, Conference: C13-07-29.1 Proceedings, arXiv:1311.1970 (2013).

[5] Y. A. Golfand and E. P. Likhtman, *Extension of the Algebra of Poincare Group Generators and Violation of p Invariance*, JETP Letters **13** (1971) 452;
D. V. Volkov and V. P. Akulov, *Possible universal neutrino interaction*, JETP Letters **16** (1972)

621;

J. Wess and B. Zumino, *A Lagrangian Model Invariant Under Supergauge Transformations*, Phys. Lett. **B49** (1974) 52.

[6] P. Fayet and S. Ferrara, *Supersymmetry*, Phys. Rept. **32** (1977) 249;
M. F. Sohnius, *Introducing Supersymmetry*, Phys. Rept. **128** (1985) 41;
H. P. Nilles, *Supersymmetry, Supergravity and Particle Physics*, Phys. Rept. **110** (1984) 1;
H. E. Haber and G. L. Kane, *The Search for Supersymmetry: Probing Physics Beyond the Standard Model*, Phys. Rept. **117** (1985) 75;
A. B. Lahanas and D. V. Nanopoulos, *The Road to No Scale Supergravity*, Phys. Rept. **145** (1987) 1.

[7] J. Wess and J. Bagger, *Supersymmetry and Supergravity*, Princeton Univ. Press, 1983;

[8] A. Salam, J. Strathdee, *Supergauge Transformations*, Nucl. Phys. **B76** (1974) 477;
S. Ferrara, J. Wess, B. Zumino, *Supergauge Multiplets and Superfields* , Phys. Lett. **B51** (1974) 239.

[9] S. J. Gates, M. Grisaru, M. Roček and W. Siegel, *Superspace or One Thousand and One Lessons in Supersymmetry*, Benjamin & Cummings, 1983;
P. West, *Introduction to supersymmetry and supergravity*, World Scientific, 1990;
S. Weinberg,*The quantum theory of fields*, Vol. 3, Supersymmetry, Cambridge, UK: Univ. Press, 2000.
H. Baer and X. Tata, *Weak Scale Supersymmetry*, Cambridge University Press, 2006.

[10] S. Coleman and J .Mandula, *All Possible Symmetries of the S Matrix*, Phys. Rev. **159** (1967) 1251.

[11] U. Amaldi, W. de Boer and H. Fürstenau, *Comparison of grand unified theories with electroweak and strong coupling constants measured at LEP*, Phys. Lett. **B260** (1991) 447.

[12] G. G. Ross and R. G. Roberts, *Minimal supersymmetric unification predictions*, Nucl. Phys. **B377** (1992) 571. V. Barger, M. S. Berger and P. Ohmann, *The Supersymmetric particle spectrum*, Phys. Rev. **D47** (1993) 1093. D. M. Pierce, J. A. Bagger, K.T. Matchev, R. Zhang, *Precision corrections in the minimal supersymmetric standard model*, Nucl.Phys. **B491** (1997) 3.

[13] H.E. Haber, *Introductory Low-Energy Supersymmetry*, Lectures given at TASI 1992, (SCIPP 92/33, 1993), `hep-ph/9306207`;
D.I. Kazakov, *Beyond the Standard Model (In search of supersymmetry)*, Lectures at the ESHEP 2000, CERN-2001-003, `hep-ph/0012288`;
D. I. Kazakov, *Beyond the Standard Model*, Lectures at the ESHEP 2004, `hep-ph/0411064`.
D. Kazakov, *Supersymmetry on the Run: LHC and Dark Matter,* Nucl.Phys.Proc.Suppl. **203-204** (2010) 118154, arXiv:1010.5419.

[14] `http://scienceblogs.com/startswithabang/files/2013/05/susyparticles_sm.png`

[15] U. Ellwanger, C. Hugonie, and A. M. Teixeira, *The Next-to-Minimal Supersymmetric Standard Model*, Phys. Rep. **496** (2010), 1-77, arXiv:0910.1785

[16] A.V. Gladyshev, D.I. Kazakov, *Supersymmetry and LHC*, Phys. Atom. Nucl. **70** (2007) 1553, `hep-ph/0606288`.

[17] P. Fayet, *Supergauge Invariant Extension of the Higgs Mechanism and a Model for the electron and Its Neutrino*, Nucl. Phys. **B90** (1975) 104;
A. Salam and J. Srathdee, *Supersymmetry and Fermion Number Conservation*, Nucl. Phys. **B87** (1975) 85.

[18] P. Fayet and J. Illiopoulos, *Spontaneously Broken Supergauge Symmetries and Goldstone Spinors*, Phys. Lett. **B51** (1974) 461.

[19] L. O'Raifeartaigh, *Spontaneous Symmetry Breaking for Chiral Scalar Superfields*, Nucl.Phys. **B96** (1975) 331

[20] L. Hall, J. Lykken and S. Weinberg, *Supergravity as the Messenger of Supersymmetry Breaking,*

Phys. Rev. **D27** (1983) 2359;

S.K. Soni and H.A. Weldon, *Analysis of the Supersymmetry Breaking Induced by N=1 Supergravity Theories*, Phys. Lett. **B126** (1983) 215;

I. Affleck, M. Dine and N. Seiberg, *Dynamical Supersymmetry Breaking in Four-Dimensions and Its Phenomenological Implications*, Nucl. Phys. **B256** (1985) 557.

[21] A.V. Gladyshev and D.I. Kazakov, *Is (Low Energy) SUSY still alive?*, C12-06-06, Lectures at the European School on High Energy Physics 2012, arXiv:1212.2548

[22] https://twiki.cern.ch/twiki/bin/view/CMSPublic/SUSYSMSSummaryPlots7TeV
https://twiki.cern.ch/twiki/bin/view/CMSPublic/PhysicsResultsSUS
https://atlas.web.cern.ch/Atlas/GROUPS/PHYSICS/CombinedSummaryPlots/SUSY/

[23] T. Cohen, et al., *SUSY simplified models at 14, 33, and 100 TeV proton colliders*, JHEP **2014** (2014) 117.

[24] G. G. Ross, *Grand Unified Theories*, Benjamin & Cummings, 1985.

[25] http://www.roma1.infn.it/people/rahatlou/

[26] A.M. Sirunyan, et al. *Search for high-mass resonances in dilepton final states in proton-proton collisions at $\sqrt{s}$ =13 TeV*. No. CMS-EXO-16-047. 2018.
G. Aad, et al., *ATLAS search for a heavy gauge boson decaying to a charged lepton and a neutrino in pp collisions at $\sqrt{s} = 7$ TeV*, The European Phys. Journ. **C 72** (2012) 2241.

[27] G. C. Branco, et al. , *Theory and phenomenology of two-Higgs-doublet models*, Phys. Rept. **516** (2012) 1-102.

[28] ATLAS collaboration, et al., *Measurements of the Higgs boson production and decay rates and constraints on its couplings from a combined ATLAS and CMS analysis of the LHC pp collision data at $\sqrt{s} = 7$ and 8 TeV*, JHEP **2016** (2016) 1-113.

[29] D. M. Asner et al., *ILC Higgs White Paper*, arXiv:1310.0763

[30] H. Baer et al., *The International Linear Collider Technical Design Report - Volume 2: Physics*, arXiv:1306.6352

[31] https://twiki.cern.ch/twiki/bin/view/CMSPublic/SummaryResultsHIG
A. M. Sirunyan, et al (CMS Collaboration), *Search for Charged Higgs Bosons Produced via Vector Boson Fusion and Decaying into a Pair of W and Z Bosons Using pp Collisions at $\sqrt{s} = 13$ TeV.*, Phys. Rev. Lett. **119** (2017) 141802.
http://cms-results.web.cern.ch/cms-results/public-results/publications/HIG-17-020/index.html
https://atlas.web.cern.ch/Atlas/GROUPS/PHYSICS/CONFNOTES/ATLAS-CONF-2016-088/

[32] R.D.Peccei and H. R. Quinn, *CP conservation in the presence of pseudoparticles.*, Phys.Rev. Lett., **38** (1977) 1440.
R.D. Peccei, and H. R. Quinn, *Constraints imposed by CP conservation in the presence of pseudoparticles*, Origin Of Symmetries, 1991. 260-266.

[33] K. A. Olive et al. (Particle Data Group), Chin. Phys. **C 38** (2014) 090001

[34] S. Schael et al., *Precision electroweak measurements on the Z resonance*, Phys. Rept. **427** (2006) 257, [hep-ex/0509008]

[35] Z. Hou et al., *Constraints on Cosmology from the Cosmic Microwave Background Power Spectrum of the 2500-square degree SPT-SZ Survey*, Astrophys. J. **782** (2014) 74, arXiv:1212.6267

[36] Y.J. Ko, et al. *Sterile neutrino search at the NEOS experiment*, Phys. Rev. Lett. **118** (2017) 121802.

[37] S. Chatrchyan, et al., CMS Collaboration *Search for a Vector-like Quark with Charge 2/3 in t + Z Events from pp Collisions at $\sqrt{s} = 7$ TeV*, Phys. Rev. Lett. **107** (2011) 271802, arXiv:1109.4985;
CMS Collaboration *Search for pair produced fourth-generation up-type quarks in pp collisions at $\sqrt{s} = 7$ TeV with a lepton in the final state*, Phys. Lett. **B718** (2012) 307, arXiv:1209.0471;
CMS Collaboration *Combined search for the quarks of a sequential fourth generation*, Phys. Rev.

D86 (2012) 112003 , arXiv:1209.1062

[38] A.D. Sakharov, *Violation of CP invariance, C asymmetry, and baryon asymmetry of the universe*, Usp.Fiz.Nauk **161** (1991) 61 [Sov. Phys. Usp. **34** (1991) 392]; Pis'ma Zh. Eksp. Teor. Fis **5** (1967) 32 [JETP Lett **5** (1967) 24].

[39] A. Strumia and F. Vissani, *Neutrino masses and mixings and...*, hep-ph/0606054

[40] C. Kraus et al, *Final results from phase II of the Mainz neutrino mass search in tritium beta decay*, Eur. Phys. J. **C40** (2005) 447, hep-ex/0412056

[41] V.M.Lobashev, *The search for the neutrino mass by direct method in the tritium beta-decay and perspectives of study it in the project KATRIN*, Nucl. Phys. **A719** (2003) 154;

[42] E. Giusarma et al., *Constraints on neutrino masses from Planck and Galaxy Clustering data*, Phys. Rev. **D88** (2013) 063515 , arXiv:1306.5544

[43] P. Minkowski, $\mu \to e\gamma$ *at a Rate of One Out of 1-Billion Muon Decays?*, Phys. Lett. **B67** (1977) 421;
T. Yanagida, *Horizontal Symmetry and Masses of Neutrinos*, Progr. Theor. Phys. **64** (1980)1103 .

[44] Yu. Zdesenko, *Colloquium: The future of double β decay research*, Rev. Mod. Phys. **74** (2002) 663.

[45] L.J. Kaufman, *Recent results in neutrinoless double beta decay*, arXiv:1305.3306 (2013).

[46] K. Alfonso, *Search for Neutrinoless Double-Beta Decay of ^{130}Te with CUORE-0 (2015)*, arXiv:1504.02454.

[47] H. Minakata, H. Nunokawa, and A. A. Quiroga, *Constraining Majorana CP phase in the precision era of cosmology and the double beta decay experiment*, PTEP **2015** (2015) 033B03, arXiv:1402.6014 [hep-ph]

[48] Đạ.L.Bennett, et al., *First-Year Wilkinson Microwave Anisotropy Probe (WMAP) Observations: Preliminary Maps and Basic Results*, The Astrophysical Journal Supplement Series **148** (2003) 1.
D.N. Spergel et al., *Astrophys. J. Suppl.* **148** (2003) 175.

[49] E. Kolb and M.S. Turner, *The Early Universe*, Frontiers in Physics, Addison Wesley, 1990.
D.S. Gorbunov, V.A. Rubakov, *Introduction to the theory of the early Universe*, Moscow, URSS, 2008 (in Russian).

[50] Modified from `http://scienceblogs.com`

[51] K.G. Begeman, A.H. Broeils, R.H. Sanders, *Extended rotation curves of spiral galaxies:Dark haloes and modified dynamics*, Mon. Not. Roy. Astron. Soc. **249** (1991) 523

[52] K. Abazajian, S.M. Koushiappas, *Constraints on Sterile Neutrino Dark Matter*, Phys.Rev. **D74** (2006) 023527, astro-ph/0605271

[53] G. Jungman, M. Kamionkowski and K. Griest, *Supersymmetric dark matter*, Phys. Rep. **267** (1996) 195;
H. Goldberg, *Constraint on the Photino Mass from Cosmology*, Phys. Rev. Lett. **50** (1983) 1419;
J.R. Ellis, J.S. Hagelin, D.V. Nanopoulos, K.A. Olive, M. Srednicki, *Supersymmetric Relics from the Big Bang*, Nucl. Phys. **B238** (1984) 453.

[54] L.Canetti, M. Drewes,, M. Shaposhnikov, *Sterile Neutrinos as the Origin of Dark and Baryonic Matter*, Phys. Rev. Lett. **110** (2013) 061801, arXiv:1204.3902

[55] J.L. Feng, *Dark Matter Candidates from Particle Physics and Methods of Detection*, Ann. Rev. Astron. Astrophys. **48** (2010) 495, arXiv:1003.0904

[56] L.D. Duffy, K. van Bibber, *Axions as Dark Matter Particles*, New J. Phys. **11** (2009) 105008, arXiv:0904.3346

[57] O. Adriani et al., PAMELA Collaboration *PAMELA results on the cosmic-ray antiproton flux from 60 MeV to 180 GeV in kinetic energy*, Phys. Rev. Lett. **105** (2010) 121101, arXiv:1007.0821

[58] Q.Yuan, X-J Bi, *Reconcile the AMS-02 positron fraction and Fermi-LAT/HESS total e $\pm$ spectra*

by the primary electron spectrum hardening, Phys. Lett. **B727** (2013) 1, arXiv:1304.2687

[59] G.A. Gomez-Vargas, et al., *Dark matter implications of Fermi-LAT measurement of anisotropies in the diffuse gamma-ray background*, Nucl. Instr. and Methods in Physics Research Section A: Accelerators, Spectrometers, Detectors and Associated Equipment **742** (2014) 149-153.

[60] G. Aad, et al., Search for invisible decays of a Higgs boson produced in association with a Z boson in ATLAS, Phys. Rev. Lett. **112** (2014) 201802.
https://atlas.web.cern.ch/Atlas/GROUPS/PHYSICS/CombinedSummaryPlots/
EXOTICS/index.html

[61] J. Aalbers, et al., *DARWIN: towards the ultimate dark matter detector*, J. of Cosmology and Astroparticle Phys. **2016** (2016) 017.

[62] V.A. Mitsou, *Overview of searches for dark matter at the LHC*, , arXiv:1402.3673[hep-ex]
http://www.quantumdiaries.org/2013/07/12/can-the-lhc-solve-the-dark-matter
mystery/

[63] M. Ablikim, et al., BESIII Collaboration, *Dark Photon Search in the Mass Range Between 1.5 and 3.4 GeV/c2*, Phys.Lett. **B774** (2017) 252, arXiv:1705.04265

[64] V.A. Rubakov, *Large and infinite extra dimensions*, hep-ph/0104152;
M. Besançon, *Experimental introduction to extra dimensions*, hep-ph/0106165;
Yu.A.Kubyshin, *Models with extra dimensions and their phenomenology*, hep-ph/0111027;
J.Hewett and M.Spiropulu, *Particle physics probes of extra spacetime dimensions*, hep-ph/0205106; A.Kisselev, *Higher dimensions in high energy collisions*, hep-ph/0303090.

[65] M. B. Green, J. H. Schwarz and E. Witten, *Superstring Theory*, Cambridge, UK: Univ. Press, 1987. Cambridge Monographs On Mathematical Physics;

[66] T. Kaluza, *Zum UnitÃd'tsproblem der Physik*, Sitzungsber. Preuss. Akad. Wiss., Phys.-Math.Kl., Berlin Math. Phys., **1921** (1921) 966.
O. Klein, *Quantum Theory and Five-Dimensional Theory of Relativity*, Z. Phys. **37** (1926) 895.

[67] T. Appelquist, A. Chodos and P.G.O. Freund, *Modern Kaluza-Klein Theories*, Reading, MA, Addison-Wesley, 1987.

[68] E.G. Adelberger, et al., *Torsion balance experiments: A low-energy frontier of particle physics*, Progress in Particle and Nuclear Physics **62** (2009)102-134.
C.D. Hoyle, et al. *Submillimeter test of the gravitational inverse-square law: a search for âĂŪJlargeâĂİ extra dimensions*, Phys. Rev. Lett. **86** (2001) 1418.

[69] N. Arkani-Hamed, S. Dimopoulos and G. Dvali, *The Hierarchy problem and new dimensions at a millimeter*, Phys. Lett. **B429** (1998) 263 [hep- ph/9803315];
N. Arkani-Hamed, S. Dimopoulos and G. Dvali, *Phenomenology, astrophysics and cosmology of theories with submillimeter dimensions and TeV scale quantum gravity*, Phys.Rev. **D59** (1999) 086004 [hep- ph/9807344].

[70] G.F. Giudice, R. Rattazzi and J.D. Wells, *Quantum gravity and extra dimensions at high-energy colliders*, Nucl. Phys. **B544** (1999) 3 [hep-ph/9811291].

[71] J.L. Hewett, *Indirect collider signals for extra dimensions*, Phys. Rev. Lett. **82** (1999) 4765 [hep-ph/9811356].

[72] T. Han, J.D. Lykken and Ren-Jie Zhang, *On Kaluza-Klein states from large extra dimensions*, Phys. Rev. **D59** (1999) 105006 [hep-ph/9811350];
E.A. Mirabelli, M. Perelstein and M.E. Peskin, *Collider signatures of new large space dimensions*, Phys. Rev. Lett. **82** (1999) 2236 [hep-ph/9811337].;

[73] T.G. Rizzo, *More and more indirect signals for extra dimensions at more and more colliders*, Phys. Rev. **D59** (1999) 115010 [hep-ph/9901209];

[74] K. Cheung, W.-Y. Keung, *Direct signals of low scale gravity at e+ e- colliders*, Phys. Rev. **D60** (1999) 112003 [hep-ph/9903294].

[75] G. Wilson, *Linear Collider Physics in the New Millennium*, LC-PHSM-2001-010.

[76] L. Randall and R. Sundrum, *A Large mass hierarchy from a small extra dimension*, Phys. Rev. Lett. **83** (1999) 3370 [hep-ph/9905221].
L. Randall and R. Sundrum, *An Alternative to compactification*, Phys. Rev. Lett. **83** (1999) 4690 [hep-th/9906064].

[77] N. Arkani-Hamed, S. Dimopoulos and J. March-Russel, *Stabilization of submillimeter dimensions: The New guise of the hierarchy problem*, Phys. Rev. **D63** (2001) 064020 [hep-th/9809124].

[78] H. Davoudiasl, J.H. Hewett and T.G. Rizzo, *Phenomenology of the Randall-Sundrum Gauge Hierarchy Model*, Phys. Rev. Lett. **84** (2000) 2080 [hep-ph/9909255];
H. Davoudiasl, J.H. Hewett and T.G. Rizzo, *Bulk gauge fields in the Randall-Sundrum model*, Phys. Lett. **B473** (2000) 43 [hep-ph/9911262].;
H. Davoudiasl, J.H. Hewett and T.G. Rizzo, *Experimental probes of localized gravity: On and off the wall*, Phys. Rev. **D63** (2001) 075004 [hep-ph/0006041].

[79] B.C. Allanach, K. Odagiri, M.A. Parker and B.R. Webber, *Searching for narrow graviton resonances with the ATLAS detector at the Large Hadron Collider*, JHEP **0009** (2000) 019 [hep-ph/0006114].

[80] C. Csáki, M.L. Graesser, L. Randall and J. Terning, *Cosmology of brane models with radion stabilization*, Phys. Rev. **D62** (2000) 045015 [hep-ph/9911406].
P. Binétruy, C. Deffayet, U. Ellwanger and D. Langlois, *Brane cosmological evolution in a bulk with cosmological constant*, Phys. Lett. **B477** (2000) 285 [hep-th/9910219].
S. Tsujikawa, K. Maeda and S. Mizuno, *Brane preheating*, Phys. Rev. **D63** (2001) 123511 [hep-ph/0012141].

[81] P. Hořava and E. Witten, *Heterotic and type I string dynamics from eleven dimensions*, Nucl. Phys. **B 460** (1996) 506-524.
A. Hanany and E. Witten, *Type II B superstrings, BPS monopoles, and three-dimensional gauge dynamics*, Nucl. Phys. **B 492** (1997) 152-190.

[82] A. Lukas, *String Phenomenology*, talk on EPS-2017, Venice (2017)

[83] J. Maldacena, *The large-N limit of superconformal field theories and supergravity*, Int.J.Theor.Phys. **38** (1999) 1113-1133, Adv.Theor.Math.Phys. **2** (1998) 231-252

Electroweak symmetry breaking after the Higgs discovery

S. Dawson
Brookhaven National Laboratory, Upton, New York, USA

Abstract

I give a pedagogical introduction to the physics of electroweak symmetry breaking. Higgs boson production and decay at the LHC and the consistency of the Higgs measurements with triviality arguments, vacuum stability, and precision electroweak measurements are discussed. Effective Lagrangian techniques are used to understand potential deviations from the Standard Model (SM) predictions.

Keywords

Lectures; Higgs boson; Oblique parameters; Triviality; Effective Field Theory

1 Introduction

The experimental discovery of the Higgs boson [1, 2] implies that the Weinberg Salam Standard Model (SM) is a valid low energy theory at the weak scale. All current measurements are consistent with this statement and physics in the electroweak symmetry breaking (EWSB) sector beyond that predicted by the SM is highly constrained by current experimental results, both at the LHC and from precision electroweak measurements. These lectures summarize the underlying theoretical framework of the SM and its experimental predictions and discuss possible high scale extensions of the theory in terms of an effective field theory.

Section 2 contains an introduction to the SM and Section 3 discusses theoretical restrictions on the EWSB sector. Section 4 presents the basics of Higgs production and decay, along with a summary of experimental results. Pedagogical discussions of the gluon fusion production rate at leading order and the determination of the Higgs width are also found in Section 4. Extensions of the SM in terms of an effective field theory are presented in Section 5 and Section 6 contains some conclusions. There are many excellent reviews of Higgs physics and the reader is referred to them for additional details and further references [3–9].

2 Weinberg-Salam Model

The Weinberg- Salam model is an $SU(2)_L \times U(1)_Y$ gauge theory containing three $SU(2)_L$ gauge bosons, W_μ^I, $I = 1, 2, 3$, and one $U(1)_Y$ gauge boson, B_μ, with kinetic energy terms,

$$\mathcal{L}_{\text{KE}} = -\frac{1}{4} W_{\mu\nu}^I W^{\mu\nu I} - \frac{1}{4} B_{\mu\nu} B^{\mu\nu} , \qquad (1)$$

where the index I is summed over and,

$$
\begin{aligned}
W_{\mu\nu}^I &= \partial_\nu W_\mu^I - \partial_\mu W_\nu^I + g\epsilon^{IJK} W_\mu^J W_\nu^K , \\
B_{\mu\nu} &= \partial_\nu B_\mu - \partial_\mu B_\nu .
\end{aligned}
\qquad (2)
$$

The $SU(2)_L$ and $U(1)_Y$ coupling constants are g and g', respectively. Coupled to the gauge fields is a complex scalar $SU(2)$ doublet, Φ,

$$\Phi = \begin{pmatrix} \phi^+ \\ \phi^0 \end{pmatrix} . \qquad (3)$$

The scalar potential is given by,

$$V(\Phi) = \mu^2 \mid \Phi^\dagger \Phi \mid + \lambda \Big(\mid \Phi^\dagger \Phi \mid \Big)^2 , \tag{4}$$

where $\lambda > 0$.

The state of minimum energy for $\mu^2 < 0$ is not at $\phi^0 = 0$ and the scalar field develops a VEV[1]. The direction of the minimum in $SU(2)_L$ space is not determined, since the potential depends only on the combination $\Phi^\dagger \Phi$ and we arbitrarily choose

$$\langle \Phi \rangle \equiv \frac{1}{\sqrt{2}} \left(\begin{array}{c} 0 \\ v \end{array} \right) . \tag{5}$$

With this choice, the electromagnetic charge is,[2]

$$Q = \frac{(\tau_3 + Y)}{2} , \tag{6}$$

where we assign hypercharge $Y = 1$ to Φ.

Therefore,

$$Q \langle \Phi \rangle = 0 \tag{7}$$

and electromagnetism is unbroken by the scalar VEV. The VEV of Equation (5) yields the desired symmetry breaking pattern,

$$SU(2)_L \times U(1)_Y \to U(1)_{EM}. \tag{8}$$

The scalar contribution to the Lagrangian is,

$$\mathcal{L}_s = (D^\mu \Phi)^\dagger (D_\mu \Phi) - V(\Phi) , \tag{9}$$

where[3]

$$D_\mu = \partial_\mu + i \frac{g}{2} \tau \cdot W_\mu + i \frac{g'}{2} B_\mu Y. \tag{10}$$

In unitary gauge there are no Goldstone bosons and only the physical Higgs scalar remains in the spectrum after spontaneous symmetry breaking. In unitary gauge,

$$\Phi = \frac{1}{\sqrt{2}} \left(\begin{array}{c} 0 \\ v + h \end{array} \right) , \tag{11}$$

which gives the contribution to the gauge boson masses from the scalar kinetic energy term of Equation (9),

$$M^2 \sim \frac{1}{2}(0, v) \left(\frac{1}{2} g \tau \cdot W_\mu + \frac{1}{2} g' B_\mu \right)^2 \left(\begin{array}{c} 0 \\ v \end{array} \right) . \tag{12}$$

The physical gauge fields are two charged fields, $W^\pm$, and two neutral gauge bosons, Z and γ.

$$W_\mu^\pm = \frac{1}{\sqrt{2}}(W_\mu^1 \mp i W_\mu^2)$$

$$Z^\mu = \frac{-g' B_\mu + g W_\mu^3}{\sqrt{g^2 + g'^2}} \equiv -\sin\theta_W B_\mu + \cos\theta_W W_\mu^3$$

---

[1]There is no mechanism or motivation for determining the $\text{sign}(\mu^2)$ in the SM.

[2]The τ_I are the Pauli matrices with $Tr(\tau_I \tau_J) = 2\delta_{IJ}$.

[3]Different choices for the gauge kinetic energy and the covariant derivative depend on whether g and g' are chosen positive or negative. There are no physical consequences of this choice.

$$A^{\mu} \quad = \quad \frac{gB_{\mu} + g'W_{\mu}^3}{\sqrt{g^2 + g'^{\,2}}} \equiv \cos\theta_W B_{\mu} + \sin\theta_W W_{\mu}^3. \tag{13}$$

Equation (13) defines a mixing angle,

$$\sin\theta_W \equiv \frac{g'}{\sqrt{g^2 + g'^{\,2}}}\,. \tag{14}$$

Since the massless photon must couple with electromagnetic strength, e, the coupling constants define the weak mixing angle θ_W,

$$\begin{aligned} e &= g\sin\theta_W \equiv gs_W \\ e &= g'\cos\theta_W \equiv g'c_W\,. \end{aligned} \tag{15}$$

The gauge bosons obtain masses from the Higgs mechanism, as demonstrated in Equation (12):

$$M_W^2 = \frac{1}{4}g^2 v^2, \qquad M_Z^2 = \frac{1}{4}(g^2 + g'^{\,2})v^2, \qquad M_A = 0\,. \tag{16}$$

If we go to a gauge other than unitary gauge, there are Goldstone bosons in the spectrum and the scalar field can be parameterized,

$$\Phi = \frac{1}{\sqrt{2}}e^{i\frac{\omega\cdot\tau}{2v}}\begin{pmatrix} 0 \\ v + h \end{pmatrix}. \tag{17}$$

In the Standard Model, there are three Goldstone bosons, $\vec{\omega} = (\omega^{\pm}, z)$, with masses M_W and M_Z in the Feynman gauge.

Fermions can easily be included in the theory. We write the fermions in terms of their left- and right-handed projections,

$$\psi_{L,R} = \frac{1}{2}(1 \mp \gamma_5)\psi\,. \tag{18}$$

From the four-Fermi theory of weak interactions [9], we know experimentally that the W-boson couples only to left-handed fermions and so we construct the $SU(2)_L$ doublet,

$$L_L = \begin{pmatrix} \nu_L \\ e_L \end{pmatrix}. \tag{19}$$

From Equation (6), the hypercharge of the lepton doublet must be $Y_L = -1$. In the limit where the neutrino is massless, it can have only one helicity state which is taken to be ν_L. Including neutrino masses requires interactions beyond the standard construction of the Weinberg-Salam model[4]. The SM is therefore constructed with no right-handed neutrinos. Further, we assume that right-handed fields do not interact with the W boson, and so the right-handed electron, e_R, must be an $SU(2)_L$ singlet with $Y_{e_R} = -2$. Using these hypercharge assignments, the leptons can be coupled in a gauge invariant manner to the $SU(2)_L \times U(1)_Y$ gauge fields,

$$\mathcal{L}_{lepton} = i\bar{e}_R\gamma^{\mu}\left(\partial_{\mu} + i\frac{g'}{2}Y_e B_{\mu}\right)e_R + i\bar{L}_L\gamma^{\mu}\left(\partial_{\mu} + i\frac{g}{2}\tau\cdot W_{\mu} + i\frac{g'}{2}Y_L B_{\mu}\right)L_L\,. \tag{20}$$

All of the known fermions can be accommodated in the Standard Model in this fashion. The $SU(2)_L$ and $U(1)_Y$ charge assignments of the first generation of fermions are given in Table 1. The quantum numbers of the 2nd and 3rd generation are identical to those of first generation.

---

[4]A pedagogical introduction to ν masses can be found in Ref. [10].

Field	SU(3)	$SU(2)_L$	$U(1)_Y$
$Q_L = \begin{pmatrix} u_L \\ d_L \end{pmatrix}$	3	2	$\frac{1}{3}$
u_R	3	1	$\frac{4}{3}$
d_R	3	1	$-\frac{2}{3}$
$L_L = \begin{pmatrix} \nu_L \\ e_L \end{pmatrix}$	1	2	-1
e_R	1	1	-2
$\Phi = \begin{pmatrix} \phi^+ \\ \phi^0 \end{pmatrix}$	1	2	1

Table 1: Quantum numbers of the SM fermions.

A fermion mass term takes the form

$$\mathcal{L}_{mass} = -m\overline{\psi}\psi = -m\left(\overline{\psi}_L\psi_R + \overline{\psi}_R\psi_L\right). \tag{21}$$

As is obvious from Table 1, the left-and right-handed fermions transform differently under $SU(2)_L$ and $U(1)_Y$ gauge transformations and so gauge invariance forbids a term like Equation (21). The Higgs boson, however, can couple in a gauge invariant fashion to the down quarks,

$$\mathcal{L}_d = -Y_d\overline{Q}_L\Phi d_R + h.c., \tag{22}$$

After the Higgs obtains a VEV, we have the effective coupling,

$$-Y_d\frac{1}{\sqrt{2}}(\overline{u}_L, \ \overline{d}_L)\begin{pmatrix} 0 \\ v+h \end{pmatrix}d_R + h.c. \tag{23}$$

which can be seen to yield a mass term for the down quark,

$$Y_d = \frac{m_d\sqrt{2}}{v}. \tag{24}$$

In order to generate a mass term for the up-type quarks we use the fact that

$$\tilde{\Phi} \equiv i\tau_2\Phi^* = \begin{pmatrix} \phi^0 \\ -\phi^- \end{pmatrix} \tag{25}$$

is an $SU(2)_L$ doublet, and write the $SU(2)_L$ invariant coupling

$$\mathcal{L}_u = -Y_u\overline{Q}_L\tilde{\Phi}u_R + h.c. \tag{26}$$

which generates a mass term for the up quark. Similar couplings can be used to generate mass terms for the charged leptons. Since the neutrino has no right handed partner in the SM, it remains massless.

For the multi-family case, the Yukawa couplings, Y_d and Y_u, become $N_F \times N_F$ matrices (where N_F is the number of families). Since the fermion mass matrices and Yukawa matrices are proportional, the interactions of the Higgs boson with the fermion mass eigenstates are flavor diagonal and the Higgs boson does not mediate flavor changing interactions. This is an important prediction of the SM.

The parameter v can be found from the charged current for μ decay, $\mu \to e\overline{\nu}_e\nu_\mu$, which is measured very accurately to be $G_F = 1.16638 \times 10^{-5} \ GeV^{-2}$. Since the momentum carried by the W boson is of order m_μ it can be neglected in comparison with M_W and we make the identification,

$$\frac{G_F}{\sqrt{2}} = \frac{g^2}{8M_W^2} = \frac{1}{2v^2}, \tag{27}$$

which gives the result

$$v = (\sqrt{2}G_F)^{-1/2} = 246 \ GeV \ . \tag{28}$$

One of the most important points about the Higgs mechanism is that all of the couplings of the Higgs boson to fermions and gauge bosons are completely determined in terms of coupling constants and fermion masses. A complete set of Feynman rules can be found in Ref. [5]. The potential of Equation (4) had two free parameters, μ and λ, which can be traded for,

$$\begin{aligned} v^2 &= -\frac{\mu^2}{2\lambda} \\ m_h^2 &= 2v^2\lambda \,. \end{aligned} \tag{29}$$

The scalar potential is now,

$$V = \frac{m_h^2}{2}h^2 + \frac{m_h^2}{2v}h^3 + \frac{m_h^2}{8v^2} \ . \tag{30}$$

The self-interactions of the Higgs boson are determined in terms of the Higgs mass. There are no remaining adjustable parameters and so Higgs production and decay processes can be computed unambiguously in terms of the Higgs mass.

3 Theoretical Constraints

3.1 Bounds from Precision Measurements

The Higgs boson enters into one loop radiative corrections in the Standard Model and precision electroweak measurements test the consistency of the theory[5] . In the electroweak sector of the SM, there are four fundamental parameters, the $SU(2)_L \times U(1)_Y$ gauge coupling constants, g and g', as well as the two parameters of the Higgs potential, which are usually taken to be the vacuum expectation value of the Higgs boson, v, and the Higgs mass, m_h. Once these parameters are fixed, all other physical quantities can be derived in terms of them (and of course the fermion masses and CKM mixing parameters, along with the strong coupling constant α_s). Equivalently, the muon decay constant, G_μ, the Z-boson mass, M_Z, and the fine structure constant, α, can be used as input parameters. Experimentally, the measured values for these input parameters are [11, 12],

$$\begin{aligned} G_\mu &= 1.16638(1) \times 10^{-5} \ GeV^{-2} \\ M_Z &= 91.1876(21) \ GeV \\ \alpha^{-1} &= 137.035999679(94) \\ m_h &= 125.09 \pm .21(stat) \pm .11(syst) \ GeV \,. \end{aligned} \tag{31}$$

The W boson mass is thus a prediction of the theory and is defined through muon decay,

$$\begin{aligned} M_W^2 &= \frac{\pi\alpha}{\sqrt{2}G_\mu(1 - M_W^2/M_Z^2)} \\ M_W^2 &= \frac{M_Z^2}{2}\left\{1 + \sqrt{1 - \frac{4\pi\alpha}{\sqrt{2}G_\mu M_Z^2}}\right\} \,. \end{aligned} \tag{32}$$

---

[5]An introductory review of precision measurements in the SM can be found in Ref. [13].

At tree level, the SM prediction from Equation (32) is,

$$M_W(tree) = 79.829 \, GeV \,, \tag{33}$$

in slight disagreement with the measured value [11],

$$M_W(experiment) = 80.379 \pm 0.012 \, GeV \,. \tag{34}$$

In order to obtain good agreement between theory and the experimental data, it is crucial to include radiative corrections. The prediction for M_W can be written as [14],

$$M_W^2 = \frac{\pi \alpha}{\sqrt{2} G_\mu s_W^2} \left[1 + \Delta r_{SM} \right] \,, \tag{35}$$

where Δr_{SM} summarizes the radiative corrections. The dependence on the top quark mass, m_t, is particularly significant as Δr_{SM} depends on m_t quadratically,

$$\Delta r_{SM}^t = -\frac{G_\mu}{\sqrt{2}} \frac{N_c}{8\pi^2} \left(\frac{c_W^2}{s_W^2} \right) m_t^2 + \log(m_t) \text{ terms} \,, \tag{36}$$

where $N_c = 3$ is the number of colors. The dependence on m_h is logarithmic,

$$\Delta r_{SM}^h \sim \frac{\alpha}{\pi s_W^2} \frac{11}{48} \log\left(\frac{m_h^2}{M_Z^2} \right) + \mathcal{O}\left(\frac{m_h^2}{M_Z^2}, \frac{v^4}{\Lambda^4} \right) \,. \tag{37}$$

The top quark does not decouple from the theory even at energies far above the top quark mass. This is because the top quark coupling to the Higgs boson is proportional to m_t.

The agreement between the radiatively corrected prediction for the W mass given by Equation (35) with the measured value is a strong test of the theory. In a similar fashion, the full set of electroweak data can be used to test the self consistency of the theory, as demonstrated in Figure 1 [15]. Similar studies have been performed by the GFITTER collaboration [16]. (The most restrictive data points are the measurements of the $Zb\bar{b}$ coupling and the W boson mass.) When the experimental values of M_W, m_t, and m_h are omitted, the fit is in good agreement with the directly measured values of the masses. Note that the fit excludes a large ($\sim 100's$ of GeV) value of m_h and so even before the Higgs boson was discovered, we knew that if there were no new physics contributions to the predictions for electroweak quantities such as M_W, the Higgs boson could not be too heavy.

3.2 Oblique Parameters

Extensions of the SM with modified Higgs sectors are significantly restricted by the requirement of consistency with the electroweak measurements. A simple way to examine whether a theory with a complicated Higgs sector is consistent with electroweak experiments is to use the oblique parameters. Using the oblique parameters to obtain limits on BSM physics assumes that the dominant contributions resulting from the expanded theory are to the gauge boson 2-point functions [17, 18]. Combinations of the $2-$ point functions define S, T and U. New physics effects are determined by subtracting the SM contribution, e.g. $\Delta S \equiv S_{BSM} - S_{SM}$.

A simple example is a model with a a real scalar singlet, S, added to the SM. After imposing a Z_2 symmetry under which $S \to -S$, the most general scalar potential is [19]

$$V = -\mu^2 \, \Phi^\dagger \Phi - m^2 S^2 + \lambda (\Phi^\dagger \Phi)^2 + \frac{a_2}{2} \, \Phi^\dagger \Phi \, S^2 + \frac{b_4}{4} S^4. \tag{38}$$

After spontaneous symmetry breaking, both Φ and S obtain VEVs and the mass eigenstates h and H are a mixture of S and Φ ($s \equiv \langle S \rangle$),

$$\begin{pmatrix} h \\ H \end{pmatrix} = \begin{pmatrix} \cos\alpha & -\sin\alpha \\ \sin\alpha & \cos\alpha \end{pmatrix} \begin{pmatrix} \sqrt{2}\phi_0 - v \\ S - s \end{pmatrix} \,, \tag{39}$$
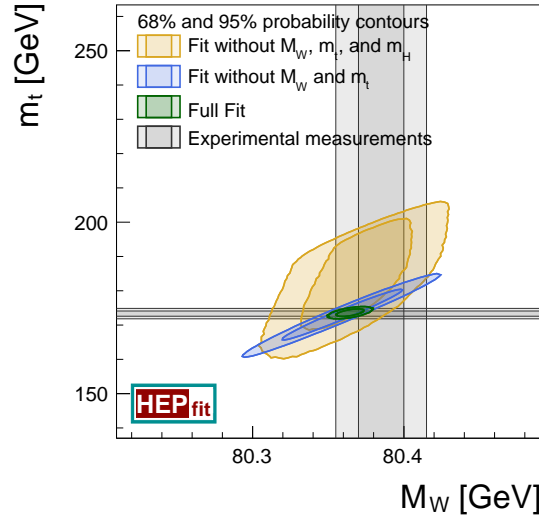
Fig. 1: Experimental limits on M_W and m_t from precision electroweak measurements. The straight bands are the direct measurements of M_W and m_t [15].

with physical masses, m_h and M_H. The singlet cannot couple directly to fermions or gauge bosons, so the only physical effect on single Higgs production is through the mixing of Equation (39). The mixing affects the SM-like Higgs couplings to both fermions and gauge bosons in an identical fashion and all SM couplings are suppressed by the factor $\cos\alpha$. This model is particularly simple since it can be studied in terms of M_H and the mixing angle α. For $m_h, M_H >> M_W, M_Z$, the contributions to the oblique parameters are,

$$
\begin{aligned}
\Delta S &= \frac{1}{12\pi}\sin^2\alpha\log\left(\frac{M_H^2}{m_h^2}\right)\\
\Delta T &= -\frac{3}{16\pi c_W^2}\sin^2\alpha\log\left(\frac{M_H^2}{m_h^2}\right)\\
\Delta U &= 0\,.
\end{aligned}
\tag{40}
$$

and for any given value of M_H, an upper limit on $\sin\alpha$ can be determined [20]. Limits from the oblique parameters are an important tool in understanding what BSM models are allowed experimentally and in restricting the parameters of the models.

3.3 Restrictions from Triviality

Theoretical bounds on the Higgs boson mass can be deduced on the grounds of *triviality*, which can be summarized as the requirement that the Higgs quartic coupling remain finite at high energy scales. If the quartic coupling becomes infinite, the theory is no longer perturbative, while if the quartic coupling goes to zero, the theory is non-interacting. The Higgs quartic coupling, λ, changes with the effective energy scale, Λ, due to the self interactions of the scalar field:

$$
\frac{d\lambda}{dt} = \frac{3\lambda^2}{4\pi^2},
\tag{41}
$$

139
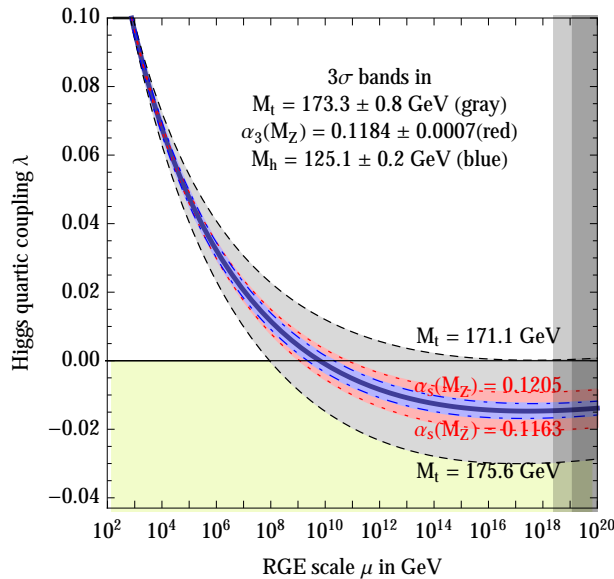
Fig. 2: Dependence of the Higgs quartic coupling on the renormalization scale [21].

where $t \equiv \log(\Lambda^2/v^2)$. In the SM, however, there are also contributions due to gauge boson and fermion loops[6]. Including the top quark contribution, Equation (42) becomes,

$$\frac{d\lambda}{dt} = \frac{3}{4\pi^2}\left\{\lambda^2 - Y_t^2\lambda - Y_t^4\right\}, \tag{42}$$

where $Y_t = m_t/v$. For small λ (small m_h), the Y_t^4 term dominates and the quartic coupling decreases with energy,

$$\lambda(\Lambda) \sim \lambda(v) - \frac{3Y_t^4}{4\pi^2}\log\left(\frac{\Lambda^2}{v^2}\right). \tag{43}$$

The scaling of λ has been performed to $2-$ loops [21], including contributions from gauge and Yukawa couplings and the result is shown in Figure 2. The quartic coupling becomes negative at a high scale that is quite sensitive to m_t and α_s, suggesting that at this scale some new physics is required to force λ to be positive which is need in order for the potential to be bounded from below.

4 Higgs Production and Decay

In this section we review the SM rates for Higgs production and decay. Numerical values, including the most precisely known higher order calculations, have been tabulated by the LHC Higgs cross section working group [22].

4.1 Higgs Decays

Expressions for the SM Higgs decay widths at leading order can be found in Ref. [5], and the QCD corrected rates, with references to the original literature, are given in Refs. [4, 8]. The QCD NLO corrected decay rates can be found using the public code, HDECAY [23].

---

[6]We neglect the gauge contributions here.

4.1.1 $\quad h \to f\bar{f}$

The Higgs couplings to fermions are proportional to fermion mass and the lowest order width for the Higgs decay to fermions of mass m_f is,

$$\Gamma(h \to f\bar{f}) = \frac{G_F m_f^2 N_{ci}}{4\sqrt{2}\pi} m_h \beta_F^3 \,, \tag{44}$$

where $\beta_F \equiv \sqrt{1 - 4m_f^2/m_h^2}$ is the velocity of the final state fermions and $N_{ci} = 1(3)$ for charged leptons (fermions). The largest fermion decay channel is $h \to b\bar{b}$, which receives large QCD corrections. A significant portion of the QCD corrections can be accounted for by expressing the decay width in terms of a running quark mass, $m_f(\mu)$, evaluated at the scale $\mu = m_h$. The QCD corrected decay width can then be approximated as [24, 25],

$$\Gamma(h \to q\bar{q}) = \frac{3G_F}{4\sqrt{2}\pi} m_q^2(m_h^2) m_h \beta_q^3 \left(1 + 5.67 \frac{\alpha_s(m_h^2)}{\pi} + \cdots \right), \tag{45}$$

where $\alpha_s(m_h^2)$ is defined in the $\overline{MS}$ scheme with 5 flavors. In leading log QCD, the running of the b quark mass is,

$$m_b(\mu^2) = m \left[\frac{\alpha_s(m^2)}{\alpha_s(\mu^2)} \right]^{(-12/23)} \left\{ 1 + \mathcal{O}(\alpha_s^2) \right\}, \tag{46}$$

where $m_b(m^2) \equiv m$ implies that the running mass at the position of the propagator pole is equal to the location of the pole. For $m_b(m_b^2) = 4.18\,GeV$, this yields an effective value $m_b(m_h = 125\,GeV)\,|_{LL} = 2.8\,GeV$ (at NLL, $m_b(m_h = 125\,GeV)\,|_{NLL} = 2.7\,GeV$). Inserting the QCD corrected mass into the expression for the width thus leads to a suppression of the width by $\sim .4$. Using the running b mass absorbs the large logarithms of the form $\log(m_h^2/m_b^2)$ and is important for numerical accuracy. The electroweak radiative corrections to $h \to f\bar{f}$ amount to only a few percent correction [26].

4.1.2 $\quad h \to WW, ZZ$

The Higgs boson can also decay to gauge boson pairs. At tree level, the decays $h \to WW^*$ and $h \to ZZ^*$ are possible (with one of the gauge bosons off-shell), while at one-loop the decays $h \to gg, \gamma\gamma$, and γZ occur.

The decay width for the off-shell decay, $h \to ZZ^* \to f_1(p_1)f_2(p_2)Z(p_3)$, is,

$$\Gamma = \int_0^{(m_h - M_Z)^2} dq^2 \int dm_{23}^2 \frac{|A|^2}{256\pi^3 m_h^3} \,, \tag{47}$$

where $m_{ij} = (p_i + p_j)^2$, $m_{12}^2 \equiv q^2$, and $m_{12}^2 + m_{23}^2 + m_{13}^2 = m_h^2 + M_Z^2$, $\lambda(m_h^2, M_Z^2, q^2) \equiv q^4 - 2q^2(m_h^2 + M_Z^2) + (m_h^2 - M_Z^2)^2$, and $m_{23}^2\,|_{max,min} \equiv \frac{1}{2}\left(m_h^2 + M_Z^2 - q^2 \pm \sqrt{\lambda} \right)$. The amplitude-squared is,

$$
\begin{aligned}
|A(h \to Zf\bar{f})|^2 &= 32\,(g_L^2 + g_R^2)\,G_F^2\,M_Z^4 \\
&\quad \cdot \left[\frac{2M_Z^2 q^2 - m_{13}^2 q^2 - m_h^2 M_Z^2 + m_{13}^2 M_Z^2 + m_{13}^2 m_h^2 - m_{13}^4}{(q^2 - M_Z^2)^2 + \Gamma_Z^2 M_Z^2} \right],
\end{aligned} \tag{48}
$$

with $g_{Lf} = T_{3f} - Q_f s_W^2$, $g_{Rf} = -Q_f s_W^2$, and $T_3 = \pm\frac{1}{2}$. We see that the amplitude is peaked at low q^2. Integrating over dm_{23}^2,

$$\frac{d\Gamma}{dq^2}(h \to Zf\bar{f}) = (g_L^2 + g_R^2)\,G_F^2\,\sqrt{\lambda(m_h^2, M_Z^2, q^2)}\frac{M_Z^4}{48\pi^3 m_h^3}$$

$$\cdot \left[\frac{(12M_Z^2 q^2 + \lambda(m_h^2, M_Z^2, q^2))}{(q^2 - M_Z^2)^2 + \Gamma_Z^2 M_Z^2} \right] . \tag{49}$$

The result for $h \to W f \overline{f'}$ can be found by making the appropriate redefinitions of the fermion - gauge boson couplings.

Performing the q^2 integral and summing over the final state fermions [27],

$$\Gamma(h \to WW^*) = \frac{g^4 m_h}{512 \pi^3} F\left(\frac{M_W}{m_h}\right)$$

$$\Gamma(h \to ZZ^*) = \frac{g^4 m_h}{2048 \cos_W^4 \pi^3} \left(7 - \frac{40}{3} s_W^2 + \frac{160}{9} s_W^4\right) F\left(\frac{M_Z}{m_h}\right), \tag{50}$$

where

$$F(x) = |1 - x^2| \left(\frac{47}{2} x^2 - \frac{13}{2} + \frac{1}{x^2}\right)$$

$$+ 3(1 - 6x^2 + 4x^4) |\ln x| + \frac{3(1 - 8x^2 + 20x^4)}{\sqrt{4x^2 - 1}} \cos^{-1}\left(\frac{3x^2 - 1}{2x^3}\right). \tag{51}$$

The NLO QCD and electroweak corrections to the off-shell decays, $h \to V^* V^* \to$ 4-fermions , $V = (W, Z)$, are implemented in the public code, PROPHECY4f [28].

4.1.3 $h \to gg$

The decay of the Higgs boson to gluons only arises through fermion loops in the SM and is sensitive to new colored particles that interact with the Higgs,

$$\Gamma(h \to gg) = \frac{G_F \alpha_s^2 m_h^3}{64\sqrt{2}\pi^3} |\sum_q F_{1/2}(\tau_q)|^2, \tag{52}$$

where $\tau_q \equiv 4m_q^2/m_h^2$ and $F_{1/2}(\tau_q)$ is defined to be,

$$F_{1/2}(\tau_q) \equiv -2\tau_q \left[1 + (1 - \tau_q) f(\tau_q)\right]. \tag{53}$$

The function $f(\tau_q)$ is given by,

$$f(\tau_q) = \begin{cases} \left[\sin^{-1}\left(\sqrt{1/\tau_q}\right)\right]^2, & \text{if } \tau_q \geq 1 \\ -\frac{1}{4}\left[\log\left(\frac{x_+}{x_-}\right) - i\pi\right]^2, & \text{if } \tau_q < 1, \end{cases} \tag{54}$$

with

$$x_\pm = 1 \pm \sqrt{1 - \tau_q}. \tag{55}$$

In the limit in which the quark mass is much less than the Higgs boson mass,

$$F_{1/2} \to \frac{2m_q^2}{m_h^2} \log^2\left(\frac{m_q}{m_h}\right). \tag{56}$$

On the other hand, for a heavy quark, $\tau_q \to \infty$, and $F_{1/2}(\tau_q)$ approaches a constant,

$$F_{1/2} \to -\frac{4}{3}. \tag{57}$$

Equations (56) and (57) make it clear that the top quark loop is the dominant contribution. QCD corrections to the decay $h \to gg$ are known at NLO for a finite top quark mass and increase the rate by roughly 60% [29].
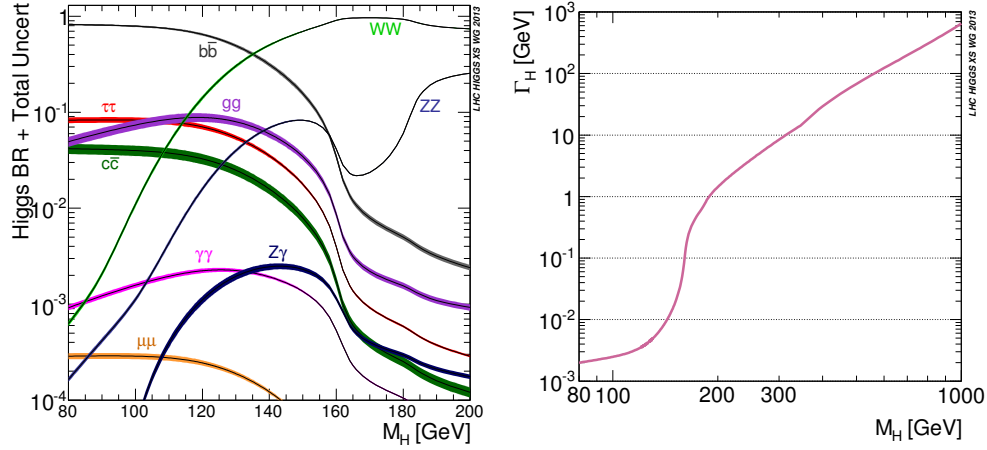
Fig. 3: SM Higgs Branching ratios (LHS) and total width for a SM-like Higgs boson of arbitrary mass (RHS) [22]. In this figure, H is the SM Higgs boson.

4.1.4 $h \rightarrow \gamma\gamma$

The decay $h \rightarrow \gamma\gamma$ arises from fermion and W loops and is an important mode for Higgs measurements at the LHC, despite the smallness of the branching ratio. At lowest order the width is, [5]

$$\Gamma(h \rightarrow \gamma\gamma) = \frac{\alpha^2 G_F}{128\sqrt{2}\pi^3} m_h^3 \mid \sum_i N_{ci} Q_i^2 F_i(\tau_i) \mid^2, \tag{58}$$

where the sum is over fermions and $W^\pm$ bosons with $F_{1/2}(\tau_q)$ given in Equation (53), and

$$F_W(\tau_W) = 2 + 3\tau_W[1 + (2 - \tau_W)f(\tau_W)], \tag{59}$$

with $\tau_W = 4M_W^2/m_h^2$, $N_{ci} = 1(3)$ for leptons (quarks), and Q_i is the electric charge in units of e. In the (unphysical) limit $\tau_W \rightarrow \infty$, $F_W \rightarrow 7$ and we see that the top quark and W contributions have opposite signs. The decay $h \rightarrow \gamma\gamma$ is therefore sensitive to the sign of the top quark Yukawa coupling through the interference of the W and t loops. Similarly, the rate for $h \rightarrow Z\gamma$ receives contributions from both fermions and the W boson. The analytic formula is given in [5] and the $Z\gamma$ width is quite small.

The Higgs branching ratios are shown in Figure 3 for a SM Higgs boson of arbitrary mass [22]. The width of the curves is an estimate of the theoretical uncertainties on the branching ratios. The branching ratios assume SM couplings and no new decay channels and include all known radiative corrections [22]. Also shown in Figure 3 is the Higgs total decay width as a function of Higgs mass. For $m_h = 125\, GeV$, the total width is very narrow, $\Gamma_h = 4\, MeV$.

4.2 Higgs Production in Hadronic Collisions

At the LHC, the dominant production mechanisms are gluon fusion, followed by vector boson fusion, shown in Figure 4. The associated production mechanisms of the Higgs with vector bosons or top quarks have smaller rates, but these channels are theoretically important and are shown in Figure 5. It is immediately apparent that gluon fusion and $t\bar{t}h$ production are sensitive to the top quark Yukawa coupling, while vector boson fusion and associated hV, $V = (W, Z)$, production probe the gauge-Higgs couplings.

The total rates for Higgs production in various channels are shown on the LHS of Figure 6 for arbitrary Higgs mass at $13\, TeV$ (LHS) and as a function of center-of-mass energy (RHS) for the physics Higgs mass. The curves include the most up-to-date theoretical calculations, and the width of the curves represents an estimate of the uncertainties [30]. We will discuss each production channel in turn in this section.
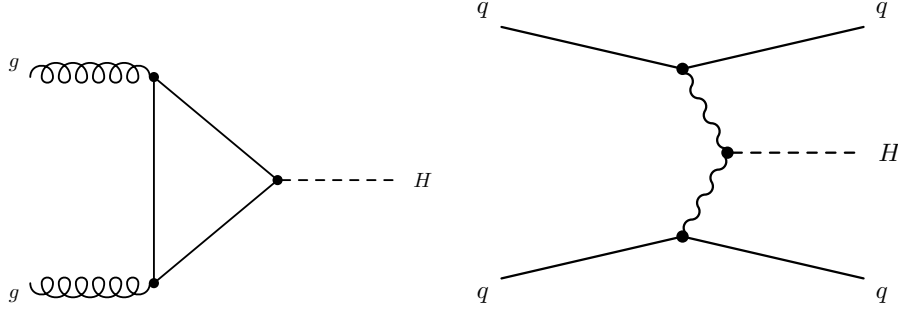
Fig. 4: Contribution to Higgs boson production from (LHS) gluon fusion and (RHS) vector boson scattering. In this figure, H is the SM Higgs boson.
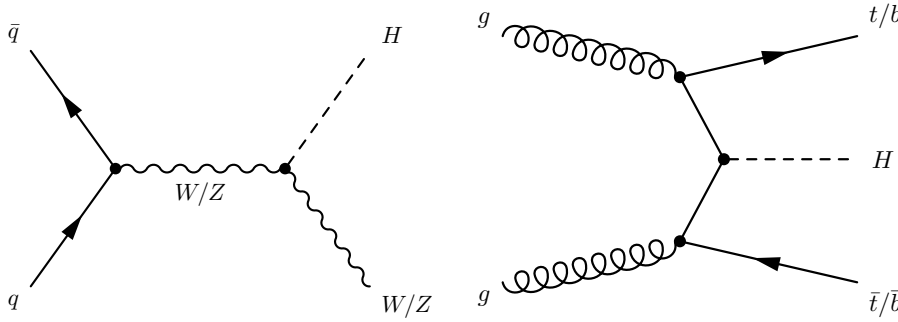

Fig. 5: Contribution to Higgs boson production from (LHS) associated Vh production and (RHS) $t\bar{t}h$ production. In this figure, H is the SM Higgs boson.
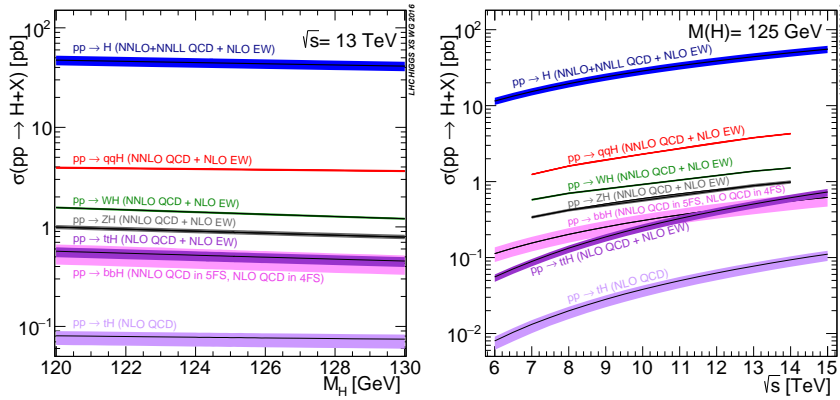

Fig. 6: Total Higgs production cross sections [30]. In this figure, H is the SM Higgs boson.

4.2.1 $gg \rightarrow h$

The primary production mechanism for a Higgs boson in hadronic collisions is through the couplings to heavy fermions, $gg \rightarrow h$, which is shown on the LHS of Figure 4. This process is dominated by the top quark loop and the loop with a bottom quark contributes roughly -5% to the SM cross section.

The lowest order (LO) amplitude for $g^{A,\mu}(p) + g^{B,\nu}(q) \rightarrow h$ from a quark of mass m_q in the loop is,

$$A^{\mu\nu}(g^A g^B \rightarrow h) = \frac{\alpha_s}{4\pi v} \delta_{AB} \left(g^{\mu\nu} \frac{m_h^2}{2} - p^\nu q^\mu \right) F_{1/2}(\tau_q) \epsilon_\mu(p) \epsilon_\nu(q)$$

$$\rightarrow \quad -\frac{\alpha_s}{3\pi v}\delta_{AB}\left(g^{\mu\nu}\frac{m_h^2}{2} - p^\nu q^\mu\right)\epsilon_\mu(p)\epsilon_\nu(q) \qquad \text{if } m_q >> m_h. \tag{60}$$

The partonic cross section can be found from the general resonance formula,

$$\hat{\sigma}(gg \rightarrow h) = \frac{16\pi^2}{m_h}(2J+1)\frac{1}{64} \cdot \frac{1}{4} \cdot 2\Gamma(h \rightarrow gg)\delta(s - m_h^2), \tag{61}$$

where the factors of $\frac{1}{64}$ and $\frac{1}{4}$ are the color and spin averages, $J = 0$ is the Higgs spin, s is the gg partonic sub-energy, and the factor of 2 undoes the identical particle factor of $\frac{1}{2}$ in the decay width $\Gamma(h \rightarrow gg)$. The lowest order partonic cross section for $gg \rightarrow h$ is,

$$\begin{aligned}
\hat{\sigma}(gg \rightarrow h) &= \frac{\alpha_s^2}{1024\pi v^2} \mid \sum_q F_{1/2}(\tau_q) \mid^2 \delta\left(1 - \frac{s}{m_h^2}\right) \\
&\equiv \hat{\sigma}_0(gg \rightarrow h)\delta\left(1 - \frac{s}{m_h^2}\right).
\end{aligned} \tag{62}$$

In the heavy quark limit, the cross section is independent of the top quark mass and becomes a constant,

$$\hat{\sigma}_0(gg \rightarrow h) \sim \frac{\alpha_s^2}{576\pi v^2}. \tag{63}$$

The heavy fermions do not decouple at high energy and the gluon fusion rate essentially counts the number of SM-like chiral quarks.

The Higgs boson production cross section at a hadron collider can be found by integrating the partonic cross section, $\sigma_0(pp \rightarrow h)$, with the gluon parton distribution functions, $g(x, \mu)$,

$$\sigma(pp \rightarrow h) = \hat{\sigma}_0 z \int_z^1 \frac{dx}{x}g(x, \mu)g\left(\frac{z}{x}, \mu\right), \tag{64}$$

where σ_0 is given in Equation (62), $z \equiv m_h^2/S$, μ is the factorization scale and S is the hadronic center of mass energy. It is particularly interesting to consider the theoretical accuracy at N^3LO [31],

$$\sigma(pp \rightarrow h)[13 \text{ TeV}] = 48.58^{+4.6\%}_{-6.7\%}(\text{theory}) \pm 3.2\%(\text{PDF} + \alpha_s), \tag{65}$$

where the theory uncertainty arises predominantly from the scale choice and the PDF+α_s uncertainty is the PDF and correlated uncertainty on α_s.

The measured Higgs rate immediately rules out the possibility of a 4th generation of SM chiral fermions. Imagine that there are heavy fermions, $\mathcal{T}$ and $\mathcal{B}$, with identical quantum numbers as the SM top and bottom quarks. The new fermions would contribute to Higgs production from gluon fusion as on the LHS of Figure 4. From Equation (63), we would have,

$$\begin{aligned}
\hat{\sigma}_0(gg \rightarrow h) &\rightarrow \frac{\alpha_s^2}{576\pi v^2}\Big[1 + 1 + 1\Big]^2 \\
&\rightarrow 9\hat{\sigma}_0(SM),
\end{aligned} \tag{66}$$

where the factors in the square bracket represent the contributions of the SM $t, \mathcal{T}$ and $\mathcal{B}$. This is obviously excluded by the measured rate for gluon fusion Higgs production, which is in good agreement with the SM prediction.

The tensor structure of Equation (60) is exactly that required for the production of a spin-0 particle from 2-gluons with momentum, $g(k_1)$ and $g(k_2)$. Starting from a $G_{\mu\nu}G^{\mu\nu}$ term in the Lagrangian and considering only the Abelian contributions for now,

$$G_{\mu\nu}G^{\mu\nu} \quad \rightarrow \quad (\partial_\mu G_\nu - \partial_\nu G_\mu)(\partial^\mu G^\nu - \partial^\nu G^\mu). \tag{67}$$
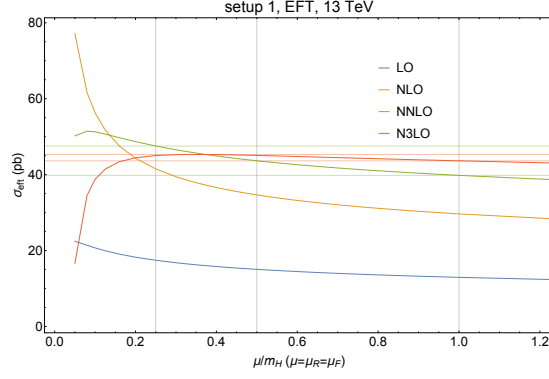
Fig. 7: QCD corrected rate for gluon fusion as a function of the factorization and renormalization scale [31].

Making the replacement $\partial_\mu \to ik_\mu$,

$$
\begin{aligned}
G_{\mu\nu}G^{\mu\nu} & \to & -(k_{1\mu}G_{1\nu} - k_{1\nu}G_{1\mu})(k_2^\mu G_2^\nu - k_2^\nu G_2^\mu) \\
& = & -2\left(k_1 \cdot k_2 G_1 \cdot G_2 - k_1 \cdot G_2 k_2 \cdot G_1\right) \\
& = & -2k_1 \cdot k_2 G_{1\mu}G_{2\nu}\left[g^{\mu\nu} - \frac{k_1^\nu k_2^\mu}{k_1 \cdot k_2}\right].
\end{aligned}
\tag{68}
$$

Comparing Equations (60) and (68)[7] suggests that the heavy quark limit for the gluon fusion production of a Higgs boson can be obtained from the effective dimension-5 Lagrangian

$$
L_{EFT} = \frac{\alpha_s}{12\pi}\frac{h}{v}G_{\mu\nu}^A G^{\mu\nu A}.
\tag{69}
$$

The effective Lagrangian of Equation (69) has been used to calculate the QCD corrections to gluon fusion to NLO, NNLO, and N³LO [31]. The result is shown in Figure 7. Note that there is a large correction (approximately a factor of 2) going from LO to NLO. The corrections at each order remain sizable and the dependence on the factorization scale, μ is reduced at higher order.

4.2.2 p_T distribution of Higgs Bosons

At LO, the Higgs boson has no p_T and a transverse momentum spectrum for the Higgs is first generated by the process, $gg \to gh$, which is an NLO contribution to the gluon fusion process [32]. As $p_T \to 0$, the partonic cross section for Higgs plus jet production diverges as $1/p_T^2$,

$$
\begin{aligned}
\frac{d\hat{\sigma}}{dt}(gg \to gh) & = & \hat{\sigma}_0\frac{3\alpha_s}{2\pi}\left\{\frac{1}{p_T^2}\left[\left(1 - \frac{m_h^2}{s}\right)^4 + 1 + \left(\frac{m_h^2}{s}\right)^4\right]\right. \\
& & \left. -\frac{4}{s}\left(1 - \frac{m_h^2}{s}\right)^2 + \frac{2p_T^2}{s}\right\},
\end{aligned}
\tag{70}
$$

where $\hat{\sigma}_0$ is the LO $gg \to h$ cross section given in Equation (62), and s, t and u are the partonic Mandelstam invariants. The p_T spectrum for Higgs plus jet at LO is shown in Figure 8, where the contributions from the gg and $qg, \bar{q}g$ initial states are shown separately. Also shown is the $m_t \to \infty$ limit of the spectrum that is derived from the effective Lagrangian of Equation (69) . The effective Lagrangian approximation fails around $p_T \sim 2m_t$. In this process, there are several distinct momentum scales (p_T, m_h, m_t), as opposed to gluon fusion where there is only a single scale (m_h/m_t) at LO. The

---

[7]The extra factor of $\frac{1}{2}$ comes from the neglected color factor, $Tr(T^A T^B) = \frac{1}{2}\delta_{AB}$.
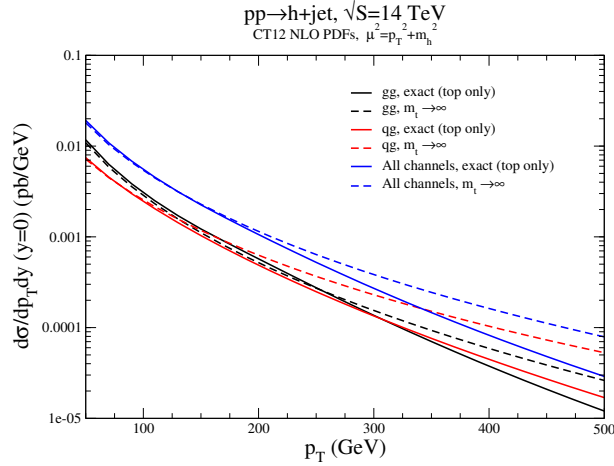
Fig. 8: Lowest order p_T spectrum for Higgs plus jet production from Equation (70) and the large m_t approximation of Equation (69).
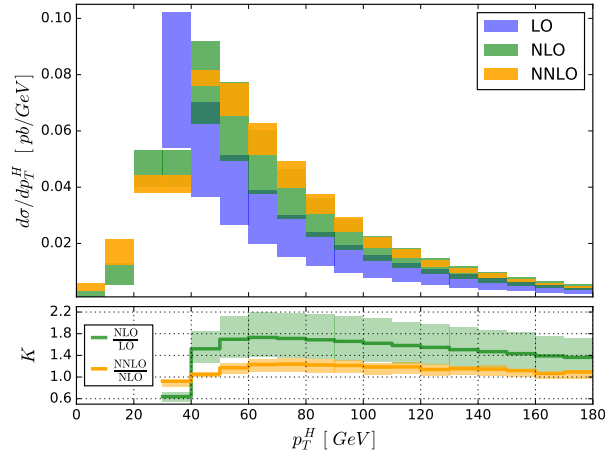

Fig. 9: QCD corrected p_T spectrum for Higgs plus jet production at $\sqrt{S} = 8\,TeV$ [33,34]. In this figure, H is the SM Higgs boson.

expansion in $\frac{m_h}{m_t}$ for $gg \to gh$ receives corrections of $\mathcal{O}(\frac{s}{m_t^2}, \frac{p_T^2}{m_t^2})$ and for $p_T \gtrsim 2m_t$, the EFT large top quark mass expansion cannot be used to obtain reliable distributions.

NLO, NNLO, and N³LO radiative corrections to Higgs plus jet production have been calculated [33–36] using the $m_t \to \infty$ approximation. The lowest order result of Equation (70) is then reweighted by a K factor derived in the $m_t \to \infty$ limit for each kinematic bin. The effects of the higher order corrections are significant and increase the rate by a factor of around 1.8 as shown in Figure 9. The singularity of the LO result at $p_T = 0$ is clearly visible in Figure 9 and we note that after the inclusion of the NLO corrections, the p_T spectrum no longer diverges as $p_T \to 0$.

The terms which are singular as $p_T \to 0$ can be isolated and the integrals performed explicitly. Considering only the gg initial state [37],

$$\frac{d\sigma}{dp_T^2 dy}(pp \to gh) \mid_{p_T^2 \to 0} \sim \hat{\sigma}_0 \frac{3\alpha_s}{2\pi} \frac{1}{p_T^2} \left[6 \log\left(\frac{m_h^2}{p_T^2}\right) - 2\beta_0 \right] g(ze^y)g(ze^{-y}) + ... \qquad (71)$$

where $z \equiv m_h^2/S$, $\beta_0 = (33 - 2n_{lf})/6$, and $n_{lf} = 5$ is the number of light flavors. Clearly when $p_T << m_h$, the terms containing the logarithms resulting from soft gluon emission can give a large
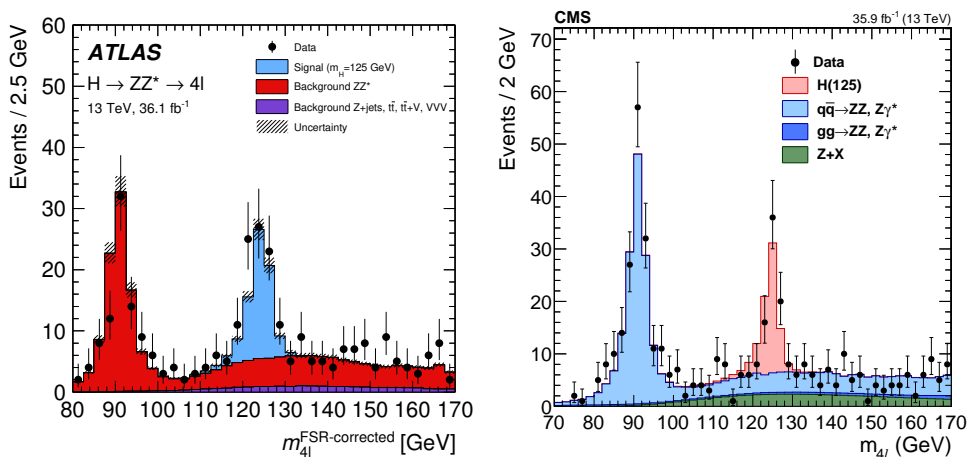
Fig. 10: $h \to ZZ \to 4$ lepton signal at $13 \, TeV$ [40, 41].

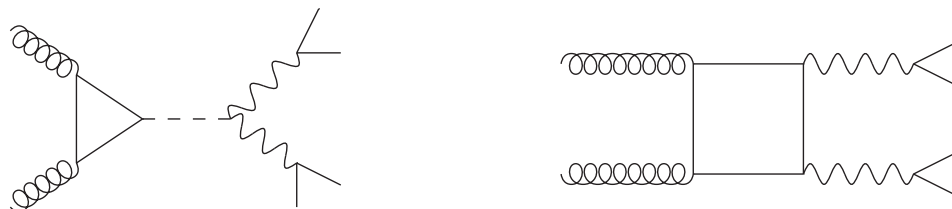**Fig. 11:** Contributions to $gg \to ZZ \to 4l$. The dominant contributions to the triangle and box diagrams are from the top quark.

numerical contribution. The logarithms of the form $\alpha_s^n \log^m(m_h^2/p_T^2)$ can be resummed [37, 38] to improve the theoretical accuracy in the regime $p_T \to 0$ [39].

4.2.3 Measuring the Higgs width with $gg \to h \to ZZ$

Gluon fusion with the subsequent Higgs decay to $ZZ \to 4$ leptons or $\gamma\gamma$ were the Higgs discovery channels. The $h \to ZZ \to 4$ lepton signals at $13 \, TeV$ are shown in Figure 10 [40, 41] and the Higgs resonance is clearly visible. Making a direct measurement of the Higgs width by fitting a Breit-Wigner function to the resonance shape is not possible since the detector resolution is $\mathcal{O}(1-2) \, GeV$, much larger than the Higgs width, $\Gamma_h \sim 4 \, MeV$.

A clever idea uses the properties of the longitudinal Z polarizations [42, 43]. Consider the process $gg \to ZZ \to 4l$ shown in Figure 11. The Higgs contribution is shown on the LHS of Figure 11 and the partonic cross section from the Higgs contribution alone is generically given by,

$$\hat{\sigma}(gg \to h \to ZZ) \sim \int ds \frac{| \, A(gg \to h) \, |^2 | \, A(h \to ZZ) \, |^2}{(s - m_h^2)^2 + \Gamma_h^2 m_h^2} \, . \tag{72}$$

We allow the effective $gg \to h$ and $h \to ZZ \to$ couplings to be scaled from the SM values by arbitrary factors $\kappa_g(s)$ and $\kappa_Z(s)$, where we explicitly note that the κ factors can in principle depend on scale,

$$| \, A(gg \to h) \, |^2 | \, A(h \to ZZ) \, |^2 \sim \kappa_g^2(s)\kappa_Z^2(s) \, | \, \epsilon_{Z1} \cdot \epsilon_{Z2} \, |^2 , \tag{73}$$

where ϵ_{Zi}^μ are the Z polarization vectors.

The interesting observation is that Equation (72) behaves very differently above the Higgs reso-

nance and near the resonance. Above the resonance, $s >> m_h^2$, Equation (72) becomes,

$$\hat{\sigma}(gg \to h \to ZZ)^{above} \sim \int ds \frac{\kappa_g^2(s)\kappa_Z^2(s) \mid \epsilon_{Z1} \cdot \epsilon_{Z2} \mid^2}{s^2} \,. \tag{74}$$

For transverse polarizations, nothing particularly interesting happens, but because of the electroweak symmetry breaking the longitudinally polarized Z bosons have a novel feature. Defining the momenta of the outgoing Z bosons as p_{Z1} and p_{Z2} and remembering that the longitudinal polarization is approximately given by,

$$\epsilon_L^\mu(p_Z) \sim \frac{p_Z^\mu}{M_Z} + \mathcal{O}\left(\frac{M_Z^2}{s}\right), \tag{75}$$

we observe that $\epsilon_L \cdot \epsilon_L \sim \frac{p_{Z1} \cdot p_{Z2}}{M_Z^2} \sim \frac{s}{M_Z^2}$. Equation (74) has the approximate form for $s >> m_h^2$,

$$\hat{\sigma}(gg \to h \to Z_L Z_L)^{above} \sim \int ds \frac{\kappa_g^2(s)\kappa_Z^2(s)}{M_Z^4} \,. \tag{76}$$

We note that Equation (76) exhibits no dependence on the Higgs width.

Near the Higgs resonance, we can use the narrow width approximation, which amounts to the replacement,

$$\frac{1}{(s - m_h^2)^2 + (m_h \Gamma_h)^2} \to \frac{\pi}{m_h \Gamma_h}\delta(s - m_h^2) \tag{77}$$

and Equation (72) is approximately,

$$\hat{\sigma}(gg \to h \to ZZ)^{on} \sim \frac{\kappa_g^2(m_h^2)\kappa_Z^2(m_h^2)}{m_h \Gamma_h} \,. \tag{78}$$

The idea is that by measuring the $gg \to h \to ZZ$ rate above and on the resonance, information can be extracted about the Higgs width. Assuming the κ factors do not depend on scale,

$$\Gamma_h \sim \frac{\hat{\sigma}^{above}}{\hat{\sigma}^{on}} \,. \tag{79}$$

At $8\,TeV$, approximately 15% of the cross section has $m_{4l} > 140\,GeV$, so this is a promising idea. If the κ factors have an energy dependence, they do not cancel in Equation (79) and the interpretation of the measurement becomes more complicated.

Of course, a real calculation needs to include both the diagrams of Figure 11, along with the interference, and this has been done by several groups with results shown in Figure 12. The importance of including the interference terms is apparent, but the long tail at high m_{4l} (shown in red) is clear. ATLAS and CMS have used this technique to place limits on the Higgs width [44, 45],

$$\Gamma_h \lesssim (4 - 5)\Gamma_h^{SM} \,. \tag{80}$$

There are some big assumptions in this extraction of the Higgs width, the most obvious of which is the assumption that the κ factors are the same on and off the Higgs resonance peak. This is clearly a false assumption, since in a quantum field theory all couplings run. If there are anomalous hZZ (or hgg) couplings, than the running could be changed significantly [46, 47]. For example, a contribution to the EFT of the form,

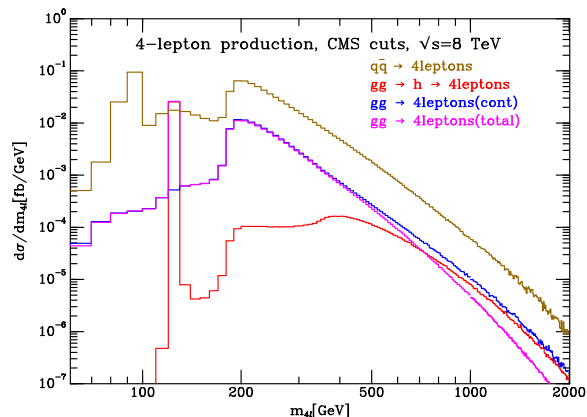$$L \sim \frac{c_Z}{\Lambda^2} \frac{h}{v} Z_{\mu\nu} Z^{\mu\nu} \tag{81}$$

Fig. 12: Contributions to $gg \to ZZ \to 4l$ at $8\,TeV$. The Higgs contributions are shown in red, while the total rate from gluon fusion including interference is given in magenta [49].

would give contributions of $\mathcal{O}\left(\frac{s}{\Lambda^2}\right)$ and would cause m_{4l} to grow above the peak, and would invalidate the extraction of Γ_h. Additional colored particles in the ggh loop would also change the interpretation of the $gg \to ZZ \to 4$ lepton result as a measurement of the Higgs width [48].

It is worth noting that an e^+e^- collider with an energy of $\sqrt{s} = 500\,GeV$ can make a 5% measurement of Γ_h with an integrated luminosity of $500\,GeV$ [50]. First the measurement of $e^+e^- \to Zh$ is made by tagging the Zh events where the recoil mass is consistent with a Higgs boson. This is done using conservation of momenta and determines $\sigma(Zh)$. Next we can measure the $h \to ZZ$ rate to determine $BR(h \to ZZ)$. The Higgs width is then determined in a model independent fashion,

$$
\begin{aligned}
\Gamma_h &= \Gamma(h \to ZZ)BR(h \to ZZ) \\
&\sim \frac{\sigma(Zh)}{BR(h \to ZZ)}.
\end{aligned}
\tag{82}
$$

4.2.4 Vector Boson Scattering

The vector boson scattering (VBS) process is shown on the RHS of Figure 4. It can be thought of as 2 incoming quarks each radiating a W or Z boson, which then form a Higgs. Vector boson fusion also offers the opportunity to observe the $2 \to 2$ scattering process, $VV \to VV$, $(V = Z, W)$, which is extremely sensitive to new physics in the electroweak sector. The $VV \to VV$ sub-process plays a special role in Higgs physics since the Higgs exchange contributions unitarize the scattering amplitude.

VBS production of a Higgs occurs through the purely electroweak process $q\bar{q}' \to q\bar{q}'h$ which has a distinctive experimental signature and vanishes in the limit $v = 0$. The outgoing jets are peaked in the forward and backward regions and can be used to tag the VBF event. This can easily be seen by considering the top leg of the RHS of Figure 4:

$$
q(p) \to q'(p')V(k).
\tag{83}
$$

In the lab frame,

$$
\begin{aligned}
p &\equiv E(1, 0, 0, 1) \\
p' &\equiv E'(1, 0, \sin\theta, \cos\theta).
\end{aligned}
\tag{84}
$$

The integral over the final state phase space for the VBS scattering cross section has a generic contribution,

$$
\sigma \sim \int \frac{(\text{Phase Space})}{[(p - p'^2)^2 - M_V^2]^2} \sim \int \frac{\theta d\theta}{[2EE'(1 - \cos\theta) - M_V^2]^2} \sim \int \frac{\theta d\theta}{[\theta^2 - M_V^2/EE']^2}
\tag{85}
$$

which is enhanced in the $\theta \to 0$ region for $E, E' >> M_V^2$. In addition, these forward tagging jets have a large invariant mass and small p_T. Typical cuts on the jets are,

$$p_{T_j} > 20 \, GeV, \; | \, y_j \, | < 5 \, , | \, y_{j_1} - y_{j_2} \, | > 3 \, , M_{jj} > 130 \, GeV \, . \tag{86}$$

The decay products from the intermediate VV scattering are mostly contained in the central rapidity region. These characteristics can be used to separate VBS scattering from QCD gluon initiated events and the non-VBS contributions can be suppressed to $\sim 1 - 2\%$ [51]. The ability to separate the Higgs signal into gluon initiated events and VBF events is crucial for the extraction of Higgs coupling constants.

4.2.5 *Associated Production*

At the LHC the process $q\bar{q} \to Vh$ offers the hope of being able to tag the Higgs boson by the V boson decay products [52], although as shown in Figure 6 the rate is significantly smaller than the dominant $gg \to h$ production mechanism. The cross section for Wh production is,

$$\hat{\sigma}(q_i\bar{q}_j \to W^\pm h) = \frac{G_F^2 M_W^6 \mid V_{ij} \mid^2}{6\pi s^2 (1 - M_W^2/s)^2} \lambda_{Wh}^{1/2} \left[1 + \frac{s\lambda_{Wh}}{12M_W^2} \right] \quad , \tag{87}$$

where $\lambda_{Wh} = 1 - 2(M_W^2 + m_h^2)/s + (M_W^2 - m_h^2)^2/s^2$ and V_{ij} is the CKM angle associated with the $q_i\bar{q}_jW$ vertex. The rate for Zh is about a factor of 3 smaller than that for Wh and analytic results can be found in Ref. [4]. The NNLO QCD and NLO electroweak corrections are known, so there is relatively little uncertainty on the prediction [53, 54].

The Vh associated channel has recently been used to observe the decay $h \to b\bar{b}$ [55, 56], using the jet substructure techniques first proposed in Ref. [57]. The idea is that by going to high transverse momentum for the Higgs, the backgrounds can be significantly reduced. Jet substructure techniques are discussed in the lectures of Schwartz at this school [58].

4.2.6 *$t\bar{t}h$ Production*

The top quark Yukawa coupling, Y_t, can be directly measured in the $t\bar{t}h$ process shown on the RHS of Figure 5. Recall that the gluon fusion production of the Higgs is also proportional to the top quark Yukawa, but in addition it can receive enhanced contributions from the bottom quark Yukawa interactions in some BSM scenarios, along with contributions from new colored scalars. The NLO QCD [59–62] and electroweak corrections [63, 64] for $t\bar{t}h$ production are known and contribute to very precise predictions [30]:

$$\sqrt{S} = 8 \, TeV \qquad \sigma_{tth} = .133 \, pb^{+4\%}_{-9\%}(scale) \pm 4.3\%(PDF + \alpha_s)$$
$$\sqrt{S} = 13 \, TeV \qquad \sigma_{tth} = .507 \, pb^{+5.8\%}(scale)_{-9.2\%} \pm 3.6\%(PDF + \alpha_s) \, . \tag{88}$$

Although numerically small, electroweak corrections spoil the direct proportionality of the lowest order cross section to Y_t^2.

This process has large backgrounds from $t\bar{t}b\bar{b}$ and $t\bar{t}jj$. In order to suppress the backgrounds, many $t\bar{t}h$ searches are done in the boosted regime, where the electroweak Sudakov logarithms become relevant. A definitive measurement of this channel has not yet been made, and will be one of the important milestones of the coming LHC run.

The associated production of $b\bar{b}h$ is not relevant in the SM, but can be important in models with enhanced b Yukawa couplings.
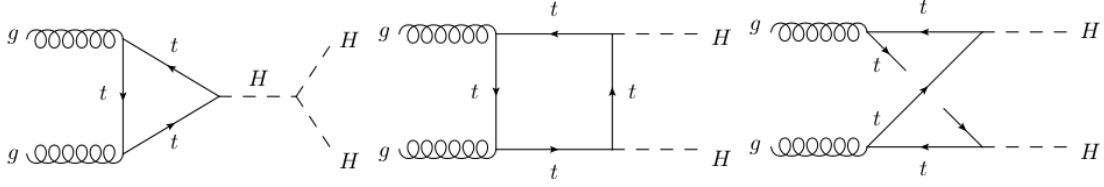
Fig. 13: Contributions to $gg \rightarrow hh$ in the SM. The dominant contribution to the triangle and box diagrams are from the top quark. In this figure, H is the SM Higgs boson.

4.2.7 Double Higgs Production

Finally, we need to measure the parameters of the Higgs potential, Equation (30), to determine if electroweak symmetry breaking really proceeds as in the SM. In the SM, the Higgs potential is,

$$V = \frac{m_h^2}{2}h^2 + \lambda_3 h^3 + \lambda_4 h^4 \,, \tag{89}$$

where $\lambda_3^{SM} = m_h^2/(2v)$ and $\lambda_4^{SM} = h^2/(8v^2)$. It is apparent that the Higgs self- couplings are weak,

$$\lambda_3^{SM} = .13v, \qquad \lambda_4^{SM} = .03 \,. \tag{90}$$

The only way to directly probe the h^3 coupling is by double Higgs production and the dominant production mechanism is gluon fusion as shown in Figure 16. The result is sensitive to new colored particles running in the loops, along with modifications to the Higgs tri-linear self-coupling and the top quark Yukawa coupling (Equations (89) and (26)).

The large m_t limit has been used to compute QCD corrections to NLO [65] and NNLO [66]. In this approach, a K factor is computed:

$$K \equiv \frac{d\sigma_{NNLO}}{d\sigma_{LO}} \,, \tag{91}$$

where the distributions in Equation (91) are computed in the $m_t \rightarrow \infty$ limit and are then used to rescale the lowest order distributions computed with finite m_t[8] [67–70]. The exact NLO result for double Higgs production including all top mass effects is now known and can be used to obtain distributions [71, 72]. The effects of including the top quark mass exactly at NLO are significant and reduce the total cross section by $\sim 14\%$ at $14\,TeV$ from the B.i. NLO HEFT limit. Including the top quark mass effects also has significant effects on distributions, as demonstrated in Figure 15.

The dependence of hh production on λ_3 from various production mechanisms is shown in Figure 16 [73] as a function of $\delta_3 \equiv \frac{\lambda_3}{\lambda_3^{SM}}$. [9]

The best current limits from the $8\,TeV$ data on double Higgs production are,

$$\frac{\sigma(pp \rightarrow hh)}{\sigma(pp \rightarrow hh) \mid_{SM}} < 29 \qquad \text{ATLAS}\,,$$
$$\frac{\sigma(pp \rightarrow hh)}{\sigma(pp \rightarrow hh) \mid_{SM}} < 19 \qquad \text{CMS}\,, \tag{92}$$

which still leaves a way to go before we get to an interesting regime. The ATLAS limit is from the $b\bar{b}b\bar{b}$ final state [74], while the CMS limit is from the $b\bar{b}\gamma\gamma$ final state [75]. ATLAS estimates that a luminosity of $3\,ab^{-1}$ will be sensitive to $\delta_3 > 8.7$ and $\delta_3 < -1.3$ [76]. This is clearly not the precision measurement we desire and the need to measure the Higgs tri-linear coupling is one of the major motivations for a $100\,TeV$ collider.

---

[8]This is termed the B.i. NLO HEFT in Figure 15.

[9]The curve labelled EFT loop-improved is identical to the B.i. NLO HEFT approximation.
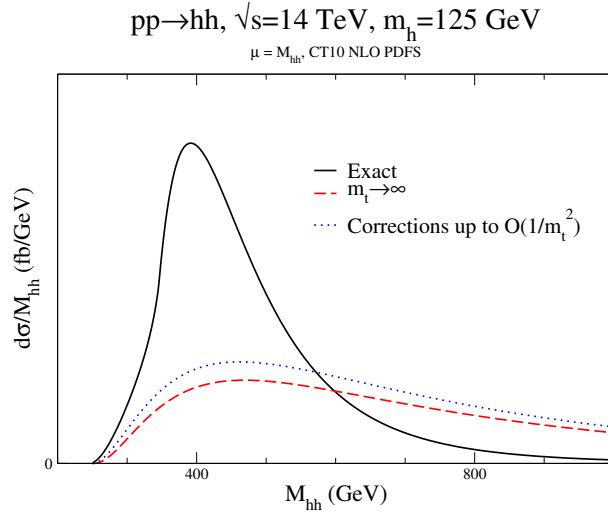
Fig. 14: LO transverse momentum distribution for double Higgs production in the SM, compared with the large m_t limit, along with the first correction of $\mathcal{O}(s/m_t^2)$.
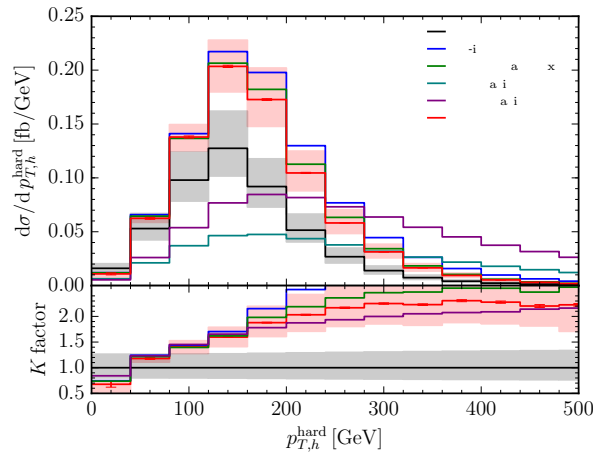

Fig. 15: Transverse momentum distribution for double Higgs production in the SM, including various approximations for the QCD corrections. The curve labelled NLO includes all finite m_t effects [72].
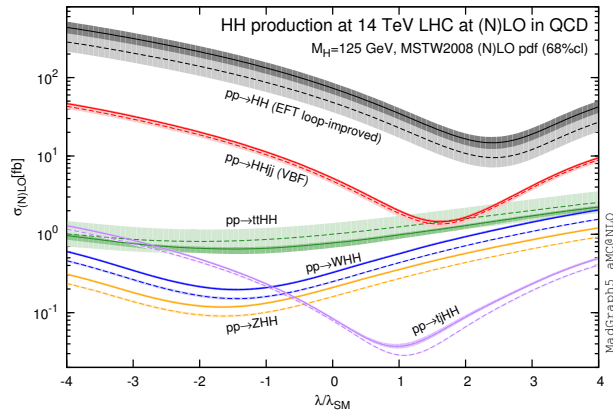

Fig. 16: Dependence of double Higgs production rates on the Higgs tri-linear self-coupling [73].
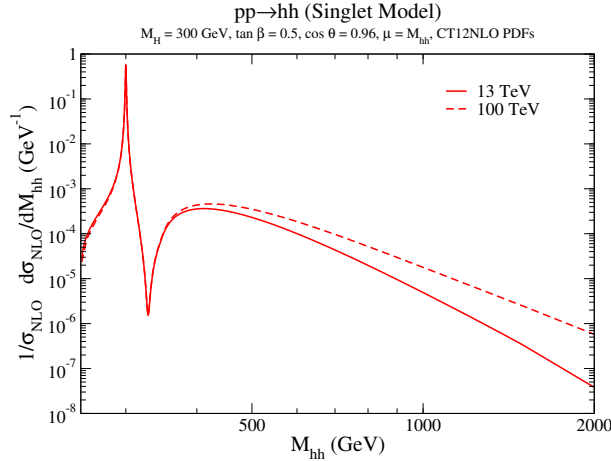
Fig. 17: Double Higgs production in the Z_2 symmetric singlet model with a heavy neutral scalar of mass $M_H = 300\,GeV$ [77].
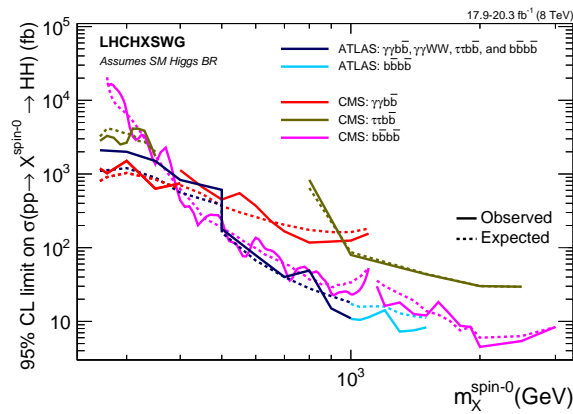

Fig. 18: Experimental limits from the LHC on hh production in a BSM theory containing an $s-$ channel scalar resonance with mass M_X [30].

The fact that the SM rate for double Higgs production is quite small makes it an ideal place to search for new physics. Many models (singlet, 2HDM, MSSM, NMSSM, etc) [77–81] contain heavy neutral scalars that can decay into 2 SM Higgs bosons with a significant ($\sim 30\%$) branching ratio. In these models, there is an $s-$ channel resonance from the heavy Higgs particle, and there will be interference between this new scalar and the SM Higgs giving the classic dip structure shown in Figure 17 for the example of the singlet model. Limits on resonant decays in the generic BSM process, $gg \rightarrow X \rightarrow hh$ for various final states are shown in Figure 18, where for heavy resonances, the most important search channel is the $4b$ final state.

It has been proposed that indirect limits on λ_3 may be extracted from the dependence of electroweak radiative corrections to single Higgs production on the Higgs tri-linear coupling. This coupling enters the rate for $gg \rightarrow h$ at $2-$ loops and contributes to the $t\bar{t}h$, Vh, and VBS processes at $1-$ loop. Of course λ_3 is not a free parameter in the SM, and some care must be taken with the renormalization prescription. Ref. [82] obtains the allowed 2σ region from a fit to single Higgs production,

$$-9.4 < \delta_3 < 16\,. \tag{93}$$

Similar allowed regions are obtained in Refs. [83–85]. The allowed parameter space from current fits to single Higgs production are not significantly different from the expected limits on λ_3 with $3\,ab^{-1}$ at the LHC.

5 Effective Field Theory and the Higgs Boson

5.1 Higgs Boson Coupling measurements

The production of the Higgs boson in Run-I at the LHC produced results which basically agree with the SM predictions at the $10 - 20\%$ level [86]. Preliminary Higgs coupling results at $13\ TeV$ [56, 87–91], are also in reasonable agreement with expectations. The rates are as predicted, and there are no non-SM like light (EW scale) particles observed.

What we need is a way to quantify small deviations from the SM predictions. The simplest way is to introduce an arbitrary scaling into the SM interactions,

$$L_\kappa = \Sigma_f \kappa_f \frac{m_f}{v} \overline{f} f h + \kappa_W g M_W W^{+\mu} W^-_\mu h + \kappa_Z g \frac{M_Z}{c_W} Z^\mu Z_\mu h. \tag{94}$$

In the SM, all κ parameters are 1, so a deviation would indicate some physics not contained in the SM. Of course, Equation (94) is not $SU(2)_L \times U(1)_Y$ gauge invariant, but it serves as a starting point for study.

For a given production and decay channel, $i \to h \to j$,

$$\kappa_i^2 = \frac{\sigma(i \to h)}{\sigma(i \to h)_{SM}}$$

$$\kappa_j^2 = \frac{\Gamma(h \to j)}{\Gamma(h \to j)_{SM}}. \tag{95}$$

The κ formalism also rescales the total width,

$$\kappa_h \equiv \frac{\Gamma_h}{\Gamma_h^{SM}}$$

$$\Gamma_h = \Sigma_X \kappa_X^2 \Gamma(h \to XX) + \Gamma(h \to \text{invisible}), \tag{96}$$

where $\Gamma(h \to \text{invisible})$ is any unobserved decay. This approach assumes that there are no new light resonances, no new tensor structures in the Higgs interactions beyond those of the SM, that the narrow width approximation for Higgs decays is valid, and is based on rescaling total rates (that is, no new dynamics is included).

A combined CMS/ATLAS fit is shown in Figure 19. This particular fit does not allow for new physics in the $gg \to h$ and $h \to \gamma\gamma$ channels, but instead parameterizes the effective couplings in terms of the SM interactions of the Higgs with the top and bottom (κ_g) and with the W and top (κ_γ) as,

$$\kappa_g^2 \sim 1.06\kappa_t^2 + .01\kappa_b^2 - .07\kappa_t\kappa_b$$

$$\kappa_\gamma^2 \sim 1.59\kappa_W^2 + .07\kappa_t^2 - .66\kappa_W\kappa_t. \tag{97}$$

Similar results are shown in Figure 20, and again the results are in general agreement with the SM predictions. With the addition of $13\ TeV$ data, the Higgs couplings should become even more constrained. In particular, the tth and bbh coupling measurements have been significantly updated from Figure 20.

ATLAS and CMS have various types of fits. In some fits, they separate Higgs bosons from different production and decay channels. Other fits allow for unobserved decay channels, or new contributions to gluon fusion or the decay to $\gamma\gamma$. None of the fits show any significant deviation from the SM predictions.

Finally, a fit to all Higgs production and decay channels yields the combined ATLAS/CMS result [86],

$$\mu \equiv \frac{\sigma_h}{\sigma_h(SM)} = 1.0 \pm 0.07(stat) \pm 0.04(syst) \pm 0.03(theory). \tag{98}$$

From Equation (98), it is clear that the accuracy of the theoretical predictions will soon be the limiting factor in the interpretation of Higgs measurements.

To improve on the fits to total rates, we need to construct an effective field theory, which is the topic of the next section.
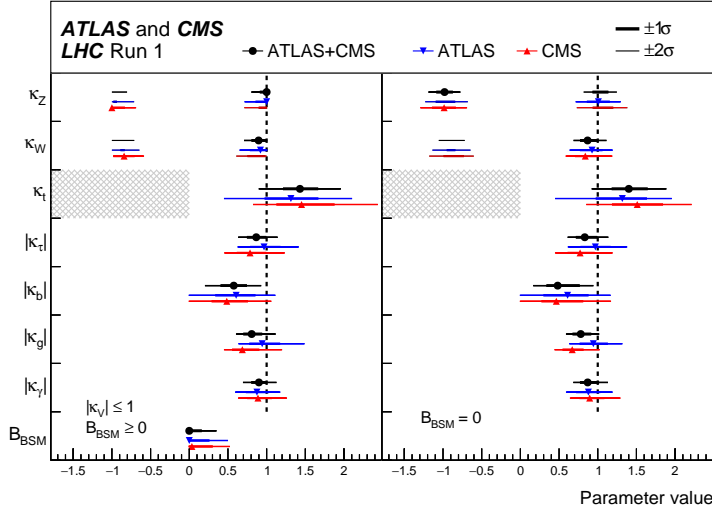
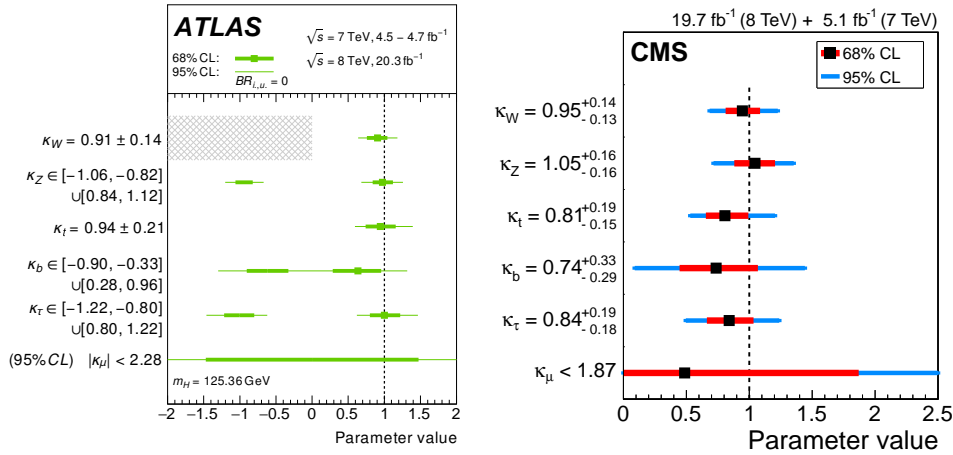**Fig. 19:** Combined ATLAS/CMS κ fits to Run-1 data [86].

Fig. 20: ATLAS κ fits to Run-1 data [92] (LHS) and CMS κ fits to Run-1 data [93] (RHS) .

5.2 Effective Field Theory Basics

The effective field theory (EFT) Lagrangian we use assumes that there are no new light degrees of freedom and is constructed by writing an $SU(2)_L \times U(1)_Y$ invariant Lagrangian as an expansion in powers of v/Λ, where Λ is some high scale where we envision that there is a UV complete theory [94, 103],

$$L_{EFT} = L_{SM} + \Sigma_i \frac{c_i^5}{\Lambda} O_i^5 + \Sigma_i \frac{c_i^6}{\Lambda^2} O_i^6 + \ldots \tag{99}$$

and O_i^n is a dimension-n operator constructed from SM fields. The EFT allows for a systematic study of BSM physics effects in a gauge invariant fashion and radiative corrections can be implemented order by order in $\frac{v}{\Lambda}$.

The only possible dimension-5 operator violates lepton number conservation and is typically neglected in studies of Higgs physics. There are many possible bases for constructing the dimension-6 operators, of which the most well-known are the Warsaw [95], HISZ [96], and SILH [97] bases. By using the equations of motion, there is a mapping from one basis to the next [98, 99]. Note that the HISZ basis does not contain fermion interactions.

There are several approaches to using the dimension-6 truncation of the EFT of Equation (99). One could calculate an amplitude to $\mathcal{O}\left(\frac{v^2}{\Lambda^2}\right)$,

$$A \sim A_{SM} + \frac{A^6_{EFT}}{\Lambda^2} \, . \tag{100}$$

Squaring the amplitude,

$$\mid A \mid^2 \sim \mid A_{SM} + \frac{A^6_{EFT}}{\Lambda^2} \mid^2 \, , \tag{101}$$

we obtain results that are guaranteed to be positive-definite. The problem is that Equation (101) contains terms $\sim \frac{(A^6_{EFT})^2}{\Lambda^4}$ that are of the same order in v^2/Λ^2 as the neglected dimension-8 terms. The expansion only makes sense if

$$\mid A^6_{EFT} \mid^2 << \mid A^*_{SM} A^8_{EFT} \mid \, , \tag{102}$$

which can be arranged in some BSM models [100] .

We begin by considering a simple EFT with just 2 non-SM terms,

$$L \sim L_{SM} + \frac{\alpha_s}{4\pi} \frac{c_g}{\Lambda^2} (\Phi^\dagger \Phi) G^A_{\mu\nu} G^{\mu\nu A} + \left(\frac{c_t Y_t}{\Lambda^2} \bar{q}_L \tilde{\Phi} q_R (\Phi^\dagger \Phi) + h.c. \right) \, . \tag{103}$$

After spontaneous symmetry breaking, the top mass is shifted,

$$m_t = \frac{Y_t v}{\sqrt{2}} \left(1 - \frac{v^2 c_t}{2\Lambda^2} \right) \, . \tag{104}$$

The Higgs coupling to the top quark is no longer proportional to m_t and Equation (103) becomes

$$L \rightarrow \frac{\alpha_s}{4\pi} \frac{c_g}{\Lambda^2} h G^A_{\mu\nu} G^{\mu\nu A} - m_t t\bar{t} \left[1 + \frac{h}{v} \left(1 - \frac{v^2 c_t}{\Lambda^2} \right) \right] + ... \tag{105}$$

When flavor indices are included in the fermion interactions, Equation (103) can generate flavor violation in the Higgs sector [101].

Both c_g and c_t contribute to $gg \rightarrow h$,[10]

$$\sigma(gg \rightarrow h) = \sigma(gg \rightarrow h)_{SM} \left(1 + 2 \frac{v^2}{\Lambda^2} (3c_g - c_t) \right) + \mathcal{O}\left(\frac{m^2_h}{m^2_t}, \frac{v^4}{\Lambda^2} \right) \, , \tag{106}$$

and so gluon fusion cannot distinguish between c_g and c_t [102–107]. The $t\bar{t}h$ process is independent of c_g at leading order and can be used to obtain a measurement of c_t. Once radiative corrections (both QCD and electroweak) are included, however, the situation becomes murkier and the $t\bar{t}h$ rate is no longer directly proportional to c_t.

We turn now to a discussion of the effects of dimension-6 operators in the electroweak sector. As an example, we consider the SILH basis relevant for gauge-Higgs interactions [97],

$$
\begin{aligned}
L_{SILH} &= \frac{c_H}{2\Lambda^2} \left(\partial^\mu \mid \Phi \mid^2 \right)^2 + \frac{c_T}{2\Lambda^2} \left(\Phi^\dagger \overleftrightarrow{D}^\mu \Phi \right)^2 + \left(\frac{c_f y_f}{\Lambda^2} \mid \Phi \mid^2 \bar{f}_L \Phi f_R + hc \right) - \frac{c_6 \lambda}{\Lambda^2} \mid \phi \mid^6 \\
&+ \frac{igc_W}{2\Lambda^2} \left(\Phi^\dagger \sigma^I \overleftrightarrow{D}^\mu \Phi \right) \left(D^\nu W^I_{\mu\nu} \right) + \frac{ig' c_B}{2\Lambda^2} \left(\Phi^\dagger \overleftrightarrow{D}^\mu \Phi \right) \left(D^\nu B_{\mu\nu} \right)
\end{aligned}
$$

---

[10]*Caveat emptor*: Practically every EFT paper uses different normalization and sign conventions for the EFT operators. The only way to check results like Equation (106) is to start from the definition of the operators in the Lagrangian.

$$+\frac{igc_{HW}}{16\pi^2\Lambda^2}\left(D^\mu\Phi\right)^\dagger\sigma^i\left(D^\nu\Phi\right)W^i_{\mu\nu}+\frac{ig'c_{HB}}{16\pi^2\Lambda^2}\left(D^\mu\Phi\right)^\dagger\left(D^\nu\Phi\right)B_{\mu\nu}$$

$$+\frac{c_\gamma g'^2g^2}{16\pi^2\Lambda^2}\mid\Phi\mid^2 B_{\mu\nu}B^{\mu\nu}+\frac{c_g g_s^2}{16\pi^2\Lambda^2}\mid\Phi\mid^2 G^A_{\mu\nu}G^{A,\mu\nu}\,. \tag{107}$$

Note that the normalization of the operators is arbitrary and merely reflects a prejudice about the origins of the new physics, $I=1,2,3$ are $SU(2)$ indices and we have not written terms involving only fermions, or terms that do not contain a Higgs field. Many of the operators of Equation (107) introduce momentum dependence into the Higgs couplings to SM fermions and so the kinematic distributions of the Higgs will be affected.

We briefly discuss some of the phenomenological effects of Equation (107). Three of the co-efficients are strongly limited by precision electroweak measurements as parameterized by the oblique parameters,

$$\begin{aligned}\Delta T &= \frac{v^2}{\Lambda^2}c_T\\ \Delta S &= \frac{M_W^2}{\Lambda^2}(c_W+c_B)\,.\end{aligned} \tag{108}$$

Using the fit from Ref. [15], $\mid c_T\mid\;\lesssim\mathcal{O}(.03)$ and $\mid c_W+c_W\mid\;\lesssim\mathcal{O}(.1)$ for $\Lambda\sim 1\,TeV$.

The coefficient c_H modifies the Higgs boson kinetic energy. The physical Higgs field needs to be rescaled,

$$h\to h\left(1-\frac{c_Hv^2}{2\Lambda^2}\right), \tag{109}$$

in order to have canonically normalized kinetic energy. This shift introduces a dependence on c_H into all of the Higgs decay widths. The tree level Higgs decay widths to $\mathcal{O}(\frac{v^2}{\Lambda^2})$ in the SILH formalism are,

$$\begin{aligned}\frac{\Gamma(h\to WW*)}{\Gamma(h\to WW^*)\mid_{SM}} &= 1-\frac{v^2}{\Lambda^2}\left[c_H-g^2\left(c_W+\frac{c_{HW}}{16\pi^2}\right)\right]\\ \frac{\Gamma(h\to ZZ*)}{\Gamma(h\to ZZ^*)\mid_{SM}} &= 1-\frac{v^2}{\Lambda^2}\left[c_H-g^2\left(c_W+\tan^2\theta_Wc_B+\frac{c_{HW}+\tan^2\theta_2c_{HB}}{16\pi^2}\right)\right]\\ \frac{\Gamma(h\to f\overline{f})}{\Gamma(h\to f\overline{f})\mid_{SM}} &= 1-\frac{v^2}{\Lambda^2}(c_H+2c_f)\,.\end{aligned} \tag{110}$$

The loop processes, $gg\to h$ and $h\to\gamma\gamma$, also receive corrections from the EFT operators. The expressions for Higgs decays in the SILH Lagrangian have been implemented into an update of the HDECAY program, EDECAY [108]. In the Warsaw basis, they can be obtained using the SMEFTsim code [109]. Fits to the EFT coefficients can be performed using total Higgs rates (as is done in the κ formalism) or including information from distributions [83, 110]. The kinematic information provides a significant improvement to the fits from using only the total rates.

Some of the operators of Equation (107) not only affect Higgs production, but they also change the WWZ and $WW\gamma$ vertices. Assuming CP conservation, the most general Lorentz invariant $3-$gauge boson couplings can be written as [111, 112]

$$\begin{aligned}L_V &= -ig_{WWV}\left[g_1^V\left(W^+_{\mu\nu}W^{-\mu}V^\nu-W^-_{\mu\nu}W^{+\mu}V^\nu\right)+\kappa^VW^+_\mu W^-_\nu V^{\mu\nu}\right.\\ &\left.+\frac{\lambda^V}{M_W^2}W^+_{\rho\mu}W^{-\mu}_{\ \ \nu}V^{\nu\rho}\right],\end{aligned} \tag{111}$$

where $V = (Z, \gamma)$, $g_{WW\gamma} = e$, and $g_{WWZ} = gc_W$. In the SM, $g_1^Z = g_1^\gamma = \kappa^Z = \kappa^\gamma = 1$, $\lambda^Z = \lambda^\gamma = 0$ and $SU(2)$ gauge invariance implies,

$$
\begin{aligned}
\lambda^\gamma &= \lambda^Z \\
g_1^Z &= \kappa^Z + \frac{s_W^2}{c_W^2}(\kappa^\gamma - 1).
\end{aligned}
\tag{112}
$$

The fields in Equation (111) are the canonically normalized mass eigenstate fields. These coefficients can be mapped to EFT coefficients in a straightforward manner and a subset of the dimension-6 coefficients contribute both to gauge boson pair production and Higgs production [110, 113, 114].

A consistent fit must include not only Higgs data, but also fits to anomalous gauge couplings. In Figure 21, we show fits to 3 of the EFT couplings that contribute to both W^+W^- and Higgs production, including only LEP data on W^+W^- pair production, only LHC data on W^+W^- and Higgs production, and the resulting fit combining the two. The LHC results have now surpassed the LEP results in terms of precision [110]. This figure includes the full set of dimension-6 squared contributions. In terms of the parameters of Equation (111),

$$
\begin{aligned}
f_W &= \frac{2\Lambda^2}{M_Z^2}(g_1^Z - 1) \\
f_B &= \frac{2\Lambda^2}{M_W^2}\left[(\kappa_\gamma - 1) - c_W^2(g_1^Z - 1)\right] \\
f_{WWW} &= \frac{4\Lambda^2}{3g^2 M_W^2}\lambda^\gamma.
\end{aligned}
\tag{113}
$$

Global fits to EFT coefficients in the SILH basis can be found in Ref. [83, 115] and in the Warsaw basis in Ref. [113]. Many of the EFT coefficients are only weakly constrained. These results illustrate, however, that fits performed to only a single operator typically significantly overestimate the sensitivity. As of this writing, the experimental collaborations have not performed such global EFT fits.

Finally, it is interesting to ask what the target precision is for measuring EFT coefficients. In any given UV complete model, these coefficients can be calculated, and the scale Λ will be of the same order of magnitude as the mass of the new particles. This suggests that as direct searches for new particles get more and more precise, it is necessary to measure the EFT coefficients more and more precisely. In a specific UV complete model, not all coefficients will be generated, and the pattern of non-zero coefficients will be a guide to the underlying model. The EFT coefficients for numerous models with heavy scalars [116–120] and heavy vector-like quarks [121, 122] are known and suggest that measurements of $\mathcal{O}(2-3\%)$ will be necessary to probe models with new particles at the $2-3\,TeV$ scale.

6 Outlook

The discovery of a SM-like Higgs boson opened a new era in particle physics. We do not yet know if we have discovered **a** Higgs boson or **the** Higgs boson. To make this determination, the measurements of Higgs interactions need to be improved to the few % level and the Higgs self-interactions need to be observed. These precision measurements will begin during the high luminosity run of the LHC, but will require a future high energy hadron collider or e^+e^- collider to reach the desired accuracy. A limiting factor will be the precision of theoretical predictions–predictions accurate at the few % level will require a dedicated effort in the coming years and improvement of our knowledge of PDFs. I have not discussed models with extra scalar particles other than the singlet model. One of the most important efforts of the Higgs program in the next few years will be the search for additional Higgs-like particles. The observation of another scalar would be the cleanest possible indication of new BSM physics in the scalar sector.
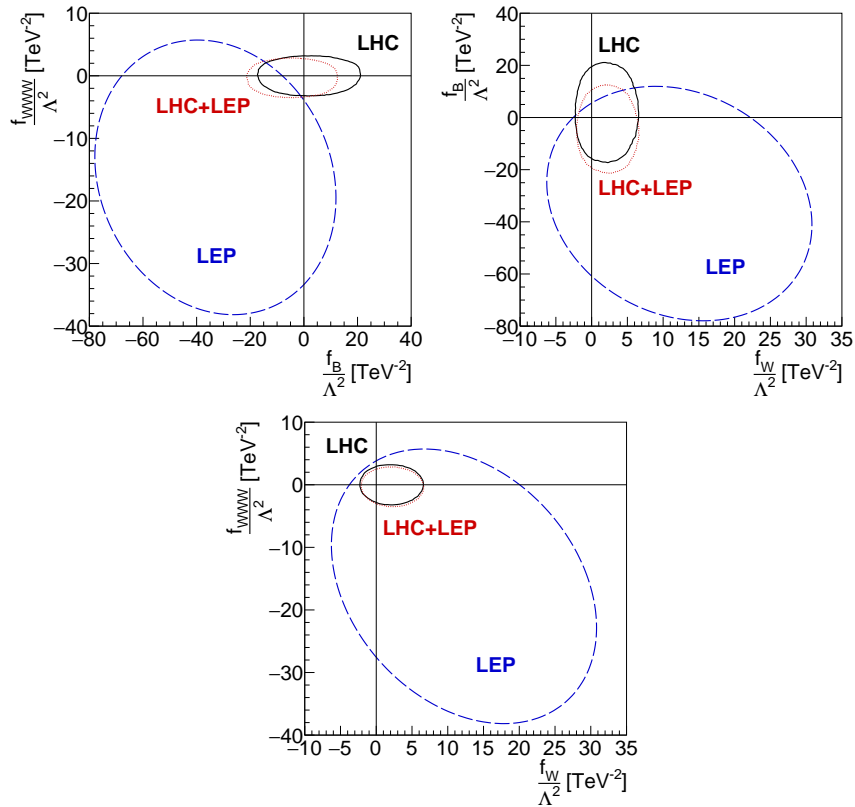
Fig. 21: Fits to LEP data, LHC data and the combination of both [110].

Acknowledgements

References

[1] Georges Aad et al. Observation of a new particle in the search for the Standard Model Higgs boson with the ATLAS detector at the LHC. *Phys. Lett.*, B716:1–29, 2012.

[2] Serguei Chatrchyan et al. Observation of a new boson at a mass of 125 GeV with the CMS experiment at the LHC. *Phys. Lett.*, B716:30–61, 2012.

[3] S. Dawson. Introduction to electroweak symmetry breaking. In *Proceedings, Summer School in High-energy physics and cosmology: Trieste, Italy, June 29-July 17, 1998*, pages 1–83, 1998.

[4] Abdelhak Djouadi. The Anatomy of electro-weak symmetry breaking. I: The Higgs boson in the standard model. *Phys. Rept.*, 457:1–216, 2008.

[5] John F. Gunion, Howard E. Haber, Gordon L. Kane, and Sally Dawson. The Higgs Hunter's Guide. *Front. Phys.*, 80:1–404, 2000.

[6] Heather E. Logan. TASI 2013 lectures on Higgs physics within and beyond the Standard Model. 2014.

[7] Laura Reina. TASI 2011: lectures on Higgs-Boson Physics. In *The Dark Secrets of the Terascale: Proceedings, TASI 2011, Boulder, Colorado, USA, Jun 6 - Jul 11, 2011*, pages 39–106, 2013.

[8] Michael Spira. Higgs Boson Production and Decay at Hadron Colliders. *Prog. Part. Nucl. Phys.*, 95:98–159, 2017.

[9] Chris Quigg. *Gauge Theories of the Strong, Weak, and Electromagnetic Interactions*. Princeton University Press, USA, 2013.

[10] Andre de Gouvea. TASI lectures on neutrino physics. In *Physics in D >= 4. Proceedings, Theoretical Advanced Study Institute in elementary particle physics, TASI 2004, Boulder, USA, June 6-July 2, 2004*, pages 197–258, 2004.

[11] C. Patrignani et al. Review of Particle Physics. *Chin. Phys.*, C40(10):100001, 2016.

[12] Georges Aad et al. Combined Measurement of the Higgs Boson Mass in pp Collisions at $\sqrt{s} = 7$ and 8 TeV with the ATLAS and CMS Experiments. *Phys. Rev. Lett.*, 114:191803, 2015.

[13] James D. Wells. TASI lecture notes: Introduction to precision electroweak analysis. In *Physics in D $\gtrsim$ 4. Proceedings, Theoretical Advanced Study Institute in elementary particle physics, TASI 2004, Boulder, USA, June 6-July 2, 2004*, pages 41–64, 2005.

[14] William J. Marciano and A. Sirlin. Testing the Standard Model by Precise Determinations of W+- and Z Masses. *Phys. Rev.*, D29:945, 1984. [Erratum: Phys. Rev.D31,213(1985)].

[15] Jorge de Blas, Marco Ciuchini, Enrico Franco, Satoshi Mishima, Maurizio Pierini, Laura Reina, and Luca Silvestrini. Electroweak precision observables and Higgs-boson signal strengths in the Standard Model and beyond: present and future. *JHEP*, 12:135, 2016.

[16] M. Baak, M. Goebel, J. Haller, A. Hoecker, D. Kennedy, R. Kogler, K. Moenig, M. Schott, and J. Stelzer. The Electroweak Fit of the Standard Model after the Discovery of a New Boson at the LHC. *Eur. Phys. J.*, C72:2205, 2012.

[17] Michael E. Peskin and Tatsu Takeuchi. Estimation of oblique electroweak corrections. *Phys. Rev.*, D46:381–409, 1992.

[18] Guido Altarelli and Riccardo Barbieri. Vacuum polarization effects of new physics on electroweak processes. *Phys. Lett.*, B253:161–167, 1991.

[19] Donal O'Connell, Michael J. Ramsey-Musolf, and Mark B. Wise. Minimal Extension of the Standard Model Scalar Sector. *Phys. Rev.*, D75:037701, 2007.

[20] Giovanni Marco Pruna and Tania Robens. Higgs singlet extension parameter space in the light of the LHC discovery. *Phys. Rev.*, D88(11):115012, 2013.

[21] Dario Buttazzo, Giuseppe Degrassi, Pier Paolo Giardino, Gian F. Giudice, Filippo Sala, Alberto Salvio, and Alessandro Strumia. Investigating the near-criticality of the Higgs boson. *JHEP*, 12:089, 2013.

[22] S. Dittmaier et al. Handbook of LHC Higgs Cross Sections: 1. Inclusive Observables. 2011.

[23] A. Djouadi, J. Kalinowski, and M. Spira. HDECAY: A Program for Higgs boson decays in the standard model and its supersymmetric extension. *Comput. Phys. Commun.*, 108:56–74, 1998.

[24] Manuel Drees and Ken-ichi Hikasa. Note on QCD corrections to hadronic Higgs decay. *Phys. Lett.*, B240:455, 1990. [Erratum: Phys. Lett.B262,497(1991)].

[25] E. Braaten and J. P. Leveille. Higgs Boson Decay and the Running Mass. *Phys. Rev.*, D22:715, 1980.

[26] Bernd A. Kniehl. Higgs phenomenology at one loop in the standard model. *Phys. Rept.*, 240:211–300, 1994.

[27] Wai-Yee Keung and William J. Marciano. Higgs Scalar Decays: $h \rightarrow W^+ W^-$. *Phys. Rev.*, D30:248, 1984.

[28] A. Bredenstein, Ansgar Denner, S. Dittmaier, and M. M. Weber. Precision calculations for H $\rightarrow$ WW/ZZ $\rightarrow$ 4fermions with PROPHECY4f. In *Proceedings, International Linear Collider Workshop (LCWS07 and ILC07) Hamburg , Germany, May 30-June 3, 2007, Vol.1-2*, pages 150–154, 2007.

[29] M. Spira, A. Djouadi, D. Graudenz, and P. M. Zerwas. Higgs boson production at the LHC. *Nucl. Phys.*, B453:17–82, 1995.

[30] D. de Florian et al. Handbook of LHC Higgs Cross Sections: 4. Deciphering the Nature of the Higgs Sector. 2016.

[31] Charalampos Anastasiou, Claude Duhr, Falko Dulat, Elisabetta Furlan, Thomas Gehrmann, Franz Herzog, Achilleas Lazopoulos, and Bernhard Mistlberger. High precision determination of the gluon fusion Higgs boson cross-section at the LHC. *JHEP*, 05:058, 2016.

[32] R. Keith Ellis, I. Hinchliffe, M. Soldate, and J. J. van der Bij. Higgs Decay to tau+ tau-: A Possible Signature of Intermediate Mass Higgs Bosons at the SSC. *Nucl. Phys.*, B297:221–243, 1988.

[33] Radja Boughezal, Christfried Focke, Walter Giele, Xiaohui Liu, and Frank Petriello. Higgs boson production in association with a jet at NNLO using jettiness subtraction. *Phys. Lett.*, B748:5–8, 2015.

[34] Radja Boughezal, Fabrizio Caola, Kirill Melnikov, Frank Petriello, and Markus Schulze. Higgs boson production in association with a jet at next-to-next-to-leading order. *Phys. Rev. Lett.*, 115(8):082003, 2015.

[35] Falko Dulat, Bernhard Mistlberger, and Andrea Pelloni. Differential Higgs production at N^3LO beyond threshold. 2017.

[36] Xuan Chen, Thomas Gehrmann, Nigel Glover, and Matthieu Jaquier. Higgs plus one jet production at NNLO. *PoS*, RADCOR2015:056, 2016.

[37] Daniel de Florian, Giancarlo Ferrera, Massimiliano Grazzini, and Damiano Tommasini. Transverse-momentum resummation: Higgs boson production at the Tevatron and the LHC. *JHEP*, 11:064, 2011.

[38] R. P. Kauffman. Higher order corrections to Higgs boson p(T). *Phys. Rev.*, D45:1512–1517, 1992.

[39] Pier Francesco Monni, Emanuele Re, and Paolo Torrielli. Higgs Transverse-Momentum Resummation in Direct Space. *Phys. Rev. Lett.*, 116(24):242001, 2016.

[40] Morad Aaboud et al. Measurement of inclusive and differential cross sections in the $H \to ZZ^* \to 4\ell$ decay channel in pp collisions at $\sqrt{s} = 13$ TeV with the ATLAS detector. *JHEP*, 10:132, 2017.

[41] Albert M Sirunyan et al. Measurements of properties of the Higgs boson decaying into the four-lepton final state in pp collisions at $\sqrt{s} = 13$ TeV. *JHEP*, 11:047, 2017.

[42] Fabrizio Caola and Kirill Melnikov. Constraining the Higgs boson width with ZZ production at the LHC. *Phys. Rev.*, D88:054024, 2013.

[43] Nikolas Kauer. Interference effects for H $\to$ WW/ZZ $\to \ell\bar{\nu}_\ell\bar{\ell}\nu_\ell$ searches in gluon fusion at the LHC. *JHEP*, 12:082, 2013.

[44] Vardan Khachatryan et al. Constraints on the Higgs boson width from off-shell production and decay to Z-boson pairs. *Phys. Lett.*, B736:64–85, 2014.

[45] Georges Aad et al. Constraints on the off-shell Higgs boson signal strength in the high-mass ZZ and WW final states with the ATLAS detector. *Eur. Phys. J.*, C75(7):335, 2015.

[46] Aleksandr Azatov, Christophe Grojean, Ayan Paul, and Ennio Salvioni. Taming the off-shell Higgs boson. *Zh. Eksp. Teor. Fiz.*, 147:410–425, 2015. [J. Exp. Theor. Phys.120,354(2015)].

[47] James S. Gainer, Joseph Lykken, Konstantin T. Matchev, Stephen Mrenna, and Myeonghun Park. Beyond Geolocating: Constraining Higher Dimensional Operators in $H \to 4\ell$ with Off-Shell Production and More. *Phys. Rev.*, D91(3):035011, 2015.

[48] Christoph Englert, Yotam Soreq, and Michael Spannowsky. Off-Shell Higgs Coupling Measurements in BSM scenarios. *JHEP*, 05:145, 2015.

[49] John M. Campbell, R. Keith Ellis, and Ciaran Williams. Bounding the Higgs width at the LHC using full analytic results for $gg \to e^-e^+\mu^-\mu^+$. *JHEP*, 04:060, 2014.

[50] Sally Dawson et al. Working Group Report: Higgs Boson. In *Proceedings, 2013 Community Summer Study on the Future of U.S. Particle Physics: Snowmass on the Mississippi (CSS2013): Minneapolis, MN, USA, July 29-August 6, 2013*, 2013.

[51] V. Del Duca, W. Kilgore, C. Oleari, C. Schmidt, and D. Zeppenfeld. Gluon fusion contributions to H + 2 jet production. *Nucl. Phys.*, B616:367–399, 2001.

[52] A. Stange, William J. Marciano, and S. Willenbrock. Associated production of Higgs and weak bosons, with $h \to b\bar{b}$, at hadron colliders. *Phys. Rev.*, D50:4491–4498, 1994.

[53] Oliver Brein, Robert V. Harlander, and Tom J. E. Zirke. vh@nnlo - Higgs Strahlung at hadron colliders. *Comput. Phys. Commun.*, 184:998–1003, 2013.

[54] Ansgar Denner, Stefan Dittmaier, Stefan Kallweit, and Alexander Muck. Electroweak corrections to Higgs-strahlung off W/Z bosons at the Tevatron and the LHC with HAWK. *JHEP*, 03:075, 2012.

[55] Albert M Sirunyan et al. Inclusive search for a highly boosted Higgs boson decaying to a bottom quark-antiquark pair. 2017.

[56] Morad Aaboud et al. Evidence for the $H \to b\bar{b}$ decay with the ATLAS detector. 2017.

[57] Jonathan M. Butterworth, Adam R. Davison, Mathieu Rubin, and Gavin P. Salam. Jet substructure as a new Higgs search channel at the LHC. *Phys. Rev. Lett.*, 100:242001, 2008.

[58] Matthew D. Schwartz. TASI Lectures on Collider Physics. 2017.

[59] S. Dawson, C. Jackson, L. H. Orr, L. Reina, and D. Wackeroth. Associated Higgs production with top quarks at the large hadron collider: NLO QCD corrections. *Phys. Rev.*, D68:034022, 2003.

[60] S. Dawson, L. H. Orr, L. Reina, and D. Wackeroth. Associated top quark Higgs boson production at the LHC. *Phys. Rev.*, D67:071503, 2003.

[61] W. Beenakker, S. Dittmaier, M. Kramer, B. Plumper, M. Spira, and P. M. Zerwas. NLO QCD corrections to t anti-t H production in hadron collisions. *Nucl. Phys.*, B653:151–203, 2003.

[62] W. Beenakker, S. Dittmaier, M. Kramer, B. Plumper, M. Spira, and P. M. Zerwas. Higgs radiation off top quarks at the Tevatron and the LHC. *Phys. Rev. Lett.*, 87:201805, 2001.

[63] S. Frixione, V. Hirschi, D. Pagani, H. S. Shao, and M. Zaro. Weak corrections to Higgs hadroproduction in association with a top-quark pair. *JHEP*, 09:065, 2014.

[64] S. Frixione, V. Hirschi, D. Pagani, H. S. Shao, and M. Zaro. Electroweak and QCD corrections to top-pair hadroproduction in association with heavy bosons. *JHEP*, 06:184, 2015.

[65] S. Dawson, S. Dittmaier, and M. Spira. Neutral Higgs boson pair production at hadron colliders: QCD corrections. *Phys. Rev.*, D58:115012, 1998.

[66] Daniel de Florian and Javier Mazzitelli. Higgs pair production at next-to-next-to-leading logarithmic accuracy at the LHC. *JHEP*, 09:053, 2015.

[67] Daniel de Florian, Massimiliano Grazzini, Catalin Hanga, Stefan Kallweit, Jonas M. Lindert, Philipp Maierhöfer, Javier Mazzitelli, and Dirk Rathlev. Differential Higgs Boson Pair Production at Next-to-Next-to-Leading Order in QCD. *JHEP*, 09:151, 2016.

[68] Daniel de Florian, Ignacio Fabre, and Javier Mazzitelli. Higgs boson pair production at NNLO in QCD including dimension 6 operators. 2017.

[69] Daniel de Florian and Javier Mazzitelli. Higgs Boson Pair Production at Next-to-Next-to-Leading Order in QCD. *Phys. Rev. Lett.*, 111:201801, 2013.

[70] Jonathan Grigo, Kirill Melnikov, and Matthias Steinhauser. Virtual corrections to Higgs boson pair production in the large top quark mass limit. *Nucl. Phys.*, B888:17–29, 2014.

[71] S. Borowka, N. Greiner, G. Heinrich, S. P. Jones, M. Kerner, J. Schlenk, and T. Zirke. Full top quark mass dependence in Higgs boson pair production at NLO. *JHEP*, 10:107, 2016.

[72] G. Heinrich, S. P. Jones, M. Kerner, G. Luisoni, and E. Vryonidou. NLO predictions for Higgs boson pair production with full top quark mass dependence matched to parton showers. *JHEP*, 08:088, 2017.

[73] R. Frederix, S. Frixione, V. Hirschi, F. Maltoni, O. Mattelaer, P. Torrielli, E. Vryonidou, and M. Zaro. Higgs pair production at the LHC with NLO and parton-shower effects. *Phys. Lett.*, B732:142–149, 2014.

[74] Search for pair production of Higgs bosons in the $b\bar{b}b\bar{b}$ final state using proton−proton collisions at $\sqrt{s} = 13$ TeV with the ATLAS detector. Technical Report ATLAS-CONF-2016-049, CERN,

Geneva, Aug 2016.

[75] Search for Higgs boson pair production in the final state containing two photons and two bottom quarks in proton-proton collisions at $\sqrt{s} = 13$ TeV. Technical Report CMS-PAS-HIG-17-008, CERN, Geneva, 2017.

[76] Higgs Pair Production in the $H(\to \tau\tau)$ and $H(\to b\bar{b})$ channel at the High-Luminosity LHC. Technical Report ATL-PHYS-PUB-2015-046, CERN, Geneva, Nov 2015.

[77] Chien-Yi Chen, S. Dawson, and I. M. Lewis. Exploring resonant di-Higgs boson production in the Higgs singlet model. *Phys. Rev.*, D91(3):035015, 2015.

[78] Alan J. Barr, Matthew J. Dolan, Christoph Englert, Danilo Enoque Ferreira de Lima, and Michael Spannowsky. Higgs Self-Coupling Measurements at a 100 TeV Hadron Collider. *JHEP*, 02:016, 2015.

[79] Raul Costa, Margarete Mühlleitner, Marco O. P. Sampaio, and Rui Santos. Singlet Extensions of the Standard Model at LHC Run 2: Benchmarks and Comparison with the NMSSM. *JHEP*, 06:034, 2016.

[80] S. Dawson and M. Sullivan. Enhanced di-Higgs Production in the Complex Higgs Singlet Model. 2017.

[81] S. Dawson and I. M. Lewis. NLO corrections to double Higgs boson production in the Higgs singlet model. *Phys. Rev.*, D92(9):094023, 2015.

[82] Giuseppe Degrassi, Pier Paolo Giardino, Fabio Maltoni, and Davide Pagani. Probing the Higgs self coupling via single Higgs production at the LHC. *JHEP*, 12:080, 2016.

[83] Stefano Di Vita, Christophe Grojean, Giuliano Panico, Marc Riembau, and Thibaud Vantalon. A global view on the Higgs self-coupling. *JHEP*, 09:069, 2017.

[84] Graham D. Kribs, Andreas Maier, Heidi Rzehak, Michael Spannowsky, and Philip Waite. Electroweak oblique parameters as a probe of the trilinear Higgs boson self-interaction. *Phys. Rev.*, D95(9):093004, 2017.

[85] Wojciech Bizon, Martin Gorbahn, Ulrich Haisch, and Giulia Zanderighi. Constraints on the trilinear Higgs coupling from vector boson fusion and associated Higgs production at the LHC. *JHEP*, 07:083, 2017.

[86] Georges Aad et al. Measurements of the Higgs boson production and decay rates and constraints on its couplings from a combined ATLAS and CMS analysis of the LHC pp collision data at $\sqrt{s} = 7$ and 8 TeV. *JHEP*, 08:045, 2016.

[87] Measurement of the Higgs boson coupling properties in the $H \to ZZ^* \to 4\ell$ decay channel at $\sqrt{s}$ = 13 TeV with the ATLAS detector. Technical Report ATLAS-CONF-2017-043, CERN, Geneva, Jul 2017.

[88] Measurements of Higgs boson properties in the diphoton decay channel with 36.1 fb^{-1} pp collision data at the center-of-mass energy of 13 TeV with the ATLAS detector. Technical Report ATLAS-CONF-2017-045, CERN, Geneva, Jul 2017.

[89] Evidence for the decay of the Higgs Boson to Bottom Quarks. Technical Report CMS-PAS-HIG-16-044, CERN, Geneva, 2017.

[90] Higgs to WW measurements with 15.2 fb^{-1} of 13 TeV proton-proton collisions. Technical Report CMS-PAS-HIG-16-021, CERN, Geneva, 2017.

[91] Measurements of properties of the Higgs boson decaying into four leptons in pp collisions at sqrts = 13 TeV. Technical Report CMS-PAS-HIG-16-041, CERN, Geneva, 2017.

[92] Georges Aad et al. Measurements of the Higgs boson production and decay rates and coupling strengths using pp collision data at $\sqrt{s} = 7$ and 8 TeV in the ATLAS experiment. *Eur. Phys. J.*, C76(1):6, 2016.

[93] Vardan Khachatryan et al. Precise determination of the mass of the Higgs boson and tests of

compatibility of its couplings with the standard model predictions using proton collisions at 7 and 8 TeV. *Eur. Phys. J.*, C75(5):212, 2015.

[94] Ilaria Brivio and Michael Trott. The Standard Model as an Effective Field Theory. 2017.

[95] W. Buchmuller and D. Wyler. Effective Lagrangian Analysis of New Interactions and Flavor Conservation. *Nucl. Phys.*, B268:621–653, 1986.

[96] Kaoru Hagiwara, S. Ishihara, R. Szalapski, and D. Zeppenfeld. Low-energy effects of new interactions in the electroweak boson sector. *Phys. Rev.*, D48:2182–2203, 1993.

[97] G. F. Giudice, C. Grojean, A. Pomarol, and R. Rattazzi. The Strongly-Interacting Light Higgs. *JHEP*, 06:045, 2007.

[98] Adam Falkowski, Benjamin Fuks, Kentarou Mawatari, Ken Mimasu, Francesco Riva, and Veronica sanz. Rosetta: an operator basis translator for Standard Model effective field theory. *Eur. Phys. J.*, C75(12):583, 2015.

[99] James D. Wells and Zhengkang Zhang. Effective theories of universal theories. *JHEP*, 01:123, 2016.

[100] Roberto Contino, Adam Falkowski, Florian Goertz, Christophe Grojean, and Francesco Riva. On the Validity of the Effective Field Theory Approach to SM Precision Tests. *JHEP*, 07:144, 2016.

[101] Roni Harnik, Joachim Kopp, and Jure Zupan. Flavor Violating Higgs Decays. *JHEP*, 03:026, 2013.

[102] Aleksandr Azatov, Christophe Grojean, Ayan Paul, and Ennio Salvioni. Resolving gluon fusion loops at current and future hadron colliders. *JHEP*, 09:123, 2016.

[103] Roberto Contino, Margherita Ghezzi, Christophe Grojean, Margarete Muhlleitner, and Michael Spira. Effective Lagrangian for a light Higgs-like scalar. *JHEP*, 07:035, 2013.

[104] Chien-Yi Chen, S. Dawson, and I. M. Lewis. Top Partners and Higgs Boson Production. *Phys. Rev.*, D90(3):035016, 2014.

[105] Florian Goertz, Andreas Papaefstathiou, Li Lin Yang, and Josǟľ Zurita. Higgs boson pair production in the D=6 extension of the SM. *JHEP*, 04:167, 2015.

[106] Aleksandr Azatov, Roberto Contino, Giuliano Panico, and Minho Son. Effective field theory analysis of double Higgs boson production via gluon fusion. *Phys. Rev.*, D92(3):035001, 2015.

[107] M. Gillioz, R. Grober, C. Grojean, M. Muhlleitner, and E. Salvioni. Higgs Low-Energy Theorem (and its corrections) in Composite Models. *JHEP*, 10:004, 2012.

[108] Roberto Contino, Margherita Ghezzi, Christophe Grojean, Margarete Mühlleitner, and Michael Spira. eHDECAY: an Implementation of the Higgs Effective Lagrangian into HDECAY. *Comput. Phys. Commun.*, 185:3412–3423, 2014.

[109] Ilaria Brivio, Yun Jiang, and Michael Trott. The SMEFTsim package, theory and tools. 2017.

[110] Anja Butter, Oscar J. P. Eboli, J. Gonzalez-Fraile, M. C. Gonzalez-Garcia, Tilman Plehn, and Michael Rauch. The Gauge-Higgs Legacy of the LHC Run I. *JHEP*, 07:152, 2016.

[111] K. J. F. Gaemers and G. J. Gounaris. Polarization Amplitudes for e+ e- —> W+ W- and e+ e- —> Z Z. *Z. Phys.*, C1:259, 1979.

[112] Kaoru Hagiwara, R. D. Peccei, D. Zeppenfeld, and K. Hikasa. Probing the Weak Boson Sector in $e^+e^- \to W^+W^-$. *Nucl. Phys.*, B282:253–307, 1987.

[113] Laure Berthier, Mikkel Bjorn, and Michael Trott. Incorporating doubly resonant $W^\pm$ data in a global fit of SMEFT parameters to lift flat directions.

[114] Adam Falkowski, Martin Gonzalez-Alonso, Admir Greljo, David Marzocca, and Minho Son. Anomalous Triple Gauge Couplings in the Effective Field Theory Approach at the LHC. *JHEP*, 02:115, 2017.

[115] Adam Falkowski and Francesco Riva. Model-independent precision constraints on dimension-6 operators. *JHEP*, 02:039, 2015.

JHEP, 09:157, 2016.

[116] Sally Dawson and Christopher W. Murphy. Standard Model EFT and Extended Scalar Sectors. *Phys. Rev.*, D96(1):015041, 2017.

[117] J. de Blas, J. C. Criado, M. Perez-Victoria, and J. Santiago. Effective description of general extensions of the Standard Model: the complete tree-level dictionary. 2017.

[118] Brian Henning, Xiaochuan Lu, and Hitoshi Murayama. How to use the Standard Model effective field theory. *JHEP*, 01:023, 2016.

[119] Johann Brehmer, Ayres Freitas, David Lopez-Val, and Tilman Plehn. Pushing Higgs Effective Theory to its Limits. *Phys. Rev.*, D93(7):075014, 2016.

[120] Martin Gorbahn, Jose Miguel No, and Veronica Sanz. Benchmarks for Higgs Effective Theory: Extended Higgs Sectors. *JHEP*, 10:036, 2015.

[121] Chien-Yi Chen, S. Dawson, and Elisabetta Furlan. Vectorlike fermions and Higgs effective field theory revisited. *Phys. Rev.*, D96(1):015006, 2017.

[122] J. A. Aguilar-Saavedra. A Minimal set of top-Higgs anomalous couplings. *Nucl. Phys.*, B821:215–227, 2009.

Neutrino Physics

S. Davidson
IN2P3,CNRS,France

Abstract

This is summary of three lectures on neutrino physics at the CERN school in Evora, Portugal, for experimental PhD students. There is a brief review of neutrino interactions in the Standard Model, Majorana and Dirac mass terms, oscillations in vaccuum and matter for 2 generations, the leptonic unitarity triangle and 3 generation mixing, and bounds on the the absolute neutrino mass scale. Follows a few topics going beyond the physics of three light active neutrinos: an introduction to a few seesaw models for Majorana masses, and leptogenesis in the type I seesaw.

Keywords

Lectures; neutrinos; leptogenesis, neutrino oscillations, mass, flavor, Majorana

1 Introduction

Neutrinos are shy particles in the laboratory, but make several relevant contributions in cosmology and astrophysics. They could be responsible for the observed matter excess of the Universe [1], and possibly also the dark matter [2]. We know that there were three species of relativistic neutrinos in thermal equilibrium in the plasma when the Univers was a few minutes old at the moment of Big Band Nuceosynthesis [3], because the observed primordial ratios of light elements depend on the energy density at the time. Additional constraints on the summed-mass, and number of light neutrinos in equilibrium are obtained from the observed anisotropies in the Cosmic Microwave Background (CMB) [4]. In the following 10^{10} years of the life of our Universe, stars were born, radiated photons and neutrinos, and died — the massive ones in supernova explosions [5] (whose explosion probably required assistance from neutrinos), thereby spreading heavy elements through the Universe and making our life possible. Humanity became acquainted with neutrinos only in the previous century, and in the last decades, they have given us laboratory evidence [14, 15] of New Physics beyond the Standard Model (SM). This has generated significant interest in the community — so many excellent review articles are available. Some review articles that I have read (much more complete than this introduction), can be found in reference [6], and useful websites in reference [8].

1.1 Notation

I use chiral (2-component) spinors, but 4-component spinor notation, where a 4-component spinor χ has 4 degrees of freedom labelled by $\{\pm E, \pm s\}$, and can be written in the chiral decomposition

$$\chi = \left(\begin{array}{c} \psi_L \\ \psi_R \end{array} \right) \ , \ \{\gamma^\alpha\} = \left\{ \left[\begin{array}{cc} 0 & I \\ I & 0 \end{array} \right], \left[\begin{array}{cc} 0 & \sigma_i \\ -\sigma_i & 0 \end{array} \right] \right\} \ , \ \{\sigma_i\} = \left[\begin{array}{cc} 0 & 1 \\ 1 & 0 \end{array} \right], \left[\begin{array}{cc} 0 & -i \\ i & 0 \end{array} \right], \left[\begin{array}{cc} 1 & 0 \\ 0 & -1 \end{array} \right] \tag{1}$$

where $\psi_L = P_L \chi, \psi_R = P_R \chi$ with $P_L = \frac{(1-\gamma_5)}{2}$. Recall that chirality is not an observable, but becomes helicity (the projection of spin along the direction of motion $\pm \hat{s} \cdot \hat{k} = \pm 1/2$) in the relativistic limit, and is simpler to calculate with than helicity.

In later sections of these notes, the chiral subscript on the fermions may suppressed (for instance, in the leptogenesis section, I write N for N_R).

The Higgs vev $v = 174$ GeV.

2 Neutrino interactions

2.1 Weak neutrino Interactions in the Standard Model

The Standard Model (SM) contains 3 generations of lepton doublets, and charged singlets:

$$\ell_{\alpha L} \in \left\{ \begin{pmatrix} \nu_{eL} \\ e_L \end{pmatrix} , \begin{pmatrix} \nu_{\mu L} \\ \mu_L \end{pmatrix} , \begin{pmatrix} \nu_{\tau L} \\ \tau_L \end{pmatrix} \right\} \quad e_{\alpha R} \in \{e_R, \mu_R, \tau_R\}$$

which here are listed in the charged lepton mass eigenstate basis, to which a greek index is commonly attributed. I do not include a ν_R in the SM because data did not require m_ν when the SM was written down, and because ν_R has no gauge interactions, so a ν_R is not required in each generation for anomaly cancellation. However, some authors consider that the SM can be defined including three ν_R and neutrino Dirac masses, in which case they do not count neutrino masses as evidence for "New Physics".

A Lagrangian which reproduces all the observed interactions of neutrinos and charged leptons is:

$$\mathcal{L} = i\overline{\ell_{L\alpha}}\gamma^\mu \mathbf{D}_\mu \ell_{L\alpha} + i\overline{e_{R\alpha}}\gamma^\mu D_\mu e_{R\alpha} - \left[(\overline{\nu_{\alpha L}}, \overline{e_{\alpha L}}) y_\alpha \begin{pmatrix} -H^+ \\ H^{0*} \end{pmatrix} e_{\alpha R} + \text{h.c.} \right] \tag{2}$$

where $\alpha \in \{e, \mu, \tau\}$ is a sum over generations, $\mathcal{L}$ is in the charged lepton mass basis, the covariant derivatives are

$$\mathbf{D}_\mu = \partial_\mu + i\frac{g}{2}\sigma^a W_\mu^a + ig'Y(\ell_L)B_\mu \ , \ D_\mu = \partial_\mu + ig'Y(e_R)B_\mu \ , \tag{3}$$

B^μ is the hypercharge gauge boson, the fermion hypercharge is $Y(f) = T_3 + Q_{em}$, and $\widetilde{H}^T = (-H^+, H^{0*})$ gives masses $m_\alpha = y_\alpha \langle H^0 \rangle$ to the charged leptons.

The first term of eqn (2) , $\overline{\ell_{L\alpha}}^T \gamma^\mu \mathbf{D}_\mu \ell_{L\alpha}$ gives:

$$\begin{pmatrix} \overline{\nu_L} & \overline{e_L} \end{pmatrix} \gamma^\mu \begin{pmatrix} \frac{g}{2\cos\theta_W} Z_\mu & \frac{g}{\sqrt{2}} W_\mu^+ \\ \frac{g}{\sqrt{2}} W_\mu^- & eA_\mu - ...Z_\mu \end{pmatrix} \begin{pmatrix} \nu_L \\ e_L \end{pmatrix} \tag{4}$$

where $s_W = \sin\theta_W$, $\tan\theta_W = g'/g$, and the photon and Z fields are defined as $A_\mu \equiv c_W B_\mu + s_W W_\mu^3$, $Z_\mu \equiv -s_W B_\mu + c_W W_\mu^3$. This gives the familiar Feynman rules illustrated in figure 1. These
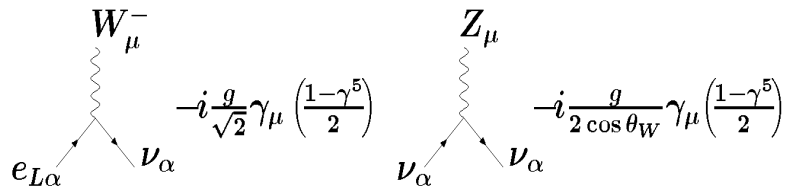

Fig. 1: W,Z Feynman rules in the SM with massless neutrinos

Feynman rules illustrate that, in the SM, there is no flavour change in the lepton sector — lepton flavour is conserved.

The Lagrangian of eqn (2) does not only reproduce all lepton interactions (except neutrino oscillations); it is also the most general renormalisable, $SU(2) \times U(1)$-invariant $\mathcal{L}$ for those particles. In order to see that, one has to show how to get rid of flavour-changing kinetic or Yukawa terms such as:

$$\left(\overline{\nu_{eL}}, \overline{e_L}\right) \not{D} \begin{pmatrix} \nu_{\mu L} \\ \mu_L \end{pmatrix} \quad , \quad \left(\overline{\nu_{eL}}, \overline{e_L}\right) \widetilde{H} \tau_R \ .$$

Since such terms are gauge invariant, the most general Lagrangian can be written as

$$i\overline{\ell_L}^{b'} Z_{bc}\gamma^\mu \mathbf{D}_\mu \ell_L^{c'} + i\overline{e_R}^f Z^{(e)}_{fg}\gamma^\mu D_\mu e_R^g - \overline{\ell}_L^{'b}[\tilde{Y}_e]_{bd}\widetilde{H}e_R^d + h.c. \tag{5}$$

and the next few paragraphs aim to show that eqn (5) can be transformed into the canonical version give in eqn (2).

The first step is to diagonalise Z, which must be hermitian because $\mathcal{L}$ should be real. It can therefore be diagonalised as $\boldsymbol{VZV^\dagger = D_Z}$ where V is unitary and $\boldsymbol{D_Z}$ diagonal, as

$$\overline{\ell_L^{'b}}\mathbf{Z}_{bc}\slashed{D}\,\ell_L^{'c} = \overline{\ell_L^{'b}}[V_Z^\dagger \mathbf{D_Z}V_Z]_{bc}\slashed{D}\,\ell_L^{'c} = \overline{\ell_L^{b''}}\mathbf{D_{Z}}_{bb}\slashed{D}\,\ell_L^{b''} = \overline{\ell_L}^b\slashed{D}\,\ell_L^b$$

where at the last equality, the eigenvalues of Z were absorbed into the definition of the fields. This is allowed, because the magnitude of a fermion field cannot be measured.

The basis transformation and field rescaling that removed the $\boldsymbol{Z}$ matrix affect the definition of the Yukawa matrix. Defining $\mathbf{Y_e} = \mathbf{D_Z^{-1/2}V_Z\widetilde{Y}_e}$ (and implicitly performing similar operations to remove $\boldsymbol{Z^{(e)}}$) , the Lagrangian now can be written

$$\mathcal{L} = i\overline{\ell_L^b}^T\slashed{D}\,\ell_L^b + i\overline{e_R^a}\slashed{D}\,e_R^a - \{\,(\overline{\ell_L^b}\,[\mathbf{Y_e}]_{bc}\widetilde{H})e_R^c + \text{h.c.}\}$$

where $[\boldsymbol{Y_e}]$ is in principle an arbitrary 3×3 matrix. A diagonal charged-lepton mass matrix can be obtained by different unitary transformations on left and right:

$$V_L[\mathbf{Y_e}]V_R^\dagger = D_e \quad .$$

(Notice that the Yukawa index order is LR in these notes). The matrices V_L, V_R can be obtained by diagonalising the hermitian matrices $[\mathbf{Y_e}][\mathbf{Y_e}]^\dagger = V_L^\dagger D_e^2 V_L$ and $[\mathbf{Y_e}]^\dagger[\mathbf{Y_e}] = V_R^\dagger D_e^2 V_R$.

2.2 Gravitational interactions

Neutrinos also have gravitational interactions, as is expected form the equivalence principle, since they carry 4-momentum. We know this because light elements (such as H, D, ^4He, and ^7Li) were produced in the first few minutes of the life of the Universe ("Big Bang Nucleosynthesis" [3]), and their primordial abundances can be infered from observation. They depend on the age of the Universe at the time, which depends on the energy density (dominated at the time by relativistic species), and allows to conclude that three or four species of neutrino were in thermal equilibrium in the Universe at that time. Current Cosmic Microwave Background data can constrain neutrino parameters [4], which also confirms that neutrinos have gravitational interactions.

2.3 Historical problems

Since a long time, neutrinos have disappeared... The solar neutrino problem is the most long-standing: the sun produces energy by a network of nuclear reactions, which should produce ν_e, which escape the sun without interacting. The photons diffuse slowly to the surface. However, the observed ν_e flux from the sun is $\sim .3 \to .5$ that expected from the solar energy output. This problem was resolved by the SNO experiment [14], who showed that the flux in all flavours was as expected from the photon output, and as predicted by solar models.

There was also an "atmospheric neutrino problem", which was a deficit in the neutrinos produced in cosmic ray interactions in the earth atmosphere: such interactions produce many pions, who generically decay ($\pi^- \to \mu\bar{\nu}_\mu \to e\bar{\nu}_e\nu_\mu\bar{\nu}_\mu$) to twice as many $\nu_\mu + \bar{\nu}_\mu$ as $\nu_e + \bar{\nu}_e$. However, there was a deficit of $\nu_\mu + \bar{\nu}_\mu$, and the community became convinced that neutrinos had mass, when the SuperKamiokande Collaboration [15] showed that there was a deficit of $\nu_\mu, \bar{\nu}_\mu$ from below, that could nicely be fit by $\nu_\mu \to \nu_\tau$ oscillations.

3   Neutrino masses

Before discussing oscillations and the kinematics of m_ν, let us first think about how to write a mass term for neutrinos in $\mathcal{L}$. Since it is known from cosmology that neutrino masses $\lesssim$ eV, we start in the effective QED and QCD invariant theory that is relevant below m_W, and neglect the SU(2) invariance of the Lagrangian. Then the only constraint on the neutrino mass is that it must be a Lorentz-scalar. The only possibility that can be constructed with two chiral fermion fields is

$$m\overline{\psi}\,\psi \;=\; m\overline{\psi_L}\,\psi_R \;+\; m\overline{\psi_R}\,\psi_L \tag{6}$$

3.1   Dirac masses

The first way to construct such a mass term for an active ν_L of the SM, is to introduce a chiral gauge singlet fermion ν_R for each SM generation. Then one can construct a fermion number conserving mass term, as for other SM fermions: $m\overline{\nu_L}\,\nu_R + m\overline{\nu_R}\,\nu_L$. In the full SU(2)-invariant SM, this can be written as :

$$\lambda(\overline{\nu_L}, \overline{e_L})\begin{pmatrix} H_0 \\ H_- \end{pmatrix}\nu_R + h.c \equiv \lambda(\overline{\ell}H)\nu_R + hc \to \; m = \lambda\langle H_0\rangle$$

In three generations, the neutrino Yukawa coupling λ generalises to an arbitrary 3×3 matrix $[\boldsymbol{\lambda}]_{\sigma I}$, which can be diagonalised like other Yukawa matrices with different unitary transformations on left and right: $U[\boldsymbol{\lambda}]U_{R\nu}^\dagger = D_\nu$. If this diagonalisation is performed in the charged lepton mass eigenstate basis, the matrix U is the leptonic version of CKM sometimes called the PMNS matrix (Pontecorvo, Maki, Nakagawa and Sakata).

3.2   Majorana masses

There is a second way to write a Lorentz-invariant mass term for ν_L, in our low-energy not-SU(2)-invariant theory. This is called a Majorana mass term. It uses the fact that the charge conjugate of ν_L is right-handed: charge conjugation on a Dirac fermion is defined as

$$\psi^c \;=\; -i\gamma_0\gamma_2\overline{\psi}^T = -i\gamma_0\gamma_2\gamma_0\psi^* = i\gamma_2^*\psi^* = \begin{bmatrix} 0 & 0 & 0 & 1 \\ 0 & 0 & -1 & 0 \\ 0 & -1 & 0 & 0 \\ 1 & 0 & 0 & 0 \end{bmatrix}\left(\begin{pmatrix} \psi_L^* \\ \psi_R^* \end{pmatrix}\right)$$

so applied to the ν_L, this gives

$$(\nu_L)^c = \left(\begin{pmatrix} 0 \\ 0 \end{pmatrix} \\ \begin{bmatrix} 0 & -1 \\ 1 & 0 \end{bmatrix}\begin{pmatrix} \nu_L^* \end{pmatrix}\right) = \left(\begin{pmatrix} 0 \end{pmatrix} \\ \begin{pmatrix} -i\sigma_2\nu_L^* \end{pmatrix}\right) \tag{7}$$

This allows to write a mass term with only ν_L (no new fields are required):

$$\begin{aligned}
\frac{m}{2}[\overline{\nu_L}(\nu_L)^c + \overline{(\nu_L)^c}\nu_L] &= \frac{m}{2}[(\nu_L)^\dagger\gamma_0(\nu_L)^c + ((\nu_L)^c)^\dagger\gamma_0\nu_L] \\
&= -i\frac{m}{2}[\nu_L^\dagger\sigma_2\nu_L^* + \nu_L^T\sigma_2\nu_L] \equiv \frac{m}{2}\nu_L\nu_L + h.c.
\end{aligned}$$

(where the second line is in 2 component notation for fermions, reviewed in appendix 12, which has the attraction of being less cluttered).

Notice that the mass term involves either the field twice[1], or its complex conjugate×charge conjugate, so this mass violates fermion number by two units, and cannot be written in this way for a fermion

---

[1] The factor of $\frac{1}{2}$ in $\mathcal{L}$ is to avoid 2s in Feynman rules and physical parameters, because I work in conventions where $\overline{\nu^c}$ and ν are considered identical. Recall that Feynman rules are obtained as $\delta^n\mathcal{L}/\delta\nu^n$, so $\delta(\overline{\nu^c}\nu)/\delta\nu = 2\nu$.

with gauge interactions (= with a conserved charge). So the simplest way to write this mass term in the full SU(2) invariant SM is to write the dimension five operator (often called Weinberg operator)

$$\mathcal{L} = ... + \frac{K}{2\Lambda}(\bar{\ell}H)(\ell^c H) + h.c. \rightarrow \frac{m}{2}\overline{\nu_L}\nu_L^c + h.c. \quad , \quad m = \frac{K}{\Lambda}\langle H_0 \rangle^2 \tag{8}$$

Since this operator is non-renormalisable, we assume it is induced by heavy new particles at the scale M, whose interactions with active neutrinos are parametrised in K.

With multiple generations, the Majorana mass matrix $\frac{1}{2}\overline{\nu_L}^\alpha[m]_{\alpha\beta}(\nu_L)^c_\beta$ is *symmetric*[2], so can be diagonalised as:

$$U^T m U = D_m . \tag{9}$$

If the eigenvalues of m are non-degenerate, the matrix U can be obtained by diagonalising $U^\dagger m^\dagger m U = D_m^2$.

The diagonalisation recipe of eqn (9) implies that the eigenvector equation for Majorana matrices is modified with respect to the familiar case of a hermitian matrix H with eigenvalues h_i and eigenvectors $\vec{v}_i$: $H\vec{v}_i = h_i \vec{v}_i$. In the Majorana case, eqn (9) implies $mU = U^* D_m$, or $m\vec{u}_i = m_i \vec{u}_i^*$, where the eigenvectors $\vec{u}_i$ are the colomns of U.

3.3 U

The leptonic mixing matrix, which lives in 3 generation space and rotates from the charged lepton mass basis (index α) to the neutrino mass basis (index i), has three angles and at least one phase:

$$
\begin{aligned}
U_{\alpha i} &= \begin{bmatrix} 1 & 0 & 0 \\ 0 & c_{23} & s_{23} \\ 0 & -s_{23} & c_{23} \end{bmatrix} \begin{bmatrix} c_{13} & & s_{13}e^{-i\delta} \\ 0 & 1 & 0 \\ -s_{13}e^{i\delta} & 0 & c_{13} \end{bmatrix} \begin{bmatrix} c_{12} & s_{12} & 0 \\ -s_{12} & c_{12} & 0 \\ 0 & 0 & 1 \end{bmatrix} P \\
&= \begin{bmatrix} c_{12}c_{13} & c_{13}s_{12} & s_{13}e^{-i\delta} \\ -c_{23}s_{12} - c_{12}s_{13}s_{23}e^{i\delta} & c_{12}c_{23} - s_{12}s_{13}s_{23}e^{i\delta} & c_{13}s_{23} \\ s_{23}s_{12} - c_{12}c_{23}s_{13}e^{i\delta} & -c_{12}s_{23} - c_{23}s_{12}s_{13}e^{i\delta} & c_{13}c_{23} \end{bmatrix} P
\end{aligned} \tag{10}
$$

where P is a diagonal matrix discussed in section 3.3.1, two of the angles are large, and the CP-violating phase δ is placed on the smallest one:

$$\theta_{23} \simeq \pi/4 \quad \theta_{12} \simeq \pi/6 \quad \theta_{13} \simeq 0.15, 8^o \quad \delta \sim 1.4\pi$$

The current experimental determinations of the angles can, for instance, be found in [10, 11]. For comparaison, the magnitudes of off-diagonal CKM matrix elements [11] are much smaller

$$V_{cb} \simeq 0.04 \quad V_{us} \simeq 0.225 \quad V_{ub} \simeq 0.004$$

One of the reasons that the PDG quotes ranges for CKM matrix elements, and for leptonic mixing angles, is that CKM matrix elements are probed in meson decays, whereas the dynamics of neutrino oscillations makes it convenient to measure the angles of the leptonic mixing matrix.

3.3.1 Majorana phases

The diagonal matrix of phases P is the identity for Dirac neutrinos, and diag$\{e^{-i\phi_1/2}, e^{-i\phi_2/2}, 1\}$ for Majorana. The origin of these phases can be understood as follows:

1. suppose that all parameters in $\mathcal{L}$ that can be complex (U and $m_{\nu i}$), are complex

---

[2]Fermion operators anti-commute, but the spinor contraction for the Majorana mass is also antisymmetric. This is easiest seen in 2-component spinor notation: $\hat{\nu}_{Li}^\rho \varepsilon_{\rho\sigma} \hat{\nu}_{Lj}^\sigma = -\hat{\nu}_{Lj}^\sigma \varepsilon_{\rho\sigma} \hat{\nu}_{Li}^\rho = \hat{\nu}_{Lj}^\sigma \varepsilon_{\sigma\rho} \hat{\nu}_{Li}^\rho$, where α, ρ are spinor indices, and $\hat{\nu}_j$ is the operator for mass eigenstare j.

2. There are 3 angles and 6 phases in a generic unitary matrix U (There are 18 real parameters in an arbitrary 3×3 complex matrix; then the Unitarity condition $UU^\dagger = 1$ reduces this to 9.)

3. There are five relative phases between the fields $e_L, \mu_L, \tau_L, \nu_1, \nu_2, \nu_3$ ...so they can chosen to remove all but one phase in the mixing matrix.

4. now check that the masses can be made real: for dirac masses, the phase of the mass can be absorbed with ν_{RI}. If ν_{L3} has a Majorana mass, between itself and anti-self, the absolute phase of ν_{L3} can be chosen to make the mass real. This fixes all LH fermion phases, so the phases from $m_{\nu 1}, m_{\nu 2}$ cannot be removed. They contribute extra CP Violation in processes where Majorana masses appear linearly (not as mm^*, so not in kinematics = not in oscillations). These phases can be left on the masses, or rotated into the diagonal P given in eqn (10).

3.3.2 *Where do mixing matrices appear?*

As in the quark sector, the mixing matrix will appear at W vertices. This can be seen by writing the $\{e_R^\alpha\}$, and $\{\nu_R^I\}$ in the mass eigenstate basis (means $U_{R\nu}$ is unphysical), and the ℓ^a in the mass basis of charged leptons:

$$\ell_L^e \equiv \begin{pmatrix} U_{ei}\nu_L^i \\ e_L \end{pmatrix} \ , \ \ell_L^\mu \equiv \begin{pmatrix} U_{\mu j}\nu_L^j \\ \mu_L \end{pmatrix} \ , \ell_L^\tau \equiv \begin{pmatrix} U_{\tau k}\nu_L^k \\ \tau_L \end{pmatrix}$$

so the Lagrangian becomes

$$i \, (U_{ej}^* \overline{\nu_L^j} \ \overline{e_L}) \, \gamma^\mu \mathbf{D}_\mu \begin{pmatrix} U_{ek}\nu_L^k \\ e_L \end{pmatrix} + i \, (U_{\mu j}^* \overline{\nu_L^j} \ \overline{\mu_L}) \, \gamma^\mu \mathbf{D}_\mu \begin{pmatrix} U_{\mu k}\nu_L^k \\ \mu_L \end{pmatrix} + ...$$

The 3×3 mixing matrix $U_{\alpha,i}$ appears at $W^\pm$ vertices

$$\rightarrow \quad -i \frac{g U_{ej}^*}{\sqrt{2}} \overline{\nu_L^j} \gamma^\mu W_\mu^+ e_L + ...$$

while the Z vertex remains flavour-diagonal:

$$\propto \sum_\alpha -i \frac{g}{2} U_{\alpha j}^* \overline{\nu_L^j} \gamma^\mu Z_\mu^+ U_{\alpha k} \nu_L^k = \delta_{jk} \frac{g}{2} \overline{\nu_L^j} \gamma^\mu Z_\mu^+ \nu_L^k \ .$$

3.4 Dirac vs Majorana

There is a *discrete* difference in the number of light degrees of freedom required for Dirac or Majorana masses: a ν_L with a Majorana (Dirac) mass requires one(two) light chiral fermions. However this distinction is not currently observable. There is also a *continuous* difference, that Majorana masses are Lepton Number Violating(LNV) so give rise to $\Delta L = 2$ processes *e.g.* $0\nu 2\beta$. There is also more CP violation in the Majorana case (all but one of the Majorana ν masses are complex), but this is only detectable in LNV processes.

In the community, it is common to present Majorana vs Dirac as a "either–or" question. Which it is, as a "model discrimination" question: are there three light majorana ν with LNV masses, or three light dirac ν with LN conserving masses. However, if its neither of those models, it seems to the author that the question is continous, not discrete, because the phenomenological question is the LNV rate (one can't measure number of light chiral fermions). For instance, if ones adds an undetectably small LNV mass to a Dirac mass matrix; does that make the neutrinos Majorana? (There would be 6 chiral fermions as for Dirac, and no observed LNV. This case has been studied recently in [16].)

4 Two generation vaccuum oscillations

This section gives three derivations of the 2-neutrino oscillation probability in vaccuum. The first is a relativistic quantum mechanics version, which in my opinion gives the right intuition and physics, but contains several twiddles so the normalisation of the result is doubtful. The second is a quantum mechanical derivation using the Schrodinger equation, which is easy to rederive and gives the correct answer, but is a doubtable formalism for studying neutrinos (One can wonder if the Schrodinger equation is appropriate for relativistic neutrinos, whether the ν propagates with fixed $\vec{k}$ and variable energy, and whether the notion of neutrino flavour eigenstate is useful, since we usually quantise mass eigenstates.). The last is a quantum field theory justification for the Schrodinger equation version, whose purpose is to justify the Schrodinger approach used for matter oscillations in a later section.

An insightful discussion clarifying many questions about neutrino oscillations can be found in [17].

4.1 Relativistic Quantum Mechanics

We are interested in a physical process, where a muon decays at the production point, then later a muon is produced in the detector. We do not know what happened between these two events, so we should sum all the possibilities at the amplitude level.

We suppose a relativistic neutrino is produced in muon decay at $t = 0$. We know how to quantise and do perturbation theory with mass eigenstate particles, so we suppose that neutrinos propagate as mass eigenstates. The amplitude to produce a mass eigenstate i is

$$\propto U_{\mu i} \ .$$

The propagator for a scalar particle of mass m_i to travel a distance L in time t to the detector is

$$G[(0,0);(L,t)] \propto \int \frac{d^3p}{(2\pi)^3} e^{i(Et-pL)} \theta(t)$$

This position-space formula (which can be found in chapter 6 of Bjorken and Drell volume II) looks unfamiliar, because propagators are usually given in momentum space. I suppose that including spin would be a straightforward complication. The amplitude to produce a charged lepton e_α at detector is then:

$$\mathcal{A}_{\mu\alpha} \propto \sum_j U_{\mu j} \times e^{-i(E_j t - k_j L)} \times U_{\alpha j}^* \ .$$

In the relativistic limit where $m_j \ll E, p$, one can take $L \simeq t$ so $-i(E_j t - p_j L) \simeq -i(E_j - p_j)L$ $= -i\frac{E_j^2 - p_j^2}{E_j + p_j} L \simeq -i\frac{m_j^2}{2E} L$ which gives

$$\mathcal{P}_{\mu\alpha} = |\mathcal{A}_{\mu\alpha}|^2 = |\sum_j U_{\mu j} e^{-im_j^2 L/(2E)} U_{\alpha j}^*|^2$$

In the 2 generation case, where the mixing matrix U is

$$U = \begin{bmatrix} \cos\theta & \sin\theta \\ -\sin\theta & \cos\theta \end{bmatrix}$$

one obtains

$$\mathcal{P}_{\mu\to\tau}(t) = \left| \sin\theta \cos\theta \left(e^{-im_2^2 L/2E} - e^{-im_3^2 L/2E} \right) \right|^2$$

173

$$= \sin^2(2\theta)\sin^2\left(L\frac{\Delta_{32}^2}{4E}\right) \quad \Delta_{32}^2 \equiv m_3^2 - m_2^2 \tag{11}$$

$$\mathcal{P}_{\mu\to\mu}(\tau) = 1 - \sin^2(2\theta)\sin^2\left(L\frac{\Delta^2}{4E}\right) = 1 - \sin^2(2\theta)\sin^2\left(1.27\frac{L}{km}\frac{\Delta^2}{\mathrm{eV}^2}\frac{\mathrm{GeV}}{4E}\right) \tag{12}$$

where E is the ν energy and L is the source-detector distance (for atmospheric νs: $E \sim 10$ GeV and $L : 20km \to 10000km$. For reactor neutrinos, $E \sim$ MeV and $L \sim km$). The probability for a muon to decay in production and reappear in the detector (sometimes called the ν_μ survival probability) is illustrated in figure 4.1.

2 generation survival probability P(μ->μ), 2 θ = 45, Δ m²_atm, E = GeV
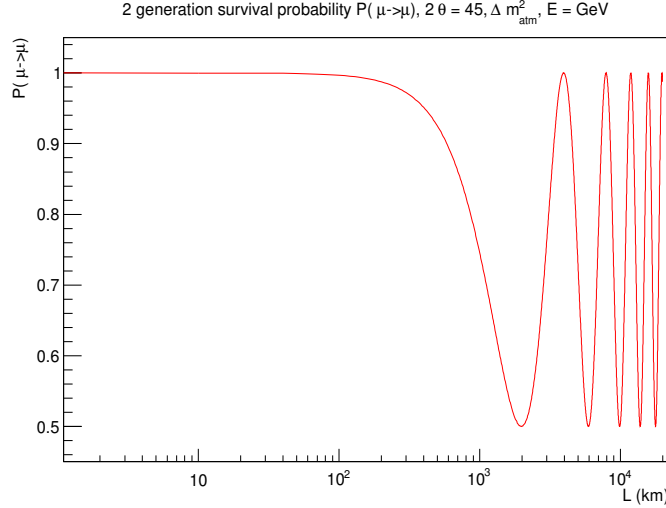
4.2 neutrino oscillations in quantum mechanics(easy to rederive)

A relativistic neutrino, with momentum $\vec{k}$, is produced in muon decay at $t = 0$ (at Tokai/edge atmosphere). It can be described as a quantum mechanical state: $|\nu(t=0)\rangle = |\nu_\mu\rangle$. After it travels a distance L in time t to the detector, it can be written $|\nu(t)\rangle$. We wish to calculate the probability with which it produces an μ in CC scattering at the detector:

$$\mathcal{P}_{\mu\to\mu}(t) = |\langle\nu_\mu|\nu(t)\rangle|^2 \quad = \quad ?$$

For two generations of massive neutrinos the flavour and mass eigenstates are related as $\nu_\alpha = U_{\alpha i}\nu_i$:

$$\begin{pmatrix} \nu_\mu \\ \nu_\tau \end{pmatrix} = \begin{pmatrix} \cos\theta & \sin\theta \\ -\sin\theta & \cos\theta \end{pmatrix} \cdot \begin{pmatrix} \nu_2 \\ \nu_3 \end{pmatrix}.$$

If time evolution in the mass basis is described by a Schrodinger-like equation

$$i\frac{d}{dt}\begin{pmatrix} \nu_2 \\ \nu_3 \end{pmatrix} = \begin{bmatrix} E_2 & 0 \\ 0 & E_3 \end{bmatrix}\begin{pmatrix} \nu_2 \\ \nu_3 \end{pmatrix} \quad , \quad E_i^2 = k^2 + m_i^2$$

then one obtains

$$|\nu(t)\rangle = \sum_j U_{\mu j}|\nu_j(t)\rangle = \sum_j U_{\mu j}e^{-iE_j t}|\nu_j\rangle$$

so the amplitude for the neutrino to produce a charged lepton α in CC scattering in detector after time t is:

$$|\langle\nu_\alpha|\nu(t)\rangle| = \left|\sum_j U_{\mu j}e^{-iE_j t}U_{\alpha j}^*\right|$$

So in the 2 generation case, using $t = L$, $E_3 - E_2 \simeq \frac{m_3^2 - m_2^2}{2E} \equiv \frac{\Delta_{32}^2}{2E}$, one obtains the probabilities already given in equations (12) and (11).

One can anticipate that if the neutrino propagates distances $L \gg E/\Delta^2$, some sort of decoherence should occur, and one should sum the probabilities to propagate the various mass eigenstates. Issues of quantum coherence and decoherence have been discussed in [17]. Here are just some simple estimates about the overlaps of wavepackets:

1. at production, the neutrino energy and momentum are not perfectly known (otherwise one could compute the masses as $\sqrt{E^2 - p^2}$), so one should sum the amplitudes for a given ν_2 and ν_3 to have various energies and momenta: this gives two wavepackets of masses m_2, m_3.

2. The group velocity of the packets is $v_i = \frac{\partial E}{\partial p} = \frac{p}{E} \simeq 1 - \frac{m_i^2}{2E^2}$, so after a distance L, the packets have separated by

$$(v_2 - v_3)L \simeq \frac{m_3^2 - m_2^2}{E^2}L \simeq \frac{L}{\ell_{osc}}\frac{1}{E}$$

3. one could expect the packets to not interfere, if they are separated by more than their size, which by the uncertainty principle should by $\sim 1/(\delta|p|)$, where $\delta|p| \sim \delta E \sim$ the energy uncertainty of the packet. So one expects the oscillating $\sin^2(\Delta^2 L/4E)$ to average to 1/2 when

$$\frac{L}{\ell_{osc}} \gtrsim \frac{E}{\delta E} \quad .$$

4.3 A skeletal QFT derivation of oscillations

One can think that since neutrinos are relativistic, one should do oscillations in Quantum Field Theory. The aim of this skeletal derivation, is to show that QFT is equivalent to the Schrodinger equation of the previous subsection.

In second quantised field theory, in the Heisenberg representation where operators are time-dependent, the equations of motion for the number operator $\hat{n}$ are

$$\frac{d}{dt}\hat{n} = +i[\hat{H}, \hat{n}] \tag{13}$$

where the Hamiltonian $\hat{H}$ for vaccuum oscillations can be taken as free $= \hat{H}_0 \sim \sum \omega \hat{n}_\omega$. Recall the free hamiltonian is the sum over all states of the number of particles $\times$ their energy. It is the integral of hamiltonian density, with which it should not be confused (the dimensions are different).

In second quantised formalism, in the conventions of Peskin and Schroeder, the neutrino field can be written:

$$\hat{\psi}^I(x) = \sum_{s=+,-} \int \frac{d^3p}{(2\pi)^3} \frac{1}{\sqrt{2E}} \left(e^{-ip \cdot x} \hat{a}_s^I(\vec{p}) u_s(p) + e^{ip \cdot x} \hat{b}_s^{I\dagger}(\vec{p}) v_s(p) \right)$$

where s is helicity, I is generation, $\hat{a}^\dagger$ creates particles, et $\hat{b}^\dagger$ creates anti-particules. The creation/annihilation operators $\hat{a}$ are defined here for energy= mass eigenstates, but the formalism is covariant.

We want to know the time/space evolution of a beam neutrinos (no $\bar{\nu}$), of positive helicity, and, to simplify the notation, the momentum is fixed to $\vec{p}$. The number operator for such modes is

$$\hat{n}_{sr}^{IJ}(\vec{p}) = \hat{a}_+^{I\dagger}(\vec{p})\hat{a}_+^J(\vec{p})$$

which is covariant in generation space (indices I, J).

The equation of motion for the number operator $\hat{n}$ is given in (13), where

$$H_0 = \sum_I \int \frac{d^3p}{(2\pi)^3}\, \omega_{II}(|\vec{p}|)\left(\hat{n}^{II}_{++}(\vec{p}) + \hat{n}^{II}_{--}(\vec{p})\right) \ , \ \omega_{II} = \sqrt{\vec{p}^2 + m_I^2} \ .$$

The commutator can then be calculated as

$$\begin{aligned}
\frac{d}{dt}\hat{n}^{IJ}_{++}(\vec{p}) &= i \int \frac{d^3k}{(2\pi)^3}\left(\omega_2(\vec{k})\hat{a}^{2\dagger}_+(\vec{k})\hat{a}^2_+(\vec{k}) + \omega_1(\vec{k})\hat{a}^{1\dagger}_+(\vec{k})\hat{a}^1_+(\vec{k})\right)\hat{a}^{I\dagger}_+(\vec{p})\hat{a}^J_+(\vec{p}) \\
&\quad - \hat{a}^{I\dagger}_+(\vec{p})\hat{a}^J_+(\vec{p})\left(\omega_2(\vec{k})\hat{a}^{2\dagger}_+(\vec{k})\hat{a}^2_+(\vec{k}) + \omega_1(\vec{k})\hat{a}^{1\dagger}_+(\vec{k})\hat{a}^1_+(\vec{k})\right) \\
&= i\left\langle \begin{bmatrix} 0 & (\omega_1 - \omega_2)\hat{a}^{1\dagger}_+(\vec{p})\hat{a}^2_+(\vec{p}) \\ (\omega_2 - \omega_1)\hat{a}^{2\dagger}_+(\vec{p})\hat{a}^1_+(\vec{p}) & 0 \end{bmatrix} \right\rangle
\end{aligned} \tag{14}$$

which turns out to be the equation one would obtain for the neutrino density matrix in the quantum mechanical formulation.

To see this connection, identify the vacuum-expectation value $\langle \hat{n}^{II}_{++}(\vec{p})\rangle \equiv [f_{++}]^{IJ}(\vec{p})$ with the density matrix for the 2-state neutrino system. The QM density matrix for $|\nu(t)\rangle = s|\nu_1(t)\rangle + c|\nu_2(t)\rangle$ can also be constructed as

$$[f_{++}] = \begin{bmatrix} s^2|\nu_1(t)\rangle\langle\nu_1(t)| & sc|\nu_1(t)\rangle\langle\nu_2(t)| \\ sc|\nu_2(t)\rangle\langle\nu_1(t)| & c^2|\nu_2(t)\rangle\langle\nu_2(t)| \end{bmatrix}$$

One can then check that the evolution of $[f_{++}]$ given by eqn (14) and by QM Hamiltonian

$$\begin{bmatrix} -\frac{m_2^2-m_1^2}{4\omega} & 0 \\ 0 & \frac{m_2^2-m_1^2}{4\omega} \end{bmatrix}$$

is identical.

5 Two generation matter oscillations

Neutrinos have weak cross sections which are very small:$\sigma \sim G_F^2 E_\nu^2$. Nonetheless, when the propagate in matter, they have an amplitude to notice the matter, which is $\propto G_F$ and can contribute an effective mass. This effect is described by *coherent* forward scattering of ν in matter, as illustrated in figure 2, which will give an extra contribution to the Hamiltonian. This effect can be relevant for neutrinos propagating in the earth, the sun or supernovae, here only the sun is discussed.
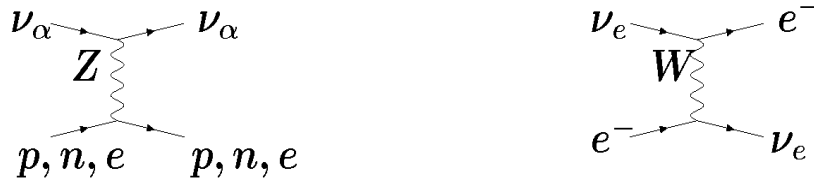

Fig. 2: Forward scattering interactions(the neutrino momentum is unchanged) of neutrinos with matter. The Z exchange diagram affects all neutrinos in the same way, so gives a contribution to the Hamiltonian $\propto$ identity. Therefore it does not induce phase differences between the propagation amplitudes of different ν_i, and can be neglected from oscillation studies.

To see how forward scattering on matter can give rise to an effective mass, one can use the Hamiltonian $H_{\mathrm{mat}} = H_0 + H_{int}$ in the QFT derivation of oscillations, with

$$H_{int} \simeq 2\sqrt{2}G_F \int d^4x (\overline{\hat{\nu}_e}(x)\gamma^\alpha P_L \hat{\nu}_e)(\overline{\hat{e}}\gamma_\alpha P_L \hat{e}(x)) \tag{15}$$

evaluated in a medium with electrons. Only the charged current interaction of ν_e with e need be included, because the NC interaction is the same for all the ν_L, so could only induce a universal a contribution to H proportional to the unit matrix. One can show that

$$\langle \mathrm{medium}|\overline{\hat{e}}\gamma_\alpha P_L \hat{e}(x)|\mathrm{medium}\rangle \to \delta_{\alpha 0}\frac{n_e}{2} \ ,$$

so that H_{mat} in the flavour basis $(\nu_e, (\nu_\tau - \nu_\mu)/\sqrt{2})$, is

$$
\begin{aligned}
H_{\mathrm{mat}} &= \ ...+ \begin{bmatrix} \cos\theta & -\sin\theta \\ \sin\theta & \cos\theta \end{bmatrix}\begin{bmatrix} 0 & 0 \\ 0 & \Delta^2/(2E) \end{bmatrix}\begin{bmatrix} \cos\theta & \sin\theta \\ -\sin\theta & \cos\theta \end{bmatrix} + \begin{bmatrix} V_e & 0 \\ 0 & 0 \end{bmatrix} \\
&= \ ...+ \begin{bmatrix} -\frac{\Delta^2}{4E}\cos 2\theta + V & \frac{\Delta^2}{4E}\sin 2\theta \\ \frac{\Delta^2}{4E}\sin 2\theta & \frac{\Delta^2}{4E}\cos 2\theta \end{bmatrix}
\end{aligned}
$$

where $V_e = \sqrt{2}G_F n_e$.

This matter hamiltonian can be diagonalised by a rotation through the angle θ_{mat}, where

$$
\begin{aligned}
\tan(2\theta_{\mathrm{mat}}) &= \frac{\Delta^2 \sin(2\theta_{12})}{2EV_e - \Delta^2 \cos(2\theta_{12})} \\
\Delta_{\mathrm{mat}}^2 &= \sqrt{(\Delta^2 c2\theta - 2EV)^2 + (\Delta^2 s2\theta)^2}
\end{aligned} \tag{16}
$$

so we see that for $V_e \ll \frac{\Delta^2}{2E}\cos(2\theta_{12})$, matter effects are negligeable. However the matter mixing angle becomes maximal ($\theta_{mat} \to \pi/4$) when $V_e \simeq \frac{\Delta^2}{2E}\cos(2\theta_{12})$, corresponding to the MSW resonance. And for $V \gg \frac{\Delta^2}{2E}\cos(2\theta_{12})$, ν_e propagates as a mass eigenstate. A useful expression for V_e, which allows to estimate where matter is relevant for which energy neutrinos, is

$$
\begin{aligned}
V_e &= \sqrt{2}G_F n_e \simeq 8 \ \mathrm{eV}\frac{\rho Y_e}{10^{14}g/cm^3} \\
Y_e &= \frac{n_e}{n_n + n_p} \ , \ \rho = \begin{cases} 10g/cm^3 & \text{earth} \\ 100g/cm^3 & \text{sun} \\ 10^{14}g/cm^3 & \text{supernova} \end{cases}
\end{aligned} \tag{17}
$$

Finally, it is important to notice that V_e is of opposite sign[3] for $\bar{\nu}$, which allows to determine the sign of the vaccuum mass difference Δ_{12}^2. In particular, since matter effects are observed in solar neutrinos, one concludes that $m_2^2 > m_1^2$.

5.1 matter of varying density

In order to understand the effect of solar matter on the neutrinos exiting the sun, one should consider matter of varying density. For varying $\rho(r)$, the matter Hamiltonian becomes time-dependent:

$$\begin{bmatrix} -\frac{\Delta^2}{4E}\cos 2\theta + V_e(t) & \frac{\Delta^2}{4E}\sin 2\theta \\ \frac{\Delta^2}{4E}\sin 2\theta & \frac{\Delta^2}{4E}\cos 2\theta \end{bmatrix}$$

---

[3] The sign arises because the interaction Hamiltonian of eqn (15) contains $\bar{\hat{\nu}}\gamma_0\hat{\nu} \supset \hat{a}^\dagger\hat{a}, \hat{b}\hat{b}^\dagger$. The negative sign arises in anti-commuting the $\hat{b}\hat{b}^\dagger$, in order to annihilate the incident $\bar{\nu}$ before creating the outgoing one.
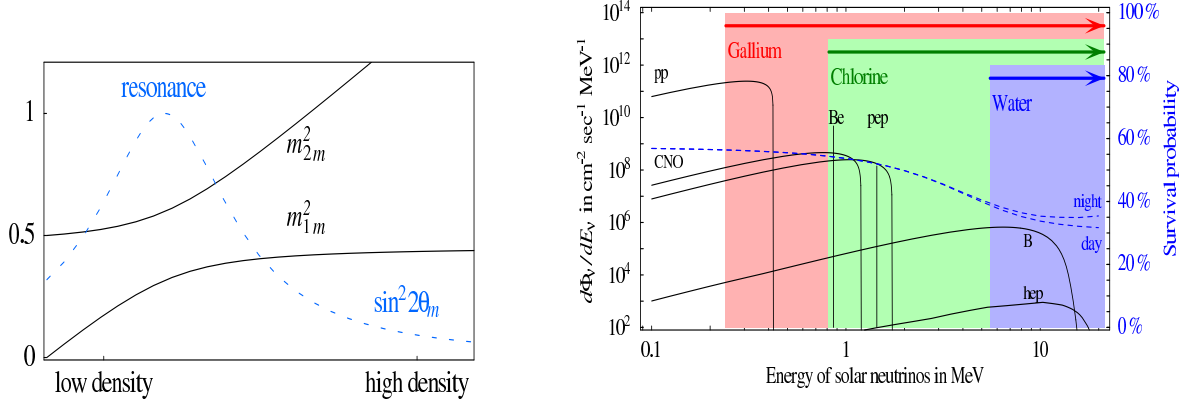
Fig. 3: On the right, solar neutrino fluxes and sensitivities of various experiments. On the left, the effective neutrino mass^2 as a function of density, normalised to $2m_{sol}^2$. Figures from hep-ph/0606054.

so the mixing angle θ_{mat} becomes time dependent. This is simple to account for in the adiabatic limit, where the time variation $\dot{\theta}_{mat}$ can be neglected compared to the oscillation timescale. Then one can imagine that if oscillations occur, they are between the instantaneous mass eigenstates. In the case of the sun, the adiabatic condition is satisfied, and it turns out that the matter effect can suppress oscillations.

The core of the sun produces ν_e in various nuclear reactions, with energies from 0.4 to 10 MeV (see [13] for a review). The principle fluxes, as well as the sensitivities of different detectors, are illustrated in figure 3.

1. From equations (16) and (17), one sees that $V_e > \Delta_{21}^2/2E$ for the $E \sim 8 MeV$ Boron neutrinos, observed in SNO and SK. So these ν_es are mass eigenstates when they are produced, and remain mass eigenstates as they exit the sun, despite that their mass is adiabatically changing. They have no amplitude to be any other state, so there no oscillations, and they exit the sun as the heavier mass eigenstate ν_2. This is illustrated in the left in figure 3 : the neutrino just tracks the mass eigenstate (upper line). The probability to produce an electron in a detector on earth is therefore $|U_{e2}|^2$:

$$P_{ee} \simeq \sin^2 \theta_{12}$$

2. On the other hand, the matter potential V_e is negligeable for the ν_e with energies $\sim$ MeV, who therefore oscillate as in vaccuum. However the vacuum oscillation length $\sim \frac{E}{\Delta^2} \ll R_{sun}$, so the oscillations decohere ($\sin^2 \frac{\Delta^2 L}{E} \to 1/2$) and the probability of producing an electron in a detector on earth is

$$P_{ee} = 1 - \frac{1}{2} \sin^2 2\theta_{12}$$

This explains why the ν_e survival probability was higher at the Davis experiment [12], than in the water cherenkov detectors [14].

6 Three generations

It is well-known that the SM has three generations. Nonetheless, in neutrino oscillations, some observables can be approximately calculated in the much simpler 2-generation formalism, because the dynamics of oscillations selects a particular mass difference and allows to measure a particular angle [4]. This is the first topic of this section.

---

[4]So in neutrino physics, one quotes experimental constraints on the angles θ_{ij}, rather than the matrix elements as is quark flavour physics.

Secondly, the CP-violating part of the 3-generation oscillation probability is introduced, and the current preference of T2K for $\delta \sim -\pi/2$ is discussed.

6.1 The drunken Unitarity triangle

The unitarity triangle is less discussed in lepton flavour physics than in quark flavour. This is perhaps because one discusses the angles rather than the matrix elements in the lepton sector, however, I use it here to illustrate why 2-flavour oscillations can be a good approximation to some observables.

The amplitude to oscillate from flavour α to β over distance L is:

$$\mathcal{A}_{\alpha\beta}(L) = U_{\alpha 1} U_{\beta 1}^* + U_{\alpha 2} U_{\beta 2}^* e^{-i(m_2^2 - m_1^2)L/(2E)} + U_{\alpha 3} U_{\beta 3}^* e^{-i(m_3^2 - m_1^2)L/(2E)} \quad . \tag{18}$$

At $L = 0$, this is just the unitarity relations $\mathcal{A}_{\alpha\beta} = 1$ for $\alpha = \beta$, $\mathcal{A}_{\alpha\beta} = 0$ for $\alpha \neq \beta$, which just say the rows of U are orthonormal. The three terms (complex numbers) can be represented as vectors adding to zero in the complex plane, as in figure 4. At $L = t \neq 0$, eqn (18) implies that two of the vectors rotate in
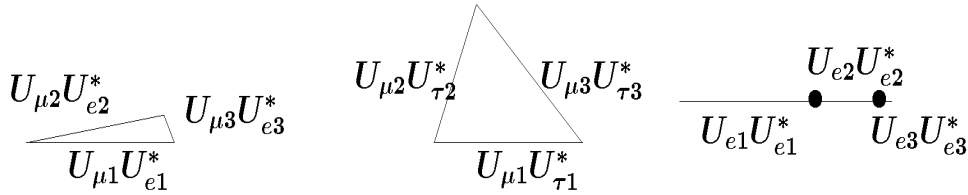

Fig. 4: Example unitarity triangles: for $\alpha = \mu$, $\beta = e$ the triangle is flattened, because $U_{e3} \sim \sin\theta_{13} \sim 0.015$ is small. For $\alpha = \mu$, $\beta = \tau$, the triangle is more equilateral.

the complex plane, with frequencies $(m_j^2 - m_1^2)/2E$, so oscillations can be visualised as time-dependent non-unitarity.

As a first example of why the two-flavour approximation works, consider the amplitude to oscillate from e to e at an energy and baseline combination such that $4E/L \simeq m_2^2 - m_1^2$. This corresponds, for instance, to reactor anti-neutrinos travelling to the Kamland detector. The amplitude is

$$\mathcal{A}_{ee}(L) = U_{e1} U_{e1}^* + U_{e2} U_{e2}^* e^{-i(m_2^2 - m_1^2)L/(2E)} + U_{e3} U_{e3}^* e^{-i(m_3^2 - m_1^2)L/(2E)} \tag{19}$$

and is illustrated on the right in figure 4. At $L \sim (m_2^2 - m_1^2)/2E$, vector 2 rotates, at a frequency $(m_2^2 - m_1^2)/2E$, whereas vector 3 spins rapidly at a frequency $(m_3^2 - m_1^2)/2E$. The two-flavour approximation works because $U_{e3} = \sin\theta_{13}$ is small, so the rapid spinning of vector 3 can be neglected.

As a second example, consider the determination of θ_{13} at reactors. The amplitude is again given in eqn (19), and the diagram is again on the right in figure (4).

However, in this case, the energy-baseline is chosen such that $4E/L \sim (m_3^2 - m_1^2)$, so only the third vector rotates. The first and second are stationary, and $U_{e3} \sim \theta_{13}$ is obtained by measuring the small $\overline{\nu}_e$ disappearance, corresponding to the decreased length of the vector in figure 4, resulting from the rotation of the short vector "3".

6.2 What is left?

Adding three generations of massive neutrinos to the SM introduces new parameters: 3 masses and a mixing matrix containing three angles and at least one phase. The three angles are measured, as are two mass-squared differences: $(m_2^2 - m_1^2)$, $|m_3^2 - m_j^2|$. From matter effects in the sun, it is also known that $(m_2^2 - m_1^2)$ is positive. Remaining to be determined are the sign of $(m_3^2 - m_j^2)$ (refered to as the "hierarchy": $m_3 > m_2 > m_1$ is the normal hierarchy, $m_2 \gtrsim m_1 > m_3$ is inverse hierarchy), the absolute mass scale, and the phase.

6.3 The phase δ

The CP-violating phase δ would be absent in 2 generations, so all three generations must contribute to the oscillation amplitude, in order to have sensitivity to δ.

To compactify the $\nu_\alpha \to \nu_\beta$ oscillation amplitude (eqn (18)), it is convenient to define[5] $x_{ji} \equiv (m_j^2 - m_i^2)L/(2E)$, and the mixing matrix combination [6] $\lambda_i = U_{\alpha i}U_{\beta i}^*$. Then

$$
\begin{aligned}
\mathcal{P}_{\alpha\beta}(L) &= |\lambda_1 + \lambda_2 + \lambda_3|^2 - \lambda_1\lambda_2^* - \lambda_1^*\lambda_2 - \lambda_1\lambda_3^* - \lambda_1^*\lambda_3 - \lambda_3\lambda_2^* - \lambda_3^*\lambda_2 \\
&\quad + \lambda_1\lambda_2^* e^{+ix_{21}} + \lambda_1^*\lambda_2 e^{-ix_{21}} + \lambda_1\lambda_3^* e^{+ix_{31}} + \lambda_1^*\lambda_3 e^{-ix_{31}} \\
&\quad + \lambda_2\lambda_3^* e^{+ix_{32}} + \lambda_2^*\lambda_3 e^{-ix_{32}} \\
&= \delta_{\alpha\beta} - 4\sum_{i<j} \mathrm{Re}\{U_{\alpha i}U_{\beta i}^* U_{\alpha j}^* U_{\beta j}\}\sin^2\frac{x_{ji}}{2} \\
&\quad + 2\sum_{i<j} \mathrm{Im}\{U_{\alpha i}U_{\beta i}^* U_{\alpha j}^* U_{\beta j}\}\sin x_{ji}
\end{aligned}
\tag{20}
$$

To make a first acquaintance with the real part of this formula, one can take the 2 generation limit ($\alpha = \mu$, $\beta = \tau$, $i = 2, j = 3$) and see that the formula (11) is recovered:

$$
\begin{aligned}
\mathcal{P}_{\mu\tau}(L) &= 0 - 4\mathrm{Re}\{-\cos\theta\sin\theta\sin\theta\cos\theta\}\sin^2\frac{x_{32}}{2} \\
&\quad + 0 \\
&= \sin^2(2\theta)\sin^2\frac{(m_3^2 - m_2^2)L}{4E}
\end{aligned}
$$

The imaginary part of the three-flavour oscillation probability (the last sum in eqn (20)) represents CP Violation, and it will give a dependence on the phase δ. To see that this term is CP Violating, one can check that it has opposite sign in the transition probabilities for $\nu_\alpha \to \nu_\beta$ vs $\overline{\nu_\alpha} \to \overline{\nu_\beta}$. The amplitude $\mathcal{A}(\nu_\alpha \to \nu_\beta)$ was obtained in section 4.1; following the same steps, but using that the Feynman rule for $\overline{e_\alpha} \to \overline{\nu_i}$ is $\sim U_{\alpha i}^*$, one sees that the Imagainary term in eqn (20) is of opposite sign in the two cases.

It can be checked that $\{U_{\alpha i}U_{\beta i}^* U_{\alpha j}^* U_{\beta j}\}$ is invariant under changes in the choices of phases of fields. made in order to remove phases from U. Recall that in section 3.3.1, the 5 relative phases of $\{e_\alpha, \nu_j\}$ were chosen in order to remove 5 phases from U. If the field phases were chosen differently, for instance $e_\alpha \to e^{-i\phi_\alpha}, \nu_j \to \nu_j e^{-i\phi_j}$, then $U_{\alpha j} \to e^{-i\phi_\alpha}U_{\alpha j}e^{i\phi_j}$, but the combination $\{U_{\alpha i}U_{\beta i}^* U_{\alpha j}^* U_{\beta j}\}$ is invariant, because $e^{\pm i\phi_\alpha}$ cancels between $U_{\alpha i}$ and $U_{\alpha j}^*$, etc.

Indeed, the combination $\{U_{\alpha i}U_{\beta i}^* U_{\alpha j}U_{\beta j}^*\}$ is proportional to the area of the unitarity triangle area, and to the Jarlskog invariant. Suppose the phases are chosen such that the base $= U_{\mu 1}U_{\tau 1}^*$ of the central triangle in figure (4) is real. Then base $\times$ height $\propto \mathrm{Im}\{U_{\mu 1}U_{\tau 1}^* U_{\mu j}^* U_{\tau j}\}$ for both $j = 2$ and $j = 3$ (its less simple to demonstrate that the third term of the imaginary sum is also $\propto$ the triangle area). To compactify the notation, it is convenient to define

$$
\widetilde{J} = 8c_{13}^2 s_{13}c_{23}s_{23}c_{12}s_{12}
\tag{21}
$$

where the area of the triangle and the Jarlskog invariant computed from the neutrino and charged lepton mass matrices are propotional to $\widetilde{J}\sin\delta$.

6.3.1 θ_{13}, δ at T2K

The current T2K data [19] has some sensitivity to the CP violating phase δ, and favours a maximal value $\delta \sim -3\pi/2$. The aim of this section is to understand this preference.

---

[5]From the review [7].

[6]The dependence on the indices α, β is suppressed because they are fixed by the physical process under consideration.

At JPARC, a beam of muons, [or anti-muons], hits a target, and produces neutrinos of energy $\simeq 0.6$ GeV, which travel 295 km underground to SuperK. In order to be sensitive to θ_{13} and δ, SuperK then searches for electrons, [or positrons]. The baseline and energy are chosen to maximise the appearance probability of electrons via the angle $\sin\theta_{13}$. So at leading order, the vaccum probability is

$$\mathcal{P}_{\mu e} \simeq \sin^2(\theta_{23})\sin^2(2\theta_{13})\sin^2(\frac{x_{31}}{2}) \quad x_{31} = \frac{(m_3^2 - m_1^2)L}{2E} \tag{22}$$

However, $s_{13}^2 \sim \Delta_{21}^2/\Delta_{31}^2$, so the x_{21} oscillations could give some detectable contribution, in which case a dependence on δ becomes possible in the three generation oscillation probability. But if CP violation from the mixing matrix is allowed in the calculation, matter effects should also be included, because, like the Imaginary term in the oscillation probability of eqn (20), they are of opposite sign for neutrinos and anti-neutrinos.

So in principle, the relevant amplitude is

$$\mathcal{A}_{\mu e} = \widetilde{U}_{\mu 1}\widetilde{U}_{e1}^* + \widetilde{U}_{\mu 2}\widetilde{U}_{e2}^* e^{-i\widetilde{x}_{21}} + \widetilde{U}_{\mu 3}\widetilde{U}_{e3}^* e^{-i\widetilde{x}_{31}}$$

where $\widetilde{x} = \Delta_{mat}^2 L/2E$, and $\widetilde{U}$ are the mass differences and mixing matrix in matter.

Matter effects in three generations are discussed, for instance, in [18]; here, the small matter effects are only included in the leading two-generation mixing term, following the discussion of section 5, so eqn (22) becomes

$$\mathcal{P}_{\mu e} \simeq \sin^2(\theta_{23})\sin^2(2\widetilde{\theta}_{13})\sin^2(\frac{\widetilde{x}_{31}}{2}) \tag{23}$$

where $2EV_e/\Delta_{31}^2 \lesssim .1$, and the mass difference and mixing angles in matter are given in eqn (16).

Then the three-generation mixing term that depends on δ can be included in perturbation theory by writing $e^{-ix_{21}} \simeq 1 - i\Delta_{21}^2 L/2E$:

$$\mathcal{P}_{\mu e} \simeq \sin^2(\theta_{23})\sin^2(2\widetilde{\theta}_{13})\sin^2(\frac{\widetilde{x}_{31}}{2}) + \widetilde{J}\frac{\Delta_{21}^2 L}{2E}\sin(\widetilde{x}_{31})\cos(\pm\delta + \frac{x_{31}}{2})$$

where $\widetilde{J}$ is defined in eqn (21).

The current T2K data contains a larger ratio of ν_e to $\overline{\nu_e}$ (electrons to positrons) than expected for any value of δ. So there is a preference for δ that flips the sign of the second term. Since T2K is on the oscillation peak $x_{31} \simeq \pi/2$, this suggests that $\delta \simeq 3\pi/2$.

If this observation is confirmed with more data, it is doubly interesting: first because it indicates that CP violation is generic, and not just a property of the CKM matrix. Secondly, leptogenesis scenarios require CP violation in the leptonic sector, so its presence supports them.

7 Mass pattern/hierarchy

Two possible mass patterns, or hierarchies, are consistent with current oscillation data:
normal hierarchy: $m_1 < m_2 \ll m_3$
inverted hierarchy: $m_3 \ll m_1 \lesssim m_2$
It is known that $m_2^2 > m_1^2$ because there are matter effects for Boron neutrinos exiting from the sun.

The sign of the big mass difference $m_3^2 - m_j^2$ appears in oscillation probability:

1. when ν and $\overline{\nu}$ travel through matter, because the matter contribution to the Hamiltonian is of opposite sign for ν and $\overline{\nu}$...

2. in 3-neutrino oscillations, where interference between Δ_{21}^2 and Δ_{31}^2 occurs, suppressed by $\sin^2\theta_{13}$

So there are proposals [20] to determine the hierarchy by studying atmospheric ν_e and $\overline{\nu}_e$ in high statistics detectors such as PINGU or ORCA [21]. Determining the hierarchy is also among the aims of the DUNE experiment [22].

8   mass scale

8.1   cosmology —a probe of the neutrino mass scale

The mass of neutrinos can have effects on the growth of Large Scale Structure, and also on the Cosmic Microwave Background (principally its evolution from recombination until today).

The participation of neutrinos in Structure formation is intuitive: they are "hot dark matter", that is, in the early Universe after matter-radiation equality, neutrinos still have non-trivial velocities. They can therefore free-stream out of over-densities, rather than collapsing with the overdensity as cold dark matter would do. However, since the neutrinos progressively slow down due to the expansion of the Universe, they only succeed in escaping from small overdensities, which suppresses the power spectrum of Large Scale Structure on small scales. The scale below which the power spectrum is suppressed allows to identify the neutrino mass. However, if neutrino masses are small, the suppression factor is small.

The effect of neutrino masses on the CMB is more subtle, because neutrinos become non-relativistic after recombination (= the moment when the CMB is born), so their masses affect the propagation of CMB photons from recombination until today. This is pedagogically explained in [4]. One of the subtleties of the CMB dependence on neutrino parameters, is that other physical processes, encoded in other parameters of the cosmological ΛCDM model, can have some of the same effects. This was explored in [23], who obtained bounds on the sum of neutrino masses $\Sigma \equiv \sum_i m_{\nu_i}$ [23]

$$
\begin{aligned}
\Sigma \quad &\lesssim \quad 0.1 \to .6 \ eV \quad \text{now} : \ \text{PLANCK}, +\text{LSS/Ly}\alpha \ (\text{in } \Lambda\text{CDM}) \\
&\lesssim \quad 0.6 \to 1 \ eV \quad \ \ \text{now} : \ \text{PLANCK} + ... \ (\text{in 12 param } \Lambda\text{CDM}) \\
\to \quad &\lesssim \quad 2 m_{atm} \quad \quad \ \text{cosmo.indep.} \ (\text{Planck} + \text{EUCLID...}) \\
&\sim \quad m_{atm} \quad \quad \ \ \Lambda\text{CDM}
\end{aligned}
$$

8.2   Beta decay

β decay provides a direct kinematic probe of the neutrino mass, because m_ν^2 distorts the e spectrum in $n \to p + e + \bar\nu$. The KATRIN experiment [24], which is running now, uses Tritium, so consider Tritium β decay:

$$^3H \to {}^3He + e + \bar\nu_e \ , \quad Q = E_e + E_\nu = 18.6\text{eV}$$

where the high-energy tail of the electron distribution turns down due to the neutrino mass $E_e = Q - E_\nu \leq Q - \text{"}m_{e_\nu}\text{"}$. The endpoint of e spectrum can be described as :

$$\frac{dN_e}{dE_e} \propto \sum_i |U_{ei}|^2 \sqrt{(18.6 \text{ keV} - E_e)^2 - m_{\nu_i}^2} \tag{24}$$

The current β-decay bound is $m_{\nu_e} \lesssim 2$ eV; the Katrin sensitivity [24] is expected to be ~ 0.3 eV.

8.2.1   *ν-capture and the Cosmic Neutrino Background*

It is known that in the early Universe at the moment of of Nucleosynthesis (BBN), there was a thermal density of SM neutrinos, comparable to the density of photons. So today there should be a Cosmic Neutrino Background, comparable to the CMB, consisting of $\sim 100\nu/\text{cm}^3$ [25]. Detecting these non-relativistic neutrinos would be interesting, and also difficult since their energy $\sim m_\nu$.

A not unpromising detection possibility [26] could be neutrino capture βdecay: $n + \nu_{CNB} \to p + e$. One can compare the ν capture rate on a nucleus N, to the usual β decay rate as the ratio of the incident CNB number density to the outgoing phase space density in β decay:

$$\frac{n_{\nu CNB}}{\nu \text{ phase space}} \simeq \frac{T_{CNB}^3}{\pi^2} \frac{1}{Q^3} \sim \left(\frac{10^{-4}\text{eV}}{20\text{keV}}\right)^3 \sim 10^{-24}$$

However, in the capture case, the electron energy is $E_e = Q + m_\nu$, so is $2m_\nu$ larger than the upper bound of the β decay spectrum. So with improved resolution, perhaps the CNB could be measured by observing electrons beyond the end-point of the β decay spectrum.

8.3 Neutrinoless double beta decay

Neutrinoless double beta decay ($0\nu2\beta$) is a Lepton *Number* Violating (LNV) process, to which Majorana neutrino masses can contribute. Other lepton number violating scenarios (such as sparticles in R-parity violating supersymmetry) can also contribute, but here only the Majorana mass contribution will be discussed.

For some nuclei, single β decay is kinematically forbidden: for instance, $^{76}_{32}Ge$ is lighter than $^{76}_{33}As$, so $^{76}_{32}Ge$ has a double beta decay to $^{76}_{34}Se + ee\bar{\nu}_e\bar{\nu}_e$, with a lifetime $\sim 10^{21}$ yrs. The lifetime is long because the matrix element is suppressed by $\sim G_F^2$ (two W are exchanged), as illustrated on the left in figure 5. In the presence of Majorana masses, double beta decay can be *neutrinoless*, as illustrated on
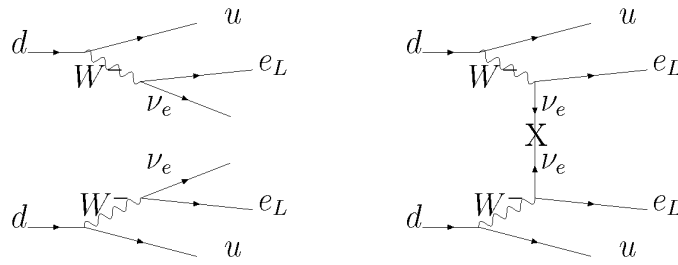

Fig. 5: Double beta decay (left) and neutrinoless double beta decay(right)

the right in figure 5. This diagram can only occur for Majorana neutrino masses, which violate lepton number, because two units of lepton number disappear into the mass insertion x on the neutrino line. As a result, the electrons emerge back-to-back, with opposite momenta and half the available energy each. So the signature of $0\nu2\beta$ is a line just beyond the end of the electron spectrum of 2ν double beta decay.

8.3.1 *The $0\nu2\beta$ matrix element*

The matrix element for $0\nu2\beta$ can schematically be written

$$|\mathcal{M}|^2 = \left| \begin{matrix} \text{nuclear} \\ \text{matrix} \\ \text{element} \end{matrix} \right|^2 \times \left| \sum_i U_{ei}^2 m_i \right|^2$$

for $m_\nu \ll Q \sim 100$ MeV (the mass of heavier Majorana neutrinos would appear downstairs in the propagator). The calculation of the nuclear matrix elements is involved; experts obtain results in different models that can differ by factors of a few [27, 28].

It is interesting to focus on the neutrino part of $|\mathcal{M}|^2$:

$$|\mathcal{M}|^2 \propto \left| c_{13}^2 c_{12}^2 e^{-i\phi_1} m_1 + c_{13}^2 s_{12}^2 e^{-i\phi_2} m_2 + s_{13}^2 e^{-i2\delta} m_3 \right|^2$$

where the majorana masses appear linearly, so accompagnied by their phases (or equivalently, by the Majorana phases from P of eqn (10)). So this Lepton Number Violating process is sensitive to the Majorana phases.
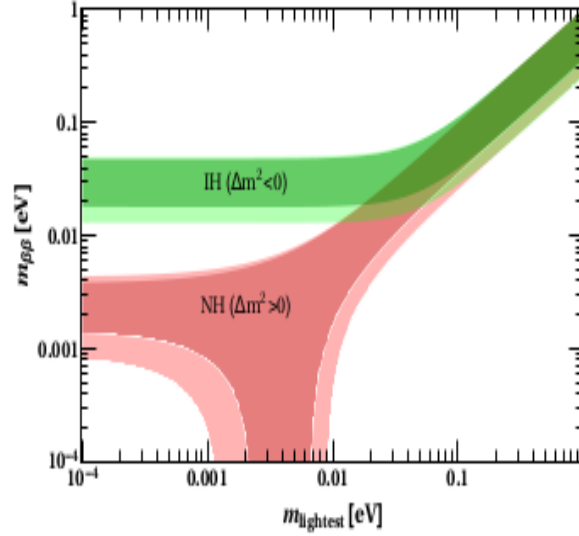
Fig. 6: $|\mathcal{M}|$ for $0\nu2\beta$ mediated by majorana neutrino masses, plotted as a function of the lightest neutrino mass. The green region is allowed for the inverse hierarchy, and the red region corresponds to the normal hierarchy.. The plot is taken from 1601.07512 by Dell'Oro *etal* [28].

8.4 What can we learn/confirm?

Suppose that the only source of lepton number violation is the majorana masses of the SM neutrinos, the largest of which is $\sim \sqrt{|m_3^2 - m_2^2|}$. Then the rate is larger for the Inverse Hierarchy $m_1 \sim m_2 > m_3$:

$$
\begin{aligned}
|\mathcal{M}|^2 &\propto |\frac{3}{4}e^{-i2\phi}m_1 + \frac{1}{4}e^{-i2\phi'}m_2 + s_{13}^2 e^{-i2\delta}m_3|^2 \\
&\to m_{atm}^2 |3 + e^{-i2(\phi'-\phi)}|^2
\end{aligned}
$$

For this hierarchy, which corresponds to the green band in figure 6, either $0\nu2\beta$ is observed, or neutrino masses are Dirac.

On the other hand, in the case of the Normal Hierarchy, ($m_1 < m_2 < m_3$), the contribution of the atmospheric mass is suppressed by s_{13}^2:

$$
\begin{aligned}
|\mathcal{M}|^2 &\to |\frac{3}{4}e^{-i2\phi}m_1 + \frac{1}{4}e^{-i2\phi'}m_{sol} + (.15)^2 e^{-i3\pi}m_{atm}|^2 \\
&\simeq m_{sol}^2 |\frac{3m_1}{m_{sol}} + e^{-i2(\phi-\phi')}|^2
\end{aligned}
$$

so the rate is lower, and for $m_1 \sim m_2/3$ and suitably chosen Majorana phases, the matrix element can vanish, despite that the neutrinos are Majorana. This case corresponds to the red region of figure 6.

8.4.1 A curious example of EFT

From an Effective Field Theory point of view, it may seem curious to set restrictive bounds on the coefficient of of the dimension 5 operator $\frac{K}{\Lambda_{NP}}\bar{\ell}H\ell^c H$, from upper bound on coefficients of dimension 9 or 11 operators such as

$$
\begin{array}{cc}
(\bar{u}\gamma^\mu P_R d)(\bar{u}\gamma_\mu P_R d)(\bar{\ell}H)(\ell^c H) & (\bar{q}\tau_i\gamma^\mu P_L q)(\bar{q}\tau_j\gamma_\mu P_L q)(\bar{\ell}\tau_i H)(\ell^c \tau_j H) \\
dim9 & (\bar{u}\gamma^\mu P_R d)(\bar{u}\gamma_\mu P_R d)\bar{e}e^c
\end{array}
$$

because New Physics is expected to appear in lower dimensional operators (those of higher dimension would be suppressed by additional powers of $1/\Lambda_{NP}$).

However, the naive expectation does not take into account the matching of the SMEFT onto a QED×QCD invariant EFT at m_W, where the Higgs gets a vev. Factors of G_F and v can change operator dimensions in this process, for instance the coefficient of the dimension 11 operator is only suppressed by one power of Λ_{NP}:

$$\sim \frac{K}{v^4\Lambda}(\bar{u}\gamma^\mu P_R d)(\bar{u}\gamma_\mu P_R d)(\bar{\ell}H)(\ell^c H)$$

Furthermore, Avogadro's number($\simeq 6 \times 10^{23}$) is large, allowing a great sensitivity to rare decays of otherwise stable particles: $0\nu2\beta$ may occur 10^{-16} times in the age of the Universe, but it still be observed by watching a tonne of material for a year.

9 Mechanisms and models for small neutrino masses

This section outlines a few models involving heavy New Particles, that are renormalisable and can generate Majorana masses for the SM neutrinos at tree level. They are refered to as "seesaw models", because the light SM neutrino masses are obtained as the ratio of larger scales. These models are attractive because they involve a minimal number of new particles and couplings.

There are three models that generate the Majorana mass operator

$$\frac{K}{2\Lambda}[\bar{\ell}H][\ell^c H] \to \bar{\nu}\nu^c \frac{K\langle H_0\rangle^2}{2\Lambda}$$

by tree-level exchange of at most one new particle per generation. The new particle can be an SU(2) singlet fermion (the Type I seesaw [29]), an SU(2) triplet fermion(the Type III seesaw [32]), or a scalar triplet (the Type II seesaw [30, 31]).

9.1 The Type I seesaw, one generation

Consider the type I seesaw [29] in one generation, where a singlet fermion N_R, with all its allowed renormalisable interactions, is added to the SM Lagrangian. It is allowed a Yukawa coupling with the doublet lepton and the Higgs, and a Majorana mass, which is not bounded above by the weak scale because the mass of N is not generated by the Higgs vev. The leptonic Lagrangian, written in terms of chiral fermions, is then:

$$\mathcal{L}_{lep}^{Yuk} = h_e(\overline{\nu_L},\overline{e_L})\begin{pmatrix} -H^+ \\ H^{0*} \end{pmatrix}e_R + \lambda(\overline{\nu_L},\overline{e_L})\begin{pmatrix} H^0 \\ H^- \end{pmatrix}N_R + \frac{M}{2}\overline{N_R^c}N_R + h.c.$$

$$m_e\overline{e_L}e_R \qquad\qquad + m_D\overline{\nu_L}N_R \qquad\qquad + \frac{M}{2}\overline{N_R^c}N_R + h.c.$$

where the second line gives the masses after the Higgs gets a vev. The neutrino mass matrix can be written (in notation where $\nu_L^c \equiv (\nu_L)^c$)

$$\begin{pmatrix} \overline{\nu_L} & \overline{N_R^c} \end{pmatrix}\begin{bmatrix} 0 & m_D \\ m_D & M \end{bmatrix}\begin{pmatrix} \nu_L^c \\ N_R \end{pmatrix}$$

Unlike a Dirac mass matrix, where different fields appear on either side, in this "Majorana" mass matrix, the same chiral degrees of freedom appear on either side: to the left are all the chiral fermions in barred-left-handed form, and to the right, the same fermions appear in unbarred right-handed form.

The eigenvectors/values are approximately ν_L with $m_\nu \sim \frac{m_D^2}{M}$ and N_R with mass $\sim M$.

9.1.1 Factors of 2 in the seesaw

A Majorana mass m_ν appears in the low-energy $\mathcal{L}$ as $\frac{m_\nu}{2}\overline{\nu_L^c}\nu_L + h.c.$. The previous section showed that in the low-energy effective theory after electroweak symmetry breaking, the type-1 seesaw gives $m_\nu = m_D^2/M$. Here we want to check that the same result is obtained with the SU(2) invariant model and operator.

The SU(2)-invariant Majorana mass operator is of dimension 5, and can be written

$$\mathcal{L} \supset \frac{K}{2\Lambda}(\overline{\ell^c}H)(\ell H) + h.c. = \frac{K}{2\Lambda}(\overline{\ell^c}_n\delta^{nN}H_N)(\ell_m\delta^{mM}H_M) + h.c.$$

where n, m, N, M are SU(2) indices that run from 1 to 2. In the high energy SM, with dynamical Higgs, this interaction has Feynman rule:

$$
\begin{aligned}
i\frac{\delta^4\mathcal{L}}{\delta\overline{\ell}_i\delta\ell^c_j\delta H_I\delta H_J} &= i\frac{K}{2\Lambda}\frac{\delta^4\mathcal{L}}{\delta\overline{\ell}_i\delta H_I\delta H_J}((\overline{\ell}H)\delta_{jN}H^N + \delta_{jM}H^M(\overline{\ell}H)) \quad (25)\\
&= i\frac{K}{2\Lambda}\frac{\delta^4\mathcal{L}}{\delta H_I\delta H_J}(\delta_{iN}\delta_{jM} + \delta_{jN}\delta_{iM})H^N H^M \\
&= -i\frac{K}{\Lambda}(\delta_{iI}\delta_{jJ} + \delta_{jI}\delta_{iJ}) \quad (26)
\end{aligned}
$$

Now to match this operator onto the seesaw model, in the seesaw model there is an s and a t channel
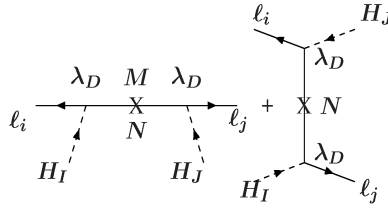

Fig. 7: Seesaw diagrams matching onto the Feynman rule for the one-generation neutrino mass operator, given in eqn (26). i, j, I, J are SU(2) doublet indices that run over 1,2.

diagram, as illustrated in figure 7, so one obtains $\frac{K}{\Lambda} = \frac{\lambda^2}{M}$ in agreement with the result from diagonalising the mass matrix.

9.2 The type I seesaw in three generations

Add 3 singlet N_Rs to the SM (the chiral projection subscript will be dropped in the following to streamline the notation). One can always choose to work in the mass eigenstate basis of the charged leptons and N_Rs, where the Lagrangian can be written

$$\mathcal{L} = \mathcal{L}_{SM} + \boldsymbol{\lambda}_{\alpha J}\overline{\ell_\alpha}\cdot HN_J - \frac{1}{2}\overline{N_J}M_JN_J^c + h.c. \quad (27)$$

The three generation type 1 seesaw adds 18 parameters to the Lagrangian: three (real) singlet masses, and 18 real parameters in the Yukawa matrix λ, from which three phases can be removed by phase choices on the doublets ℓ_α.

In the presence of electroweak symmetry breaking, for $M \gg m_D = \lambda v$, the mass matrix for SM neutrinos is

$$[m_\nu] = \boldsymbol{\lambda}M^{-1}\boldsymbol{\lambda}^T v^2 \ , \quad v = \langle H^0 \rangle \ .$$

In the effective low-energy Lagrangian, where the SM neutrinos have this Majorana mass matrix, there are nine new parameters in the Lagrangian: the three neutrino masses m_1, m_2, m_3 , and the 3 angles and 3 phases of U_{MNS}. There are therefore 9 free parameters of the high-scale model which are inaccessible at low energy, so in a later section of these lectures, it will not come as a surprise that they can be chosen to reproduce the Baryon Asymmetry of the Universe.

An attractive feature of the seesaw, is that one can easily obtain the observed neutrino masses for reasonable choices of the singlet masses M and Yukawas λ. For instance, if the neutrino Yukawa matrix ressembles that of the up-type quarks, with $\lambda \sim h_t$, then $m_\nu \sim .1$ eV is obtained for $M \sim 10^{15}$ GeV. Or if one prefers an electroweak scale $M \sim$ TeV, then $\lambda \sim 10^{-6}$ ($\sim$ the electron Yukawa coupling) generates $m_\nu \sim .1$ eV.

However, a disadvantage of the type I seesaw, is that even if the singlets are kinematically accessible at the LHC, their only coupling to the SM is their Yukawa, which is small and suppresses the production rate.

Another drawback of the non-supersymmetric seesaw is that the neutrino loop contributions to the Higgs mass can be uncomfortably large. A one-loop diagram is illustrated in figure 8. The loop is finite
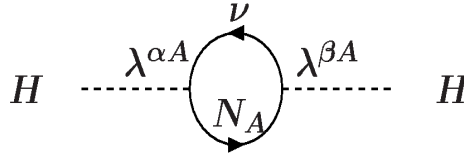

Fig. 8: Loop contribution to the Higgs mass in the seesaw model .

and calculable [33]:

$$\delta m_H^2 \quad \simeq \quad -\sum_I \frac{[\boldsymbol{\lambda}^\dagger \boldsymbol{\lambda}]_{II}}{8\pi^2} M_I^2 \sim \frac{m_\nu M_I^3}{8\pi^2 v^4} v^2 \tag{28}$$

so for $M \gtrsim 10^7$ GeV, this loop gives a larger contribution to the Higgs mass-squared than its observed value. Of course, the Higgs mass sitting in the Lagrangian is unknown, so a cancellation is possible but requires a "tuning" for which no justification is known. Alternatively, the loop contribution can be cancelled by another loop contribution, as arises in, for instance, supersymmetric models.

9.3 A low-scale tree model detectable at the LHC: the inverse seesaw

The "inverse seesaw" [34] is a model that gives Majorana masses of the observed magnitude to the SM neutrinos, and contains heavy singlets that could be found at the LHC. There are more new particles than in the type 1 seesaw.

For each generation, add two gauge-singlet, chiral fermions N, S, which share a $\sim$ TeV-scale Dirac mass. In the one generation case:

$$\mathcal{L} = \mathcal{L}_{SM} + \boldsymbol{\lambda}\overline{N}\ell \cdot H - \overline{N}MS - \frac{1}{2}\overline{S}\mu S^c \tag{29}$$

where N is the usual "right-handed neutrino" who interacts with the SM doublet leptons via the Yukawa coupling, and N and S share a TeV-scale Dirac mass M. Then a small ($\sim$ keV) Majorana mass μ is added for S. In the limit $\mu = 0$, lepton number conserved, and L=1 for ℓ, N, S^c. However $m_\nu = 0$ in

this limit, as can by writing the 1 generation mass matrix in Majorana form

$$
\begin{pmatrix} \overline{\nu_L} & \overline{N^c} & \overline{S} \end{pmatrix}
\begin{bmatrix} 0 & m_D & 0 \\ m_D & 0 & M \\ 0 & M & \mu \end{bmatrix}
\begin{pmatrix} \nu_L^c \\ N \\ S^c \end{pmatrix} \ .
$$

For $\mu = 0$ the determinant vanishes, but S and N share a Dirac mass M, so ν_L must be massless. For $\mu \neq 0$, the determinant is μm_D^2, so for $M > m_D \gg \mu$, the three masses are $M, M, m_D^2 \mu / M^2$. It is straightforward to check that for $\lambda \sim 0.1$, $M \sim$ TeV, and $\mu \sim 0.1$ keV, $m_\nu \sim .1$eV is obtained. So as advertised, this model gives naturally small m_ν, and singlets with TeV masses and with $\mathcal{O}(1)$ yukawa couplings.

The three generation light neutrino mass matrix in this model:

$$
[m_\nu] \;\; = \;\; [\boldsymbol{\lambda}][M]^{-1}[\mu][M]^{-1}[\boldsymbol{\lambda}]^T v^2 \sim .05 \text{ eV}
$$

(in square brackets are matrices) can be obtained diagrammatically from figure 9, where one distributes the various mass insertions upstairs in the fraction if they are small, and downstairs if they are large.
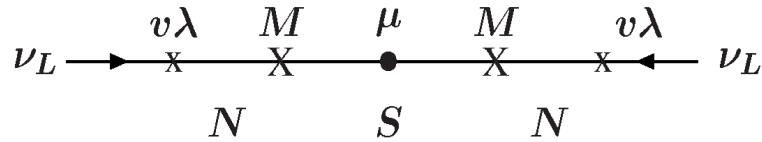

Fig. 9: Diagram for the SM neutrino mass in the inverse seesaw model

10 Leptogenesis

Leptogenesis [1, 41] is a class of recipes, that use majorana neutrino mass models to generate the matter excess of the Universe. The model generates a lepton asymmetry (before the Electroweak Phase Transition), and the non-perturbative SM B+L violation reprocesses it to a baryon excess.

10.1 The Matter Excess of the Universe

If you step out the door in the countryside at night, the sky is decorated with stars. Like us, they are all made of matter, and the puzzle is to understand the origin of this excess of matter over anti-matter in our Universe.

Stars are mostly made of Hydrogen, containing a proton(baryon) and an electron. So the matter excess is equivalent to an excess of baryons over anti-baryons. Leptons are neglected in this discussion, because (despite that every Hydrogen contains an electron), there should be a Cosmic Background of Neutrinos whose density is far higher than that of electrons, which could contain a significant (and difficult-to-observable) lepton asymmetry today.

We define the nucleons that we are made of to be baryons (as opposed to anti-baryons), then by touching objects around us, we observe that they are also made of baryons (as opposed to anti-baryons) because matter combined with anti-matter becomes a puff of photons. This argument can be extended to the solar system (bathed in the solar wind), and to the scale of galaxy clusters, because if a cluster of matter brushing against a cluster of anti-matter, photons would be produced by proton-antiproton annihilation, and these are not observed in the cosmological spectrum. So we assume that all the Universe *we see* is made of matter (dark matter, of course, can be matter-antimatter symmetric).

The matter density of the Universe ($\sim 5\%$ of the energy budget today) can be quantified [35] as

$$Y_B \equiv \left.\frac{n_B - n_{\bar{B}}}{s}\right|_0 = 3.86 \times 10^{-9}\Omega_B h^2 \simeq (8.53 \pm 0.11) \times 10^{-11}$$

where s is the entropy density (conserved during most the Universe history) whose value today s_0 is about $7\times$ the number density of CMB photons, and $n_B, (n_{\bar{B}})$ is the number density of (anti)baryons. So in practise, there are 6 baryons for every 10^{10} photons in our Universe today.

A first question about the baryon asymmetry, is "where did it come from?"

1. For instance, maybe the Universe is matter-anti-matter symmetric, but composed of islands of matter and anti-matter? The islands would need to be larger than galaxy clusters, in order to agree with the photon background, and it appears more difficult to make a model that spatially separates baryons from anti-baryons than to make a model that generates an asymmetry. So this idea is not pursued.

2. Putting the baryon excess as an initial condition at the birth of the Universe does not work to well either, because a period of inflation is required to explain the large-scale coherent temperature fluctuations in the CMB. After "60 e-folds" of inflation, the volume of the Universe has grown by $\sim (10^{30})^3$, so any pre-existing density of baryons is decreased by $\sim 10^{-90}$...and the energy density that drives inflation usually appears as entropy after inflation, so it seems difficult to obtain $Y_B \sim 10^{-10}$ this way.

So it seems that the baryon asymmetry needs to be generated in the early Universe after inflation.

10.2 Required Ingredients

There are many recipes for making the baryon asymmetry, but they all share three required ingredients, initially given by Sakharov [36] and sometimes called Sakharov conditions:

1. Baryon number violation : if the Universe starts in a state of $n_B - n_{\bar{B}} = 0$, then $\not{B}$ is required to evolve to $n_B - n_{\bar{B}} \neq 0$.

2. C and CP violation : it is clear that particles need to behave differently from anti-particles. Otherwise the particles would make a baryon asymmetry, the anti-particles would make an anti-baryon asymmetry of the same magnitude, and no net asymmetry would be created.
   C is maximally violated in the SM, and CP violation is present in the SM quarks, observed in Kaons and Bs, and current neutrino oscillation data favours a non-zero phase in the leptonic mixing matrix.

3. departure from thermal equilibrium: the generation of the baryon asymmetry is a dynamical process, so cannot occur in thermal equilibrium, which is static. An alternate way to see this, is that there are no asymmetries in un-conserved quantum numbers in equilibrium (and B is not conserved, by condition 1).
   In the standard cosmological model, departures from equilibrium can be obtained by interactions that occur on timescales of order or longer than the age of the Universe, or at phase transitions.

10.2.1 B non-conservation in the SM

The second and third Sakharov conditions are realised in the Standard Model (of particle physics and cosmology). And contrary to superficial expectations, it turns out that B+L violation is also present in the SM, and rapid at temperatures above m_W.

B and L are global symmetries of the SM Lagrangian, in which appear terms of the form

$$\mathcal{L}_{SM} \supset \bar{q}\not{D}q \ , \ \bar{\ell}\not{D}\ell \ , \ \bar{\ell}He \ , \ \bar{q}\widetilde{H}u \ , \ \bar{q}Hd$$

where q, ℓ are the quark and lepton SU(2) doublets, e, u, and d are the SU(2) singlets. So it is clear that there are symmetries under phase rotations of all the leptons, or all the quarks, or equivalently, that all the Feynman rules conserve B and L. This is reassuring, because the lower bound on the proton lifetime, for decays such as $p \to e^+ \pi_0$ is $\gtrsim 10^{33}$ years (to be compared with the age of the Universe $\gtrsim 10^{10}$ yrs).

Nonetheless, the SM *does not conserve* $B + L$. This is a consequence of the axial anomaly [37] in QFT, which says that axial currents (containing a γ_5, which count the number of left minus right fermions) which appear conserved at the classical level, are not conserved at one loop.

We are interested in $B + L$. This is not a pure axial current (left - right), but it is classically conserved and has an axial component because the SM is a chiral theory. As a result of the anomaly, one obtains for one generation(α is colour)

$$\sum_{\substack{SU(2) \\ singlets}} \partial^\mu(\overline{\psi}\gamma_\mu\psi) + \partial^\mu(\overline{\ell}\gamma_\mu\ell) + \partial^\mu(\overline{q}^\alpha\gamma_\mu q_\alpha) \propto \frac{1}{64\pi^2} W^A_{\mu\nu}\widetilde{W}^{\mu\nu A}.$$

where integrating the RHS over space-time counts the "winding number" of the SU(2) gauge field configuration. As a result, W field configurations of non-zero winding number are sources of a doublet lepton and three (for colour) doublet quarks for each generation (no singlets because they do not have SU(2) interactions). These field configurations therefore change baryon and lepton number by three units (one for each generation).

It is curious that this (non-perturbative) effect does not appear in the Feynman rules. Some intuition for what is happening can be obtained in the Dirac sea picture of the fermion vacuum, illustrated in the following figure(for which I think V Rubakov). At $t \to -\infty$, on the left of the figure, is a vacuum. Then at $t = 0$, is a W field configuration of finite winding number — for each doublet field of the SM, one of the negative energy states from the sea becomes a positive energy state.

Left−handed fermions
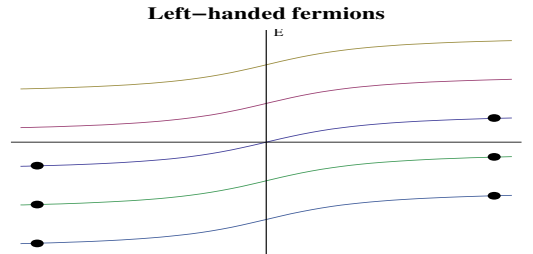
For baryogenesis, it is important to know the rate for this SM non-perturbative B+L violation. At zero temperature, it is tunneling process (from a vaccuum with one winding number to the next), and exponentially suppressed [38] $\Gamma \propto e^{-8\pi/g^2}$ (this is usually negligeable). At finite temperature, $0 < T < m_W$, the fields can climb over the barrier and the rate is only Boltzmann suppressed [39]: $\Gamma_{\not{B}\not{+}\not{L}} \sim e^{-m_W/T}$, and finally most interestingly, $\Gamma_{\not{B}\not{+}\not{L}} \sim \alpha^5 T$ for $T > m_W$ so SM $\not{B}\not{+}\not{L}$ is "in equilibrium (=fast) for $m_W < T < 10^{12}$ GeV. This SM $\not{B}\not{+}\not{L}$ is sometimes called "sphalerons", and in the presence of a lepton asymmetry, they partially transform it to a baryon asymmetry.

10.2.2   *Summary of preliminaries:*

There are three required ingredients to generate the Baryon asymmetry of the Universe :$\not{B}$, $\mathcal{CP}$, and $\not{T}\mathcal{E}$. They are all present in the Standard Models of particle physics and cosmology, but to my knowledge noone has succeeded[7] to combine them so as to obtain a big enough asymmetry Y_B. So the baryon asymmetry is usually taken to be evidence for New Physics from Beyond the Standard Model. However,

---

[7]The cold electroweak baryogenesis mechanism of Tranberg *etal* [40] is interesting.

since there is only one number to fit, and NP models have many parameters, it is motivated to try to make the baryon asymmetry in models that are introduced for some other reason... such as the type 1 seesaw, which can fit the observed neutrino masses and mixings, and will be discussed next.

10.3   Leptogenesis in the type I seesaw

This section sketches how leptogenesis occurs in seesaw models with mediators of mass $M \gtrsim, \gg$ TeV. To be concrete, the type 1 seesaw is discussed ; the details are different in the type 2 and 3 seesaws, but the general picture is similar.

The type one seesaw Lagrangian is given in eqn (27). Recall first that for $\lambda \sim 1$, the singlets should have masses $\lesssim 10^{15}$ GeV. So here, suppose that the lightest singlet, N_1, has a mass $M_1 \sim 10^9$ GeV, and that the reheat temperature of the Universe after inflation $T_{reheat} \gtrsim M_1$. Different mass spectra for the singlets will be discussed afterwards. Recall also that the 3 generation type-1 seesaw has 18 parameters in the high-scale Lagrangian, to be compared with the 3 masses, 3 mixing angles and 3 phases of the low-energy majorana mass matrix for SM neutrinos. This implies that there are numerous parameters in the high-energy Lagrangian that can be ajusted to obtain the correct baryon asymmetry, without observable consequences. Leptogenesis in the type 1 seesaw (originally proposed by [41]) with heavy singlets is therefore something of a fairy tale for physicists, and its as a fairy tale that it is presented here.

10.3.1   *The Fairy Tale*

Once upon a time, a Universe was born. So all the fairies came to the christening of the Universe...

... and gave to the Universe the Standard Model and the Seesaw (heavy sterile N_j with $\not{L}$ masses and $\not{CP}$ interactions).

The adventure begins after inflationary expansion of the Universe:

1. If its hot enough, a population of Ns appear(they like heat).
2. The temperature drops below M, and the N population decays away.
3. In the $\not{CP}$ and $\not{L}$ interactions of the N, an asymmetry in SM leptons is created.
4. If this asymmetry can escape the big bad wolf of thermal equilibrium...
5. ...the lepton asym gets partially reprocessed to a baryon asymmetry by non-perturbative $B + L$ -violating SM processes ("sphalerons").

And the Universe lived happily ever after, containing many photons. And for every 10^{10} photons, there were 6 extra baryons (wrt anti-baryons).

10.3.2 To calculate something?

There are a very large number of bayogenesis scenarios, and in some cases the state of the art in calculating the dynamics is advanced (quantum field theory of oscillations at finite temperature in curved space-time). The aim here is simpler: given a baryogenesis scenario at the "fairy tale" level, how does one estimate whether it could work? For this, it is helpful to focus on the Sakharov conditions, calculate a suppression factor for each Sakharov condition, then multiply them together to get Y_B:

$$\frac{n_B - n_{\bar{B}}}{s} \sim \frac{1}{3g_*}\epsilon\eta \sim 10^{-3}\epsilon\eta \qquad (\text{want } 10^{-10}) \tag{30}$$

where the entropy density in the early Universe at temperature T is $s \sim g_* n_\gamma$ (g_* counts the number of light modes, the definition can be found in table A.1 of [1]), ϵ is the lepton asymmetry generated in the CP and L violating interactions, and η is some measure of the departure from thermal equilibrium.

As an illustration, we estimate η and ϵ for the fairy tale. Suppose at $T \gtrsim M_1$, an N_1 density $\sim T^3$ is produced. Later, at the temperature drops below M_1 the N_1 population starts to decay away. We assume that a lepton asymmetry is always generated in these decays; however, it can only *survive* if it is not washed out by inverse decays $H\ell \to N_1$. Or equivalently, the asymmetry can only survive after the inverse decays go out of equilibrium

$$\Gamma_{ID}(H\ell \to N) \simeq \Gamma(N \to H\ell)e^{-M_1/T} = \frac{[\lambda\lambda^\dagger]_{11}M_1}{8\pi}e^{-M_1/T} < \mathcal{H} \sim \frac{10T^2}{m_{pl}} \tag{31}$$

where the out-of-equilibrium condition is that the rate is small compared to $\mathcal{H}$, the expansion rate of the Universe[8].

Since the interactions of the Ns are in equilbrium, they should follow a thermal Boltzmann distribution, so the fraction of N_1 remaining at T_{ID} (=when the inverse decays turn off), is

$$\frac{n_N}{n_\gamma}(T_{ID}) \simeq e^{-M_1/T_\alpha} \simeq \frac{\mathcal{H}}{\Gamma(N \to \ell_\alpha H)} \equiv \eta \tag{32}$$

where $\mathcal{H}$ is the Hubble expansion rate $\sim 10T^2/m_{pl}$. This is the density of N_1 whose decays can contribute to the baryon asymmetry of the Universe.

Now estimate ϵ, the CP asymmetry in decays. The constraints from unitarity and CPT and general results of about CP violation are clearly presented in the Appendix of [42]. Recall that the CP transformation is defined, in the **S**-matrix as

$$CP : \langle H\ell|\boldsymbol{S}|N\rangle \to \langle \overline{H\ell}|\boldsymbol{S}|\overline{N}\rangle = \langle \overline{H\ell}|\boldsymbol{S}|N\rangle \tag{33}$$

---

[8]equivalently, one can say that the interaction timescale is long compared to the age of the Universe

where overline means the CP-conjugate particle (anti-particle). N is its own anti-particle because it is Majorana.

In leptogenesis, we are interested in the $\cancel{CP}$, $\cancel{L}$ interactions of N_I. In the fairy tale, we only included decays, so consider the asymmetry:

$$\epsilon_1^\alpha \;=\; \frac{\Gamma(N_1 \to H\ell_\alpha) - \Gamma(\bar{N}_1 \to \bar{H}\bar{\ell}_\alpha)}{\Gamma(N_1 \to H\ell) + \Gamma(\bar{N}_1 \to \bar{H}\bar{\ell})} \qquad (\text{recall } N_1 = \bar{N}_1) \tag{34}$$

which represents the fraction of N_1 decays producing excess leptons. It is labelled by lepton flavour, because the flavour is relevant in detailed calculations, but from now on here, we sum on α and drop the α index.
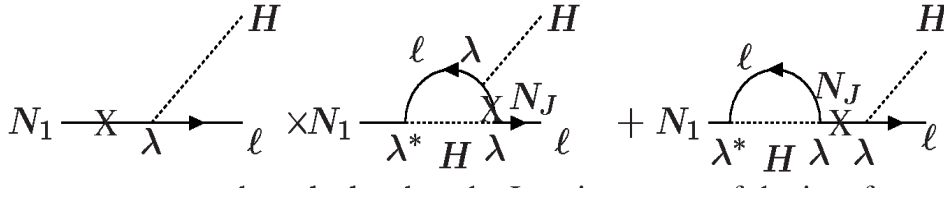

Fig. 10: Tree×loop diagrams generating a CP asymmetry ϵ in the decay of the heavy singlet N_1.

The asymmetry ϵ_1 can be calculated as the Imaginary part of the interference of tree $\times$ loop diagrams illustrated in figure 10 [43]. The $\cancel{CP}$ arises from complex coupling, and must be multiplied by an imaginary part of the amplitude (sometimes refered to as a "strong phase") arising from some particles in the loop being on-shell. So in practise, it arises from the Imaginary part of the Feynman parameter integration that one performs in evaluating a loop integral in dimensional regularisation. This is not very intuitive, so lets try to estimate ϵ without doing a loop calculation. This is possible because some of the loop particles need to be on-shell in order to give the strong phase.

The unitarity and CPT invariance of S-matrix elements can be used to calculate ϵ from tree amplitudes. However, here we just estimate diagrammatically. Consider $M_1 \ll M_{2,3}$, so in the loop diagrams contributing to ϵ, the internal N_J can be replaced by the SM neutrino mass matrix $\frac{[K]_{\alpha\beta}}{\Lambda} \equiv \frac{[m_\nu]_{\alpha\beta}}{v^2}$. This works because the momentum in the loop is of order M_1 (so can be neglected compared to $M_{2,3}$), and N_1 on the internal line does not contribute because the coupling constant combination must be Imaginary. Then can estimate

$$\epsilon_1 \sim \frac{1}{16\pi^2} \frac{\lambda^2 K}{\lambda^2 \Lambda} M_1 \;\;<\;\; \frac{3}{8\pi} \frac{m_\nu^{max} M_1}{v^2} \;\sim\; 10^{-6} \frac{M_1}{10^9 \text{GeV}}$$

where in the first estimate, the $1/16\pi^2$ is for the loop (but for the Im part of the loop, one should really take $1/8\pi$), the $|\lambda|^2$ downstairs is because ϵ is normalised to Γ, and the mass factor M_1 is to make the dimensions work. The second inequality is a $\sim$ in our approach here, it gives an idea of the magnitude of ϵ, assuming that the phases cooperate. However, in a more careful derivation, the inequality is an upper bound, which combined with eqn (30):

$$\frac{n_B - n_{\bar{B}}}{s} \;\sim\; 10^{-3} \epsilon \eta \sim 10^{-3} \frac{\mathcal{H}}{\Gamma} 10^{-6} \frac{M_1}{10^9 \text{GeV}}$$

implies that one needs $M_1 \gtrsim 10^9$ GeV to get a sufficient asymmetry $Y_B \sim 10^{-10}$ for hierarchical singlets in the type 1 seesaw.

10.3.3 Leptogenesis for $M_1 < 10^9$ GeV?

Singlets with $M \gtrsim 10^9$ GeV have some undesirable features: they are not kinematically accessible at upcoming colliders, and overcontribute to the Higgs mass (see eqn 28). The contribution to the Higgs mass can be cancelled by considering the SUSY seesaw, but in some low-scale (< 10 TeV) SUSY models, gravitinos are over-produced in the early Universe if the reheat temperature is above $\sim 10^5$ GeV (so heavy supersymmetric Ns may have troubles too). Fortunately it is simple to do leptogenesis with TeV $< M_K < 10^7$ GeV: for $M_I \sim M_J$ the second loop diagram of figure 10 resonantly enhances ϵ, allowing to reach $\epsilon \lesssim 1/8\pi$.

In the leptogenesis scenario discussed here, where the asymmetry is produced in N decay, there is a lower bound on the singlet mass from requiring that the asymmetry be produced before the Electroweak Phase Transition (in order to profit from sphalerons):

$$\Gamma_{ID} \sim e^{-M/T}\Gamma(N \to \phi\ell) < H \quad \Rightarrow \quad M \gtrsim 10T_c$$

where $T_c \sim 100$ GeV is the critical temperature of the electroweak phase transition (a cross-over in the SM). So in summary, the fairy tale can work for N_I with $M_I \gtrsim$ TeV.

Leptogenesis can also work with lighter singlets (who decay after the electroweak phase transition), provided that the asymmetry is generated as the singlets are produced. The scenario outlined here relies in oscillations among the singlets, so they must be sufficiently degenerate ($m_{N_2} \simeq m_{N_3}$). This was initially explored in [44], then revisited in the context of the νM(inimal)SM — see for instance [45, 46]. Here is presented only a superficial summary.

The singlets N are "light" (suppose 1 GeV), so the Yukawas λ are necessarily small: $\lambda \sim \sqrt{\frac{m_\nu * \text{GeV}}{v^2}} \lesssim 10^{-7}$. The N_2, N_3 start being produced at temperatures $T \lesssim$ TeV, via their Yukawa interactions. Then they oscillate, among themselves and can transform back to doublet leptons via the Yukawa interactions. These three processes occur coherently, so CP violation in $\lambda\Delta M^2\lambda^T$ generates lepton flavour asymmetries in the $\nu_{L\alpha}$ (Notice that lepton number in $\ell_L + N_R$, defined as $L|_{SM}$ + helicity of N, is conserved in these processes.). The sphalerons only see the lepton number in the SM doublets, and partially transform it to a baryon asymmetry. From the time oscillations start, until the sphalerons turn off at the electroweak phase transition, the asymmetries in the $\nu_{L\alpha}$ seed asymmetries in the N which give larger asymmetries in the $\nu_{L\alpha}$. Recent calculations (see *e.g.* [47]) show that a sufficiently large baryon asymmetry can be obtained.

11 The End

Most of the students at the school work at hadron colliders, where neutrinos are missing energy. However, neutrino physics might by interesting for two reasons: the observed neutrino masses are evidence for Beyond-the Standard Model Physics (and its encouraging to know that BSM exists somewhere, despite being shy at the LHC), and secondly, the Standard Model neutrino lives in an SU(2) doublet, so there should be BSM physics involving charged leptons — we just need to find it.

12 Appendix: To convert from 4- to 2-component fermion notation

A 4-component fermion ψ_D can be written as two chiral 2-comp fermions (LeftHanded = χ, and RightHanded = $\bar{\eta}$):

$$\psi_D = \begin{pmatrix} \chi_\alpha \\ \bar{\eta}^{\bar{\beta}} \end{pmatrix}$$

where usual dotted indices of the right-handed fermion are here written barred. The 2-comp indices α and $\bar{\beta}$ run from 1..2, and are contracted with the anti-symmetric epsilon tensor

$$\varepsilon_{\bar{\alpha}\bar{\beta}} = \varepsilon^{\alpha\beta} = \begin{pmatrix} 0 & 1 \\ -1 & 0 \end{pmatrix}, \; \varepsilon^{\bar{\alpha}\bar{\beta}} = \varepsilon_{\alpha\beta} = -\varepsilon^{\alpha\beta}$$

Notice the sign flip in going from dotted to undotted indices.

Undotted indices are always contracted up-down:

$$\chi\rho = \chi^\alpha \rho_\alpha = \varepsilon^{\alpha\beta}\chi_\beta\rho_\alpha = -\rho_\alpha\chi^\alpha = \rho^\alpha\chi_\alpha$$

and dotted indices down-up, and the ε flips sign in getting bars (sign flip because of up-down vs down-up summing conventions: $\bar{\rho}^{\bar{\beta}} = \bar{\rho}_{\bar{\alpha}}\varepsilon^{\bar{\alpha}\bar{\beta}}$, but $\bar{\rho}^{\bar{\beta}} = (\rho^\beta)^* = (\rho_\alpha\varepsilon^{\beta\alpha})^*$. This perverse set of conventions is so that one can copy Wess+Bagger(W+B) 2-component spinor results, and also Peskin and Schroeder. W+B define

$$\begin{aligned} (\eta\rho)^* &= (\eta\rho)^\dagger = (\varepsilon^{\alpha\beta}\eta_\alpha\rho_\beta)^* = (-\varepsilon^{\bar{\alpha}\bar{\beta}})\bar{\rho}_{\bar{\beta}}\bar{\eta}_{\bar{\alpha}} \\ &= \bar{\rho}_{\bar{\alpha}}\bar{\eta}^{\bar{\alpha}} \end{aligned}$$

So, eg

$$\bar{\psi}_D = \begin{pmatrix} \bar{\chi}_{\bar{\alpha}}\eta^\beta \end{pmatrix} \begin{pmatrix} 0 & \delta^{\bar{\alpha}}_{\bar{\rho}} \\ \delta^\omega_\beta 0 \end{pmatrix} = \begin{pmatrix} \eta^\omega & \bar{\chi}_{\bar{\rho}} \end{pmatrix} \tag{35}$$

In practice, there is a -ve sign from interchanging fermion fields in an operator, but not when you take cc of the op.

References

[1] chapter 4 of S. Davidson, E. Nardi and Y. Nir, "Leptogenesis," Phys. Rept. **466** (2008) 105 doi:10.1016/j.physrep.2008.06.002 [arXiv:0802.2962 [hep-ph]].
See also, for instance, W. Buchmuller, P. Di Bari and M. Plumacher, "Leptogenesis for pedestrians," Annals Phys. **315** (2005) 305 [arXiv:hep-ph/0401240].

[2] A. Boyarsky, A. Neronov, O. Ruchayskiy and M. Shaposhnikov, "Restrictions on parameters of sterile neutrino dark matter from observations of galaxy clusters," Phys. Rev. D **74** (2006) 103506 doi:10.1103/PhysRevD.74.103506 [astro-ph/0603368].

[3] F. Iocco, G. Mangano, G. Miele, O. Pisanti and P. D. Serpico, "Primordial Nucleosynthesis: from precision cosmology to fundamental physics," Phys. Rept. **472** (2009) 1 doi:10.1016/j.physrep.2009.02.002 [arXiv:0809.0631 [astro-ph]].

[4] Neutrino Cosmology, J Lesgourgues, G Mangano, S Pastor, Cambridge University Press, (or other reviews by the same authors).

[5] See G. Raffelt's website: http://wwwth.mpp.mpg.de/members/raffelt/

[6] A. Strumia and F. Vissani, "Neutrino masses and mixings and...," hep-ph/0606054.
See also the next reference, and later reviews by some of the authors.

[7] M. C. Gonzalez-Garcia and Y. Nir, "Neutrino masses and mixing: Evidence and implications," Rev. Mod. Phys. **75** (2003) 345 doi:10.1103/RevModPhys.75.345 [hep-ph/0202058].

[8] Giunti website "neutrino unbound": http://www.nu.to.infn.it/
fits: http://www.nu-fit.org/
Recent summaries at the CERN ν platform kickoff:
https://indico.cern.ch/event/572831/

[9] A. Cervera, A. Donini, M. B. Gavela, J. J. Gomez Cadenas, P. Hernandez, O. Mena and S. Rigolin, "Golden measurements at a neutrino factory," Nucl. Phys. B **579** (2000) 17 Erratum: [Nucl. Phys. B **593** (2001) 731] doi:10.1016/S0550-3213(00)00606-4, 10.1016/S0550-3213(00)00221-2 [hep-ph/0002108]. See also later papers refering to this.

[10] see the website www.nu-fit.org, or I. Esteban, M. C. Gonzalez-Garcia, M. Maltoni, I. Martinez-Soler and T. Schwetz, JHEP **1701** (2017) 087 doi:10.1007/JHEP01(2017)087 [arXiv:1611.01514 [hep-ph]].
See also *etal* and Tortola, *eg* P. F. de Salas, D. V. Forero, C. A. Ternes, M. Tortola and J. W. F. Valle, "Status of neutrino oscillations 2017," arXiv:1708.01186 [hep-ph].

[11] C. Patrignani et al. (Particle Data Group), Chin. Phys. C, 40, 100001 (2016).

[12] B. T. Cleveland, T. Daily, R. Davis, Jr., J. R. Distel, K. Lande, C. K. Lee, P. S. Wildenhain and J. Ullman, "Measurement of the solar electron neutrino flux with the Homestake chlorine detector," Astrophys. J. **496** (1998) 505. doi:10.1086/305343

[13] J. N. Bahcall and R. K. Ulrich, "Solar Models, Neutrino Experiments and Helioseismology," Rev. Mod. Phys. **60** (1988) 297. doi:10.1103/RevModPhys.60.297

[14] Q. R. Ahmad *et al.* [SNO Collaboration], "Direct evidence for neutrino flavor transformation from neutral current interactions in the Sudbury Neutrino Observatory," Phys. Rev. Lett. **89** (2002) 011301 doi:10.1103/PhysRevLett.89.011301 [nucl-ex/0204008].

[15] Y. Fukuda *et al.* [Super-Kamiokande Collaboration], "Evidence for oscillation of atmospheric neutrinos," Phys. Rev. Lett. **81** (1998) 1562 doi:10.1103/PhysRevLett.81.1562 [hep-ex/9807003].

[16] G. Anamiati, R. M. Fonseca and M. Hirsch, "Quasi Dirac neutrino oscillations," arXiv:1710.06249 [hep-ph].

[17] E. K. Akhmedov and A. Y. Smirnov, "Paradoxes of neutrino oscillations," Phys. Atom. Nucl. **72** (2009) 1363 doi:10.1134/S1063778809080122 [arXiv:0905.1903 [hep-ph]].

[18] M. Blennow and A. Y. Smirnov, "Neutrino propagation in matter," Adv. High Energy Phys. **2013** (2013) 972485 doi:10.1155/2013/972485 [arXiv:1306.2903 [hep-ph]].

[19] L. Escudero [T2K Collaboration], "Initial Probe of δ_{CP} by the T2K Experiment with ν_μ Disappearance and ν_e Appearance," Nucl. Part. Phys. Proc. **273-275** (2016) 1814. doi:10.1016/j.nuclphysbps.2015.09.292
See also the talk of A.Y. Smirnov at Padua (link on Giunti's webpage of ref [7], under lectures, pheno):
http://active.pd.infn.it/g4/seminars/2016/files/smirnov.pptx

[20] E. K. Akhmedov, S. Razzaque and A. Y. Smirnov, "Mass hierarchy, 2-3 mixing and CP-phase with Huge Atmospheric Neutrino Detectors," JHEP **1302** (2013) 082 Erratum: [JHEP **1307** (2013) 026] doi:10.1007/JHEP02(2013)082, 10.1007/JHEP07(2013)026 [arXiv:1205.7071 [hep-ph]].

[21] M. G. Aartsen *et al.* [IceCube PINGU Collaboration], "Letter of Intent: The Precision IceCube Next Generation Upgrade (PINGU)," arXiv:1401.2046 [physics.ins-det].
U. F. Katz [KM3NeT Collaboration], "The ORCA Option for KM3NeT," [arXiv:1402.1022 [astro-ph.IM]].

[22] R. Acciarri *et al.* [DUNE Collaboration], "Long-Baseline Neutrino Facility (LBNF) and Deep Underground Neutrino Experiment (DUNE) : Volume 2: The Physics Program for DUNE at LBNF," arXiv:1512.06148 [physics.ins-det].

[23] E. Di Valentino, A. Melchiorri and J. Silk, "Beyond six parameters: extending ΛCDM," Phys. Rev.

D **92** (2015) no.12, 121302 doi:10.1103/PhysRevD.92.121302 [arXiv:1507.06646 [astro-ph.CO]].

[24] http://www.katrin.kit.edu/

[25] A. Ringwald and Y. Y. Y. Wong, "Gravitational clustering of relic neutrinos and implications for their detection," JCAP **0412** (2004) 005 doi:10.1088/1475-7516/2004/12/005 [hep-ph/0408241].

[26] A. G. Cocco, G. Mangano and M. Messina, "Probing low energy neutrino backgrounds with neutrino capture on beta decaying nuclei," JCAP **0706** (2007) 015 doi:10.1088/1475-7516/2007/06/015 [hep-ph/0703075].
There is also a (proposed?) experiment, PTOLEMY, see arXiv:1307.4738 [astro-ph.IM].

[27] J. D. Vergados, H. Ejiri and F. Simkovic, "Theory of Neutrinoless Double Beta Decay," Rept. Prog. Phys. **75** (2012) 106301 doi:10.1088/0034-4885/75/10/106301 [arXiv:1205.0649 [hep-ph]].

[28] S. Dell'Oro, S. Marcocci, M. Viel and F. Vissani, "Neutrinoless double beta decay: 2015 review," Adv. High Energy Phys. **2016** (2016) 2162659 doi:10.1155/2016/2162659 [arXiv:1601.07512 [hep-ph]].

[29] The original seesaw references are:
P. Minkowski, Phys. Lett. B **67** (1977) 421; M. Gell-Mann, P. Ramond and R. Slansky, *Proceedings of the Supergravity Stony Brook Workshop*, New York 1979, eds. P. Van Nieuwenhuizen and D. Freedman; T. Yanagida, *Proceedinds of the Workshop on Unified Theories and Baryon Number in the Universe*, Tsukuba, Japan 1979, ed.s A. Sawada and A. Sugamoto; R. N. Mohapatra, G. Senjanovic, *Phys.Rev.Lett.* **44** (1980)912.

[30] R. N. Mohapatra and G. Senjanovic, "Neutrino Masses and Mixings in Gauge Models with Spontaneous Parity Violation," Phys. Rev. D **23** (1981) 165. doi:10.1103/PhysRevD.23.165
M. Magg and C. Wetterich, "Neutrino Mass Problem and Gauge Hierarchy," Phys. Lett. **94B** (1980) 61. doi:10.1016/0370-2693(80)90825-4

[31] J. Schechter and J. W. F. Valle, "Neutrino Masses in SU(2) x U(1) Theories," Phys. Rev. D **22** (1980) 2227. doi:10.1103/PhysRevD.22.2227

[32] R. Foot, H. Lew, X. G. He and G. C. Joshi, "Seesaw Neutrino Masses Induced by a Triplet of Leptons," Z. Phys. C **44** (1989) 441. doi:10.1007/BF01415558 E. Ma and D. P. Roy, "Heavy triplet leptons and new gauge boson," Nucl. Phys. B **644** (2002) 290 doi:10.1016/S0550-3213(02)00815-5 [hep-ph/0206150].

[33] F. Vissani, "Do experiments suggest a hierarchy problem?," Phys. Rev. D **57** (1998) 7027 doi:10.1103/PhysRevD.57.7027 [hep-ph/9709409].

[34] An early inverse seesaw reference is M. C. Gonzalez-Garcia, A. Santamaria and J. W. F. Valle, "Isosinglet Neutral Heavy Lepton Production in Z Decays and Neutrino Mass," Nucl. Phys. B **342** (1990) 108. doi:10.1016/0550-3213(90)90573-V
more details can be found in A. Pilaftsis, "Radiatively induced neutrino masses and large Higgs neutrino couplings in the standard model with Majorana fields," Z. Phys. C **55** (1992) 275 doi:10.1007/BF01482590 [hep-ph/9901206].

[35] P. A. R. Ade *et al.* [Planck Collaboration], "Planck 2015 results. XIII. Cosmological parameters," Astron. Astrophys. **594** (2016) A13 doi:10.1051/0004-6361/201525830 [arXiv:1502.01589 [astro-ph.CO]].

[36] A. D. Sakharov, "Violation of CP Invariance, c Asymmetry, and Baryon Asymmetry of the Pisma Zh. Eksp. Teor. Fiz. **5** (1967) 32 [JETP Lett. **5** (1967 SOPUA,34,392-393.1991 UFNAA,161,61-64.1991) 24].

[37] A clear introduction to the anomaly can be found in section 6.3 of Polyakov, "Gauge Fields + Strings".

[38] G. 't Hooft, "Symmetry Breaking Through Bell-Jackiw Anomalies," Phys. Rev. Lett. **37** (1976) 8. doi:10.1103/PhysRevLett.37.8

[39] The original "sphaleron" paper is : F. R. Klinkhamer and N. S. Manton, "A Saddle Point Solution

in the Weinberg-Salam Theory," Phys. Rev. D **30** (1984) 2212. doi:10.1103/PhysRevD.30.2212

The rates above and below the phase transition are discussed in : Y. Burnier, M. Laine and M. Shaposhnikov, "Baryon and lepton number violation rates across the electroweak crossover," JCAP **0602** (2006) 007 doi:10.1088/1475-7516/2006/02/007 [hep-ph/0511246].

[40] See other references by the same author, and *eg* A. Tranberg, "Standard Model CP-violation and Cold Electroweak Baryogenesis," Phys. Rev. D **84** (2011) 083516 doi:10.1103/PhysRevD.84.083516 [arXiv:1009.2358 [hep-ph]].

[41] The original leptogenesis paper: M. Fukugita and T. Yanagida, "Baryogenesis Without Grand Unification," Phys. Lett. B **174** (1986) 45.

[42] E. W. Kolb and S. Wolfram, "Baryon Number Generation in the Early Universe," Nucl. Phys. B **172** (1980) 224 Erratum: [Nucl. Phys. B **195** (1982) 542]. doi:10.1016/0550-3213(80)90167-4, 10.1016/0550-3213(82)90012-8

Or see also the CP chapter of the Physics Reports in reference 1.

[43] L. Covi, E. Roulet and F. Vissani, "CP violating decays in leptogenesis scenarios," Phys. Lett. B **384** (1996) 169 doi:10.1016/0370-2693(96)00817-9 [hep-ph/9605319].

[44] E. K. Akhmedov, V. A. Rubakov and A. Y. Smirnov, "Baryogenesis via neutrino oscillations," Phys. Rev. Lett. **81** (1998) 1359 doi:10.1103/PhysRevLett.81.1359 [hep-ph/9803255].

[45] T. Asaka and M. Shaposhnikov, "The nuMSM, dark matter and baryon asymmetry of the universe," Phys. Lett. B **620** (2005) 17 doi:10.1016/j.physletb.2005.06.020 [hep-ph/0505013].

[46] L. Canetti, M. Drewes, T. Frossard and M. Shaposhnikov, "Dark Matter, Baryogenesis and Neutrino Oscillations from Right Handed Neutrinos," Phys. Rev. D **87** (2013) 093006 doi:10.1103/PhysRevD.87.093006 [arXiv:1208.4607 [hep-ph]].

[47] J. Ghiglieri and M. Laine, "GeV-scale hot sterile neutrino oscillations: a derivation of evolution equations," JHEP **1705** (2017) 132 doi:10.1007/JHEP05(2017)132 [arXiv:1703.06087 [hep-ph]].

S. Eijima and M. Shaposhnikov, "Fermion number violating effects in low scale leptogenesis," Phys. Lett. B **771** (2017) 288 doi:10.1016/j.physletb.2017.05.068 [arXiv:1703.06085 [hep-ph]].

T. Hambye and D. Teresi, "Baryogenesis from L-violating Higgs-doublet decay in the density-matrix formalism," Phys. Rev. D **96** (2017) no.1, 015031 doi:10.1103/PhysRevD.96.015031 [arXiv:1705.00016 [hep-ph]].

Practical Statistics for High Energy Physics

E. Gross
Weizmann Institute of Science, Rehovot, Israel

Abstract
In these lecture notes the frequentist methods used in the Higgs search, discovery and measurement are reviewed. The idea is that the reader will be able to understand what lies beneath the surface of the results and the plots shown in the experiments publications. Though the results shown are mainly from ATLAS and CMS, the methods and the lessons can be propagated to other fields such as Astro-Particles and fixed target experiments.

1 Introduction

These lecture notes are based on statistics lectures given in the European CERN school for High Energy Physics, 2017. The frequentist approach used in the Higgs search, discovery and measurement are reviewed. Examples from real data analysis are given to clarify the methods. This is a revised version of the proceedings of the same school from 2015 [1]

2 The Search for the Higgs Boson

From Wikipedia: On 4 July 2012, the discovery of a new particle with a mass between 125 and 127 GeV/c2 was announced; physicists suspected that it was the Higgs boson. Since then, the particle has been shown to behave, interact, and decay in many of the ways predicted by the Standard Model.

High Energy Physicists (HEP) rely on a hypothesis: The Standard Model. This model relies on the existence of the 2012 discovery of the Higgs Boson. The minimal content of the Standard Model includes the Higgs Boson, the Quarks, the Leptons and the force mediating Bosons including the photons, gluons, W and Z. However, the Standard Model suffers from some problems, e.g. the hierarchy and naturality problems that are solved by various extensions of the Model and include other particles that are yet to be discovered. The challenge of HEP is to generate tons of data and to develop powerful analyses to tell if the data indeed contains evidence for new particles. Once the new particle, such as the 2012 scalar, has been discovered, the next step would have been to measure its mass, and confirm that it has the expected properties of the Higgs Boson (Spin, CP). Perhaps it is not the expected Standard Model Higgs Boson, but a member of a family of Scalar Bosons, the rest, yet to be discovered.

The statistical challenge is obvious: to tell in the most powerful way, and to the best of our current scientific knowledge, if, in our data, there is new physics, beyond what is already known. In that sense, what is already known is the background. The complexity of the apparatus and the physics (both signal and background) suffer from large systematic errors that should be taken care of in a correct statistical way.

Though the Higgs Boson has been already discovered, in these lecture notes, for pedagogic reasons, it is assumed, that, the so-called Standard Model, contains no Higgs Boson, serve as the background to the signal, which is the Higgs Boson. The Higgs Boson cannot exist without the Standard Model, so there are two nested hypotheses tested against each other. The Standard Model (denoted by b for background) and the Standard Model containing a Higgs Boson with a mass m_H, i.e. the signal+background, denoted by $s(m_H) + b$.

3 Essential Terminology

3.1 A Tale of Two Hypotheses

From Wikipedia: A hypothesis (plural hypotheses) is a proposed explanation for a phenomenon. For a hypothesis to be a scientific hypothesis, the scientific method requires that one can test it. Scientists generally base scientific hypotheses on previous observations that cannot satisfactorily be explained with the available scientific theories.

The expected signal and background are determined by the corresponding cross sections, luminosity delivered by the accelerator and the detectors response (efficiency and geometrical acceptance). $s(m_H)$ is given by

$$s(m_H) = L \cdot \sigma_{SM}(m_H) \cdot \epsilon \cdot A. \tag{1}$$

where L is the luminosity delivered by the accelerator, $\sigma_{SM}(m_H)$ is the Standard Model (SM) production cross section of the Higgs Boson, and ϵ and A are the efficiency and geometrical acceptance of the detector. For simplicity, let's assume a counting experiment and let n be the number of observed events, then

$$n = \mu s(m_H) + b. \tag{2}$$

b is the expected background, and μ is the signal strength given by

$$\mu = \frac{\sigma_{obs}}{\sigma_{SM}}. \tag{3}$$

There are therefore two hypotheses. One is the background only (b), and the other is the $\mu s(m_H) + b$ hypothesis, i.e., a Higgs Boson with a strength μ on top of the background. For a Standard Model Higgs Boson, we expect to measure $\mu = 1.0$. The background only hypothesis is denoted by H_0 while H_μ is the Higgs Boson hypothesis with H_1 being the SM Higgs Boson hypothesis.

3.2 Testing an Hypothesis

From Wikipedia: A statistical hypothesis test is a method of statistical inference. Commonly, two statistical data sets are compared, or a data set obtained by sampling is compared against a synthetic data set from an idealized model. A hypothesis is proposed for the statistical relationship between the two data sets, and this is compared as an alternative to an idealized null hypothesis that proposes no relationship between two data sets. The comparison is deemed statistically significant if the relationship between the data sets would be an unlikely realization of the null hypothesis according to a threshold probability the significance level. Hypothesis tests are used in determining what outcomes of a study would lead to a rejection of the null hypothesis for a pre-specified level of significance.

The first step in any hypothesis testing is to identify and state the relevant null, H_{null} and alternative H_{alt} hypotheses. The next step is to define a test statistic, q, under the null hypothesis (the tested hypothesis). We then compute from the observations the observed value q_{obs} of the test statistic q. Finally, decide (based on q_{obs}) to either fail to reject the null hypothesis or reject it in favour of an alternative hypothesis.

3.3 Discovery and Exclusion in a Nut Shell

To establish a discovery we define the null hypothesis as the background only hypothesis, $H_{null} = H_0$, and test it. We either fail to reject it or manage to reject it in favour of the alternative hypothesis, $H_{alt} = H_\mu$. Rejection of the null H_0 hypothesis at the level of 5σ (see 3.5) is considered a discovery. Defining the null hypothesis as $H_{null} = H_\mu$ enables the exclusion of the signal. For example, if we define the null hypothesis as the Standard Model Higgs with a mass m_H, $H_{null} = H_1$, testing and rejecting this hypothesis at the 95% Confidnece Level (see 3.5) is considered an exclusion of the Standard Model Higgs with a mass m_H.

3.4 A Test Statistic

As defined in Wikipedia: A hypothesis test is typically specified in terms of a test statistic, considered as a numerical summary of a data-set that reduces the data to one value that can be used to perform the hypothesis test. In general, a test statistic is selected or defined in such a way as to quantify, within observed data, behaviours that would distinguish the null from the alternative hypothesis, where such an alternative is prescribed, or that would characterise the null hypothesis if there is no explicitly stated alternative hypothesis, which often occurs when performing a measurement.

One example for using a test statistic is the discovery of the Higgs, when the data of Billions of Collisions is summarised in one number which determines if LHC rejected the background only hypothesis in favour of the Higgs Boson with a mass m_H or not.

There are many ways to define a test statistic based on the nature of the required test. Test statistics for discovery or exclusion are commonly based on Likelihood ratios.

Note that the likelihood is a function of the data, i.e.

$$L(H_0) = Prob(x|H_0) \tag{4}$$

where x is the data.

Before classifying the test statistics in a formal way, let us take a simplified approach. The two most common test statistics in High Energy Physics are the Neyman-Pearson (NP) and Profile Likelihood (PL). The NP test statistic given by

$$q^{NP} = -2ln\frac{L(H_0)}{L(H_1)}. \tag{5}$$

$L(H_0)$ and $L(H_1)$ are the likelihoods of the null (b) and alternative ($s(m_H) + b$) hypotheses. Note that inverting the roles of the null and alternative hypotheses, simply swap the sign of the NP test statistic. The PL test statistic depends on the tested hypothesis and for a simple counting experiment (see Equation 2), when testing the b-only hypothesis, H_0, the test statistic is given by

$$q_0 = -2ln\frac{L(b)}{L(\hat{\mu}s(m_H) + b)}. \tag{6}$$

$\hat{\mu}$ is the Maximul Likelihood Estimators (MLE) of μ. In this simplified example b is assumed to be known. The probability distribution function (PDF) of both test statistics under the null $f(q^{NP}|b), f(q_0|b)$ and the alternative $f(q^{NP}|s(m_H) + b), f(q_0|s(m_H) + b)$ hypotheses are shown in Figure 1.

3.5 What is the p-value

As defined in Wikipedia: An important property of a test statistic is that its sampling distribution under the null hypothesis must be calculable, either exactly or approximately, which allows p-values to be calculated.

The observed $p - value$ is a measure of the compatibility of the data with the tested hypothesis. It is the probability, under assumption of the null hypothesis H_{null}, of finding data of equal or greater incompatibility with the predictions of H_{null}. This is clearly illustrated in Figure 1 for the PL test statistic by the light blue area (right plot). Here H_0 is the tested null hypothesis (b only) and the $p - value$ is given by

$$p = \int_{q_{0,obs}}^{\infty} f(q_0|b)dq_0. \tag{7}$$

One can regard the hypothesis as excluded if its p-value is observed below a specified threshold (usually denoted by α).

Now, depending on the nature of the statistical test, one considers a one-sided or two-sided p-value. When performing a measurement, any deviation above or below the mean is drawing our attention
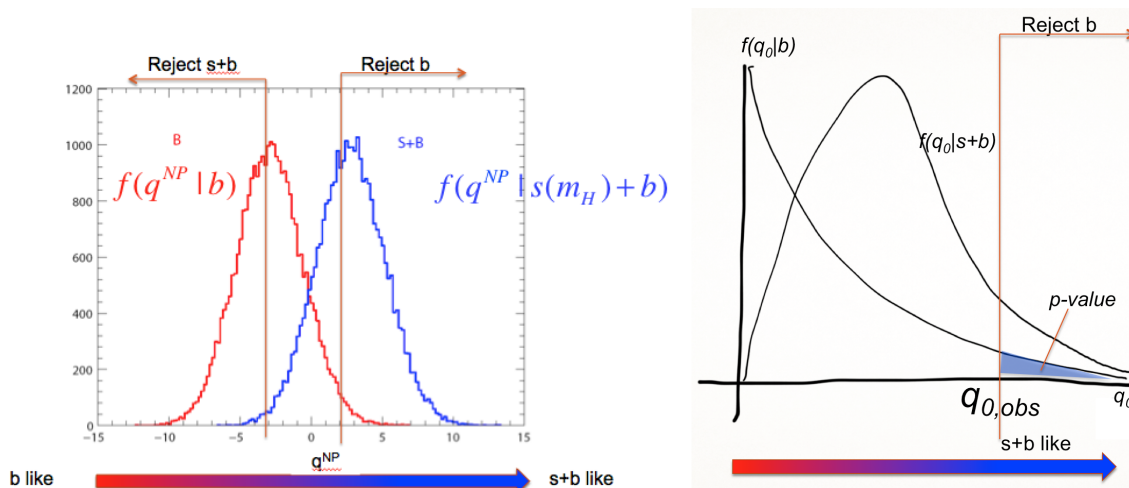
Fig. 1: The pdf of the Neyman-Pearson q^{NP} (left) and PL (Profile-Likelihood), q_0 (right) test statistics, under the null (b) and alternative ($s(m_H) + b$) hypotheses.

and might serve an indication of some anomaly or new physics. Here we consider a two sided p-value. However, when trying to reject an hypothesis while performing searches, one usually considers only one-sided tail probabilities. When the null hypothesis is the b-only hypothesis, downward fluctuations of the background, are not considered as an evidence against the background. Likewise, when deriving a limit, upward fluctuations of the hypothesised signal are not considered as an evidence against the signal. In both cases only one-sided tail probabilities are considered.

In particle physics, when performing searches, one usually converts the p-value into an equivalent significance, Z defined such that a Gaussian distributed variable, which is found Z standard deviations above its mean, has an upper-tail probability equal to p (Figure 2). That is,

$$Z = \Phi^{-1}(1 - p), \tag{8}$$

where Φ^{-1} is the quantile (inverse of the cumulative distribution) of the standard Gaussian. For a signal
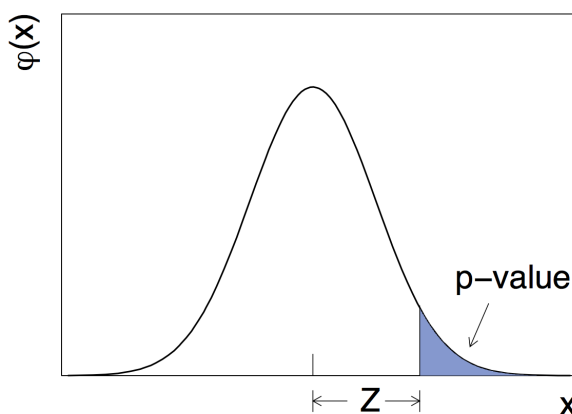

Fig. 2: The relationship between a p-value and a significance of Z sigma.

process such as the Higgs boson, the particle physics community has a tendency to regard rejection of the background hypothesis with a significance of at least $Z = 5$, as an appropriate level to constitute

a discovery. This corresponds to $p = 2.87 \times 10^{-7}$. For purposes of excluding a signal hypothesis, a threshold p-value of 0.05 (i.e., 95% confidence level) is often used, which corresponds to $Z = 1.64$. This should not be confused with a 1.96σ fluctuation of a Gaussian variable that gives 0.05 for the two-sided tail area.

Note that, for a sufficiently large data sample, one would obtain a p-value of 0.5 for data in perfect agreement with the expected background. With the definition of Z given above, this gives $Z = 0$.

3.6   Expected Significance and the Asimov Data Set

As defined in Wikipedia: The use of a single representative individual to stand in for the entire population can help in evaluating the sensitivity of a statistical method. Franchise, a science fiction short story by Isaac Asimov, was cited as the inspiration of the term "Asimov data set", where an ensemble of simulated experiments can be replaced by a single representative one.

It is often useful to quantify the sensitivity of an experiment by reporting the expected significance one would obtain with a given measurement under the assumption of various hypotheses. For example, the sensitivity to discovery of a given signal process H_1 could be characterized by the expectation value, under the assumption of H_1, of the value of Z obtained from a test of H_0. This would not be the same as the Z obtained using Eq. (8) with the expectation of the p-value, however, because the relation between Z and p is nonlinear. The median Z and p will, however, satisfy Eq. (8) because this is a monotonic relation. Therefore we take the term 'expected significance' to refer to the median.

In the Standard Model there is only one Higgs Boson with well defined couplings. To find the discovery sensitivity of an experiment, one needs to generate one ensemble of experiments containing the Higgs Boson at the tested mass. However, if one goes beyond the Standard Model, e.g., supersymmetric models, one faces a multi-dimensional parameter space where the Higgs Boson's couplings, and hence its production cross section and decay properties (both related to the signal strength) vary as a function of the parameters. For each point in parameter space one needs to estimate the experiment's discovery sensitivity. One faces the need to generate an enormous number of ensembles of experiments and evaluate the median sensitivity for each ensemble.

In [2] it was shown that one can replace each ensemble of the alternate-hypothesis experiments with one data set that represents the typical experiment. This "Asimov" data set delivers the desired median sensitivity. Hence, one is exempted from the need to perform an ensemble of experiments for each set of parameters.

The Asimov data set is constructed such that when one uses it to evaluate the estimators for all parameters, one obtains the true parameter values.

As intuitively used for years till proven at [2], the Asimov data set can trivially be constructed from the true parameters values. For example, in a counting experiment (see Eq. 2) the Asimov data set corresponding to the H_1 hypothesis is $n_A = s + b$. and the one correspond to the H_0 hypothesis is $n_A = b$. As strange as it reads, the Asimov data set is not necessarily an integer.

3.7   Nuisance Parameters.

From Wikipedia: In statistics, a nuisance parameter is any parameter which is not of immediate interest but which must be accounted for in the analysis of those parameters which are of interest.

A widely used procedure to establish discovery (or exclusion) in particle physics is based on a frequentist significance test using a likelihood ratio as a test statistic. In addition to parameters of interest such as the rate (cross section) of the signal process, the signal and background models will contain in general *nuisance parameters* whose values are not taken as known *a priori* but rather must be fitted from the data.

It is assumed that the parametric model is sufficiently flexible so that for some value of the param-

eters it can be regarded as true. The additional flexibility introduced to parametrise systematic effects results, as it should, in a loss in sensitivity. To the degree that the model is not able to reflect the truth accurately, an additional systematic uncertainty will be present that is not quantified by the statistical method presented here.

Here, nuisance parameters are denoted by θ. The likelihood is then a function of the parameter of interest, say, μ. Then $L = L(\mu, \theta)$. When testing H_μ, the Profile Likelihood test statistic in the presence of nuisance parameters, become

$$q_\mu = -2ln\frac{L(\mu, \hat{\hat{\theta}}_\mu)}{L(\hat{\mu}, \hat{\theta})}. \tag{9}$$

μ is the parameter of interest, θ represent the nuisance parameters (including b). A hat stands for the MLE (Maximum Likelihood Estimator) while a double hat is the constrained MLE, i.e. the MLE of θ, fixing μ. It is common to say that θ is profiled.

3.8 Confidence Interval, Confidence Level and Coverage.

From Wikipedia: A confidence interval (CI) is a type of interval estimate of a population parameter. It is an observed interval (i.e., it is calculated from the observations), in principle different from sample to sample, that frequently includes the value of an unobservable parameter of interest if the experiment is repeated. How frequently the observed interval contains the (true) parameter is determined by the confidence level... Whereas two-sided confidence limits form a confidence interval, their one-sided counterparts are referred to as lower or upper confidence bounds.

Say, the result of a measurement is given by $\mu = 1.1 \pm 0.3$. This means that the Confidence Interval, CI, is $\mu = [0.8, 1.4]$ at the 68% Confidence Level (CL). I.e., in an ensemble of repeated experiments, each producing a CI, 68% of the Confidence Intervals contain the unknown true value of the parameter of interest μ.

There are many ways to derive a CI at a given CL. If, the method produces a CI that contains the true value of the parameter of interest (p.o.i) more than the CL (e.g. in our example, more than 68%), the method is said to over-cover, and is considered conservative. If, however, the CI contains the true value of the p.o.i. less than the claimed Confidence Level, the method is considered to under-cover, which means, one cannot trust the CL, and the true CL might be lower than the claimed one.

3.9 Upper Limits and Confidence Levels.

If one deduces that the CI of μ contains $\mu = 0$, i.e. $\mu = [0, \mu_{up}]$ at the 95% CL, then one says that $\mu < \mu_{up}$ at the 95% CL.

If $\mu < 1$ at the 95% CL, and μ is given by Eq. 3, i.e.

$$\mu = \frac{\sigma_{obs}(m_H)}{\sigma_{SM}(m_H)} < 1 \tag{10}$$

one concludes that $\sigma_{obs}(m_H) < \sigma_{SM}(m_H)$, i.e. a SM Higgs with a mass m_H is excluded at the 95% CL.

3.10 The Neyman Pearson Lemma.

Wikipedia: In statistics, the Neyman Pearson lemma, named after Jerzy Neyman and Egon Pearson, states that when performing a hypothesis test between two simple hypotheses H_{null} and H_{alt}, the likelihood-ratio test which rejects H_{null} in favour of H_{alt} is the most powerful test at (a given) significance level...

When we reject the null hypothesis H_{null} based on a very small p-value, we also take a risk. We might be wrong (this is referred to as a type I error, see section 3.11). The null hypothesis can still be true

and the p-value is a measure for this risk. The p-value can therefore be interpreted as the false-positive rate and it satisfies

$$p \leq Prob(reject\ H_{null}|H_{null} = TRUE) \tag{11}$$

However, if while rejecting the null hypothesis, the probability for the alternative hypothesis to be true is small.... the test statistic is probably not doing its job, i.e. it is not powerful. The power of a test is therefore related to the probability that $H_{alt} = TRUE$ while rejecting H_{null}, i.e.

$$POWER = Prob(rejectH_{null}|H_{alt} = TRUE). \tag{12}$$

Neyman and Pearson showed [4], that (in the absence of nuisance parameters) the most powerful test statistic is the likelihood ratio defined in Eq. 5.

3.11 Type I & Type II Errors, the Modified Frequentist p-value, or, the CLs Technique.

Wikipedia: CLs (from Confidence Levels) is a statistical method for setting upper limits (also called exclusion limits) on model parameters, a particular form of interval estimation used for parameters that can take only non-negative values...... ......it differs from standard confidence intervals in that the stated confidence level of the interval is not equal to its coverage probability. The reason for this deviation is that standard upper limits based on a most powerful test necessarily produce empty intervals with some fixed probability when the parameter value is zero, and this property is considered undesirable by most physicists and statisticians.

For the sake of clarity let us define now type I and type II errors. Type I error is the probability to reject the null hypothesis, when the null hypothesis is true. This is referred to as "False Positive". It is usually denoted by α, i.e. $\alpha = Prob(rejectH_{null}|H_{null} = TRUE)$. Type II error, referred to as "False Negative", is when we accept the null hypothesis, when the alternative hypothesis is true. It is usually denoted by β. $\beta = Prob(AcceptH_{null}|Hnull = FALSE) = Prob(AcceptH_{null}|H_{alt} = TRUE)$. Quoting Birnbaum [5]: *A concept of statistical evidence is not plausible unless it finds strong evidence for H_{alt} against H_{null}, with small probability α when H_{null} is true, and with much larger probability $(1 - \beta)$) when H_{alt} is true.* $1 - \beta = Prob(rejectH_{null}|H_{alt} = TRUE)$ is defined as the power of the statistical test. Since rejecting H_{null} is accepting H_{alt} by definition, we find

$$POWER = 1 - \beta = Prob(acceptH_{alt}|H_{alt} = TRUE) = 1 - Prob(rejectH_{alt}|H_{alt} = TRUE). \tag{13}$$

Let $H_{null} = H_{s+b}$, i.e. the $s + b$ hypothesis, then, given an observation, H_{s+b} is rejected if the p-value$= p_{s+b} \leq \alpha$. At the threshold we find

$$p_{s+b} = Prob(reject\ H_{s+b}|H_{s+b} = TRUE). \tag{14}$$

with a power (Equation 13) of

$$Power = 1 - p_b. \tag{15}$$

A situation occurs when the power is very small and the experiment has no sensitivity to reject with high power the $s + b$ hypothesis, because it almost rejects the b-only hypothesis as well, as seen in Figure 3. A way out, was suggested by the CL_s technique [6] which is based on Birnbaum [5]. Birnbaum suggested in 1962 that the the $\{p - value\}/\{power\}$ should be used as a measure of the strength of statistical evidence provided by significance tests, rather than the $p - value$ alone. This translates into using a modified $p - value$

$$p'_{s+b} = \frac{p_{s+b}}{1 - p_b} \tag{16}$$

Equation 16 can also be interpreted as a normalised p-value, where p_{s+b} is normalised to the acceptance probability of H_b. Obviously if, while rejecting H_{s+b} one does not accept H_b , one does not have a
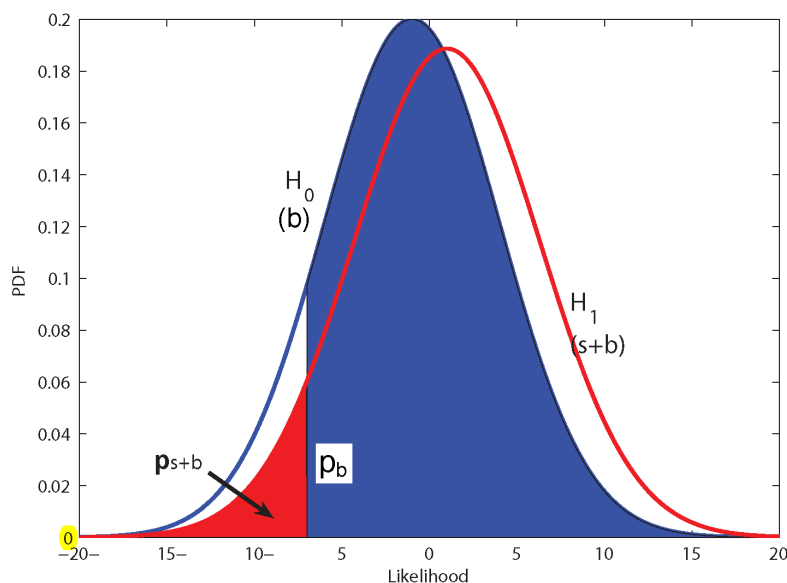
Fig. 3: An illustration showing the reasoning of the CL_s method. In this situation a signal+background hypothesis might be rejected though the experiment has no sensitivity to observe that particular signal.

sensitivity to exclude the $s + b$ hypothesis.

$$p'_{s+b} = \frac{Prob(reject\ H_{s+b}|H_{s+b} = TRUE)}{Prob(accept\ H_b|H_b = TRUE)} \qquad (17)$$

The CL_s method lacks a frequentist coverage. However, it lacks it in places where the experiment is insensitive to the expected signal! And this is not necessarily a disadvantage from the physicists point of view! Here is what happens: One uses the Neyman-Pearson likelihood ratio as a test statistics. When the expected signal is very low the two pdf are almost overlapping (see Figure 3). The background might fluctuate down resulting in a very small p_{s+b}. As a result we are tempted to exclude the signal hypothesis. However, it is not the signal hypothesis s, that is excluded, but the signal+background hypothesis $s + b$. It is the small expected signal $s << s + b$ that is leading to a false exclusion. To protect against such an inference one uses the modified $p - value$ (Eq. 16) as a criterion for taking a decision of rejecting the signal hypothesis.

As a result, for heavy Higgses with low cross section, where the experiment lacks sensitivity, the false exclusion rate is too low and the method over-covers. This is conservative because it avoids excluding when there is no sensitivity. When the signal cross section is high (light m_H), the coverage is close to full.

3.12 Feldman-Cousins: Ensuring Coverage by Neyman Construction.

Wikipedia: Neyman construction is a frequentist method to construct an interval at a confidence level $CL\%$, that if we repeat the experiment many times the interval will contain the true value a fraction $CL\%$ of the time, this way, one guarantees full coverage by construction.

As said, the Neyman construction is a method of parameter estimation that ensures coverage. One scans over all the possible true values of some parameter s and defines an acceptance interval for each s, based on the known pdf, $f(s_m|s)$, of the measured s_m given a possible true s (there is only ONE unknown true s though). The (e.g.) 68% acceptance interval $[s_l, s_h](s)$ is defined via the integration $[s_l, s_h](s) = \{s_m| \int_{s_l}^{s_h} f(s_m|s)ds_m = 68\%\}$ (Figure 4). Even in the simplest case where f is a Gaussian,

there is an ambiguity in the choice of the integration boundaries, which will lead to two-sided intervals, or one-sided integral bounded from below or above. To sort out the integration limits one needs to specify an ordering rule (i.e. which measurements should be considered within the integration boundaries and which should stay out). The construction of the acceptance intervals for all s forms a belt from which one can easily get the corresponding (e.g.) 68% confidence interval $[s_d, s_u](s_o)$, given one measurement s_o via inversion (Figure 4).
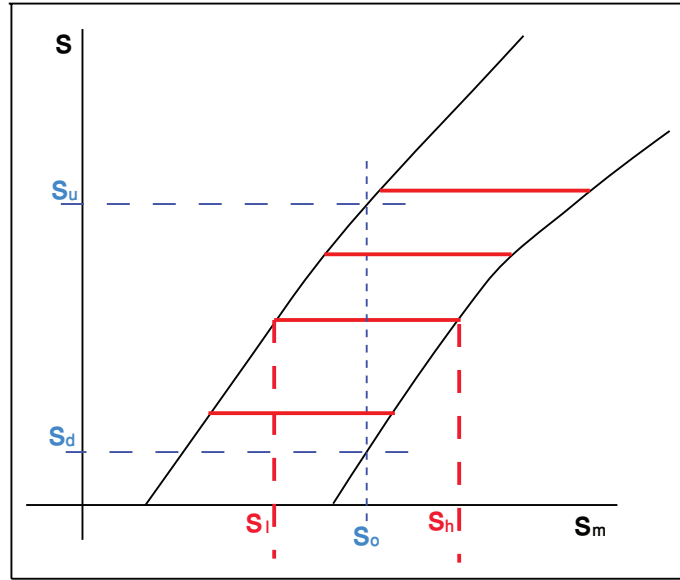

Fig. 4: An illustration showing the Neyman belt. The horizontal lines are the acceptance intervals in the measured parameter space s_m for a given possible true s, $[s_l, s_h](s)$. Given an observation s_o one can construct the confidence interval $[s_d, s_u]$ via inversion, as indicated in the Figure.

3.12.1   The Feldman-Cousins Method

The full Neyman construction was introduced to HEP by Feldman and Cousins [7]. The test statistic is the likelihood ratio $q(s) = \frac{L(s+b)}{L(\hat{s}+b)}$ where $\hat{s}$ is the MLE of s (in $L(\hat{s}+b)$) under the constraint that s is physically allowed (i.e. positive). To avoid negative signals, if $\hat{s} < 0$, one alters the test statistic to $q(s) = \frac{L(s+b)}{L(b)}$. To construct a 68% acceptance interval in the number of observed events, $[n_1, n_2]$, one is using q as an ordering rule, i.e. $\sum_{n_1}^{n_2} p(n|s,b) \geq 68\%$ where only terms with decreasing order of $q(n)$ are included in the sum, till the sum exceeds the 68% confidence (see Fig. 4). When n_o events are observed, one is using this constructed Neyman belt to derive a confidence interval, which, depending on the observation, might be a one-sided or a two-sided interval. This method is therefore called the unified method, because it avoids a flip-flop of the inference (i.e. one decides to flip from a limit to an interval if the result is significant enough...).

One can clearly see in Fig. 4 that depending on the observation, s_o, one gets either a one sided bound, or a two sided interval.

A noted difficulty with this approach is that an experiment with higher expected background which observes no events might set a better upper limit than an experiment with lower or no expected background. This would never occur with the CL_s method.

Another difficulty is that this approach does not incorporate a treatment of nuisance parameters. However, it can either be plugged in "by hand", using the hybrid Cousins and Highland method [8] or in the LHC way, i.e. using the Profile Likelihood [2] as described above.

4 Classification of Test Statistics.

Depending on the nature of the test, one can classify the various test statistics, all based on Likelihood ratios, where the nuisance parameters are profiled (e.g. Eq. 9). The classification is based on [2] and is shown in Table 1. It is to be noted that $\tilde{t}_0$ is equivalent to q_0.

Table 1: Classification of Test Statistics

Test Stat.	Purpose	Expression	LR
q_0	discovery of positive signal	$q_0 = \begin{cases} -2\ln\lambda(0) & \hat{\mu} \geq 0 \\ 0 & \hat{\mu} < 0 \end{cases}$	$\lambda(0) = \frac{L(0,\hat{\hat{\theta}})}{L(\hat{\mu},\hat{\theta})}$
t_μ	2-sided measurement	$t_\mu = -2ln\lambda(\mu)$	$\lambda(\mu) = \frac{L(\mu,\hat{\hat{\theta}})}{L(\hat{\mu},\hat{\theta})}$
$\tilde{t}_\mu$	avoid negative signal (Feldman-Cousins)	$\tilde{t}_\mu = -2ln\tilde{\lambda}(\mu)$	$\tilde{\lambda}(\mu) = \begin{cases} \frac{L(\mu,\hat{\hat{\theta}}(\mu))}{L(\hat{\mu},\hat{\theta})} & \hat{\mu} \geq 0 \\ \frac{L(\mu,\hat{\hat{\theta}}(\mu))}{L(0,\hat{\hat{\theta}}(0))} & \hat{\mu} < 0 \end{cases}$
q_μ	exclusion	$q_\mu = \begin{cases} -2\ln\lambda(\mu) & \hat{\mu} \leq \mu \\ 0 & \hat{\mu} > \mu \end{cases}$	
$\tilde{q}_\mu$	exclusion of positive signal	$\tilde{q}_\mu = \begin{cases} -2\ln\frac{L(\mu,\hat{\hat{\theta}}(\mu))}{L(0,\hat{\hat{\theta}}(0))} & \hat{\mu} < 0 , \\ -2\ln\frac{L(\mu,\hat{\hat{\theta}}(\mu))}{L(\hat{\mu},\hat{\theta})} & 0 \leq \hat{\mu} \leq \mu \\ 0 & \hat{\mu} > \mu \end{cases}$	

5 Wald and Wilks Asymptotic Approximation

Abraham Wald showed [10] that given the likelihood ratio $\lambda(\mu) = \frac{L(\mu,\hat{\hat{\theta}}_\mu)}{L(\hat{\mu},\hat{\theta})}$, the test statistic $t_\mu = -2ln\lambda(\mu)$ satisfies

$$-2ln\lambda(\mu) = \frac{(\mu - \hat{\mu})^2}{\sigma_{\hat{\mu}}^2} + O(1/\sqrt{N}) \tag{18}$$

where $\hat{\mu}$ follows a Gaussian distribution with a mean μ' and a standard deviation $\sigma_{\hat{\mu}}$, and N is the sample size. Following this result, the statistics t_μ distribution $f(t_\mu|\mu')$, follows a non central Chi Square distribution for one degree of freedom where the non-cenrality parameter Λ is, $\Lambda = \frac{(\mu - \mu')^2}{\sigma^2}$. In the special case $\mu' = \mu$, $\Lambda = 0$ and $f(t_\mu|\mu)$ follows a Chi Square Distribution with one degree of freedom, a result attributed to Samuel Wilks [9]. Since the Asimov data set correspond to $\hat{\mu} = \mu'$, one finds that Equation 18 becomes an identity and therefore

$$-2ln\lambda_A(\mu) = \frac{(\mu - \mu')^2}{\sigma_{\hat{\mu}}^2}. \tag{19}$$

It follows that when testing H_μ for exclusion (with q_μ, see Table 1), let $< \hat{\mu} >= \mu' = 0$, one finds [2]

$$\sigma_{\hat{\mu}} = \frac{\mu}{\sqrt{q_{\mu,A}}}. \tag{20}$$

6 Asymptotic Formulae

Wikipedia: In mathematics and statistics, an asymptotic distribution is a distribution that is in a sense the "limiting" distribution of a sequence of distributions. One of the main uses of the idea of an asymptotic distribution is in providing approximations to the cumulative distribution functions of statistical estimators.

The frequentist approach of statistics requires the knowledge of the probability distribution functions (PDFs) of the test statistic under the null and alternative hypotheses. These PDFs are used to find both the significance for a specific data set and the expected significance. However, obtaining these PDFs, can involve Monte Carlo generations that are computationally expensive. Ref [2] developed the asymptotic formulae based on results due to Wilks [9] and Wald [10] by which one can obtain both the significance for given data as well as the full sampling distribution of the significance under the hypothesis of different signal models, all without recourse to Monte Carlo. In this way one can find, for example, the median significance and also a measure of how much one would expect this to vary as a result of statistical fluctuations in the data. Obtaining the same things with Monte Carlo is sometimes impossible. One LHC collision might take $o(10mins)$ to generate, and one needs over 10^7 events to calculate a 5σ tail of a PDF. Moreover, the test statistics involve heavy duty fits which also take time. Combining AT-LAS and CMS results in over 4000 Nuisance Parameters. Repeated fits of that many parameters result often in failure fits. Some we are not even aware of. It could be that the PDF generated by toys is subject to unknown failure of fits and is not reliable for $p-value$ calculations. In most cases, the number of events involved is satisfying the condition for the asymptotic approximation to work.

All of the asymptotic approximations of the PDFs of the test statistics shown in Table 1 have been calculated under the null and alternative hypotheses [2]. There is no point in reproducing them all here. Three common uses are for exclusion, discovery and measurement.

6.1 Exclusion

For exclusion one can either use q_μ or $\tilde{q}_\mu$ (Table 1) as a test statistic. In numerical examples we have found that the difference between the two tests is negligible, but use of q_μ leads to important simplifications. Furthermore, in the context of the asymptotic approximation, the two statistics are equivalent. That is, assuming the approximations below, q_μ can be expressed as a monotonic function of $\tilde{q}_\mu$ and thus they lead to the same results. We will therefore recommend the use of q_μ for the derivation of exclusion.

Using the asymptoric formulae of [2] we find that $f(q_\mu|\mu)$ distributes as a half-chi-square:

$$f(q_\mu|\mu) = \frac{1}{2}\delta(q_\mu) + \frac{1}{2}\frac{1}{\sqrt{2\pi}}\frac{1}{\sqrt{q_\mu}}e^{-q_\mu/2} \ . \tag{21}$$

It is therefore recommended to verify that $f(q_\mu|\mu) \sim \chi_1^2$. This is usually the case, in particular when combining channels.

The cumulative distribution is

$$F(q_\mu|\mu) = \Phi\left(\sqrt{q_\mu}\right) \ . \tag{22}$$

6.1.1 The $p-value$

The p-value of the hypothesized μ is

$$p_\mu = 1 - F(q_\mu|\mu) = 1 - \Phi\left(\sqrt{q_\mu}\right) \tag{23}$$

and therefore the corresponding significance is

$$Z_\mu = \Phi^{-1}(1 - p_\mu) = \sqrt{q_\mu} \ . \tag{24}$$

If the p-value is found below a specified threshold α (often one takes $\alpha = 0.05$), then the value of μ is said to be excluded at a confidence level (CL) of $1 - \alpha$. The upper limit on μ is the largest μ with $p_\mu \leq \alpha$. Here this can be obtained simply by setting $p_\mu = \alpha$ and solving for μ. One finds

$$\mu_{\text{up}} = \hat{\mu} + \sigma \Phi^{-1}(1 - \alpha) \ . \tag{25}$$

For example, $\alpha = 0.05$ gives $\Phi^{-1}(1 - \alpha) = 1.64$. Any point μ_0 satisfying $\mu_0 \leq \mu_{\text{up}}$ is excluded at the $100(1 - \alpha)\%$ Confidence Level. (for $\alpha = 0.05$ the 95% Confidence Interval does not contain $\mu = \mu_0$). Also as noted above, σ depends in general on the hypothesized μ. Thus in practice one may find the upper limit numerically as the value of μ for which $p_\mu = \alpha$.

6.1.2   Expected Limit and Error Bands

To find the expected limit, one should plug in the Asimov data which represents the alternative hypothesis, which in this case is the expected background (with no fluctuations). The signal strength is set to zero (in a simple counting experiment $n = b$). One then gets $q_{\mu,A}$ and the corresponding μ_{up}^{med} is given by solving $q_{\mu_{up}^{med},A} = 1.64^2$ (for $\alpha = 0.05$). The error bands are given by

$$\mu_{up+N} = \sigma(\Phi^{-1}(1 - \alpha) + N) \tag{26}$$

with

$$\sigma^2 = \frac{\mu^2}{q_{\mu,A}} \tag{27}$$

following Equation (20). μ can be taken as μ_{up}^{med} in the calculation of σ.

6.2   Expected Limit and Error Bands a-la "(CL$_s$)"

To avoid setting limits when the experiment is not sensitive to the signal, one might use the modified p-value defined above, "p'_{s+b}"

$$p'_{s+b} = \frac{p_{s+b}}{1 - p_b} \tag{28}$$

We find

$$p'_\mu = \frac{1 - \Phi(\sqrt{q_\mu})}{\Phi(\sqrt{q_{\mu,A}} - \sqrt{q_\mu})} \tag{29}$$

The median and expected error bands will therefore be

$$\mu_{up+N} = \sigma(\Phi^{-1}(1 - \alpha\Phi(N)) + N) \tag{30}$$

with

$$\sigma^2 = \frac{\mu^2}{q_{\mu,A}} \tag{31}$$

To get the 95% expected upper limit, set $\alpha = 0.05$. μ can be taken as μ_{up}^{med} in the calculation of σ..

Note that for $N = 0$ we find the median limit

$$\mu_{up}^{med} = \sigma \Phi^{-1}(1 - 0.5\alpha) \tag{32}$$

The expected μ and the expectation for error band N is shown in Figure 5. one can clearly see the shrinkage of the error band, $\mu_{up+N\sigma} - \mu_{up+(N-1)\sigma}$, when $N \to -\infty$

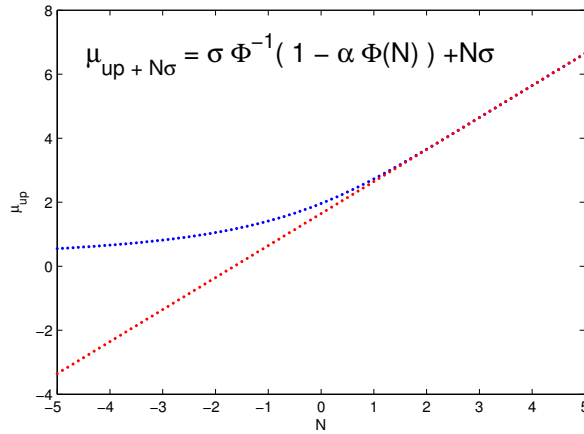**Fig. 5:** $\mu_{up+N\sigma}$ as a function of N (in units of σ). Red is based on p_{s+b} blue is based on p'_{s+b} (CL_s).

6.3 Example from the Higgs Boson Search

Figure 6 taken from [11] shows μ_{up} as a function of m_H at one of the stages of the Higgs search. The
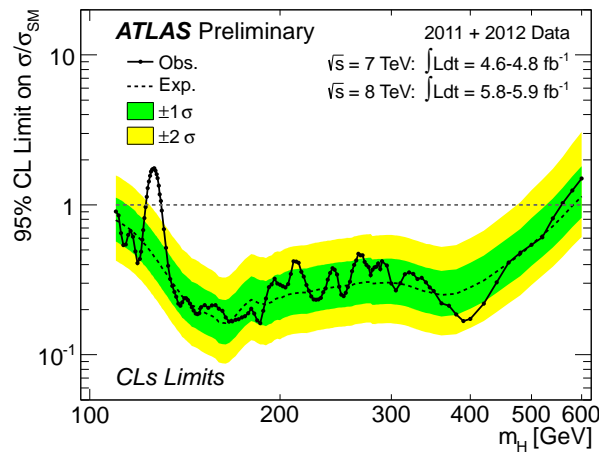

Fig. 6: The observed (full line) and expected (dashed line) 95% CL combined upper limits on the SM Higgs boson signal strength (μ_{up}) in the full mass range m_H considered in this analysis. The dashed curves show the median expected limit in the absence of a signal and the green and yellow bands indicate the corresponding 68% and 95% intervals.

mass range where $\mu_{up}(m_H) \leq 1$ is where a SM Higgs Boson with a mass m_H is excluded. Obviously one cannot exclude the Higgs around $m_H = 125$ GeV, where a real signal is being built up with luminosity $\mu_{up} > 1$. The median expected is given by the dashed line (following Equation 32 with $\alpha = 0.05$). The error bands are derived using Equation 30, with $N = \pm 1$ (Green) and $N = \pm 2$ (yellow).

Figure 7 taken from the same reference, shows p'_{s+b} (labeled in the Figure as CL_s), as a function of m_H. Mass regions where $p'_{s+b} \leq 0.05$ are excluded at, at least, the 95% CL.

6.4 Measurement

Let the statistic be $t_\mu = -2 \ln \lambda(\mu)$ (Table 1) as the basis of the statistical test of a hypothesized value of μ. This could be a test of $\mu = 0$ for purposes of establishing existence of a signal process, or non-
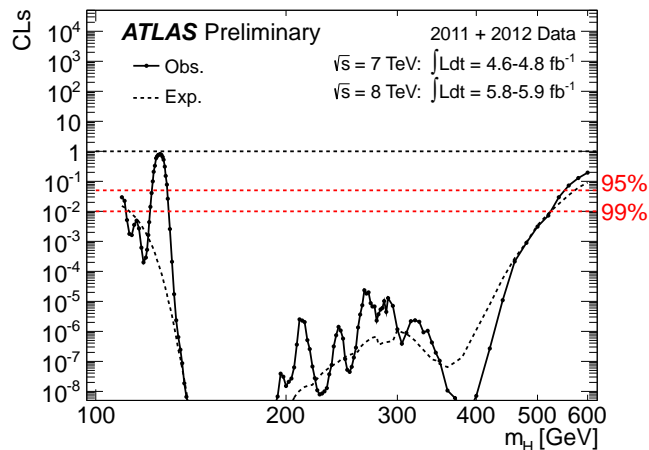
Fig. 7: The value of the combined CL_s (p'_{s+b}), testing the Standard Model Higgs boson hypothesis, as a function of m_H in the full mass range of this analysis. The expected CL_s is shown in the dashed curves. The regions with $CL_s < 0.05$ are excluded at least at 95% CL. The 95% and 99% CL values are indicated as dashed horizontal lines.

zero values of μ for purposes of obtaining a confidence interval. In the asymptotic regime the pdf of t_μ distributes like a χ^2 with one degree of freedom, under the H_μ hypothesis.

$$f(t_\mu|\mu) = \frac{1}{\sqrt{2\pi}} \frac{1}{\sqrt{t_\mu}} e^{-t_\mu/2} \ . \tag{33}$$

To measure μ, one scans the test statistics, finds $\hat{\mu}$ and σ^{up}, σ^{lo} by substituting $t_\mu = 1$. The 68% Confidence Interval of μ is then estimated to be $[\hat{\mu} - \sigma^{lo}, \hat{\mu} + \sigma^{up}]$. If one wants to estimate with how many standard deviations a specific value of μ, e.g. $\mu = 0$. is unlikely, one calculates $\sqrt{t_0}$.

To get the expcted μ one repeats the above procedure, calculating t_μ with the Asimov data set, for which $\hat{\mu} = \mu$.

A formulation of the asymptotic properties of t_μ is given in [2].

6.5 Discovery

To establish a discovery one tries to reject the background only hypothesis. We use the q_o test statistics (Table 1). Since we do not want downward fluctuations of the background to serve as an evidence against the background we define the test statistics such that $q_0 = 0$ if $\hat{\mu} < 0$. The test statistic is therefore given by (Table 1):

$$q_0 = \begin{cases} -2 \ln \frac{L(0)}{L(\hat{\mu})} & \hat{\mu} \geq 0, \\ 0 & \hat{\mu} < 0 \ , \end{cases} \tag{34}$$

Under the background only hypothesis, H_0, q_0 is asymptotically distributed as half a chi squared with one degree of freedom, i.e.

$$f(q_0|0) = \frac{1}{2}\delta(q_0) + \frac{1}{2}\frac{1}{\sqrt{2\pi}}\frac{1}{\sqrt{q_0}} e^{-q_0/2} \ . \tag{35}$$

The significance of the observation is given by

$$Z_0 = \Phi^{-1}(1 - p_0) = \sqrt{q_0} \, . \tag{36}$$

The p_0 value can easily be calculated using

$$p_0 = 1 - F(q_0|0) \, , \tag{37}$$

where

$$F(q_0|0) = \Phi\left(\sqrt{q_0}\right) \, . \tag{38}$$

A significance of 3σ is considered as an observation, while a significance exceeding 5σ is regarded as a discovery. The reason for using such a large number to establish a discovery is because of the Look Elsewhere Effect, discussed in section 8.

6.6 Discovery Example

In Figure 10 we show the $p - value$ as a function of the mass, taken from the ATLAS discovery conference note [11]. Both, the $p - value$ and its corresponding significance are indicated. One clearly sees an upward fluctuation of the background (downward fluctuation in $p - value$) around a mass of 125 GeV. The fluctuation is at the level of 5σ. For other masses the $p - value$ fluctuates around 0.5, meaning a significance of 0σ. The expected $p - value$ is given by the dashed line. One can clearly see that only around $m_H = 125$ GeV, the expected and the observed $p - value$ are similar, indicating a signal strength $\mu \sim 1$, as can clearly be seen in Figure 11.

6.6.1 Significance in a nut-shell.

Many people use a thumbnail formula $Z = \frac{s}{\sqrt{b}}$ to estimated the significance of an apparent signal. s represents here $n - b$, where b is the expected background, and n is the number of observed events.

Using the profile likelihood formalism we can get a much more accurate estimation for the apparent observed significance [2].

If we regard b as known, the data consist only of n and thus the likelihood function is

$$L(\mu) = \frac{(\mu s + b)^n}{n!} e^{-(\mu s + b)} \, , \tag{39}$$

The test statistic for discovery q_0 can be written

$$q_0 = \begin{cases} -2 \ln \frac{L(0)}{L(\hat{\mu})} & \hat{\mu} \geq 0, \\ 0 & \hat{\mu} < 0 \, , \end{cases} \tag{40}$$

where $\hat{\mu} = n - b$. For sufficiently large b we can use the asymptotic formula [2] to obtain

$$Z_0 = \sqrt{q_0} = \begin{cases} \sqrt{2 \left(n \ln \frac{n}{b} + b - n\right)} & \hat{\mu} \geq 0, \\ 0 & \hat{\mu} < 0. \end{cases} \tag{41}$$

To approximate the median significance assuming the nominal signal hypothesis ($\mu = 1$) we replace n by the Asimov value $s + b$ to obtain

$$\text{med}[Z_0|1] = \sqrt{q_{0,\text{A}}} = \sqrt{2 \left((s + b) \ln(1 + s/b) - s\right)} \, . \tag{42}$$

Expanding the logarithm in s/b one finds

$$\text{med}[Z_0|1] = \frac{s}{\sqrt{b}}\left(1 + \mathcal{O}(s/b)\right) \ . \tag{43}$$

Although $Z_0 \approx s/\sqrt{b}$ has been widely used for cases where $s + b$ is large, one sees here that this final approximation is strictly valid only for $s \ll b$. We therefore recommend to use Eq. 42 to estimate a significance in a nut shell. It is much more accurate.

7 Testing an hypothesis with boundaries.

In [7] Feldman and Cousins derive the test statistics with the physical condition, namely, the true value of μ must be positive, i.e. $\mu > 0$. In [2] the $\tilde{t}_\mu$ test statistic is introduced (see Table 1) in order to avoid a negative non-physical signal. As a result, depends on the observation, a two sided (measurement) or one sided (limit) Confidence Interval is obtained. This is the equivalence of the Feldman-Cousins test statistic with the advantage of taking care of the nuisance parameters. The original Feldman-Cousins test statistic is not considering systematics. In [2] the asymptotic formula of $\tilde{t}_\mu$ is derived. In a later paper [12] the same authors improve the test statistic by taking into account two sided boundaries. This is the case, for example when one wants to measure or set limits on the measurement of a Branching Ratio, which must be $0 < BR < 1$ by definition. The revised $\tilde{t}_\mu$ is defined by

$$\tilde{t}_\mu = \begin{cases} -2\ln\frac{L(\mu,\hat{\hat{\theta}}(\mu))}{L(\mu_-,\hat{\hat{\theta}}(\mu_-))} & \hat{\mu} \leq \mu_- \\ -2\ln\frac{L(\mu,\hat{\hat{\theta}}(\mu))}{L(\hat{\mu},\hat{\theta})} & \mu_- < \hat{\mu} < \mu_+ \\ -2\ln\frac{L(\mu,\hat{\hat{\theta}}(\mu))}{L(\mu_+,\hat{\hat{\theta}}(\mu_+))} & \hat{\mu} \geq \mu_+ \ , \end{cases} \tag{44}$$

$\hat{\hat{\theta}}$ represent the nuisance parameters, $\hat{\hat{\theta}}(\mu)$ is the conditional maximum likelihood estimate of θ given μ. μ_- and μ_+ are the physical boundaries. The Feldman-Cousins test statistic is retrieved for $\mu_- = 0$ and no upper boundary, μ_+. The asymptotic formulas are derived in [12].

7.1 Pull

The pull of a nuisance parameter θ, with an expectation θ_0 is defined as:

$$pull(\theta) = \frac{\hat{\theta} - \theta_0}{\sigma_\theta} \tag{45}$$

the pull quantifies how far from its expected value we had to "pull" the parameter while finding the MLE. A healthy situation is when the pull average is zero with a standard deviation close to 1, if this is not the case, further investigation is required. The expected value of a nuisance parameter and its assumed standard deviation will be based on an auxiliary measurement or MC studies.

7.2 Impact

the impact of a nuisance parameter is defined as:

$$impact(\theta) = \Delta\mu^\pm = \hat{\hat{\mu}}_{\theta_0 \pm \sigma_\theta} - \hat{\mu} \tag{46}$$

where $\hat{\hat{\mu}}_{\theta_0 \pm \sigma}$ is the MLE of μ when we profile every parameter except θ, and set the value of θ to its expectation value plus or minus one standard deviation. The impact gives a measure of how much our parameter of interest varies as we change the nuisance parameter. Obviously not all nuisance parameters are equally important, so a nuisance parameter with low impact may be possibly discarded (or "pruned") to simplify the fit procedure.

7.3 Example of pull and impact

To illustrate the use of impact and pull, consider a simple counting experiment which measures n events, with $n = \mu \cdot s \cdot A \cdot \epsilon + b$, where s is the number of signal events, μ is the p.o.i and A (acceptance) ϵ (efficiency) and b (background) are nuisance parameters with gaussian distributions.
The likelihood is given by:

$$L(\mu, A, \epsilon, b) = \frac{(\mu s A \epsilon + b)^n}{n!} exp\left(-(\mu s A \epsilon + b)\right) \cdot$$

$$exp\left(-\frac{(b - b_{obs})^2}{\sigma_b}\right) exp\left(-\frac{(A - A_{obs})^2}{\sigma_A}\right) exp\left(-\frac{(\epsilon - \epsilon_{obs})^2}{\sigma_\epsilon}\right) \tag{47}$$

For each nuisance parameter, there is an "observed" value which could come from some auxiliary measurement. In this simplified case all nuisance parameters are measured by their MLEs, i.e. ($\hat{\theta} = \theta_{obs}$). We assume the "true" value of the parameters are known to be θ_0.

The pulls are calculated straightforward from equation 45. The impact is calculated with the test statistic $t_\mu(\epsilon) = -2ln\frac{L(\hat{\hat{\mu}}, \hat{\hat{A}}, \epsilon, \hat{\hat{b}})}{L(\hat{\mu}, \hat{A}, \hat{\epsilon}, \hat{b})}$ (for the nuisance parameter ϵ), with double hat indicating that the fit is constrained to ϵ, as was described above. Table 2 shows the values of the parameters used in the toy calculation. The measured value for n, was picked from a poisson distribution with expectation value of $n_{exp} = \mu \cdot s \cdot A \cdot \epsilon + b$ (the true, Asimov, values) and ϵ_{obs} A_{obs} and b_{obs} were picked from gaussian distributions.

Figure 8 shows a typical overlay plot of pull and impact (right plot for Asimov and left plot for some toy data set). Note the different x-axis (top for the impact, bottom for the pull). Figure 9 shows in more detail the calculation of the impact - it shows the scan of $t_\mu(\epsilon)$, $\hat{\mu}(\epsilon)$ and the procedure leading from $\hat{\epsilon} \pm \sigma_\epsilon$ points to the Impact range (right plot for Asimov and left plot for some toy data set).

Parameter	Asimov	Measured
s	90	-
n	131.5	132
μ	1	1.4
ϵ	0.5	0.465
σ_ϵ	0.05	-
A	0.7	0.487
σ_A	0.2	-
b	100	103.21
σ_b	10	-

Table 2: Parameters for toy experiment

8 The Look Elsewhere Effect (LEE).

Wikipedia: The look-elsewhere effect is a phenomenon in the statistical analysis of scientific experiments, particularly in complex particle physics experiments, where an apparently statistically significant observation may have actually arisen by chance because of the size of the parameter space to be searched. Once the possibility of look-elsewhere error in an analysis is acknowledged, it can be compensated for by careful application of standard mathematical techniques [3].

8.1 The LEE with one parameter (m) undefined under the null hypothesis.

When searching for a new resonance somewhere in a possible mass range, the significance of observing a local excess of events must take into account the probability of observing such an excess *anywhere* in
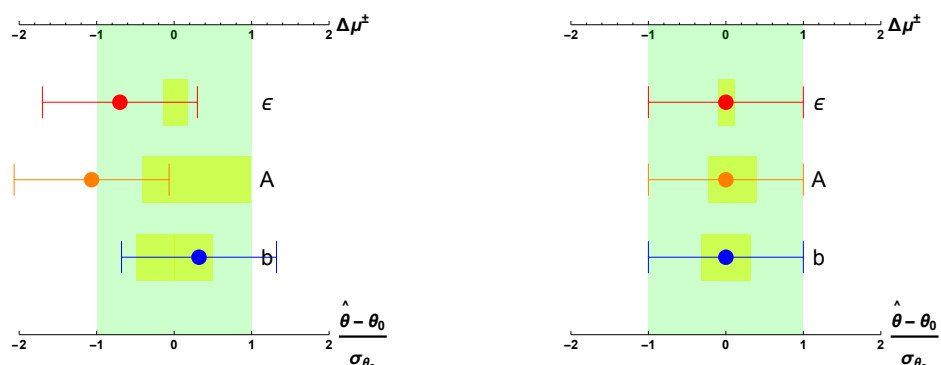
Fig. 8: Impact and pull for the three nuisance parameters (right plot for Asimov and left plot for some toy data set). The yellow rectangles show the impact range (upper x-axis) and the coloured dots show the pull (lower x-axis) with one σ error bars
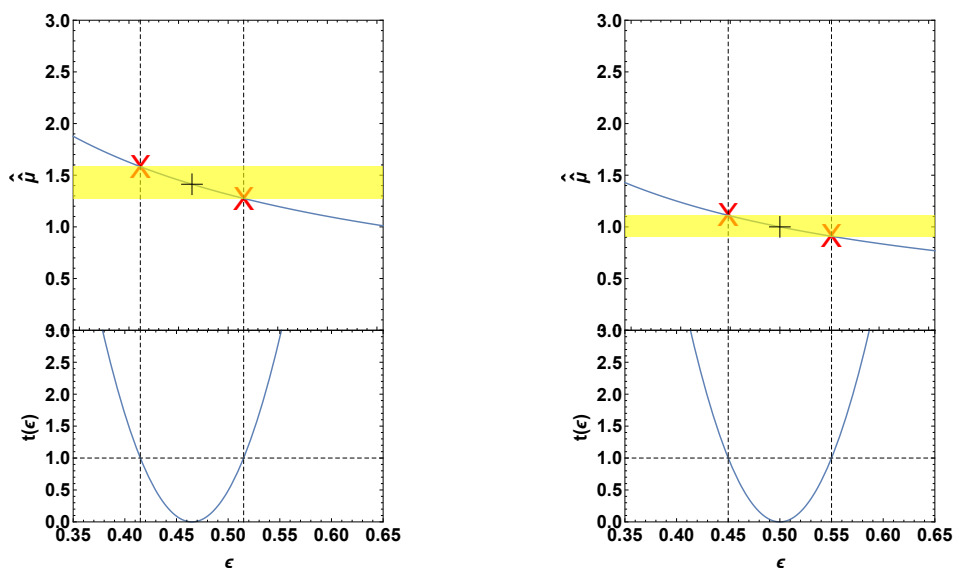

Fig. 9: Calculation of the impact of the nuisance parameter ϵ (right plot for Asimov and left plot for some toy data set). The upper plot shows the MLE of μ when profiling all parameters except ϵ (the blue curve) and the red X's show the point where $\hat{\hat{\mu}}(\epsilon)$ intersects with the $\hat{\epsilon} \pm \sigma_\epsilon$ points (the dashed vertical lines), which marks the end points of the impact. The bottom plot shows the scan of the test statistic $t_\mu(\epsilon) = -2ln\frac{L(\hat{\hat{\mu}},\hat{\hat{A}},\epsilon,\hat{\hat{b}})}{L(\hat{\mu},\hat{A},\hat{\epsilon},\hat{b})}$ and shows that the $\hat{\epsilon} \pm \sigma_\epsilon$ points correspond to $min(t_\mu(\epsilon)) \pm 1$

the range. This is the so called "look elsewhere effect". The effect can be quantified in terms of a trial factor, which is the ratio between the probability of observing the excess at some fixed mass point (local $p-value$), to the probability of observing it anywhere in the range (global $p-value$). The question we try to answer with a $p-value$ is *What is the probability of observing an excess anywhere in the search range".* For years it was a common knowledge that in order to convert the local probability into a global probability one has to apply a trial factor which is simply the number of possible independent search regions, i.e. $trial\# = \frac{p_{float}}{p_{fix}} = \frac{search\ range}{mass\ resolution}$. In [3] it was shown that an important factor was missing from this rule of thumb estimation. The trial number is linearly dependent on the local significance. This can be intuitively understood by the possibility of havung a look elsewhere effect within the independent search range, where the number of possibilities peak can arrange itself is proportional to the significance. The trial number is therefore asymptotically (for small $p-values$, i.e. large significance) given by

$$trial\# \approx 1 + \sqrt{\frac{\pi}{2}} \mathcal{N} Z_{fix} \tag{48}$$

where $\mathcal{N}$ is the number of independent search regions.

The trial factor is thus asymptotically linear with both the effective number of independent regions, and with the fixed-mass significance.

The number of independent search region is not a trivial quantity. The resolution might not be well defined and is usually depending on the mass. We applied the formula obtained by Davies [13] for an hypothesis testing when a nuisance parameter (the mass) is known only under the alternative hypothesis. The mass is not defined under the null (background only) hypothesis.

Let $q_0(m, \theta)$ be the discovery test statistics (following Equation 34). m is undefined under the null hypothesis ($\mu = 0$). Nevertheless, there is a dependence of q_0 on the mass through the denominator.

$$q_0(m) = \begin{cases} -2\ln\frac{L(0)}{L(\hat{\mu}, m)} & \hat{\mu} \geq 0, \\ 0 & \hat{\mu} < 0 \, , \end{cases} \tag{49}$$

Given some data set, we scan $q_0(m)$ and find the maximal one (smallest $p-value$ over all possible masses). We define it as

$$\hat{q}_0 \equiv max_m[q_0(m)] = q_0(\hat{m}) \tag{50}$$

Since for any given m, $q_0(\hat{m} \geq q_0(m)$, the global $p-value$, $p_{global} \geq p_{local}$. Hence, the trial number is always greater or equal to one, $Trial\# \geq 1$. We find that for high local significance (at the tail of the pdf distributions), the following relation exists between the global and local $p-value$:

$$P(q_0(\hat{m}) > u) \approx \frac{1}{2} P(\chi_1^2 > u) + \mathcal{N} P(\chi_2^2 > u) \tag{51}$$

where in the tail $u \to \infty$. $\mathcal{N}$ is the number of independent search regions. To obtain this we find the average number of upcrossings at a level $u = Z^2$, n_u, i.e. $E[n_u] = \mathcal{N}e^{-u/2}$.

Since we are interested to know the global significance for high level , normally $u = Z^2 > 16$, the number of upcrossings is very small and one needs to generate expensive toys to estimate $E[n_u]$. One then renormalize the upcrossings level. Let us pick a low level u_0 where the number of upcrossings is relatively large and the statistical error on the estimation is therefore small (normally one picks $u_0 = 0$ or $u_0 = 0.5^2$). We find $E(n_{u_0}) = \mathcal{N}e^{-u_0/2}$ and therefore

$$E(n_u) = E(n_{u_0})e^{\frac{u_0-u}{2}} \tag{52}$$

Finally we find that the answer to the question: *What is the probability to have a fluctuation with a significance bigger than $Z = \sqrt{u}$ all over a given mass range?* is given by

$$P_{global}(u) \approx p_{local}(u) + E(n_{u_0})e^{\frac{u_0-u}{2}} \tag{53}$$

where u_0 is some low reference level, where the estimation of the number of upcrossings $E(n_{u_0})$ is easy and fast.

To illustrate it let us look at a real example from the Higgs Boson search and discovery. In the following Figures we show the p_0 (Figure 10) and the signal strength μ (Figure 11) as a function of the Higgs mass. The plots are taken from the ATLAS discovery conference note [11]. $Z = 0$ corresponds
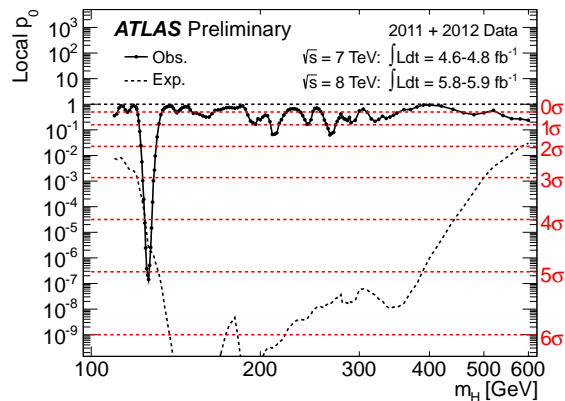

Fig. 10: The local probability p_0 for a background-only experiment to be more signal-like than the observation in the full mass range of this analysis as a function of m_H. The dashed curves show the median expected local p_0 under the hypothesis of a Standard Model Higgs boson production signal at that mass. The horizontal dashed lines indicate the p-values corresponding to significances of 1σ to 6σ.
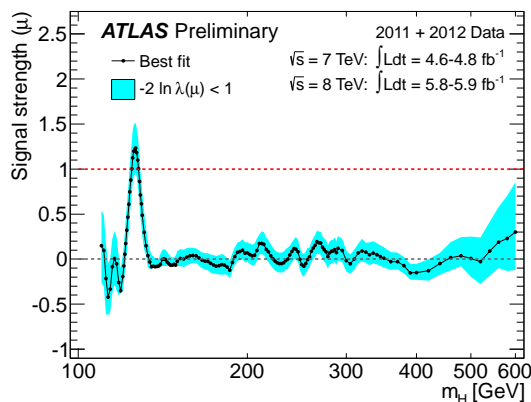

Fig. 11: The combined best-fit signal strength $\hat{\mu}$ as a function of the Higgs boson mass hypothesis in the full mass range of this analysis

to either $p_0 = 0.5$ or $\hat{\mu} = 0$. Se we have to count the number of up-crossings at 0σ. We should have performed a few Momte Carlo experiments and count the average number of up-crossings at $u = 0$. But this seems to be not practical when we combine all the channels. Instead we could simply take the data itself and count $n_{u_0} = 9 \pm 3$. This accuracy is sufficient for the estimation of the trial number. Following Equation 53, substituting $u_0 = 0$ and $u = 5^2 = 25$, we find

$$p_{global} = O(10^{-7}) + 9 \times e^{-25/2} = 3.3 \times 10^{-5} \tag{54}$$

The trial number is about $trial\# \approx \frac{10^{-5}}{10^{-7}} \approx 100$ and it reduces the significance from 5σ to 4σ.

8.2 The LEE with two parameters (m, Γ) undefined under the null hypothesis.

In cases where there are two parameters undefined under the null hypothesis, such as mass (m) and width (Γ) the Look Elsewhere Effect is broader. Ref [14] solved the case for a multi-dimensional search.

Suppose we would like to estimate the global significance of some observed excess. When allowing both the mass and the width float, we observe that the highest significance of $Z\sigma$ occurs for some specific mass and width. This observation corresponds to a local background fluctuation with a p-value of p_{local}. However, any fluctuation at any mass and width in the 2D search plane of m and Γ would have drawn our attention. The increased probability to observe a fluctuation of $Z\sigma$ or more anywhere in the mass-width plane $A = (m, \Gamma)$ (LEE) is given by the global p-value, p_{global}. The local p-value is based on scanning the $q_0(m, \Gamma)$ test statistic, $q_0(m, \Gamma)$ given by

$$q_0(m, \Gamma) = -2 \log \frac{L(0, m, \Gamma, \hat{\hat{\theta}})}{L(\hat{\mu}, \hat{m}, \hat{\Gamma}, \hat{\theta})}. \tag{55}$$

The distribution of the maximum local significance $u = Z^2 = \max_{m, \Gamma} q_0(m, \Gamma)$ was studied in [14]. The global p-value is given by

$$p_{global} \approx E[\phi(A_u)] = p_{local} + e^{-u/2}(N_1 + \sqrt{u}N_2) \tag{56}$$

where N_1 and N_2 are coefficients that are estimated by calculating the average Euler characteristic of the plane A. To solve for N_1 and N_2, it is convenient to set two reference levels u_0 and u_1, find the Euler characteristics for each level, and solve the consequent system of two linear equations. In a 2D manifold with closed islands, some with holes, each disconnected full island takes the value $+1$. Each hole contributes -1. In that sense a full round shape has the Euler characteristic of $+1$. If you dig a hole in it, its Euler characteristics becomes $+1 - 1 = 0$ (Figure 12).
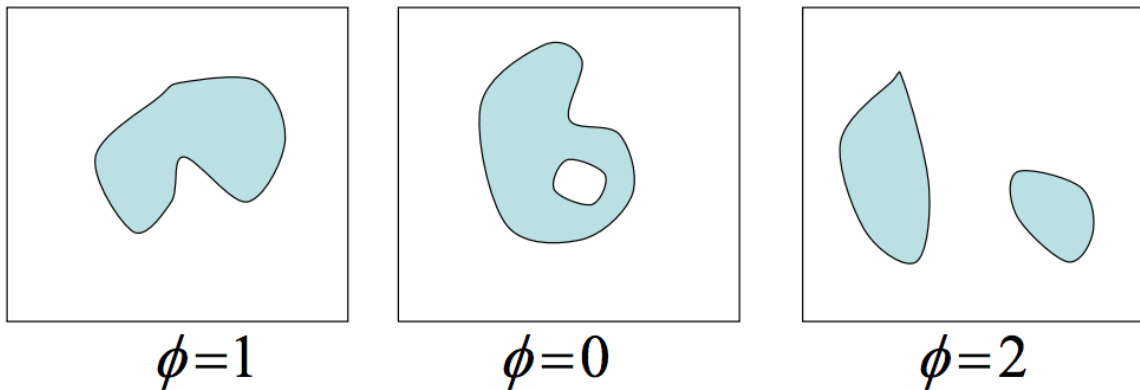

$\phi=1$ $\phi=0$ $\phi=2$

Fig. 12: Illustration of the Euler characteristic of some 2-dimensional manifold.

An example can be taken from the search for di-photon in ATLAS [15]. In Figure 13 one sees the 2D $(m_X, \Gamma_X/m_X)$ plane. The manifold A_u is obtained by slicing this plane at a level $u = Z^2$. The Euler characteristic is the number of "disconnected" islands in that slice.
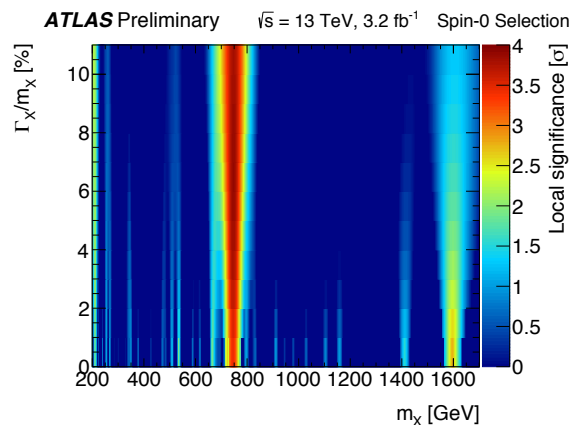
Acknowledgements

Fig. 13: The 2D $(m_X, \Gamma_X/m_X)$ plane. The colors are the significance Z, where the level u is given by $u = Z^2$

References

[1] Proceedings of the 2015 European School of High-Energy Physics, ESHEP2015, CERN-2017-008-SP, Mulders, Martijn (ed.) (CERN) ; Zanderighi, Giulia (ed.) (CERN), e-proceedings: 10.23730/CYRSP-2017-004.

[2] G. Cowan, K. Cranmer, E. Gross and O. Vitells, Eur. Phys. J. C **71** (2011) 1554 [Eur. Phys. J. C **73** (2013) 2501] doi:10.1140/epjc/s10052-011-1554-0, 10.1140/epjc/s10052-013-2501-z [arXiv:1007.1727 [physics.data-an]].

[3] E. Gross and O. Vitells, Eur. Phys. J. C **70**, 525 (2010) doi:10.1140/epjc/s10052-010-1470-8 [arXiv:1005.1891 [physics.data-an]].

[4] Neyman, Jerzy; Pearson, Egon S. (1933). "On the Problem of the Most Efficient Tests of Statistical Hypotheses". Philosophical Transactions of the Royal Society A: Mathematical, Physical and Engineering Sciences 231 (694ï£¡706): 289ï£¡337. Bibcode:1933RSPTA.231..289N. doi:10.1098/rsta.1933.0009. JSTOR 91247.

[5] Birnbaum, Allan (1962). "On the foundations of statistical inference". Journal of the American Statistical Association 57 (298): 269ï£¡326. doi:10.2307/2281640. JSTOR 2281640. MR 0138176.

[6] Presentation of search results: the CLs technique, A L Read 2002 J. Phys. G: Nucl. Part. Phys. 28 2693-2704, **doi:10.1088/0954-3899/28/10/313**

[7] G. J. Feldman and R. D. Cousins, Phys. Rev. D **57** (1998) 3873 doi:10.1103/PhysRevD.57.3873 [physics/9711021 [physics.data-an]].

[8] R. D. Cousins and V. L. Highland, "Incorporating systematic uncertainties into an upper limit," Nuclear Instruments and Methods A.320 (1992) 331-335

[9] S.S. Wilks, *The large-sample distribution of the likelihood ratio for testing composite hypotheses*, Ann. Math. Statist. **9** (1938) 60-2.

[10] A. Wald, *Tests of Statistical Hypotheses Concerning Several Parameters When the Number of Observations is Large*, Transactions of the American Mathematical Society, Vol. **54**, No. 3 (Nov., 1943), pp. 426-482.

[11] [ATLAS Collaboration], "Observation of an Excess of Events in the Search for the Standard Model Higgs boson with the ATLAS detector at the LHC," ATLAS-CONF-2012-093.

[12] G. Cowan, K. Cranmer, E. Gross and O. Vitells, "Asymptotic distribution for two-sided tests with lower and upper boundaries on the parameter of interest," arXiv:1210.6948 [physics.data-an].

[13] R. B. Davies, *Hypothesis testing when a nuisance parameter is present only under the alternative*, Biometrika **74** (1987), 33-43.

[14] O. Vitells and E. Gross, "Estimating the significance of a signal in a multi-dimensional search," Astropart. Phys. **35**, 230 (2011) doi:10.1016/j.astropartphys.2011.08.005 [arXiv:1105.4355 [astro-ph.IM]].

[15] The ATLAS collaboration, "Search for resonances in diphoton events with the ATLAS detector at $\sqrt{s}$ = 13 TeV," ATLAS-CONF-2016-018.

Organizing Committee

T. Donskova (Schools Administrator, JINR)
N. Ellis (CERN)
M. Mulders (CERN)
A. Olchevsky (JINR)
K. Ross (Schools Administrator, CERN)
G. Zanderighi (CERN/Oxford Univ.)

Local Organizing Committee

N. Antunes (LIP)
G. Barreira (LIP)
M. Bezzeghoud (Evora Univ.)
R. Conceição (LIP)
P. Conde Muíño (LIP/FCUL)
M. Gallinaro (LIP)
R. Gonçalo (LIP)
I. Lopes (Univ. de Coimbra/LIP)
J. Maneira (LIP/FCUL)
A. Onofre (Univ. do Minho/LIP)
J. Romão (CFTP/IST)
J. Varela (LIP/IST)

International Advisors

F. Gianotti (CERN)
V. Matveev (JINR)
A. Skrinsky (BINP)
N. Tyurin (IHEP)

Lecturers

A. Arbuzov (JINR)
M. Beneke (TUM)
C. Boehm (IPPP/Annecy)
S. Davidson (CNRS)
S. Dawson (BNL)
D. Fursaev (Dubna Univ/JINR)
E. Gross (Weizmann)
D. Kazakov (JINR)
K. Melnikov (KIT)
G. Milhano (LIP-Lisbon)
P. Silva (CERN)

Discussion Leaders

A. Bednyakov (JINR)
A. Gladyshev (JINR)
I. Ivanov (CFTP/IST)
M. Nardecchia (CERN)
E. Re (CERN)
R. Santos (ISEL)

Students

Fernando ABUDINEN

Chiara AMENDOLA

Claire ANTEL

Joan ARNAU ROMEU

Olga BAKINA

Maria Del Mar BARRIO LUNA

Matteo BEDOGNETTI

Lisa BENATO

Andrea BESCHI

Diallo BOYE

Klaudia BURKA

Douglas John Paul BURNS

Po-Hsun CHEN

Yu-Heng CHEN

Evgeniya CHEREMUSHKINA

Vincenzo CIRIOLO

Andre CORTEZ

Elena DALL'OCCO

Pablo DE CASTRO MANZANO

Charles Eliaz DELPORTE

Kevin DE VASCONCELOS CORGA

Stephan DUELL

Ulrich EINHAUS

Karim EL MORABIT

Saskia FALKE

Davide FAZZINI

Susanna GAGINYAN

Bruno GALINHAS

Mazuza Mohammad A GHNEIMAT

Carlo Alberto GOTTARDO

Emanuel GOUVEIA

Antinéa GUERGUICHON

Guillermo Nicolas HAMITY

Robert HANKACHE

Nikolai HARTMANN

Jaana HEIKKILAE

Alexander HELD

Marketa JANSOVA

Johannes Josef JUNGGEBURTH

Ellis KAY

Evangelos KOURLITIS

Magdalena KUICH

Johannes LANGE

Maria LAVROVA

Xuanhong LOU

Tatiana LYUBUSHKINA

Oliver MAJERSKY

Petr MANDRIK

Emily MCDONALD

Cedric MEAUX

Hualin MEI

Claudia MERLASSINO

Fabrizio MIANO

Irakli MINASHVILI

Elisa MINUCCI

Philipp MOGG

Seth MOORTGAT

Harry MOSS

Aleksandr MUDROKH

Mick MULDER

John MYERS

Adam PARKER

Ana Paula PEREIRA PEIXOTO

Malgorzata Maria PIKIES

Alessio PIUCCI

Navid K. RAD

Johnny RAINE

Andres RAMIREZ MORALES

Evan RANKEN

Tasneem RASH

Haifa REJEB SFAR

Victor RENAUDIN

Sebastien RETTIE

Jan Oliver RIEGER

Andrea RODRIGUEZ PEREZ

Krystian ROSLON

Elias RUTTINGER

Despoina SAMPSONIDOU

Andrea SCARPELLI

Cristina SCHLESIER

Cristiano SEBASTIANI

Michal SEFCIK

Andrea SELCE

Tina SFILIGOJ

Yu-Ting SHEN

Rostislav SOTENSKY

Carl Joseph Edmund SUSTER

Grigore TARNA

Stefanie TODT

Oleksii TOLDAIEV

Fabio TRESOLDI

Tiago VALE

Marco VALENTE

Maarten VAN VEGHEL

Viesturs VECKALNS

Emma WINKELS

Robert WOLFF

Michael ZAMKOVSKY

Zukhaimira Binti ZOLKAPLI

Posters

Presenter	Poster title
ABUDINÉN, F.	CP Violation sensitivity at BELLE II
AMENDOLA, C.	The CMS Level-1 tau lepton and Vector Boson Fusion triggers for the LHC Run II
ANTEL, C.	Dark Matter bumphunting at Trigger Level with ATLAS
ARNAU ROMEU, J.	Search for Lepton Flavor Violation at LHCb
BARRIO, M.	Evidence for the Standard Model tZq production in three-lepton events at 13 TeV in CMS
BEDOGNETTI, M.	Search for Lepton Flavour Violation with the ATLAS detector: a hunt for $\tau \rightarrow 3\mu$
BENATO, L.	Search for heavy resonances decaying into a Z boson and a vector boson in the $(\ell\bar{\ell}, \nu\bar{\nu})q\bar{q}$ final states at CMS
BESCHI, A.	The CMS electron and photon trigger for the LHC Run 2
BOYE, D.	Search for Higgs decays to beyond the standard model light gauge bosons in four-lepton events with the ATLAS detector at $\sqrt{s} =$13 TeV
BURKA, K.	Measurement of the azimuthal anisotropy in Pb+Pb collisions at $\sqrt{s_{\mathrm{NN}}} = 5.02$ TeV with the ATLAS detector at the LHC
BURNS, D.	Differential $t\bar{t}$ Production Cross Sections with respect to Global Event Distributions at CMS
CHEREMUSHKINA, E.	Excited lepton search in the semileptonic ($l\nu qq$) final state in pp collisions data at 13 TeV with the ATLAS detector at the LHC
CORTEZ, A.	New Developments in Gas Detectors Dual-Stage Proportional Scintillation Counter
DALL'OCCO, E.	Sensor Characterisation for the LHCb VELO Upgrade
DUELL, S.	Semileptonic B decays with the Belle II experiment

Presenter	Poster title
EINHAUS, U.	ROPPERI - A novel TPC readout with GEMs, pads and Timepix
FALKE, S.	In situ scale factors from $Z \rightarrow ee$ events for the electron and photon energy calibration with the ATLAS detector
GAGINYAN, S.	Investigation of nuclear reactions on separated lead isotopes at 2.2 GeV/nucleon energies of the deuteron beams
GOUVEIA, E.	Probing the CP nature of the Higgs coupling in $t\bar{t}h$ events at the LHC
GALINHAS, B.	Heavy Flavor Production at $\sqrt{s} =$ 13 TeV
GHNEIMAT, M.	Cross section measurement of $t\bar{t} + \gamma$ production in pp collisions with the ATLAS detector
GOTTARDO, C. A.	Search for Lepton Flavour Violation in top quark decays with the ATLAS detector
HAMITY, G.	Limits on neutral Higgs bosons decaying to $\tau^+\tau^-$ with ATLAS
HARTMANN, N.	Search for gluinos and squarks in events with one isolated lepton, at least 2-9 jets and missing transverse momentum at $\sqrt{s} =$ 13 TeV with the ATLAS Detector
IRAKLI, M.; ROSTISLAV, S.	Micromegas chambers for ATLAS upgrade
JANSOVÁ, M.	Search for top squark pair production in the single lepton channel at CMS
JUNGGEBURTH, J.	Search for Supersymmetry in multileptonic final states
KAY, E.	Search for a New Heavy Charged Gauge Boson with ATLAS
KOURLITIS, E.	Search for production of supersymmetric particles in final states with missing transverse momentum and multiple b-jets at $\sqrt{s} =$ 13 TeV p-p collisions.
KUICH, M.	Search for signals of onset of deconfinement: Be+Be collisions at CERN SPS.
LANGE, J.	Top quark mass measurement in the $t\bar{t}$ all-jets final state with the CMS experiment at $\sqrt{s} =$ 13 TeV
LAVROVA, M.	The TUS space experiment

Presenter	Poster title
Lou, X.	Search for Dark Matter Produced in Association with a Hadronically Decaying Vector Boson at $\sqrt{s}$ =13 TeV with the ATLAS Detector
Lyubushkina, T.	Search for excited B_c^+ meson states with the ATLAS Detector
Mandrik, P.	The evaluation of the systematic uncertainties for finite MC samples in the presence of negative weights
Méaux, C.	Lepton flavour in FCNC transitions: prospects at the LHC
Mei, H.	Higgs mass measurement using H $\rightarrow$ ZZ* $\rightarrow$ 4l decay mode with the CMS detector
Merlassino, C.	Characterisation of irradiated silicon sensors with the Transient Current Technique
Miano, F.	The Performance of the ATLAS Inner Detector Trigger System
Mogg, P.	Search for Supersymmetric Partners of the Top Quark in the Fully Hadronic Final State with ATLAS at $\sqrt{s}$ =13 TeV
Moortgat, S.	Identification of c-quark jets at the CMS experiment
Moss, H.	QCD Multijet Background Estimation in Run-II SUSY Searches with the ATLAS Detector
Mudrokh, A.	Particle Identification (PID) for MPD
Mulder, M.	Understanding rare beauty: the effective lifetime and branching fraction of $B_s^0 \rightarrow \mu^+\mu^-$
Parker, A.	Searches for Higgs boson pair-production in the $b\bar{b}\tau\tau$ decay channel with the ATLAS detector
Peixoto, A.	Search for tZ production via Flavour Changing Neutral Currents with the ATLAS Experiment at 13 TeV
Piucci, A.	A focus on the LHCb Upgrade
Rad, N. K.	Search for top squark pair-production in the single-lepton channel in models with highly compressed mass spectra with the CMS experiment
Ranken, E.	Reconstructing Neutrino Momenta in Dilepton $t\bar{t}$ Decays

Presenter	Poster title
RASHID, T.	Irradiation Damage Studies for ATLAS Inner Tracker (ITK) Upgrade at the HL-LHC
RAINE, J.	Search for $t\bar{t}H \rightarrow b\bar{b}$ at $\sqrt{s}$=13 TeV with ATLAS
RENAUDIN, V.	Semitauonic B decays at LHCb
ROSLON, K.	Cooling System for the Slow Control System RACKs
RODRIGUEZ PEREZ, A.	Search for the supersymmetric partner of the top quark in full hadronic final states at 13 TeV
SAMPSONIDOU, D.	Study of the WZ production at 13 TeV at the ATLAS experiment
SCARPELLI, A.	Track/shower separation in a Dual-phase liquid Argon TPC using a Convolutional Neural Network
SEBASTIANI, C.	Search for long-lived neutral particles decaying into Lepton-Jets with the ATLAS detector in p-p collision data at $\sqrt{s}$=13 TeV
SUSTER, C.	Single top-quark tW production at ATLAS
TARNA, G.	Electron Identification with the ATLAS detector
TAYLOR, A.	Prospects for observing ttHH production with the ATLAS experiment at the HL-LHC
VALE, T.	Search for vector-like quarks decaying to a Z boson with the ATLAS experiment
VALENTE, M.	Online Track-based Pileup subtraction for the ATLAS HL-LHC Upgrade
VECKALNS, V.	Colour flow between jets in top quark decays. Observations at the CERN CMS experiment.
VAN VEGHEL, M.	Search for the lepton-flavour violating decays $B_s^0 \rightarrow e^{\pm}\mu^{\mp}$
WINKELS, E.	Search for boosted $t\bar{t}H(H \rightarrow b\bar{b})$ at ATLAS
WOLFF, R.	The ATLAS experiment: LAr trigger readout electronics upgrade and associated Higgs boson production with a top quark pair
ZOLKAPLI, Z.	Search for Neutral MSSM Higgs Boson Decaying to $\mu^+\mu^-$ in pp Collisions at $\sqrt{s}$ =13 TeV